UNIVERSITAT DE BARCELONA

FACULTAT DE FARMÀCIA I CIÈNCIES DE L'ALIMENTACIÓ

LABORATORI DE QUÍMICA FARMACÈUTICA

DEPARTAMENT DE FARMACOLOGIA, TOXICOLOGIA I QUÍMICA TERAPÈUTICA

NEW POLYCYCLIC SMALL MOLECULES AS ION CHANNEL MODULATORS

MARTA BARNIOL I XICOTA

Gener 2017

UNIVERSITAT DE BARCELONA

FACULTAT DE FARMÀCIA I CIÈNCIES DE L'ALIMENTACIÓ

PROGRAMA DE DOCTORAT:
Química Orgànica Experimental i Industrial

New polycyclic small molecules as ion channel modulators

Memòria presentada per Marta Barniol i Xicota per optar al títol de Doctora per la Universitat de Barcelona

Director i tutor:

Dr. Santiago Vázquez Cruz

Marta Barniol i Xicota

Gener 2017

Als meus pares

i a la meva germana

" L'èxit comença amb la voluntat.

La batalla de la vida no sempre la guanya

la persona més forta o més lleugera

Per que tard o d'hora la persona que guanya

És aquella que creu que pot fer-ho"

- R. Kippling

AGRAÏMENTS

Durant el transcurs d'aquesta Tesi, he tingut la sort d'haver coincidit i d'haver comptat amb persones meravelloses a les que em sento molt agraïda. M'agradaria no oblidar-me a ningú però és impossible, per tant a tots els esmentats a continuació com als que em deixi, moltes gràcies!

En primer lloc voldria donar les gràcies al meu director de tesi, per haver-me donat l'oportunitat de fer investigació, des del primer treball dirigit al 2009 fins ara al finalitzar la Tesi Doctoral al 2017. Santi, GRACIAS por todo lo que me has enseñado, por darme libertad para llevar a cabo mis ideas, por todos los consejos químicos y no, por estar ahí en los momentos de estrés, pero sobretodo gracias por confiar en mí desde el primer dia. Eres un gran director de tesis y una gran persona.

Seguidament agrair als altres professors del Departament de Química Farmacèutica, dels que també he après molt durant aquests anys. A Pelayo Camps, per ser un exemple de tenacitat i una font de coneixement químic; a Diego Muñoz-Torrero, per sempre estar disposat a ajudar, escoltar y tener esa capacidad misteriosa de entrar en el lab justo cuando estoy de cháchara (me tienes que contar cómo lo haces) i a la Carmen Escolano, per no tenir pèls a la llengua i ser un exemple a seguir – suerte que has venido a poner orden en el lab..!

No voldria oblidar-me tots aquells grups de recerca que han contribuït científicament en els projectes d'aquesta Tesi; en el camp de la grip: al grup de la Prof. Lieve Naesens, del Rega Institute for Medicinal Research (Leuven, Bèlgica), al Prof. Lawrence Pinto de la Northwestern University (Evanston, Illinois, US), als Drs. Jun Wang i Michael Caffrey de la University of Arizona (Tucson, US), a la Prof. Anna Moroni i la Dra. Sabrina Gazzarrini, de la Università degli Studi di Milano i especialment al grup del Prof. Javier Luque de la Universitat de Barcelona per la realització dels càlculs de docking i dinàmica molecular. En relació als projectes de NMDA al Prof. Francesc Sureda (Universitat Rovira i Virgili) i al Prof. David Soto, per a més a més haver tingut l'amabilitat d'ensenyar-me *patch*. Finalment en relació als projectes de $P2X_7$ mencionar els grups del Prof. Yong-Chul Kim al Gwangju Institute of Science and Technology (GIST, Korea) i el del Prof. Lin-Hua Jiang a la University of Leeds (Leeds, UK), especialment a la Dra. Emily Caseley.

Mencionar també aquelles persones que amb la seva feina han facilitat el meu dia a dia al lab: la Maite, l'Ana, l'Asun, l'Armando, el Josep Galdon i el Javier.

Un gràcies molt gran al grup SVC. Primer de tot a l'Eva, mi mentora, gràcies per la paciència d'ensenyar-me des de zero, pels teus bons consells, saber escoltar, ser algú amb qui sé que puc comptar i en definitiva, per ser una bona amiga! Al Salv*e* - ets molt gran - no podria haver trobat ningú millor amb qui començar! Al Matías pels riures i els seus consells als que (a vegades) feia cas – *¿dónde está la lista?* i a l'Elena per estar sempre disposada a ajudar. Como no, a la Rous, per ser la meva veïna de vitrina i la meva *cómplice* dels bailes del divendres, amb la que ens hem donat suport en els moments de *pou* però també hem compartit molt bons moments, has sigut un puntal en aquests últims anys, et trobaré a faltar *mapache*! A l'Eugènia, l'última – gran - incorporació al grup i als treballs dirigits i altres estudiants que han passat aquests anys pel lab, en especial a la Maria, a la Marta Frigolé i a l'Enric. Finalment a les meves *mindus* de les que he après molt i a les que

espero haver ensenyat alguna cosa: la Marta M., l'Anna Ruíz – ets única -, la Blanca, la Marta Baran, l'Olga i finalment a les que ahí siguen: Sandra i Andreea – confio en vosotras, vosotras podéis!!

A tots els meus companys del laboratori de Química Farmacèutica – que després de tots aquests anys al lab, en són uns quants-. Començant pel principi, a la Tània, la meva primera companya de vitrina, moltes gràcies per ajudar-me sempre i fer el meu inici molt més fàcil; a l'Eli, per tenir sempre un somriure a la cara i per ser la millor event organizer que he conegut! Al Carles, *er genio*, per tenir un modus operandi i manera de veure les coses bastant semblant a la meva, i perquè sé que sempre puc comptar amb tu, tant si és per a un simple cafè com perquè em donis una opinió políticament incorrecta quan no te la demano. A la Irene, amb la que he compartit més temps de tesi, hem passat juntes tot el procés de mindus a doctores i hem viscut mil moments imborrables durant aquest temps, *xurri ets un sol!*. Al David, pels nostres insubstituïbles *ganivets*, al Javi por los lab-breaks i tus "*eso es así*", i als dos per ser clarament pitjors que jo a la *fiball* – se siente -, us considero dos bons amics i adoro que haguem coincidit al lab! A l'Ane, la meva compi d'habitació a València, per tots els bons moments i perquè semblava que no arribaria mai i ja ets doctora!!, a la Orne, por tu perseverancia y tu madurez; a la Katia, perquè es pot parlar de tot amb tu, *ánimo, que si se puede*!; a la Sònia, *xica*, ets l'alegria de la huerta; a l'Arnau, el teu *escolta* ha creat escola i a tants altres que pot ser han passat més temporalment, però han deixat un bon record, com el Toni – que veient el percal de lab vas fugir ràpidament a computacional -, l'Albert, la Eugenia, l'Andrea E., els de Salvat o el Raül i l'Andrés de CIDQO.

Nombrar també els meus companys del màster de València, en especial a l'Alberto – el mejor cocinero-, a Fabri, Manu, Javi y, faltaría más, a Juan Andrés – por tus disertaciones en RMN -; a tots els companys de Química Orgànica de la facultat de Farmàcia; así como a "los de la IQM" con los que empezamos a montar el Simposio de la SEQT: Mario, Pili, Marta, Gemma y especialmente a Oskía y a Paula.

Durant aquest temps he tingut l'oportunitat de conèixer i treballar a altres laboratoris i grups de recerca, als que tinc molt que agrair. First at Dr. Hilton's group at UCL, thank you Steve for all I learned, your kindness, to be so easy to talk to and, of course, to correct my English - *quéee?*. Also to all the amazing people working in that group, especially to Bhaven, Zi and Ale. Of course to Zen, *cani*, a friendship like yours is invaluable, and to her family. For my time in San Francisco, to Bill and Susan, to be my adoptive parents for a month – thank you for your kind hospitality, fantastic cooking and great conversations. Thank again Prof. DeGrado (Bill), for accepting me in his research group where I could grew as a scientist and for all the wise pieces of advice. Also to all the members of the DeGrado lab at UCSF, specially to Kathleen, Sid and Gözde, Haifan, Bobo – to convince me to go climbing, to be able to (almost) defeat my stubbornness and always be ready to listen to me and give me smart advice- and Bruk, besides for teaching me in the lab, for being a really good friend with who I can talk about everything – listen, please, move to Europe. Finalment agrair al Prof. Xavi Gomis-Rüth per acollir-me al seu grup a l'IBEC durant els meus últims mesos de Tesi, així com als membres del seu grup, molt especialment a la Mar – espero que tot t'estigui anant genial per Àustria! Agrair també a tota la gent que he

conegut durant les estades a l'estranger i han fet que es fes molt més fàcil ser lluny de casa – Bia – my *fav* roomie, Júlia, Sol, Ester...

Agrair també als meus amics d'aquí – m'agradaria nombrar-vos un(a) per un(a) però és una mica complicat- per la vostra comprensió i per haver estat allà en tot moment, sempre disposats a ajudar i amb una paraula d'ànim a punt! Mil gràcies per seguir fent-me costat.

Als meus pares, que m'ho han donat tot, per recolzar-me, ajudar-me i ser allà sempre, incondicionalment. Per ser un model a seguir i ser les persones més vàlides i fortes que conec; no tinc paraules d'agraïment suficients per a vosaltres. A la meva germana per escoltar-me, fer els seus anàlisis de psicòloga de totes les situacions i per compartir amb mi la passió pels acudits dolents. Al Bat, per ser la millor companyia en la fase d'escriptura de la Tesi.

Finally to Jef, to have been there for me – and survived – first, during the fellowships and, right after, during the final Thesis period, I know it has not been easy. Thank you so much for sticking by my side through thick and thin, showing me that distance means nothing and to see the best side of every situation. Thanks for being such a marvellous person.

El treball experimental recollit en aquesta memòria s'ha realitzat en el Laboratori de Química Farmacèutica de la Facultat de Farmàcia i Ciències de l'Alimentació de la Universitat de Barcelona, sota la direcció del Dr. Santiago Vázquez Cruz.

Aquest treball ha estat finançat pel Ministerio de Ciencia e Innovación (projectes CTQ2008-03768 i CTQ2011-22433). Per la realització de la present Tesi Doctoral he gaudit d'una beca per la finalització de la Tesi Doctoral del Institut de Biomedicina de la Universitat de Barcelona (IBUB) durant l'any 2015, així com de l'ajut per estades pre-doctorals a l'estranger de la Fundació Pedro i Pons (09/2014-12/2014), l'ajut per a la realització d'estades formatives a estranger de la fundació Montcelimar i la Universitat de Barcelona i la beca EMBO Short-Term de l'European Molecular Biology Organization, ASTF-453-2015, (09/2015-11/2015).

PRÒLEG

Aquesta Tesi Doctoral es presenta com a Compendi de publicacions. El treball es troba dividit en 9 capítols que, d'acord amb la normativa vigent, inclouen: un apartat d'introducció general on es justifica la temàtica i posen en context els articles presentats a continuació (**capítol 1**); un apartat amb els objectius generals de la Tesi, així com els objectius específics de cada un dels projectes descrits (**capítol 2**); una secció explicativa prèvia a cada article que fa de resum d'aquests i a l'hora de discussió dels resultats obtinguts (**capítols 3-8**) i finalment un apartat de conclusions finals (**capítol 9**).

Cal fer palès que els capítols es troben ordenats cronològicament i per grups temàtics, essent així els capítols del 3 al 6, un bloc temàtic relacionat amb el virus de la Influenza A, el capítol 7 fa relació al receptor $P2X_7$ i el capítol 8 representa tant el bloc temàtic de $P2X_7$ com de NMDA.

En el bloc tematic de compostos anti-Influenza A s'inclouen i es discuteixen els articles: "3-Azatetracyclo[5.2.1.1^{5,8}.0^{1,5}]undecane Derivatives: From Wild-Type Inhibitors of the M2 Ion Channel of Influenza A Virus to Derivatives with Potent Activity against the V27A Mutant" (Rey-Carrizo, M., Torres, E., Ma, C., Barniol-Xicota, M., Wang, J., Wu, Y., Naesens, L., DeGrado, W. F., Lamb, R. A., Pinto, L. H. & Vázquez, S. *Journal of Medicinal Chemistry*. **2013**, *56*, 9265-9274.), en el **capítol 3**.

"Easily Accessible Polycyclic Amines that Inhibit the Wild-Type and Amantadine-Resistant Mutants of the M2 Channel of Influenza A Virus" (Rey-Carrizo, M., Barniol-Xicota, M., Ma, C., Frigolé-Vivas, M., Torres, E., Naesens, L., Llabrés, S., Juárez-Jiménez, J., Luque, F.J, DeGrado, W. F., Lamb, R. A., Pinto, L. H. & Vázquez, S. *Journal of Medicinal Chemistry*. **2014**, *57(13)*, 5738-5747) i "Dimerization of Pyramidalized 3,4,8,9-Tetramethyltetracyclo [4.4.0.0^{3,9}.0^{4,8}]dec-1(6)-ene to a Hydrocarbon Featuring Four Cyclohexane Rings in Boat Conformations" (Rey-Carrizo, M., Barniol-Xicota, M., Font-Bardia, M. & Vázquez, S. *Angewandte Chemie International Edition*. **2014**, *53*, 8195-8199) en el **capítol 4**. Cal tenir en compte que aquest capítol 4 consta de dues parts, A i B, que responen al fet que el treball presentat en la part B, és derivat directe del treball presentat en la part A.

Finalment en aquest primer bloc hi ha els dos manuscrits "Slow but steady wins the race: dissimilarities among new dual inhibitors of the wild-type and the V27A mutant M2 channels of influenza A virus." (Barniol-Xicota, M., Gazzarrini, S., Torres, E., Hu, Y., Wang, J., Naesens, L., Moroni, A. & Vázquez, S. *Manuscrit enviat a la revista*) en el

capítol 5 i "Redesigning old anti-influenza compounds: synthesis and evaluation of novel anilines with activity against the 2009 H1N1 influenza virus" (Leiva, R., Barniol-Xicota, M., Codony, S., Ginex, T., Vanderlinden, E., Montes, M., Caffrey, M., Naesens, L., Luque, F. J. & Vázquez, S. *Manuscrit enviat a la revista*) en el **capítol 6**, igualment resumits i comentats.

En el bloc temàtic de compostos antagonistes del receptor $P2X_7$ s'hi inclou el manuscrit "Escape from adamantane: Scaffold optimization of novel $P2X_7$ antagonists featuring complex polycycles" (Barniol-Xicota, M., Caseley, E., Valverde, E., Kim, Y-C., Jiang, L-H. & Vázquez, S. *Manuscrit enviat a la revista*) així com un breu resum i discussió del mateix.

L'últim bloc està format pel **capítol 8** en el que s'hi troba el manuscrit "Multi-target directed ligands to the NMDA and $P2X_7$ receptors, of interest for the treatment of Alzheimer's Disease" (Karou, O., Kim, Y-C., Sureda, F. X., Vázquez, S. & Barniol-Xicota, M. *Manuscrit enviat a la revista*) i el seu resum i discussió.

La memòria també inclou un apartat de difusió dels resultats on s'hi fa constar els articles presentats en el context d'aquesta Tesi, així com d'altres no recollits en aquest treball.

RESULTS DISSEMINATION

PUBLICATIONS

1. **'Inhibitors of the M2 channel of influenza A virus'.** Duque,MD.; Torres,E.; Valverde,E.; Barniol,M.; Guardiola,S.; Rey,M.; Vázquez,S. *Recent Advances in Pharmaceutical Sciences* (Transworld Research Network). **2011**, 37/661 (2). Kerala (INDIA). ISBN: 978-81-7895-528-5

2. **'3-Azatetracyclo[5.2.1.1^{5,8}.0^{1,5}]undecane derivatives: from wild-type inhibitors of the M2 ion channel of influenza A virus to derivatives with potent activity against the V27A mutant'.** Rey-Carrizo, M.; Torres, E.; Ma, C.; Barniol-Xicota, M.; Wang, J.; Wu, Y.; Naesens, L.; DeGrado, W. F.; Lamb, R. A.; Pinto, L. H.; Vázquez, S. *Journal of Medicinal Chemistry*. **2013**, *56*, 9265-9274.

3. **'Direct reductive alkylation of amine hydrochlorides with aldehyde bisulfite adducts'.** Barniol-Xicota, M.; Turcu, A.L.; Codony, S.; Escolano, C.; Vázquez, S. *Tetrahedron Letters*. **2014**, *55*, 2548-2550.

4. **'Easily accessible polycyclic amines that inhibit the wild-type and amantadine-resistant mutants of the M2 channel of influenza A virus'.** Rey-Carrizo, M.; Barniol-Xicota, M.; Ma, C.; Frigolé-Vivas, M.; Torres, E.; Naesens, L.; Llabrés, S.; Juárez-Jiménez, J.; Luque, F.J; DeGrado, W. F.; Lamb, R. A.; Pinto, L. H.; Vázquez, S. *Journal of Medicinal Chemistry*. **2014**, *57(13)*, 5738-5747.

5. '**Dimerization of pyramidalized 3,4,8,9-tetramethyltetracyclo [4.4.0.0^{3,9}.0^{4,8}]dec-1(6)-ene to a hydrocarbon featuring four cyclohexane rings in boat conformations'**. Rey-Carrizo, M.; Barniol-Xicota, M.; Font-Bardia, M.; Vázquez, S. *Angewandte Chemie International Edition*. **2014**, *53*, 8195-8199.

6. '**Antibacterial activity of novel benzopolycyclic amines**'. Barniol-Xicota, M.; Escandell, A.; Valverde, E.; Julian, E.; Torrents, E.; Vázquez, S. *Bioorganic & Medicinal Chemistry*. **2015,** *23*, 290-296.

7. '**Stopping the flu in its tracks: New approaches to influenza A inhibition'**. Barniol-Xicota, M.; *Proceedings 35th European School of Medicinal Chemistry (ESMEC)*. **2015**, 1, 14-15.

8. '**Synthesis of cinacalcet: an enantiopure active pharmaceutical ingredient (API)**'. Barniol-Xicota, M.; Leiva, R.; Escolano, C.; Vázquez, S. Synthesis. **2016**, *48*, 783-803.

9. '**Heme-Regulated eIF2α Kinase Modulates Hepatic FGF21 and is Activated by PPARβ/δ Deficiency**'. Zarei, M.; Barroso, E.; Leiva, R.; Barniol-Xicota, M.; Escolano, C.; Vázquez, S.; Palomar, X.; Pardo, V.; González-Rodríguez, A.; Valverde, A. M.; Wahili, W.; Vazquez-Carrera, M. *Diabetes*. **2016**, 65(10), 3185-99.

CONFERENCES

I. Poster. **Barniol, M**.; Rey, M.; Torres, E.; Ma, C.; Pinto, L. H.; Vázquez, S.; *New Influenza A M2 Channel Inhibitors Featuring Tetracyclic Scaffolds*; 7th Balticum Organicum Syntheticum (BOS), Tallin (ESTONIA), **June-2012**

II. Oral communication. Torres, E.; Rey, M.; **Barniol, M.**; Vázquez, S.; *Synthesis of polycyclic amines with anti-influenza A virus* activity, XXIV Reunión Bienal de Química Orgánica, San Sebastián (Spain), **July-2012**

III. Poster. Torres, E.; **Barniol, M.**; Vázquez, S.; Rey, M.; *Synthesis and anti-influenza A activity of novel polycyclic amines*, XXIV Reunión Bienal de Química Orgánica, San Sebastián (Spain), **July-2012**

IV. Poster. **Barniol-Xicota, M.**; Torres, E.; Ma, C.; Pinto, L.H.; Vázquez, S.; *Novel anti-influenza drugs: inhibitors of the V27A mutant M2 channel*, VI Mediterranean Organic Chemistry Meeting (REQOMED), Granada (Spain), **May-2013**

V. Poster. **Barniol-Xicota, M.**; Rey-Carrizo, M.; Torres, E.; Ma, C.; Frigolé, M.; Llabrés, S.; Juárez-Jiménez, J.; Luque, F. J.; Pinto, L.H.; Vázquez, S.; *Novel polycyclic compounds with potent activity against the amantadine-resistant L26F and V27A mutant M2 channels of influenza A virus*, XVII Congreso de la Sociedad Española de Química Terapéutica, Madrid (Spain), **October-2013**

VI. Oral communication. **Barniol-Xicota, M.**; Leiva, R.; *Fighting the flu: design of new potential antiviral compounds*; Jornada d'Investigadors Predoctorals Interdisciplinària (JIPI), Barcelona (Spain), **January-2014**

VII. Poster. Leiva, R.; Gazzarrini, S.; Torres, E.; Rey-Carrizo, M.; **Barniol-Xicota, M.**; Moroni, A.; Naesens, L.; Vázquez, S.; *Hemagglutinin as a new target to fight the flu*. I Simposio de Jóvenes Investigadores (Sociedad Española de Química Terapéutica), Madrid (Spain), **May- 2014**

VIII. Poster. Rey-Carrizo, M.; Frigolé-Vivas, M.; **Barniol-Xicota, M.**; Leiva, R.; Gazzarrini, S.; Ma, C.; Moroni, A.; Pinto, L.H.; Vázquez, S.; *Exploring new polycyclic scaffolds targeting the V27A mutant M2 channel of influenza A virus* I Simposio de Jóvenes

Investigadores (Sociedad Española de Química Terapéutica), Madrid (Spain), **May-2014**

IX. Oral communication. **Barniol-Xicota, M.**; *Influenza A virus: a wolf in sheep's clothing. Recent advances in new anti-influenza compounds*; I Simposio de Jóvenes Investigadores (Sociedad Española de Química Terapéutica), Madrid (Spain), **May-2014**

X. Poster. **Barniol-Xicota, M**; Vázquez, S; *New polycyclic scaffolds: light on P2X7 receptors*, II Simposio de Jóvenes Investigadores (Sociedad Española de Química Terapéutica), Madrid (Spain), **June- 2015**

XI. Poster. **Barniol-Xicota, M**.; *Stopping the flu in its tracks: New approaches to influenza A inhibition*; European School of Medicinal Chemistry (EFMC-ESMEC), Urbino (Italy), **June-2015**

XII. Oral communication (selected by scientific comitee). **Barniol-Xicota, M**.; *Stopping the flu in its tracks: New approaches to influenza A inhibition*; European School of Medicinal Chemistry (EFMC-ESMEC), Urbino (Italy), **June-2015**

XIII. Poster. Rey-Carrizo, M.; **Barniol-Xicota, M.**; Vázquez, S.; *Dimerization of a highly pyramidalized alkene to a hydrocarbon featuring four cyclohexane rings in boat conformations*, XXXV Reunión Bienal de Química Orgànica (RSEQ), A Coruña (Spain), **July-2015**

XIV. Poster. **Barniol-Xicota, M.**, Vázquez, S.; DeGrado, W.; Gazzarrini, S.; Torres, E.; Rey-Carrizo, M.; Moroni, A.; Naesens, L. *New approaches to influenza A inhibition*. Eli Lilly-EUACC (XIII Awards for PhD students), Madrid (Spain), **September-2015**

XV. Poster. Turcu, A. L.; **Barniol-Xicota, M.**; Codony, S.; Escolano,C; Vázquez, S.; *Direct reductive alkylation of amine hydrochlorides with aldehyde bisulfite adducts*. Simposio de Investigadores Jóvenes, Barcelona (Spain), **November-2015**

XVI. Poster. Vázquez, S.; DeGrado, W.; Wu, Y.; Gazzarrini, S.; Torres, E.; Rey-Carrizo, M.; Moroni, A.; Naesens, L.; **Barniol-Xicota, M.;** *Inhibiting the M2 channel of the influenza A virus: looking for the right stopper,* Chemical Biology Symposium (RSC), London (UK), **April-2016**

XVII. Seminar. **Barniol-Xicota, M.**, Torres, E.; Leiva, R.; Rey-Carrizo, M.; Vázquez, S.; *Combatent del virus de la influenza: noves estructures i dianes terapèutiques.* Research seminars at the Faculty of Pharmacy, Barcelona (Spain), **May-2016**

XVIII. Poster. **Barniol-Xicota, M.**; Leiva, R.; Codony, S.; Montes, M.; Naesens, L.; Ginex, T.; Luque, F. J.; DeGrado, W. F.; Moroni, A.; Vázquez, S.; *New horizons in Influenza*

A therapeutics. V SEQT Summer School - "Medicinal Chemistry in Drug Discovery: The Pharma Perspective", Sant Feliu de Llobregat (Spain), **June-2016**

XIX. Poster. Turcu, A. L.; **Barniol-Xicota, M.**; Sureda, F. X.; Coll-Llauradó, M.; Vázquez, S; *New benzopolycyclic cage amines with potent activity as NMDA receptor antagonists.* Simposio de Jóvenes Investigadores (Sociedad Española de Química Terapéutica), Barcelona (Spain), **June-2016**

XX. Poster. **Barniol-Xicota, M.**; Torres, E.; Llabres, S.; Wu, Y.; Naesens, L.; Luque, F. J.; DeGrado, W. F.; Moroni, A.; Vázquez, S.; *Influenza A drugs: towards monotherapy*. XVII Tetrahedron Symposium, Sitges (Spain), **July-2016**

XXI. Poster. **Barniol-Xicota, M.**; Leiva, R.; Codony, S.; Montes, M.; Naesens, L.; Ginex, T.; Luque, F. J.; DeGrado, W. F.; Moroni, A.; Vázquez, S.; *New horizons in Influenza A therapeutics*. V SEQT Summer School - "Medicinal Chemistry in Drug Discovery: The Pharma Perspective", Sant Feliu de Llobregat (Spain), **September-2016**

XXII. Poster. Turcu, A. L.; **Barniol-Xicota, M.**; Sureda, F. X.; Martinez-Falguera, D.; Vázquez, S; *Novel analogues of memantine with potent activity as glutamate N-methyl-D-aspartate receptor antagonists*. XIII Simposio de Investigadores Jóvenes de la Real Sociedad Española de Química, Logroño (Spain), **November-2016**

RESEARCH STAYS

1. **University College London** (UCL), School of Pharmacy, Supervisor: Dr. Stephen Hilton. Research topic: Intramolecular acylal cyclisations (IAC) towards the synthesis of natural products and substituted pyrrolidine and piperidine heterocycles. (01/09/2014-28/01/2015)

2. **University of California San Francisco** (UCSF), Supervisor: Prof. William F. DeGrado. Research topics: (i) M2 protein binding studies and high throughput pharmacological evaluation methodology development and (ii) Synthesis of a novel family of dual peptidic conjugates with glucocorticoid and S1P1 receptor antagonist activity (30/07/2015-21/12/2015)

3. **Institute for Bioengineering of Catalonia** (IBEC), Supervisor: Prof. Xavier Gomis-Rüth. Research topic: Structure solving of the M2 V27A mutant channel of influenza A virus (01/04/2016-01/07/2016).

INDEX

Chapter 1

Introduction

1.1. ELS CANALS IÒNICS

1.1.1. Característiques generals dels canals iònics

Els anomenats canals iònics són proteïnes transmembrana especialitzades que es troben en les cèl·lules de pràcticament tots els éssers vius i virus. Són proteïnes multimèriques, contenen dues o més cadenes polipeptídiques, que s'organitzen formant un porus ple d'aigua o canal iònic d'una banda a altra de la membrana plasmàtica, fent de filtre[1].

L'estructura típica d'aquests canals consta de[2]: el vestíbul extracel·lular, que fa de receptacle d'ions; el filtre selectiu, que consisteix en una seqüència d'aminoàcids (aa) molt conservada; una cavitat central hidrofòbica plena d'aigua, que permet la resolvatació dels ions per tal que continuïn el seu pas sense interaccionar amb la superfície de la proteïna; i la comporta intracel·lular, que consisteix en un cabdell d'hèlix de les subunitats proteiques que formen el canal, infranquejable quan aquest es troba tancat. (Figura 1)

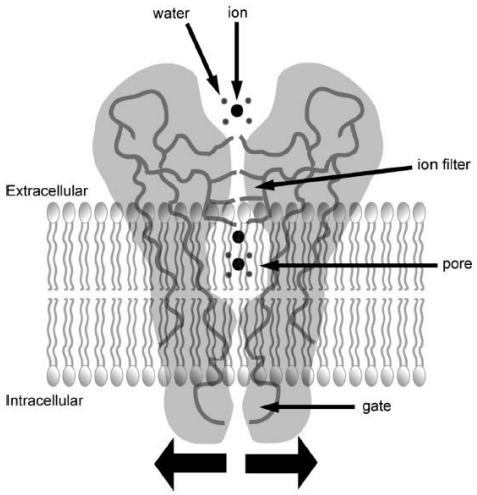

Figura 1. Estructura d'un canal iònic model. Les parts principals es troben detallades.

Dues característiques fonamentals d'aquests canals permeten la permeació organitzada d'ions a través de la membrana: la selectivitat i el mecanisme de comporta[3].

La *selectivitat* fa referència a l'habilitat de deixar pas només a un tipus determinat d'espècie iònica - típicament Na^+, Ca^{2+}, K^+ o Cl^- - a través de la membrana lipídica impermeable[4,5]. En la majoria de canals això s'aconsegueix gràcies a l'anomenat filtre

[1] Minor, D. L. An Overview of Ion Channel Structure, Functioning of Transmembrane Receptors in Cell Signalling; Elsevier Inc.: San Diego, CA, **2011**.
[2] Hebert, S. C. General principles of the structure of ion channels. *Am. J. Med*. **1998**, 104 (1), 87–98.
[3] Armstrong, C. M. Packaging Life: The Origin of Ion-Selective Channels. *Biophys. J.*, **2015**, 109 (2), 173–177.
[4] Tang, L., Gamal El-Din, T. M., Payandeh, J., Martinez, G. Q., Heard, T. M., Scheuer, T., Zheng, N. & Catterall, W. A. Structural basis for Ca^{2+} selectivity of a voltage-gated calcium channel. *Nature* **2013**, 505, 56–61.

selectiu que permet que les molècules que puguin interactuar favorablement amb els aa que el formen, vencin la barrera energètica per desprendre's de les aigües d'hidratació, dessolvatant-se[6]. Així doncs aquestes entraran dins el filtre a través del qual es mouran fins a solvatar-se novament a l'altre cantó de la membrana. D'altra banda les molècules que no siguin prou afins a aquests residus, no podran vèncer el penal energètic requerit i no es podran dessolvatar per entrar dins el filtre. En el costat oposat hi ha les molècules altament afins que, si bé podran dessolvatar-se i entrar dins el porus, un cop al filtre quedaran retingudes, bloquejant el canal[7]. A banda de la capacitat d'establir interaccions afins, l'amplada del porus permet una selecció de les molècules en funció de la seva mida.

El *mecanisme de comporta*[8,9,10] dels canals és el responsable d'activar o desactivar la permeació de les molècules afins a través del porus en funció de la resposta a un estímul determinat. Aquests poden ser elèctrics (canals dependents de voltatge) o bé químics (canals dependents de lligand). Quan no hi ha un senyal extern, típicament el porus es troba en estat basal, és a dir, tancat. Un cop davant de l'estímul correcte, aquest provocarà un canvi conformacional, fent que el canal s'obri per un període de temps en el rang dels mil·lisegons, per després tornar a la seva forma tancada; primer en període refractari irresponsiu i finalment en estat basal[11].

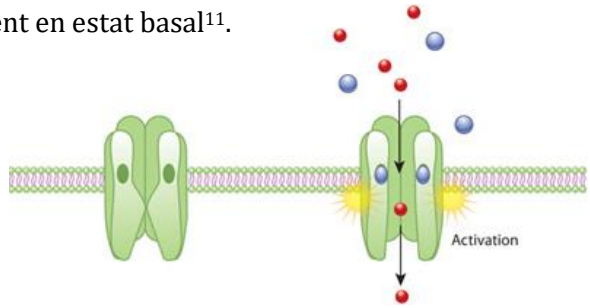

Figura 2. Representació esquemàtica de la localització en la membrana i la funció selectiva d'un canal iònic.

[5] MacKinnon, R. Potassium channels and the atomic basis of selective ion conduction (Nobel Lecture). *Angew. Chem. Int. Ed. Engl.* **2004**, 43 (33), 4265-77.
[6] Piasta, K. N.,Theobald, D. L. & Christopher, C. Potassium-selective block of barium permeation through single KcsA channels. *J. Gen. Physiol*. **2011**, 138, 421.
[7] Morais-Cabral, J. H., Zhou, Y. & MacKinnon, R. Energetic optimization of ion conduction rate by the K+ selectivity filter. *Nature* **2001**, 414, 37.
[8] Uysal, S., Cuello, L.G., Cortes, D. M., Koide, S., Kossiakoff, A. A. & Perozo, E. Mechanism of activation gating in the full-length KcsA K+ channel. *Proc. Natl. Acad. Sci. U S A*. **2011**, 108 (29), 11896-9.
[9] Rothberg, B. S., Shin, K. S. & Yellen, G. Movements near the Gate of a Hyperpolarization-activated Cation Channel. *J. Gen. Phys.* **2003**, 122 (5), 501–510.
[10] Webster, S.M., Del Camino, D., Dekker, J.P. & Yellen, G. Intracellular gate opening in Shaker K+ channels defined by high-affinity metal bridges. *Nature* **2004**, 428 (6985), 864-8.
[11] Zhou, Y., Morais-Cabral, J. H., Kaufman, A. & MacKinnon, R. Chemistry of ion coordination and hydration revealed by a K+ channel- Fab complex at 2.0 Å resolution. *Nature* **2001**, 414 (6859), 43−48.

La regulació dels canals iònics té conseqüències directes sobre la fisiologia de la membrana i indirectes en múltiples processos de regulació de l'organisme al que pertany[12,13]. Aquestes són:

- generació de potencials de membrana
- transmissió de senyals elèctrics
- manteniment del balanç electrolític de la membrana i del volum cel·lular
- generació de senyals reguladors a la cèl·lula

En resum, els canals iònics permeten el flux d'ions, generant senyals elèctrics i químics que desencadenaran processos de senyalització a través de diferents cascades bioquímiques, tenint efectes a nivells d'organisme.

1.1.2. Classificació

Els canals iònics dels éssers vius es solen classificar bé en funció de la seva selectivitat, trobant canals de sodi, de potassi, de calci i de clorurs, o bé en funció del seu mecanisme d'activació o comporta - en el que ens basarem d'ara en endavant - trobant dos grans grups: els canals dependents de voltatge i els canals dependents de lligand[14]. (Figura 3)

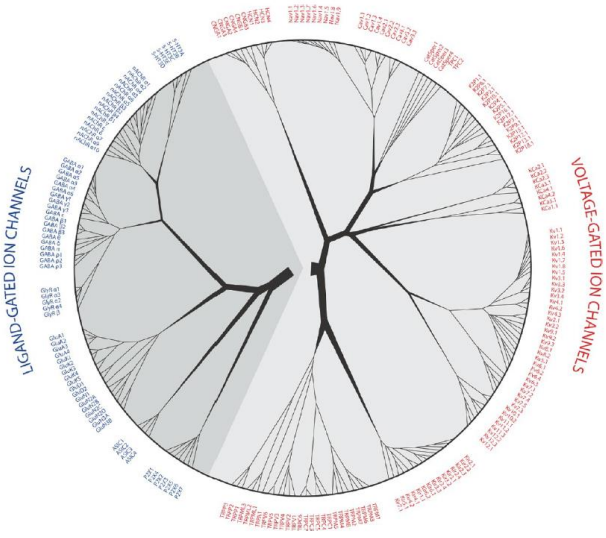

Figura 3. Arbre filogenètic dels canals iònics segons el seu mecanisme d'activació.

[12] Gouaux, E. & Mackinnon, R. Principles of selective ion transport in channels and pumps. *Science* **2005**, 310 (5753), 1461-5.
[13] Barnett, M. W. & Larkman, P. M. The action potential. *Pract. Neurol*. **2007**, 7 (3), 192-7.
[14] Bagal, S. K., Brown, A. D., Cox, P. J., Omoto, K., Owen, R. M., Pryde, D. C., Sidders, B., Skerratt, S. E., Stevens, E. B., Storer, I. R. & Swain, N. A. Ion Channels as Therapeutic Targets: A Drug Discovery Perspective. *J. Med. Chem.* **2013**, 56, 593-624.

Els **canals dependents de voltatge** (DDV) s'obren i es tanquen en resposta a potencials de membrana. Es tracta d'un grup de proteïnes complexes que comparteixen la mateixa unitat bàsica, consistent en una única unitat proteica amb dos dominis transmembrana (2-TM) separats per un colze que defineix un porus. Mentre que aquesta unitat constitueix la majoria dels canals iònics voltatge dependents en procariotes, en el cas dels canals eucariòtics aquest motiu 2-TM bàsic consta normalment de quatre segments transmembrana addicionals (6-TM)[15]. (Figura 4)

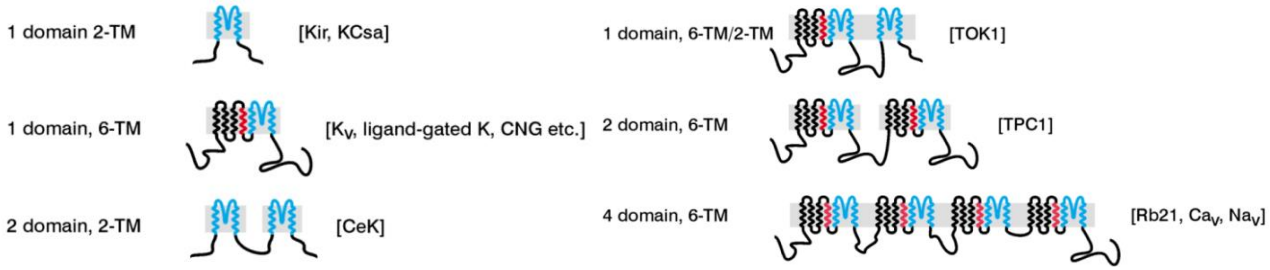

Figura 4. Varietat de motius estructurals en els canals dependents de voltatge.

Dins de la *topologia 4TM* trobem els canals de potassi rectificador-intern (Kir) i de porus bessó (K2P). Tot i que ambdós presenten una estructura primària de dos dominis transmembrana (2TM), aquesta és insuficient per formar un canal iònic complert i funcional, pel que s'ensamblen, adquirint una estructura tetramèrica (4TM)[16].

Canals de potassi rectificador-intern, **Kir**

Aquesta amplia família de canals es troba distribuïda per múltiples tipus de teixit, estant implicada en una gran varietat de funcions fisiològiques, com ara la regulació homeostàtica del potassi (Kir1.1)[17]. Actualment no hi ha cap molècula de baix pes molecular moduladora d'aquests canals que presenti la suficient selectivitat[18] o bé potència[19] per ser candidata a fàrmac. (Figura 5)

[15] Anderson, P. A. V & Greenberg, R. M. Phylogeny of ion channels: Clues to structure and function. *Comp. Biochem. Physiol. B Biochem. Mol. Biol*. **2001**, 129 (1), 17–28.
[16] Hibino, H., Inanobe, A., Furutani, K., Murakami, S., Findlay, I. & Kurachi, Y. Inwardly Rectifying Potassium Channels: Their Structure, Function, and Physiological Roles. *Physiol. Rev*. **2010**, 90 (1), 291-366.
[17] Welling, P. A. & Ho, K. A comprehensive guide to the ROMK potassium channel: form and function in health and disease. *Am. J. Physiol*. **2009**, 297, F849–F863.
[18] Tang, H., Walsh, S. P., Yan, Y., de Jesus, R. K., Shahripour, A., Teumelsan, N., Zhu, Y., Ha, S., Owens, K. A., Thomas-Fowlkes, B. S., Felix, J. P., Liu, J., Kohler, M., Priest, B. T., Bailey, T., Brochu, R., Alonso-Galicia, M., Kaczorowski, G. J., Roy, S., Yang, L., Mills, S. G., Garcia, M. L. & Pasternak, A. Discovery of selective small molecule ROMK inhibitors as potential new mechanism diuretics. *ACS Med. Chem. Lett*. **2012**, 3 (5), 367–372.
[19] Raphemot, R., Lonergan, D. F., Nguyen, T. T., Utley, T., Lewis, L. M., Kadakia, R., Weaver, C. D., Gogliotti, R., Hopkins, C., Lindsley, C. W. & Denton, J. S. Discovery, characterization, and structure–activity relationships of an

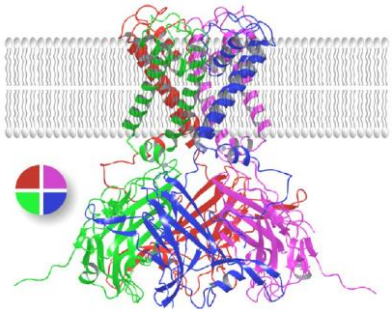

Figura 5. Estructura d'un canal Kir de potassi (KirBac3.1, codi PDB 2WLK), amb la topologia representativa 4TM (dibuixat al costat).

Canal de porus bessó, **K2P**[20]

Els canals K2P es troben a les neurones, cèl·lules musculars i cèl·lules endocrines, on regulen la secreció de neurotransmissors i hormones. Els compostos capaços d'activar a aquest grup de proteïnes, com ara els ésters de l'àcid cafeic, **CDC** i **CAPE**, tenen potencial per tractar malalties cardíaques i neurològiques[21]. D'altra banda els bloquejadors com ara **1** poden ser usats com a reguladors del son[22,23].

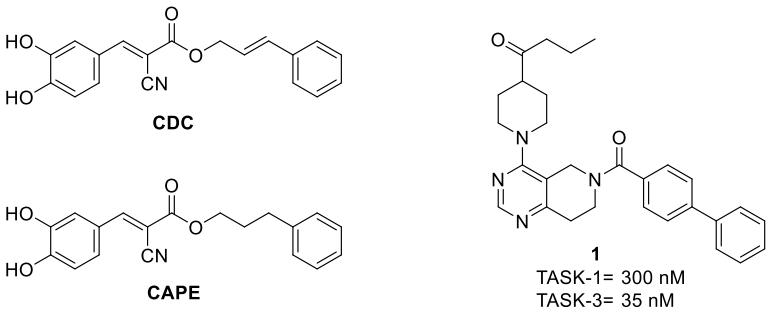

Figura 6. Estructures dels agonistes de TREK-1 ($K2P_{2.1}$) derivats de l'àcid cafeic i de l'antagonista de TASK-1/3 ($K2P_{3.1}$/ $K2P_{9.1}$) desenvolupat per Merck.

inhibitor of inward rectifier potassium (Kir) channels with preference for Kir2.3, Kir3.X, and Kir7.1. *Front. Pharmacol*. **2011**, 2, 75/1–75/18.

[20] Mathie, A., Al-Moubarak, E. & Veale, E. L. Gating of two pore domain potassium channels. *J. Physiol.* **2010**, 588 (17), 3149–3156.

[21] Danthi, S., Enyeart, J. A. & Enyeart, J. J. Caffeic acid esters activate TREK-1 potassium channels and inhibit depolarization-dependent secretion. *Mol. Pharmacol*. **2004**, 65 (3), 599–610.

[22] Wilke, B. U., Lindner, M., Greifenberg, L., Albus, A., Kronimus, Y., Bünemann, M., Leitner, M. G. & Oliver, D. Diacylglycerol mediates regulation of TASK potassium channels by Gq-coupled receptors. *Nature Commun.* **2014**, 5, 5540.

[23] Coburn, C. A., Luo, Y., Cui, M., Wang, J., Soll, R., Dong, J., Hu, B., Lyon, M. A., Santarelli, V. P., Kraus, R. L., Gregan, Y., Wang, Y., Fox, S. V., Binns, J., Doran, S. M., Reiss, D. R., Tannenbaum, P. L., Gotter, A.L., Meinke, P. T. & Renger, J. J. Discovery of a Pharmacologically Active Antagonist of the Two-Pore-Domain Potassium Channel K2P9.1 (TASK-3). *ChemMedChem* **2012**, 7 (1), 123–133.

Els canals dependents de voltatge amb una *topologia 6TM* són els més estudiats d'entre els canals iònics. Es pensa que el seu mecanisme de comporta funciona gràcies al moviment d'un residu hidrofòbic del porus que col·lapsa per tancar-lo, seguit del moviment del sensor de voltatge cap al canal. Davant de l'estímul adequat aquest sensor s'allunya, estirant el residu hidrofòbic del porus cap a ell i provocant l'obertura del canal.

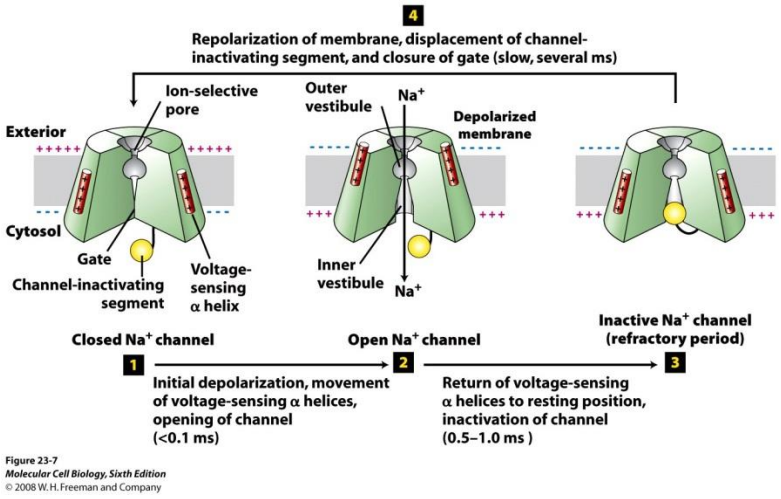

Figura 7. Mecanisme de comporta dels canals iònics DDV, representat per un canal de sodi DDV.

El coneixement de la seva estructura ha experimentat un salt qualitatiu gràcies a l'aparició a la literatura de diverses estructures cristal·lines[24], com ara el canal bacterià NavAb10b[25]; tot i així el lloc d'unió de les molècules de baix pes molecular es troba poc definit. La hipòtesi actual contempla tres possibles llocs d'unió: el porus, una escletxa en el sensor de voltatge i el lloc de fenestració. Els components d'aquest grup han estat objecte d'estudi en múltiples programes de química mèdica[26] i són:

Canals de sodi dependents de voltatge, **Nav**

Es tracta d'una família composta per nou membres, Nav 1.1 – Nav1.9, responsable de la creació i propagació de potencials d'acció. La seva distribució en neurones, cor i teixit muscular, fa que siguin dianes desitjables per controlar l'excitabilitat cel·lular[27]. Dins d'aquesta categoria trobem múltiples fàrmacs comercials com ara la lamotrigina

[24] Long, S. B., Tao, X., Campbell, E. B. & MacKinnon, R. Atomic structure of a voltage-dependent K+ channel in a lipid membrane-like environment. *Nature* **2007**, 450 (7168), 376–382.
[25] Payandeh, J., Scheuer, T., Zheng, N. & Catterall, W. A. The crystal structure of a voltage-gated sodium channel. *Nature* **2011**, 475 (7356), 353–358.
[26] Triggle, D. J. Calcium channel antagonists: clinical uses - past, present and future. *Biochem. Pharmacol*. **2007**, 74 (1), 1–9.

(anticonvulsiu), la carbamazepina (antiepilèptic) i els anestèsics locals lidocaïna, benzocaïna i bupivacaïna. Tenint en compte que el potencial terapèutic d'aquests canals va des del tractament del dolor a actuar com a possibles dianes antineoplàsiques, actualment es treballa pel desenvolupament de compostos selectius per un sol subtipus de canal de sodi, evitant així el gran nombre d'efectes secundaris que es presenten en aquest grup.

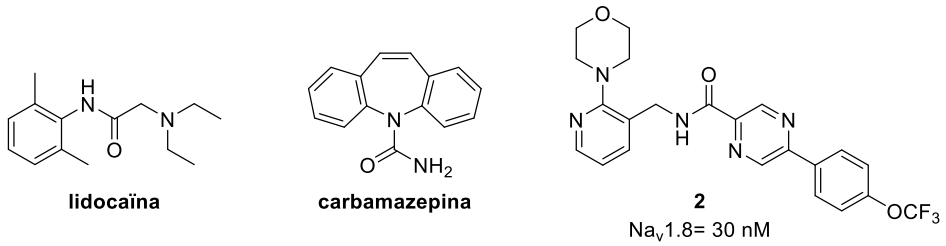

Figura 8. Moduladors dels canals Na_V no selectius (lidocaïna i carbamazepina) i primers compostos amb relativa selectivitat pel canal $Na_V1.8$ desenvolupat per Abbot i Icagen.

Canals de potassi dependents de voltatge, **Kv**

La família dels canals de potassi és la més extensa, comptant amb més de 40 membres diferents. La seva funció és principalment repolaritzar la membrana cel·lular després que es generi un potencial d'acció. Tot i que com a moduladors d'aquests canals trobem fàrmacs àmpliament coneguts com ara la fluoxetina o norfluoxetina, que tenen acció sobre els canals Kv1.1[28] i Kv4.3[29], el membre més destacable és sens dubte el canal hERG (Human ether-a-go-go-related gene) o Kv11.1. Aquest és un canal de potassi promiscu que juga un paper fonamental en el potencial d'acció de repolarització cardíac. Els inhibidors d'hERG poden induir el síndrome de QT elongat, incrementant enormement el risc d'arrítmies ventriculars i mort sobtada[30]. Com a conseqüència de la retirada del mercat de múltiples medicaments com ara l'astemizol o la cisaprida, ja que podien actuar com a lligands d'aquest canal, actualment es mira la selectivitat front a hERG a tots els candidats a fase clínica[31].

[28] Tytgat, J., Maertens, C., & Daenens, P. Effect of fluoxetine on a neuronal, voltage-dependent potassium channel (Kv1.1). *Br. J. Pharmacol*. **1997**, 122 (7), 1417–24.
[29] Jeong, I., Choi, J. S., & Hahn, S. J. Effects of fluoxetine on cloned Kv4.3 potassium channels. *Brain Res.* **2013**, 1500, 10–18.
[30] Vandenberg, J.I., Perry, M.D., Perrin, M.J., Mann, S.A., Ke, Y. & Hill, A.P. hERG K(+) channels: structure, function, and clinical significance. *Physiol. Rev*. **2012**, 92 (3), 1393-478.
[31] Redfern, W.S., Carlsson, L., Davis, A.S., Lynch, W.G., MacKenzie, I., Palethorpe, S., Siegl, P.K., Strang, I., Sullivan, A.T., Wallis, R., Camm, A.J. & Hammond, T.G. Relationships between preclinical cardiac electrophysiology, clinical QT interval prolongation and torsade de pointes for a broad range of drugs: evidence for a provisional safety margin in drug development. *Cardiovasc. Res*. **2003**, 58, 32-45.

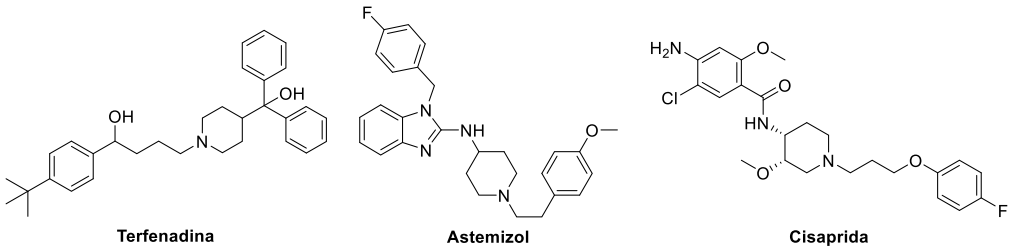

Figura 9. Moduladors d'hERG, fàrmacs retirats del mercat.

Canals de calci dependents de voltatge, **Cav**

Aquests canals són el nexe molecular entre els potencials de membrana i les vies de senyalització intracel·lulars dependents de calci, és a dir, funcionen entre l'excitació muscular i la contracció o entre l'excitació neuronal i l'alliberació de neurotransmissor. Conseqüentment, són la diana terapèutica per múltiples desordres neurològics (gabapentina i pregabalina) i cardiovasculars (dilitiazem, amlodipí i nifedipí)[26].

Canals de potassi activats per calci

Es tracta d'un grup molt divers que consta de 8 membres i que presenten una activació doble: per voltatge i per un ió intracel·lular, en la gran majoria dels casos calci. Tot i que en el mercat trobem fàrmacs que actuen sobre aquests canals, el coneixement del seu mecanisme d'acció i la selectivitat d'aquests compostos és més aviat pobre. En aquesta línia Pfizer ha desenvolupat el senicapoc[32] per a l'asma i l'anèmia falciforme[33,34]. Recentment s'ha vist que aquests canals es troben expressats al SNC i podrien tenir un efecte beneficiós en processos d'aprenentatge i memòria, per això es treballa en la millora de la selectivitat dins aquest subgrup.

[32] Liegeois, J. F., Mercier, F., Graulich, A., Graulich-Lorge, F., Scuvee-Moreau, J. & Seutin, V. Modulation of small conductance calcium- activated potassium (SK) channels: a new challenge in medicinal chemistry. *Curr. Med. Chem*. **2003**, 10 (8), 625–647.

[33] Ataga, K. I., Smith, W. R., De Castro, L. M., Swerdlow, P., Saunthararajah, Y., Castro, O., Vichinsky, E., Kutlar, A., Orringer, E. P., Rigdon, G. C. & Stocker, J. W. Efficacy and safety of the Gardos channel blocker, senicapoc (ICA-17043), in patients with sickle cell anemia. *Blood* **2008**, 111 (8), 3991–3997.

[34] Ataga, K.I. & Stocker, J. Senicapoc (ICA-17043): a potential therapy for the prevention and treatment of hemolysis-associated complications in sickle cell anemia. *Expert Opin. Investig. Drugs*. **2009**,18 (2), 231-9.

Canals de receptor de potencial transitori, **TRP**[35,36]

Els TRP són canals catiònics amb diversos mètodes d'activació, mentre que alguns semblen estar constitutivament oberts, altres són dependents de voltatge, de calci intracel·lular, de pH, d'estat RedOx, d'osmolaritat o d'estirament mecànic. Comprenen una gran varietat de funcions que van des de la percepció del dolor i temperatura, fins a l'absorció de magnesi i calci. Es troben classificats en 6 subfamílies en funció de la seva homologia: clàssica (TRPC), receptor vainilloid (TRPV), melastatina (TRPM), policistines (TRPP), mucolipines (TRPML) i la proteïna transmembrana ankyrin 1 (TRPA).

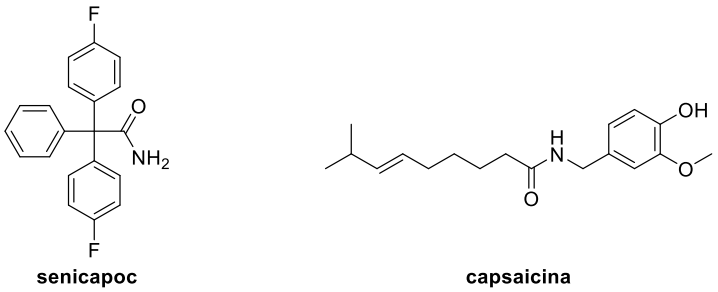

senicapoc **capsaicina**

Figura 10. Estructures dels moduladors dels canals de Ca^{2+} activats per K^+ (senicapoc) i dels TRP (capsaicina).

Els **canals dependents de lligand (DDL)** o canals ionotròpics[37] s'obren i es tanquen en resposta a la unió d'una molècula específica o lligand en el seu domini extracel·lular. La unió d'aquest lligand provoca un canvi conformacional en l'estructura del canal, obrint-lo i permetent el flux d'ions a través d'aquest. Trobem tres classes principals de canals ionotròpics en funció de la seva topologia: els canals pentamèrics de la família del colze de cisteïna; els canals tetramèrics selectius de glutamat i de nucleòtids diversos i finalment els canals trimèrics sensors d'àcid (ASIC) i receptors purinèrgics (P2X).

[35] Nilius, B. TRP channels in disease. *Biochim. Biophys. Acta*. **2007**, 1772 (8), 805–812.
[36] Viana, F. & Ferrer-Montiel, A. TRPA1 modulators in preclinical development. *Expert Opin. Ther. Pat.* **2009**, 19 (12), 1787–1799.
[37] Alexander, S. P. H., Davenport, A. P., Kelly et al. The concise guide to pharmacology 2015 / 16: ligand-gated ion channels. *Br. J. Pharm.* **2015**, 5744–5869.

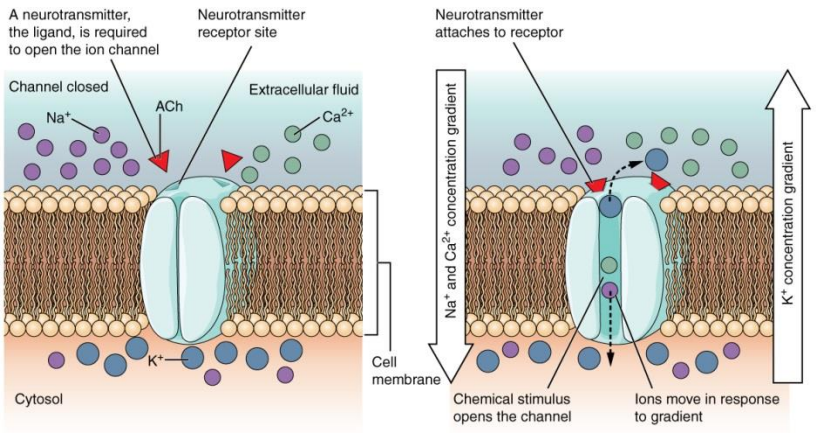

Figura 11. Mecanisme de comporta dels canals iònics DDL, representat per un canal d'Ach.

Canals de colze de cisteïna

Els constituents d'aquesta família s'encarreguen de controlar la transmissió sinàptica ràpida. En els vertebrats trobem els receptors de GABA-A, els receptors nicotínics d'acetilcolina, els receptors 5-HT3 i els receptors de glicina.

Els **receptors de GABA-A**[38] tenen com a lligand endogen el neurotransmissor àcid γ-aminobutíric (GABA), tot i que s'ha vist que altres molècules com ara el muscimol poden unir-se al lloc d'unió d'aquest NT. Les molècules de baix pes molecular lligands d'aquest canal tenen efectes ansiolítics i sedants, podent-ne fer prevaldre l'un sobre l'altre a través d'un lligand selectiu sobre una de les 5 subunitats que formen el receptor. Els fàrmacs més coneguts i antics per a aquest tipus de dianes són les benzodiazepines, com ara el diazepam o el flumazenil. En l'actualitat la recerca en aquest canal està dirigida a millorar-ne la selectivitat per tal de desenvolupar medicaments ansiolítics no sedants[39], com per exemple **3** (Figura 12).

El neurotransmissor acetilcolina és el lligand endogen pels **canals AChR**[40], que es troben àmpliament distribuïts al cervell. Els seus agonistes – com la nicotina - o agonistes parcials tenen un enorme potencial terapèutic per al tractament de processos de deteriorament cognitiu (**4**) i per deixar de fumar (vareniclina).

[38] Sieghart, W. Structure, pharmacology, and function of GABAA receptor subtypes. *Adv. Pharmacol*. **2006**, 54, 231−263

[39] Atack, J. R. GABAA receptor subtype-selective modulators. I.α2, α3-Selective agonists as non-sedating anxiolytics. *Curr. Top. Med. Chem*. **2011**, 11 (9), 1176−1202.

[40] Arias, H. R. Localization of agonist and competitive antagonist binding sites on nicotinic acetylcholine receptors. *Neurochem. Int*. **2000**, 36 (7), 595−645.

El canal **5-HT3** té la serotonina com a lligand endogen. Aquest receptor està associat a la transmissió excitatòria sinàptica i es troba expressat a nivell de SNC, SNP i intestí. Cal mencionar que el desenvolupament de fàrmacs antagonistes basats en la serotonina ha estat especialment fructífer, trobant al mercat la família dels –setron, indicats com antiemètics en processos de quimioteràpia[41].

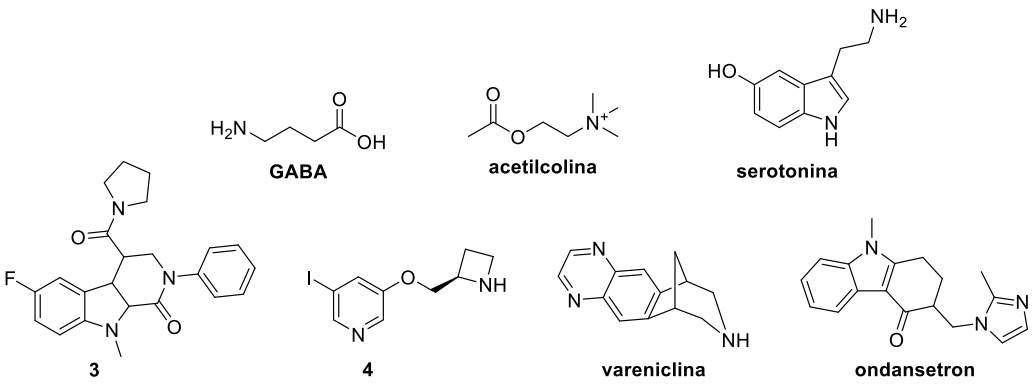

Figura 12. Lligands dels canals de colze de Cys; endògens (a dalt) i sintètics (a baix).

Receptors ionotròpics de glutamat, **iGluR**[42]

Els iGluR funcionen com a complex de quatre subunitats individuals i són una de les classes més ben enteses de canals iònics. Aquests intervenen en la neurotransmissió excitatòria, jugant un paper fonamental en el desenvolupament i funció del SNC en mamífers. La seva desregulació està relacionada amb un ampli ventall de trastorns neurològics com ara l'epilèpsia o la malaltia d'Alzheimer. Dins d'aquest grup, trobem tres categories en funció de la seva afinitat pels agonistes sintètics[43]: àcid α-amino-3-hidroxil-5-metil-4-isoxazolepropiònic (els canals **AMPA**), àcid kaïnic (canals **KA**) i *N*-metil-D-aspartat (canals de **NMDA**). Aquests últims presenten trets únics: requereixen l'acció d'un co-agonista, bé glicina o bé D-serina, per tal de ser activats i, a més, són bloquejats per Mg^{2+} extracel·lular que surt del canal davant una despolarització de la membrana que el conté.

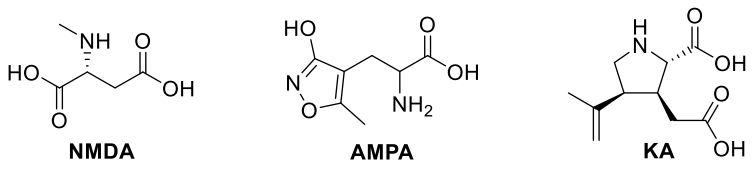

Figura 13. Agonistes sintètics que defineixen els subtipus d'iGluR.

[41] Chong, Y. & Choo, H. 5-HT(3) antagonists under development. *Expert Opin. Invest. Drugs*. **2010**, 19 (11), 1309–1319.
[42] Madden, D. R. The Structure and Function of Glutamate Receptor Ion Channels. *Nat. Rev. Neuroscience* **2002**, 3(2), 91–101.
[43] Hollmann, M. & Heinemann, S. Cloned glutamate receptors. *Annu. Rev. Neurosci*. **1994**, 17, 31–108.

Canals sensors d'àcid i receptors de purines, **ASIC** i **P2X**

Els receptors d'aquest grup formen trímers en els que cada subunitat presenta una topologia 2TM, un colze extracel·lular gran i dominis amino i carboxi intracel·lulars curts. Ambdós subgrups són relativament desconeguts estructural i mecanísticament, tot i que les seves implicacions en el SNC i en la nocicepció ha despertat un gran interès entre la comunitat científica, resultant-ne un gran nombre de projectes amb l'objectiu del seu estudi.

Els subtipus **ASIC**[44] són activats per canvis de pH i el seu interès rau en la possibilitat d'usar-los com a dianes pel dolor crònic relacionat amb la inflamació. Com a antagonista no selectiu dèbil, trobem el fàrmac comercial amiloride.

El subtipus **P2X** es tracta d'una enorme família que consta de 7 subtipus de receptors purinèrgics dependents d'ATP extracel·lular[45]. Tot i que avui en dia no hi ha cap fàrmac comercial per a aquesta família, la recerca d'antagonistes dels receptors $P2X_{2/3}$ i $P2X_{7,}$ per al tractament del dolor, i dels $P2X_4$ per a malalties cutànies, està començant a albirar horitzons prometedors[46].

Per últim trobem un grup de canals iònics que no es comporta com cap dels casos mencionats anteriorment. Aquests, coneguts amb el nom de *viroporines*[47], es troben en els virus i consisteixen en proteïnes petites del voltant dels 100 aa que formen un porus selectiu a través de la membrana viral[48]. Dins d'aquesta família trobem, entre d'altres, el canal M2 del virus de la grip, que va ser la primera viroporina descoberta, la proteïna p7 del virus de l'hepatitis i la proteïna HIV-1-Vpu del virus de la immunodeficiència humana. Tot i que les característiques estructurals i de funcionament difereixen notablement entre els membres d'aquest grup, comparteixen una característica comú: són essencials pel cicle vital del virus, és a dir, són factors de virulència. L'interès pel seu estudi és doncs, per una banda, el seu potencial com a dianes terapèutiques per les malalties associades a la infecció del patogen corresponent[49] i per l'altra, la possibilitat de ser usades com a model

[44] Wemmie, J. A., Price, M. P. & Welsh, M. J. Acid-sensing ion channels: advances, questions and therapeutic opportunities. *Trends Neurosci*. **2006**, 29 (10), 578−586.
[45] Burnstock , G. Purinergic nerves. *Pharmacol Rev*. **1972**, 24, 509–581.
[46] North, R. A. & Jarvis, M. F. P2X receptors as drug targets. *Mol. Pharmacol.* **2013**, 83 (4), 759–69.
[47] Scott, C. & Griffin, S. Viroporins: Structure, function and potential as antiviral targets. *J. Gen. Virol.* **2015**, 96 (8), 2000–2027.
[48] Wang, K., Xie, S. & Sun, B. Viral proteins function as ion channels. Biochim. Biophys. Acta. **2011**, 1808 (2), 510–515.
[49] To, J., Surya, W. & Torres, J. Targeting the Channel Activity of Viroporins. *Advances in Protein Chemistry and Structural Biology* (1st ed., Vol. 104). Elsevier Inc, **2015**.

per a l'estudi de canals iònics més complexes, com ara els eucariòtics[50]. Cal recalcar que, sorprenentment, només hi ha una viroporina que sigui la diana de medicaments, aquesta és el canal M2 amb l'amantadina i la rimantadina com a fàrmacs comercials.

1.1.3 Canals iònics i processos patogènics en l'ésser humà

En l'ésser humà els canals iònics són la quarta família més abundant de proteïnes, per la que codifiquen un 1% dels gens humans[51,52]. A més a més aquests canals es troben en les membranes de cèl·lules de tot tipus, desenvolupant funcions clau per a una gran varietat de processos fisiològics.

La seva gran distribució i varietat de funcions fa que es trobin implicats en nombrosos processos patològics. Segons la seva implicació es poden distingir tres tipus de patogènia: malalties infectives, canalopatíes i co-efectors de malalties multifactorials; en la taula següent es mostra un petit resum.

Tipus de patogènia	Implicació del canal	Exemple
Malalties infectives	Les viroporines implicades són claus per a la correcta infecció viral	canal M2 – malaltia de la influenza (grip)
Canalopatíes	La mutació heretada o adquirida d'un determinat canal, és la causa principal que es desenvolupi un determinat procés patològic.	canal P2X7 – Percepció alterada del dolor[53]
Co-efectors de malalties multifactorials	La desregulació del canal contribueix a l'agreujament dels símptomes d'una determinada malaltia o bé contribueix al desenvolupament o progrés del procés patogènic	canal NMDA – Malaltia d'Alzheimer

Taula 1. Tipus de patogènia associada a canals iònics.

[50] Pinto, L. H. & Lamb, R. A. Viral ion channels as models for ion transport and targets for antiviral drug action. *FEBS Letters.* **2004**, 560, 1-2.
[51] Harte, R. & Ouzounis, C. A. Genome-wide detection and family clustering of ion channels. *FEBS Letters*. **2002**, 514 (2–3), 129–134.
[52] Venter, J. C., Adams, M. D., Myers et al. The Sequence of the Human Genome. Science **2001**, 291 (5507), 1304–1351.
[53] Cregg, R., Momin, A., Rugiero, F., Wood, J. N. & Zhao, J. Pain Channelopathies. *J. Physiol*. **2010**, 588, 1897–904.

En l'actualitat la implicació d'aquesta família de proteïnes en processos patogènics és enorme, constant de més de 300 malalties diferents. Tot i així la xifra no deixa d'incrementar a causa del progrés de la comprensió del mecanisme i funció d'aquests canals iònics.

1.1.4 Gamma de fàrmacs actuals i direccions futures

Tot i el gran potencial dels canals iònics com a diana terapèutica, ja per la seva implicació en múltiples processos patològics, com per la gran presència d'aquestes proteïnes en l'ésser humà, en l'actualitat només són la diana d'un 7% dels fàrmacs disponibles[54].

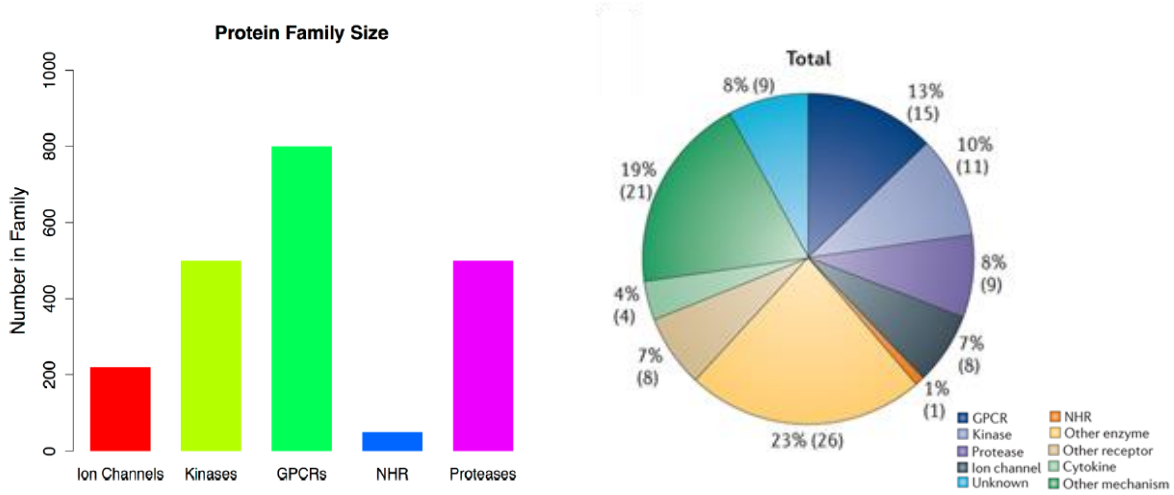

Figura 14. Mida relativa de la família de canals iònics respecte a altres famílies de proteïnes (esquerra). Nombre de fàrmacs comercials classificats segons la naturalesa de la seva diana terapèutica (dreta).

Aquest desajust s'atribueix al desconeixement relatiu dels canals iònics. Actualment, no s'ha pogut determinar el lligand d'un 40% dels canals coneguts, a més a més, tant l'estructura com el mecanisme d'acció i el lloc d'unió de lligand de la gran majoria dels canals, resten com a enigmes per a la comunitat científica. Això fa que el procés de descobriment de fàrmacs entorn aquest tipus de proteïnes sigui especialment costós, provocant en moltes ocasions el fracàs d'aquests compostos un cop en fase clínica. Tot i així alguns casos d'èxit com el de la vareniclina (Champix®), llançada al mercat l'any 2006, ha fet que la investigació se centri en aquells subtipus amb una biologia més coneguda, generant al seu torn, més recursos d'investigació cap a aquelles famílies per descobrir.

[54] Overington, J. P., Al-Lazikani, B. & Hopkins, A. L. How many drug targets are there? *Nat. Rev. Drug Discov.* **2006**, 5 (12), 993–6.

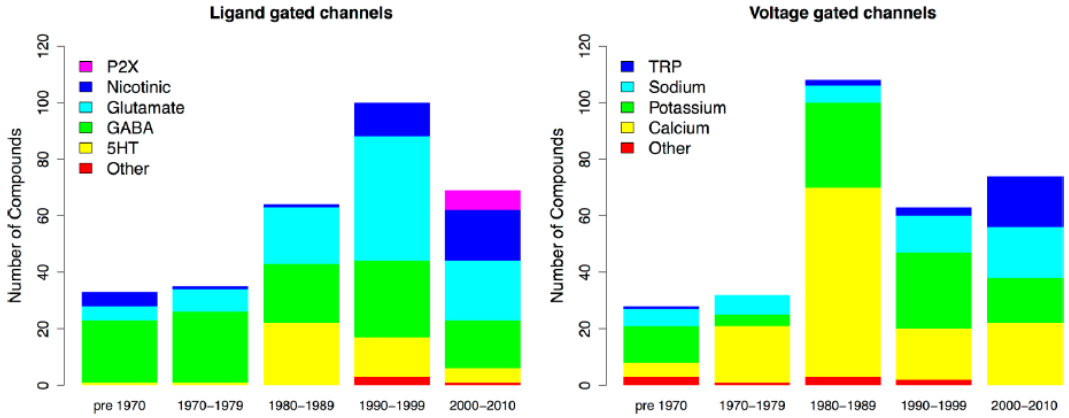

Figura 15. Lligands de canals iònics en desenvolupament, classificats per tipus de canal i dècada.

Es creu que en els pròxims anys els fàrmacs que tenen per diana els canals iònics, experimentaran un auge important, similar al que van patir els receptors acoblats a proteïnes-G (GPCRs) al voltant de l'any 2000[55]. Per a que aquest fet ocorri haurà d'anar lligat a una millora del coneixement de l'estructura i funció d'aquests canals; per a aquesta tasca, el desenvolupament de molècules de baix pes molecular dirigides a canals iònics, jugarà un paper fonamental. Les molècules de baix pes molecular, doncs, poden ser usades com a eines per obtenir noves idees i un coneixement més profund de la biologia.

En línia amb aquesta idea, la present Tesi ha estat enfocada al desenvolupament de molècules de baix pes molecular que tenen com a diana els canals iònics que es comenten a continuació. La finalitat d'aquestes noves molècules és modular l'activitat de les proteïnes objectiu, bé amb fins terapèutics o bé per tal de ser emprades com a eines per al seu estudi. Perseguint aquesta idea, s'han dissenyat, preparat i avaluat farmacològicament: inhibidors de la viroporina M2, antagonistes del receptor de purines $P2X_7$ i antagonistes parcials del canal ionotròpic d'NMDA.

[55] Kaczorowski, G. J., Mcmanus, O. B., Priest, B. T. & Garcia, M. L. Ion Channels as Drug Targets: The Next GPCRs. *J. Gen. Physiol*. **2008**, 399–405.

1.2. EL VIRUS DE LA INFLUENZA A

A mode d'aclariment i per tal d'entendre la proteïna M2 i l'hemaglutinina, explicades a continuació, cal conèixer alguns trets rellevants del virus al que pertanyen.

1.2.1. Característiques

El virus de la influenza A (o virus de la grip) és un virus enbolcallat de la família *Orthomyxoviridae*, caracteritzat per presentar el seu genoma en vuit fragments d'ARN monocatenari de sentit negatiu i que codifica 11 proteïnes virals. De l'exterior a l'interior del virus, aquestes proteïnes són: l'hemaglutinina i la neuraminidasa, que són glicoproteïnes antigèniques que es troben a la membrana lipídica del virus, la proteïna M2, que travessa aquest embolcall formant un canal selectiu de protons i, a l'interior del virus, trobem la nucleoproteina (NP), la proteina de matriu M1, el complex de polimerasa viral format per les subunitats PA, PB1 i PB2, la proteïna no estructural NS1 i la proteïna d'exportació nuclear (NEP)[56].

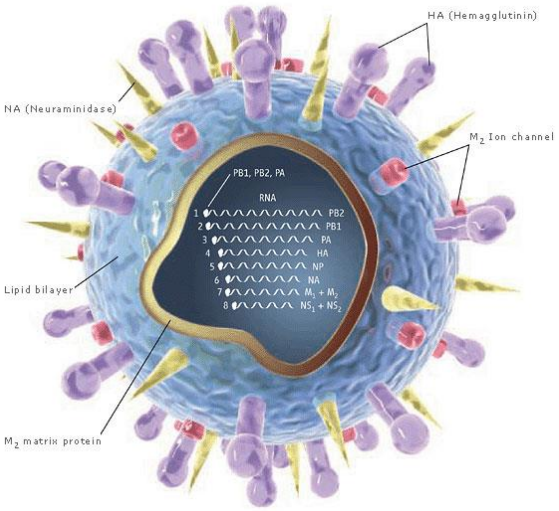

Figura 16. Estructura i disposició de les proteïnes del virus de la Influenza A.

La nomenclatura estàndard per a les soques d'aquest virus[57] inclou: tipus de virus/ espècie d'on va ser aïllat (en cas que no sigui humà)/ lloc d'aïllament/ nombre d'aïllat/ any d'aïllament/ tipus d'hemaglutinina i tipus de neuraminidasa. Per exemple A/Panama/2007/1999(H3N2) ens estaria indicant que és un virus de la influenza A trobat

[56] Ghedin, E., Sengamalay, N. A., Shumway, M., Zaborsky, J., Feldblyum, T., Subbu, V., Spiro, D. J., Sitz, J., Koo, H., Bolotov, P., Dernovoy, D., Tatusova, T., Bao, Y., St George, K., Taylor, J., Lipman, D. J., Fraser, C. M., Taubenberger, J. K. & Salzberg, S. L. Large-scale sequencing of human influenza reveals the dynamic nature of viral genome evolution. *Nature* **2005**, 437 (7062), 1162-6.

[57] WHO. Bull. A revision of the system of nomenclature for influenza viruses: a WHO Memorandum. *World Health Organ*. **1980,** 58, 585.

en humans a Panamà, que és l'ordre d'aïllat 2007 de l'any 1999 i que presenta una HA tipus 3 i una NA tipus 2.

Dos dels trets més destacats d'aquest virus són la seva alta infectivitat, fet que fa que el seu contagi, per via aèria o via mans-boca, sigui extremadament fàcil i la seva habilitat per mutar.[58]

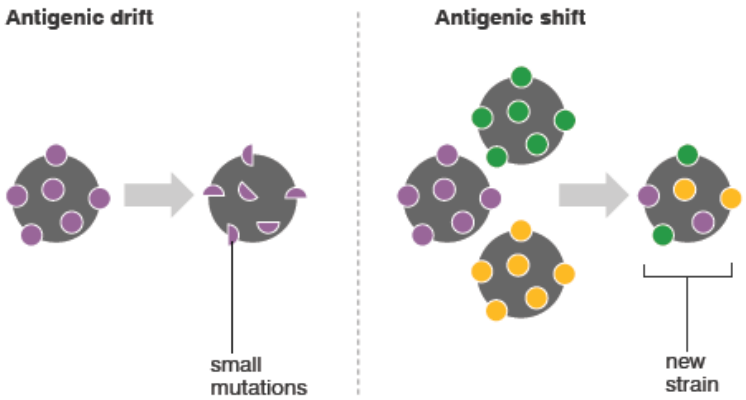

Figura 17. Mecanismes de mutació del virus de la Influenza A: deriva antigènica (esquerra) i rotació antigènica (dreta).

Les mutacions es poden donar a través de dos mecanismes diferents: La deriva antigènica, consistent en mutacions puntuals en l'estructura del virus que permeten que aquest variï lleugerament les seves propietats fent que, per exemple, adquireixi resistència als tractaments per aturar-lo. L'altre camí de mutació és l'anomenada rotació antigènica, consistent en el reordenament genètic entre dos o més soques del virus de la influenza A diferents, donant lloc a una soca nova amb característiques mesclades de les dues anteriors. Per exemple, a través d'aquest mecanisme un virus pròpiament animal, pot adquirir la capacitat d'infectar a humans[59].

[58] Centers for Disease Control and Prevention: http://www.cdc.gov/flu/about/viruses/change.htm (consultat el 21 Oct 2016).
[59] Bouvier, N. M. & Palese, P. The biology of influenza viruses. *Vaccine* **2008**, 26, D49.

1.2.2 El cicle viral

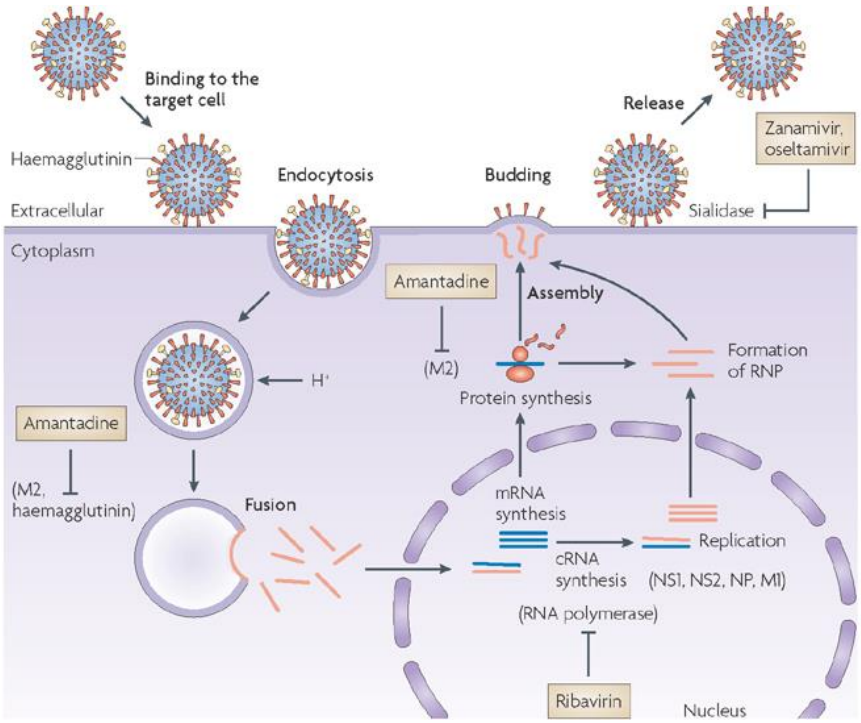

Figura 18. Cicle viral de l'Influenza A.

Entrada del virus

El cicle comença quan el virus entra en l'organisme i reconeix els àcids siàlics de la superfície de les cèl·lules del tracte respiratori de l'hoste, als que s'uneix gràcies a la proteïna de superfície HA[60].

Endocitosis

Seguidament el virus entra a les cèl·lules a través d'una endocitosis facilitada per receptor, normalment per clatrina, tot i que s'han descrit rutes alternatives d'internalització del virus per macropinocitosis[61]. El virus doncs, és internalitzat en un endosoma primerenc que presenta un pH al voltant de 6.

Fusió

L'endosoma primerenc és transportat i es converteix en un endosoma tardà, en el que el pH és disminuït altre cop gràcies a l'ATPasa vacuolar (V-ATPasa). Això fa que l'HA pateixi un canvi conformacional irreversible en el que expulsa el domini *N*-terminal de la

[60] Skehel, J. J. & Wiley, D. C. Receptor binding and membrane fusion in virus entry: the influenza hemagglutinin. *Annu. Rev. Biochem.* **2000**, 69, 531-69.
[61] de Vries, E., Tscherne, D. M., Wienholts, M. J., Cobos-Jiménez, V., Scholte, F., García-Sastre, A., Rottier, P. J. M. & de Haan, C. A. M. Dissection of the influenza a virus endocytic routes reveals macropinocytosis as an alternative entry pathway. *PLoS Pathog*. **2011**, 7, e1001329.

subunitat HA2, anomenat pèptid de fusió[62,63]. Aquest s'insertarà a la membrana de l'endosoma provocant una fusió d'ambdues membranes, la viral i l'endosòmica.

El canvi de pH activa també el canal M2 que comença a deixar passar protons, acidificant així l'interior del virus. Això provoca la dissociació de la proteïna M1 del complex de la ribonucleoproteïna viral (vRNP), fent que aquestes vRNP siguin alliberades al citoplasma des d'on seran importades al nucli per mitjà de factors d'importació nuclear. Per altra banda, la proteïna M1 complexarà en endosomes tardans des d'on serà importada, igualment, al nucli[64].

Replicació i transcripció viral

Un cop al nucli la polimerasa viral catalitza: la síntesi d'una còpia de sentit positiu del RNA viral, l'anomenat ARN complementari, que serà copiada fins a produir grans quantitats de ARN viral (vARN) i la síntesi d'un ARN missatger, també de sentit positiu.

Els nous vARN seran encapsulats per la nucleoproteïna i gràcies a la NEP formaran el complex d'exportació nuclear, que permetrà creuar una de les nucleoporines, passant al citoplasma.

Per altra banda els mARN s'uniran a la nucleoproteïna per ser exportats a través de la via del factor d'exportació nuclear 1 (NXF1), que és la que usa la cèl·lula hoste per exportar el seu propi ARN.

Traducció

Els mARN segresten els mecanismes cel·lulars de traducció de la cèl·lula hoste, evitant mecanismes de resposta d'aquest hoste gràcies a l'acció de la proteïna NS1[65]. Un cop alliberats de la NP són traduïts en els ribosomes a proteïnes virals. La NP, NS1, NEP i la proteïna M1 passen altre cop al nucli per donar lloc a més ARN viral.

En canvi, la NA, l'HA i la proteïna M2 són transportades al reticle endoplasmàtic i a l'aparell de Golgi, per passar a proteïnes madures gràcies a modificacions post-translacionals. Cal mencionar que durant el pas per l'aparell de Golgi, que consta d'un pH àcid, la proteïna M2 s'encarrega de incrementar el pH dins les vesícules de transport per evitar el canvi de conformació de l'HA[66].

[62] Lin, X., Noel, J. K., Wang, Q., Ma, J. & Onuchic, J. N. Lowered pH Leads to Fusion Peptide Release and a Highly Dynamic Intermediate of Influenza Hemagglutinin. *J. Phys. Chem. B.* **2016**, 5, 6775.

[63] Carr, C. M. & Kim, P. S. A spring-loaded mechanism for the conformational change of influenza hemagglutinin. *Cell* **1993**, 73(4), 823–832.

[64] Samji, T. Influenza A: Understanding the viral life cycle. *Yale J. Biol. Med.* **2009**, 82(4), 153–159.

[65] De Clercq, E. Antiviral agents active against influenza A viruses. *Nat. Rev. Drug Discov*. **2006**, 5, 1015.

[66] Takeuchi, K. & Lamb, R. A. Influenza virus M2 protein ion channel activity stabilizes the native form of fowl plague virus hemagglutinin during intracellular transport. *J. Virol*. **1994**, 68, 911.

Empaquetament, formació del virió i alliberació de virus madurs

Un cop acabat el procés de maduració les proteïnes de superfície HA, NA i la proteïna transmembrana M2, s'agreguen en rais lipídics de la membrana plasmàtica. Seguidament, els ARN virals s'uneixen a l'HA gràcies a l'acció de la proteïna M1. L'alta concentració de HA i NA alteren la curvatura de la membrana, permetent la polimerització de la proteïna M1 per tal de continuar amb la formació del nou virió. Simultàniament la proteïna M2 passa al coll d'aquest virió alterant un cop més la membrana plasmàtica, fins que aquesta es separa del virió[67] que queda unit a la cèl·lula hoste només per enllaços de l'HA amb els àcids siàlics receptors. Finalment, gràcies a l'escissió d'aquest enllaç per la NA, els nous virus influenza, són alliberats[68].

Com es pot inferir del cicle viral, totes les proteïnes de la influenza A, juguen un paper fonamental. Per tant el mal funcionament o la inhibició de qualsevol d'aquestes, permetria aturar la infecció; així doncs, totes són susceptibles a ser la diana de fàrmacs anti-influenza[69].

[67] Schmidt, N. W., Mishra, A., Wang, J., DeGrado, W.F. & Wong, G.C. Influenza virus A M2 protein generates negative Gaussian membrane curvature necessary for budding and scission. *J. Am. Chem. Soc*. **2013**, 135 (37), 13710-9.

[68] Palese, P., Tobita, K., Ueda, M. & Compans, R. W. Characterization of temperature sensitive influenza virus mutants defective in neuraminidase. *Virology* **1974**, 61 (2), 397-410.

[69] Das, K., Aramini, J.M., Ma, L., Krug, R. M. & Arnold, E. Structures of influenza A proteins and insights into antiviral drug targets. *Nat. Str. Mol. Bio*. **2010**, 17, 530-538.

1.3. El CANAL M2

1.3.1. Estructura

La viroporina M2 del virus de la Influenza A es tracta d'una proteïna transmembrana de 97 aa que s'acobla en forma tetramèrica formant un canal en la membrana viral. Cada filament d'aquest canal està construït en forma de dues hèlix α disposades amb un paral·lelisme orientat cap al costat esquerra respecte a la regió N-terminal. Aquest desviament és degut a una lleugera flexió, amb una inclinació de 30-35 graus, prop del residu glicina 34[70]. Les regions que podem distingir en cada filament són les següents:

Residus	Part	Funció	Estructura
1-24	Regió N-terminal (extracel·lular, desordenada)	Incorporació de la proteïna en el virió	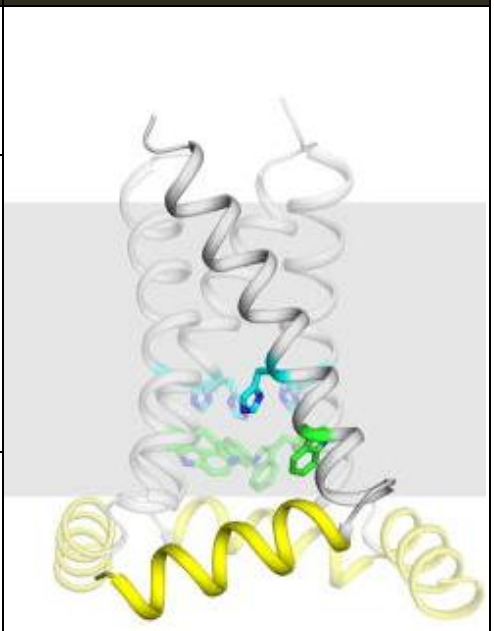
25-46	Domini transmembrana (TM, hèlix α tetramèrica)[71]	- Tetramerització de la proteïna - Conducció de protons - Lloc d'unió a fàrmacs	
47-61	Regió citoplasmàtica amfipàtica (intracel·lular, hèlix α)	- localització de la membrana - brot i l'escissió de virions acabats de formar - estabilització de la proteïna	
62-97	Regió C-terminal (intracel·lular, desordenada)	- interacció amb la proteïna de matriu M1 del virus[72]	

Taula 2. Estructura, regions i funcions del canal M2.

[70] Wang, J., Qiu, J. X., Soto, C. & DeGrado, W. F. Structural and dynamic mechanisms for the function and inhibition of the M2 proton channel from influenza A virus. *Curr. Opin. Struct. Biol*. **2011**, 21, 68.
[71] Wang, J., Kim, S., Kovacs, F. & Cross, T. A. Structure of the transmembrane region of the M2 protein H(+) channel. *Protein Sci*. **2001**, 10, 2241.
[72] Martin, K. & Heleniust, A. Nuclear transport of influenza virus ribonucleoproteins: The viral matrix protein (M1) promotes export and inhibits import. *Cell* **1991**, 67, 117–130.

La resolució per RMN en solució[73] i per mitjà de cristal·lografia de Raig X[74] de l'estructura del canal M2 l'any 2008, va marcar un abans i un després en l'estudi d'aquest canal. Des de llavors, fins a 15 estructures de diferents fragments del canal i per mitjà de tècniques diverses (X-raig, RMN en solució, RMN en estat sòlid) s'han dipositat al Protein Data Bank (PDB). Tot i així no va ser fins l'any 2014 que es va produir el següent descobriment revolucionari, si bé el canal M2 es tracta d'un tetràmer, aquest és doblement simètric, consistent en una dimerització de dímers funcionals[75,76].

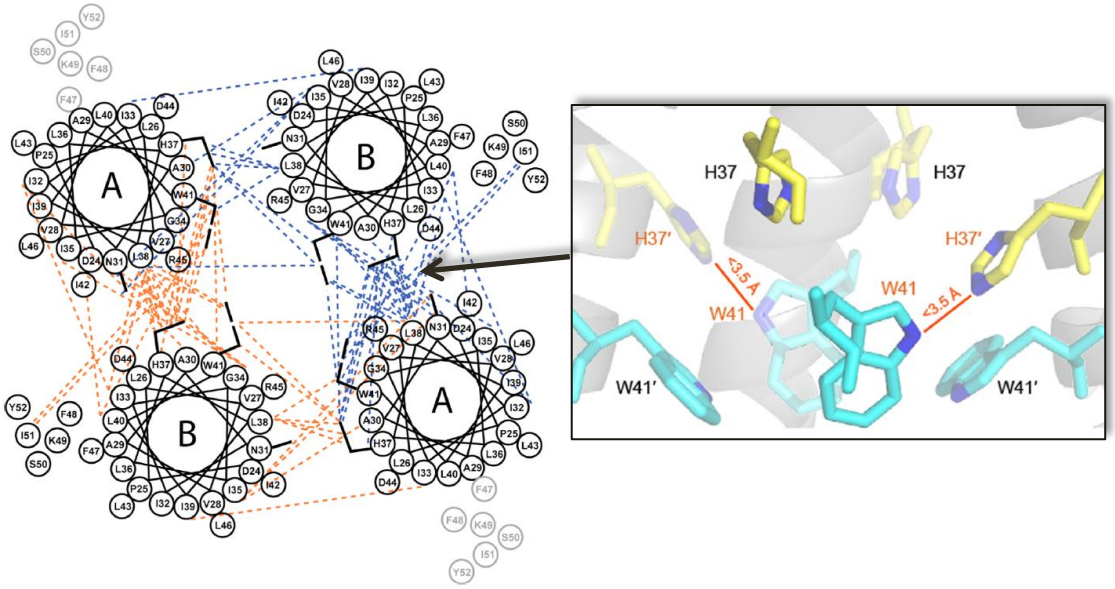

Figura 19. Esquerra: Representació de la doble simetria del canal tetramèric M2. Les cadenes laterals dels residus rellevants N31, H37 i W41 estan representades per les línies negres. Dreta: Enssamblatge dels 4 residus H37 i W41 en el dímer de dímers. La distància intermolecular entre l'H37' del dímer amb el W41 del mateix dímer és curta, d'entre 3-3.5 Å.

[73] Schnell, J. R. & Chou, J. J. Structure and mechanism of the M2 proton channel of influenza A virus. *Nature* **2008**, *451*, 591.
[74] Stouffer, A. L., Acharya, R., Salom, D., Levine, A. S., Di Costanzo, L., Soto, C. S., Tereshko, V., Nanda, V., Stayrook, S. & DeGrado, W. F. Structural basis for the function and inhibition of an influenza virus proton channel. *Nature* **2008**, *451*, 596.
[75] Kawano, K., Yano, Y., & Matsuzaki, K. A dimer is the minimal proton-conducting unit of the influenza a virus M2 channel. *J. Molec. Bio.* **2014**, 426(14), 2679–2691.
[76] Andreas, L. B., Reese, M., Eddy, M. T., Gelev, V., Ni, Q. Z., Miller, E. A., Emsley, L., Pintacuda, G., Chou, J. & Griffin, R. G. Structure and Mechanism of the Influenza A M218-60 Dimer of Dimers. *J. Am. Chem. Soc.* **2015**, 137(47), 14877–14886.

1.3.2 Funció[15]

La funció fonamental del canal M2 és conduir protons. És a dir, actua de canal regulador de pH per tal de permetre, durant el cicle del virus: la difusió de protons a l'interior de l'endosoma que conté el virus, per tal que aquest passi a un estat madur permetent la fusió de la membrana viral en l'endosoma i el correcte desempaquetament del genoma viral de la proteïna M1[77]; el retard de l'acidificació de les vesícules de transport a l'aparell de Golgi[78] per tal de permetre la correcta formació i posterior alliberament del virus.

El domini transmembrana del canal (residus 25-46) és la unitat funcional d'aquest, comprenent els residus essencials per a la conducció de protons. Aquests són: les histidines de la posició 37 (His37), el pKa de les quals controla la velocitat de conducció[79,80]; els triptòfans de la posició 41 (Trp41), que controlen el flux unidireccional de protons[81]; la valina de la posició 27 (Val27), que forma una petita vàlvula que controla l'entrada de protons i finalment l'àcid aspàrtic de la posició 44 (Asp44), que forma un pont d'hidrogen indirecte amb el grup NH de l'anell d'indole del Trp41, a través d'un agrupament d'aigües al final del canal. Així doncs mentre que la sanefa HxxxW formada per H37 i el W41 és el cor funcional del canal, la V27 i el D44 són les comportes a cada banda d'aquest.

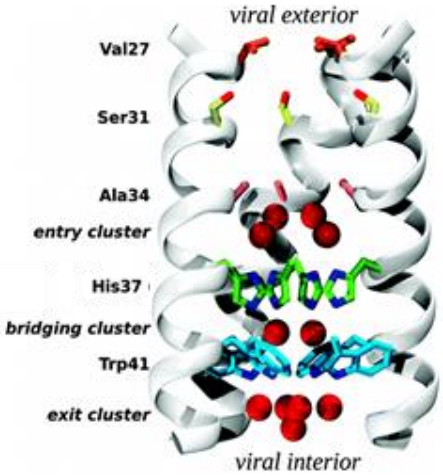

Figura 20. Representació esquemàtica del domini TM. Els residus importants per a la seva funció es troben indicats.

[77] Helenius, A. Unpacking the incoming influenza virus. *Cell* **1992**, 69, 577–578.
[78] Sakaguchi, T., Leser, G. P. & Lamb, R. A. The ion channel activity of the influenza virus M2 protein affects transport through the Golgi apparatus. *J. Cell. Biol*. **1996**, 133, 733–747.
[79] Hu, F., Schmidt-Rohr, K. & Hong, M. NMR Detection of pH-Dependent Histidine–Water Proton Exchange Reveals the Conduction Mechanism of a Transmembrane Proton Channel. *J. Am. Chem. Soc*. **2012**, 134, 3703.
[80] Hu, J., Fu, R., Nishimura, K., Zhang, L., Zhou, H. X., Busath, D. D., Vijayvergiya, V. & Cross, T. A. Histidines, heart of the hydrogen ion channel from influenza A virus: toward an understanding of conductance and proton selectivity. *Proc. Natl. Acad. Sci. USA* **2006**, 103, 6865.
[81] Tang, Y., Zaitseva, F., Lamb, R. A. & Pinto, L. H. The gate of the influenza virus M2 proton channel is formed by a single tryptophan residue. *J. Biol. Chem*. **2002**, 277, 39880.

El canal M2 és classificat com a canal lent ja que a pH fisiològic (pH=7.4) condueix a una velocitat d'uns 100-1000 protons per segon, considerada lenta respecte a la constant de conducció de protons a través d'un porus aquós de dimensions semblants, que és de 10^8 protons per segon[82]. Aquest fet s'explica ja que a pH fisiològic la concentració de protons és baixa, trobant-se al voltant d'un ordre de magnitud de la velocitat de difusió, però quan el pH extern s'acidifica, essent més baix que el pH de l'interior del virus (pHout<pHin) aquesta conducció es torna molt més elevada, fins a multiplicar la velocitat de difusió per una constant de velocitat de segon ordre; així doncs, el màxim de conducció es troba a pHs baixos[83]. Aquest comportament és el que fa que la conducció de protons a través del canal presenti una dependència sigmoide respecte al pH.

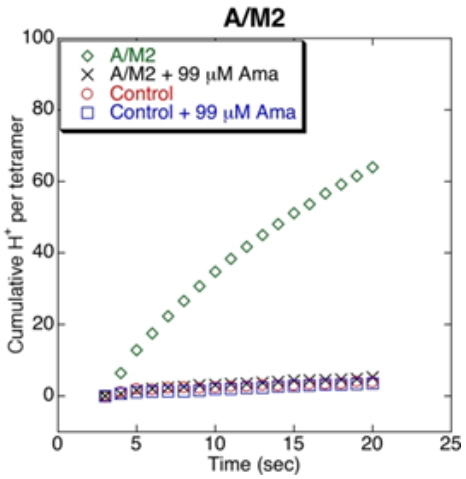

Figura 21. Velocitat de conducció del canal M2 (en verd) respecte al pH.

El mecanisme a través del qual es produeix el pas de protons a través del canal ha estat objecte de controvèrsia en els últims anys[15,84,85,86,87,88]. Tot i així, la determinació de l'estructura doblement dimèrica del canal ha permès una explicació plausible[20,21].

[82] Decoursey, T. E. Voltage-gated proton channels and other proton transfer pathways. *Physiol. Rev.* **2003**, 83, 475–579.
[83] Ma, C., Polishchuk, A. L., Ohigashi, Y., Stouffer, A. L., Schon, A., Magavern, E., Jing, X., Lear, J.D., Freire, E., DeGrado, W. F. & Lamb, R. A. Identification of the functional core of the influenza A virus A/M2 proton-selective ion channel. *Proc. Natl. Acad. Sci. USA* **2009**, 106, 12283–12288.
[84] Acharya, R., Carnevale, V., Fiorin, G., Levine, B. G., Polishchuk, A. L., Balannik, V., Samish, I., Lamb, R. A., Pinto, L. H., DeGrado, W. F. & Klein, M. L. Structure and mechanism of proton transport through the transmembrane tetrameric M2 protein bundle of the influenza A virus. *Proc. Natl. Acad. Sci. USA*. **2010**, 107, 15075.
[85] Phongphanphanee, S., Rungrotmongkol, T. & Yoshida, N. Proton Transport through the Influenza A M2 Channel: Three-Dimensional Reference Interaction Site Model Study. *J. Am. Chem. Soc*. **2010**, 9, 9782–9788.
[86] Ivanovic, T., Rozendaal, R., Floyd, D. L., Popovic, M., Van Oijen, A. M. & Harrison, S. C. Kinetics of Proton Transport into Influenza Virions by the Viral M2 Channel *PLos One* **2012**, *7*, e31566, 1-9.
[87] Okada, A., Miura, T. & Takeuchi, H. Protonation of histidine and histidine-tryptophan interaction in the activation of the M2 ion channel from influenza a virus. *Biochemistry* **2001**, *40*, 6053-60.
[88] Carnevale, V., Fiorin, G., Levine, B. G., DeGrado, W. F. & Klein, M. L. Multiple Proton Confinement in the M2 Channel from the Influenza A Virus. *J. Phys. Chem. C* **2010**, *114*, 20856-20863.

Els protons entren al canal previ pas de la comporta de V27. Un cop a l'interior hidrofílic els protons es transporten a través d'una translocació intermolecular, gràcies a la proximitat dels residus hidrofílics que es troben de cara al porus. En primer lloc els protons s'uneixen a la H37 més N-terminal i després a la H37 més C-terminal del dímer, que es troben formant un pont d'hidrogen entre els nitrògens δ i ε respectivament. Tot seguit té lloc la transferència del protó de la His al Trp i l'alliberament d'aquest a l'interior del virus. Gràcies a una tautomeria de la His37, la proteïna torna a l'estat original. Per tant, cada un dels dímers que formen el canal, són funcionals per a la conducció de protons[33]. Cal destacar que la proximitat de les H37 i el W41 que es troben formant una xarxa estable d'interaccions catió–π dins de l'hèlix i entre hèlix veïnes, és la responsable de la tetramerització de la proteïna.

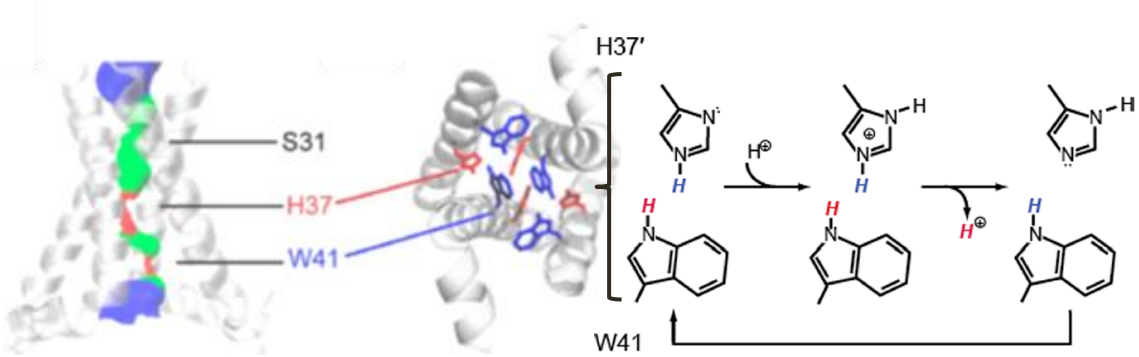

Figura 22. Estructura del dímer de dímers. Esquerra: Amplada de la superfície del porus, blau=espai per més d'una aigua, verd=espai per una molècula d'aigua, vermell = no hi caben aigües. Centre: Domini C-terminal del porus, el triptòfan (blau) adopta la conformació "indole in" en una hèlix i "indole out" en l'altra, permetent un bon empaquetament del dímer. Dreta: Possible mecanisme de conducció entre H37 i W41. L'H en negre, representa un protó que entra al canal des del domini N-terminal. L'H blau representa un protó transferit de H37 a W41. L'H vermell representa un protó que és alliberat ràpidament a l'interior del virus. La tautomerització de les cadenes laterals d'H37, tornen la proteïna a l'estat original.

1.3.3 Malalties relacionades

La malaltia de la influenza, comunament coneguda com la grip, consta d'un període d'incubació d'uns dos dies, després dels quals apareix un quadre simptomatològic de malestar general amb febre alta, dolor muscular, mal de cap i rinorrea. En la població immunològicament competent, és tracta d'una malaltia autolimitada que desapareix al cap d'una setmana. Tot i així el virus de la influenza pot ser especialment agressiu donant lloc

a complicacions mortals quan apareix una soca especialment virulenta o quan infecta als anomenats grups de risc, dins els que trobem infants, persones de la tercera edat i persones immunocompromeses.

El virus de la grip es transmet en forma d'epidèmies estacionals que tenen lloc durant la tardor i l'hivern en les zones temperades. Les repercussions d'aquestes a nivell mundial es tradueixen anualment en entre 3 i 5 milions de casos severs i al voltant de 250.000-500.000 de morts, essent un clar problema de salut pública[89]. A més a més té una repercussió a nivell econòmic a causa de la pèrdua de productivitat de les empreses per l'absentisme laboral, la saturació dels centres sanitaris durant els períodes epidèmics i la infecció zoonòtica d'aquest virus a animals de granja que farà que aquests no siguin aptes per a l'explotació ramadera[90].

El problema més important és però, la capacitat d'aquest virus de generar pandèmies. Aquestes es poden donar a través del mecanisme de rotació antigènica, anteriorment comentat, pel qual una soca especialment infectiva es pot combinar amb una d'especial virulència, originant una pandèmia mortal imparable tal i com va passar l'any 1918 amb l'anomenada grip espanyola. La pandèmia de 1918 va acabar amb 40 milions de vides arreu del món, essent la més devastadora de la història de la humanitat[91]. Tenint en compte aquest fet i que aquestes pandèmies presenten caràcter periòdic, la necessitat de desenvolupar fàrmacs per fer front a aquest virus, és evident.

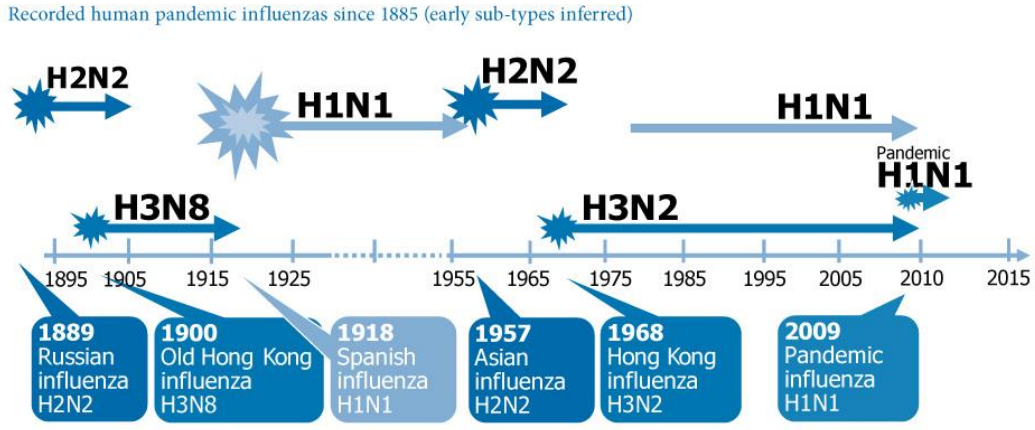

Figura 23. Pandèmies del virus de la influenza A al llarg de la història.

[89] Rossman, J. S. & Lamb, R. A. Influenza virus assembly and budding. *Virology* **2011**, 411, 229.
[90] Molinari, N. A. M., Ortega-Sanchez, I. R., Messonnier, M. L., Thompson, W. W., Wortley, P. M.,Weintraub, E. & Bridges, C. B. The annual impact of seasonal influenza in the US: measuring disease burden and costs. *Vaccine* **2007**, 25, 5086.
[91] Taubenberger, J. K. & Morens, D.M. 1918 Influenza: the Mother of All Pandemics. Centers for Disease Control and Prevention. **2006**.

1.3.4 Gamma de fàrmacs

El canal M2 és la diana de dos fàrmacs comercials: l'amantadina (Symmetrel®, Mantadix®) i la rimantadina (Flumadine®).

Amantadina IC_{50}= 16.0 μM

Rimantadina IC_{50}= 10.8 μM

Figura 24. Fàrmacs comercials amb el canal M2 com a diana i IC_{50} d'ambdós.

La manera com l'amantadina (Amt) bloqueja el canal va suscitar molta controvèrsia en el passat[92], tot i així, avui en dia es reconeix que una sola molècula d'amantadina s'uneix dins el porus entre els residus Val27 i Gly34 (anomenat lloc d'unió al porus), quan el canal es troba obert a pH àcid. El mecanisme pel que aquestes estructures adamantàniques inhibeixen l'activitat del canal es tracta d'un bloqueig físic en el que el fàrmac clou el porus evitant: la transferència de protons, el canvi conformacional de la proteïna, així com la tetramerització d'aquesta.

L'orientació del grup polar de l'adamantà dins del canal M2 ha estat igualment tema de debat i forta controvèrsia entre dues modalitats possibles: en la primera, coneguda com a forma-*down*[93], la caixa hidrofòbica de l'adamantà estableix interaccions de Van der Waals amb els grups metil de les Val27 i Ala30, mentre que el grup polar es troba dirigit a l'interior del porus. Contràriament, en la segona modalitat o forma-*up*, el grup polar es troba apuntant cap a la porta de Val27 on es troba més solvatat.

El debat es va resoldre després de provar que aquestes dues formes fluctuen, depenent de l'estat de protonació en el que es trobi el canal M2[94].

[92] Kozakov, D., Chuang, G., Beglov, D. & Vajda, S. Where does amantadine bind to the influenza virus M2 proton channel? *Trends Biochem. Sci*. **2010**, 35(9), 471–475.
[93] Cady, S. D., Wang, J., Wu, Y., Degrado, W. F. & Hong, M. Specific Binding of Adamantane Drugs and Direction of Their Polar Amines in the Pore of the Influenza M2 Transmembrane Domain in Lipid Bilayers and Dodecylphosphocholine Micelles Determined by NMR Spectroscopy. *J. Am. Chem. Soc*. **2011**, 2, 4274–4284.
[94] Khurana, E., Devane, R. H., Dal Peraro, M. & Klein, M. L. Computational study of drug binding to the membrane-bound tetrameric M2 peptide bundle from influenza A virus. *Biochim. Biophys. Acta*. **2011**, 1808, 530.

1.3.4.1 Situació actual: Canal M2 com a diana antiviral

Avui en dia l'aparició de soques resistents i els efectes secundaris a nivell de sistema nerviós central de l'amantadina, amb coneguda activitat com a antagonista del receptor d'NMDA, han fet que es desaconselli l'ús d'aquests fàrmacs[95]. Aquest fet enlloc de produir un abandonament del canal M2 com a diana, ha desencadenat una forta recerca de bloquejadors del canal M2, ja que aquest representa una diana farmacològica idònia, doncs presenta:

- *Biologia ben coneguda.*

Els avanços en els darrers anys gràcies a estudis teòrics, estructurals i funcionals de la proteïna M2 han fet que es tracti del canal iònic més ben conegut avui en dia. Aquest fet el fa ideal per al disseny racional de fàrmacs.

- *Paper fonamental en el cicle viral.* (Veure secció 1.3.2)

- *Taxa de mutació baixa.*

Tot i que el virus de la grip presenta una taxa de mutació especialment elevada, en el cas del canal M2 només hi ha un nombre molt limitat de mutants viables i infectius. De fet, en les soques circulants se'n troben majoritàriament 3 tipus[96]:

V27A (Valina $\rightarrow$ Alanina)

En aquest canal mutant en la posició 27 hi ha un canvi de valina, la cadena lateral de la qual és un grup isopropil, per una alanina amb un grup metil per cadena. Això genera que es perdi la comporta d'entrada al canal, incrementant la velocitat de conducció de protons i que es debiliti l'empaquetament de les hèlix α, traduint-se en un canal eixamplat uns 2 Å respecte a la forma salvatge. Així doncs tot i que els inhibidors són capaços d'unir-se al porus, no hi ha cap resistència energètica que els hi impedeixi la sortida, fent que aquests es desuneixin del canal de manera ràpida i la conducció de protons no s'aturi. Cal destacar que el V27A és l'únic mutant originat com a resposta a l'ús de fàrmacs[97,98].

[95] Hubsher, G., Haider, M. & Okun, M. S. Amantadine: the journey from fighting flu to treating Parkinson disease. *Neurology* **2012**, 78, 1096.
[96] Leonov, H., Astrahan, P., Krugliak, M. & Arkin, I. T. How Do Aminoadamantanes Block the Influenza M2 Channel , and How Does Resistance Develop? *J. Am. Chem. Soc*. **2011**, 133, 9903–9911.
[97] Furuse, Y., Suzuki, A., Kamigaki, T. & Oshitani, H. Evolution of the M gene of the influenza A virus in different host species: large-scale sequence analysis*. J. Virol*. **2009**, 6(1), 67.
[98] Furuse, Y., Suzuki, A. & Oshitani, H. Large-scale sequence analysis of M gene of influenza A viruses from different species: Mechanisms for emergence and spread of amantadine resistance. *Antimicrob. Agents Chemother*. **2009**, 53(10), 4457–4463.

L26F (Leucina $\longrightarrow$ Fenilalanina)

En aquest cas el canvi de la leucina, amb un grup isobutil, per una fenilalanina, amb un grup benzil, que es col·loca en la interfície interhelical, produeix una desestabilització de l'estructura general del canal. Com a resultat l'empaquetament del porus serà menys compacte fent que incrementi el seu diàmetre en uns 0.5 Å. Els efectes de l'eixamplament són semblants als de la mutació V27A.

S31N (Serina $\longrightarrow$ Asparragina)

El mutant S31N és el més rellevant clínicament[99] ja que es troba en un 95% de les soques circulants. La serina (-CH_2OH) de la soca salvatge és substituïda per una asparagina (-CH_2CONH_2 provocant un canvi més notable que en els casos anteriors en el canal: s'eixampla 0.5 Å prop de la porta de Val27 i s'estreny uns 1.5 Å al lloc de la mutació (Asn31). En el canal salvatge la serina 31 s'orienta cap als lípids de membrana, conformació que no s'adopta en el canal mutant ja que la cadena lateral de metilcarboxamida de l'Asn31 és més llarga i hidrofílica i per tant, es produiran interaccions desfavorables. Això provoca una reestructuració global del canal que destrueix el lloc d'unió a amantadina. En el cas que amantadina entri al canal establirà interaccions desestabilitzats amb la cadena de metilcarboxamida, orientada cap al porus en el S31N. Tot i que això justificaria la resistència del canal S31N a Amt, cal mencionar que el mecanisme de resistència encara no ha estat completament esclarit i que n'existeixen altres hipòtesis [19,100,101].

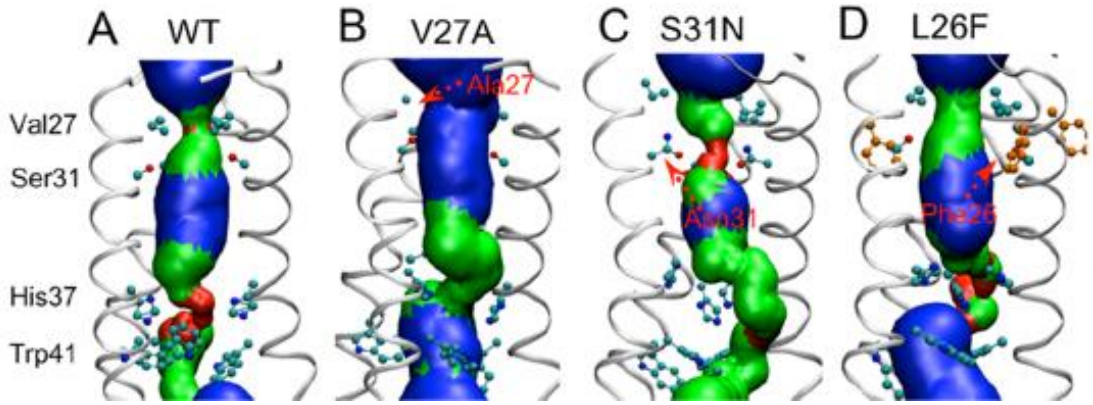

Figura 25. Comparació dels porus dels canals d'influenza A de les soques circulants actuals.

[99] Dong, G., Peng, C., Luo, J., Wang, C., Han, L., Wu, B., Ji, G. & He, H. Adamantane-resistant influenza A viruses in the world (1902-2013): frequency and distribution of M2 gene mutations. *PLoS One*. **2015**, 10, e0119115.
[100] Pielak, R. M., Oxenoid, K. & Chou, J. J. Structural investigation of rimantadine inhibition of the AM2-BM2 chimera channel of influenza viruses. *Structure* **2011**, 19, 1655.
[101] Can, T. V., Sharma, M., Hung, I., Gor'kov, P. L., Brey, W. W. & Cross, T. A. Magic Angle Spinning and Oriented Sample Solid-State NMR Structural Restraints Combine for Influenza A M2 Protein Functional Insights. *J. Am. Chem. Soc.* **2012**, 134, 9022.

Gràcies a tot el coneixement actual sobre la biologia del virus, el disseny de nous inhibidors contra les soques resistents està començant a donar els seus fruits.

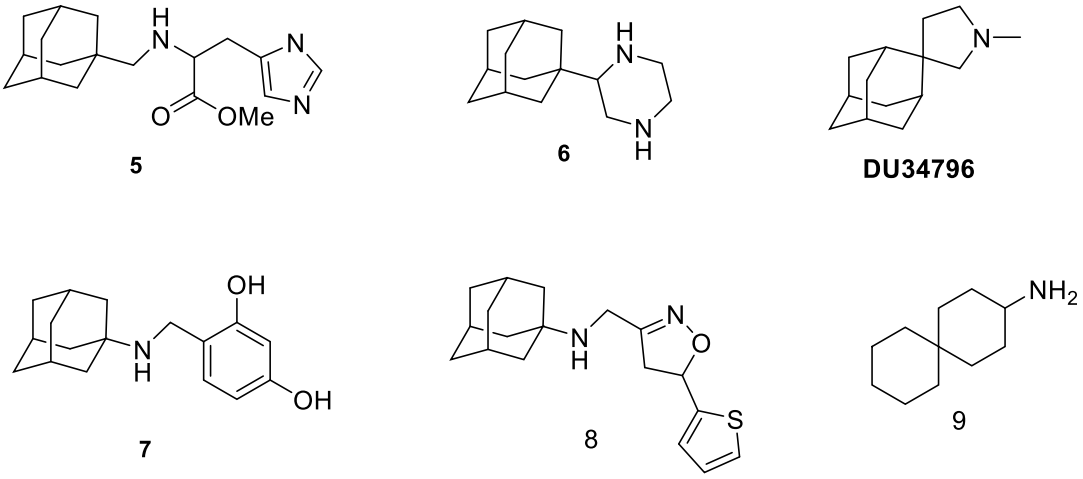

Figura 26. Inhibidors del canal M2 desenvolupats recentment

Cal destacar el gran interès que s'ha despertat durant els darrers anys al voltant del desenvolupament d'una teràpia antiviral combinada per fer front al virus de la grip[102,103]. Aquesta, de manera similar al tractament actual contra el VIH, consistiria en administrar un còctel de fàrmacs que poguessin actuar a diferents punts del cicle del virus, és a dir sobre diferents dianes. Per aquest fet, en la present Tesi s'explora, tot i trobar-se fora del grup de canals iònics, la proteïna viral hemaglutinina com a potencial diana terapèutica.

[102] Nguyen, J. T., Smee, D. F., Barnard, D. L., Julander, J. G., Gross, M., de Jong, M. D. & Went, G. T. Efficacy of Combined Therapy with Amantadine, Oseltamivir, and Ribavirin In Vivo against Susceptible and Amantadine-Resistant Influenza A Viruses. *PLoS One* **2012**, 7, e31006.

[103] Seo, S., Englund, J. A., Nguyen, J. T., Pukrittayakamee, S., Lindegardh, N., Tarning, J., Tambyah, P. A., Renaud, C., Went, G. T., de Jong, M. D. & Boeckh, M. Combination therapy with amantadine, oseltamivir and ribavirin for influenza A infection: safety and pharmacokinetics. *J. Antivir. Ther.* **2013**, 18, 377.

1.4. L'HEMAGLUTININA

1.4.1 Estructura

L'hemaglutinina (HA) és la proteïna més abundant en la superfície del virus de la influenza A. Està formada per uns 550 aminoàcids i es tracta d'una glicoproteïna de membrana de tipus I, constant d'una seqüència senyal *N*-terminal que és tallada al reticle endoplasmàtic (RE), un domini transmembrana hidrofòbic que fa d'àncora prop del domini *C*-terminal i una cua citoplasmàtica curta[104]. L'HA es plega formant homotrímers associats al RE i finalment és modificada post-translacionalment amb l'addició de grups acil, a tres de les cisteïnes de la seva cua citoplasmàtica i zona transmembrana[105] i amb la *N*-glicosilació de set residus d'Asn en l'ectodomini[106,107]. L'ectodomini madur, s'extén al voltant de 130 Å des de la membrana viral i el seu radi varia entre 15 i 40 Å en diferents punts. El tronc de la proteïna consta d'un cabdell enrotllat de triple filament, format per les hèlix de cada monòmer. Els dominis més distals de la membrana són globulars i contenen el lloc d'unió al receptor i les regions antigèniques més importants[108].

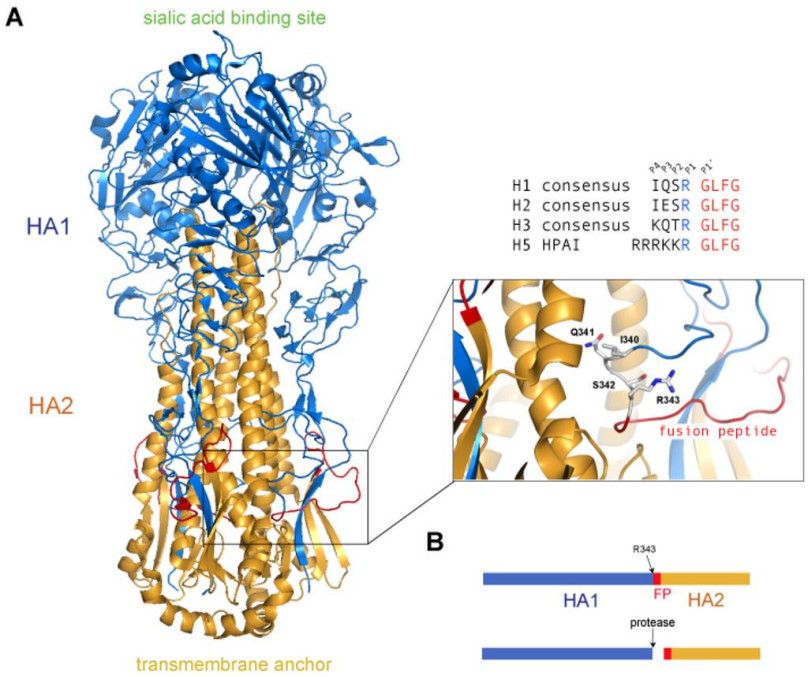

[104] Wang, Q. & Tao, Y. J. Influenza: Molecular Virology. *Caister Academic Press*. **2010**, 196.
[105] Kordyukova, L.V., Serebryakova, M.V., Baratova, L.A. & Veit, M. S-acylation of the hemagglutinin of influenza viruses: mass spectrometry reveals site-specific attachment of stearic acid to a transmembrane cysteine. *J. Virol.* **2008**, 82 (18), 9288–9292.
[106] Ward, C.W. & Dopheide, T. A. Amino acid sequence and oligosaccharide distribution of the haemagglutinin from an early Hong Kong influenza virus variant A/Aichi/2/68 (X-31). *Biochem. J.* **1981,** 193 (3), 953–962.
[107] Wilson, I. A., Skehel, J. J. & Wiley, D. C. Structure of the haemagglutinin membrane glycoprotein of influenza virus at 3 Å resolution. *Nature* **1981**, 289 (5796), 366–373.
[108] Schmidt, M., Schmidt, M.F & Rott, R. Chemical identification of cysteine as palmitoylation site in a transmembrane protein (Semliki Forest virus E1). *J. Biol. Chem.* **1988**, 263 (35), 18635–18639.

Figura 27. A. Estructura de l'HA trimèrica sense tallar (PDB:1RD8). El lloc d'escissió es mostra ampliat, així com les cadenes laterals dels residus de tall. B. Representació esquemàtica de la divisió de l'HA0 en HA1 (lloc d'unió al receptor) i HA2. El nou domini *N*-terminal d'HA2 és el primer residu del pèptid de fusió[109].

Durant el cicle de vida del virus, l'HA passa per tres conformacions separades[51,110,111,112]. L'HA és sintetitzada en forma de polipèptid precursor, l'HA0. Aquest és tallat extracel·lularment en el primer pas de la infecció[113], per les proteases de la mucosa respiratòria de l'hoste, donant lloc al domini *C* terminal de la subunitat HA1 i el domini *N* terminal de la subunitat HA2 que quedaran unides per ponts disulfur. El trímer cilíndric doncs quedarà format per:

- un *cap globular* amb residus d'HA1, que conté el lloc d'unió pels àcids siàlics de la superfície de les cèl·lules epitelials de l'hoste i és el que permet el reconeixement del virus i posterior internalització en l'endosoma.
- un *domini tija* format per HA1 i HA2, proximal a la membrana.
- una *regió frontissa* que el connecta a la membrana.

A pH neutre, és a dir, en la forma no activada o nativa de l'HA, el pèptid de fusió (HA2) es troba enterrat en el trímer en la zona de la tija. Davant una acidificació del pH, provocada pel canal M2[114], aquest pèptid s'allibera i promou la fusió de l'embolcall del virus i la membrana de l'endosoma[115]. Aquesta fusió permet l'alliberament del genoma viral al citoplasma (veure secció 1.2.2).

[109] Hamilton, B. S., Whittaker, G. R. & Daniel, S. Influenza Virus-Mediated Membrane Fusion: Determinants of Hemagglutinin Fusogenic Activity and Experimental Approaches for Assessing Virus Fusion. *Viruses* **2012**, 4 (7), 1144-1168.

[110] Bizebard, T., Gigant, B., Rigolet, P., Rasmussen, B., Diat, O., Bösecke, P., Wharton , S. A., Skehel, J.J. & Knossow, M. Structure of influenza virus haemagglutinin complexed with a neutralizing antibody. *Nature* **1995**, 376 (6535), 92-4.

[111] Bullough, P.A., Hughson, F.M., Skehel, J.J. & Wiley, D.C. Structure of influenza haemagglutinin at the pH of membrane fusion. *Nature*. **1994**, 371 (6492), 37-43.

[112] Chen, J., Lee, K. H., Steinhauer, D. A., Stevens, D. J., Skehel, J. J. & Wiley, D. C. Structure of the hemagglutinin precursor cleavage site, a determinant of influenza pathogenicity and the origin of the labile conformation. *Cell* **1998**, 95 (3), 409-17.

[113] D. C. Wiley & J. J. Skehel. The structure and function of the hemagglutinin membrane glycoprotein of influenza virus. *Annu. Rev. Biochem.* **1987**, *56*, 365-394.

[114] Zhu, Lei, et al. Inhibition of influenza A virus (H1N1) fusion by benzenesulfonamide derivatives targeting viral hemagglutinin. *PloS one* **2011** (6.12): e29120.

[115] Skehel, J. J. & Wiley, D. C. Receptor binding and membrane fusion in virus entry: the influenza hemagglutinin. *Ann. Rev. Biochem.* **2000,** (69.1), 531-569.

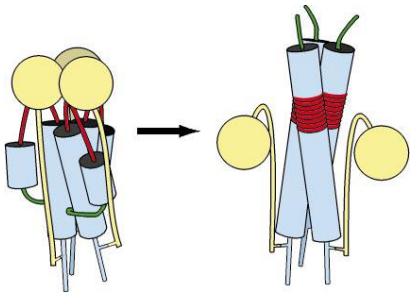

Figura 28. Mecanisme de fusió de la membrana viral. En la conformació nativa HA0, les subunitats HA1 (grogues) ocupen l'extrem distal de l'estructura sobre una regió trimèrica enrotllada d'HA2 (blau). Els pèptids de fusió (verd) es troben enterrats al nucli de l'estructura. Davant una davallada del pH, tenen lloc els canvis conformacionals (estructura de la dreta): es debiliten les interaccions no covalents entre HA1 i HA2, els colzes d'HA2 (vermell) salten cap a conformacions en hèlix, propulsant els pèptids de fusió al cim de l'estructura per tal que puguin interactuar amb la membrana objectiu[116].

Des de la publicació de la primera estructura de raig X de l'HA al 1981[54], més de 25 estructures de raig X han sigut resoltes[117,118], incloent les tres conformacions moleculars principals, anteriorment comentades: el precursor HA0, la forma metastable a pH neutre (HA1/HA2) i l'estructures de l'HA un cop alliberat el pèptid de fusió. A més a més han estat també publicades estructures d'HA unida a lligands, així com dels diferents subtipus d'HA.

[116] Han, X., Bushweller, J. H., Cafiso, D. S. & Tamm, L. K. Membrane structure and fusion-triggering conformational change of the fusion domain from influenza hemagglutinin. *Nat. Struct. Mol. Biol.* **2001**, *8*, 715-720.
[117] Gamblin, S.J., Haire, L. F., Russell, R. J., Stevens, D. J., Xiao, B., Ha, Y., Vasisht, N., Steinhauer, D. A., Daniels, R. S., Elliot, A., Wiley, D. C. & Skehel J. J. The structure and receptor binding properties of the 1918 influenza hemagglutinin. *Science* **2004**, 303 (5665), 1838-42.
[118] Stevens, J., Corper, A. L., Basler, C. F., Taubenberger, J. K., Palese, P. & Wilson, I. A. Structure of the uncleaved human H1 hemagglutinin from the extinct 1918 influenza virus. *Science*. **2004**, 303 (5665), 1866-70.

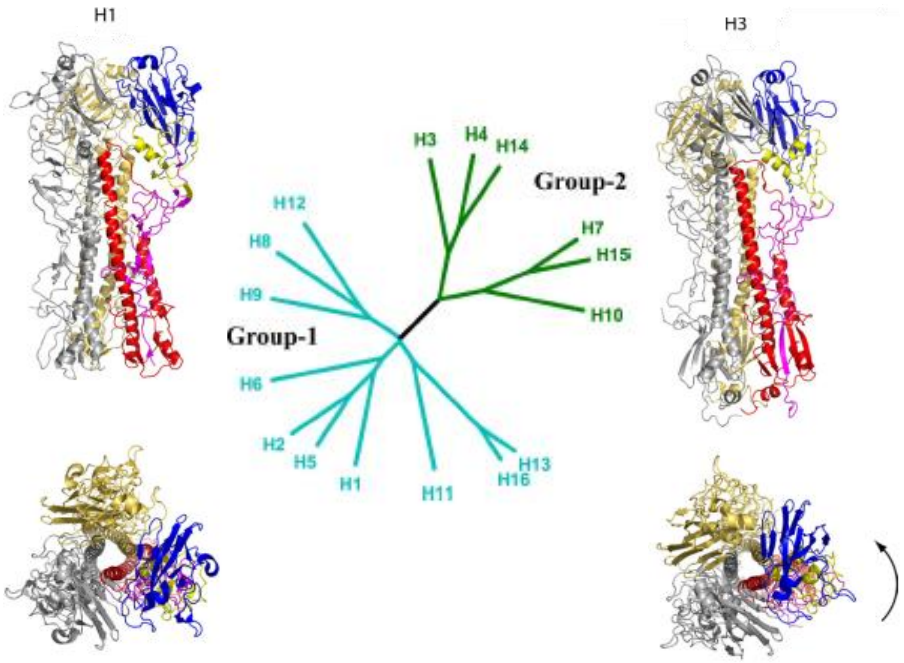

Figura 29. Organització filogenètica de les HA i estructures cristal·lines d'H1 i H3, representants dels dos grups principals. En daurat i platejat trobem dos dels monòmers que formen el trímer i en el tercer monòmer, se'n troben detallades les parts - blau: lloc d'unió al receptor; groc: esterasa vestigial; magenta i vermell: subdominis de fusió. Les diferències entre H1 i H3 es troben en variacions locals de l'estructura, així com en l'orientació dels subdominis: la fletxa indica la rotació dels subdominis distals a la membrana del grup 2 (H3), respecte al grup 1 (H1).

Hi ha 16 subtipus diferents d'HA que es divideixen en 5 clados o grups monofilètics que en funció dels residus específics de grup HA1 17 i HA2 106 i 111 del pèptid de fusió, es poden separar en dos grans grups. El primer grup està representat per l'HA1 i conté els clados H1-, H9- i H-13, caracteritzats per presentar tirosina en HA1 17, histidina en HA2 111 i un residu bàsic de lisina o arginina a l'HA2 106[119]. El segon grup està representat per l'HA3 i inclou HA del tipus H3 i H7, que presenten His en HA1 17 i HA2 106 i treonina a HA2 111.

[119] Thoennes, S., Li, Z. N., Lee, B. J., Langley, W. A., Skehel, J. J., Russell, R. J. & Steinhauer, D. A. Analysis of Residues Near the Fusion Peptide in the Influenza Hemagglutinin Structure for Roles in Triggering Membrane Fusion. *Virology* **2008**, *370*, 403-414.

1.4.2 Funció

Les funcions de l'HA són les següents:

1. Actuar d'antigen.

Les HA són reconegudes pels receptors dels àcids siàlics de la superfície de les cèl·lules epitelials[62,120] del tracte respiratori, gràcies als quals entren a la cèl·lula per endocitosi i la infecció viral comença.

2. Especificitat interespècie

Relacionada amb la característica anterior, l'especificitat per un tipus concret de receptor d'àcid siàlic és el que determina si el virus infectarà principalment aviram (amb àcids siàlics d'enllaç α-2,3) o bé humans (amb àcids siàlics d'enllaç α-2,6 al tracte respiratori superior). Aquest tret és especialment rellevant ja que les infeccions més virulentes per als humans es donen quan una HA d'especificitat α-2,3, adquireix capacitat d'infectar humans, donant lloc a una soca que provocarà simptomatologia a nivell de vies aèries inferiors, on es troben receptors d'àcid siàlics tipus α-2,3 en els humans, i per tant molt més severa. Aquest salt entre espècies està estretament lligat amb la generació de pandèmies i ocorre durant els processos de recombinació, els quals es solen donar en els porcs, ja que aquests animals presenten receptors amb ambdós tipus d'enllaç en el seu tracte respiratori.

[120] Ha, Y., Stevens, D. J., Skehel, J. J. & Wiley, D. C. X-ray structures of H5 avian and H9 swine influenza virus hemagglutinins bound to avian and human receptor analogs. *Proc. Natl. Acad. Sci. USA* **2001**, *98*, 11181-11186.

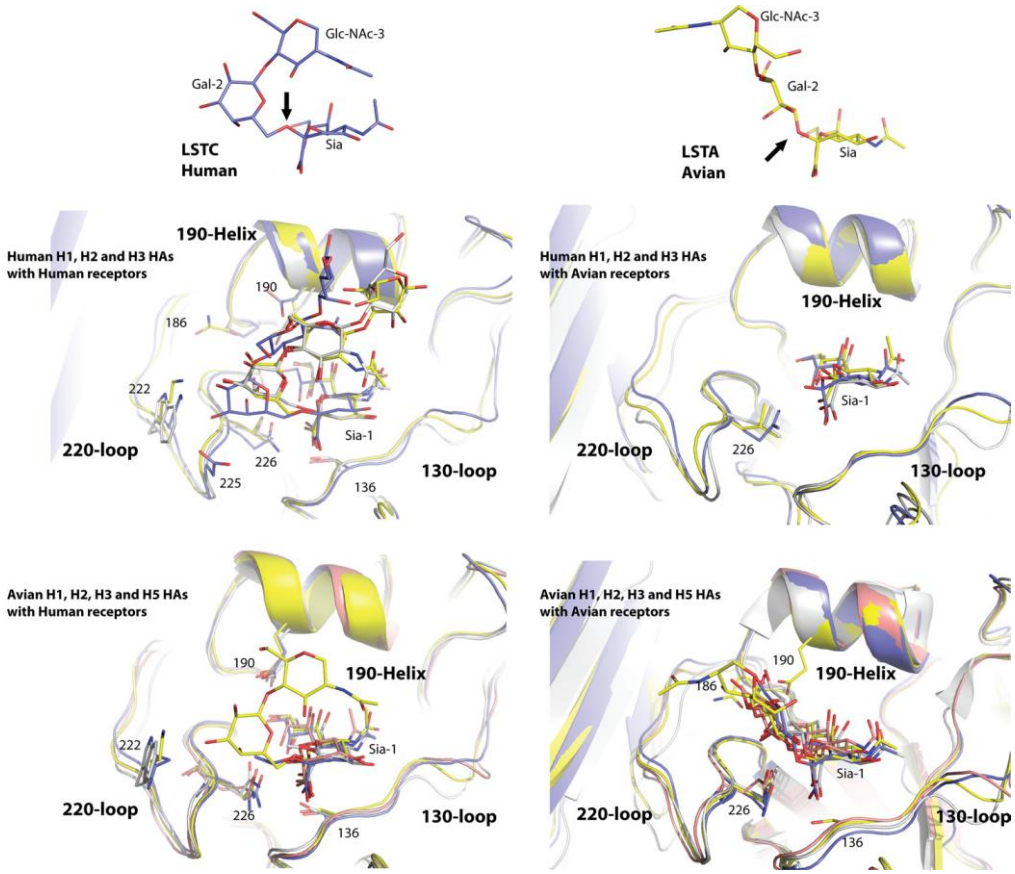

Figura 30. Estructures cristal·lines dels complexes entre l'HA i receptors. A dalt: àcid siàlic unit a l'anàleg del receptor humà α-2,6 LSTc (esquerra; carbonis en blau) i aviar α-2,3 LSTa (dreta; carbonis en groc). Les fletxes negres indiquen l'oxigen glicosídic. Centre i a baix: Solapaments del lloc d'unió a receptor d'HA de diferents espècies i subtipus, en complex amb el receptor humà (esquerra) i aviar (dreta). L'HA i els àtoms de carboni del lligand són: blau-H1; groc-H2; salmó-H5.

3. *Media la fusió* de les membranes virals i endosomals, essencial per l'alliberació del genoma viral al citoplasma.

1.4.3 Malalties relacionades

Al pertànyer al mateix agent patogen que la proteïna M2, anteriorment comentada, la malaltia a la que està associada és, de la mateixa manera, la grip (veure secció 1.3.3).

1.4.4 Gamma de fàrmacs

La recerca al voltant d'aquesta proteïna s'ha centrat principalment en el desenvolupament d'anticossos, per ser usats com a vacunes profilàctiques[121,122,123,124].

Pel que fa a fàrmacs avui en dia no se'n troba cap que tingui com a diana aquesta proteïna. Tot i així la recerca en aquesta direcció ha donat a conèixer alguns resultats inicials encoratjadors. Un dels primers exemples és la *tert*-butilhidroquinona (TBHQ), que inhibeix el canvi conformacional de l'HA i conseqüentment la infectivitat viral a concentracions de 10 μM[125].

Les noves molècules actives poden presentar tres mecanismes d'acció en funció del seu punt d'intervenció: inhibidors de l'escissió d'HA0, inhibidors del lloc d'unió a la membrana o inhibidors de la fusió de membranes. A l'hora de dissenyar aquestes molècules, caldrà tenir en compte els tres llocs d'unió a la proteïna més conservats[126]:

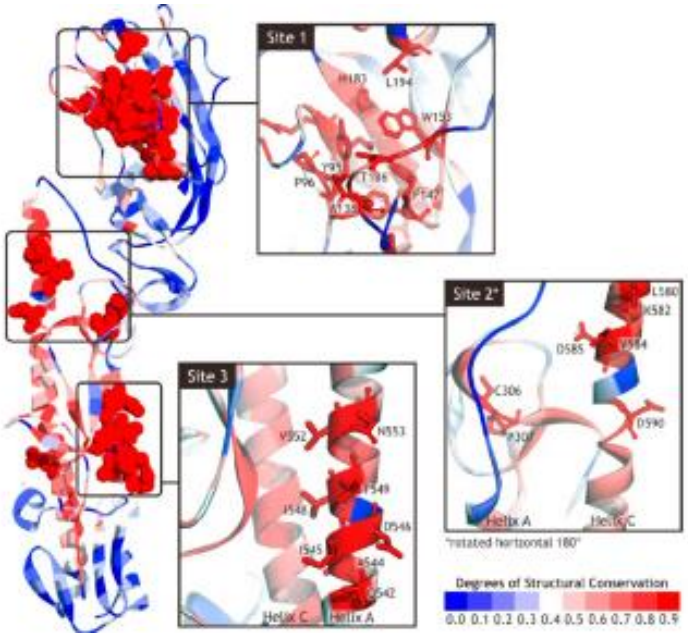

Figura 31. Representació dels llocs d'unió més conservats en la proteïna HA.

[121] Laursen, N. S. & Wilson, I. A. Broadly neutralizing antibodies against influenza viruses. *Antiviral Res*. **2013**, 98, (3), 476-483.

[122] Kirchenbaum, G. A. & Ross, T.M. Eliciting broadly protective antibody responses against influenza. *Curr. Opin. Immunol*. **2014**, 28, 71-76.

[123] Gutierrez, A. F. & El-Sahly, H. Recombinant hemagglutinin protein vaccine: a new option in immunization against influenza. *Future Virol.* **2015**, 10(9), 1057-1067.

[124] Rossignol, J. F., LaFrazia, S., Chiappa, L., Ciucci, A. & Santero, M. G. Thiazolides, a new class of anti-influenza molecules targeting viral hemagglutinin at the post-translational level. *J. Biol. Chem.* **2009**, *284*, 29798-29808.

[125] Bodian, D., Yamasaki, R., Buswell, R., Stearns, J., White, J. & Kuntz, I. Inhibition of the fusion-inducing conformational change of infleunza hemagglutinin by benzoquinones and hydroquinones. *Biochem.* **1993**, 32(12), 2967-2978.

[126] Yusuf, M., Konc, J., Sy Bing, C., Trykowska Konc, J., Ahmad Khairudin, N. B., Janezic, D. & Wahab, H. A. Structurally conserved binding sites of hemagglutinin as targets for influenza drug and vaccine development. *J. Chem. Inf. Model.* **2013**, 53 (9), 2423–2436.

En el *lloc 1* hi trobem un seguit de residus conservats i, per tant, podrà ser usat per a l'optimització de la unió a HA de lligands multivalents.

El *lloc 2* es troba a l'hèlix C, en la interfase entre HA1 i HA2, presentant les zones més conservades als residus C306 i C307 (de la subunitat HA1) i L580, K582, V584 i D585 (de la subunitat HA2). En el grup 1 hi ha un gir de l'hèlix A que fa inaccessible la butxaca hidrofòbica de l'hèlix C (lloc d'unió) als lligands. Es creu que és el lloc idoni per desenvolupar nous inhibidors de la fusió i per eliminar les diferències d'inhibició entre el grup 1 i grup 2, a través d'un disseny racional de compostos dirigits a aquesta regió.

El *lloc 3* es troba a l'hèlix A i és d'interès a l'hora de desenvolupar lligands amb un mecanisme d'inhibició divers contra diferents subtipus i soques d'HA.

Recentment la recerca de compostos anti HA, majoritàriament impulsada per companyies farmacèutiques com ara Roche o Bristol-Myers Squibb, ha aconseguit desenvolupar noves molècules de baix pes molecular amb una activitat potent anti HA.

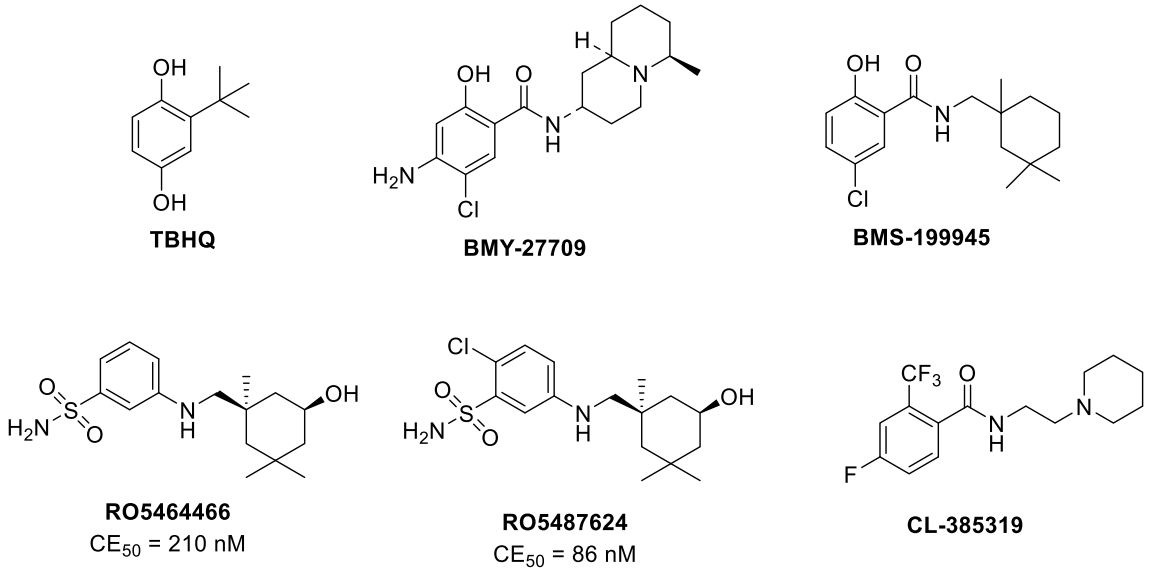

Figura 32. Compostos amb activitat anti HA. Es mostra la TBHQ i alguns dels antivirals desenvolupats per Bristol-Myers Squibb (BMS, BMY), Roche (RO) i Wyeth-Ayerst (CL).

Tot i així tots aquests nous compostos presenten un problema de selectivitat de grup, és a dir, o bé són efectius per a les soques que pertanyen al grup 1 d'HA o al grup 2. El desenvolupament d'un fàrmac capaç d'inhibir l'HA dels dos grups, resta com a repte per al futur.

1.5. RECEPTOR PURINÈRGIC IONOTRÒPIC $P2X_7$

1.5.1 Estructura

La senyalització purinèrgica va ser descoberta per Burnstock a l'any 1972[127], quan va proposar que l'ATP i altres nucleòtids i nucleòsids jugaven un paper fonamental en la senyalització extracel·lular, formant una xarxa complexa[128]. La xarxa purinèrgica està formada d'un gran nombre de receptors de membrana i ectoenzims, incloent el receptor $P2X_7$. La família de receptors P2X està formada per set tipus de canals de cations dependents de lligand, d'entre els que el $P2X_7$[129] destaca per ser el més gran.

El receptor purinèrgic $P2X_7$ ($RP2X_7$) està format per 595 aminoàcids, el gen del qual està format per 13 exons i es troba en el braç curt del cromosoma 12, compartint la localització amb el $RP2X_4$. En comparació amb altres subtipus de RP2X, el $RP2X_7$ és altament polimòrfic, constant amb més de 260 polimorfismes d'un sol nucleòtid.

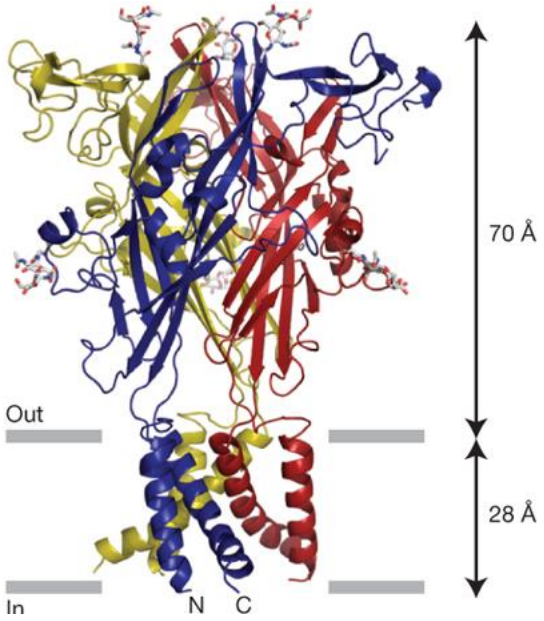

Figura 33. Arquitectura dels receptors P2X. Cada subunitat està representada per un color diferent.

La seva estructura és trimèrica i cada una de les subunitats que la formen consten de:

Domini *intracel·lular aminoterminal curt* (aa 1-25)

Domini *intracel·lular carboxiterminal llarg* (aa 356-595)

[127] Burnstock, G. Purinergic nerves. *Pharmacol. Rev.* **1972**, 24, 509–581.
[128] Burnstock, G. Pathophysiology and therapeutic potential of purinergic signaling. *Pharmacol Rev*. **2006**, 58, 58–86.
[129] Coddou, C., Yan, Z., Obsil, T., Huidobro-Toro, J.P. & Stojilkovic, S. S. Activation and regulation of purinergic P2X receptor channels. *Pharmacol. Rev*. **2011**, 63, 641–683.

Aquest domini és essencial per a la formació del porus i per a l'estabilització del receptor a la membrana plasmàtica.

Dominis *transmembrana*

Són dos dominis hidrofòbics que inclouen els aminoàcids 26-46 i 335-355, separats pel domini extracel·lular.

Domini *extracel·lular* (aa 47-334)

Es tracta d'una regió extracel·lular glicosilada que separa els dominis transmembrana i conté el lloc d'unió a l'ATP extracel·lular.

Actualment l'estructura del $RP2X_7$ no està totalment descrita ja que no ha pogut ser cristal·litzada. Tot i així gràcies a la cristal·lització del receptor $P2X_4$ del peix zebra ($zfRP2X_4$)[130,131], s'ha pogut generar models informàtics d'homologia que han permès una aproximació acurada al $RP2X_7$[132,133,134]. És sabut que el $RP2X_7$ és homotrimèric, és a dir format per tres subunitats iguals i gràcies a la informació complementària d'aquests models, s'hipotetitza que el conjunt de les diferents subunitats que el formen li donen forma de dofí[135]. En el model de dofí els dominis TM farien de cua i el domini extracel·lular del cos del dofí.

Els dominis TM tenen una mida aproximada de 28 Å i estan formats per sis hèlix α TM, dues de cada subunitat. Dins de cada subunitat, les hèlix α es troben orientades de manera antiparal·lela aproximadament, i es troben en un angle de 45º respecte a la membrana. Les hèlix α que formen el domini TM2 es creuen entre elles a mig camí al llarg del seu domini, provocant la constricció del porus, i per tant definint el receptor en repòs.

El domini extracel·lular té una mida relativament gran, arribant aproximadament a 70 Å per sobre de la membrana. El cos del domini extracel·lular està caracteritzat per làmines β, semblants a l'estructura de la pre-albúmina, que interaccionen en múltiples punts

[130] Kawate, T., Michel, J. C., Birdsong, W.T. & Gouaux, E. Crystal structure of the ATP-gated P2X4 ion channel in the closed state. *Nature*. **2009**, 460, 592–598.
[131] Gonzales, E. B., Kawate, T. & Gouaux, E. Pore architecture and ion sites in acid sensing ion channels and P2X receptors. *Nature*. **2009**, 460, 599–604.
[132] Caseley, E. A., Muench, S. P., Baldwin, S. A., Simmons, K., Fishwick, C. W. & Jiang, L.-H. Docking of competitive inhibitors to the P2X7 receptor family reveals key differences responsible for changes in response between rat and human. *Bioorg. Med. Chem. Lett*. **2015**, 25 (16), 3164–3167.
[133] Caseley, E. A., Muench, S. P., Fishwick, C. W. & Jiang, L.-H. Structure-based identification and characterisation of structurally novel human P2X7 receptor antagonists. *Biochem. Pharmacol.* **2016**, 116, 130–139.
[134] Ahmadi, M., Nowroozi, A. & Shahlaei, M. Constructing an atomic-resolution model of human P2X7 receptor followed by pharmacophore modeling to identify potential inhibitors. *J. Mol. Graph. Model*. **2015**, 61, 243–261.
[135] Jiang, L.-H., Baldwin, J. M., Roger, S. & Baldwin, S. Insights into the Molecular Mechanisms Underlying Mammalian P2X7 Receptor Functions and Contributions in Diseases, Revealed by Structural Modeling and Single Nucleotide Polymorphisms. *Front. Pharmacol.* **2013**, 4, 55.

conferint rigidesa a l'estructura. Tot i que les làmines de la regió distal respecte a la membrana estan interactuant amb subunitats adjacents, la part proximal al domini TM no està en contacte amb cap subunitat. Aquesta conformació podria possibilitar que les hèlix del domini TM canviïn de conformació obrint el canal mitjançant inducció per lligand d'un canvi en la conformació de les regions superiors del domini extracel·lular. Adjuntat al cos del receptor hi ha el cap amb un plegament definit per tres làmines β antiparal·leles i una hèlix α.

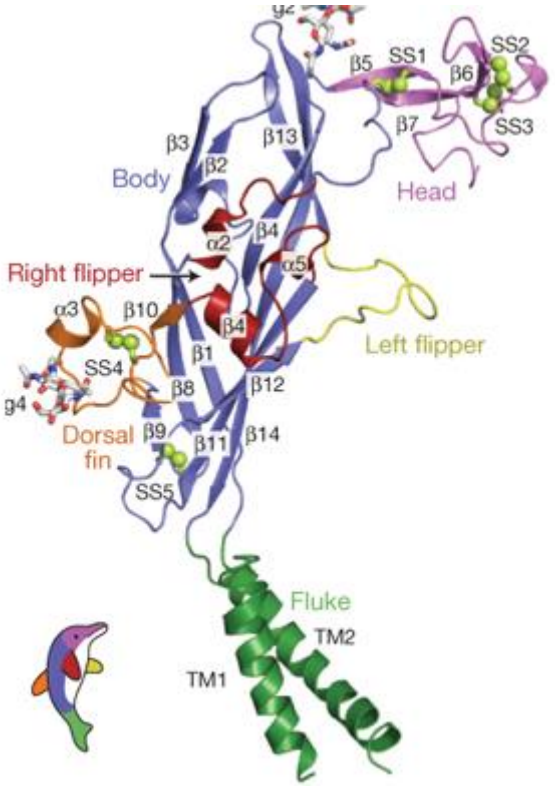

Figura 34. Estructura d'una subunitat de l'homotrímer en forma de dofí. Estan indicades les hèlix α (TM1-2 i α2-5), les làmines β (β1-14), els ponts disulfur (SS1-5) i els glicans units (g2 i g4).

Les interaccions dins d'una subunitat es donen principalment entre els dominis extracel·lulars, essent del tipus: cos-cos, cap-cos, aleta esquerra-aleta dorsal. Els residus que formen el nucli de làmines β en el cos es troben altament conservats, suggerint que les interaccions cos-cos es troben en tots els RP2X. En la determinació de l'estructura del receptor zfRP2X$_4$ es va suggerir que els llocs d'unió del ATP al trímer es troben a uns 45 Å del canal iònic, en profunds solcs extracel·lulars que comprenen subunitats adjacents.

1.5.2 Funció

L'activació del $RP2X_7$ requereix la unió de dues molècules d'adenosina-5'-trifosfat (ATP) extracel·lular que estimulen l'obertura del canal iònic, afavorint l'intercanvi bidireccional de cations de mida petita - sortida de Na^+ i K^+ i entrada de Ca^{2+} - a través de la membrana plasmàtica[136,137].

L'entrada d'ions es pot donar per dues vies. La primera a través de fenestracions localitzades per sobre els dominis TM proximals a la membrana plasmàtica; amb una obertura de 8 Å de diàmetre, aquestes fenestracions permeten l'accés al canal a ions com Ca^{2+}, Na^+ i K^+. Una segona via d'entrada seria a través del domini extracel·lular i de dos grans vestíbuls rics en residus acídics que podrien crear un potencial electrostàtic que concentrés cations a l'entrada extracel·lular del canal. En l'estat tancat del receptor els ions no poden passar per la zona contreta del primer vestíbul ja que és massa petita (~2,3 Å). Tot i així la unió d'un agonista pot induir canvis conformacionals entre les subunitats, produint una petita dilatació que permetria l'accés dels ions al medi intracel·lular.

En condicions d'exposició sostinguda a ATP el $RP2X_7$ es dessensibilitza i dóna lloc a la formació d'un macroporus no selectiu. Aquest deixa passar, a través d'ell, molècules orgàniques d'alt pes molecular, d'entre 600 i 900 Da, incloent aminoàcids, com el glutamat. Tot i que la formació d'aquest porus permet ser estudiada amb tints com el Yo-Pro-1 o bromur d'etidi, el seu mecanisme de formació roman sense determinar [138,139]. Actualment les dues hipòtesis que tenen més força són:

- Dilatació progressiva del canal

En aquesta proposta es contempla la unió d'una tercera molècula d'ATP al receptor, provocant un canvi conformacional del $RP2X_7$. Aquest canvi farà de base estructural per la dilatació del canal tal i com passa en el $RP2X_2$ i el $RP2X_4$

- Via Pannexina-1

Aquest mecanisme involucra l'acció de la Pannexina-1 que és proteïna formadora de porus, l'hemicanal Panx1. Tot i així sembla ser que l'activació d'aquesta proteïna és un

[136] Surprenant, A., Rassendren, F., Kawashima, E., North, R. A. & Buell, G. The cytolytic P2Z receptor for extracellular ATP identified as a P2X receptor (P2X7). *Science* **1996**, 272, 735–738.
[137] Rassendren, F., Buell, G. N., Virginio, C., Collo, G., North, R. A. & Surprenant, A. The permeabilizing ATP receptor, P2X7. Cloning and expression of a human cDNA. *J. Biol. Chem*. **1997**, 272, 5482–5486.
[138] Valera, S., Hussy, N., Evans, R. J., Adami, N., North, A., Surprenant, A. & Buellet, G. A new class of ligand-gated ion channel defined by P2X receptor for extra-cellular ATP. *Nature* **1994**, 371, 516–519.
[139] Sperlágh, B. & Illes, P. P2X7 receptor: an emerging target in central nervous system diseases. *Trends Pharmacol. Sci*. **2014**, 35 (10), 537–547.

efecte de la creació del porus que actua reforçant-lo, però no un requisit per a que aquest es formi[140,141].

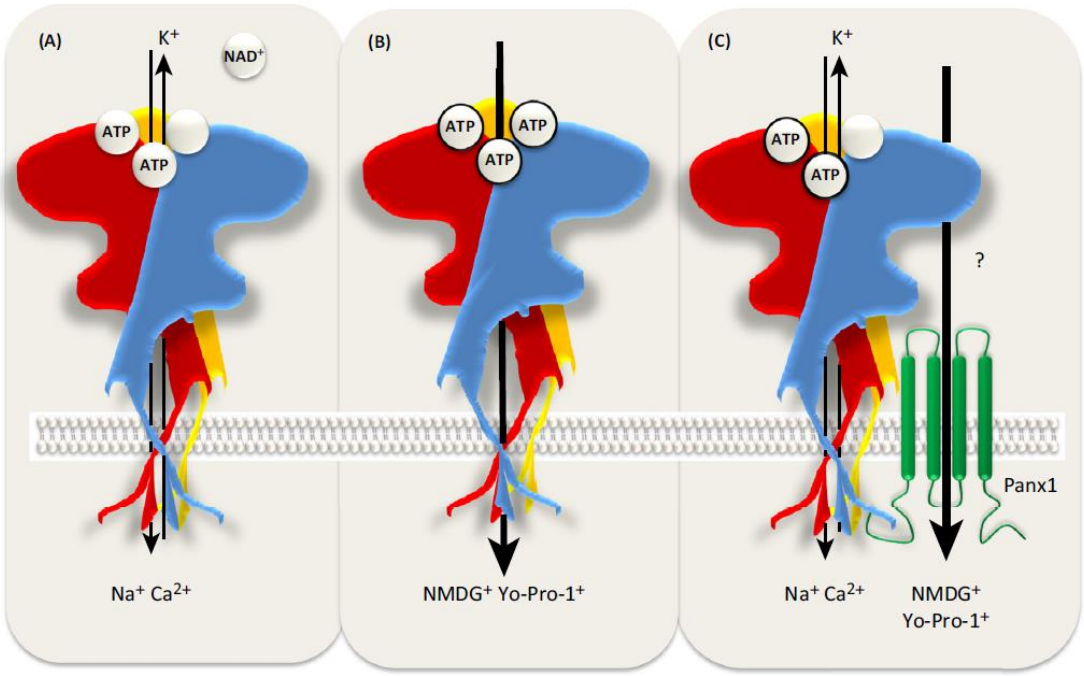

Figura 35. Estructura esquemàtica del $RP2X_7$ en forma oberta (A) i durant la formació del porus (B-hipòtesi de dilatació progressiva, C-Via Pannexina).

La formació d'aquest macroporus donarà lloc a la deformació de la membrana, a l'activació de processos citotòxics i finalment a la mort cel·lular.

L'obertura fisiològica del canal activa cascades bioquímiques relacionades amb la inflamació. En macròfags, l'entrada citosòlica de Ca^{2+} a través del canal iònic compensa la sortida de K^+; aquest influx activa la caspasa-1 que provoca l'activació i alliberació de citocina inflamatòria IL-1β en la seva forma inactiva, pro-IL-1β. La concentració de IL-1β desencadena la inflamació com a resposta i podria estimular altres mediadors de la inflamació, per exemple l'òxid nítric sintasa (NOS), la ciclooxigenasa 2 (COX-2), el Factor Necròtic Tumoral alfa (TNF-α), la fosfolipasa-D (PLD), la fosfolipasa A_2 (PLA_2), el Factor Nuclear Kappa-B (NK-κB) o la protein-quinasa activada per mitògens (MAPKs). Per tant, es

[140] Alberto, A.V.P., Faria, R. X., Couto, C. G. C., Ferreira, L. G. B., Souza, C. A. M., Teixeira, P. C. N., Fróes, M. M. & Alves, L. A. Is pannexin the pore associated with the P2X7 receptor? *Naunyn Schmiedebergs Arch. Pharmacol*. **2013**, 386, 775–787.

[141] Xu, X. J., Boumechache, M., Robinson, L. E., Marschall, V., Gorecki, D. C., Masin, M. & Murrell-Lagnado, R. D. Splice variants of the P2X7 receptor reveal differential agonist dependence and functional coupling with pannexin-1. *J. Cell Sci.* **2012**, 125 (16), 3776-3789.

pot dir que tots els mediadors esmentats anteriorment contribueixen a les vies de senyalització inflamatòries desencadenades per l'activació del $RP2X_7$[142] .

Els lisosomes secretors són alliberats a l'espai pericel·lular pinçant la membrana plasmàtica mitjançant un procés que requereix pèrdua de K^+, i per tant un increment d'ions Ca^{2+}, i l'activació de la PLC.

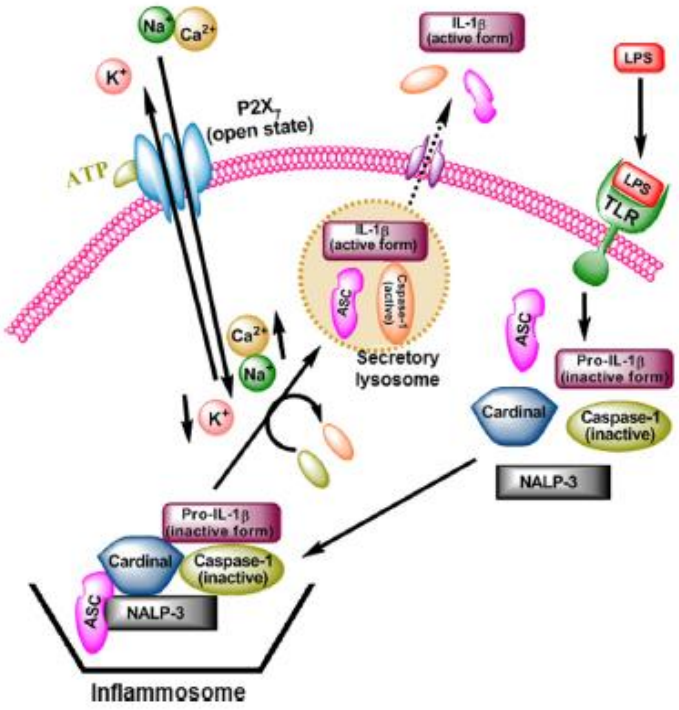

Figura 36. Activació del receptor $P2X_7$: Formació de l'inflamasoma.

Cal mencionar que el $RP2X_7$ té unes propietats farmacològiques característiques que el diferencien de la resta de receptors ionotròpics purinèrgics (P2), aquestes són:

1. Baixa afinitat per l'ATP. Calen concentracions de l'ordre micromolar alt (~100 μM) per activar-lo.

2. L'agonista 2,3-O-(4-benzoilbenzoil)-ATP (BzATP) que és 10 vegades més potent que l'ATP, activa els $RP2X_7$ selectivament[143].

3. Després d'aplicacions repetides del mateix agonista les constants de velocitat de tancament del canal i amplitud de resposta canvien dràsticament, fent que el receptor no es dessensibilitzi.

[142] Garcia-Marcos, M., Pochet, S., Marino, A. & Dehaye, J-P. P2X7 and phospholipid signalling: The search of the "missing link" in epithelial cells. *Cell. Signal.* **2006**, 18(12), 2098–2104.
[143] S. Alloisio, S., Di Garbo, A., Barbieri, R., Bozzo, L., Ferroni, S. & Nobile, M. Evidence for two conductive pathways in P2X receptor: differences in modulation and selectivity. *J. Neurochem.* **2010**, 113, 796–806.

1.5.3 Malalties relacionades[144]

El $RP2X_7$ es troba àmpliament distribuït per l'organisme fent que la seva malfunció estigui relacionada amb múltiples processos patològics, a través de l'activació de processos inflamatoris i de toxicitat cel·lular. Tot i que inicialment la presència d'aquests receptors en el SNC va generar molta controvèrsia, avui en dia la seva implicació en malalties neurològiques està totalment acceptada i és l'àrea més prometedora a nivell terapèutic[145,146,147]. Algunes de les implicacions d'aquest receptor ionotròpic es troben en:

La inducció, i manteniment del *dolor neuropàtic i inflamatori*. El $RP2X_7$ juga un paper clau en la regulació, l'expressió i secreció de varies citocines i altres mediadors inflamatoris.

El *sistema immunològic*. Es troben implicats en la formació de granulomes, com ara les cèl·lules gegants multinucleades (MGC) o en la protecció davant de micobacteris.

Processos apoptòtics. Com s'ha dit anteriorment, una estimulació excessiva del receptor comporta la mort cel·lular, ja que pot activar la via de la caspasa, moduladora essencial en la mort induïda de la cèl·lula.

Diabetis tipus II. El $RP2X_7$ està involucrat en l'alliberament de IL-Ra per part de les cèl·lules pancreàtiques β, no només per a l'alliberament de citocines sinó també per l'alliberament d'insulina. En individus obesos el $RP2X_7$ es troba sobreexpressat, mentre que en persones amb diabetis tipus I aquests receptors són quasi bé indetectables; és per això que es pensa que el $RP2X_7$ realitza un mecanisme compensatori en resposta a un augment en la demanda d'insulina.

Malalties infeccioses. Els $RP2X_7$ es troben involucrats en mecanismes de l'hoste per eliminar microorganismes que parasiten els macròfags com ara el *Mycobacterium*, la *Leishmania* i la *Chlamydia*.

Càncer. S'han associat els alts nivells de TNF-α i de IL-1β, dels quals el $RP2X_7$ en regula l'alliberació, amb l'increment d'incidència de càncer prostàtic i gàstric, respectivament.

---

[144] De Marchi, E., Orioli, E., Dal Ben, D. & Adinolfini, E. P2X7 receptor as a therapeutic target. *Adv. Protein Chem. Struct. Biol*. **2016,** 104, 39-79

[145] Rech, J. C., Bhattacharya, A., Letavic, M. A., & Savall, B. M. The evolution of P2X7 antagonists with a focus on CNS indications. *Bioorg. Med. Chem. Lett.* **2016**, 26(16), 3838–3845.

[146] Tewari, M. & Seth, P. Emerging role of P2X7 receptors in CNS health and disease. *Ageing Res. Rev*. **2015**, 24, 328–342.

[147] Skaper, S. D., Debetto, P. & Giusti, P. The P2X7 purinergic receptor: from physiology to neurological disorders. *FASEB J*. **2010**, 24(2), 337–345.

Cal afegir que s'està investigant l'ús d'antagonistes dels $RP2X_7$ en altres patologies inflamatòries com ara la Malaltia Pulmonar Obstructiva Crònica (MPOC) o la inflamació de la bufeta.

Malalties del SNC. Els receptors $P2X_7$ es troben expressats a les terminals nervioses, als astròcits i a la microglia, on prenen part en múltiples vies bioquímiques relacionades amb processos patològics d'etiologia diversa en el SNC. A més a més s'ha vist que en molts d'aquests processos, es troben sobreexpresats.

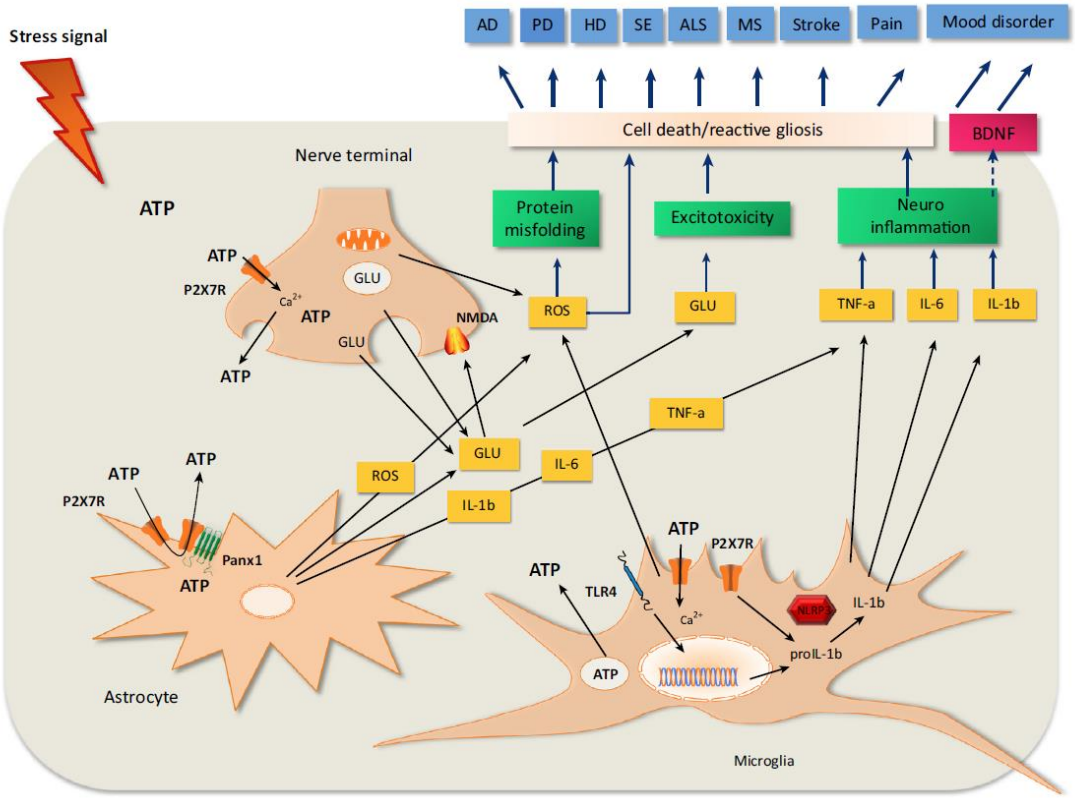

Figura 37. Cascades bioquímiques de mort cel·lular activades pel $RP2X_7$ en el SNC.

Davant de senyals d'estrès com ara en condicions d'hipòxia, lesió mecànica o toxicitat química o bacteriana, es produeix l'activació endògena del $RP2X_7$. Aquesta activació és capaç d'autoamplificar-se, provocant l'alliberació de més ATP que anirà a activar els $RP2X_7$ de les cèl·lules veïnes. Així doncs s'alliberaran grans quantitats de Ca^{2+} a través del canal, que provocaran:

- Alliberació de glutamat des de les terminals nervioses i astròcits. Aquest pot arribar a nivells excitotòxics provocant la mort neuronal, per exemple per sobreactivació dels RNMDA. (veure Capítol 8)

- Maduració de les IL-β i alliberació d'aquestes per la NLRP3 de l'inflamasoma, que a la vegada alliberarà altres citocines que contribuiran a una major neuroinflamació.

- Increment de la producció d'espècies d'oxigen reactives (ROS), per tant agreujarà les lesions neuronals i el mal plegament de proteïnes.

- La conducció directa- o indirectament a la mort neuronal i a l'astrogliosi reactiva.

- Disminució de la producció del factor neurotròfic cerebral (BDNF) i conseqüentment de la plasticitat neuronal.

Tots aquests mecanismes derivats de l'activació del receptor $P2X_7$ poden ser els desencadenants o agreujants de: la malaltia d'Alzheimer (AD), la malaltia de Parkinson (PD), la malaltia de Huntington (HD), epilèpsia (SE), esclerosi lateral amiotròfica (ALS), esclerosi múltiple (MS), infart, dolor i alteració de l'estat d'ànim.

1.5.4 Gamma de fàrmacs

Actualment no es disposa de cap fàrmac comercial que tingui com a diana el receptor $P2X_7$. Tot i així les incomptables oportunitats d'intervenció terapèutica que ofereix aquest receptor, han fet que en els últims deu anys hi hagi hagut un increment exponencial de la recerca en aquest camp. Això ha donat a conèixer múltiples molècules de baix pes molecular capaces d'exercir una activitat biològica potent sobre aquest receptor.

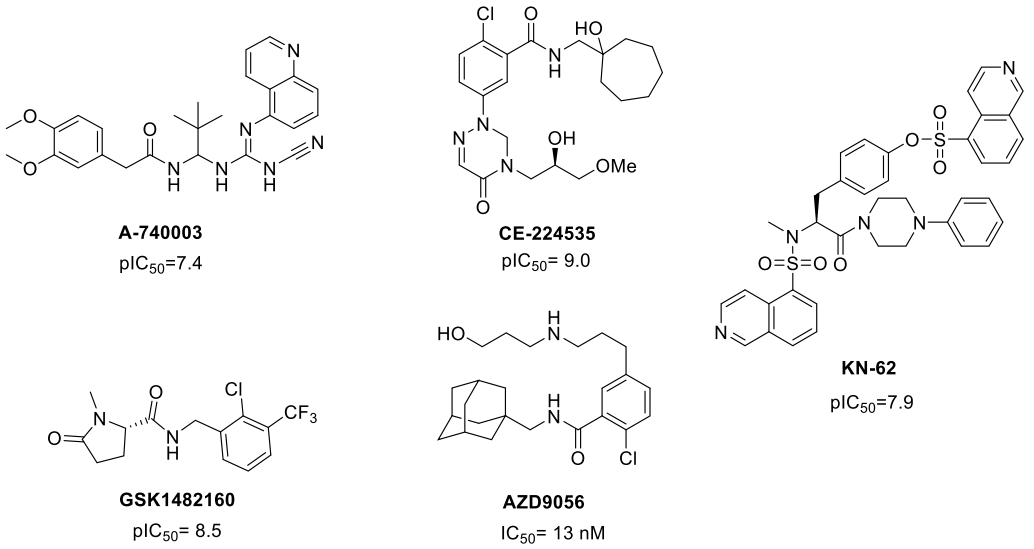

Figura 38. Compostos antagonistes del $RP2X_7$.

Inicialment la recerca estava dirigida en el desenvolupament de compostos amb caràcter antiinflamatori perifèric o pel tractament de l'artritis reumatoide, fent que durant el període d'entre el 2008 i el 2013 apareguessin més de 50 patents per a aquestes

indicacions[148,149]. Tot i així amb l'estrepitós fracàs en fase clínica IIb del compost AZD9056[150], desenvolupat per AstraZeneca pel tractament de l'artritis reumatoide, ha fet que en aquest últim període es busqui una acció a nivell de SNC o càncer[19]. En aquesta línia trobem els anticossos desenvolupats per Biosceptre (BIL010t, BIL03s i BIL06v), que actualment es troben en fase clínica.

Segons l'anteriorment esmentat el $RP2X_7$ es tracta d'una diana farmacologica molt versàtil i relativament inexplorada. Per a aquest motiu i tenint en compte l'interès del nostre grup en el desenvolupament de molècules de baix pes molecular com a moduladors de canals iònics, així com el fet que múltiples compostos amb activitat sobre el $RPP2X_7$ presenten una estructura adamantànica, la qual el nostre grup n'és expert en modificar, ens va fer iniciar una nova línia de recerca basada en aquest receptor, els primers resultats de la qual s'han obtingut durant la present Tesi.

[148] Friedle, S. A., Curet, M. A, & Watters, J. J. Recent patents on novel $P2X_7$ receptor antagonists and their potential for reducing central nervous system inflammation. *Recent Pat. CNS Drug Discovery* **2010**, 5(1), 35–45.
[149] Nagy, J. Recent Patents on Novel P2X7 Receptor Antagonists Potentially Effective for Treatment of Inflammatory Diseases. *Recent Pat. Biomarkers* **2013**, 1–24.
[150] Keystone, E. C., Wang, M. M., Layton, M., Hollis, S. & McInnes, I. B. Clinical evaluation of the efficacy of the P2X7 purinergic receptor antagonist AZD9056 on the signs and symptoms of rheumatoid arthritis in patients with active disease despite treatment with methotrexate or sulphasalazine. *Ann. Rheum. Dis.* **2012**. 71 (10), 1630–1635.

1.6. RECEPTOR GLUTAMATÈRGIC IONOTRÒPIC NMDA

El glutamat és el principal neurotransmissor excitatori a nivell de SNC en els mamífers i juga un paper fonamental en nombroses funcions fisiològiques, participant en processos de percepció sensorial primària i de cognició[151,152,153,154,155]. La neurotransmissió glutamatèrgica en el SNC és el resultat de l'alliberament presinàptic de glutamat en l'escletxa sinàptica. El glutamat alliberat interacciona amb nombrosos tipus de receptors, que poden ser ionotròpics i/o metabotròpics, localitzats en les membranes plasmàtiques presinàptica i postsinàptica (Figura 39)[156,157,158] .

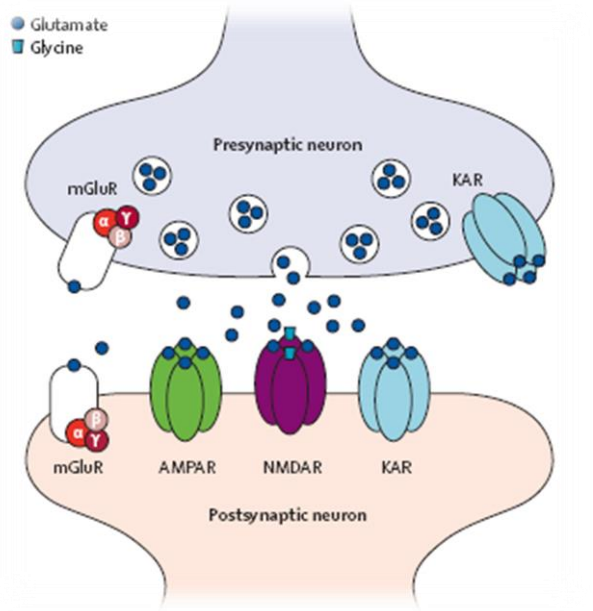

Figura 39. Sinapsi excitatòria del SNC: el glutamat és alliberat per vesícules presinàptiques en l'escletxa sinàptica on actuen sobre dos tipus de receptors: els receptors ionotròpics i els receptors metabotròpics.

Els receptors metabotròpics (mGluR) estan acoblats a proteïnes G i n'hi ha de tres tipus: grup I (mGlu1 i mGlu5), grup II (mGlu2 i mGlu3) i grup III (mGlu4, mGlu6, mGlu7 i mGlu8).

[151] Bräuner-Osborne, H., Egebjerg, J., Nielsen, E. O., Madsen, U. & Krogsgaard-Larsen, P. Ligands for glutamate receptors: design and therapeutic prospects. *J. Med. Chem.* **2000**, *43*, 2609-2645.
[152] Newcomer, J. W. & Krystal, J. H. NMDA receptor regulation of memory and behavior in humans. *Hippocampus* **2001**, *11*, 529-542.
[153] Danbolt, N. C. Glutamate uptake. *Prog. Neurobiol.* **2001**, *65*, 1-105.
[154] Bleich, S., Römer, K., Wiltfang, J. & Kornhuber, J. Glutamate and the glutamate receptor system: a target for drug action. *Int. J. Geriatr. Psychiatry* **2003**, *18*, S33-S40.
[155] Featherstone, D. E. Intercellular glutamate signalling in the Nervous System and beyond. *ACS Chem. Neurosci.* **2010**, *1*, 4-12.
[156] Kalia, L. V., Kalia, S. K. & Salter, M. W. NMDA receptors in clinical neurology: excitatory times ahead. *Lancet Neurol.* **2008**, *7*, 742.
[157] Ozawa, S. Kamiya, H. & Tsuzuki, K. Glutamate receptors in the mammalian central nervous system. *Prog. Neurobiol.* **1998**, *54*, 581-618.
[158] Dingledine, R., Borges, K., Bowie, D. & Traynelis, S. F. The glutamate receptor ion channels. *Pharmacol. Rev.* **1999**, *51*, 7-61.

Els receptors ionotròpics són canals iònics dependents de lligand i permeables als cations monovalents Na^+ i K^+ i, dependent del subtipus, també a Ca^{2+}. Fins el moment, s'han identificat tres tipus de receptors ionotròpics en base a l'afinitat selectiva per agonistes específics: receptors NMDA (*N*-metil-D-aspartat)[159,160,161,162], receptors kainat[163,164,165], i receptors AMPA [àcid α-amino-3-(3-hidroxi-5-metil-4-isoxazolil)propiònic][166,167]. Més recentment, s'ha descobert una quarta família de receptors ionotròpics: els receptors delta (GluD1 i GluD2)[168,169].

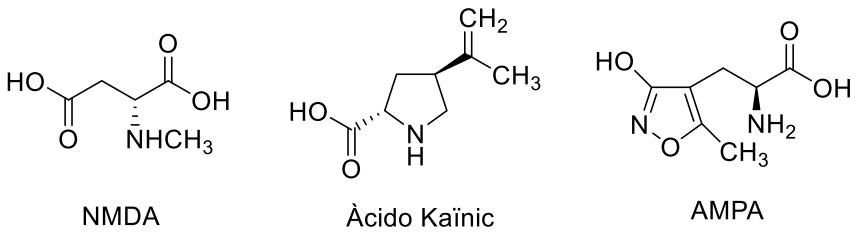

Figura 40. Agonistes que permeten la classificació dels receptors ionotròpics.

1.6.1 Estructura dels receptors NMDA

Els receptors de N-metil-D-aspartat (NMDA) són tetràmers heterogenis, formats per dos heterodímers, del voltant dels 1500 aminoàcids. La proteïna necessita de dos parells de subunitats diferents en la seva estructura per ser funcional[170], normalment aquestes són GluN1, que conté el lloc d'unió a glicina i GluN2, que conté el lloc d'unió a glutamat[171]. Cal mencionar que existeixen també heterodímers de GluN1 amb GluN3 (lloc d'unió per D-serina) expressats àmpliament pel sistema nerviós, tot i així la funció d'aquests receptors està menys definida i no els tractarem aquí.

[159] Yamakura, T. & Shimoji, K. Subunit- and site-specific pharmacology of the NMDA receptor channel. *Prog. Neurobiol.* **1999**, *59*, 279-298

[160] Chazot, P. L. & Hawkins, L. M. NMDA receptor subtypes- rationale for future CNS therapies. *Drugs* **1999**, *2*, 1313.

[161] Cull-Candy, S., Brickley, S. & Farrant, M. NMDA receptor subunits: diversity, development and disease. *Curr. Opin. Neurobiol.* **2001**, *11*, 327-335

[162] Paoletti, P. & Neyton, J. NMDA receptor subunits: function and pharmacology. *Curr. Opin. Pharmacol.* **2007**, *7*, 39-47.

[163] Huettner, J. E. Kainate receptors and synaptic transmission. *Prog. Neurobiol.* **2003**, *70*, 387-407.

[164] Isaac, J. T. R., Mellor, J., Hurtado, D. & Roche, K. W. Kainate receptor trafficking: physiological roles and molecular mechanisms. *Pharmacol. Ther.* **2004**, *104*, 163-172.

[165] Jane, D. E., Lodge, D. & Collingridge, G. L. *Neuropharmacol.* **2009**, *56*, 90-113.

[166] Lees, G. J. Kainate receptors: pharmacology, function and therapeutic potential. *Drugs* **2000**, *59*, 33-78.

[167] Jayakar, S. S. & Dikshit, M. AMPA receptor regulation mechanisms: future target for safer neuroprotective drugs. *Intern. J. Neurosci.* **2004**, *114*, 695-734.

[168] Suryavanshi, P. S., Gupta, S. C., Yadav, R., Kersherwani, V., Liu, J. & Dravid, S. M. Glutamate Delta-1 receptor regulates metabotropic glutamate receptor 5 signaling in the hippocampus. *Mol. Pharmacol.* **2016**, *90*, 96-105.

[169] Orth, A., Tapken, D. & Hollmann, M. The delta subfamily of glutamate receptors: characterization of receptor chimeras and mutants. *Eur. J. Neurosci.* **2013**, *37*, 1620-1630.

[170] Prof. Jon Johnson (Pittsburgh Center for Pain Research, University of Pittsburgh), lecture at Faculty of Pharmacy (Universitat de Barcelona). 16th March 2016.

[171] Moriyoshi, K., Masu, M., Ishii, T., Shigemoto, R., Mizuno, N. & Nakanishi, S. Molecular cloning and characterization of the rat NMDA receptor. *Nature*. **1991**, 354 (6348), 1-7.

Al llarg del receptor NMDA, podem distingir-ne les següents parts:

- un *domini carboxi-terminal intracel·lular* (CTD) que s'associa amb proteïnes post-sinàptiques, facilitant la senyalització intracel·lular.

- un *domini transmembrana* (TMD) que forma el canal iònic o porus.

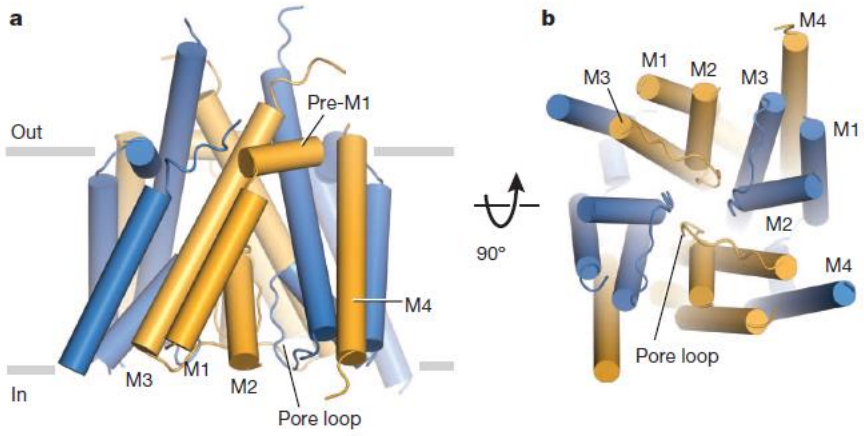

Figura 41. Arquitectura del domini transmembrana (GluN1 en blau i GluN2B en taronja). Esquerra: Esquema del TMD paral·lel a la membrana. Dreta: Vista del porus que forma el TMD des de la regió citoplasmàtica (des de dins de la cèl·lula).

- dos dominis extracel·lulars:

el *domini amino-terminal* (ATD) que contribueix al control de la velocitat d'obertura i desactivació del canal iònic. Conté llocs d'unió per als moduladors al·lostèrics de NMDA. Cada subtipus presenta una especificitat diferent per al modulador al·lostèric, trobant-ne el zinc (GluN2A i 2B), l'ifenprodil (GluN2B) i poliamines diverses (GluN2B)[172]. L'ATD és la principal regió de control de les propietats farmacològiques i biofísiques del canal[173].

el *domini d'unió del lligand* (LBD) en el que trobem els llocs d'unió per al magnesi i per a les molècules de baix pes molecular que regulen l'obertura i el tancament del porus.

Les regions de la proteïna queden doncs, disposades en tres capes; de fora a dintre (de més allunyat de la membrana fins a arribar a aquesta): ATD, LBD i TMD.

[172] Yuan, H., Hansen, K. B., Vance, K. M., Ogden, K. K. & Traynelis, S. T. Control of N-methyl-D-aspartate Receptor Function by the NR2 Subunit Amino-Terminal Domain. *J Neurosci.* **2009**, 29 (39), 12045–12058.
[173] Gielen, M., Siegler, B., Retchless, L. M., Johnson, J. W. & Pierre Paoletti. Mechanism of differential control of NMDA receptor activity by NR2 subunits. *Nature Lett.* **2009**, 459, 703-707.

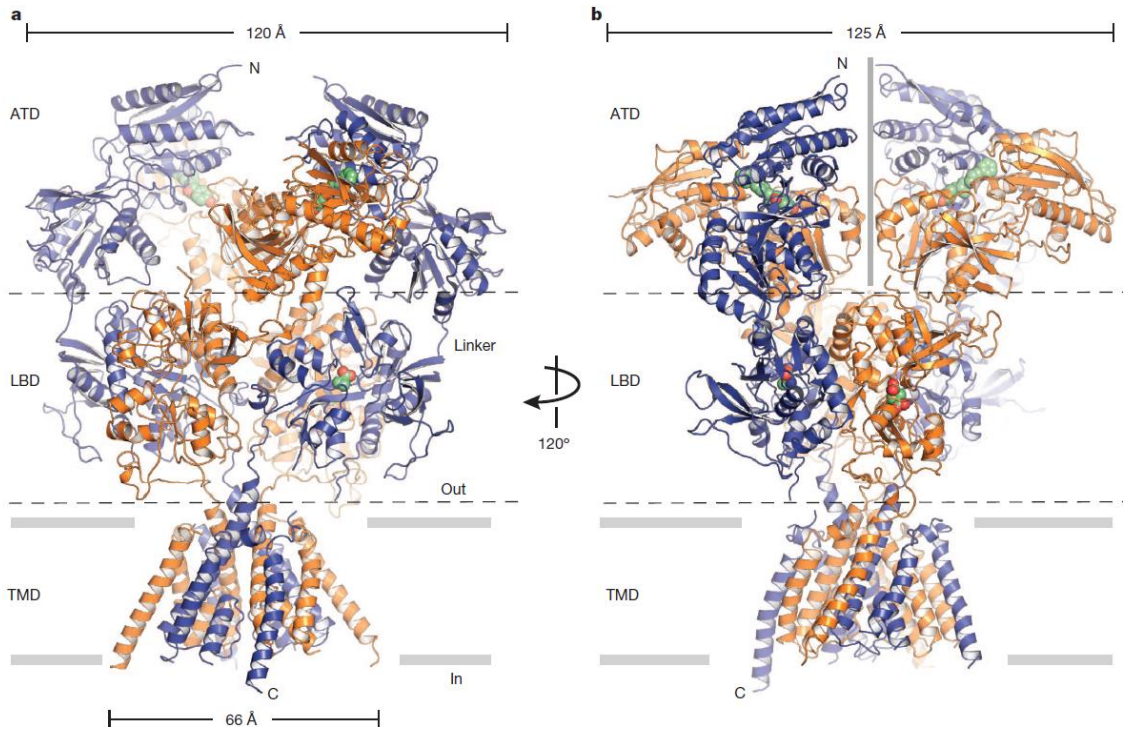

Figura 42. Arquitectura, simetria i organització del receptor d'NMDA de glutamat GluN1 (de color blau) - GluN2B (de color groc). Esquerra: Receptor paral·lel a la membrana. Dreta: Rotació de 120º sobre l'eix de simetria del receptor. Veure figura 43 per una representació esquemàtica i millor comprensió de les estructures cristal·lines.

L'estructura i el mecanisme de comporta d'aquesta enorme proteïna no són encara entesos en la seva totalitat. Tot i així la determinació per Raig X de l'estructura de l'NMDA l'any 2014 pels grups de Furukawa[174] i Gouaux[175] va marcar un abans i un després en la seva comprensió estructural. Dos anys més tard, al 2016, aquests dos mateixos grups van aclarir-ne el mode de funcionament mitjançant la resolució d'estructures amb moduladors units a NMDA, emprant la innovadora tècnica de crio-microscòpia electrònica[176] ajudada de ressonància de doble electró-electró[177], en el cas del grup de Gouaux[178], i de cristal·lografia de raig X i electrofisiologia, en el cas de Furukawa[179].

[174] Karakas, E. & Furukawa, H. Crystal structure of a heterotetrameric NMDA receptor ion channel. *Science*. **2014**, 344 (6187), 992–997.
[175] Lee, C.-H., Lü, W., Michel, J. C., Goehring, A., Du, J., Song, X. & Gouaux, E. NMDA receptor structures reveal subunit arrangement and pore architecture. *Nature*. **2014**, 511(7508), 191–197.
[176] Cheng, Y. Leading Edge Review: Single particle cryo-EM at crystallographic resolution. *Cell*. **2015**, 161, 450-457.
[177] Mchaourab, H. S., Steed, P. R. & Kazmier, K. Structure. Toward the Fourth Dimension of Membrane Protein Structure: Insight into Dynamics from Spin-labeling EPR Spectroscopy. *Structure*. **2011**, 19 (11), 1549–1561.
[178] Zhu, S., Stein, R. A., Yoshioka, C., Lee, C. H., Goehring, A., McHaourab, H. S. & Gouaux, E. Mechanism of NMDA Receptor Inhibition and Activation. *Cell*. **2016**, 165 (3), 704–714.
[179] Tajima, N., Karakas, E., Grant, T., Simorowski, N., Diaz-Avalos, R., Grigorieff, N. & Furukawa, H. Activation of NMDA receptors and the mechanism of inhibition by ifenprodil. *Nature*. **2016**, 534 (7605), 1–17.

Gràcies aquests estudis se sap que el receptor d'NMDA de glutamat (GluN1–GluN2B) té una forma que s'assembla a la d'un bolet, amb una alçada de 150 A° i amplades de 123 per 120 A°. La seva estructura general presenta una simetria doble gràcies a la disposició doblement dimèrica del tipus GluN1-2-1-2, en la qual els dominis extracel·lulars ATD i LBD formen parells de dímers (simetria 2x) i el domini transmembrana (TMD) queda en forma de porus pseudotetramèric (simetria pseudo 4x).

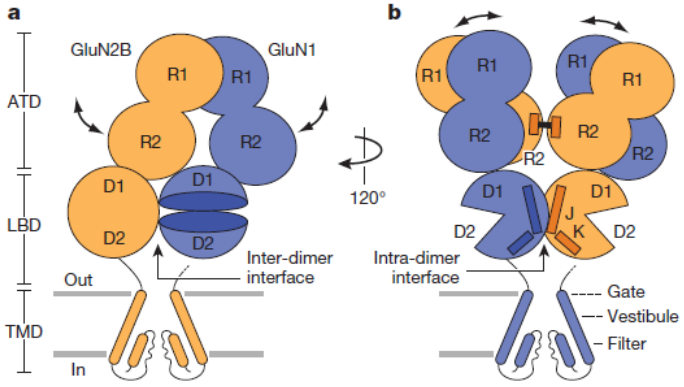

Figura 43. Representació esquemàtica del receptor NMDA.

1.6.2 Funció dels receptors NMDA[180]

Els receptors NMDA (RNMDA) regulen la funcionalitat i plasticitat estructural de sinapsis individuals, dendrites i neurones, per mitjà de l'activació de cascades de senyalització dependents de Ca^{2+} i, a diferència d'altres iGlu, no són fonamentals per a la transmissió sinàptica basal. L'explicació es troba en el seu mecanisme d'acció. El canal NMDA és classificat com a tipus Hebbian[181], ja que la seva activació requereix una prèvia despolarització de la membrana per eliminar el blocatge voltatge dependent del magnesi sobre el canal. Un cop lliure de magnesi el canal NMDA requereix la unió de dues molècules dels co-agonistes glutamat i glicina per ser activat, permetent així l'entrada de Ca^{2+} a l'espai intracel·lular[182]. És a dir, el RNMDA presenta dependència a voltatge i a lligand.

[180] Hardingham, G. E. & Bading, H. Synaptic versus extrasynaptic NMDA receptor signalling: implications for neurodegenerative disorders. *Nat. Rev. Neurosci*. **2010**, 11(10), 682–696.
[181] Hebb, D.O. The Organization of Behavior. New York: Wiley & Sons. **1949**.
[182] Lipton, S. Paradigm shift in neuroprotection by NMDA receptor blockade: memantine and beyond. Nat. Rev. *Drug Discov.* **2006**, 5(2), 160–170.

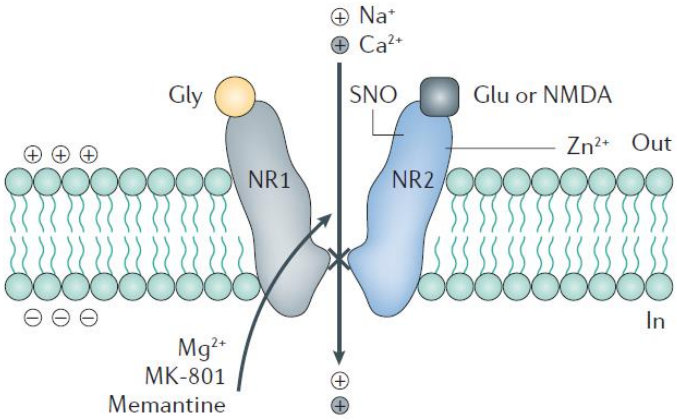

Figura 44. Representació esquemàtica dels llocs d'unió i modulació del receptor de NMDA.

La glicina és un aa que es sol trobar en concentracions del rang mil·limolar baix en el medi extracel·lular del sistema nerviós (SN); per exemple el fluid cerebroespinal conté 4.2 μM de Gly. Aquest fet fa que els llocs d'unió a glicina (EC_{50} ~ 1 μM) en el receptor NMDA, es trobin normalment ocupats. Per tant, el que regula l'activació del receptor és el glutamat extracel·lular. El glutamat es tracta del neurotransmissor (NT) més important del SNC i és alliberat des de les terminals presinàptiques a les sinapsis glutamatèrgiques, unint-se en el LBD de la subunitat GluN2 del receptor NMDA pel que té una EC_{50} de 2.9 μM[183]. Es creu que l'efecte de la unió dels co-agonistes glutamat i glicina, és l'estabilització del LBD heterodimèric i l'anell de comporta, permetent la correcta estructura per a l'activació del receptor[9].

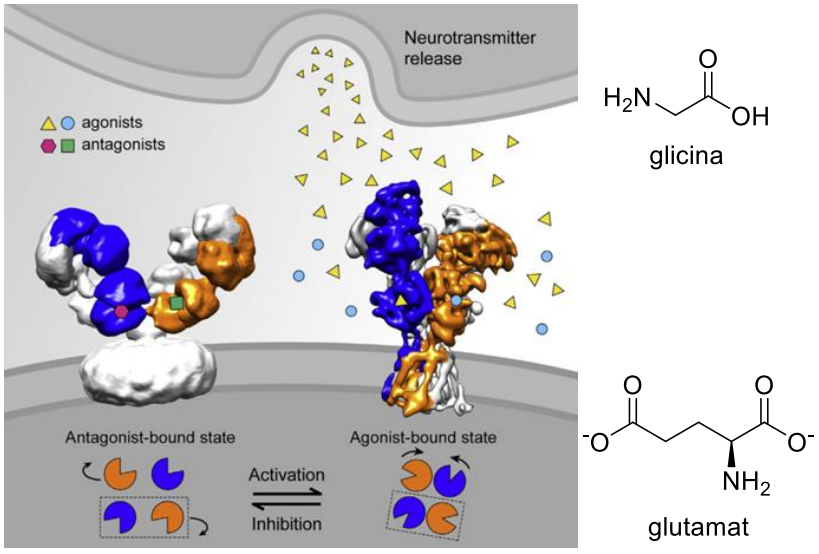

Figura 45. Co-agonistes del receptor NMDA i canvis de conformació d'aquest.

[183] Vyklicky, V., Korinek, M., Smejkalova, T., Balik, A., Krausova, B., Kaniakova, M., Lichnerova, K., Cerny, J., Krusek, J., Dittert, I., Horak, M. & Vyklicky, L. Structure, function, and pharmacology of NMDA receptor channels. *Physiol. Res*. **2014**. 63 (Suppl. 1): S191-S203.

En condicions fisiològiques la concentració d'aquests aa a les sinapsis és del rang de nM. Quan té lloc l'alliberació de glutamat, aquest arriba a una concentració màxima del voltant de 1mM i, en qüestió de mil·lisegons, és eliminat de la sinapsis per mitjà de difusió i sistemes de recaptació. Aquesta breu exposició al glutamat és suficient per activar el canal NMDA unit a glicina, coneguda com a activació fàsica i que contribueix a la transmissió sinàptica normal. Tot i així aquesta excitació sinàptica no donarà lloc a l'entrada de Ca^{2+} ja que, com s'ha mencionat prèviament, els RNMDA també són voltatge dependents.

Quan ens trobem en potencial de membrana de repòs (-70mV) els cations de Mg^{2+} que es troben en concentracions mM a l'espai extracel·lular de les neurones, entren al porus del receptor NMDA ja que les concentracions de Mg^{2+} dins d'aquestes neurones són del rang μM. Un cop al porus s'hi uneixen de manera forta, evitant-ne la permeació a través d'ell. Davant d'una despolarització forta i sostinguda (suficient amplitud i duració), aquests cations Mg^{2+} són desplaçats del porus, permetent l'activació del canal NMDA i el pas selectiu a cations, conegut com a activació tònica. En concret el receptor de NMDA és especialment permeable a Ca^{2+}, missatger clau en processos de plasticitat neuronal i memòria[184].

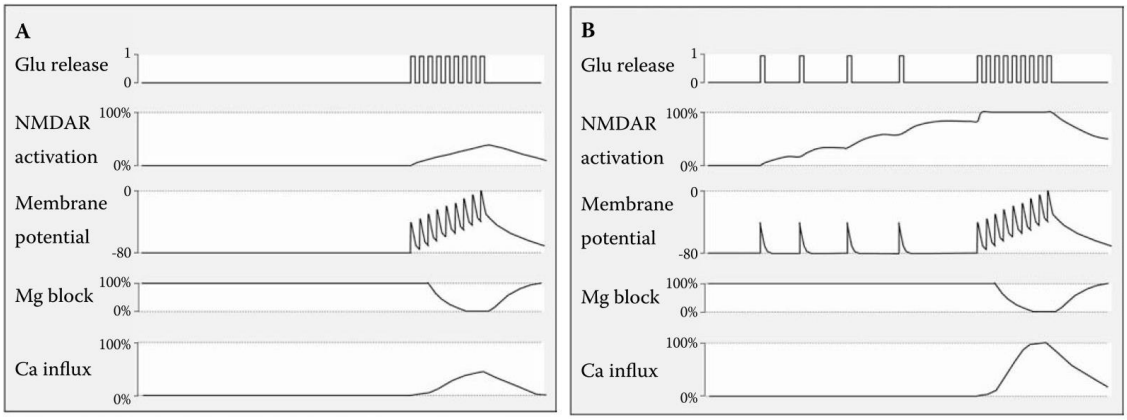

Figura 46. Exemplificació dels estímuls sinàptics rebuts pel receptor NMDA. A causa de l'alta afinitat pel glutamat i la cinètica d'activació i desactivació lenta del receptor, aquests poden "memoritzar" estímuls sinàptics de baixa freqüència, que no generen pas d'ions a través del receptor a causa del bloqueig per Mg^{2+}. Això farà que davant la despolarització de la membrana, el pas de calci sigui molt més gran en el cas que hi hagi hagut estimulació sinàptica prèvia (B vs A), permetent la creació de memòria[185].

[184] Traynelis, S. F., Wollmuth, L. P., McBain, C. J., Menniti, F. S., Vance, K. M., Ogden, K. K., Hansen, K. B., Yuan, H., Myers, S. J. & Dingledine, R. Glutamate receptor ion channels: structure, regulation, and function. *Pharmacol. Rev.* **2010**, 62 (3), 405-96.
[185] Van Dongen, A. M. Biology of the NMDA Receptor. Boca Raton (FL): CRC Press/Taylor & Francis; **2009**.

Seguidament, el receptor passarà a un estat de dessensibilització induït per l'entrada de calci a les neurones i es mantindrà, més o menys temps, en aquest estat en funció del calci extracel·lular. La glicina també pot conduir a una dessensibilització del receptor; aquesta però, es reverteix a concentracions de saturació de gly. Finalment el canal tornarà al seu estat de repòs amb la cessació de la presència sostinguda de glutamat[14].

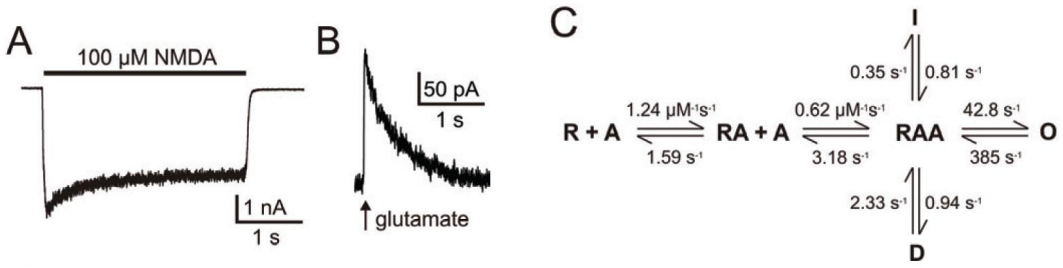

Figura 47. A: Activació tònica (NMDA aplicat 3s): Després d'una activació ràpida, comença la dessensibilització que es va fent més gran amb el temps. Quan el NMDA és retirat, el receptor es desactiva. B: Activació fàsica (alliberació sinàptica de glutamat): Després d'una activació ràpida, el receptor NMDA es desactiva amb una cinètica de velocitat de doble exponencial. C: Esquema de la cinètica d'activació del receptor (R= receptor; A= agonista; O= canal obert; I = canal dessensibilitzat pel calci; D = canal dessensibilitzat per la glicina).

1.6.3 Malalties associades

Com ja s'ha comentat prèviament, els RNMDA es troben majoritàriament a l'espai perisinàptic, on juguen un paper fonamental en la plasticitat neuronal, essent el màxim regulador dels processos d'aprenentatge i memòria. Tot i així també hi ha receptors NMDA pre- o extra-sinàptics, la funció fisiològica dels quals no ha estat totalment esclarida.

Els efectes globals de l'activació d'aquest receptor són paradoxals; per una banda poden ser neuroprotectors i per l'altra excitotòxics, provocant la mort neuronal[186]. Aquest fet ha estat explicat durant molt de temps per la teoria que diu que les respostes neuronals a l'activitat RNMDA segueixen una corba en forma de campana. Segons això tant una resposta desmesurada com una resposta insuficient, resultarien nocives[187,188].

[186] Lipton, S. A. & Kater, S. B. Neurotransmitter regulation of neuronal outgrowth, plasticity and survival. *Trends Neurosci*. **1989**, 12, 265–270.
[187] Lipton, S. A. & Nakanishi, N. Shakespeare in Love - with NMDA receptors? *Nature Med*. **1999**, 5, 270–271.
[188] Hardingham, G. E. & Bading, H. The Yin and Yang of NMDA receptor signalling. *Trends Neurosci.* **2003**, 26, 81–89.

Els estudis més recents han detallat aquesta teoria, demostrant que l'efecte de l'activació del RNMDA depèn de dos factors: de la localització d'aquest receptor[189] i del temps d'exposició a glutamat. Així doncs, mentre que l'estimulació dels RNMDA sinàptics promou la salut neuronal, l'activació dels extrasinàptics, pot activar vies de mort neuronal[190]. Tenint en compte això, la sobreexposició dels RNMDA extrasinàptics a glutamat, causa una activació excessiva del receptor que indueix excitotoxicitat mitjançada pel calci. Per tant, no és només la sobreexposició indiscriminada al glutamat el que promou la mort neuronal, sinó el fet que aquesta tingui lloc sobre un tipus concret de receptor NMDA.

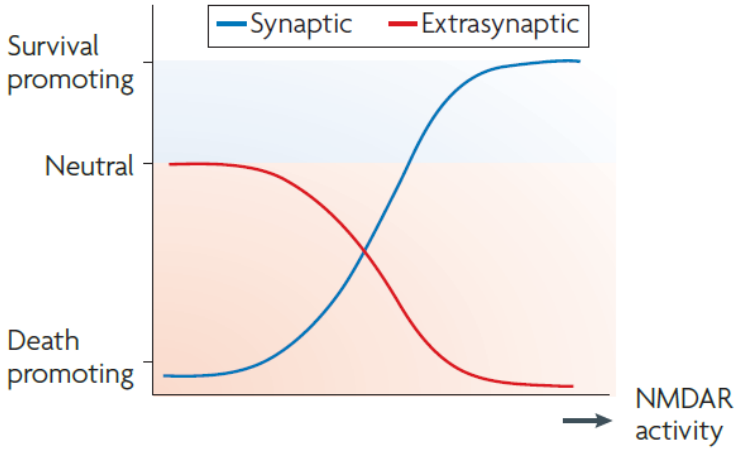

Figura 48. Model en X de l'excitotoxicitat depenent de NMDA. S'il·lustra els efectes de l'activació dels RNMDA sinàptics (blau) i extrasinàptics (vermell): Mentre que en els sinàptics una activació per sota del normal és nociva per a les neurones, una gran activitat d'aquests, resulta beneficiosa. En canvi pels extrasinàptics la poca activació no té un efecte rellevant, però la sobre activació és neurotòxica.

Cal puntualitzar que mentre que l'activació sinàptica és de naturalesa fàsica (temps de mS), l'activació extrasinàptica requereix un agonisme crònic (activació sostinguda). A concentracions equivalents de calci per a les dues vies, els efectes són oposats:

<u>Activació sinàptica</u>

És ben tolerada per les neurones de l'hipocamp i per mitjà de la inducció de gens de supervivència i supressió de gens de mort, fa que les neurones siguin més resistents a l'estrès oxidatiu i a l'apoptosi.

[189] Carter, B. C. & Jahr, C. E. Postsynaptic, not presynaptic NMDA receptors are required for spike-timing-dependent LTD induction. *Nat. Neurosci.* **2016**, 19(9), 1218–24.
[190] Hardingham, G. E., Fukunaga, Y. & Bading, H. Extrasynaptic NMDARs oppose synaptic NMDARs by triggering CREB shut-off and cell death pathways. *Nat. Neurosci.* **2002**, 5, 405–414.

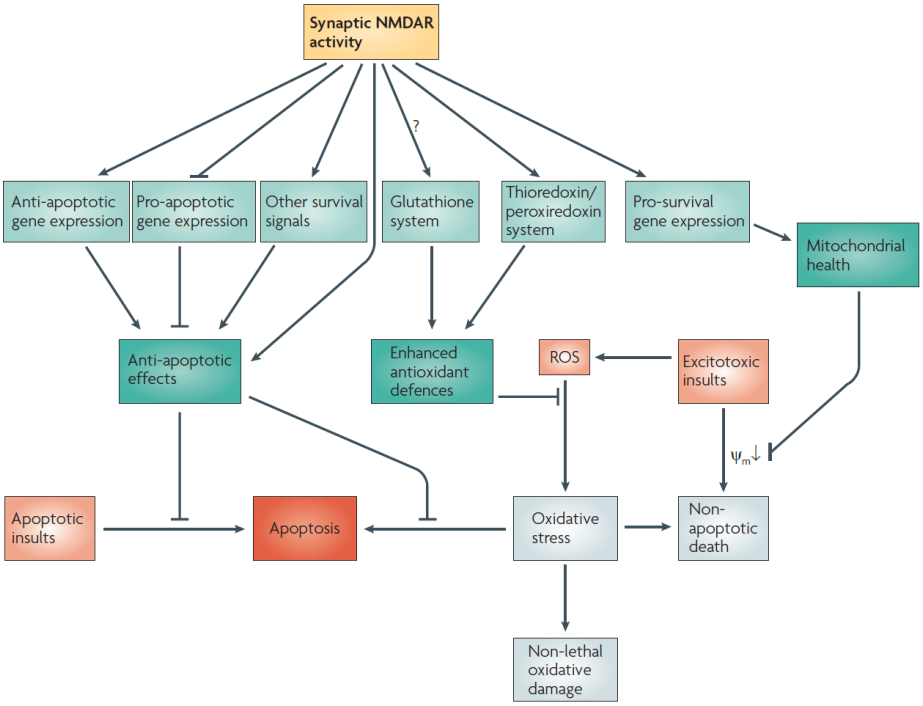

Figura 49. Vies neuroprotectores relacionades amb l'activitat RNMDA sinàptica.

Activació extrasinàptica

Les altes concentracions de calci condueixen a la disfunció de les mitocòndries i a la mort cel·lular, a través de diverses cascades bioquímiques com ara l'activació de FOXO o de Calapaïna i la inactivació de ERK1/2 o de CREB. La cascada bioquímica excitotòxica dependrà del tipus de cèl·lula i de la intensitat de l'estímul.

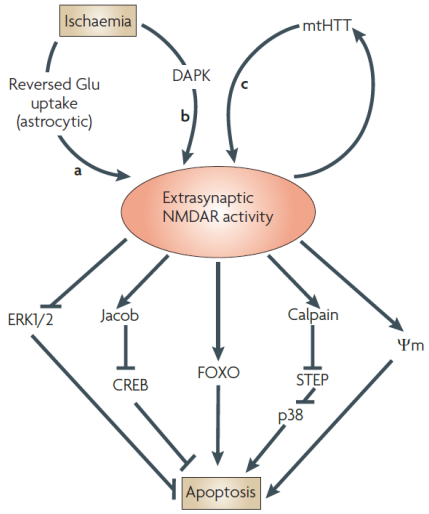

Figura 50. Activadors i efectors de l'activitat NMDAR extrasinàptica.

Com a resultat d'aquests processos, tant la hiper- com la hipoactivació dels receptors NMDA està implicada en múltiples processos patogènics, com ara l'esquizofrènia, la

depressió, quadres de dolor crònic, l'epilèpsia i la malaltia d'Alzheimer[191,192], aquesta última essent la més estudiada.

La malaltia d'Alzheimer[193] (AD, per el seu nom en anglès) és un procés patològic neurodegeneratiu el major símptoma del qual, és la pèrdua gradual de la funció cognitiva i que desemboca en la mort. La patofisisologia de l'AD és complexa i el seu origen no ha estat determinat. Tot i així és acceptat que un dels majors causants d'aquesta és la formació de les plaques senils al cervell per acumulació de pèptid β-amiloide[194]. Aquestes plaques activen múltiples processos de senyalització i cascades bioquímiques neurocitotòxiques, que tenen com a resultat final la mort neuronal. Una de les vies de progressió de l'AD és la desregulació del receptor de NMDA. En els primers estadis de la malaltia hi ha una sobre activació del RNMDA a causa d'una presència excessiva de glutamat a les sinapsis, que fa que s'aboleixi la funció de filtre del magnesi i s'activin vies neurotòxiques, que finalment deriven en mort neuronal i pèrdua de memòria. Es creu que aquesta sobreestimulació per glutamat respon majoritàriament a una malfunció dels mecanismes de recaptació d'aquest aa, encara que pot tenir altres orígens, com ara una alliberació incrementada de glutamat induïda per l'activació de diverses cascades neurotòxiques[195].

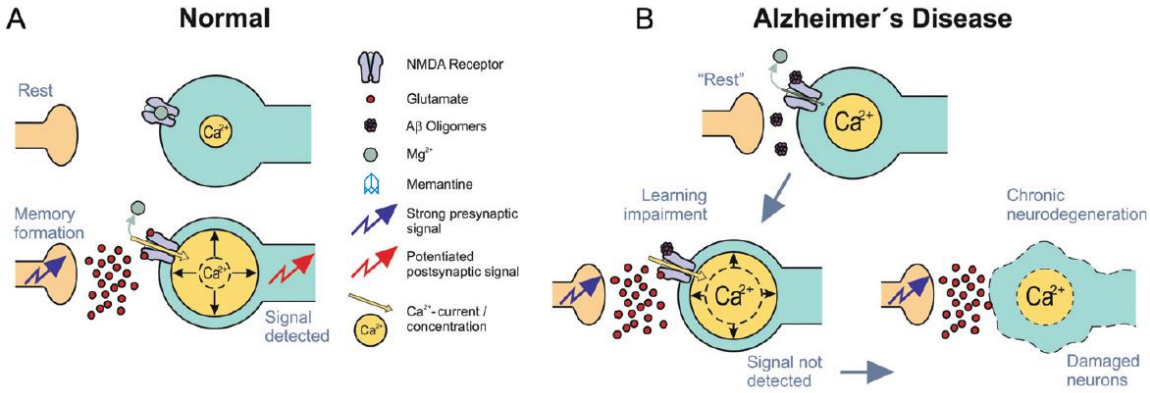

Figura 51. Comparació de la transmissió sinàptica fisiològica (A) i en la malaltia d'Alzheimer (B).

A banda d'això les mutacions heretades o adquirides dels receptors NMDA estan associades amb problemes de desenvolupament cognitiu, epilèpsia afàsica i altres

[191] Butterfield, D. A. & Pocernich, C. B. The glutamatergic system and Alzheimer's disease: Therapeutic implications. *CNS Drugs*. **2003**, 17 (9), 641–652.
[192] Danysz, W. & Parsons, C. G. Alzheimer's disease. β-amyloid, glutamate, NMDA receptors and memantine - Searching for the connections. *Br. J. Pharmacol*. **2012**, 167(2), 324–352.
[193] Ballard, C., Gauthier, S., Corbett, A., Brayne, C., Aarsland, D. & Jones, E. Alzheimer's disease. *Lancet* **2011**, 377, 1019–1031.
[194] Murphy, M. P. & LeVine, H. Alzheimer's Disease and the β-Amyloid Peptide. *J. Alzheimers Dis*. **2010**, 19(1), 1–17.
[195] Lalo, U., Palygin, O., Verkhratsky, A., Grant, S. G. N. & Pankratov, Y. ATP from synaptic terminals and astrocytes regulates NMDA receptors and synaptic plasticity through PSD-95 multi-protein complex. Sci. Rep. **2016**, 33609.

canalopaties[196], la majoria incloses dins el grup de les anomenades malalties minoritàries[197,198].

1.6.4 Gamma de fàrmacs

Tant agonistes com antagonistes del canal NMDA són coneguts avui en dia, tot i així són els d'aquest últim grup els d'interès per al tractament de la malaltia d'Alzheimer[199].

Mentre que els antagonistes competitius (selfotel, midafotel) bloquegen tant la funció normal com la neurotòxica donant lloc a efectes secundaris greus no acceptables[200], els antagonistes no competitius, capaços de bloquejar el porus del RNMDA quan aquest es troba en forma oberta (unit als seus co-agonistes), presenten potencial terapèutic.

Aquest comportament, paral·lel al del magnesi, es troba així mateix en altres estructures catiòniques (a pH fisiològic). Segons les diferents interaccions amb el porus del RNMDA podem classificar els antagonistes no competitius en tres grans grups:

Blocadors atrapants o d'alta afinitat

Queden atrapats dins el canal un cop aquest es tanca. Trobem el MK-801 (dizocilpina) i les conegudes com a substàncies d'abús, fenilciclidina (PCP) i ketamina.

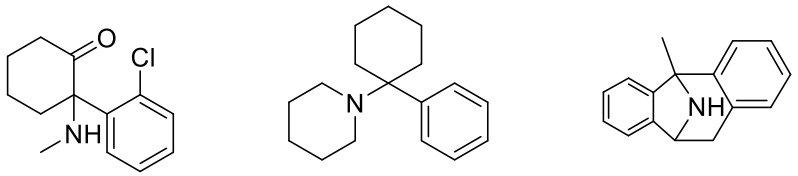

Figura 52. Blocadors atrapants de NMDA.

Inhibidors seqüencials o de blocadors de falca

El mecanisme d'acció d'aquests consisteix en evitar el tancament del canal, un cop s'han unit a la seva forma oberta. Trobem el tetraetilamoni, l'aminoacridina i els seus derivats.

[196] Kim, J. B. *Channelopathies*. *Korean J. Pediatr.* **2014**, 57(1), 1–18.
[197] Lesca, G., Rudolf, G., Bruneau, N. *et al*. GRIN2A mutations in acquired epileptic aphasia and related childhood focal epilepsies and encephalopathies with speech and language dysfunction. *Nat. Genet.* **2013**, 45 (9), 1061-6.
[198] Endele, S., Rosenberger, G., Geider, K. *et al.* Mutations in GRIN2A and GRIN2B encoding regulatory subunits of NMDA receptors cause variable neurodevelopmental phenotypes. *Nat. Genet.* **2010**, 42 (11), 1021-6.
[199] Kemp, J. A. & McKernan, R. M. NMDA receptor pathways as drug targets. *Nat. Neurosci*. **2002**, 5, 1039–1042.
[200] Lipton, S. A. Prospects for clinically tolerated NMDA antagonists: open-channel blockers and alternative redox states of nitric oxide. *Trends Neurosci*. **1993**, 16, 527–532.

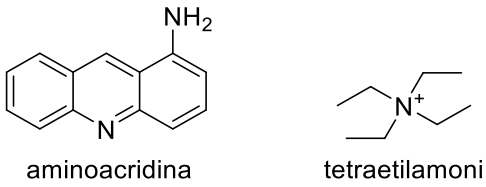

Figura 53. Blocadors de falca.

Blocadors atrapants parcials

Aquests blocadors tenen propietats mixtes dels dos grups anteriors: impedeixen temporalment el tancament del canal, és a dir, són reversibles[201]. En aquest grup trobem l'amantadina i la memantina, aquest últim més potent. Estructuralment s'ha vist que els grups metil de la memantina són crucials per a una millora del bloqueig de NMDA ja que li confereixen més hidrofobicitat i, el que és més important, una estructura asimètrica que permet que encaixi millor al lloc d'unió del receptor[202].

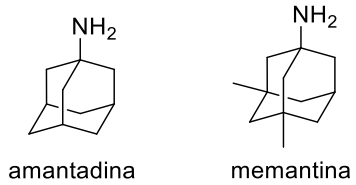

Figura 54. Antagonistes no competitius reversibles del canal de NMDA.

Tot i així, avui en dia la memantina és l'únic lligand del receptor NMDA que ha estat aprovat per al tractament de la malaltia d'Alzheimer[203]. Aquest compost va ser sintetitzat i patentat per Eli Lilly & Co. al 1968 com a anàleg de l'amantadina, coneguda per la seva acció antiviral. Igual que l'anterior la memantina presenta una estructura tricíclica (adamantànica) amb una amina a la posició de cap de pont, que es troba protonada a pH fisiològic, fent que es pugui unir al lloc d'unió del magnesi.

Els seus efectes en pacients amb AD consten d'una millora de la comunicació, comprensió i memòria, millorant així les condicions de vida de les persones afectades per la malaltia. Les propietats terapèutiques s'expliquen ja que la memantina inhibeix preferentment els RNMDA extrasinàptics, que són els que inicien processos neurotòxics a causa de la sobre

[201] Mori, H. & Mishina, M. Structure and function of the NMDA receptor channel. *Neuropharmacol.* **1995**, 34(10), 1219–1237.
[202] Limapichat, W., Yu, W. Y., Branigan, E., Lester, H. & Dougherty, D. Key binding interactions for memantine in the NMDA receptor. *ACS Chem. Neurosci*. **2013**, 4, 255–260.
[203] Parsons, C. G., Danysz, W. & Quack, G. Memantine is a clinically well tolerated N-methyl-D-aspartate (NMDA) receptor antagonist — a review of preclinical data. *Neuropharmacol*. **1999**, 38, 735–767.

activació, permetent així restaurar la potenciació a llarg termini (activació tònica del RNMDA) responsable de la cognició i memòria.

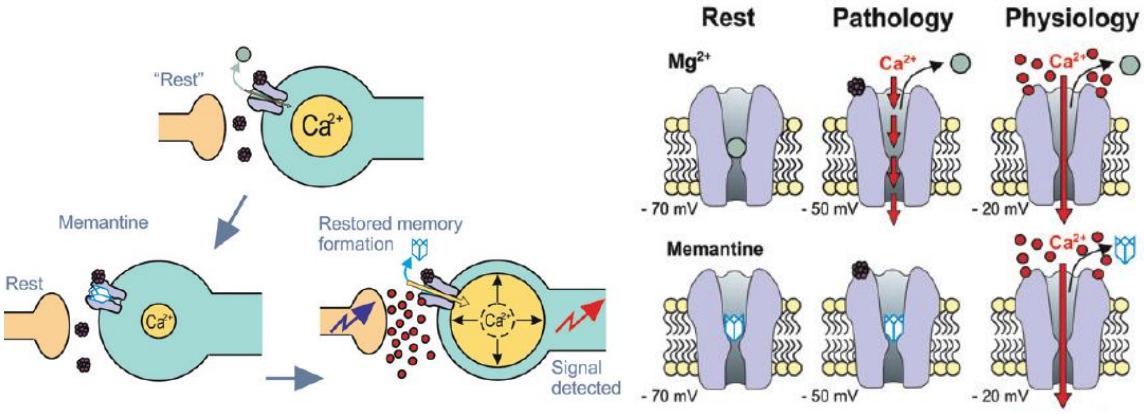

Figura 55. Efectes de la memantina sobre el receptor NMDA. Esquerra: La memantina fa una funció de filtre, similar a la del Mg^{2+}, però essent més efectiva que aquest i bloquejant l'efecte del glutamat patològic a les sinapsis. La plasticitat neuronal és restablerta i s'evita la mort neuronal. Dreta: Il·lustració esquemàtica del bloqueig voltatge dependent per memantina.

El mecanisme d'acció de la memantina és el que permet que aquest fàrmac pugui bloquejar els efectes exocitotòxics de l'activació del RNMDA sense afectar-ne la seva activació fisiològica[204]. La memantina és un antagonista no competitiu, voltatge dependent i d'afinitat relativament baixa, que li permet mostrar una cinètica de bloqueig ràpida. Aquestes característiques permeten que en condicions de repòs (-70 mV) ocupi el canal de NMDA, però davant d'una despolarització potent (-20 mV) gràcies a la cinètica voltatge depenent ràpida, el pot desbloquejar, permetent la conducció sinàptica fisiològica. D'altra banda, al presentar una afinitat pel receptor més elevada que el magnesi, enfront d'una despolarització crònica però moderada (-50 mV), com la que es produeix en la AD, la memantina, a diferència del magnesi, no abandona el canal i n'evita així l'entrada citotòxica de Ca^{2+}.

Tot i el bon perfil terapèutic que aquest fàrmac ofereix, és l'únic de la seva classe disponible al mercat actualment. Per a aquest motiu, el disseny de nous compostos d'acció similar però amb propietats millorades, gràcies als nous descobriments funcionals i estructurals, són desitjables.

Cal afegir que la memantina, així com altres antagonistes de NMDA han estat emprats en l'estratègia de lligands dirigits a múltiples dianes (MTDLs, per les seves sigles en angles).

[204] Johnson, J. W., Glasgow, N. G. & Povysheva, N. V. Recent insights into the mode of action of memantine and ketamine. *Curr. Opin. Pharmacol*. **2015**, 20, 54–63.

Aquesta estratègia consisteix en una alternativa a la polimedicació i es basa en el desenvolupament d'una única entitat química capaç d'actuar sobre dianes diferents, normalment unint dos fragments que, de manera independent, mostren activitat farmacològica sobre dianes que estan relacionades amb una mateixa malaltia. La MTDL és especialment apropiada per a malalties d'etiologia complexa, com és el cas de la malaltia d'Alzheimer[205].

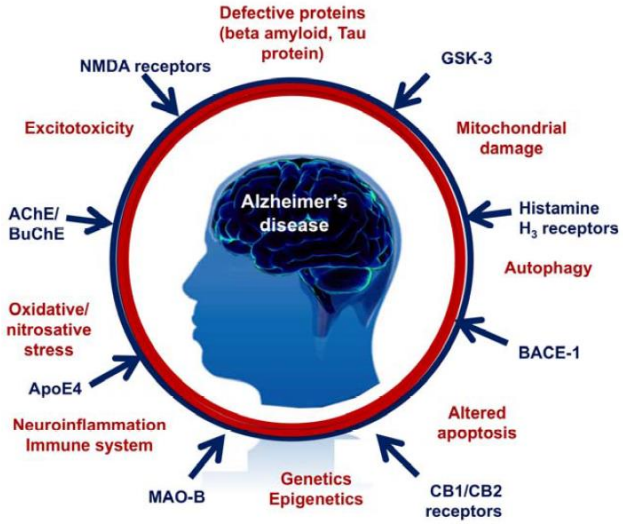

Figura 56. Factors que contribueixen a la fisiopatologia de la AD (vermell) i possibles dianes terapèutiques (blau)

En aquest context la combinació de fàrmacs que actuen sobre el sistema glutamatèrgic, com la memantina, amb fàrmacs que realitzen la seva acció sobre el sistema colinèrgic, com ara la tacrina, ha guanyat força com a estratègia per combatre l'AD. Així doncs mentre que la inhibició del RNMDA actuaria contrarestant la neurodegeneració, la inhibició de l'acetilcolinesterasa (AChE) ajudaria a la restauració de la memòria i la cognició, estimulant les neurones restants. Seguint aquesta idea recentment han aparegut la carbacrina i el memagal, compostos que actuen sobre les dues dianes i que ofereixen propietats farmacològiques millorades respecte als seus fragments per separat[206].

Així doncs els antagonistes del RNMDA presenten un gran potencial per ser inclosos en futurs MTDL per al tractament de la malaltia de l'AD.

[205] Perez, D. I., Martinez, A., Gil, C. & Campillo, N. E. From Bitopic Inhibitors to Multitarget Drugs for the Future Treatment of Alzheimer's Disease. *Curr. Med. Chem.* **2015**, 22(33), 3789–3806.
[206] Rosini, M., Simoni, E., Minarini, A. & Melchiorre, C. Multi-target Design Strategies in the Context of Alzheimer's Disease: Acetylcholinesterase Inhibition and NMDA Receptor Antagonism as the Driving Forces. *Neurochem. Res.* **2014**, 1–10.

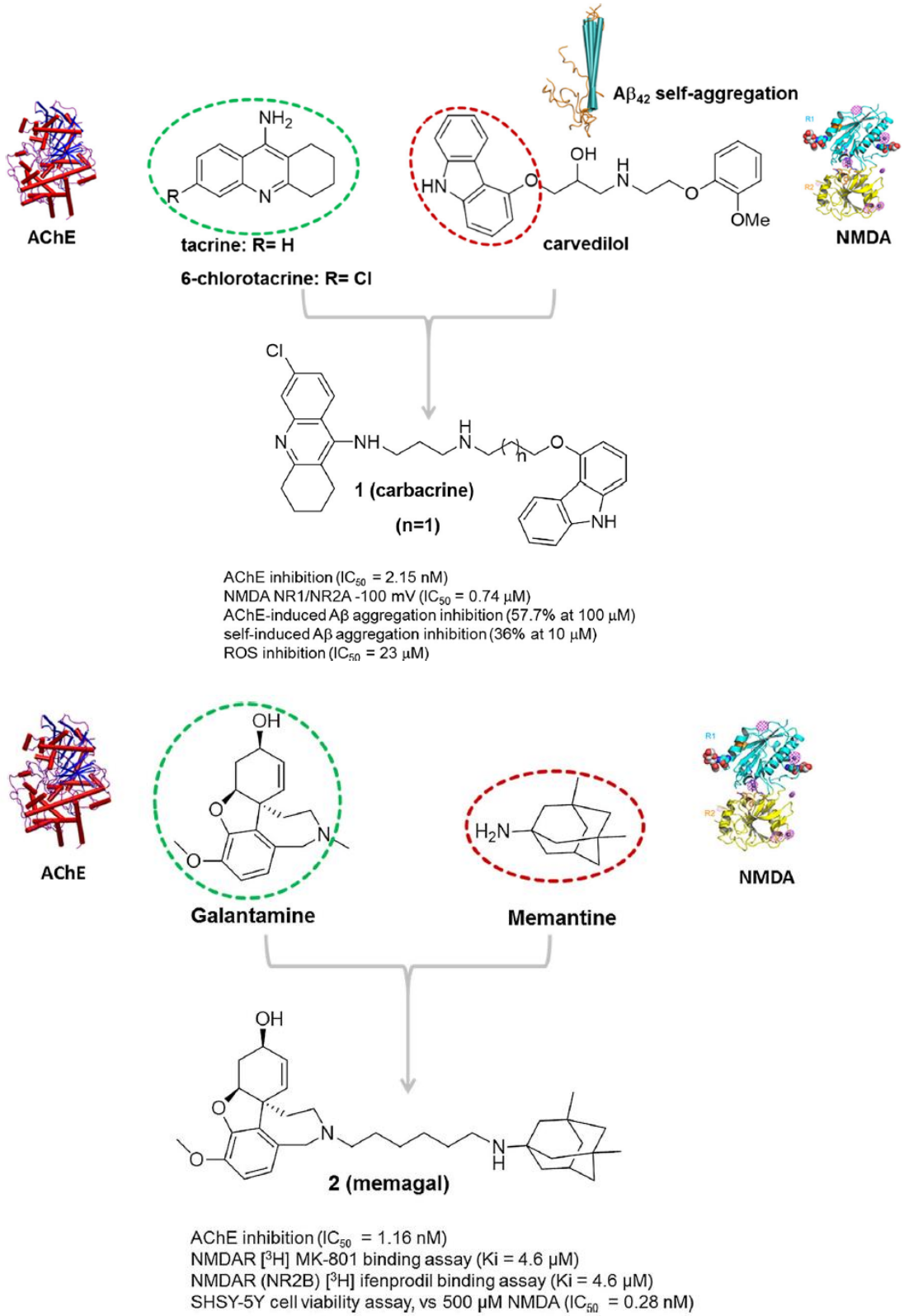

Figura 57. Disseny i activitat farmacològica del memagal i de la carbacrina.

Chapter 2

Objectives

2.1 Objectives

As already mentioned in the introduction (section 1.1.4) in the present Thesis the objective is to target three ion channels being: influenza A M2, $P2X_7$ and NMDA, with small molecules that are able to modulate them in the appropriate manner to avoid or ameliorate their related diseases or to be used as investigational tools.

Besides this and tacking into account the wide pure organic chemical background of the group, the study of chemical structures arising from the previous projects and with theoretical interest, was also taken into consideration. In addition, although not set as a main purpose of this Thesis, the optimization of the chemical reactions involved in the preparation of the bioactive products has also been carried out.

The specific objectives follow:

M2 channel of Influenza A virus

1. Synthesis and pharmacological evaluation of the 3-azatetracyclo[5.2.1.$1^{5,8}$.$0^{1.5}$] undecane, **I**, and its derivatives, as ring contracted analogues of amantadine and rimantadine. (**Chapter 3**)

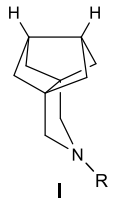

I

2. Synthesis and pharmacological evaluation of the 4-azatetracyclo[5.4.2.$0^{2,6}$.$0^{8.11}$] trideca-9,12-diene and related compounds, **II**, as synthetically more accessible M2 channel inhibitors. (**Chapter 4A**)

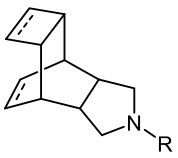

II

3. Synthesis of 4-(2-adamantyl)piperidines, **III**, 4-(2-adamantylmethyl)piperidines, **IV**, and related compounds as longer analogues of amantadine and rimantadine. (**Chapter 5**)

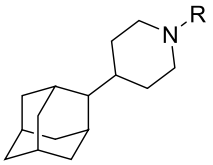

III

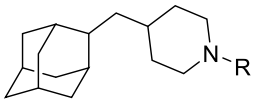

IV

4. Due to the observation that some of the previous compounds were presenting an antiviral mechanism unrelated to the M2 channel, putatively inhibiting the influenza A surface glycoprotein hemagglutinin, the exploration of this viral target was set as an additional objective. The synthesis and the pharmacological evaluation of a large family of 1-adamantylmethylanilines, **V**, and related compounds, **VI** and **VII**, was developed. (**Chapter 6**)

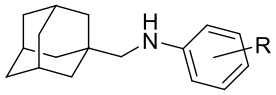

V

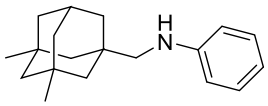

VI

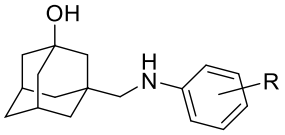

VII

P2X$_7$ ionotropic purinergic receptor

5. Synthesis and pharmacological evaluation of pentacyclododecylcarbohydrazides, **VIII**, and reduced derivatives, **IX**, in order to start building our group's own SAR information for this new target. (**Chapter 7**)

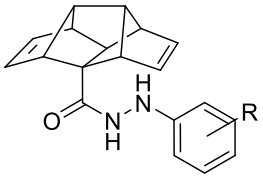

VIII

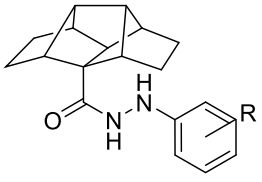

IX

NMDA ionotropic glutamate receptor

6. Synthesis and pharmacological evaluation of 3-amino-N'-phenyladamantane-1-carbohydrazides, **X**, as Multi-Target Directed Ligands for NMDA-P2X$_7$, with possible implications in the Alzheimer's disease treatment. (**Chapter 8**)

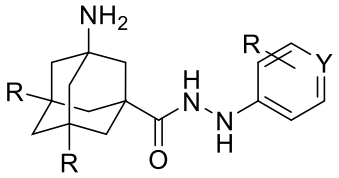

X

Pure organic chemistry

7. Generation of the highly pyramidalized alkene **XII** and structural study of its dimer **XIII**. (**Chapter 4b**)

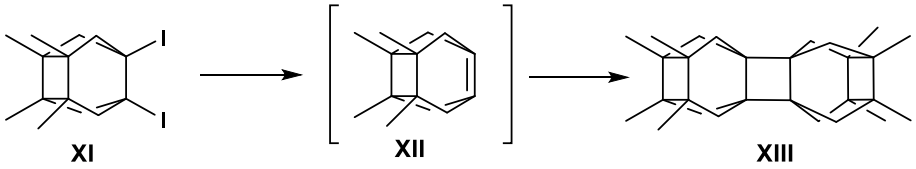

XI **XII** **XIII**

2.2 Objectius

Tal i com s'ha mencionat en la introducció (secció 1.1.4) l'objectiu de la present Tesi és desenvolupar molècules que tinguin com a diana els tres canals iònics següents: la proteïna M2 del virus de la influenza A, el $RP2X_7$ i el RNMDA, per tal de modular-los d'una manera tal que se'n millorin els estats patològics associats o bé per ser emprades com a eines de recerca.

A part d'això i tenint en compte l'expertesa en química orgànica pura que té el grup, s'ha inclòs com a objectiu l'estudi d'estructures químiques d'interès teòric, provinents dels projectes anteriors. A més a més, tot i no tractar-se del propòsit principal d'aquesta Tesi, s'ha dut a terme l'optimització d'algunes reaccions químiques involucrades en la preparació dels productes bioactius objectiu.

A continuació es presenten els objectius específics:

Canal M2 del virus de la Influenza A

1. Síntesi i avaluació farmacològica del 3-azatetraciclo[5.2.1.$1^{5,8}$.$0^{1.5}$]undecà, **I**, així com dels seus derivats, com a anàlegs per contracció d'anell d'amantadina i rimantadina. (**Capítol 3**)

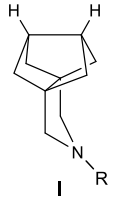

I

2. Síntesi i avaluació farmacològica del 4-azatetraciclo[5.4.2.$0^{2,6}$.$0^{8.11}$]trideca-9,12-dià i compostos relacionats, **II**, com a inhibidors del canal M2 fàcilment accessibles sintèticament. (**Capítol 4a**)

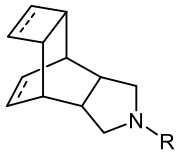

II

3. Síntesi de 4-(2-adamantil)piperidines, **III**, 4-(2-adamantilmetil)piperidines, **IV**, i compostos relacionats, com a anàlegs més llargs d'Amt i Rmt. (**Capítol 5**)

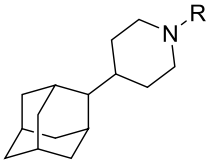

III

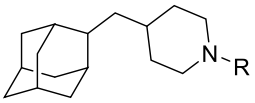

IV

4. A causa de l'observació que alguns dels compostos prèviament desenvolupats presentaven un mecanisme antiviral no relacionat amb el canal M2, sinó que presumptament inhibien la proteïna de superfície HA, l'estudi d'aquesta va ser establert com a un objectiu addicional. Per aquest motiu es va sintetitzar i avaluar farmacològicament una gran família d'1-adamantilmetilanilines, **V**, i compostos relacionats, **VI** i **VII.** (**Capítol 6**)

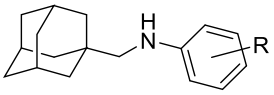

V

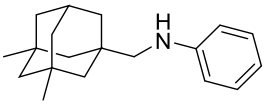

VI

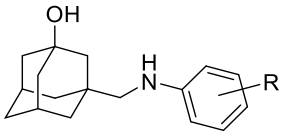

VII

Receptor ionotròpic de purines $P2X_7$

5. Síntesi i avaluació farmacològica de pentaciclododecilcarbohidrazides, **VIII**, i els seus derivats reduïts, **IX**, per tal de començar a construir una informació de relació estructura activitat, pròpia del grup per a aquesta nova diana. (**Capítol 7**)

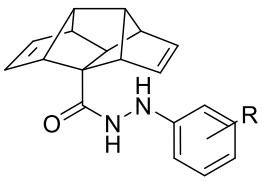

VIII

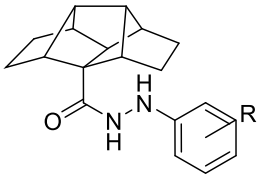

IX

Receptor ionotròpic de glutamat NMDA

6. Síntesi i avaluació farmacològica de 3-amino-N'-feniladamantano-1-carbohidrazides, **X**, com a Lligands Dirigits a Múltiples Dianes per NMDA-$P2X_7$, amb possibles implicacions en el tractament de la malaltia d'Alzheimer. (**Capítol 8**)

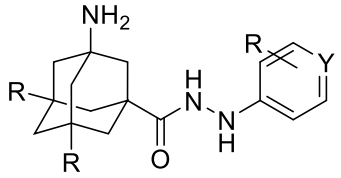

X

Química Orgànica Pura

7. Generació de l'alquè altament piramidalitzat **XII** i estudi estructural del seu dímer **XIII**. (**Capítol 4b**)

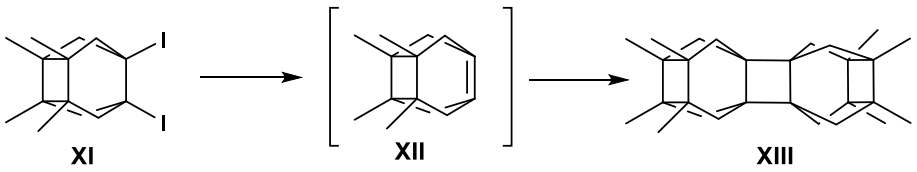

XI **XII** **XIII**

Chapter 3

3-Azatetracyclo[5.2.1.1^{5,8}.0^{1,5}]undecane derivatives as *wt* and V27A Influenza A/M2 channel blockers

3.1 Rationale and previous work

The M2 channel is a short transmembrane protein essential for the viability of the virus Influenza A[1], causing agent of the flu. Its function as viral pH regulator[2,3] is inhibited by the commercial drugs Amantadine (Amt)[4] and Rimantadine (Rmt)[5], which bind the channel blocking the proton flow through it[6]. One of the most particular characteristics of this short proton channel is the ability to vary its pore width, by means of point mutations that replace one pore facing amino acid for another one with different properties[7]. These pore variations are the responsible for the increasing drug resistance to adamantane like drugs (Amt, Rmt)[8]. As nowadays 99% of the circulating strains of Influenza carry mutant channels[9], it is of paramount importance to develop new drugs which with to fight this virus[10,11]. Noteworthy the main mutant channels are the S31N[12], which is narrower than the wt, and the wider L26F[13] and V27A[14], this last one being the only originated by drug selection pressure[15,13]. (see introduction, sections 1.2.2 and 1.2.3)

[1] Cady, S. D., Luo, W., Hu, F. & Hong, M. Structure and Function of the Influenza A M2 Proton Channel. *Biochem.* **2009**, 6, 7356–7364.
[2] Shimbo, K., Brassard, D. L., Lamb, R. A. & Pinto, L. H. Selectivity and Activation of the M2 Channel of Influenza Virus. *Biophys. J.* **1996**, 70(3), 1335-46.
[3] Hong, M. & Degrado, W. F. Structural basis for proton conduction and inhibition by the influenza M2 protein. *Protein Sci*. **2012**, 21(11), 1620–1633.
[4] Wang, C., Takeuchi, K. & Pinto, L. H. Ion Channel Activity of Influenza A Virus M2 Protein : Characterization of the Amantadine Block. *J. Virol.* **1993**, 67(9), 5585–5594.
[5] Wright, A. K., Batsomboon, P., Dai, J., Hung, I., Zhou, H. X., Dudley, G. B. & Cross, T. A. Differential Binding of Rimantadine Enantiomers to Influenza A M2 Proton Channel. *J. Am. Chem. Soc*. **2016**. 138(5), 1506–1509.
[6] Pinto, L. H. & Lamb, R. A. Controlling influenza virus replication by inhibiting its proton channel. *Mol Biosyst*. **2007**, 3(1):18-23.
[7] Le, L. & Leluk, J. Study on Phylogenetic Relationships, Variability, and Correlated Mutations in M2 Proteins of Influenza Virus A. *PLoS One*. **2011**, 6(8), e22970.
[8] Leonov, H., Astrahan, P., Krugliak, M. & Arkin, I. T. How Do Aminoadamantanes Block the Influenza M2 Channel, and How Does Resistance Develop? *J. Am. Chem. Soc*. **2011**, 133, 9903–9911.
[9] Dong, G., Peng, C., Luo, J., Wang, C., Han, L., Wu, B., Ji, G. & He, H. Adamantane-resistant influenza a viruses in the world (1902-2013): Frequency and distribution of M2 gene mutations. *PLoS ONE*, **2015** 10(3), 1–20.
[10] Naesens, L., Stevaert, A. & Vanderlinden, E. Antiviral therapies on the horizon for influenza. *Curr. Opin. Pharmacol*. **2016**, 30, 106–115.
[11] Wang, J., Li, F. & Ma, C. Recent progress in designing inhibitors that target the drug-resistant M2 proton channels from the influenza A viruses. *Biopolymers.* **2015**, 104(4), 291–309.
[12] Wang, J., Wu, Y., Ma, C., Fiorin, G., Wang, J., Pinto, L. H. & Lamb, R. A. Structure and inhibition of the drug-resistant S31N mutant of the M2 ion channel of in fluenza A virus. *Proc Natl Acad Sci USA*. **2013**, 110(4),1315-20.
[13] Furuse, Y., Suzuki, A. & Oshitani, H. Large-Scale Sequence Analysis of M Gene of Influenza A Viruses from Different Species: Mechanisms for Emergence and Spread of Amantadine Resistance. *Antimicrob. Agents Chemother.* **2009**, 53(10), 4457-63.
[14] Pielak, R. M. & Chou, J. J. Solution NMR structure of the V27A drug resistant mutant of influenza A M2 channel. *Biochem. Biophys. Res. Commun.* **2010**, 401(1), 58–63.
[15] Furuse, Y., Suzuki, A., Kamigaki, T. & Oshitani, H. Evolution of the M gene of the influenza A virus in different host species: large-scale sequence analysis. *Virol. J*. **2009**, 6(1), 67.

The project presented in this chapter is the follow up work of the namely first influenza project of the research group[16]. Steaming from the compound **10**, which was found to be an Influenza A inhibitor in a wide pharmacological activity assay of Amt ring-contracted analogues prepared in the group[17], several ring expanded and ring contracted derivatives of Amt were synthesized and evaluated with the aim to explore the effect of modifying the inhibitor's size in the different M2 channels (at the time of unknown structure).

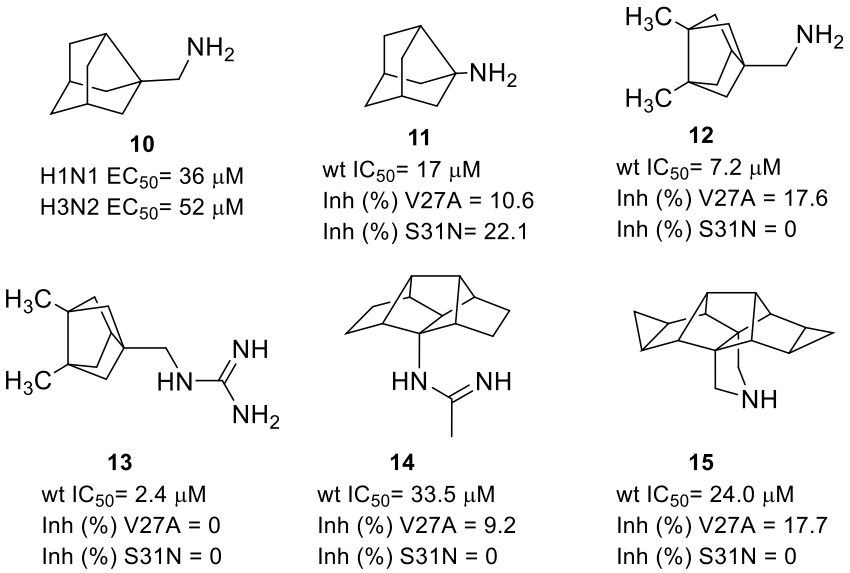

Figure 58. Ring contracted and ring expanded analogues prepared in a previous project. Antiviral EC_{50} values are shown for **10**. IC_{50} values are shown for wt M2 channel, while % of inhibition of the channel function by 100 μM of inhibitor for 2 min, are given for A/V27A and A/S31N mutant channels.

Resulting from this first work, several inhibitors against the *wt* channel of Influenza A virus were identified. Moreover it could be seen that the ring expanded analogues, featuring the pentacyclo[6.4.0.0^{2,10}.0^{3,7}.0^{4,9}]dodecane scaffold (**14** and **15**) were able to show marginal inhibition values against the mutant V27A. More interesting were the ring contracted analogues (**11** and **12**), which in some cases, were able to mildly inhibit the three relevant channels of the virus.

These results promoted a further exploration of the ring contracted analogues of Amt, detailed in this chapter. With the aim to target the three main channels we envisaged a

[16] Duque, M. D., Ma, C., Torres, E., Wang, J., Naesens, L., Juárez-Jiménez, J., Camps, P., Luque, F. J., DeGrado, W. F., Lamb, R. A., Pinto, L. H. & Vázquez, S. Exploring the size limit of templates for inhibitors of the M2 ion channel of influenza A virus. *J. Med. Chem.* **2011**, 54(8), 2646–2657.

[17] Camps, P., Duque, M. D., Vázquez, S., Naesens, L., Clercq, E. De, Sureda, F. X., López-Querol, M., Camins, A., Pallàs, M., Prathalingam, S. R., Kelly, J. M., Romero, V., Ivorra, M. D. & Cortés, D. Synthesis and pharmacological evaluation of several ring-contracted amantadine analogs. *Bioorg. Med. Chem.* **2008**, 16(23), 9925–9936.

series of modified bisnoradamantane scaffolds, being 3-azatetracyclo[5.2.1.1^{5,8}.0^{1,5}]undecanes, which were modified to be greater in length than Amt –feature that had been seen beneficial when targeting the wider V27A- but with a slight width reduction compared to this commercial drug –thought to be required to inhibit the narrower mutant S31N- (Figure 59).

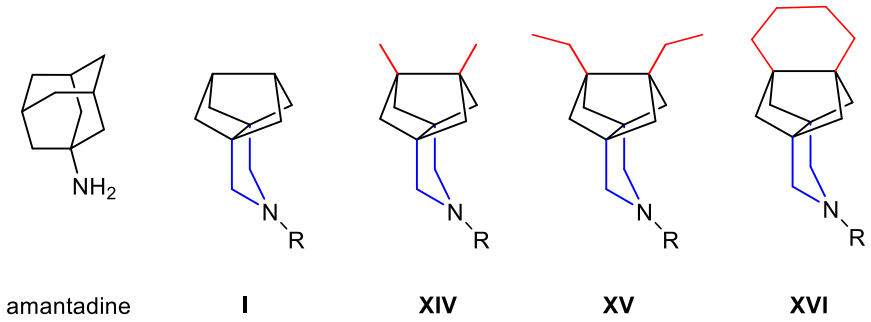

Figure 59. Analogues prepared in this project. From the bisnoradamantane scaffold (black), the length is increased in both directions with a pyrrolidine ring (blue) and with a variety of alkyl substituents (red), which confer greater length and bulkiness to the basic centre distal side.

In addition, for this family of derivatives, the basic centre was introduced in a pyrrolidine scaffold. This modification had three main purposes:

1. Increase the compound's length in the basic centre proximal site.
2. Confer a fixed orientation to this basic centre.
3. Reduce the conformational freedom of the basic centre.

3.2 Theoretical discussion

In the present Thesis the compounds featuring the general scaffold **I** were prepared, yielding the pharmacologically assayed compounds **25**, **26** and **27**.

To access the bisnoradamantane diacid, key precursor of the depicted compounds, a synthetic route previously described in the group was followed[18,19] (Scheme 1).

[18] Camps, P., Iglesias, C., Rodríguez, M. J., Grancha, M. D., Gregori, M. E., Lozano, R., Miranda, M. A., Figueredo, M. & Linares, A. A short synthesis of dimethyl tricyclo[3.3.0.03,7]octane-1,5-dicarboxylate and its 3,7-dimethyl derivative. A new route to the tricyclo[3.3.0.03,7]octane skeleton . *A. Chem. Ber*. **1988**, 121, 647-654.
[19] Camps, P., Font-Bardia, M., Pérez, F., Solans, X. & Vázquez, S. Synthesis, Chemical Trapping, and Dimerization of 3,7-Dimethyltricyclo[3.3.0.03, 7]oct-1(5)-ene:[2+ 2] Retrocycloaddition of the Cyclobutane Dimer. *Angew. Chem., Int. Ed. Engl*. **1995**, 34, 912–914.

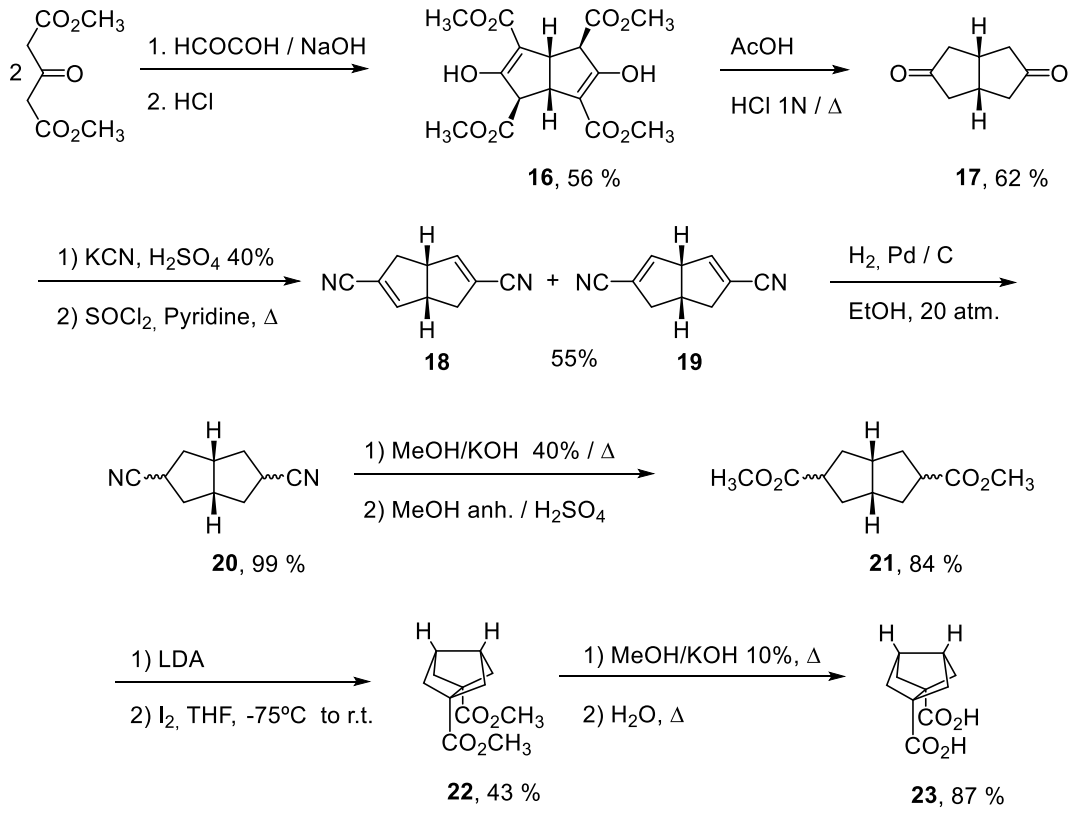

Scheme 1. Preparation of the key bisnoradamantane diacid **23**

The synthesis started with a Weiss reaction[20,21], which implies the condensation of the α-dicarbonylic compound glyoxal with two equivalents of dimethyl 1,3-acetonedicarboxylate, in basic media. Interestingly this unique reaction consists in two aldol condensations, two dehydrations and two Michael reactions that afford the bicyclic adduct **16** in moderate yields. The dienol-tetraester **16** is then treated with acetic and hydrochloric acids in water, undergoing a hydrolysis and decarboxylation to the symmetric diketone **17**[22]. In aqueous media with neutral pH - regulated by dropwise addition of 40% sulphuric acid - the diketone intermediate was reacted with potassium cyanide to give a stereoisomeric mixture of bis-cyanohydrines. This mixture was readily dehydrated using thionyl chloride in pyridine at reflux, to the regioisomeric mixture of dinitriles **18** and **19**. After sublimation of the mixture of **18** and **19**, in order to remove sulfur traces, a catalytic hydrogenation, using 10 % Pd/C as catalyst and 20 atm of pressure, yielded the stereoisomeric mixture **20**, composed of the three possible reduced products. Following, this mixture was hydrolysed with KOH in a methanol/water media

[20] Fu, X. & Cook, J. M. *Aldrichimica Acta*. **1992**, 25(2), 43-54.
[21] Gupta, A. K., Fu, X., Snyder, J. P. & Cook, J. M. General approach for the synthesis of polyquinenes via the Weiss reaction. *Tetrahedron* **1991**, 47, 3665-3710.
[22] Bertz, S. H., Cook, J. M., Gawish, A. & Weiss, U. *Org. Synth. Coll. Vol. VII*, Wiley: New York, **1990**, 50-56.

and the bicyclic diacid obtained was immediately esterified, using Fisher's conditions, to the regiomeric ester mixture **21**.

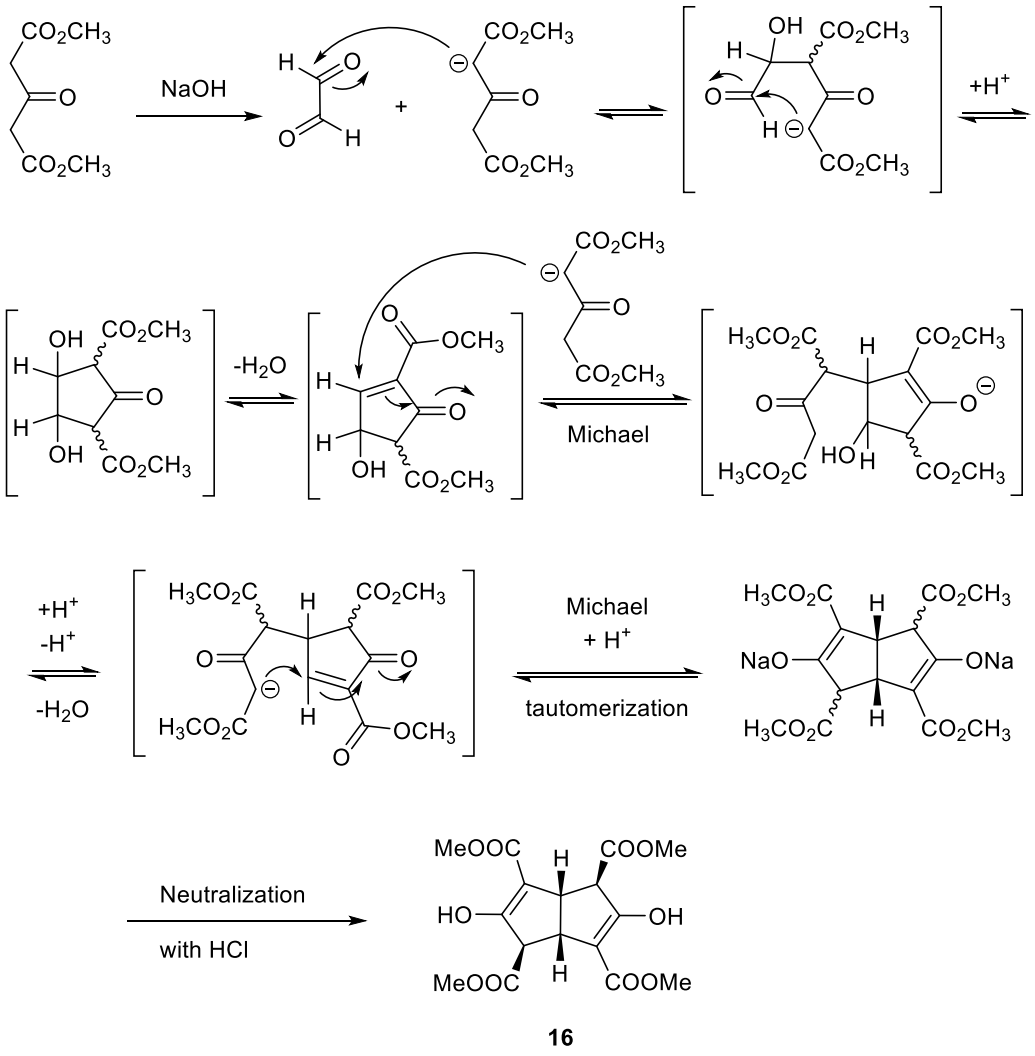

Scheme 2. Weiss reaction mechanism.

Upon reaction of **21** with the basic non-nucleophile lithium diisopropylamide (LDA), the lithium bis-enolates were coupled by a iodine-mediated oxidation (Scheme 3). This cyclization step was key in order to build up the bisnoradamantane scaffold, immediate precursor of the target compounds.

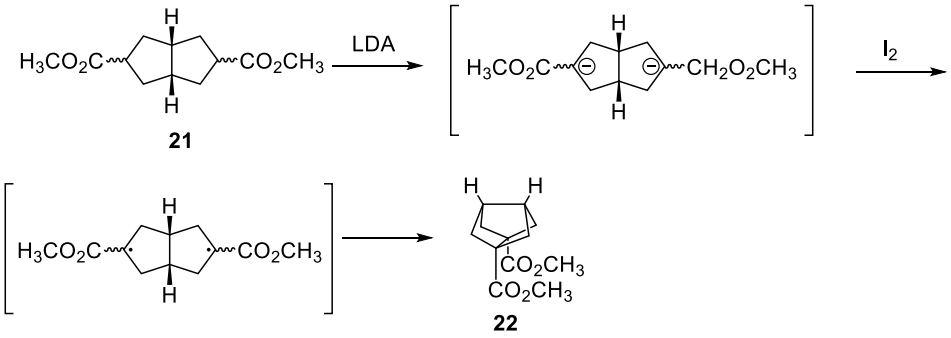

Scheme 3. Key oxidative coupling mechanism.

Of note, despite this step was a minefield of side-reactions, all the optimization attempts were unsuccessful. A final hydrolysis in basic media furnished the desired bisnoradamantane diacid **14**, upon which we started the envisaged 3-step synthetic route towards our first 3-azatetracyclo[5.2.1.1^{5,8}.0^{1,5}]undecane product (Scheme 4) .

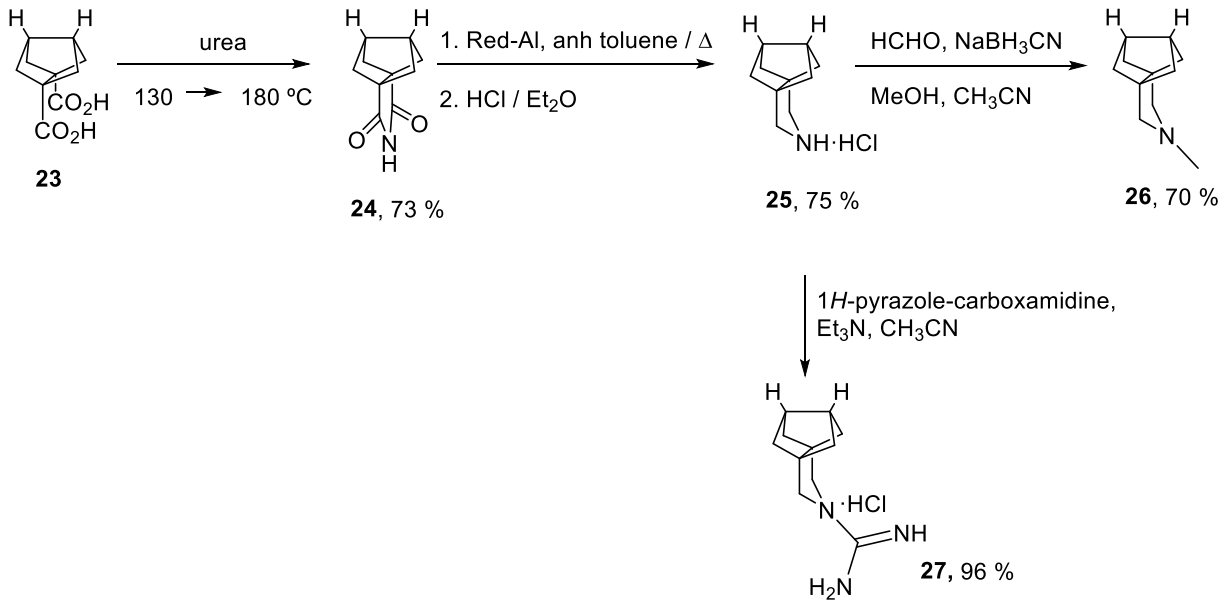

Scheme 4. Route towards compounds **25**, **26** and **27.**

As described in the article, reaction of **23** with urea at 180ºC furnished the imide **24**, which was reduced using Red-Al® to **25**. From this amine **25**, the guanidine derivative **27** and the tertiary amine **26** were prepared.

The compounds **25**, **26** and **27** prepared and the results of the inhibition of the *wt* and Amt-Resistant A/M2 Ion Channels, tested by the groups of Prof. Lawrence H. Pinto (Northwestern University, Evanston) and Prof. William F. DeGrado (University of California San Francisco) are gathered in table 3.

	A/M2 WT		A/M2 S31N		A/M2 V27A	
	Inh (%)[a]	**IC_{50}[b]**	**Inh (%)[a]**	**IC_{50}[b]**	**Inh (%)[a]**	**IC_{50}[b]**
 **25[c]**	93.8	9.7	0	ND	26.0	ND
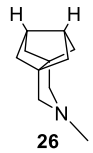 **26**	87.9	16.3	0	ND	12.3	ND
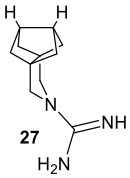 **27**	92.4	6.1	1.0	ND	84.2	11.4
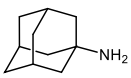 **Amt**	91.0	16.0	35.6	199.9	10.8	ND

Table 3. [a]Inhibition of A/M2 channels expressed in Xenopus oocytes using the TEV technique. All inhibitors were initially tested at 100 μM for 2 min. [b]Determined only for compounds having >75% inhibition. [c]Antiviral EC_{50} determined by microscopic scoring of the CPE at 72 h post infection = 16 μM in the influenza A/HongKong/7/87 H3N2 strain (carrying a *wt* M2 channel).

All three compounds were equipotent (**26**) or more potent (**25**, **27**) than the commercial drug (**Amt**). Of note, **25** displayed antiviral activity in the CPE assay. The guanidine **27** was found to be a dual potent inhibitor of the *wt* and the V27A mutant channel; together with other compounds comprehended in this project, *this was the first non-adamantane compound endowed with this dual activity reported in the literature*.

Journal of Medicinal Chemistry

Article

pubs.acs.org/jmc

3-Azatetracyclo[5.2.1.1^{5,8}.0^{1,5}]undecane Derivatives: From Wild-Type Inhibitors of the M2 Ion Channel of Influenza A Virus to Derivatives with Potent Activity against the V27A Mutant

Matias Rey-Carrizo,[†] Eva Torres,[†] Chunlong Ma,[‡,⊥] Marta Barniol-Xicota,[†] Jun Wang,[§] Yibing Wu,[§] Lieve Naesens,[∥] William F. DeGrado,[§] Robert A. Lamb,[⊥,#] Lawrence H. Pinto,[‡] and Santiago Vázquez*[,†]

[†]Laboratori de Química Farmacèutica (Unitat Associada al CSIC), Facultat de Farmàcia, and Institute of Biomedicine (IBUB), Universitat de Barcelona, Av. Joan XXIII s/n, Barcelona E-08028, Spain

[‡]Department of Neurobiology and Physiology, Northwestern University, Evanston, Illinois 60208-3500, United States

[§]Department of Pharmaceutical Chemistry, University of California, San Francisco, California 94158, United States

[∥]Rega Institute for Medical Research, KU Leuven, 3000 Leuven, Belgium

[⊥]Department of Molecular Biosciences, and [#]Howard Hughes Medical Institute, Northwestern University, Evanston, Illinois 60208-3500, United States

Supporting Information

ABSTRACT: We have synthesized and characterized a series of compounds containing the 3-azatetracyclo[5.2.1.1^{5,8}.0^{1,5}]undecane scaffold designed as analogues of amantadine, an inhibitor of the M2 proton channel of influenza A virus. Inhibition of the wild-type (WT) M2 channel and the amantadine-resistant A/M2-S31N and A/M2-V27A mutant ion channels were measured in *Xenopus* oocytes using two-electrode voltage clamp (TEV) assays. Most of the novel compounds inhibited the WT ion channel in the low micromolar range. Of note, several compounds inhibited the A/M2 V27A mutant ion channel, one of them with submicromolar IC$_{50}$. None of the compounds was found to inhibit the S31N mutant ion channel. The antiviral activity of three novel dual WT and A/M2-V27A channels inhibitors was confirmed by influenza virus yield assays.

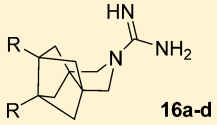

16a-d

INTRODUCTION

The influenza A virus M2 protein is a 97 residues long integral membrane protein with a transmembrane (TM) domain of 19 residues, a small ectodomain of 23 residues, and a 54 residues long cytoplasmic tail.[1] This M2 protein is encoded by a spliced mRNA derived from viral RNA segment 7.[2] The A/M2 proton channel activity is required for viral replication.[3] Influenza A virus particles enter the host cells by endocytosis (mainly via the clathrin-mediated route).[4] Within the endosome, release of the viral ribonucleoprotein (RNPs) complexes from the matrix M1 protein depends on acidification of the viral interior. This lowering of the pH is accomplished by the M2 proton channel, which facilitates the flow of protons from the acidic endosomal lumen into the interior of the virion.[5] This proton channel function of M2 has been found to be essential in all influenza A subtypes thus far studied. In some virus strains, e.g., H7N1 fowl plague virus, the A/M2 protein also equilibrates the pH of the trans-Golgi network to prevent a premature conformational change of the viral hemagglutinin (HA).[6]

Influenza A viruses are important pathogens which are capable of causing significant morbidity and mortality in humans. Two classes of antiviral drugs are currently available: the M2 ion channel inhibitors (amantadine (Amt) and rimantadine) and the neuraminidase (NA) inhibitors (oseltamivir and zanamivir).[6] However, the usefulness of Amt and rimantadine dropped sharply in recent years due to the widespread of resistant viruses, which prompted the Centers for Disease Control to recommend discontinuing the use of Amt-based drugs.[7,8] Also, resistance to oseltamivir has been frequently observed in recent flu seasons.[9,10] Therefore, there is an urgent need to develop the next generation of antiviral drugs that are active against drug-resistant influenza viruses. Systematic mutational analysis of the pore-line residues of the A/M2 TM domain identified many Amt-resistance mutations.[11] However, only a few of these mutations (i.e., L26F, V27A, and S31N) have been observed in transmissible viruses, with the S31N mutation being the most frequently occurring Amt-resistance mutation.[12] The channel properties (ion selectivity and activity) of these mutants appear to be very similar to those of the WT M2 channel, suggesting that the channel properties need to be finely tuned in order for the virus to be transmissible.

Many efforts have been made to discover new small molecular inhibitors of Amt-resistant mutant forms of A/M2. For example, Wang et al. reported several spiro compounds such as **1**−**3**. Spiroadamantane **3** inhibits the L26F and V27A A/M2 mutants with good efficacy in electrophysiological and virus plaque reduction assays.[13−15] Most recently, this group also discovered new compounds, such as **4** and **5**, that inhibit the most prevalent drug-resistant A/M2 mutant, S31N (Chart 1).[16−18]

Received: September 6, 2013
Published: November 4, 2013

Chart 1. Structures of Amantadine, Rimantadine, and Recently Developed Analogues with Potent Activity against Mutant A/M2 Channels[a]

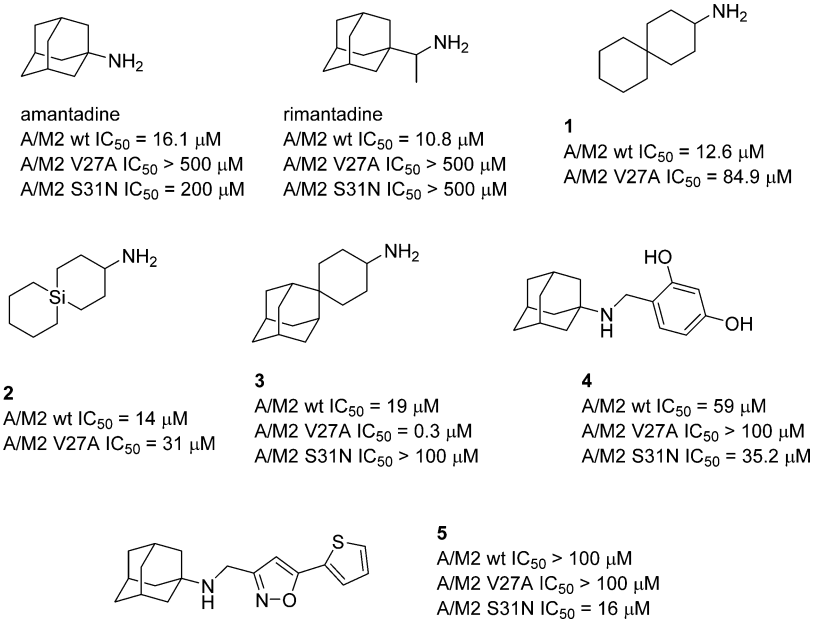

[a]The IC_{50} values shown are reported 50% inhibitory concentrations obtained in the TEV assay.[13−18]

Chart 2. Structures of Known Ring-Contracted and Ring-Rearranged Analogues of Amantadine

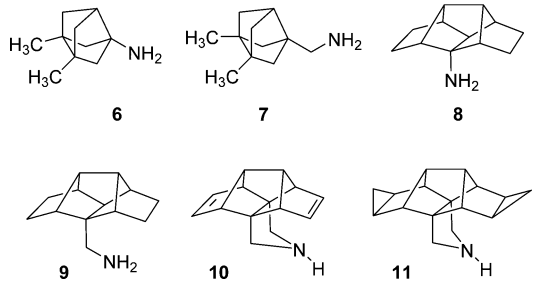

In this study, we report some novel scaffolds designed to inhibit the A/M2 channel. Several pyrrolidine derivatives were found to inhibit the WT channel as well as the M2-V27A mutant ion channel. The best compound, guanidine **16d**, has a low micromolar activity against the WT channel (IC_{50} = 3.4 μM) and submicromolar activity against the M2-V27A mutant (IC_{50} = 0.29 μM).

CHEMISTRY

During the past years, our group has synthesized several polycyclic Amt analogues containing different scaffolds, including ring-contracted, ring-rearranged, and 2,2-dialkyl

Table 1. Inhibitory Effect of the Synthesized Compounds on A/M2 WT, S31N, or V27A Proton Channel Functions[a]

	A/M2 WT (mean ± SE)		A/M2 S31N (mean ± SE)		A/M2 V27A (mean ± SE)	
compd	inhibition by 100 μM for 2 min (%)	IC_{50} (μM)	inhibition by 100 μM for 2 min (%)	IC_{50} (μM)	inhibition by 100 μM for 2 min (%)	IC_{50} (μM)
amantadine	91.0 ± 2.1	16.0 ± 1.2	35.6 ± 1.5	199.9 ± 13.5	10.8 ± 2.0	ND[b]
6	93.6 ± 0.9	17.0 ± 1.0	22.1 ± 0.2	252.2 ± 13.2	10.6 ± 0.7	ND
7	97.3 ± 0.4	7.2 ± 0.3	0	ND	17.6 ± 1.8	ND
8	4.8 ± 2.8	ND	0	ND	0	ND
9	12.8 ± 1.0	ND	0	ND	0	ND
10	82.5 ± 0.8	33.5 ± 1.6	0	ND	9.2 ± 1.0	ND
11	86.5 ± 0.8	24.0 ± 2.1	0	ND	17.7 ± 0.5	ND
14a	93.8 ± 0.8	9.7	0	ND	26.0 ± 0.3	ND
15a	87.9 ± 0.6	16.3	0	ND	12.3 ± 1.6	ND
16a	92.4 ± 0.6	6.1	1.0 ± 1.0	ND	84.2 ± 1.0	11.4
14b	93.9 ± 0.2	11.7	6.2 ± 0.7	ND	5.6 ± 1.5	ND
15b	88.3 ± 0.2	25.2	0	ND	0	ND
16b	95.7 ± 1.5	1.05	0	ND	0	ND
14c	65.0 ± 1.7	ND	13.1 ± 1.7	ND	15.8 ± 2.7	ND
16c	42.8 ± 1.8	ND	10.8 ± 1.2	ND	79.2 ± 0.4	13.8
14d	85.3 ± 0.8	4.5	11.9 ± 1.0	ND	76.2 ± 0.3	20.5
16d	93.1 ± 2.5	3.4	5.7 ± 2.0	ND	93.8 ± 0.9	0.29

[a]Isochronic (2 min) values for IC_{50} are given. See text and Experimental Section for details. [b]ND: not determined.

dx.doi.org/10.1021/jm401340p | J. Med. Chem. 2013, 56, 9265−9274

Scheme 1. Synthesis of Polycyclic Pyrrolidine Derivatives

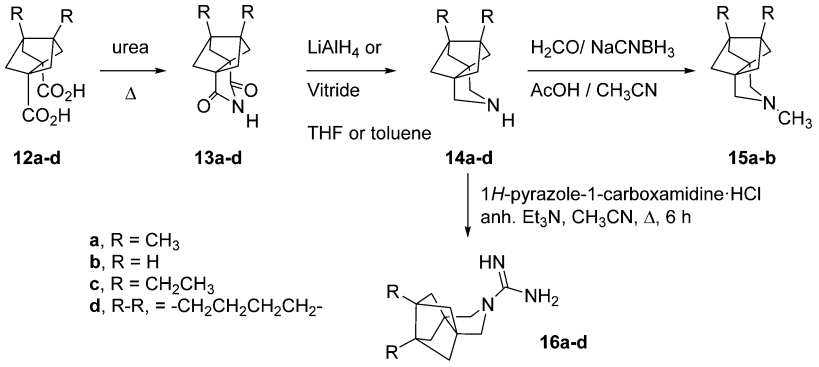

Scheme 2. Synthesis of Diesters 22c−d

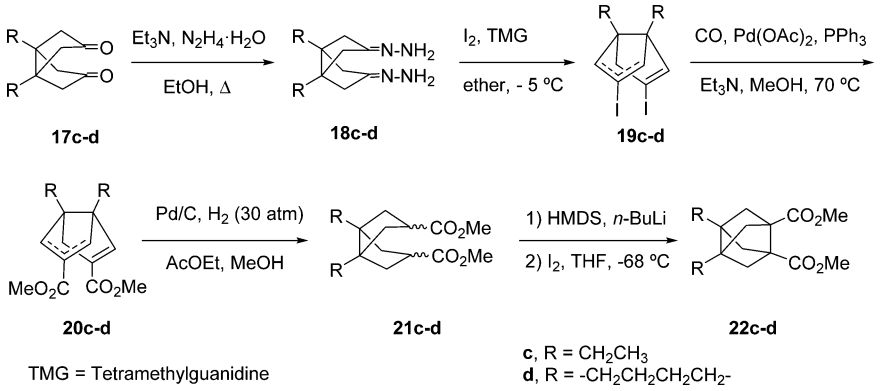

derivatives of Amt (Chart 2).[19−22] Several ring-contracted analogues of Amt, such as amines **6** and **7**, were evaluated for inhibition of A/M2 proton channel activity by using the conductance assay in M2-expressing oocytes. They displayed similar IC_{50} values for WT A/M2 as Amt but, unfortunately, were inactive against the Amt-resistant S31N or V27A mutant forms of A/M2.[20] We have also explored the activity of larger, ring-rearranged analogues of Amt using the pentacyclo-[6.4.0.0^{2,10}.0^{3,7}.0^{4,9}]dodecane scaffold. Very interestingly, while primary amines **8** and **9** and several derivatives, including secondary and tertiary amines, amidines, and guanidines, did not inhibit A/M2 proton channel activity, the conformationally more rigid pyrrolidine-based derivatives **10** and **11** did show a promising activity against the WT A/M2 channel, being only slightly less active than Amt. Moreover, while the primary amines **8** and **9** did not show any activity against the V27A mutant form of A/M2, both pyrrolidine derivatives showed a marginal activity against this mutant (Table 1).[20,22]

On the basis of these promising results, we reasoned that the synthesis of pyrrolidine analogues of the already active bisnoradamantane **7**, featuring an unprecedented 3-azatetracyclo[5.2.1.1^{5,8}.0^{1,5}]undecane ring, may lead to compounds with higher activity against the WT and the V27A mutant of A/M2.

The reaction of the known[23,24] diacids **12a,b** with urea at 180 °C for 30 min yielded imides **13a,b**, which were subsequently reduced to give the secondary amines **14a,b** in good overall yields. Reductive alkylation of the secondary amines with formaldehyde and $NaCNBH_3$ led to the corresponding tertiary amines **15a,b** in good yields. Taking into account our observation that some of the corresponding guanidines derived from our previously synthesized amines were also inhibitors of the A/M2 channel,[20] we synthesized guanidines **16a,b** from amines **14a,b** and 1*H*-pyrazole-1-carboxamidine monohydrochloride (Scheme 1).

Recent experimental and computational studies have shown that the mutation of Val27 to a residue with a smaller side chain such as alanine (A/M2-V27A mutant) destroyed the hydrophobic gate formed by this residue and increased the pore radius by ∼2 Å at the *N*-terminal end.[14,25,26]

The amine **14a** and guanidine **16a** displayed higher inhibitory activity against the M2-V27A mutant channel than their corresponding smaller analogues, **14b** and **16b** (see below). Also, because recent MD calculations suggested that larger, more hydrophobic molecules may fill the pore of the V27A mutant better,[14] we designed two novel, larger analogues of the dual inhibitor **16a**, i.e., **16c** and **16d**.

For the synthesis of pyrrolidines **14c,d** and **16c,d**, following the route outlined in Scheme 1, novel diacid derivatives **12c,d** were required. Thus, we synthesized diacids **12c,d** from easily available diketones **17c,d**, following the synthetic sequence shown in Scheme 2 that we had previously developed for related bisnoradamantane derivatives.[27]

To homologate diketones **17c−d**,[28−30] they were transformed into a mixture of the corresponding bis-vinyl iodides *syn*- and *anti*-**19c−d**, via the corresponding bis-hydrazones, **18c−d**, following the Barton procedure, in 41 and 56%, respectively, overall yield.[31,32] Then, palladium (0) catalyzed methoxycarbonylation of **19c−d** afforded **20c−d** in 62 and 64% yield, respectively, as a mixture of *syn* and *anti* regioisomers. Catalytic hydrogenation (Pd/C) of the mixture of *syn*- and *anti*-**20c−d** gave an stereoisomeric mixture of diesters **21c−d** in 77 and 74% yield, respectively. Reaction of diesters **21c−d** with two equivalents of LiHMDS in anhydrous THF, followed by

dx.doi.org/10.1021/jm401340p | J. Med. Chem. 2013, 56, 9265−9274

reaction of the corresponding bis-enolate with one equivalent of iodine gave **22c−d** in 47 and 57% yield, respectively. Finally, hydrolysis of diesters **22c−d** gave the diacids **12c−d** in, 63% and 80% yield, respectively (Scheme 2).

From diacids **12c−d**, and following the synthetic sequence shown in Scheme 1, we prepared the amines **14c−d** and the guanidines **16c−d** in good overall yields (see Supporting Information for details).

All the pharmacologically evaluated compounds were fully characterized as salts (hydrochlorides or tartrates) through their spectroscopic data and elemental analyses.

PHARMACOLOGICAL ACTIVITY AND STRUCTURE−ACTIVITY RELATIONSHIPS

Inhibition of WT and Amt-Resistant A/M2 Ion Channels. The inhibitory activity of the compounds was tested on A/M2 channels expressed in *Xenopus* oocytes using the TEV technique. All inhibitors were initially tested at 100 μM; those that inhibited the WT A/M2 channel activity by more than 75% were chosen for measurement of their 50% inhibitory concentration (IC_{50}). The results are given in Table 1.

Amt inhibited WT A/M2 channel with an IC_{50} of 16.0 μM in an isochronic (2 min) inhibition assay. It has been suggested that in designing Amt analogues, pyrrolidine or piperidine derivatives may result in a more favorable orientation inside the M2 channel pore as compared to freely rotating alkylamine chains.[33] Thus, we had previously tested tetracyclic derivatives **8** and **9** and conformationally more rigid amines **10** and **11** (Table 1).[20] In sharp contrast with the poor performance of primary amines **8** and **9**, diene **10** was shown to be able to inhibit WT A/M2 channel by more than 80%, showing an IC_{50} of 33.5 μM. Bis-cyclopropanation slightly increased the potency because derivative **11** showed an IC_{50} of 24.0 μM. Interestingly, **11** (at a concentration of 100 μM) inhibited the A/M2 V27A channel activity by 17.7%, which is superior to Amt (10.8%), yet much less than **1−3**.[13−15]

On the basis of these results, we synthesized compounds **14a**, **15a**, and **16a** as conformationally more rigid analogues of **7**. In agreement with the previous trend observed in going from **8** and **9** to **10** and **11**, pyrrolidines **14a** and **16a** were potent inhibitors of the WT channel (IC_{50} of 9.7 and 6.1 μM, respectively) and, very interestingly, were better inhibitors of the V27A mutant channel than **7**, with the guanidine **16a** showing an IC_{50} of 11.4 μM. Alkylation of **14a** to **15a** reduced the inhibitory potency both for the WT and the V27A mutant.

We also synthesized smaller and larger analogues of **14a** and **16a**. As expected, in going from **14a** and **16a** to the smaller analogues **14b** and **16b**, an important reduction of the activity against the V27A mutant was observed, although both compounds kept the inhibitory activity against the WT. Again, the tertiary amine **15b** was less potent than the corresponding secondary amine **14b**. For this reason, no further tertiary amines were synthesized.

In going from the dimethyl derivatives **14a** and **16a** to their corresponding diethyl derivatives, **14c** and **16c**, the activity against both the WT and the V27A mutant channels diminished, probably because the freely rotating ethyl chains of **14c** and **16c** make destabilizing contacts with the backbone of the protein. These contacts should be more evident in the narrower WT channel, as reflected in the lower inhibitory activities of **14c** and **16c** against the WT channel compared to **14a** and **16a**. In the conformationally more rigid amine **14d** and guanidine **16d**, the low micromolar inhibitory activity against the WT channel was restored and, pleasingly, good inhibition of the V27A mutant channel was observed, with **16d** showing an IC_{50} of 0.29 μM.

Binding of Guanidine 16d. To determine the binding affinity of this class of compounds, we chose one of the most potent inhibitor against WT M2, **16d**, and measured its affinity by solution NMR drug titration. A peptide spanning the transmembrane domain (22−46) of M2, designated as M2TM, was reconstituted in dodecylphosphocholine (DPC) micelles in a 1:50 peptide to detergent ratio, under which condition M2TM forms tetramer predominantly. **16d** was titrated into the solution, and the characteristic peak of W41 $H^{\varepsilon 1}$ was monitored in 1D ^{1}H NMR (Supporting Information Figure S1). It was found that drug-bound form of M2 is in slow exchange with the apo-form: a new peak at 10.9 ppm, corresponding to W41 $H^{\varepsilon 1}$, emerges upon drug addition and continuously increases with drug titration while the peak at 10.4 ppm associated with the apo-form becomes weaker. Previously, we observed that this peak correlates with the binding of drugs to the pore of the channel.[34] A plot of the peak integral at 10.9 ppm against increasing drug concentrations is shown in Figure 1. The data were fitted using the nonlinear least-squares fitting

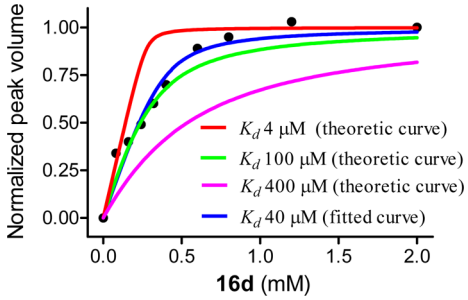

Figure 1. Binding affinity of **16d** to WT M2TM as determined by solution NMR drug titration. Normalized peak volume of the W41 $H^{\varepsilon 1}$ in the drug-bound form was plotted as a function of **16d** concentration. The fitting yields a stoichiometry ratio of 1.37 ± 0.28 drug/tetramer with a K_d of 40 ± 24 μM (curve shown in blue). In comparison, theoretical curve fittings with fixed stoichiometry (N = 1) and K_d of 4, 100, and 400 μM are shown in red, green, and pink, respectively. Details about curve fitting can be found in the Supporting Information.

equation as described earlier.[34] The best fit gave a stoichiometry ratio of 1.37 ± 0.28 drug per tetramer and a dissociation constant K_d of 40 ± 24 μM. It should be noted that the titration was conducted at a protein concentration (1.6 mM) that is significantly above K_d, thus the actual K_d is difficult to be determined. However, theoretical curve fittings with fixed stoichiometry (N = 1, meaning one drug per tetramer binding) and different K_d (4, 100, and 400 μM) showed the K_d to be significantly less than 100 μM (see Figure 1).

It is worth noting that the difference between the IC_{50} and K_d reflects the differences in the experimental assays used to determine these properties. It has long been known that M2 channel blockers are very slow binders, as noted in the second-order rate constant of amantadine (i. e., 600 to 900 M^{-1} s^{-1} for the Udorn strain).[35] So, the IC_{50} depends on the amount of time the drug is exposed to the target.

Antiviral Activity and Cytotoxicity in Cell Culture. All novel compounds were subjected to antiviral evaluation against a wide range of DNA and RNA viruses, using CPE reduction

dx.doi.org/10.1021/jm401340p | J. Med. Chem. 2013, 56, 9265−9274

Table 2. Antiviral Activity in Influenza Virus-Infected MDCK[a] Cells

	antiviral EC_{50}[b] (μM)							
	influenza A/H1N1		influenza A/H3N2		influenza B		cytotoxicity (μM) at 72 h	
compd	CPE	MTS	CPE	MTS	CPE	MTS	CC_{50}[c]	MCC[d]
14a	>100	>100	1.6	>100	>100	>100	59	100
15a	>100	>100	>100	>100	>100	>100	49	≥20
16a	>100	>100	>100	>100	>100	>100	1.4	4
14b	>100	>100	7.9	7.2	>100	>100	≥59	100
15b	>100	>100	>100	>100	>100	>100	>100	≥100
16b	>50	>50	>50	>50	>50	>50	10	8.5
14c	>100	>100	>100	>100	>100	>100	49	20
16c	>100	>100	>100	>100	>100	>100	6.2	4.0
14d	>100	>100	>100	>100	>100	>100	6.8	4.0
16d	>100	>100	>100	>100	>100	>100	3.1	4.0
amantadine	34	38	0.84	0.82	>500	>500	>500	>500
rimantadine	18	4.3	0.62	0.12	>500	>500	203	500

[a]MDCK: Madin-Darby canine kidney cells. [b]Virus strains: A/PR/8/34 (A/H1N1); A/HK/7/87 (A/H3N2) and B/HK/5/72. The EC_{50} represents the 50% effective concentration, or compound concentration producing 50% inhibition of virus replication, as determined by microscopic scoring of the CPE at 72 h post infection, or by the MTS cell viability test. [c]MCC: minimum cytotoxic concentration, or concentration producing minimal alterations in cell morphology after 72 h incubation with compound. [d]CC_{50}: 50% cytotoxic concentration, as determined by the MTS cell viability test. Values shown are the mean of 2−3 determinations.

assays in relevant cell lines. None of the compounds displayed activity against the enveloped DNA viruses herpes simplex virus (type 1 or type 2) or vaccinia virus, the enveloped RNA viruses feline coronavirus, parainfluenza-3 virus, respiratory syncytial virus, vesicular stomatitis virus, Sindbis virus, or Punta Toro virus, or the nonenveloped RNA viruses Coxsackievirus B4 and Reovirus-1 (data not shown).

In our basic CPE reduction assays with influenza virus, performed in MDCK cell cultures, three virus strains were used: the A/PR/8/34 strain, an A/H1N1 virus with two amantadine-resistance mutations (S31N and V27T) in the A/M2 protein, the A/HK/7/87 strain, which has a WT A/M2 protein, and the B/HK/5/72 strain. The antiviral data obtained by microscopic scoring of the virus-induced CPE were confirmed by the colorimetric MTS cell viability assay. In parallel, the compounds were applied to uninfected MDCK cells to estimate the cytotoxicity by microscopy or MTS cell viability assay (Table 2).

In agreement with the TEV assays (see above), all the compounds were not active against the amantadine-resistant A/PR/8/34 strain that carries the M2-S31N mutation. For compounds **14a**, **14b**, and Amt, a correlation was seen between their cell culture activities for the A/HK/7/87 virus (EC_{50} values: 1.6 μM for **14a** and 7.9 μM for **14b**) and their IC_{50} values against A/M2 WT proton channel function. This was, however, not the case for the amine **14d** and for the guanidines **16a**,**b**,**d**. These four compounds had quite pronounced cytotoxicity in the MDCK cells in our three-day CPE reduction assay (i.e., minimum cytotoxic concentrations of 8 μM or lower), and this may have masked the potential inhibitory effect of the compounds toward the A/HK/7/87 virus (Table 2).

It is difficult to speculate on the cause of the toxicity. These are amphiphilic compounds that might well cause a membrane disrupting effect given sufficient time of exposure. The CPE test is a 3-day assay and, hence, some compounds may display toxic effects that make it impossible to assess the potential antiviral effect. On the other hand, compounds with favorable activity and selectivity are easily identified in the CPE assay, i.e., **14a** and **14b**.

Table 3. Activity of 16a,b,d and 14d in Influenza Virus Yield Assay

	activity[a] (μM) against A/HK/7/87		cytotoxicity at 24 h
compd	EC_{90} (μM)	EC_{99} (μM)	MCC (μM)[b]
16a	0.46	0.79	>50
16b	20	≥38	>50
14d	0.85	>10	>50
16d	0.37	>2	≥10
Amt	0.22	1.1	≥500
rimantadine	0.10	>4	≥500
ribavirin	4.6	11	>100

[a]Antiviral activity was determined by a qRT-PCR-based virus yield assay to quantify the virus in the supernatant at 24 post infection.[35] EC_{90} and EC_{99}: concentrations causing 1 $\log_{10}$ and 2 $\log_{10}$ reduction in virus yield, respectively. [b]MCC: minimum cytotoxic concentration, or concentration producing minimal alterations in cell morphology after 24 h incubation with compound.

We therefore evaluated amine **14d** and the guanidines **16a**,**b**,**d** in a virus yield assay with strain A/HK/7/87 (carrying a WT A/M2), in which the virus released in the supernatant at 24 h after infection was quantified by real-time RT-PCR.[36] As shown in Table 3, amine **14d** and guanidines **16a** and **16d** had an EC_{90} value (i.e., concentration causing 10-fold reduction in virus yield) below 1 μM, which is the same order of magnitude as the values noted for Amt and rimantadine. Of these, **16a** and Amt were able to afford a 100-fold reduction in virus yield, with EC_{99} values of ∼1 μM.

CONCLUSIONS

The present works showed that, starting from compounds active against the WT A/M2 channel, it is possible to design compounds active against both the WT and the V27A mutant A/M2 channels. In fact, some of them inhibit both channels more effectively than amantadine inhibits the WT. The low micromolar antiviral activity of the three dual inhibitors identified, amine **14d** and guanidines **16a** and **16d**, was confirmed by an influenza virus yield assay. Interestingly, the

dx.doi.org/10.1021/jm401340p | J. Med. Chem. 2013, 56, 9265−9274

compounds reported here are the first examples of non-adamantane derivatives endowed with low micromolar activity against the V27A/M2 mutant channel, opening the way to the design of novel M2 inhibitors structurally based on non-adamantane scaffolds. Taking into account the broad utility of the adamantane scaffold in medicinal chemistry, the novel azapolycyclic ring reported here may be of interest for other therapeutic areas where the adamantane derivatives are of medicinal interest.

EXPERIMENTAL SECTION

Plasmid, mRNA Synthesis, and Microinjection of Oocytes. The cDNA encoding the influenza A/Udorn/72 (A/M2) was inserted into pGEM3 vector for the expression on oocyte plasma membrane. A/M2 S31N and A/M2 V27A mutants were generated by QuikChange site-directed mutagenesis kit (Agilent Technologies). The synthesis of mRNA and microinjection of oocytes have been described previously.[37]

Two-Electrode Voltage Clamp Analysis. Macroscopic membrane current was recorded 48−72 h after injection as described previously.[13] The tested compounds were applied at pH 5.5 at various concentrations when the inward current reaches maximum. The compounds were applied for 2 min, and residual membrane current was compared with the membrane current before the application of compounds. Membrane currents were analyzed with pCLAMP 10.0 software package (Axon Instruments, Sunnyvale, CA).

NMR of Drug Titration. The M2TM peptide corresponding to the transmembrane domain of the Udorn M2, SSDPLVVAASII-GILHLILWILDRL, was synthesized using an optimized protocol as described before.[34] The NMR sample was prepared starting from mixing peptide and DPC in the desired molar ratio in ethanol, followed by removal of ethanol by nitrogen flush and lyophilization to ensure completely removal. The resulting film was dissolved in NMR buffer consisting of 50 mM sodium phosphate in 10% D_2O and 90% H_2O, pH 7.5. Drug, **16d**, was dissolved in H_2O and added to the NMR sample gradually. The final dilution was less than 2%.

Cell Culture Assays for Antiviral Activity and Cytotoxicity. The antiviral activity of the compounds was determined in established CPE reduction assays, using a diverse set of DNA and RNA viruses as indicated and including three (sub)types of influenza virus: A/Puerto Rico/8/34 (A/H1N1), A/Hong Kong/7/87 (A/H3N2), and B/Hong Kong/5/72.[38,39] Briefly, Madin−Darby canine kidney cells seeded in 96-well plates were exposed to influenza virus (multiplicity of infection: 50 $CCID_{50}$ (50% cell culture infective dose) per well) together with the test compounds. After three days incubation at 35 °C, microscopy was performed to score the virus-induced cytopathic effect (CPE) as well as compound cytotoxicity. These data were confirmed by the colorimetric formazan-based MTS cell viability assay. Antiviral activity was expressed as the EC_{50} value, or compound concentration producing 50% inhibition of the virus-induced CPE, as determined by microscopy or MTS assay. Compound cytotoxicity was expressed as the minimum inhibitory concentration (MCC), i.e., the concentration producing minimal changes in cell morphology, or the CC_{50} value, i.e., the concentration causing 50% reduction in cell viability by MTS assay.

To determine the effect of the compounds on virus yield, MDCK cells were incubated with influenza virus (strain A/HongKong/7/87) and compounds as above. After 24 h incubation, the supernatants were collected and frozen. The virus released in these supernatants was quantified by real-time qRT-PCR, as described.[36] Antiviral activity was expressed as the EC_{90} or EC_{99} value, i.e., the compound concentration producing a virus yield reduction of 1 $\log_{10}$ or 2 $\log_{10}$, respectively.

Chemical Synthesis. General Methods. Melting points were determined in open capillary tubes with a MFB 595010 M Gallenkamp melting point apparatus. 300 MHz ^1H/75.4 MHz ^{13}C NMR spectra, 400 MHz ^1H/100.6 MHz ^{13}C NMR spectra, and 500 MHz ^1H NMR spectra were recorded on Varian Gemini 300, Varian Mercury 400, and Varian Inova 500 spectrometers, respectively. The chemical shifts are reported in ppm (δ scale) relative to internal tetramethylsilane, and coupling constants are reported in hertz (Hz). Assignments given for the NMR spectra of the new compounds have been carried out on the basis of DEPT, COSY $^1H/^1H$ (standard procedures), and COSY $^1H/^{13}C$ (gHSQC and gHMBC sequences) experiments. An asterisk (*) in the NMR data means interchangeable signals. IR spectra were run on a Perkin-Elmer Spectrum RX I spectrophotometer. Absorption values are expressed as wavenumbers (cm^{-1}); only significant absorption bands are given. The GC/MS analysis was carried out in an inert Agilent Technologies 5975 gas chromatograph equipped with an Agilent 122−5532 DB-5MS 1b (30 m × 0.25 mm) capillary column with a stationary phase of phenylmethylsilicon (5% diphenyl−95% dimethylpolysiloxane), using the following conditions: initial temperature of 50 °C (1 min), with a gradient of 10 °C/min up to 300 °C, and a temperature in the source of 250 °C, *Solvent Delay* (SD) of 4 min and a pressure of 7.35 psi. Column chromatography was performed on silica gel 60 A C.C (35−70 mesh, SDS, ref 2000027). Thin-layer chromatography was performed with aluminum-backed sheets with silica gel 60 F_{254} (Merck, ref 1.05554), and spots were visualized with UV light and 1% aqueous solution of $KMnO_4$. The analytical samples of all of the new compounds which were subjected to pharmacological evaluation possessed a purity ≥95% as evidenced by their elemental analyses.

7,8-Dimethyl-3-azatetracyclo[5.2.1.1^{5,8}.0^{1,5}]undeca-2,4-dione (13a). A mixture of known[23] diacid **12a** (3.0 g, 13.4 mmol) and urea (4.2 g, 95% purity, 67.0 mmol) was heated slowly to 135 °C. When the mixture melted, it was heated to 180 °C for 30 min and cooled. Water (66 mL) was added, and the suspension was extracted with CH_2Cl_2 (6 × 40 mL). The combined organic extracts were washed with brine (1 × 45 mL), dried with anhydrous Na_2SO_4, filtered, and concentrated in vacuo to dryness to give imide **13a** as a white solid (2.07 g, 75% yield). An analytical sample of **13a** was obtained by crystallization from $CHCl_3$, mp 209−210 °C. IR (KBr) ν 3194 (N−H), 1766 and 1711 (C═O st) cm^{-1}. ^1H NMR (400 MHz, $CDCl_3$) δ 1.23 [s, 6 H, C7(8)-C$\underline{H}_3$], 1.88 [dd, J = 9.8 Hz, J' = 1.9 Hz, 4 H, 6(9,10,11)-H_α], 1.92 [dd, J = 9.8 Hz, J' = 2.0 Hz, 4 H, 6(9,10,11)-H_β], 8.24 (bs, 1 H, NH). ^{13}C NMR (100.6 MHz, $CDCl_3$) δ 16.1 [CH_3, C7(8)-CH_3], 51.8 [C, C7(8)], 55.2 [CH_2, C6(9,10,11)], 57.5 [(C, C1(5)], 177.4 (C, CO). GC/MS (EI), m/e (%): 205 ($M^{\cdot+}$, 4), 134 (83), 120 (100), 119 (53), 150 (48), 117 (10), 105 (17), 92 (22), 91 (38), 79 (15), 77 (23). HRMS-ESI+ m/z $[M + H]^+$ calcd for $[C_{12}H_{15}NO_2 + H]^+$, 206.1176; found, 206.1185.

7,8-Dimethyl-3-azatetracyclo[5.2.1.1^{5,8}.0^{1,5}]undecane Hydrochloride (14a·HCl). To a stirred solution of imide **13a** (0.36 g, 1.8 mmol) in anhydrous toluene (8 mL) at 0 °C, sodium bis-(2-methoxyethoxy)aluminum hydride (2.7 mL, 65% in toluene, 8.8 mmol) was added dropwise. When the addition was finished, the solution was heated under reflux for 72 h. The mixture was cooled to 0 °C (ice−water bath), treated with 30% aq solution of KOH until basic pH, and stirred at room temperature for 1 h. The organic layer was separated, and the aqueous one was extracted with CH_2Cl_2 (3 × 15 mL). The combined organic layers were dried with anhydrous Na_2SO_4, filtered, and evaporated in vacuo. The obtained solid residue was dissolved in Et_2O (20 mL) and treated with excess of HCl in Et_2O to give the hydrochloride of **14a** (0.41 g, 99% yield) as a solid that was collected by filtration. An analytical sample of **14a·HCl** was obtained as a white solid by crystallization from MeOH/Et_2O, mp 248−249 °C. IR (KBr) ν 3527, 2953, 2883, 2767, 2702, 2588, 2536, 2413, 2241, 1902, 1610, 1594, 1508, 1483, 1457, 1444, 1379, 1363, 1297, 1260, 1183, 983, 871 cm^{-1}. ^1H NMR (400 MHz, CD_3OD) δ 1.19 [s, 6 H, C7(8)-CH_3], 1.67 [m, 8 H, 6(9,10,11)-H_2], 3.26 [bs, 4 H, C2(4)-H_2]. ^{13}C NMR (100.6 MHz, CD_3OD) δ 16.7 [CH_3, C7(8)-CH_3], 47.5 [CH_2, C2(4)], 52.4 [C, C7(8)], 56.6 [CH_2, C6(9,10,11)], 58.7 [C, C1(5)]. MS (EI), m/e (%): 177 ($M^{\cdot+}$, 6), 135 (21), 134 ($C_{10}H_{14}^{\cdot+}$, 100), 133 (35), 122 (29), 119 (22), 107 (22), 106 (35), 105 (48), 93 (32), 92 (21), 91 (64), 80 (23), 79 (24), 77 (34), 55 (21).

3,7,8-Trimethyl-3-azatetracyclo[5.2.1.1^{5,8}.0^{1,5}]undecane Hydrochloride (15a·HCl). To a suspension of **14a** (0.5 g, 2.4 mmol) in acetonitrile (10 mL), $NaBH_3CN$ (95% content, 0.46 g, 6.9 mmol), AcOH (0.4 mL), and formaldehyde (37% aqueous solution 0.6 mL,

dx.doi.org/10.1021/jm401340p | J. Med. Chem. 2013, 56, 9265−9274

7.3 mmol) were added and the mixture was magnetically stirred at room temperature for 8 h. Then, more $NaBH_3CN$ (95% content, 0.46 g, 6.9 mmol) and formaldehyde (37% aqueous solution 0.6 mL, 7.3 mmol) were added, and stirring at room temperature was continued for 18 h more. The mixture was concentrated in vacuo, the residue was suspended in water (20 mL), and the solution was made basic with aqueous solution of 2 N NaOH (4 mL) and extracted with EtOAc (3 × 20 mL). The combined organic extracts were dried (anhydrous Na_2SO_4), filtered, treated with an excess of an ethereal solution of HCl, and concentrated in vacuo to give the hydrochloride of **15a** (0.4 g, 73% yield) as a white solid. An analytical sample of **15a·HCl** was obtained by crystallization from 2-propanol, mp 280−281 °C (dec.). IR (KBr) ν 3384, 3007, 2953, 2882, 2591, 2564, 2474, 2449, 1644, 1480, 1462, 1446, 1419, 1378, 1349, 1293, 1257, 1248, 1193, 1173, 1123, 1105, 1068, 1025, 967, 893 cm^{-1}. ^1H NMR (500 MHz, $CDCl_3$) δ 1.09 (s, 3 H) and 1.11 (s, 3 H) (C7-CH_3 and C8-CH_3), 1.47 [d, J = 8.5 Hz, 2 H, 9(11)-H_α], 1.52 [dd, J = 7.2 Hz, J' = 2.0 Hz, 2 H, 6(10)-H_β], 1.63 [d, J = 8.0 Hz, 2 H, 6(10)-H_α], 2.18 [dd, J = 8.0 Hz, J = 2.0 Hz, 2 H, 9(11)-H_β], 2.79 [m, 2 H, C2(4)-H_a], 2.82 (d, J = 3.5 Hz, 3 H, N-CH_3), 3.64 [d, J = 7.5 Hz, 2 H, C2(4)-H_b] and 12.65 (bs, 1H, NH). ^{13}C NMR (125.7 MHz, $CDCl_3$) δ 16.0 (CH_3) and 16.2 (CH_3) (C7-CH_3) and (C8-CH_3), 40.7 (CH_3, N-CH_3), 50.2 (C, C7)*, 51.9 (C, C8)*, 54.7 [CH_2, C9(11)]*, 56.3 [CH_2, C6(10)]*, 56.5 [CH_2, C2(4)], 57.2 [C, C1(5)]. MS (EI), m/e (%): 191 ($M^{\cdot+}$, 43), 190 (40), 148 (100), 136 (35), 134 (32), 133 (31), 107 (22), 106 (28), 105 (28), 94 (20), 91 (41), 77 (21), 58 (50), 57 (37).

3-Amidino-7,8-dimethyl-3-azatetracyclo[5.2.1.1^{5,8}.0^{1,5}]-undecane Hydrochloride (16a·HCl). A suspension of **14a·HCl** (0.37 g, 1.73 mmol), Et_3N (0.44 mL, 2.79 mmol) and 1*H*-pyrazole-1-carboxamidine hydrochloride (0.31 g, 2.11 mmol) in CH_3CN (5 mL) was heated at 70 °C for 6 h. Then, the suspension was allowed to stand overnight in the freezer (4 °C), and the solid was separated by filtration in vacuo and washed with diethyl ether to give **16a·HCl** as a beige solid (450 mg, 61% yield), mp 276−277 °C (dec). IR (KBr) ν 3295, 3093, 2937, 2876, 2723, 1634, 1531, 1478, 1456, 1361, 1293, 1189, 1161, 1133, 1116, 1045, 955, 737, 604, 540 cm^{-1}. ^1H NMR (400 MHz, CD_3OD) δ 1.18 [s, 6 H, C7(8)-CH_3], 1.63 [d, J = 6.9 Hz, 4 H, 6(9,10,11)-H_α], 1.69 [d, J = 6.9 Hz, 4 H, 6(9,10,11)-H_β], 3.49 [s, 4 H, C2(4)-H_2]. ^{13}C NMR (100.6 MHz, CD_3OD) δ 16.7 [CH_3, C7(8)-CH_3], 49.5 [CH_2, C2(4)], 52.3 [C, C7(8)], 58.0 [CH_2, C6(9,10,11)], 58.4 [C, C1(5)], 156.7 (C, C═N). MS (EI), m/e (%): 220 (54), 219 ($M^{\cdot+}$, 41), 166 (66), 165 (100), 164 (68), 163 (23), 145 (33), 134 ($C_{10}H_{14}^{\cdot+}$, 29), 133 (21), 123 (23), 122 (26), 120 (23), 119 (24), 114 (26), 113 (34), 112 (24), 107 (23), 106 (29), 105 (65), 91 (58), 79 (22), 77 (31), 74 (41), 73 (51), 72 (23).

3-Azatetracyclo[5.2.1.1^{5,8}.0^{1,5}]undeca-2,4-dione (13b). From known[24] diacid **12b** (0.5 g, 2.6 mmol) and urea (0.8 g, 95% purity, 12.7 mmol) and following the same procedure as reported for **13a**, imide **13b** was obtained as a white solid (0.33 g, 73% yield). An analytical sample of **13b** was obtained by crystallization from CH_2Cl_2, mp 131−132 °C. IR (KBr) ν 3189 (N−H), 1749 and 1715 (C═O st), 1346, 1135, 1054, 833 cm^{-1}. ^1H NMR (400 MHz, $CDCl_3$) δ 1.85 [dd, J = 9.6 Hz, J' = 2.4 Hz, 4 H, 6(9,10,11)-H_α], 2.05 [dd, J = 7.6 Hz, J' = 1.6 Hz, 4 H, 6(9,10,11)-H_β], 2.68 [m, 2 H, 7(8)-H], 7.74 (bs, 1 H, NH). ^{13}C NMR (100.6 MHz, $CDCl_3$) δ 40.3 [CH, C7(8)], 49.5 [CH_2, C6(9,10,11)], 57.1 [C, C1(5)], 176.8 (C, C═O). GC/MS (EI), m/e (%): 177 ($M^{\cdot+}$, 3), 106 (100), 105 (21), 93 (13), 92 (22), 91 (39), 79 (10), 78 (22), 77 (12), 65 (16). HRMS-ESI− m/z [M−H]$^-$ calcd for [$C_{10}H_{11}NO_2$-H]$^-$, 176.0717; found, 176.0725.

3-Azatetracyclo[5.2.1.1^{5,8}.0^{1,5}]undecane Hydrochloride (14b·HCl). To a stirred solution of imide **13b** (0.41 g, 2.3 mmol) in anhydrous THF (15 mL) at 0 °C, $LiAlH_4$ (0.9 g, 23.1 mmol) was added portionwise. When the addition was finished, the solution was heated under reflux for 72 h. The mixture was cooled to 0 °C (ice−water bath), treated with 10 N aq solution of NaOH til basic pH (8 mL), and stirred at room temperature for 1 h. The mixture was filtered through Celite, and the filtrate was thoroughly washed with CH_2Cl_2. The organic layer was separated, dried with anhydrous Na_2SO_4, filtered, and evaporated in vacuo. The obtained solid residue was dissolved in Et_2O (20 mL) and treated with excess of HCl in Et_2O to give the hydrochloride of **14b** (0.32 g, 75% yield). An analytical sample of **14b·HCl** was obtained as a white solid by crystallization from MeOH/Et_2O, mp 218−219 °C. IR (KBr) ν 3421, 2989, 2961, 2887, 2739, 2530, 2493, 1560, 1481, 1458, 1450, 1420, 1388, 1353, 1294, 1248, 1228, 1115, 1082, 1007, 988, 949, 924, 901, 881, 853, 771, 657, 604, 495 cm^{-1}. ^1H NMR (400 MHz, CD_3OD) δ 1.60 [broad d, J = 7.6 Hz, 4 H, 6(9,10,11)-H_α], 1.76 [dd, J = 7.6 Hz, J' = 2.0 Hz, 4 H, 6(9,10,11)-H_β], 2.48 [m, 2 H, 7(8)-H], 3.32 [bs, 4 H, C2(4)-H_2]. ^{13}C NMR (100.6 MHz, CD_3OD) δ 41.3 [CH, C7(8)], 47.0 [CH_2, C2(4)], 50.2 [CH_2, C6(9,10,11)], 58.3 [C, C1(5)]. MS (EI), m/e (%): 149 ($M^{\cdot+}$, 29), 108 (53), 107 ($C_8H_{11}^+$, 100), 106 (29), 105 (30), 95 (31), 94 (86), 92 (26), 91 (46), 80 (27), 79 (62), 77 (37), 71 (21), 70 (20).

3-Methyl-3-azatetracyclo[5.2.1.1^{5,8}.0^{1,5}]undecane Hydrochloride (15b·HCl). To a suspension of **14b** (0.32 g, 2.1 mmol) in acetonitrile (13 mL), $NaBH_3CN$ (95% content, 0.28 g, 4.3 mmol), AcOH (1.2 mL), and formaldehyde (37% aqueous solution, 1.1 mL, 14.1 mmol) were added and the mixture was magnetically stirred at room temperature for 8 h. Then, more $NaBH_3CN$ (95% content, 0.28 g, 4.3 mmol) and formaldehyde (37% aqueous solution 1.1 mL, 14.1 mmol) were added, and stirring at room temperature was continued for 18 h more. The mixture was concentrated in vacuo, the residue was suspended in water (20 mL), and the solution was made basic with aqueous solution of 2 N NaOH (4 mL) and extracted with EtOAc (3 × 25 mL). The combined organic extracts were dried (anhydrous Na_2SO_4), filtered, treated with an excess of an ethereal solution of HCl, and concentrated in vacuo to give the hydrochloride of **15b** (0.24 g, 70% yield) as a white solid. An analytical sample of **15b·HCl** was obtained by crystallization from MeOH/Et_2O, mp 223−224 °C (dec.). IR (KBr) ν 3003, 2962, 2889, 2572, 2462, 1628, 1508, 1482, 1465, 1349, 1293, 1269, 1228, 1177, 1129, 1106, 1079, 1060, 965, 890 cm^{-1}. ^1H NMR (400 MHz, CD_3OD) δ 1.61 (dd, J = 8.2 Hz, J' = 3.3 Hz, 2 H), 1.60−1.73 (complex signal, 4 H) and 1.79 (dd, J = 8.5 Hz, J = 2.4 Hz, 2H) [C6(10)-H_2 and C9(11)-H_2], 2.46 [m, 2H, C7(8)-H], 2.96 (s, 3H, N-CH_3), 3.18 (d, J = 12.0 Hz, 2 H) and 3.70 [d, J = 12.0 Hz, 2 H) [C2(4)-H_2]. ^{13}C NMR (100.6 MHz, CD_3OD) δ 39.9 [CH, C7(8)], 40.7 (CH_3, N-CH_3), 41.7 [CH, C7(8)], 49.7 [CH_2, C9(11)]*, 50.5 [CH_2, C6(10)]*, 57.3 [CH_2, C2(4)], 58.0 [C, C1(5)]. MS (EI), m/e (%): 163 ($M^{\cdot+}$, 57), 162 (100), 121 (26), 120 (35), 108 (30), 105 (11), 94 (13), 91 (19), 79 (17), 77 (14), 58 (22). HRMS-ESI+ m/z [M + H]$^+$ calcd for [$C_{11}H_{17}N$ + H]$^+$, 164.1434; found, 164.1432.

3-Amidino-3-azatetracyclo[5.2.1.1^{5,8}.0^{1,5}]undecane Hydrochloride (16b·HCl). From a suspension of **14b·HCl** (0.13 g, 0.7 mmol), Et_3N (0.17 mL, 1.08 mmol), and 1*H*-pyrazole-1-carboxamidine hydrochloride (0.12 g, 0.8 mmol) in CH_3CN (5 mL) and following the same procedure as reported for **16a·HCl**, guanidine **16b·HCl** was obtained as a beige solid (150 mg, 96% yield), mp 254−255 °C (dec) (CH_2Cl_2). IR (KBr) ν 3401, 3323, 3153, 2981, 2966, 2933, 2886, 1652, 1635, 1615, 1471, 1456, 1373, 1297, 1196, 1085, 565 cm^{-1}. ^1H NMR (400 MHz, CD_3OD) δ 1.55 [broad d, J = 7.2 Hz, 4 H, 6(9,10,11)-H_α], and 1.79 [broad d, J = 8.8 Hz, 4 H, 6(9,10,11)-H_β], 2.44 [s, 2 H, C7(8)], 3.55 [s, 4 H, C2(4)-H_2]. ^{13}C NMR (100.6 MHz, CD_3OD) δ 41.2 [CH, C7(8)], 48.9 [CH_2, C2(4)], 51.5 [CH_2, C6(9,10,11)], 57.8 [C, C1(5)], 156.7 (C, C═NH). MS (EI), m/e (%): 194 (43), 193 (40), 192 [(M + H)$^+$, 14], 153 (22), 152 (84), 151 (67), 150 (28), 139 (100), 138 (62), 117 (44), 115 (53), 114 (35), 109 (27), 108 (29), 107 (53), 106 (29), 105 (23), 96 (32), 95 (54), 94 (26), 92 (25), 91 (73), 81 (25), 80 (24), 79 (54), 78 (28), 77 (65), 75 (32), 74 (23), 71 (20), 65 (24), 63 (25), 53 (26). Anal. Calcd for $C_{11}H_{17}N_3$·HCl (227.73): C 58.01, H 7.97, N 18.45. HRMS-ESI+ m/z [M + H]$^+$ calcd for [$C_{11}H_{17}N_3$ + H]$^+$, 192.1495; found, 192.1494.

7,8-Diethyl-3-azatetracyclo[5.2.1.1^{5,8}.0^{1,5}]undeca-2,4-dione (13c). From diacid **12c** (1.12 g, 4.44 mmol) and urea (1.33 g, 22.2 mmol) and following the same procedure as reported for **13a**, imide **13c** was obtained as a white solid (0.91 g, 87% yield). An analytical sample of **13b** was obtained by crystallization from CH_2Cl_2/*n*-pentane, mp 204−205 °C. IR (KBr) ν 3404, 3198, 3072, 2962, 1761, 1707, 1464, 1353, 1210, 1143, 1061, 830, 725, 618, 506 cm^{-1}. ^1H NMR (400 MHz, $CDCl_3$) δ 0.92 [t, J = 7.6 Hz, 6 H, C7(8)-$CH_2C\underline{H}_3$], 1.63 [q, J = 7.6 Hz, 4 H, C7(8)-C$\underline{H}_2CH_3$], 1.80 [broad d, J = 7.2 Hz, 4 H,

dx.doi.org/10.1021/jm401340p | J. Med. Chem. 2013, 56, 9265−9274

6(9,10,11)-H_a], 1.96 [broad d, J = 7.2 Hz, 4 H, 6(9,10,11)-H_b], 8.13 (broad s, 1H, NH). ^{13}C NMR (100.6 MHz, $CDCl_3$) δ 10.0 [CH_3, C7(8)-$CH_2\underline{C}H_3$], 22.8 [CH_2, C7(8)-$\underline{C}H_2CH_3$], 52.1 [CH_2, C6-(9,10,11)], 56.6 [C, C7(8)], 57.2 [C, C1(5)], 177.7 (C, CO). GC/MS, m/z (%); main ions: 233 ($M^{\cdot+}$, 34), 163 (16), 162 (96), 148 (100), 147 (20), 133 (80), 106 (18), 105 (35), 91 (40), 77 (16). HRMS-ESI+ m/z [M + H]$^+$ calcd for [$C_{14}H_{19}NO_2$ + H]$^+$, 234.1489; found, 234.1499.

7,8-Diethyl-3-azatetracyclo[5.2.1.1^{5,8}.0^{1,5}]undecane (2*R*,3*R*)-Tartrate, [14c·(2*R*,3*R*)-Tartrate]. To a stirred solution of imide **13c** (907 mg, 3.89 mmol) in anhydrous toluene (32 mL) at 0 °C, sodium bis-(2-methoxyethoxy)aluminum hydride (5.95 mL, 65% solution in toluene, 5.95 mmol) was added dropwise. When the addition was finished, the solution was heated under reflux for 72 h. The mixture was cooled to 0 °C (ice−water bath), treated with 30% aq solution of KOH until basic pH, and stirred at room temperature for 1 h. The organic layer was separated, and the aqueous one was extracted with CH_2Cl_2 (3 × 30 mL). The combined organic layers were dried with anhydrous Na_2SO_4, filtered, and evaporated in vacuo to give amine **14c** as an orange oil (326 mg). The amine was dissolved in methanol (5 mL) and treated with (2*R*,3*R*)-tartaric acid (170 mg, 1.13 mmol) dissolved in the minimum amount of methanol. The mixture was concentrated in vacuo to yield **14c** as its (2*R*,3*R*)-tartrate as a yellow solid (459 mg, 33% yield). An analytical sample of **14c**·(2*R*,3*R*)-tartrate was obtained by crystallization from MeOH/Et_2O, mp 165−166 °C. IR (KBr) ν 3422, 3321, 2958, 2882, 1718, 1585, 1455, 1407, 1303, 1263, 1210, 1130, 1068, 899, 834, 784, 680, 618 cm^{-1}. ^{1}H NMR (400 MHz, CD_3OD) δ 0.93 [t, J = 7.6 Hz, 6 H, C7(8)-$CH_2C\underline{H}_3$], 1.53 [broad d, J = 7.2 Hz, 4 H, 6(9,10,11)-H_a], 1.61 [q, J = 7.6 Hz, 4 H, C7(8)-$C\underline{H}_2CH_3$], 1.76 [broad d, J = 7.2 Hz, 4 H, 6(9,10,11)-H_b], 3.27 [s, 4 H, 2(4)-H2], 4.39 [s, 2 H, C$\underline{H}$(OH)-CO_2H]. ^{13}C NMR (100.6 MHz, CD_3OD) δ 10.5 [CH_3, C7(8)-$CH_2\underline{C}H_3$], 24.2 [CH_2, C7(8)-$\underline{C}H_2CH_3$], 47.6 [CH_2, C2(4)], 53.3 [CH_2, C6(9,10,11)], 57.9 [C, C1(5)]*, 58.0 [C, C7(8)]*, 74.4 [CH, $\underline{C}$H(OH)], 177.6 (C, CO_2H). GC/MS, m/z (%); main ions: 205 [($C_{14}H_{23}N$)$^{\cdot+}$, 7], 190 (11), 176 (16), 163 (21), 162 (100), 161 (14), 147 (27), 136 (20), 133 (21), 120 (15), 119 (21), 107 (15), 105 (23), 91 (37).

3-Amidino-7,8-diethyl-3-azatetracyclo[5.2.1.1^{5,8}.0^{1,5}]-undecane Hydrochloride (16c·HCl). From a suspension of **14c**·**HCl** (459 mg, 1.29 mmol), Et_3N (0.30 mL, 2.06 mmol), and 1*H*-pyrazole-1-carboxamidine hydrochloride (226 mg, 1.54 mmol) in CH_3CN (10 mL) and following the same procedure as reported for **16a**·**HCl**, guanidine **16c**·**HCl** was obtained as a yellow solid (242 mg, 76% yield). An analytical sample was obtained by crystallization from *t*-butanol, mp 231−232 °C (dec). IR (KBr) ν 3291, 3220, 3173, 3102, 2957, 2877, 2364, 2337, 1603, 1556, 1455, 1369, 1290, 1112, 1077, 946, 899, 677 cm^{-1}. ^{1}H NMR (400 MHz, CD_3OD) δ 0.93 [t, J = 7.6 Hz, 6 H, C7(8)-$CH_2C\underline{H}_3$], 1.58 [broad d, J = 6.6 Hz, 4 H, 6(9,10,11)-H_a], 1.61 [q, J = 7.6 Hz, 4 H, C7(8)-$C\underline{H}_2CH_3$], 1.72 [broad d, J = 6.6 Hz, 4 H, 6(9,10,11)-H_b], 3.51 [s, 4 H, 2(4)-H]. ^{13}C NMR (100.6 MHz, CD_3OD) δ 10.5 [CH_3, C7(8)-$CH_2\underline{C}H_3$], 24.2 [CH_2, C7(8)-$\underline{C}H_2CH_3$], 49.8 [CH_2, C2(4)], 54.6 [CH_2, C6(9,10,11)], 57.5 [C, C1(5)]*, 57.9 [C, C7(8)]*, 156.7(C, C═NH). MS, m/z (%); main ions: 247 ($C_{15}H_{25}N_3^{\cdot+}$, 34), 246 (26), 232 (100), 192 (33), 178 (33), 177 (20), 162 (18), 159 (14), 119 (28), 112 (24), 105 (20), 91 (35), 79 (15), 72 (68).

12-Azapentacyclo[6.5.1.1^{3,10}.0^{1,10}.0^{3,8}]pentadeca-11,13-dione (13d). From diacid **12d** (520 mg, 2.10 mmol) and urea (624 mg, 10.4 mmol) and following the same procedure as reported for **13a**, imide **13d** was obtained as a white solid (400 mg, 83% yield). An analytical sample of **13d** was obtained by crystallization from CH_2Cl_2/*n*-pentane, mp 202−203 °C. IR (ATR) ν 3404, 3189, 3079, 2934, 1758, 1706, 1473, 1396, 1354, 1213, 1140, 1061, 840, 733, 618 cm^{-1}. ^{1}H NMR (400 MHz, $CDCl_3$) δ 1.58 [m, 4 H, 5(6)-H_2], 1.70 [m, 4 H, 4(7)-H_2], 1.83 [d, J = 7.2 H, 4 H, 2(9,14,15)-H_a], 1.99 [d, J = 7.2 Hz, 4 H, 2(9,14,15)-H_b], 8.09 [broad s, 1 H, N$\underline{H}$]. ^{13}C NMR (100.6 MHz, $CDCl_3$) δ 18.7 [CH_2, C5(6)], 25.5 [CH_2, C4(7)], 52.2 [C, C3(8)], 53.0 [CH_2, C2(9,14,15)], 56.9 [C, C1(10)], 177.5 [C, C11(13)]. MS, m/z (%); main ions: 231 ($M^{\cdot+}$, 27), 160 (23), 146 (100), 145 (49), 131 (15), 118 (21), 117 (35), 91 (31). HRMS-ESI+ m/z [M + H]$^+$ calcd for [$C_{14}H_{17}NO_2$ + NH_4]$^+$, 249.1598; found, 249.1607.

12-Azapentacyclo[6.5.1.1^{3,10}.0^{1,10}.0^{3,8}]pentadecane (2*R*,3*R*)-Tartrate, [14d·(2*R*,3*R*)-tartrate]. From imide **13d** (378 mg, 1.51 mmol) in dry toluene (14 mL) and sodium bis-(2-methoxyethoxy) aluminum hydride (2.30 mL, 65% solution in toluene, 7.55 mmol) and following the same procedure as reported for **14c**·(2*R*,3*R*)-tartrate, amine **14d** as its (2*R*,3*R*)-tartrate was obtained as a pale-yellow solid (442 mg, 83% yield). An analytical sample of **14d**·(2*R*,3*R*)-tartrate was obtained by crystallization from CH_2Cl_2/CH_3OH, mp 124−125 °C. IR (KBr) ν 3377, 2931, 2542, 2360, 1715, 1585, 1475, 1450, 1351, 1296, 1118, 1069, 983, 897, 834, 690 cm^{-1}. ^{1}H NMR (400 MHz, CD_3OD) δ 1.57−1.72 [complex signal, 12 H, 5(6)-H_2, 4(7)-H_2 and 2(9,14,15)-H_a], 1.75 [broad d, J = 6.8 Hz, 4 H, 2(9,14,15)-H_b], 3.27 [s, 4 H, 11(13)-H_2], 4.36 [s, 2 H, C$\underline{H}$(OH)-CO_2H]. ^{13}C NMR (100.6 MHz, CD_3OD) δ 20.0 [CH_2, C5(6)], 26.8 [CH_2, C4(7)], 47.3 [CH_2, C11(13)], 52.9 [C, C3(8)], 54.3 [CH_2, C2(9,14,15)], 58.2 [C, C3(8)], 74.7 (CH, $\underline{C}$H(OH)], 178.2 (C, CO_2H). GC/MS, m/z (%); main ions: 203 [($C_{14}H_{21}N$)$^{\cdot+}$, 62], 202 (43), 188 (100), 175 (21), 160 (39), 148 (77), 146 (28), 134 (95), 133 (43), 132 (34), 131 (33), 121 (79), 120 (36), 119 (26), 118 (23), 117 (40), 106 (24), 105 (29), 94 (19), 93 (19), 92 (20), 91 (79), 82 (26), 80 (29), 79 (29), 77 (30), 70 (29). HRMS-ESI+ m/z [M + H]$^+$ calcd for [$C_{14}H_{21}N$ + H]$^+$, 204.1747; found, 204.1748.

12-Amidino-12-azapentacyclo[6.5.1.1^{3,10}.0^{1,10}.0^{3,8}]-pentadecane Hydrochloride (16d·HCl). From a suspension of **14d** (249 mg, 1.22 mmol), Et_3N (0.14 mL, 0.98 mmol), and 1*H*-pyrazole-1-carboxamidine hydrochloride (215 mg, 1.47 mmol) in CH_3CN (9.5 mL) and following the same procedure as reported for **16a**·**HCl**, guanidine **16d**·**HCl** was obtained as a yellow solid (215 mg, 63% yield). An analytical sample was obtained by crystallization from *t*-butanol, mp 254−255 °C (dec). IR (ATR) ν 3303, 3178, 2926, 2871, 2371, 1647, 1616, 1464, 1361, 1293, 1127, 1035, 958, 929, 775, 701, 609, 559 cm^{-1}. ^{1}H NMR (400 MHz, CD_3OD) δ 1.55−1.65 [complex signal, 8 H, 5(6)-H_2 and 2(9,14,15)-H_a], 1.69 [m, 4 H, 4(7)-H_2], 1.80 [broad d, J = 6.8 Hz, 4 H, 2(9,14,15)-H_b], 3.50 [s, 4 H, 11(13)-H_2]. ^{13}C NMR (100.6 MHz, CD_3OD) δ 20.0 [CH_2, C5(6)], 26.8 [CH_2, C4(7)], 49.4 [CH_2, C11(13)], 52.8 [C, C3(8)], 55.6 [CH_2, C2(9,14,15)], 57.8 [CH_2, C1(10)], 156.7 (C, CN). MS, m/z (%); main ions: 245 [($C_{15}H_{23}N_3$)$^{\cdot+}$, 91], 230 (39), 217 (72), 190 (100), 171 (21), 162 (58), 148 (38), 143 (23), 131 (31), 129 (25), 120 (30), 117 (27), 112 (56), 111 (27), 105 (27), 91 (69), 79 (29), 77 (32), 72 (39), 60 (30).

■ ASSOCIATED CONTENT

Ⓢ Supporting Information

^{1}H spectra showing chemical shift of W41 $H^{\varepsilon 1}$ as a function of drug concentration. NMR titration assay. Experimental procedures and characterization data for compounds **12c−d** and **18c−d** to **22c−d**. Elemental analysis data of the new compounds. This material is available free of charge via the Internet at http://pubs.acs.org.

■ AUTHOR INFORMATION

Corresponding Author

*Phone: +34 934024533. Fax: +34 934035941. E-mail: svazquez@ub.edu.

Author Contributions

The manuscript was written through contributions of all authors. All authors have given approval to the final version of the manuscript. M.R.-C. and E.T. contributed equally.

Notes

The authors declare no competing financial interest.

■ ACKNOWLEDGMENTS

E.T. and S.V. thank the Spanish Ministerio de Ciencia e Innovación (FPU fellowship to E.T.; grant CTQ2011-22433 to S.V.) and the Generalitat de Catalunya (grant SCG-2009-294) for financial support. M.R.C. acknowledges a predoctoral grant from the Government of Andorra (ATCR2012/2013-00XX-AND). L.N. acknowledges financial support from the Geconcerteerde Onderzoeksacties (GOA/10/014) and the technical assistance from W. van Dam. W.F.D. acknowledges support from GM56423 from the NIH.

■ ABBREVIATIONS USED

Amt, amantadine; BSA, bovine serum albumin; CD, circular dichroism; DMEM, Dulbecco's Modified Eagle Medium; DMPC, dimyristoylphosphatidylcholine; DPC, dodecylphosphocholine; LiHMDS, lithium bis(trimethylsilyl)amide; MDCK, Madin–Darby canine kidney; MD, molecular dynamics; MTS, 3-(4,5-dimethylthiazol-2-yl)-5-(3-carboxymethoxyphenyl)-2-(4-sulfophenyl)-2*H*-tetrazolium; NMR, nuclear magnetic resonance; PBS, phosphate buffered saline; TEV, two-electrode voltage clamps; TM, transmembrane; WT, wild-type

■ REFERENCES

(1) Lamb, R. A.; Zebedee, S. L.; Richardson, C. D. Influenza virus M2 protein is an integral membrane protein expressed on the infected-cell surface. *Cell* **1985**, *40*, 627–633.

(2) Lamb, R. A.; Lai, C.-J.; Choppin, P. W. Sequences of mRNAs derived from genome RNA segment 7 of influenza virus: colinear and interrupted mRNAs code for overlapping proteins. *Proc. Natl. Acad. Sci. U. S. A.* **1981**, *78*, 4170–4174.

(3) Takeda, M.; Pekosz, A.; Shuck, K.; Pinto, L. H.; Lamb, R. A. Influenza a virus M2 ion channel activity is essential for efficient replication in tissue culture. *J. Virol.* **2002**, *76*, 1391–1399.

(4) Vanderlinden, E.; Naesens, L. Emerging antiviral strategies to interfere with influenza virus entry. *Med. Res. Rev.* **2013**, *33*, DOI: 10.1002/med.21289.

(5) Zhirnov, O. P. Solubilization of matrix protein M1/M from virions occurs at different pH for orthomyxo- and paramyxoviruses. *Virology* **1990**, *176*, 274–279.

(6) Grambas, S.; Hay, A. J. Maturation of influenza A virus hemagglutinin—estimates of the pH encountered during transport and its regulation by the M2 protein. *Virology* **1992**, *190*, 11–18.

(7) Bright, R. A.; Shay, D. K.; Shu, B.; Cox, N. J.; Klimov, A. I. Adamantane resistance among influenza A viruses isolated early during the 2005–2006 influenza season in the United States. *JAMA, J. Am Med. Assoc.* **2006**, *295*, 891–894.

(8) Fiore, A. E.; Shay, D. K.; Haber, P.; Iskander, J. K.; Uyeki, T. M.; Mootrey, G.; Bresee, J. S.; Cox, N. J. Prevention and control of influenza. Recommendations of the Advisory Committee on Immunization Practices (ACIP), 2007. *MMWR Recomm. Rep.* **2007**, *56*, 1–54.

(9) Moscona, A. Global transmission of oseltamivir-resistant influenza. *N. Engl. J. Med.* **2009**, *360*, 953–956.

(10) Baz, M.; Abed, Y.; Papenburg, J.; Bouhy, X.; Hamelin, M. E.; Boivin, G. Emergence of oseltamivir-resistant pandemic H1N1 virus during prophylaxis. *N. Engl. J. Med.* **2009**, *361*, 2296–2297.

(11) Balannik, V.; Carnevale, V.; Fiorin, G.; Levine, B. G.; Lamb, R. A.; Klein, M. L.; DeGrado, W. F.; Pinto, L. H. Functional studies and modeling of pore-lining residue mutants of the influenza a virus M2 ion channel. *Biochemistry* **2010**, *49*, 696–708.

(12) Furuse, Y.; Suzuki, A.; Oshitani, H. Large-scale sequence analysis of M gene of influenza A viruses from different species: mechanisms for emergence and spread of amantadine resistance. *Antimicrob. Agents Chemother.* **2009**, *53*, 4457–4463.

(13) Balannik, V.; Wang, J.; Ohigashi, Y.; Jing, X.; Magavern, E.; Lamb, R. A.; DeGrado, W. F.; Pinto, L. H. Design and pharmacological characterization of inhibitors of amantadine-resistant mutants of the M2 ion channel of influenza A virus. *Biochemistry* **2009**, *48*, 11872–11882.

(14) Wang, J.; Ma, C.; Fiorin, G.; Carnevale, V.; Wang, T.; Hu, F.; Lamb, R. A.; Pinto, L. H.; Hong, M.; Klein, M. L.; DeGrado, W. F. Molecular dynamics simulation directed rational design of inhibitors targeting drug-resistant mutants of influenza A virus M2. *J. Am. Chem. Soc.* **2011**, *133*, 12834–12841.

(15) Wang, J.; Ma, C.; Wu, Y.; Lamb, R. A.; Pinto, L. H.; DeGrado, W. F. Exploring organosilane amines as potent inhibitors and structural probes of influenza A virus M2 proton channel. *J. Am. Chem. Soc.* **2011**, *133*, 13844–13847.

(16) Wang, J.; Wu, Y.; Ma, C.; Fiorin, G.; Wang, J.; Pinto, L. H.; Lamb, R. A.; Klein, M. L.; DeGrado, W. F. Structure and inhibition of the drug-resistant S31N mutant of the M2 ion channel of influenza A virus. *Proc. Natl. Acad. Sci. U. S. A.* **2013**, *110*, 1315–1320.

(17) Wang, J.; Ma, C.; Wang, J.; Jo, H.; Canturk, B.; Fiorin, G.; Pinto, L. H.; Lamb, R. A.; Klein, M. L.; DeGrado, W. F. Discovery of Novel Dual Inhibitors of the Wild-Type and the Most Prevalent Drug-Resistant Mutant, S31N, of the M2 Proton Channel from Influenza A Virus. *J. Med. Chem.* **2013**, *56*, 2804–2812.

(18) Williams, J. K.; Tietze, D.; Wang, J.; Wu, Y.; DeGrado, W. F.; Hong, M. Drug-induced conformational and dynamical changes of the S31N mutant of the influenza M2 proton channel investigated by solid-state NMR. *J. Am. Chem. Soc.* **2013**, *135*, 9885–9897.

(19) Camps, P.; Duque, M. D.; Vázquez, S.; Naesens, L.; De Clercq, E.; Sureda, F. S.; López-Querol, M.; Camins, A.; Pallàs, M.; Prathalingam, S. R.; Kelly, J. M.; Romero, V.; Ivorra, D.; Cortés, D. Synthesis and pharmacological evaluation of several ring-contracted amantadine analogs. *Bioorg. Med. Chem.* **2008**, *16*, 9925–9936.

(20) Duque, M. D.; Ma, C.; Torres, E.; Wang, J.; Naesens, L.; Juárez-Jiménez, J.; Camps, P.; Luque, F. J.; DeGrado, W. F.; Lamb, R. A.; Pinto, L. H.; Vázquez, S. Exploring the size limit of templates for inhibitors of the M2 ion channel of influenza A virus. *J. Med. Chem.* **2011**, *54*, 2646–2657.

(21) Torres, E.; Vanderlinden, E.; Fernández, R.; Miquet, S.; Font-Bardia, M.; Naesens, L.; Vázquez, S. Synthesis and anti-influenza activity of 2,2-dialkylamantadines and related compounds. *ACS Med. Chem. Lett.* **2012**, *3*, 1065–1069.

(22) Torres, E.; Duque, M. D.; Vanderlinden, E.; Ma, C.; Pinto, L. H.; Camps, P.; Froeyen, M.; Vázquez, S.; Naesens, L. Role of the viral hemagglutinin in the anti-influenza virus activity of newly synthesized polycyclic amine compounds. *Antiviral Res.* **2013**, *99*, 281–291.

(23) Camps, P.; Font-Bardia, M.; Pérez, F.; Solans, X.; Vázquez, S. Synthesis, chemical trapping and dimerization of 3,7-dimethyltricyclo-[3.3.0.0^{3,7}]oct-1(5)-ene: [2 + 2] retrocycloaddition of the cyclobutane dimer. *Angew. Chem., Int. Ed. Engl.* **1995**, *34*, 912–914.

(24) Camps, P.; Luque, F. J.; Orozco, M.; Pérez, F.; Vázquez, S. Synthesis, chemical trapping and dimerization of tricyclo[3.3.0.0^{3,7}]-oct-1(5)-ene, the consummate member of a series of pyramidalized alkenes. *Tetrahedron Lett.* **1996**, *37*, 8605–8608.

(25) Pielak, R. M.; Chou, J. J. Solution NMR structure of the V27A drug resistant mutant of influenza A M2 channel. *Biochem. Biophys. Res. Commun.* **2010**, *401*, 58–63.

(26) Gu, R.-X.; Liu, L. A.; Wang, Y.-H.; Xu, Q.; Wei, D. H. Structural comparison of the wild-type and drug-resistant mutants of the influenza A M2 proton channel by molecular dynamics simulations. *J. Phys. Chem. B* **2013**, *117*, 6042–6051.

(27) Ayats, C.; Camps, P.; Duque, M. D.; Font-Bardia, M.; Muñoz, M. R.; Solans, X.; Vázquez, S. Alternative syntheses of the new D_{2d} symmetric tetramethyl tricyclo[3.3.0.0^{3,7}]octane-1,3,5,7-tetracarboxylate. *J. Org. Chem.* **2003**, *68*, 8715–8718.

(28) Makhseed, S.; McKeown, N. B. Novel spiro-polymers with enhanced solubility. *Chem. Commun.* **1999**, 255–256.

(29) Weiss, U.; Edwards, J. M. A one-step synthesis of ketonic compounds of the petalane, [3.3.3]- and [4.3.3]propellane series. *Tetrahedron Lett.* **1968**, *47*, 4885–4887.

(30) Bertz, S. H.; Cook, J. M.; Gawish, A.; Weiss, U. Condensation of dimethyl 1,3-acetonedicarboxylate with 1,2-dicarbonyl compounds: *cis*-

bicyclo[3.3.0]octane-3,7-diones. *Organic Syntheses*; Wiley: New York, 1990; Collected Vol. *VII*, pp 50−59.
(31) Barton, D. H. R.; Bashiardes, G.; Fourrey, J.-L. Studies on the oxidation of hydrazones with iodine and with phenylselenenyl bromide in the presence of strong organic bases; an improved procedure for the synthesis of vinyl iodides and phenyl-vinyl selenides. *Tetrahedron* **1988**, *44*, 147−162.
(32) Barton, D. H. R.; Chen, M.; Jaszberenyi, J. Cs.; Taylor, D. K. Preparation and reactions of 2-*tert*-butyl-1,1,3,3-tetramethylguanidine: 2,2,6-trimethylcyclohexen-1-yl iodide. *Organic Syntheses*; Wiley: New York, 1998; Collected Vol. *IX*, pp 147−150.
(33) Kolocouris, A.; Spearpoint, P.; Martin, S. R.; Hay, A. J.; López-Querol, M.; Sureda, F. X.; Padalko, E.; Neyts, J.; De Clercq, E. Comparisons of the influenza virus A M2 channel binding affinities, anti-influenza virus potencies and NMDA antagonistic activities of 2-alkyl-2-aminoadamantanes and analogues. *Bioorg. Med. Chem. Lett.* **2008**, *18*, 6156−6160.
(34) Cady, S. D.; Wang, J.; Wu, Y.; DeGrado, W. F.; Hong, M. Specific binding of adamantane drugs and direction of their polar amines in the pore of the influenza M2 transmembrane domain in lipid bilayers and dodecylphosphocholine micelles determined by NMR Spectroscopy. *J. Am. Chem. Soc.* **2011**, *133*, 4274−4284.
(35) Wang, C.; Takeuchi, K.; Pinto, L. H.; Lamb, R. A. Ion channel activity of influenza A virus M2 protein: characterization of the amantadine block. *J. Virol.* **1993**, *67*, 5585−5594.
(36) Stevaert, A.; Dallocchio, R.; Dessì, A.; Pala, N.; Rogolino, D.; Sechi, M.; Naesens, L. Mutational analysis of the binding pockets of the diketo acid inhibitor L-742,001 in the influenza virus PA endonuclease. *J. Virol.* **2013**, *87*, 10524−10538.
(37) Ma, C.; Soto, C. S.; Ohigashi, Y.; Taylor, A.; Bournas, V.; Glawe, B.; Udo, M. K.; DeGrado, W. F.; Lamb, R. A.; Pinto, L. H. Identification of the pore-lining residues of the BM2 ion channel protein of influenza B virus. *J. Biol. Chem.* **2008**, *283*, 15921−15931.
(38) Vanderlinden, E.; Göktas, F.; Cesur, Z.; Froeyen, M.; Reed, M. L.; Russell, C. J.; Cesur, N.; Naesens, L. Novel inhibitors of influenza virus fusion: structure−activity relationship and interaction with the viral hemagglutinin. *J. Virol.* **2010**, *84*, 4277−4288.
(39) Naesens, L.; Vanderlinden, E.; Roth, E.; Jeko, J.; Andrei, G.; Snoeck, R.; Pannecouque, C.; Illyes, E.; Batta, G.; Herczegh, P.; Sztaricskai, F. Anti-influenza virus activity and structure−activity relationship of aglycoristocetin derivatives with cyclobutenedione carrying hydrophobic chains. *Antiviral Res.* **2009**, *82*, 89−94.

Supporting Information

3-Azatetracyclo[5.2.1.1^{5,8}.0^{1,5}]undecane derivatives: from wild-type inhibitors of the M2 ion channel of influenza A virus to derivatives with potent activity against the V27A mutant

Matias Rey-Carrizo,[ǂ,‡] Eva Torres,[ǂ,‡] Chunlong Ma,[#,§] Marta Barniol-Xicota,[ǂ] Jun Wang,[†] Yibing Wu,[†] Lieve Naesens,[⊥] William F. DeGrado,[†] Robert A. Lamb,[§,∫] Lawrence H. Pinto,[#] Santiago Vázquez[ǂ]*

Table of contents

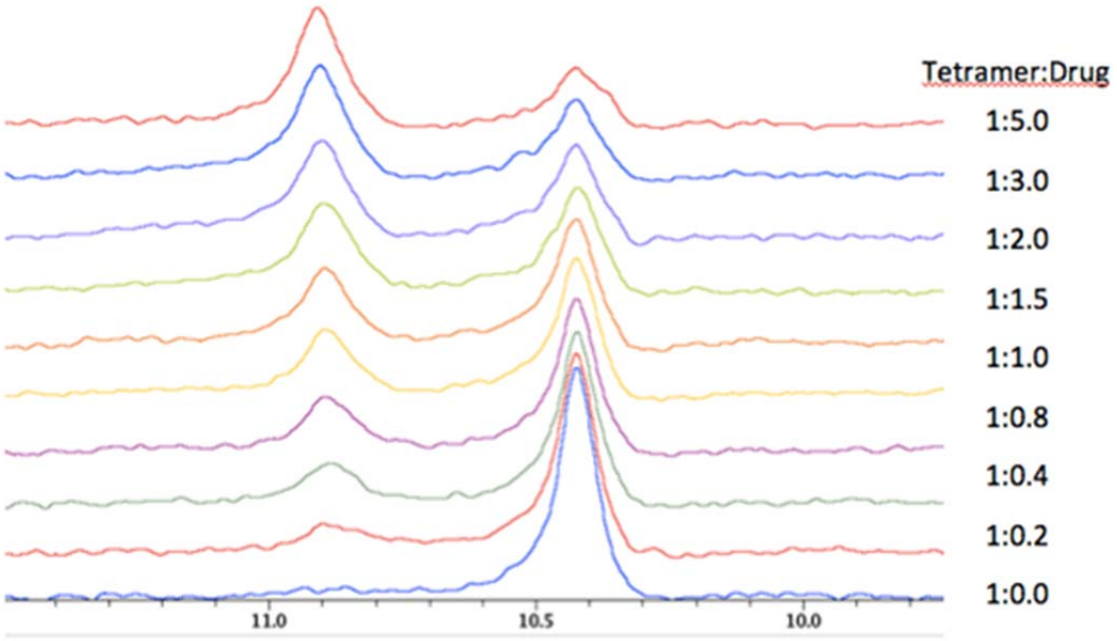

Figure S1. ^{1}H spectra showing chemical shift of W41 $H^{\varepsilon 1}$ as a function of drug concentration. The spectra were recorded for 1.6 mM M2TM in 80 mM DPC, 50mM phosphate buffer pH 7.5 at 313K on a Bruker Avance-I 800 MHz spectrometer. The stepwise titration was performed by addition of high concentration **16d** (250mM).

We used the same approach applied for rimantadine drug binding study on the wt M2.[1]

$$\frac{[\text{Tetra}\bullet\text{Drug}]}{[\text{Tetra}]_T} = \frac{K_D + [\text{Tetra}]_T \times N + [\text{Drug}]_T - \sqrt{\left(K_D + [\text{Tetra}]_T \times N + [\text{Drug}]_T\right)^2 - 4[\text{Tetra}]_T \times N \times [\text{Drug}]_T}}{2[\text{Tetra}]_T \times N}$$

where $[\text{Tetra}]_T$ and $[\text{Drug}]_T$ are the total drugable tetramer and drug concentrations, respectively, N represents the number of drugs per tetrameter, K_D is the dissociation constant. N and K_D were fitted to the fraction of $[\text{Tetra}\bullet\text{Drug}]/ [\text{Drug}]_T$, which was obtained by dividing the peak volume of W41 $H^{\varepsilon 1}$ at certain titration point by the maximum volume during the course of titration. Summary of the fitting is shown in Table S1.

[1] Cady, S. D.; Wang, J.; Wu, Y.; DeGrado, W. F.; Hong, M. *J. Am. Chem. Soc.* **2011**, *133*, 4274-4284.

Table S1. Summary of fitting results

Best-fit Values				
N	1.37 ± 0.28	1[a]	1[a]	1[a]
K_D (μM)	40 ± 24	4[a]	100[a]	400[a]
Goodness of fit R^2	0.963	0.679	0.942	0.369
Absolute sum of squares	0.037	0.333	0.059	0.647

[a]: Values are fixed in the fitting.

***Cis*-1,5-diethylbicyclo[3.3.0]octane-3,7-dione bishydrazone (18c)**. To a solution of known[2] diketone **17c** (15.0 g, 77.2 mmol) in absolute EtOH (225 mL) was added triethylamine (173 mL, 1.25 mmol) and hydrazine monohydrate (39.9 mL, 0.82 mmol). The mixture was heated to reflux for 3 hours. The dark yellow solution obtained was allowed to cool down to room temperature, it was then concentrated to a third of its volume and it was left at 4 ºC overnight. The white precipitate was filtered, washed with cold 96% ethanol and dried under vacuum to give **18c** (*anti* isomer) as white needles (14.95g, 87%), mp 139-140 ºC. IR (KBr) ν 3390, 3372, 3193, 2962, 2939, 2876, 2827, 1636, 1459, 1423, 1338, 1291, 1223, 1056, 826, 791, 675, 591, 513 cm^{-1}. ^1H NMR (400 MHz, $CDCl_3$) δ: 0.90 [t, J = 7.4 Hz, 6 H, C1(5)-$CH_2C\underline{H}_3$], 1.38 [q, J = 7.4 Hz, 4 H, C1(5)-$C\underline{H}_2CH_3$], 2.11 [dd, J = 18.0 Hz, J' = 0.8 Hz, 2H, 4(8)-H_{endo}], 2.23 [dd, J = 18.0 Hz, J' = 1.6 Hz, 2H, 4(8)-H_{exo}], 2.37 [dd, J = 17.0 Hz, J' = 0.8 Hz, 2H, 2(6)-H_{endo}] , 2.46 [dd, J = 17.0 Hz, J' = 1.6 Hz, 2H, 2(6)-H_{exo}], 4.84 (s, 4 H, 2 NH_2). ^{13}C NMR (100.6 MHz, $CDCl_3$) δ: 9.8 [CH_3, C1(5)-$CH_2\underline{C}H_3$], 26.0 [CH_2, C1(5)-$\underline{C}H_2CH_3$], 35.2 [CH_2, C4(8)], 42.2 [CH_2, C2(6)], 52.4 [C, C1(5)], 157.7 [C=N, C3(7)]. MS, m/e (%); main ions: 222 ($M^{\cdot+}$, 11), 206 (100), 193 (27), 152 (19), 151 (29), 150 (13), 149 (12), 91 (14).

Mixture of *cis*-1,5-diethyl-3,7-diiodobicyclo[3.3.0]octan-2,7-diene and *cis*-1,5-diethyl-3,7-diiodobicyclo[3.3.0]octan-2,6-diene (*syn*- and *anti*-19c). To a stirred suspension of bis-hydrazone **18c** (1.0 g, 4.5 mmol) in dry diethyl ether (72 mL) under an argon atmosphere, tetramethylguanidine (8.5 ml, 67.5 mmol) was added. The mixture was cooled to −18 ºC and solid iodine (6.88 g, 27.1 mmol) was added in small portions during 1 hour. When the addition was over, the mixture was allowed to warm to room temperature and stirring was continued for 15 hours. The organic layer was washed with $Na_2S_2O_3$ (10% aqueous solution, 5 × 30 ml) and brine (2 × 30 ml). The organic layer was dried (Na_2SO_4), filtered and concentrated under reduced pressure to give an orange solid that was purified by column chromatography (silica gel, *n*-hexane) to give a mixture of ***syn*-** and ***anti*-19c** (876 mg, 47% yield). From some selected fractions, pure ***syn*-19c** was obtained that was fully characterized, mp 63–64 ºC (*n*-hexane); IR (KBr) ν 3446, 2960, 2926, 2874, 1601, 1457, 1430, 1377, 1281, 1148, 1097, 1034, 1015, 964, 893, 853, 805, 790, 745 cm^{-1}; ^1H NMR (400 MHz, $CDCl_3$) δ 0.90 [t, J = 7.2 Hz, 3 H, C1-$CH_2C\underline{H}_3$]*, 0.91 [t, J = 7.6 Hz, 3 H, C5-$CH_2C\underline{H}_3$]*, 1.42 [q, J = 7.2 Hz, 2 H, C1-$C\underline{H}_2CH_3$]*, 1.43 [q, J = 7.2 Hz, 2 H, C5-$C\underline{H}_2CH_3$]*, 2.50 [dd, J = 16.4 Hz, J' = 2 Hz, 2 H, 4(6)-H_{endo}], 2.62 [dd, J = 16.4 Hz, J' = 2 Hz, 2 H, 4(6)-H_{exo}], 6.01 [t, J = 2 Hz, 2 H, 2(8)-H]; ^{13}C NMR (100.6 MHz, $CDCl_3$) δ 9.5 [CH_3, C1-$CH_2\underline{C}H_3$]*, 9.9 [CH_3, C5-$CH_2\underline{C}H_3$]*, 25.7 [CH_2, C1-$\underline{C}H_2CH_3$]*, 26.0 [CH_2, C5-$\underline{C}H_2CH_3$]*, 54.8 [CH_2, C4(6)], 58.0 (C, C5), 70.8 (C, C1), 92.5 [C-I, C3(7)], 142.4 [CH, C2(8)]. GC/MS (GC), m/e (%); main ions (*syn* and *anti*): rt (19.5 min): 414 ($M^{\cdot+}$, 15), 287 [$(M\text{-}I)^+$, 56], 160 [$(M\text{-}2I)^{\cdot+}$, 100], 145 [$(C_{11}H_{13})^+$, 31], 131 [$(C_{10}H_{11})^+$, 48], 115 (20), 91 [$(C_7H_7)^+$, 21]; rt (19.6 min): 414 ($M^{\cdot+}$, 15), 385 [$(M\text{-}C_2H_5)^+$, 100], 258 [$(M\text{-}2C_2H_5)^{\cdot+}$, 10], 131 [$(C_{10}H_{11})^+$, 22], 115 (11), 91 [$(C_7H_7)^+$, 21].

Mixture of dimethyl 1,5-diethyl-*cis*-bicyclo[3.3.0]octa-2,7-diene-3,7-dicarboxylate and dimethyl 1,5-diethyl-*cis*-bicyclo[3.3.0]octa-2,6-diene-3,7-dicarboxylate (*syn*- and *anti*-20c). A mixture of **19c** (5.65 g, 13.65 mmol), triphenylphosphine (706 mg, 2.69 mmol), $Pd(OAc)_2$ (316 mg, 1.41 mmol), methanol (175 mL) and triethylamine (11.4 mL, 82.2 mmol) was purged with CO for 10 min and stirred and heated under

[2] Makhseed, S.; McKeown, N. B. Novel spiro-polymers with enhanced solubility. *Chem. Commun.* **1999**, 255-256.

reflux for 22 h under CO (about 1 atm). The black suspension was allowed to cool to room temperature and was evaporated in vacuo to dryness. The residue was taken in dichloromethane (200 mL) and filtered. The orange filtrate was washed with HCl (10% aqueous solution, 3 × 200 mL), $NaHCO_3$ (saturated aqueous solution, 3 × 200 mL) and brine (200 mL). The organic layer was dried (anhydrous Na_2SO_4), filtered and concentrated in vacuo to dryness to give a mixture of *syn*- and *anti*-**20c** as a brown oil. Column chromatography (silica gel, hexanes to ethyl acetate / hexanes mixture 2/8) gave a mixture of *syn*- and *anti*-**20c** (in the approx. ratio of 1:1, ^{1}H NMR or GC/MS) as a yellowish oil (2.36 g, 62% yield). IR (ATR) ν 2964, 2851, 1713, 1634, 1460, 1435, 1381, 1352, 1317, 1239, 1217, 1190, 1159, 1128, 1076, 961, 908, 892, 855, 797, 773, 749, 738, 687, 554 cm^{-1}; ^{1}H NMR (400 MHz, $CDCl_3$) δ *syn*-**20c** 0.93 (t, *J* = 7.4 Hz, 3 H, C1-$CH_2C\underline{H}_3$), 0.97 (t, J = 7.4 Hz, 3 H, C5-$CH_2C\underline{H}_3$), 1.36-1.64 (complex signal, 4 H, C1-$C\underline{H}_2CH_3$ and C5-$C\underline{H}_2CH_3$), 2.45 [dd, *J* = 16.4 Hz, *J'* = 1.8 Hz, 2 H, 4(6)-H_a], 2.58 [dd, *J* = 16.4 Hz, *J'* = 1.8 Hz, 2 H, 4(6)-H_b], 3.70 [s, 6 H, C3(7)-$CO_2\underline{C}H_3$], 6.59 [t, *J* = 1.8 Hz, 2 H, 2(8)-H]; *anti*-**20c** 0.93 [t, *J* = 7.4 Hz, 6 H, C1(5)-$CH_2C\underline{H}_3$], 1.36-1.64 [complex signal, 4 H, C1(5)-$C\underline{H}_2CH_3$], 2.49 [dd, *J* = 16.4 Hz, *J'* = 2.8 Hz, 2 H, 4(8)-H_a], 2.68 [broad d, *J* = 17.2 Hz, 2 H, 4(8)-H_b], 3.71 [2 s, 6 H, C3(7)-$CO_2\underline{C}H_3$], 6.60 [d, *J* = 1.6 Hz, 2 H, 2(6)-H]; ^{13}C NMR (100.6 MHz, $CDCl_3$) δ *syn*-**20c** 9.4 (CH_3, C1-$CH_2\underline{C}H_3$)*, 9.8 (CH_3, C5-$CH_2\underline{C}H_3$)*, 25.5 (CH_2, C1-$\underline{C}H_2CH_3$)*, 26.3 (CH_2, C5-$\underline{C}H_2CH_3$)*, 42.5 [CH_2, C4(6)], 51.5 (CH_3, 2 $CO_2\underline{C}H_3$), 55.6 (C, C5), 68.4 (C, C1), 134.9 [C, C3(7)-*syn*], 150.3 [CH, C2(6)], 165.6 (C, $\underline{C}O_2CH_3$); *anti*-**20c** 9.9 [CH_3, C1(5)-$CH_2\underline{C}H_3$], 27.6 [CH_2, C1(5)-$\underline{C}H_2CH_3$-*anti*], 40.7 [CH_2, C4(8)], 51.4 (CH_3, 2 $CO_2\underline{C}H_3$), 61.2 [C, C1(5)], 132.9 [C, C3(7)], 144.0 [CH, C2(8)], 165.6 (C, $\underline{C}O_2CH_3$). GC/MS, m/e (%); main ions (*syn* and *anti*): rt (19.9 min): 278 ($M^{\cdot+}$, 23), 249 [$(M\text{-}C_2H_5)^+$, 14], 247 (49), 246 [$(M\text{-}CH_3OH)^{\cdot+}$, 100], 219 (27), 218 [$(M\text{-}HCO_2CH_3)^{\cdot+}$, 92], 217 (57), 203 (18), 193 [$(C_{12}H_{17}O)^+$, 91], 189 [$(M\text{-}C_2H_5\text{-}HCO_2CH_3)^+$, 69], 187 (29), 186 (16), 161 (37), 159 [$(C_{12}H_{16})^+$, 87], 157 (25), 145 (20), 133 (20), 131 (32), 130 (22), 129 [$(C_{10}H_{10})^+$, 57], 128 (27), 117 (22), 115 (38), 105 (26), 93 (22), 91 [$(C_7H_7)^+$, 37], 77 (18); rt (20.0 min): 278 ($M^{\cdot+}$, 12), 249 [$(M\text{-}C_2H_5)^+$, 26], 247 (20), 219 (46), 218 [$(M\text{-}HCO_2CH_3)^{\cdot+}$, 100], 217 (27), 189 [$(M\text{-}C_2H_5\text{-}HCO_2CH_3)^+$, 31], 159 [$(C_{12}H_{16})^+$, 49], 129 [$(C_{10}H_{10})^+$, 28], 115 (16), 91 [$(C_7H_7)^+$, 15]. HRMS-ESI+ m/z [*M*+H]$^+$ calcd for $[C_{16}H_{22}O_4+H]^+$: 279.1591, found: 279.1593.

Mixture of *endo,endo*-, *endo,exo*- and *exo,exo*- dimethyl 1,5-diethyl-*cis*-bicyclo[3.3.0]octane-3,7-dicarboxylate (21c). A mixture of **20c** (4.45 g, 15.99 mmol) was dissolved in absolute ethanol (120 mL), Pd on charcoal (1.34 g, 54% water content, ca. 5% Pd, equivalent to 30.9 mg of Pd) was added and the resulting mixture was hydrogenated at 400 psi at room temperature for 7 days. The suspension was filtered, and the solvent was evaporated in vacuo to give a mixture of *endo,endo*-, *endo,exo*- and *exo,exo*- stereoisomers of **21c** (3.47 g, 77% yield) as an oil. IR (ATR) ν 2959, 2878, 1730, 1458, 1434, 1364, 1265, 1192, 1171, 1042, 1027, 930, 830, 761, 668 cm^{-1}; ^{1}H NMR (500 MHz, $CDCl_3$) δ *endo,endo*-**21c** 0.87 [t, *J* = 7.5 Hz, 3 H, C1(5)-$CH_2C\underline{H}_3$], 1.24 [q, *J* = 7.5 Hz, 4 H, C1(5)-$C\underline{H}_2CH_3$], 1.89 [dd, *J* = 13.5 Hz, *J'* = 10.0 Hz, 4 H, 2(4,6,8)-H_a], 1.98 [dd, *J* = 13.5 Hz, *J'* = 8.5 Hz, 4 H, 2(4,6,8)-H_b], 2.88 [m, 2 H, 3(7)-H], 3.67 [s, 6 H, 3(7)-$CO_2C\underline{H}_3$]; *endo,exo*-**21c** and *exo,exo*-**21c** 0.88 [t, *J* = 7.5 Hz, 3 H, C1(5)-$CH_2C\underline{H}_3$], 0.89 [t, *J* = 7.5 Hz, 3 H, C1(5)-$CH_2C\underline{H}_3$], 1.26-1.39 (complex signal, C1(5)-$C\underline{H}_2CH_3$], 1.54 (d, *J* = 12.5 Hz), 1.59 (d, *J* = 11.0 Hz), 1.75 (t, *J* = 12.5 Hz), 1.88 (m) and 2.03 (dd, *J* = 14.5 Hz, *J'* = 7.0 Hz) (CH_2), 2.59 (tt, 1 H, *J* = 14.0 Hz, *J'* = 9.0 Hz), 2.75 (tt, 1 H, J = 14.5 Hz, J' = 9.0 Hz) and 2.87 (m) (CH), 3.66 (s, 6 H, $OC\underline{H}_3$), 3.67 (s, 6 H, $OC\underline{H}_3$); ^{13}C NMR (100.6 MHz, $CDCl_3$) δ *endo,endo*-**21c** 9.9 [CH_3, C1(5)-$CH_2\underline{C}H_3$], 25.8 [CH_2, C1(5)-$\underline{C}H_2CH_3$-*anti*], 38.2 [CH_2, C2(4,6,8)], 51.7 (CH_3, 2

$CO_2\underline{C}H_3$), 57.3 [C, C1(5)], 177.2 (C, $\underline{C}O_2CH_3$); *endo,exo*-**21c** and *exo,exo*-**21c** 10.0 (CH_3), 10.2 (CH_3), 28.0 (CH_2), 30.9 (CH_2), 40.2 (CH), 40.5 (CH_2), 41.5 (CH), 41.9 (CH_2), 42.7 (CH), 43.1 (CH_2), 51.60 (CH_3), 51.62 (CH_3), 55.2 (C), 55.3 (C), 176.1 (C), 176.2 (C), 176.5 (C). GC/MS (GC), m/e (%); main ions (only two peaks were observed): rt (19.6 min): 282 ($M^{\cdot+}$, 2), 251 (37), 250 [$(M\text{-}CH_3OH)^{\cdot+}$, 100], 222 (36), 221 (22), 218 [$(M\text{-}2CH_3OH)^{\cdot+}$, 61], 193 (55), 191 (41), 190 (98), 183 (27), 163 (43), 162 (34), 161 (42), 142 (18), 136 (17), 135 (38), 134 (16), 133 [$(C_{10}H_{14})^+$, 78], 122 (21), 121(39), 110 (18), 107 [$(C_8H_{10})^+$, 53], 105 (30), 93 (39), 91 (33), 79 (34), 77 (18), 59 (18), 55 (24); rt (19.7 min): 282 ($M^{\cdot+}$, 2), 251 (28), 250 [$(M\text{-}CH_3OH)^{\cdot+}$, 73], 222 (48), 221 (38), 218 [$(M\text{-}2CH_3OH)^{\cdot+}$, 56], 193 (47), 191 (31), 190 (28), 181 (16), 163 (66), 162 (26), 161 (47), 158 (98), 149 (21), 142 (32), 136 (24), 135 (38), 133 [$(C_{10}H_{14})^+$, 100], 126 (21), 124 (29), 123 (31), 121 (60), 110 (20), 107 [$(C_8H_{10})^+$, 90], 105 (43), 95 (27), 93 (64), 91 (52), 81 (35), 79 (59), 77 (32), 67 (27), 59 (34), 55 (44). HRMS-ESI+ m/z $[M+H]^+$ calcd for $[C_{16}H_{26}O_4+H]^+$: 283.1904, found: 283.1897.

Dimethyl 3,7-diethyltricyclo[3.3.0.0^{3,7}]octane-1,5-dicarboxylate (22c). A solution of LiHMDS was prepared by reacting a solution of HMDS (3.56 mL, 17.0 mmol) in anhydrous THF (14 mL) with *n*-butyllithium (8.0 mL, 2.0 M in hexanes, 16.0 mmol) at -68ºC under argon for 1 h. Then, a solution of a stereoisomeric mixture of diesters **21c** (2.0 g, 7.08 mmol) in anhydrous THF (14 mL) was added dropwise keeping the temperature at -68ºC. Stirring was continued for 1 h at this temperature and then a solution of iodine (1.80 g, 7.08 mmol) in anhydrous THF (32 mL) was added dropwise. The mixture was maintained 1 h at -68ºC and then allowed to warm to room temperature over 15 h. The mixture was acidified with HCl (10% aqueous solution) until pH 2 (10 mL) and the THF was removed *in vacuo*. The remaining aqueous phase was extracted with diethyl ether (4 × 50 mL) and the combined organic extracts were washed with $Na_2S_2O_3$ (10% aqueous solution, 3 × 100 mL) and brine (2 × 100 mL), dried (Na_2SO_4), filtered and evaporated to dryness under reduced pressure to furnish a dark red oil. Column chromatography of this residue (silica gel, hexanes / ethyl acetate, 9 / 1) gave diester **22c** (930 mg, 47% yield) as an orange oil. IR (ATR) ν 2962, 2891, 1732, 1479, 1459, 1435, 1378, 1325, 1301, 1285, 1219, 1192, 1155, 1132, 1081, 1063, 1042, 1002, 942, 915, 775, 763, 730, 647 cm^{-1}; ^{1}H NMR (400 MHz, $CDCl_3$) δ 0.90 [t, J = 7.4 Hz, 6 H, C3(7)-$CH_2C\underline{H}_3$], 1.57 [d, J = 7.0 Hz, 4 H, 2(4,6,8)-H_a], 1.59 [q, J = 7.4 H, 4 H, C3(7)-$C\underline{H}_2CH_3$], 2.01 [d, J = 7.0 Hz, 4 H, 2(4,6,8)-H_b], 3.67 [s, 6 H, $CO_2C\underline{H}_3$]; ^{13}C NMR (100.6 MHz, $CDCl_3$) δ 10.0 [CH_3, C3(7)-$CH_2\underline{C}H_3$], 22.7 [CH_2, C3(7)-$\underline{C}H_2CH_3$], 51.6 (CH_3, 2 $CO_2\underline{C}H_3$), 52.9 [CH_2, C2(4,6,8)], 53.0 [C, C3(7)], 57.3 [C, C1(5)], 173.6 (C, $\underline{C}O_2CH_3$). GC/MS, m/z (%); main ions: 280 ($M^{\cdot+}$, 1), 249 (41), 248 (25), 220 (100), 191 (67), 189 (28), 181 (72), 180 (25), 179 (44), 161 (87), 160 (27), 149 (88), 133 (20), 131 (37), 121 (60), 119 (30), 105 (38), 93 (31), 91 (49), 77 (21). HRMS-ESI+ m/z $[M+H]^+$ calcd for $[C_{16}H_{24}O_4+H]^+$: 281.1753, found: 281.1750.

3,7-Diethyltricyclo[3.3.0.0^{3,7}]octane-1,5-dicarboxylic acid (12c). A mixture of **22c** (2.32 g, 8.28 mmol) and a solution of KOH (40%) in MeOH (24 mL) was heated under reflux for 3 h. Water (24 mL) was added and heating under reflux was continued for 6 h more. The solution was made acidic with conc. aqueous HCl (25 mL) and concentrated in vacuo. The dark solid was extracted with boiling diethyl ether (6 × 50 mL). The combined organic extracts were dried (Na_2SO_4), filtered and evaporated to dryness under reduced pressure to furnish **12c** (1.32 g, 63% yield) as a pale yellow solid, mp 205-206 ºC; IR (KBr) ν 2971, 2930, 2705, 2604, 1702, 1420, 1312, 1235, 1151, 1091, 938, 729 cm^{-1}; ^{1}H NMR (400 MHz, $CDCl_3$) δ 0.91 [t, J = 7.2 Hz, 6 H, C3(7)-$CH_2C\underline{H}_3$], 1.56-1.64 [complex signal, 8 H, C3(7)-$C\underline{H}_2CH_3$ and 2(4,6,8)-H_a], 2.03 [d, J = 7.6 Hz, 4 H, 2(4,6,8)-H_b], 10.65 (broad s, 2 H, $CO_2\underline{H}$); ^{13}C NMR (100.6 MHz, $CDCl_3$) δ 10.0

[CH_3, C3(7)-$CH_2\underline{C}H_3$], 22.7 [CH_2, C3(7)-$\underline{C}H_2CH_3$], 52.7 [CH_2, C2(4,6,8)], 53.3 [C, C3(7)], 57.9 [C, C1(5)], 180.1 [C=O, C9(11)]. MS, m/z (%); main ions: 234 [(M-H_2O), 5]$^{\cdot+}$, 206 [(M-HCO_2H)$^{\cdot+}$, 55], 177 (67), 167 (100), 166 (37), 165 (31), 163 (33), 162 (47), 149 (63), 137 (18), 133 (28), 131 (23), 121 (54), 119 (23), 107 (21), 105 (40), 93 (46), 91 (60), 79 (34), 77 (38), 69 (19), 57 (29). HRMS-ESI+ m/z [*M*+H]$^+$ calcd for [$C_{14}H_{20}O_4$+H]$^+$: 253.1434, found: 253.1428.

Tricyclo[4.3.3.0^{1,6}]dodecane-8,11-dione bishydrazone (18d). From known[3] diketone **17d** (37.3 g, 0.19 mol), triethylamine (431 mL, 3.11 mmol) and hydrazine monohydrate (97.4 mL, 2.02 mmol) in absolute EtOH (525 mL) and following the same procedure as reported for **18c**, **18d** was obtained as an orange sticky solid (42.5 g, 99% yield). An analytical sample of **18d** (*anti* isomer) was obtained by crystallization from chloroform, mp 142-143 ºC. IR (KBr) ν 3353, 3195, 2921, 2862, 2841, 1654, 1444, 1420, 1339, 1267, 1225, 1079, 872, 862, 813, 687, 507 cm^{-1}; ^{1}H NMR (400 MHz, $CDCl_3$) δ 1.45 [broad s, 8 H, 3(4)-H_2 and 2(5)-H_2], 2.15 [dd, J = 18.0 Hz, J' = 1.6 Hz, 2 H, 9(12)-H_a], 2.32 [dd, J = 17.0 Hz, J' = 1.6 Hz, 2 H, 7(10)-H_b], 2.34 [dd, J = 18.0 Hz, J' = 1.8 Hz, 2 H, 9(12)-H_b], 2.47 [broad d, J = 17.2 Hz, 2 H, 7(10)-H_a], 4.85 (broad s, 4 H, NH_2); ^{13}C NMR (100.6 MHz, $CDCl_3$) δ 21.3 (CH_2, C3)*, 21.6 (CH_2, C4)*, 30.4 (CH_2, C2)*, 32.1 (CH_2, C5)*, 37.5 [broad CH_2, C9(12)], 42.5 [broad CH_2, C7(10)], 46.4 (C, C1)*, 47.6 (C, C5)*, 157.5 [C=N, C3(7)]. MS, m/z (%); main ions: 220 (M$^{\cdot+}$, 19), 204 (100), 191 (18), 188 (25), 150 (39), 149 (39), 148 (23), 105 (16), 91 (30), 79 (17). HRMS-ESI+ m/z [*M*+H]$^+$ calcd for [$C_{12}H_{20}N_4$+H]$^+$: 221.1761, found: 221.1756.

Mixture of 8,11-diiodotricyclo[4.3.3.0^{1,6}]dodecan-7,11-diene and 8,11-diiodotricyclo[4.3.3.0^{1,6}]dodecan-7,10-diene (*syn*- and *anti*-19d). From bis-hydrazone **18d** (1.0 g, 4.54 mmol), tetramethylguanidine (8.6 ml, 68.1 mmol) and iodine (9.22 g, 36.3 mmol) in dry diethyl ether (50 mL) and following the same procedure as reported for **19c**, **19d** was obtained as an pink solid (1.07 g, 57% yield). An analytical sample of **19d** (*syn* and *anti* mixture) was obtained by crystallization from *n*-pentane, mp 91-92 ºC. IR (KBr) ν 3404, 3042, 2916, 2843, 1599, 1436, 1270, 1210, 1097, 1074, 989, 856, 790, 739, 594 cm^{-1}; ^{1}H NMR (400 MHz, $CDCl_3$) δ *anti*-**19d** 1.25-1.72 [complex signal, 8 H, 2(5)-H_2 and 3(4)-H_2], 2.51 [dd, J = 16.4 Hz, J' = 1.6 Hz, 2 H, 9(12)-H_a], 2.62 [dd, J = 16.4 Hz, J' = 2.4 Hz, 2 H, 9(12)-H_b], 5.85 [m, 2 H, 7(10)-H]; δ *syn*-**19d** 1.25-1.55 [complex signal, 8 H, 2(5)-H_2 and 3(4)-H_2], 2.54 [m, 4 H, 9(10)-H_2], 5.88 [t, J = 2.0 Hz, 2 H, 7(12)-H]; ^{13}C NMR (100.6 MHz, $CDCl_3$) δ *anti*-**19d** 19.0 [CH_2, C3(4)], 31.0 [CH_2, C2(5)], 52.6 [CH_2, C9(12)], 59.0 [C, C1(6)], 91.1 [C, C8(11)], 148.5 [CH, C7(10)]; δ *syn*-**19d** 19.7 (CH_2, C3)*, 20.8 (CH_2, C4)*, 31.4 (CH_2, C2)*, 31.8 (CH_2, C5)*, 53.2 (C, C1), 55.9 [CH_2, C9(10)], 65.9 (C, C6), 92.6 [C, C8(11)], 143.9 [CH, C7(12)]. GC/MS, m/z (%); main ions (*syn* and *anti*): rt (20.2 min): 412 (M$^{\cdot+}$, 26), 285 [(M-I)$^+$, 40], 158 [(M-2I)$^{\cdot+}$, 100], 157 (51), 143 (24), 130 (34), 129 (48), 128 (28), 117 (27), 116 (22), 115 (49), 102 (23), 91 (40); rt (20.3 min): 412 (M$^{\cdot+}$, 13), 285 [(M-I)$^+$, 84], 158 [(M-2I)$^{\cdot+}$, 100], 143 (17), 130 (26), 129 (35), 128 (23), 117 (18), 115 (34), 102 (11), 91 (23).

Mixture of dimethyl tricyclo[4.3.3.0^{1,6}]dodecan-7,11-diene-8,11-dicarboxylate and dimethyl tricyclo[4.3.3.0^{1,6}]dodecan-7,10-diene-8,11-dicarboxylate (*syn*- and *anti*-20d). From a mixture of **19d** (5.70 g, 13.70 mmol), triphenylphosphine (719 mg, 2.74 mmol), $Pd(OAc)_2$ (308 mg, 1.37 mmol) and triethylamine (11.4 mL, 82.2 mmol) in methanol (180 mL) and following the same procedure as reported for **20c**, **20d** was obtained as a black oil. Column chromatography (silica gel, hexanes to ethyl acetate / hexanes mixture 2/8) gave a mixture of *syn*- and *anti*-**20d** (in the approx. ratio of 1:1, ^{1}H

[3] Weiss U.; Edwards, J. M. A one-step synthesis of ketonic compounds of the pentalane, [3.3.3]- and [4.3.3]propellane series. *Tetrahedron Lett.* **1968**, *47*, 4885-4887.

NMR) as a white solid (2.43 g, 64% yield), mp 71-72 ºC (hexane). IR (KBr) ν 3026, 3001, 2954, 2921, 2899, 2853, 1713, 1627, 1609, 1437, 1352, 1282, 1264, 1244, 1224, 1206, 1194, 1106, 1084, 979, 950, 898, 777, 749, 602, 552 cm^{-1}; ^1H NMR (400 MHz, $CDCl_3$) δ *anti*-**20d** 1.20-1.83 [complex signal, 8 H, 2(5)-H_2 and 3(4)-H_2], 2.58 [dd, J = 16.2 Hz, J' = 1.6 Hz, 2 H, 9(12)-H_a], 2.65 [dd, J = 16.4 Hz, J' = 2.8 Hz, 2 H, 9(12)-H_b], 3.70 (s, 6 H, $CO_2C\underline{H}_3$), 6.47 [m, 2 H, 7(10)-H]; δ *syn*-**20d** 1.25-1.60 [complex signal, 8 H, 2(5)-H_2 and 3(4)-H_2], 2.50 [m, 4 H, 9(10)-H_2], 3.71 (s, 6 H, $CO_2C\underline{H}_3$), 6.47 [m, 2 H, 7(12)-H]; ^{13}C NMR (100.6 MHz, $CDCl_3$) δ *anti*-**20d** 19.7 [CH_2, C3(4)], 31.4 [CH_2, C2(5)], 43.6 [CH_2, C9(12)], 51.5 (CH_3, $CO_2\underline{C}H_3$), 56.0 [C, C1(6)], 135.2 [C, C8(11)], 151.9 [CH, C7(10)], 165.9 (C, $\underline{C}O_2CH_3$); δ *syn*-**20d** 20.5 (CH_2, C3)*, 21.0 (CH_2, C4)*, 31.6 (CH_2, C2)*, 32.3 (CH_2, C5), 39.6 [CH_2, C9(10)], 50.7 (C, C1), 51.5 (CH_3, $CO_2\underline{C}H_3$), 63.2 (C, C6), 132.2 [C, C8(11)], 145.5 [CH, C7(12)], 166.0 (C, $\underline{C}O_2CH_3$). MS, m/z (%); main ions: 276 (M^+, 40), 244 (100), 217 (48), 216 (42), 185 (34), 184 (18), 157 (47), 131 (16), 129 (29), 128 (17), 117 (21), 115 (28), 91 (21). HRMS-ESI+ m/z $[M+H]^+$ calcd for $[C_{16}H_{20}O_4+H]^+$: 277.1434, found: 277.1435.

Mixture of *endo,endo*- and *endo,exo*- dimethyl tricyclo[4.3.3.0^{1,6}]dodecan-8,11-dicarboxylate (21d). A mixture of **20d** (5.43 g, 19.7 mmol) was dissolved in absolute ethanol (120 mL), Pd on charcoal (1.09 g, 54% water content, ca. 5% Pd, equivalent to 25.1 mg of Pd) was added and the resulting mixture was hydrogenated at 400 psi at room temperature for 14 days. The suspension was filtered, and the solvent was evaporated in vacuo to give a mixture of *endo,endo*- and *endo,exo*- stereoisomers of **21d** (4.06 g, 74% yield) as a yellow oil. IR (ATR) ν 2924, 2861. 1730, 1700, 1460, 1434, 1364, 1308, 1278, 1192, 1167, 1121, 1020, 930, 890, 830, 761, 722 cm^{-1}; ^1H NMR (400 MHz, $CDCl_3$) δ 1.20-1.52 [complex signal, 8 H, 2(5)-H_2 and 3(4)-H_2], 1.87-2.02 [complex signal, 8 H, 7(9,10,12)-H_2], 2.93-3.11 [complex signal, 2 H, 8(11)-H], 3.67 (s, 6 H, $CO_2C\underline{H}_3$); ^{13}C NMR (100.6 MHz, $CDCl_3$) δ *endo,exo*-**21d** 20.8 [CH_2, C3(4)], 31.1 [CH_2, C2(5)], 39.6 (CH) and 40.9 (CH) (C8 and C11), 40.1 (CH_2) and 41.1 (CH_2) [C7(9) and C10(12)], 51.69 [C, C1(6)], 51.8 (CH_3, $CO_2\underline{C}H_3$), 177.3 (C, $\underline{C}O_2CH_3$); δ *endo,endo*-**21d** 21.6 [CH_2, C3(4)], 32.3 [CH_2, C2(5)], 40.1 [CH, C8(11)], 40.7 [CH_2, C7(9,10,12)], 50.7 (C, C1), 51.6 [C, C1(6)], 51.72 (CH_3, $CO_2\underline{C}H_3$), 177.3 (C, $\underline{C}O_2CH_3$). GC/MS, m/z (%); main ions: 280 ($M^{\cdot+}$, 2), 248 [$(M-CH_3OH)^{\cdot+}$, 100], 220 [$(M-HCO_2H)^{\cdot+}$, 82], 216 (59), 189 (36), 188 (58), 179 (52), 161 (83), 158 (30), 147 (25), 134 (55), 121 (59), 119 (87), 105 (37), 93 (52), 91 (76), 79 (45), 77 (25). HRMS-ESI+ m/z $[M+H]^+$ calcd for $[C_{16}H_{24}O_4+H]^+$: 281.1747, found: 281.1747.

Dimethyl tetracyclo[6.2.1.1^{3,10}.0^{3,8}]dodecane-1,10-dicarboxylate (22d). From a solution of HMDS (2.50 mL, 11.73 mmol) in anhydrous THF (10 mL), *n*-butyllithium (5.0 mL, 2.0 M in hexanes, 10.0 mmol) a stereoisomeric mixture of diesters **21d** (1.37 g, 4.89 mmol) in anhydrous THF (10 mL) and a solution of iodine (1.24 g, 4.89 mmol) in anhydrous THF (22 mL) and following the same procedure as reported for **22c**, a dark red oil containing **22d** was obtained. Column chromatography of this residue (silica gel, from hexanes to hexanes / ethyl acetate, 87 / 13) gave diester **22d** (771 mg, 57% yield) as a yellow solid, mp 72–73 ºC (hexanes). IR (ATR) ν 3432, 2937, 2856, 1734, 1455, 1436, 1301, 1198, 1176, 1115, 1080, 1031, 930, 799, 758, 566 cm^{-1}; ^1H NMR (400 MHz, $CDCl_3$) δ 1.57 [m, 4 H, 5(6)-H_2], 1.65 [m, 4 H, 4(7)-H_2], 1.77 [d, J = 7.2 H, 4 H, 2(9,11,12)-H_a], 1.87 [d, J = 7.2 Hz, 4 H, 2(9,11,12)-H_b], 3.66 [s, 6 H, $CO_2C\underline{H}_3$]; ^{13}C NMR (100.6 MHz, $CDCl_3$) δ 18.8 [CH_2, C5(6)], 25.4 [CH_2, C4(7)], 48.0 [C, C3(8)], 51.6 (CH_3, 2 $CO_2\underline{C}H_3$), 53.9 [CH_2, C2(9,11,12)], 57.5 [C, C1(10)], 173.5 (C, $\underline{C}O_2CH_3$). GC/MS, m/z (%); main ions: 279 [$(M+H)^+$, 13], 247 (32), 246 (51), 237 (31), 219 (25), 205 (17), 203 (19), 196 (13), 188 (18), 179 (53), 177 (30), 164 (55), 159 (37), 147 (63), 133 (16), 131 (25), 119 (100), 117 (29), 115 (19), 105 (25), 91 (64), 79 (21),

77 (21). HRMS-ESI+ m/z $[M+H]^+$ calcd for $[C_{16}H_{22}O_4+H]^+$: 279.1591, found: 279.1588.

Tetracyclo[6.2.1.1^{3,10}.0^{3,8}]dodecane-1,10-dicarboxylic acid (12d). From **22d** (722 mg, 2.59 mmol) and a solution of KOH (40%) in MeOH (7 mL) and following the same procedure as for **12c**, diacid **12d** (520 mg, 80% yield) was obtained as a pale yellow solid, mp 239-240 ºC; IR (ATR) ν 2931, 2859, 2693, 2592, 1696, 1418, 1299, 1236, 1201, 1083, 1038, 885, 714, 600 cm^{-1}; ^{1}H NMR (400 MHz, $CDCl_3$) δ 1.58 [m, 4 H, 5(6)-H_2], 1.66 [m, 4 H, 4(7)-H_2], 1.81 [d, J = 7.4 H, 4 H, 2(9,11,12)-H_a], 1.91 [d, J = 7.4 Hz, 4 H, 2(9,11,12)-H_b], 9.88 [very broad s, 2 H, $CO_2\underline{H}$]; ^{13}C NMR (100.6 MHz, $CDCl_3$) δ 18.8 [CH_2, C5(6)], 25.3 [CH_2, C4(7)], 48.3 [C, C3(8)], 53.7 [CH_2, C2(9,11,12)], 58.0 [C, C1(10)], 179.9 (C, $\underline{C}O_2CH_3$). GC/MS, m/z (%); main ions: 250 ($M^{\cdot+}$, 3), 232 [$(M-H_2O)^{\cdot+}$, 48], 204 (37), 165 (78), 164 (28), 160 (30), 159 (36), 150 (67), 147 (53), 146 (26), 145 (26), 131 (44), 119 (89), 117 (53), 115 (28), 105 (30), 93 (17), 92 (20), 91 (100), 79 (33), 77 (40), 65 (20). HRMS-ESI– m/z $[M–H]^-$ calcd for $[C_{14}H_{18}O_4–H]^-$: 249.1132, found: 249.1135.

Elemental analysis data:

Compound	**Molecular Formula**	**Calculated**				**Found**			
		C	H	N	X	C	H	N	X
14a·HCl·0.5H_2O	$C_{12}H_{19}N$·HCl·0.5H_2O	64.70	9.50	6.29	15.91	64.73	9.36	6.68	16.11
15a·HCl·0.2H_2O	$C_{13}H_{21}N$·HCl·0.2H_2O	67.48	9.76	6.05	15.32	67.57	9.57	6.33	15.42
16a·HCl·0.33Et_2O	$C_{13}H_{21}N_3$·HCl·0.33Et_2O	61.37	9.10	14.99	12.65	61.70	9.07	14.62	13.04
14b·HCl·0.35H_2O	$C_{10}H_{15}N$·HCl·0.35H_2O	62.56	8.77	7.30	18.46	62.67	9.08	7.44	18.46
16b·1.75HCl	$C_{11}H_{17}N_3$·1.75HCl	51.80	7.41	16.47	nd	52.03	7.72	16.79	nd
14c·$C_4H_6O_6$·0.25H_2O	$C_{14}H_{23}N$·$C_4H_6O_6$·0.25H_2O	60.06	8.26	3.89	-	60.06	8.51	4.06	-
16c·HCl·0.3H_2O	$C_{15}H_{25}N_3$·HCl·0.3H_2O	62.29	9.27	14.53	12.26	61.90	9.16	14.93	12.31
14d·$C_4H_6O_6$·1CH_3OH	$C_{14}H_{21}N$·$C_4H_6O_6$·1CH_3OH	59.20	8.11	3.63	-	59.41	8.08	3.47	-
16d·HCl·0.25H_2O	$C_{15}H_{25}N_3$·HCl·0.25H_2O	62.92	8.62	14.68	nd	63.04	8.55	14.49	nd
18c	$C_{12}H_{14}N$	64.83	9.97	25.20	-	64.78	10.09	25.11	-
***syn*- and *anti*-19c**	$C_{12}H_{16}I_2$·0.1hexane	35.80	4.15	-	60.05	35.51	3.95	-	60.43
***syn*- and *anti*-19d**	$C_{12}H_{14}I_2$	34.98	3.42	-	61.60	34.87	3.34	-	61.49

Chapter 4

Part A

Easily Accessible Polycyclic Amines as *wt* and mutant Influenza A/M2 channel blockers

4A.1 Rationale and previous work

The endeavour described herein has its origins in our previous project in which we observed that the polycyclic amines, which were greater in length but featured a reduction in the polycyclic core width in respect to amantadine, were endowed with dual activity against the *wt* and the V27A mutant channels from Influenza A virus (see chapter 3).

With the objective of further exploring this strategy and taking into account that:

- Several structures of the M2 *wt* channel were available at the time[1,2], which allowed a tailoring of our compounds to the binding site.
- The structure of the V27A mutant had been disclosed, reporting wider diameters of the pore[3].
- Our hypothesis that, in order to target the V27A mutant, greater lengths might be required. Presumably this would allow the basic centre of our molecules to establish interactions with the Gly34 in the lower binding site of the channel, disrupting the deeper water clusters and blocking the pore[4].
- Coming from a resource consuming synthetic route of 12 steps, which included challenging reactions and the use of hazardous reagents to reach the first bioactive compound, this time we aimed for ready-access compounds, this is, the new bioactive polycycles should be prepared in few synthetic steps[5].

The following three polycyclic scaffolds: 4-azatetracyclo[5.3.2.$0^{2,6}$.$0^{8,10}$]dodecanes (**XVII**), 4-azatetracyclo[5.4.2.$0^{2,6}$.$0^{8.11}$]trideca-9,12-diene (**II**) and 7,8,9,10-tetramethyl-3-azapentacyclo[7.2.1.$1^{5,8}$.$0^{1,5}$.$0^{7,10}$]tridecane (**XVIII**), were envisaged at the start of this work (Chart 1).

[1] Cady, S. D., Schmidt-Rohr, K., Wang, J., Soto, C. S., Degrado, W. F. & Hong, M. Structure of the amantadine binding site of influenza M2 proton channels in lipid bilayers. *Nature*. **2010**, 463(7281), 689–692.
[2] Acharya, R., Carnevale, V., Fiorin, G., Levine, B. G., Polishchuk, A. L., Balannik, V., Samish, I., Lamb, R. A., Pinto, L. H., DeGrado, W. F. & Klein, M. L. Structure and mechanism of proton transport through the transmembrane tetrameric M2 protein bundle of the influenza A virus. *Proc. Nat. Acad. Sci. USA*. **2010**, 107, 15075-15080.
[3] Pielak, R. M. & Chou, J. J. Solution NMR structure of the V27A drug resistant mutant of influenza A M2 channel. *Biochem. Biophys. Res. Commun*. **2010**, 401, 58-63.
[4] Hong, M. & DeGrado, W. F. Structural basis for proton conduction and inhibition by the influenza M2 protein. *Protein Sci*. **2012**, 21, 1620.
[5] Rey-Carrizo, M., Barniol-Xicota, M., Ma, C., Frigolé-Vivas, M., Torres, E., Naesens, L., Llabrés, S., Juárez-Jiménez, J., Luque, F. J., DeGrado, W. F., Lamb, R. A., Pinto, L. H. & Vázquez, S. Easily accessible polycyclic amines that inhibit the wild-type and amantadine-resistant mutants of the M2 channel of influenza A virus. *J Med Chem*. **2014**, 57(13), 5738-47.

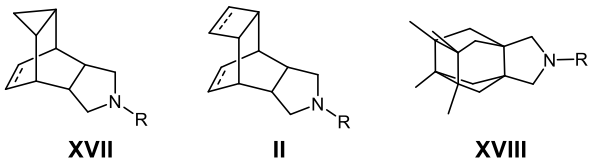

XVII **II** **XVIII**

Chart 1. Designed polycycles with putative anti-influenza A activity.

These structures were meeting the sought criteria, being greater in length than our previous family of compounds and the first bioactive compound of each series was accessible in only 2 synthetic steps in the case of **XVII** and **II** or 5 steps in the case of **XVIII**. In addition, these scaffolds offered diverse chemically modifiable points, which allowed us to prepare a family of derivatives for each series.

4A.2 Theoretical discussion

The 4-azatetracyclo[5.4.2.$0^{2,6}$.$0^{8,11}$]trideca-9,12-diene and related compounds (**II**), were prepared in the present thesis.

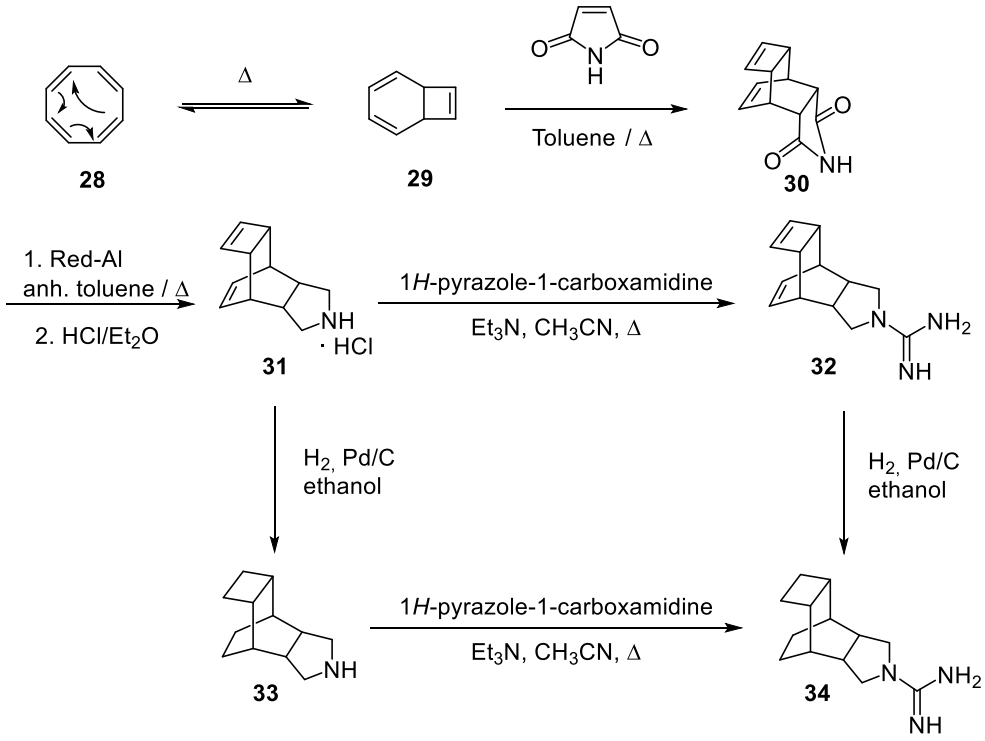

Scheme 5. Synthetic route to 4-azatetracyclo[5.4.2.$0^{2,6}$.$0^{8,11}$]trideca-9,12-diene derivatives with antiviral activity.

The synthesis started with the reaction of cyclooctatetraene and maleimide in a heated sealed tube. Interestingly in this Diels-Alder cycloaddition - previously reported by Abou-Gharbia and co-workers[6] - the cyclooctatetraene, under high temperatures, isomerizes to its tautomer or valence isomer bicyclo[4.2.0]octa-2,4,7-triene by means of a by thermal 6e- electrocyclic pericyclic reaction[7,8,9]. This *in situ* formed specie is the diene that reacts with the dienophile maleimide, yielding the tetracyclic endo-adduct **30**. Of note, the formation of the endo adduct responds to the effect of the bonding interaction between the carbonyl group and the forming π-bond of the bicyclo[4.2.0]octa-2,2,7-triene[10] (Scheme 6).

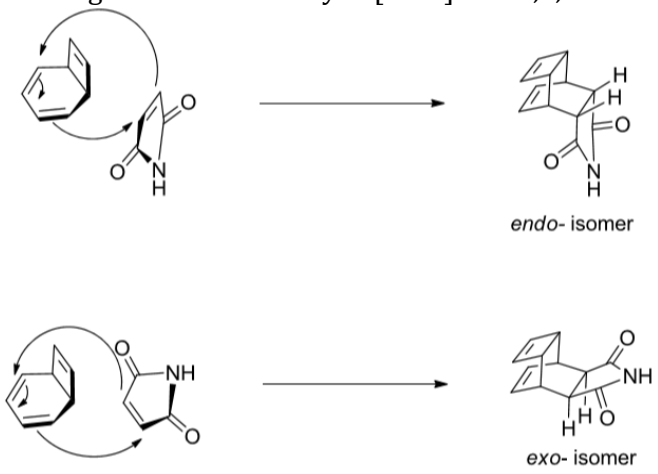

Scheme 6. Theoretical exo- and endo- products arising from the Diels-Alder reaction of cyclooctatetraene and maleimide.[11]

As described in the journal article, a double reduction of the imide **30** carbonyl groups using Red-Al®, lead to the first bioactive product, the pyrrolidine **31**. From this key intermediate **31** the desired saturated derivative, **33**, and their corresponding guanidines, **32** and **34**, were accessed through an hydrogenation with Pd/C as catalyst and a reaction with 1*H*-pyrazole-1 -carboxamidine, respectively.

[6] Abou-Gharbia, M., Patel, U. R., Webb, M. B., Moyer, J. A., Andree, T. H. & Muth, E. A. Polycyclic aryl- and heteroarylpiperazinyl imides as 5-HT1A receptor ligands and potential anxiolytic agents: synthesis and structure-activity relationship studies. *J. Med. Chem.* **1988**, 31, 1382.
[7] Huisgen, R. & Mietzsch, F. The Valence Tautomerism of Cyclooctatetraene. *Angew. Chem. Intl. Ed. English.* **1964**, 3(2), 83.
[8] Vogel, E., Kiefer, H. & Roth, W. R. Bicyclo[4,2,0]octa-2,4,7-triene. *Angew. Chem. Intl. Ed. English*. **1964**, 3(6), 442–443.
[9] Huisgen, R., Konz, W. E. & Gream, G. E. Evidence for different valence tautomers of bromocyclooctatetraene. *J. Am. Chem. Soc*. **1970**, 92 (13), 4105.
[10] Lane, C. F. Sodium Cyanoborohydride - A Highly Selective Reducing Agent for Organic Functional Groups. *Synthesis*. **1975**, 135.
[11] Borch, R. F. Bernstein, M. D. & Durst, H. D. The Cyanohydridoborate Anion as a Selective Reducing Agent. *J. Am. Chem. Soc.* **1971**, 93, 2897.

As for the previous family of amines, compounds **31-34** were evaluated as M2 channel blockers by the groups of Profs. Pinto and DeGrado. Moreover its antiviral activity was assessed by the group of Prof. Lieve Naesens (Rega Institute for Medical Research, KU Leuven, Belgium). The results are collected in table 4.

	A/M2 WT		A/M2 S31N		A/M2 V27A	
	Inh (%)[a]	IC_{50}[b]	Inh (%)[a]	IC_{50}[b]	Inh (%)[a]	IC_{50}[b]
31[c]	92.9	5.54	3.9	ND	5.5	ND
32	94.5	1.24	3.9	ND	17.2	ND
33	91.8	4.93	14.2	ND	33.8	ND
34	94.5	2.03	2.6	ND	75.9	22.61
Amt	91.0	16.0	35.6	199.9	10.8	ND

Table 4. [a] Inhibition of A/M2 channels expressed in Xenopus oocytes using the TEV technique. All inhibitors were initially tested at 100 μM for 2 min. [b] Determined only after >75% inhibition. [c] Antiviral EC_{50} determined by microscopic scoring of the CPE at 72 h post infection of A/PR/8/34 = 1.3 μM.

Pleasingly, these results outperformed the corresponding analogues derived from the slightly smaller scaffold **XVII**, synthesized in the Thesis of Matías Rey-Carrizo (see article for further details).

4A.3 Follow up work

Steaming from the results of this work, other related projects branched out:

The first one was developed in the present thesis and was devoted to the preparation of further derivatives from the scaffold **II**, which resulted to be, among the more synthetically accessible ones, the most suitable for the preparation of potent anti-influenza A compounds (**XVII** vs **II**, see article for further details).

As already mentioned, experimental and computational studies had confirmed the wider pore diameter of M2/V27A mutant channel; after further evidence came out from the structures **II** and in order to get access to longer and wider compounds, which could fill better this cavity, we designed the analogues **35** and **36**. The introduction of the epoxide group was designed *in silico* by the group of Prof F. Javier Luque (Universitat de Barcelona) aimed to, besides meeting the aforementioned structural requirements, also modify the polarity of the derivatives. This modification was unforeseen in previous influenza A inhibitors and the effect of the insertion of such a polar oxygen atom was

prone to significantly change the activity of our antivirals. As it was worth further exploring this hypothesis we also envisaged the preparation of **38**, isoster of the cyclopropane **6**, previously synthesized by our group[12] (Chart 2).

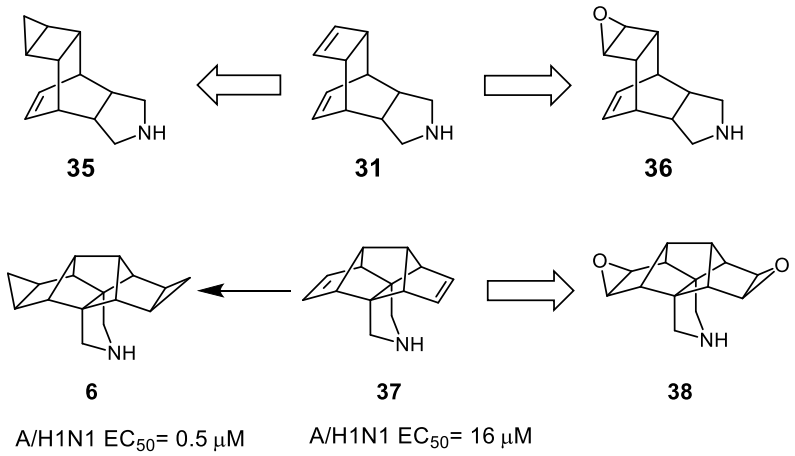

Chart 2. Polarity changed derivatives. An analogous cyclopropanation modification had already reported successful results in our group[12].

Starting from the imide precursor **30** and in order to prepare **35,** several cyclopropanation attempts were carried out. First of all we used diazomethane and palladium acetate, in an analogous way in which **6** was obtained. This methodology, despite known to be suitable for strained alkenes, had no effect in this case, recovering pure starting material. Alternatively, we tried the classical cyclopropanation protocols reported by Simmons-Smith[13,14] and the Furukawa modification[15,16,17] which source of iodomethylzinc reagent comes from the alkyl exchange reaction between an alkyl zinc (diethylzinc in our case) and a 1,1-dimethyliodine. Unfortunately, all the attempts were fruitless (Scheme 7).

[12] Duque, M. D., Ma, C., Torres, E., Wang, J., Naesens, L., Juárez-Jiménez, J., Camps, P., Luque, F. J., DeGrado, W. F., Lamb, R. A., Pinto, L. H. & Vázquez, S. Exploring the size limit of templates for inhibitors of the M2 ion channel of influenza A virus. *J. Med. Chem.* **2011**, 54(8), 2646–2657.
[13] Simmons, H. E. & Smith, R. D. A new synthesis of cyclopropanes from olefins. *J.Am.Chem.Soc.***1958**, 80 ,5323.
[14] Simmons, H. E. & Smith, R. D. A new Synthesis of Cyclopropanes. *J. Am. Chem. Soc*. **1959**, 81, 4256.
[15] Furukawa, J., Kawabata, N. & Nishimura, J. A novel route to cyclopropanes from olefins. *Tetrahedron Lett*. **1966**, 3353.
[16] Furukawa, J., Kawabata, N. & Nishimura, J. Synthesis of cyclopropanes by the reaction of olefins with dialkylzinc and methylene iodide. *Tetrahedron*. **1968**, 24, 53.
[17] Nishimura, J., Furukawa, J., Kawabata, N. & Kitayama, M. The relative reactivity of olefins in cycloaddition with zinc carbenoid. *Tetrahedron*. **1971**, 27, 1799.

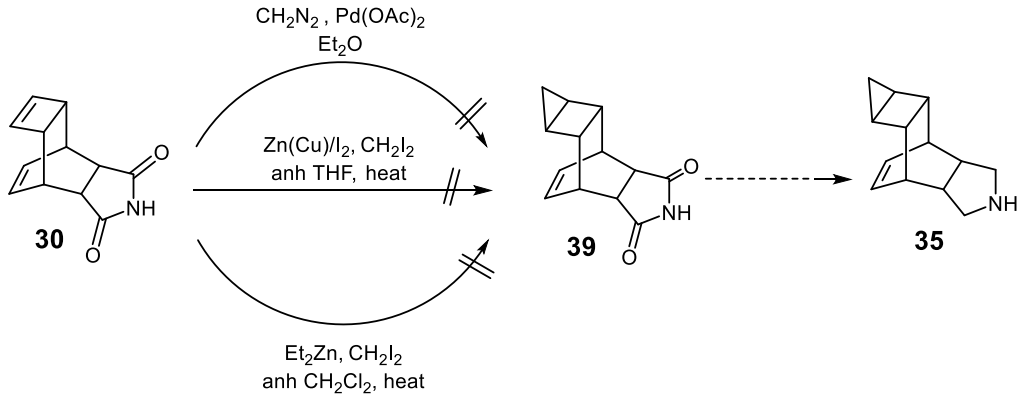

Scheme 7. Cyclopropanation attempts.

Starting from the precursor imines, **30** and **42,** and using the *in situ* prepared dimethyldioxirane as the epoxidizing agent, epoxides **40** and **43** were successfully prepared in a 94% and quantitative yield, respectively. Not fully unexpectedly the reduction of imide **43** was accompanied of epoxides opening to give a mixture of alcohols **44**, that could not be separated. In **40**, we expected that the remaining double bond below the epoxide may somehow protect the epoxide from the hydride attack. However the reduction of the imide group did not furnish the desired product **36** but a complex mixture of ring-opening alcohol isomers that could not be separated (Scheme 8).

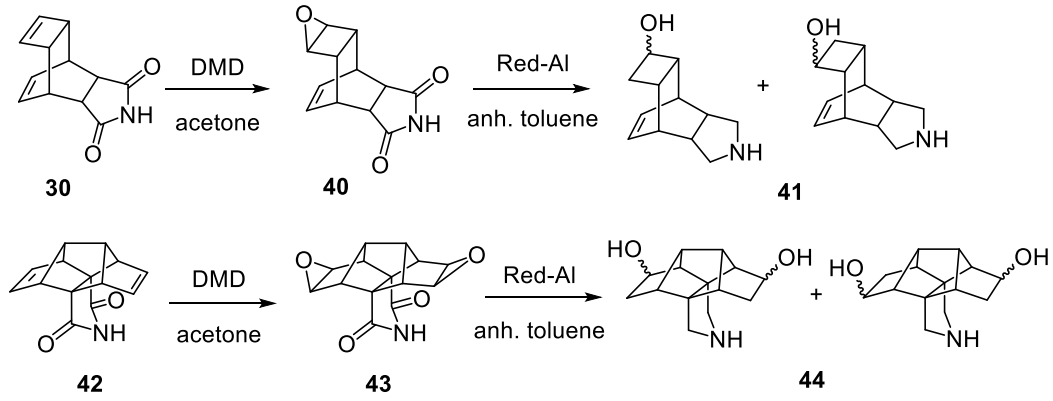

Scheme 8. Epoxidization route.

In light of the discouraging results, this project was abandoned.

The second follow up project, was carried out in the thesis of Dr. Matías Rey-Carrizo. He successfully prepared several polycyclic compounds using imine **30** as starting point. From his work, several new anti-influenza A agents, were identified[18] (Scheme 9).

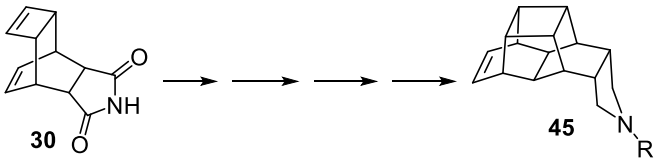

Scheme 9. Polycyclic compounds developed by Dr. Matías Rey-Carrizo.

The final project that arouse from this work is related to the general structure **XVIII**, prepared in the thesis context of Dr. Matias Rey-Carrizo. Unlike the previous two works, this endeavour is not related to medicinal chemistry but to pure organic chemistry (see chapter 4-part B).

4A.4 Experimental data of the unpublished work

4-Oxa-10-azapentacyclo[5.5.2.0^{2,6}.0^{3,5}.0^{8,12}]tetradeca-13-en-9,11-dione, 40.

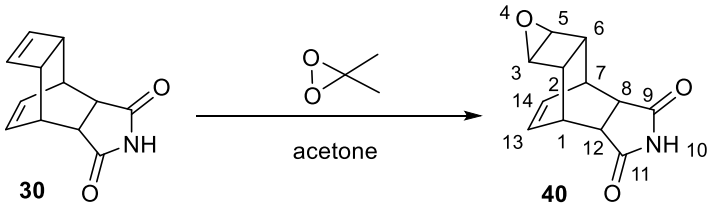

In a 100 mL 1 neck round bottom flask a solution of dione **30** (1.00 g; 4.96 mmol) and DMD in acetone solution (64.5 mL, 0.1 N, 6.45 mmol) was prepared. After capping it was left stirring overnight at room temperature, giving a mixture of starting material and epoxidized product in an approximate ratio of 1:1.4. Then, more of DMD (40 mL, 0.1 N, 4.0 mmol) were added and the same reaction procedure was followed to obtain the epoxide **40** pure in a 94% yield. ^{1}H NMR (400 MHz, $CDCl_3$) δ 2.41 [dd, *J* = 4.5 Hz, *J* = 2.4 Hz, 2 H, 9(11)-H], 2.82 [t, *J* = 1.5 Hz, 2 H, 1(7)-H], 3.30 [m, 2H, 8(12)-H], 3.58 [d, *J* = 2.7 Hz, 2 H, 2(6)-H], 6.26 [m, 2 H, 13(14)-H], 8.10 (s, 1H, NH).

[18] Rey-Carrizo, M., Gazzarrini, S., Llabrés, S., Frigolé-Vivas, M., Juárez-Jiménez, J., Font-Bardia, M., Naesens, L., Moroni, A., Luque, J. & Vázquez, S. New polycyclic dual inhibitors of the wild type and the V27A mutant M2 channel of the influenza A virus with unexpected binding mode. *Eur. J. Med. Chem*. **2015**, 96, 318–329.

3-Aza-8,15-dioxaoctacyclo[8.7.0.0^{1,5}.0^{5,13}.0^{6,11}.0^{7,9}.0^{12,17}.0^{14,16}]heptadecane-2,4-dione, 43.

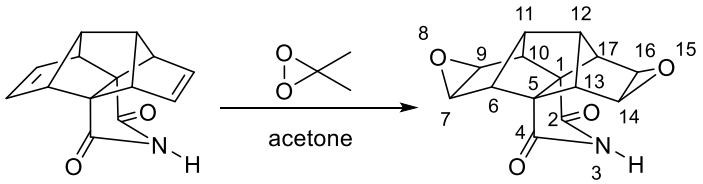

42 **43**

In a 100 mL 1 neck round bottom flask a solution of **42** (1.00 g; 4.44 mmol) and DMD in acetone solution (57 mL, 0.09 N, 5.13 mmol) was prepared. After capping it was left stirring overnight at room temperature, giving a mixture of starting material, ene-epoxide and diepoxide in ratio 6:4:1. According to the results more acetone solution of DMD was added and the same reaction procedure was followed three more times (30 mL; 75 mL; 19 mL) until the diepoxide **43** was obtained pure in quantitative yield. ^{1}H NMR (400 MHz, $CDCl_3$) δ 2.27 [s, 2 H, 11(12)-H], 3.16 [s, 4 H, 7(9, 14, 15)-H], 3.39 [s, 4 H, 6(10,13,17)-H], 8.10 [s, 1 H, NH].

Journal of Medicinal Chemistry

ACS AuthorChoice

Article

pubs.acs.org/jmc

Terms of Use

Easily Accessible Polycyclic Amines that Inhibit the Wild-Type and Amantadine-Resistant Mutants of the M2 Channel of Influenza A Virus

Matias Rey-Carrizo,[†] Marta Barniol-Xicota,[†] Chunlong Ma,[‡,#] Marta Frigolé-Vivas,[†] Eva Torres,[†] Lieve Naesens,[∥] Salomé Llabrés,[⊥] Jordi Juárez-Jiménez,[⊥] Francisco J. Luque,[⊥] William F. DeGrado,[§] Robert A. Lamb,[#,▽] Lawrence H. Pinto,[‡] and Santiago Vázquez*[,†]

[†]Laboratori de Química Farmacèutica (Unitat Associada al CSIC), Facultat de Farmàcia, and Institute of Biomedicine (IBUB), Universitat de Barcelona, Av. Joan XXIII s/n, Barcelona E-08028, Spain

[‡]Department of Neurobiology and Physiology, Northwestern University, Evanston, Illinois 60208-3500, United States

[§]Department of Pharmaceutical Chemistry, University of California, San Francisco, California 94158, United States

[∥]Rega Institute for Medical Research, KU Leuven, 3000 Leuven, Belgium

[⊥]Departament de Fisicoquímica, Facultat de Farmàcia, and Institute of Biomedicine (IBUB), Universitat de Barcelona, Av. Prat de la Riba 171, Santa Coloma de Gramenet E-08921, Spain

[#]Department of Molecular Biosciences, and [▽]Howard Hughes Medical Institute, Northwestern University, Evanston, Illinois 60208-3500, United States

Supporting Information

ABSTRACT: Amantadine inhibits the M2 proton channel of influenza A virus, yet most of the currently circulating strains of the virus carry mutations in the M2 protein that render the virus amantadine-resistant. While most of the research on novel amantadine analogues has revolved around the synthesis of novel adamantane derivatives, we have recently found that other polycyclic scaffolds effectively block the M2 proton channel, including amantadine-resistant mutant channels. In this work, we have synthesized and characterized a series of pyrrolidine derivatives designed as analogues of amantadine. Inhibition of the wild-type M2 channel and the A/M2-S31N, A/M2-V27A, and A/M2-L26F mutant forms of the channel were measured in *Xenopus* oocytes using two-electrode voltage clamp assays. Most of the novel compounds inhibited the wild-type ion channel in the low micromolar range. Of note, two of the compounds inhibited the amantadine-resistant A/M2-V27A and A/M2-L26F mutant ion channels with submicromolar and low micromolar IC_{50}, respectively. None of the compounds was found to inhibit the S31N mutant ion channel.

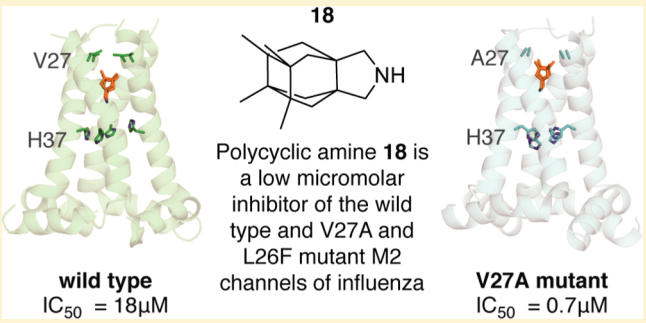

INTRODUCTION

Amantadine (Amt) and rimantadine (Rmt), two polycyclic aminoadamantane derivatives, have been in clinical use as anti-influenza virus agents for decades. However, the efficacy of these two drugs dropped sharply in recent years due to the global distribution of mutant viruses carrying Amt resistance mutations, prompting the Centers for Disease Control to recommend discontinuing the use of amantadine-based drugs.[1,2] Therefore, there is an urgent need to develop novel antiviral drugs that are active against drug-resistant influenza viruses.

The mechanism of action of Amt and Rmt is based on the inhibition of the M2 proton channel of the influenza A virus. The M2 protein is a 97 residues long integral membrane protein with a transmembrane (TM) domain of 19 residues, a small ectodomain of 23 residues, and a 54 residues long cytoplasmic tail.[3−5] Detailed mutational studies indicated that several point mutations of pore-lining residues of the A/M2 TM domain result in Amt-resistance.[6] However, only a few of these mutations (i.e., L26F, V27A, and S31N) have been observed in transmissible viruses, with the S31N mutation being the most frequently occurring Amt-resistance mutation.[7] In 2011, Wang et al. reported that spiro compound **1** is able of inhibiting the L26F and V27A M2 mutants with good efficacy in electrophysiological and plaque reduction assays.[8−10] More recently, our group has reported the first non-adamantane inhibitor of the V27A mutant, the polycyclic pyrrolidine **2** (Chart 1).[11]

Received: April 15, 2014
Published: June 18, 2014

   dx.doi.org/10.1021/jm5005804 | *J. Med. Chem.* 2014, 57, 5738−5747

Chart 1. Structures of Amt, Rmt, and Recently Developed Compounds with Potent Activity against A/M2-V27A Mutant Channels[a]

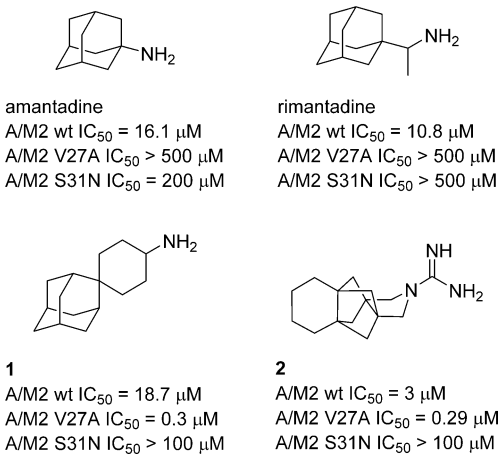

[a]The IC_{50} values denote the reported 50% inhibitory concentrations on A/M2 wt, S31N, and V27A proton channel function.[8−11]

A common problem of **1** and **2** is that their syntheses involves several steps (e.g., up to 11 steps for **2**),[11] which means that the synthesis of novel analogues of these two compounds would be challenging. In the present study, we report novel scaffolds designed to inhibit the A/M2 channel. We have found that the wild-type (wt) channel can be inhibited by several easy-accessible pyrrolidine derivatives. Furthermore, we have identified two compounds, **18** and **19**, that are capable of inhibiting the M2-V27A mutant ion channel with submicromolar IC_{50} values. In addition, both compounds are able to inhibit the M2 wt channel with an IC_{50} value similar to that of Amt, and both are also low micromolar inhibitors of the M2-L26F mutant channel.

CHEMISTRY

During the past years, our group has synthesized several polycyclic Amt analogues containing different scaffolds, including ring-contracted, ring-rearranged, and 2,2-dialkyl derivatives of Amt.[12−15] Several of them displayed similar IC_{50} values for wt A/M2 as Amt but, unfortunately, were inactive against the Amt-resistant S31N or V27A mutant forms of A/M2.[13] More recently, we have reported on the synthesis of polycyclic pyrrolidines and on their inhibitory effect on the A/M2 proton channel activity by using the conductance assay in M2-expressing oocytes. Again, several of these novel compounds displayed similar IC_{50} values for wt A/M2 as Amt, and, interestingly, we found three guanidine derivatives that displayed low micromolar to submicromolar IC_{50} values against the V27A mutant channel.[11]

On the basis of our previous insights that polycyclic scaffolds other than adamantane effectively inhibit the M2 proton channel and that the synthesis of guanidine **2** and related compounds involved a very long synthetic sequence, we have searched for novel synthetic strategies able to yield polycyclic amines that are structurally diverse and easily available by short synthetic sequences.

The reduction of known imide **3**, easily accessible in multigram quantities by the reaction of commercially available cycloheptatriene with maleimide,[16] furnished amine **4** in 79% yield. The catalytic hydrogenation of **4** led to fully saturated compound **6** in 95% yield. Both pyrrolidines were transformed

Scheme 1. Synthesis of Novel Polycyclic Pyrrolidine Derivatives

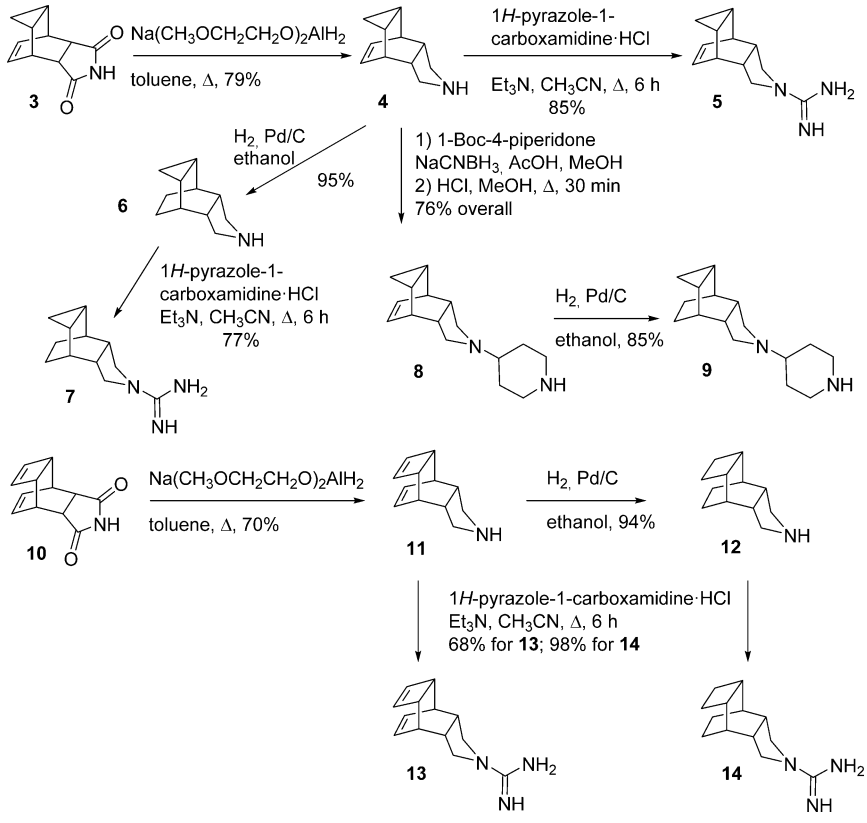

dx.doi.org/10.1021/jm5005804 | J. Med. Chem. 2014, 57, 5738−5747

Scheme 2. Synthesis of Compounds 18 and 19

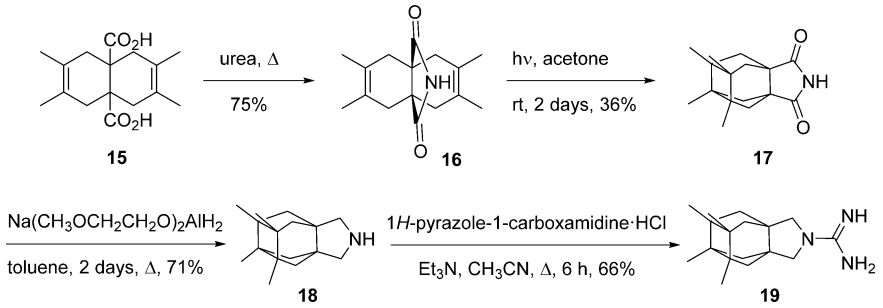

Table 1. Inhibitory Effect of the Synthesized Compounds on A/M2 wt, S31N, or V27A Proton Channel Functions[a,b]

	A/M2 wt (mean ± SE)		A/M2 S31N (mean ± SE)		A/M2 V27A (mean ± SE)	
compd	inhibition by 100 μM for 2 min (%)	IC_{50} (μM)	inhibition by 100 μM for 2 min (%)	IC_{50} (μM)	inhibition by 100 μM for 2 min (%)	IC_{50} (μM)
amantadine	91.0 ± 2.1	16.0 ± 1.2	35.6 ± 1.5	199.9 ± 13.5	10.8 ± 2.0	ND[e]
4	88.8 ± 1.3	2.92	0	ND	2.4 ± 1.3	ND
5	90.7 ± 0.9	1.50	0	ND	9.5 ± 0.6	ND
6	90.9 ± 1.0	3.38	5.7 ± 0.9	ND	3.4 ± 2.2	ND
7	93.4 ± 1.2	1.64	2.5 ± 0.4	ND	14.5 ± 1.7	ND
11	92.9 ± 1.2	5.54	3.9 ± 1.3	ND	5.5 ± 0.1	ND
12	94.5 ± 0.8	1.24	3.9 ± 1.8	ND	17.2 ± 5.2	ND
13	91.8 ± 0.8	4.93	14.2 ± 2.5	ND	33.8 ± 2.3	ND
14	94.5 ± 1.6	2.08	2.6 ± 1.4	ND	75.9 ± 1.2	22.61
18[c]	90.2 ± 0.9	18.0	1.1 ± 1.1	ND	96.4 ± 0.5	0.70
19[d]	91.7 ± 1.2	10.7	2.7 ± 1.5	ND	96.7 ± 0.5	0.50

[a]The activity of the inhibitors was measured using the TEV technique on A/M2 channels expressed in *Xenopus* oocytes; percentage of inhibition was average of at least three experiments. For IC_{50} experiments, 7–9 concentrations were measured, and, at each concentration, experiments were run at least three times. [b]Isochronic (2 min) values for IC_{50} are given. See text and Supporting Information for details. [c]The inhibition by 100 μM for 2 min of **18** on A/M2 L26F mutant channel was 90.6% ± 1.1 with an IC_{50} of 8.6 μM. [d]The inhibition by 100 μM for 2 min of **19** on A/M2 L26F mutant channel was 88.4% ± 0.6 with an IC_{50} of 7.5 μM. [e]ND, not determined.

into their corresponding guanidines, **5** and **7**, by reaction with 1*H*-pyrazole-1-carboxamidine. Taking into account that recent experimental and computational studies have shown that the M2-V27A mutant channel has a larger cavity than the wt M2 channel,[9,17−19] we also synthesized larger compounds derived from **4** and **6**. Thus, reductive alkylation of amine **4** with 1-Boc-4-piperidone followed by deprotection led to piperidine **8** in 75% overall yield. The catalytic hydrogenation of **8** furnished piperidine **9** in 85% yield (Scheme 1). Similarly, starting from known imide **10**, easily available from cyclooctatetraene and maleimide,[16] amines **11** and **12** and their guanidine derivatives **13** and **14**, were synthesized in good yields (Scheme 1).

To increase the chemical diversity of the compounds, while preserving the synthetic easiness, two more compact pyrrolidine derivatives, **18** and **19**, were designed (Scheme 2). For the synthesis of these aesthetically appealing compounds that include one four-membered ring, three five-membered rings, and two six-membered rings, we started from known diacid **15**, easily available from acetylene dicarboxylic acid and 2,3-dimethylbutadiene.[20,21] The reaction of **15** with urea at 180 °C for 30 min yielded imide **16** in 75% yield. Photolysis of imide **16** at room temperature in acetone with a 125 W Hg lamp for 2 days gave a mixture of the starting imide and the tetracyclic imide **17**. Column chromatography of this mixture through silica gel afforded pure **17** in 36% yield (based on recovered starting material, brsm). The imide was subsequently reduced using sodium bis(2-methoxyethoxy)-aluminum hydride to give the secondary amine **18** in 71% yield. Finally, reaction of **18** with 1*H*-pyrazole-1-carboxamidine monohydrochloride in acetonitrile led to guanidine **19** in 66% yield (Scheme 2).

Previously, we have seen that, in related polycyclic compounds, on going from secondary to tertiary amines, the inhibitory effect on either wt or V27A mutant M2 channels diminished.[6,11,15] For this reason, in this work we have not synthesized alkylated derivatives of the novel secondary amines herein reported.

All the new compounds were fully characterized as hydrochlorides through their spectroscopic data and elemental analyses.

Pharmacological Activity and Structure−Activity Relationships. *Inhibition of wt and Amt-Resistant A/M2 Ion Channels.* The inhibitory activity of the compounds was tested on A/M2 channels expressed in *Xenopus* oocytes using the two-electrode voltage clamp (TEV) technique. All inhibitors were initially tested at 100 μM; those that inhibited the wt A/M2 channel activity by more than 80% were chosen for measurement of their IC_{50} value in an isochronic (2 min) inhibition assay. The results are given in Table 1.

Amt inhibited wt A/M2 channel with an IC_{50} of 16.0 μM while being inactive against the V27A mutant channel. Unfortunately, piperidine derivatives **8** and **9** did not display any activity. Tetracyclo amines **4**, **6**, **11**, and **12** and their corresponding guanidines **5**, **7**, **13**, and **14** were potent low-micromolar inhibitors of the wt channel. Regarding the activity against the V27A M2 mutant channel, three trends were found,

dx.doi.org/10.1021/jm5005804 | J. Med. Chem. 2014, 57, 5738−5747

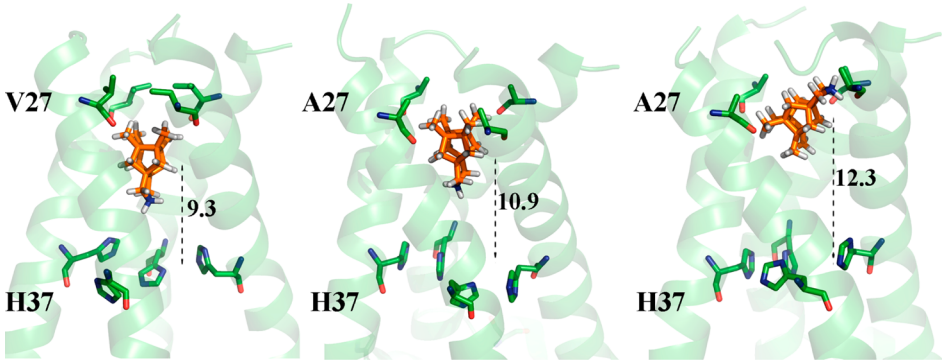

Figure 1. Representation of compound **18** bound to (left) the wild-type M2 channel and its V27A variant (*down* and *up* orientations shown in middle and right panels, respectively). The dashed line indicates the distance (Å) from the center-of-mass of the inhibitor to the plane formed by the Cα atoms of His37.

Table 2. Cross-Diagonal Distances (Å) between Helices A−C and B−D in the Apo Form of the wt and V27A Channels[a]

	wt		V27A		
	d1	d2	d1	d2	Δ^b
Val27	10.3 ± 0.5 (8.3 ± 0.6)	10.6 ± 0.5 (8.6 ± 0.6)	11.6 ± 0.7 (10.0 ± 0.9)	11.5 ± 0.8 (9.9 ± 0.9)	+1.1 (+1.5)
Ser31	11.0 ± 0.4 (11.2 ± 0.5)	10.7 ± 0.4 (10.8 ± 0.5)	11.4 ± 0.6 (12.0 ± 0.7)	11.3 ± 0.6 (12.0 ± 0.7)	+0.5 (+1.0)
Gly34	10.1 ± 0.4	9.3 ± 0.5	9.6 ± 0.6	9.4 ± 0.6	−0.2
His37	13.4 ± 0.5 (10.6 ± 0.5)	12.3 ± 0.8 (9.9 ± 0.9)	12.3 ± 0.6 (9.6 ± 0.6)	11.8 ± 0.8 (9.2 ± 0.9)	−0.8 (−1.0)

[a]Values measured from the Cα atoms of residues in the tetrad; values determined from the Cβ atoms are given in parentheses. [b]Difference between cross-diagonals in wt and V27A channels (positive values imply a widening of the pore in the V27A channel).

i.e., guanidine performed better than its corresponding amine (e.g., **7** vs **6** or **13** vs **11**), the fully saturated compounds were more potent than their corresponding unsaturated analogues (e.g., **7** vs **5** or **14** vs **13**), and the cyclobutane/cyclobutene analogues were more potent than the cyclopropane derivatives (e.g., **12** vs **6** or **14** vs **7**). Altogether, guanidine **14** emerged as the more promising compound, being more potent than Amt against the wt M2 channel and endowed with fair activity against the V27A mutant channel. None of the compounds was found to inhibit the S31N mutant ion channel. Finally, amine **18** and guanidine **19** also proved to be active against the wt channel, with similar IC_{50} values as Amt (18.5 and 10.7 μM, respectively) while being endowed with submicromolar IC_{50} against the V27A mutant (0.7 and 0.5 μM, respectively). Moreover, both compounds were low micromolar inhibitors of the L26F mutant (8.6 and 7.5 μM, respectively).

Molecular Modeling. To gain insight into the inhibitory data of the more compact pyrrolidine derivatives, the interaction of **18** with the wt M2 channel and its V27A variant was examined by means of molecular dynamics (MD) simulations and compared with the trends found for the binding of Amt.

The analysis of the three replicas run for **18** bound to the wt channel shows a consistent binding mode, where the center-of-mass (COM) of the inhibitor is located close to the plane formed by the Cα atoms of Ser31, the amine nitrogen is pointing toward the plane formed by the His37 residues (average distance of 6.1 Å), and the tilt angle (i.e., the deviation of the amine nitrogen from the pore axis) is 16.1°, which partly reflects the twisted geometry of the pyrrolidine ring (Figure 1; see also Supporting Information Figure S1). This orientation (denoted *down* hereafter) is also found for Amt bound to the wt channel (Supporting Information Figure S2). In two replicas of the V27A−**18** complex, the inhibitor adopts the *down* orientation, but in the third replica it turns over at the beginning of the trajectory and the inhibitor adopts the opposite (*up*) orientation (the distance of the amine nitrogen to the His37 plane and the tilt angle are, on average, 14.9 Å and 145.3°; Figure 1 and Supporting Information Figure S3). Remarkably, Amt was found in the *up* orientation in the three replicas run for the V27A channel (Supporting Information Figure S4), and even in one case Amt was released to the solvent after few nanoseconds.

To explore the molecular basis of the exchange between *down* and *up* orientations found in the V27A channel, additional MD simulations were run for the apo forms of both wt and V27A channels. The root-mean-square deviation (RMSD) of the protein backbone for the transmembrane helices between the wt channel and its V27A variant amounts to 1.4 Å, which compare with the typical range of RMSD values obtained for the ligand-bound forms of the two channels (between 1.2 and 1.7 Å; Supporting Information Table S1). This suggests that the gross structural features of the channel are not drastically altered by the Val27 → Ala mutation, in agreement with previous studies.[9,18] Nevertheless, inspection of the interhelical cross-diagonals distances (measured from either the Cα or the Cβ atoms) for distinct tetrads of residues shows that the mutation widens the pore at the Ala27 plane, an effect associated with the narrowing of the pore at the His37 plane (Table 2). This structural rearrangement likely contributes to the displacement of the amine nitrogen of compound **18** in the V27A channel, which is pushed away from the His37 plane by 1.6 Å (from 6.1 Å in the wt channel to 7.7 Å in the V27A variant for the inhibitor in the *down* orientation) and might facilitate the exchange between *down* and *up* arrangements of the inhibitor. Compared to compound **18**, the lower, more compact size of Amt should likely enhance the exchange rate between the two ligand orientations, eventually leading to an easier release from the pore that could account for the reduction in inhibitory potency against the V27A channel (Table 1).

dx.doi.org/10.1021/jm5005804 | J. Med. Chem. 2014, 57, 5738−5747

Table 3. Antiviral Activity in Influenza Virus-Infected MDCK[a] Cells

	antiviral activity (μM)						
	A/PR/8/34		A/HK/7/87			cytotoxicity (μM)	
compd	EC_{50} (CPE)[b]	EC_{50} (MTS)[b]	EC_{50} (CPE)[b]	EC_{50} (MTS)[b]	EC_{99} (virus yield)[c]	CC_{50}[d]	MCC[e]
4	>100	>100	6.2	8.0	20	54	100
5	>100	>100	>100	>100	ND	39	100
6	>100	>100	6.0	2.7	<0.4	49	100
7	>100	>100	>100	>100	ND	41	100
8	≤0.80	<0.80	>100	>100	ND	46	100
9	>100	>100	>100	>100	ND	9.0	20
11	1.3	<0.80	>100	>100	>10	4.9	15
12	>100	>100	>100	>100	<0.08	1.9	4
13	>100	>100	>100	>100	>10	9.4	20
14	>100	>100	>100	>100	4.6	1.9	4
18	1.8	3.0	>100	>100	>50	49	100
19	>100	>100	>100	>100	>10	15	≥4
amantadine	30	34	1.4	1.4	1.1	>500	≥500
rimantadine	7.6	5.1	0.81	0.15	>4	230	500

[a]MDCK: Madin–Darby canine kidney cells; virus strains: A/PR/8/34 (A/H1N1) and A/HK/7/87 (A/H3N2). [b]50% effective concentration, or compound concentration producing 50% inhibition of virus replication, as determined by microscopic scoring of the CPE at 72 h post infection or by the MTS cell viability test. [c]EC_{99}: compound concentration giving 2 $\log_{10}$ reduction in virus yield, as determined by quantifying the virus in the supernatant at 24 post infection, using an qRT-PCR based virus yield assay.[25] [d]CC_{50}: 50% cytotoxic concentration, as determined by the MTS cell viability test. Values shown are the mean of 2–3 determinations. [e]MCC: minimum cytotoxic concentration, or concentration producing minimal alterations in cell morphology after 72 h incubation with compound. ND, not determined.

The lack of inhibitory potency of compound **18** against the S31N variant can be realized from the comparison of the inhibitor bound to the wt M2 channel and the solid-state NMR-derived structural data available for the complex of the S31N channel bound to the 5-thienyl isoxazole derivative containing a 1-(1-adamantylamino)-methylene group in position 3 (PDB entry 2LY0).[22] It was noted that the structure of the S31N variant closely resembled previous structures of the wt M2 channel, showing most similarity to the Amt-bound channel structure solved by solid-state NMR.[23] Similar structural resemblance is also found upon comparison with the snapshots sampled for the wt channel bound to compound **18** (see Supporting Information Figure S6), which rules out the existence of drastic structural alterations in the arrangement of the transmembrane helices triggered upon binding of the two compounds. Both NMR and MD simulations revealed that binding of the isoxazole derivative involved water-mediated contacts between the protonated amine group with two Asn31 side chains as well as by a direct interaction between the amide unit of a third Asn31 and the charged amine group. This network of interactions was facilitated by the fact that the adamantylamino group was oriented with the amine facing away the His37 plane. However, the position of the protonated amine unit in the isoxazole derivative is replaced by the hydrophobic cage of compound **18** (see Supporting Information Figure S6), which would thus be unable of forming a similar pattern of stabilizing interactions. On the other hand, adoption of the reverse arrangement of compound **18** (i.e., adopting an amine-up orientation) should not only alter the contacts with Asn31 due to the distinct orientation of the amine group but would also trigger unfavorable clashes between the terminal methyl groups with the tetrad of Gly37 residues.

Antiviral Activity. The anti-influenza virus activity of the compounds was first assessed in a relatively stringent three-day cytopathic effect (CPE) reduction assay in MDCK cells (Table 3). All the guanidines showed to be inactive, probably reflecting a permeability problem or, particularly for **13**, **14**, and **19**, as a consequence of their cytotoxicity. Compounds **4** and **6** displayed favorable activity (i.e., antiviral EC_{50} values in the range of 3–8 μM) against the A/HK/7/87 virus strain, which possesses a wt M2 channel. Three other compounds, i.e., **8**, **11**, and **18**, showed strong activity against the A/PR/8/34 strain, an A/H1N1 virus with two mutations (S31N and V27T) in the M2 protein. We previously found that A/PR/8/34 appears particularly sensitive to a slight increase in endosomal pH as induced by some polycyclic amine compounds.[15] This effect may explain, at least in part, the antiviral activity of these compounds, although they were devoid of activity against the S31N M2 mutant channel. A similar behavior has very recently been observed by Kolocouris et al. in a set of novel aminoadamantanes.[24]

We subsequently performed a 24 h virus yield assay and a plaque reduction assay, both using the WT-M2 A/HK/7/87 virus. These experiments confirmed the activity of **4** and **6** (Table 3 and Figure 2), which, in terms of cell culture activity, emerged as the two most promising molecules among the synthesized series. Compounds **12** and **14** were shown to reduce virus yield, with EC_{99} values of <0.08 μM (**12**) and 4.6 μM (**14**). These compounds caused a clear (**12**) or modest (**14**) reduction in plaque size or number at a compound concentration of 0.5 μM (Figure 2). However, because both were visibly toxic at 2–8 μM, their selectivity index (i.e., ratio of cytotoxic to antivirally effective concentration) appears limited. Finally, **11**, **13**, and **18** caused visible inhibition of plaque formation (Figure 2) at 0.5–2 μM, but the activity of these three compounds was not confirmed in the CPE or virus yield assay (Table 3). As expected, neither the novel compounds nor the reference agents Amt and Rmt were active against influenza B virus (data not shown).

CONCLUSIONS

The present work shows the feasibility of designing easily accessible compounds able to successfully inhibit the wt and the

dx.doi.org/10.1021/jm5005804 | J. Med. Chem. 2014, 57, 5738–5747

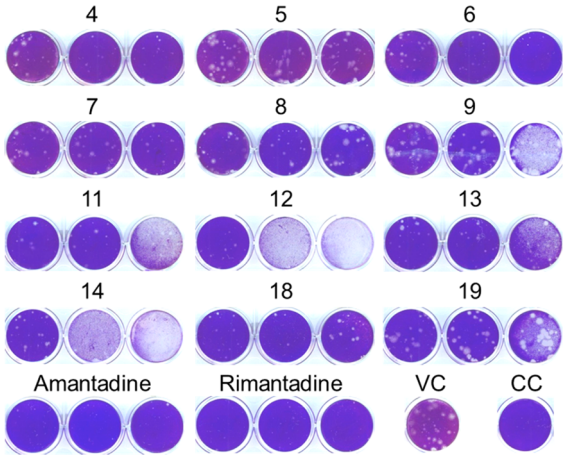

Figure 2. Activity of the compounds in an influenza virus plaque reduction assay. MDCK cells were infected with influenza virus (strain A/HK/7/87; 25 PFU per well) in the presence of the test compounds (concentrations, from left to right: 0.5, 2, and 8 μM). After 72 h incubation, plaques were visualized by crystal violet staining. VC: mock-treated virus control. CC: uninfected cell control.

V27A and L26F variants of the A/M2 channels of influenza A virus. In fact, some of the newly designed compounds inhibit the three channels similarly or even more effectively than Amt inhibits the wt proton channel. In particular, amine **18** and guanidine **19** emerged as promising compounds, being low micromolar inhibitors against the wt channel and the L26F mutant, while being endowed with submicromolar IC_{50} against the V27A variant. Furthermore, compound **18** showed strong activity against the A/PR/8/34 strain, an A/H1N1 virus with two mutations (S31N and V27T) in the M2 protein. Overall, these results suggest that compounds **18** and **19** are suitable templates to explore novel candidates against influenza virus.

EXPERIMENTAL SECTION

Plasmid, mRNA Synthesis, and Microinjection of Oocytes. The cDNA encoding the influenza A/Udorn/72 (A/M2) was inserted into pGEM3 vector for the expression on oocyte plasma membrane. A/M2 S31N and A/M2 V27A mutants were generated by QuikChange site-directed mutagenesis kit (Agilent Technologies). The synthesis of mRNA and microinjection of oocytes have been described previously.[26]

Two-Electrode Voltage Clamp Analysis. Macroscopic membrane current was recorded 48−72 h after injection as described previously.[8] The tested compounds were applied at pH 5.5 at various concentrations when the inward current reaches maximum. The compounds were applied for 2 min, and residual membrane current was compared with the membrane current before the application of compounds. Membrane currents were analyzed with pCLAMP 10.0 software package (Axon Instruments, Sunnyvale, CA).

Antiviral Assays. To determine the anti-influenza virus activity in Madin−Darby canine kidney (MDCK) cells, CPE reduction and virus yield assays were performed as described.[25,27] Briefly, MDCK cells grown in 96-well plates were infected with influenza virus (strains A/PR/8/34 (A/H1N1); A/HK/7/87 (A/H3N2) or B/HK/5/72), and at the same time the test compounds were added in serial dilutions. After 72 h incubation at 35 °C, microscopy was performed to score the compounds' inhibitory effect on the viral cytopathic effect (CPE) or cytotoxicity. These data were verified by measuring the cell viability with the formazan-based MTS assay. In separate experiments, supernatants were harvested from the infected and compound-treated cells at 24 h post infection, and virus yield in these samples was determined by qRT-PCR. To perform plaque reduction assays, influenza virus A/HK/7/87 was incubated (1 h at 4 °C) with different concentrations of the compounds and then added to confluent MDCK cells in 12-well plates. After 1 h incubation at 35 °C, excess virus was removed and replaced by fresh medium containing the compounds and 0.8% agarose. After 72 h incubation, plaques were visualized by cell fixation with 3.7% formaldehyde and staining with 0.1% crystal violet.

Chemical Synthesis. General Methods. Melting points were determined in open capillary tubes with a MFB 595010 M Gallenkamp. 400 MHz ^{1}H/100.6 MHz ^{13}C NMR spectra, and 500 MHz ^{1}H NMR spectra were recorded on Varian Gemini 300, Varian Mercury 400, and Varian Inova 500 spectrometers, respectively. The chemical shifts are reported in ppm (δ scale) relative to internal tetramethylsilane, and coupling constants are reported in hertz (Hz). Assignments given for the NMR spectra of the new compounds have been carried out on the basis of DEPT, COSY ^{1}H/^{1}H (standard procedures), and COSY ^{1}H/^{13}C (gHSQC and gHMBC sequences) experiments. IR spectra were run on PerkinElmer Spectrum RX I spectrophotometer. Absorption values are expressed as wavenumbers (cm^{-1}); only significant absorption bands are given. The GC/MS analysis was carried out in an inert Agilent Technologies 5975 gas chromatograph equipped with an Agilent 122-5532 DB-5MS 1b (30 m × 0.25 mm) capillary column with a stationary phase of phenylmethylsilicon (5% diphenyl−95% dimethylpolysiloxane), using the following conditions: initial temperature of 50 °C (1 min), with a gradient of 10 °C/min up to 300 °C, and a temperature in the source of 250 °C, solvent delay (SD) of 4 min and a pressure of 7,35 psi. Column chromatography was performed on silica gel 60 AC.C (35−70 mesh, SDS, ref 2000027). Thin-layer chromatography was performed with aluminum-backed sheets with silica gel 60 F_{254} (Merck, ref 1.05554), and spots were visualized with UV light and 1% aqueous solution of $KMnO_4$. The analytical samples of all of the new compounds which were subjected to pharmacological evaluation possessed purity ≥95% as evidenced by their elemental analyses.

4-Azatetracyclo[5.3.2.0^{2,6}.0^{8,10}]dodec-11-ene Hydrochloride, 4·HCl. A solution of imide **3** (8.00 g, 42.3 mmol) in dry and degassed toluene (280 mL) was cooled down to 5 °C with an ice bath. Sodium bis(2-methoxyethoxy) aluminum hydride (64.5 mL, 65% solution in toluene, 211.4 mmol) was added dropwise, and the resulting solution was heated to reflux and stirred for 2 days. The solution was allowed to cool down to room temperature, and 30% aqueous KOH (300 mL) was added dropwise. The organic phase was separated and the aqueous layer was extracted with dichloromethane (3 × 250 mL). The combined organic extracts were dried over Na_2SO_4, filtered, and concentrated under vacuo to give a red oil. This oil was dissolved in EtOAc and treated with an excess of a 1.2 N ethereal solution of HCl and was allow to stand at 0 °C for 24 h. The suspension was filtered to get **4·HCl** as a white solid (6.54 g, 79%). An analytical sample of **4·HCl** was obtained by crystallization from MeOH/Et_2O, mp 197−198 °C. IR (KBr) ν 3430, 2932, 2894, 2765, 2519, 2640, 1569, 1466, 1450, 1422, 1395, 1383, 1355, 1301, 1281, 1245, 1170, 1132, 1068, 1026, 1016, 936, 902, 841, 824, 758, 731, 649, 591, 580 cm^{-1}. ^{1}H NMR (400 MHz, CD_3OD) δ 0.23 (complex signal, 2 H, 9-H_2), 1.05 [m, 2 H, 8(10)-H], 2.75 [m, 2 H, 2(6)-H], 2.82 [dm, J = 12.0 Hz, 2 H, 3(5)-H_a], 2.95 [m, 2 H, 1(7)-H], 3.38 [dd, J = 12.0 Hz, 2 H, 3(5)-H_b], 5.91 [m, 2 H, 11(12)-H]. ^{13}C NMR (100.6 MHz, CD_3OD) δ 5.5 (CH_2, C9), 11.1 [CH, C8(10)], 35.5 [CH, C1(7)], 44.8 [CH, C2(6)], 50.4 [CH_2, C3(5)], 130.7 [CH, C11(12)]. MS (DI), m/e (%). Main ions: 161 ($M^{\bullet+}$, 5), 94 (14), 93 (16), 92 (19), 91 (47), 81 (12), 80 (20), 68 (100), 67 (35).

4-Azatetracyclo[5.3.2.0^{2,6}.0^{8,10}]dodecane Hydrochloride, 6·HCl. To a solution of **4·HCl** (200 mg, 1.00 mmol) in absolute EtOH (35 mL), Pd on activated charcoal (5%, 40 mg) was added. The black suspension was set in a hydrogenator at 150 psi of H_2 and was stirred at room temperature overnight. The black suspension was filtered, and **6·HCl** was recovered as an off-white solid (190 mg, 95%). An analytical sample was obtained by crystallization from 2-propanol, mp 227−228 °C. IR (KBr) ν 3421, 3073, 2935, 2755, 2646, 2585, 2460, 2363, 1590, 1447, 1423, 1347, 1100, 1058, 1028, 999, 902, 881, 812, 798, 752, 723, 662, 526 cm^{-1}. ^{1}H NMR (400 MHz, CD_3OD) δ 0.59 (dt, J = 6.0 Hz, J' = 7.6 Hz, 1 H, 9-H_a), 0.97 (dt, J = 6.0 Hz, J' = 3.6

dx.doi.org/10.1021/jm5005804 | J. Med. Chem. 2014, 57, 5738−5747

Hz, 1 H, 9-H_b), 1.04 [m, 2 H, 8(10)-H], 1.25 [broad d, J = 8.8 Hz, 2 H, 11(12)-H_a], 1.42 [broad d, J = 8.8 Hz, 2 H, 11(12)-H_b], 1.96 [broad s, 2 H, 1(7)-H], 2.68 [m, 2 H, 2(6)-H], 3.16 [dd, J = 12.0 Hz, J' = 6.8 Hz, 2 H, 3(5)-H_a], 3.42 [dd, J = 12.0 Hz, J' = 8.6 Hz, 2 H, 3(5)-H_b]. ^{13}C NMR (100.6 MHz, CD_3OD) δ 6.9 [CH_2, C9], 16.7 [CH, C8(10)], 17.9 [CH_2, C11(12)], 28.1 [CH, C1(7)], 41.2 [CH, C2(6)], 48.6 [CH_2, C3(5)]. MS (DI), m/e (%). Main ions: 163 ($M^{\bullet+}$, 35), 162 (15), 134 (73), 105 (12), 94 (14), 93 (13), 92 (12), 91 (35), 80 (20), 79 (30), 77 (25), 70 (100), 68 (62), 67 (21).

_t_-Butyl 4-[4-Azatetracyclo[5.3.2.0^{2,6}.0^{8,10}]dodec-11-ene]-piperidine-1-carboxylate. To a solution of **4·HCl** (1.15 g, 5.8 mmol) in water (30 mL) was added a 10 N aqueous solution of NaOH. It was then extracted with EtOAc (3 × 50 mL), and the organic phase was dried over Na_2SO_4, filtered, and concentrated under vacuo (yellowish oil, 945 mg, quantitative yield). This oil was dissolved in MeOH (20 mL), and sodium cyanoborohydride (1.06 g, 16.9 mmol), 1-Boc-4-piperidone (1.39 g, 7.0 mmol), and glacial acetic acid (0.67 mL) were added to the solution. The solution was stirred at room temperature for 8 h, and a second portion of sodium cyanoborohydride (1.06 g, 16.9 mmol) and 1-Boc-4-piperidone (1.39 g, 7.0 mmol) were added. The yellow solution was further stirred at room temeprature overnight. It was concentrated under vacuo, and the yellow oil was redissolved in water (50 mL) and extracted with EtOAc (3 × 50 mL). The organic phase was dried over Na_2SO_4, filtered, and concentrated under vacuo (clear sticky solid, 3.90 g). Column chromatography of the solid (silica gel, EtOAc) gave the pure carbamate as an off-white solid (1.52 g, 76%). An analytical sample was prepared by crystallization from MeOH/Et_2O, mp 176−177 °C. IR (KBr) ν 3004, 2980, 2683, 2612, 2330, 2203, 2163, 1684, 1455, 1420, 1364, 1264, 1170, 1150, 1113, 1068, 1047, 1016, 974, 944, 866, 841, 814, 768, 733 cm^{-1}. ^{1}H NMR (500 MHz, $CDCl_3$) δ 0.21 (dt, J = 5.5 Hz, J' = 3.0 Hz, 1 H, 9-H_b), 0.27 (dt, J = 5.5 Hz, J' = 7.5 Hz, 1H, 9-H_a), 1.01 [m, 2 H, 8(10)-H], 1.44 [s, 9 H, C(C$\underline{H}_3$)$_3$], 1.65 [dq, J = 12.5 Hz, J' = 2.5 Hz, piperidine-C3(5)-H_{ax}], 1.94 [dm, J = 12.5 Hz, 2 H, piperidine-C3(5)-H_{eq}], 2.39 [broad s, 2 H, 3(5)-H_a], 2.68 [m, 2 H, piperidine-C2(6)-H_a], 2.81 [m, 2 H, 2(6)-H], 2.93 [complex signal s, 3 H, 1(7)-H and piperidine-C4-H], 3.60 [broad s, 2 H, 3(5)-H_b], 4.21 [broad s, 2 H, piperidine-C2(6)-H_b], 5.86 [m, 2 H, 11(12)-H]. ^{13}C NMR (125.6 MHz, $CDCl_3$) δ 5.4 (CH_2, C9), 9.9 [CH, C8(10)], 28.0 [broad CH_2, C3(5)-piperidine], 28.3 [CH_3, C($\underline{C}H_3$)$_3$], 33.3 [CH, C1(7)], 41.7 [broad CH_2, C2(6)-piperidine], 42.1 [CH, C2(6)], 54.6 [CH_2, C3(5)], 62.2 (CH, C4-piperidine), 80.4 [C, $\underline{C}(CH_3)_3$], 129.4 [CH, C11(12)], 154.1 [C═O, $\underline{C}O_2C(CH_3)_3$]. MS (DI), m/e (%). Main ions: 344 ($M^{\bullet+}$, 26), 287 [(M-C_4H_9)$^+$, 35], 271 (12), 243 [(M-$CO_2C_4H_9$)$^+$,12], 207 (14), 195 (100), 188 (14), 151 (15), 94 (19), 57 (27). HRMS-ESI+ m/z [M + H]$^+$ calcd for [$C_{21}H_{32}N_2O_2$ + H$^+$], 345.2537; found, 345.2533.

4-(4-Piperidinyl)-4-azatetracyclo[5.3.2.0^{2,6}.0^{8,10}]dodec-11-ene Dihydrochloride, 8·2HCl. To a solution of the carbamate previously reported (760 mg, 2.20 mmol) in methanol (25 mL), a 0.8 N HCl solution in methanol (30 mL) was added. The resulting clear solution was heated to reflux and stirred for 30 min. It was then allowed to cool down to room temperature and was concentrated under vacuo to give a white solid that was crystallized from MeOH/Et_2O to give **8·2HCl** as a white solid (700 mg, quantitative), mp >250 °C (dec.). IR (KBr) ν 3479, 3405, 2945, 2804, 2733, 2642, 2585, 2496, 2363, 1630, 1458, 1437, 1239, 1157, 1044, 974, 842, 766, 727, 679, 583 cm^{-1}. ^{1}H NMR (400 MHz, CD_3OD) δ 0.28 (m, 2 H, 9-H_2), 1.04 [m, 2 H, 8(10)-H_2], 2.00 [dm, J = 13.6 Hz, 2 H, piperidine-C3(5)-H_{ax}], 2.35 [d, J = 13.6 Hz, 2 H, piperidine-C3(5)-H_{eq}], 2.59 [broad s, 2 H, 3(5)-H_a], 2.76 [broad s, 2 H, 2(6)-H], 2.96 [broad s, 2 H, 1(7)-H], 3.07 [td, J = 13.2 Hz, J' = 2.8 Hz, 2 H, piperidine-C2(6)-H_{ax}], 3.40 (tt, J = 13.0 Hz, J' = 4.0 Hz, 1 H, piperidine−C4-H), 3.54 [dm, J = 13.2 Hz, 2 H, piperidine-C3(5)-H_{eq}], 3.78 [broad s, 2 H, 3(5)-H_b], 5.90 [m, 2 H, 11(12)-H]. ^{13}C NMR (100.6 MHz, CD_3OD) δ 5.8 (CH_2, C9), 10.9 [CH, C8(10)], 26.7 [CH_2, C3(5)-piperidine], 34.4 [CH, C1(7)], 43.5 [CH_2, C2(6)-piperidine], 43.8 [CH, C2(6)], 56.6 [CH_2, C3(5)], 60.1 (CH, C4-piperidine), 130.5 [CH, C11(12)]. MS (DI), m/e (%). Main ions: 244 ($M^{\bullet+}$, 23), 200 (14), 189 (27), 188 (25), 164 (18), 163 (57), 162 (33), 160 (14), 152 (100), 151 (43), 120 (12), 108 (43), 107 (26), 97 (35), 96 (15), 95 (15), 94 (50), 91 (35), 86 (15), 85 (58), 84 (50), 83 (41), 82 (20), 69 (27), 68 (44), 58 (16), 57 (28), 55 (26).

4-(4-Piperidinyl)-4-azatetracyclo[5.3.2.0^{2,6}.0^{8,10}]dodecane Dihydrochloride, 9·2HCl. To a solution of **8·2HCl** (200 mg, 0.63 mmol) in absolute EtOH (35 mL), Pd on charcoal (40 mg, ca. 10% Pd) was added and the resulting suspension was hydrogenated at room temperature and at 150 psi of H_2 overnight. The black suspension was filtered, and **9·2HCl** was recovered as a white solid (170 mg, 85%). An analytical sample was obtained by crystallization from MeOH, mp >300 °C (dec.). IR (KBr) ν 3422, 2929, 2889, 2840, 2779, 2726, 2646, 2608, 2495, 2453, 2419, 2371, 1609, 1473, 1399, 1364, 1288, 1098, 1078, 879, 841, 800, 610, 510 cm^{-1}. ^{1}H NMR (400 MHz, CD_3OD) δ 0.59 (td, J = 7.6 Hz, J' = 6 Hz, 1 H, 9-H_a), 1.00 (m, 1 H, 9-H_b), 1.04 [m, 2 H, 8(10)-H], 1.26 [broad d, J = 8.8 Hz, 2H, 11(12)-H_a], 1.55 [broad d, J = 8.8 Hz, 2 H, 11(12)-H_b], 1.98 [s, 2 H, 1(7)-H], 2.07 [m, 2 H, piperidine-3(5)-H_{ax}], 2.45 [d, J = 13.2 Hz, 2 H, piperidine-3(5)-H_{eq}], 2.69 [broad s, 2 H, 2(6)-H], 3.07 [broad s, 2 H, 3(5)-H_a], 3.12 [td, J = 13.2 Hz, J' = 2.8 Hz, 2H, piperidine-2(6)-H_{ax}], 3.58 [d, J = 13.2 Hz, 2 H, piperidine-2(6)-H_{eq}], 3.63 (m, 1 H, piperidine-4-H), 3.78 [broad s, 2 H, 3(5)-H_b]. ^{13}C NMR (100.6 MHz, CD_3OD) δ 7.0 (CH_2, C9), 16.7 [CH, C8(10)], 17.7 [CH_2, C11(12)], 26.9 [CH_2, C3(5)-piperidine], 27.0 [CH, C1(7)], 40.4 [CH, C2(6)], 43.6 [CH_2, C2(6)-piperidine 54.5 [CH_2, C3(5)], 60.2 (CH, C4-piperidine). MS (DI), m/e (%). Main ions: 205 (47), 204 (28), 112 (100), 111 (36), 110 (30), 91 (19), 79 (16), 72 (17), 68 (41).

4-Amidino-4-azatetracyclo[5.3.2.0^{2,6}.0^{8,10}]dodec-11-ene Hydrochloride, 5·HCl. A solution of **4·HCl** (1.15 g, 5.83 mmol) in water (30 mL) was basified to pH = 14 with a 10 N aqueous solution of NaOH. It was then extracted with EtOAc (3 × 50 mL), and the joined organic phase was dried over Na_2SO_4, filtered off, and concentrated under vacuo (yellow oil, 900 mg, 5.55 mmol, 95% yield). To a suspension of this oil in acetonitrile (35 mL), 1_H_-pyrazole-1-carboxamidine monohydrochloride (1.08 g, 7.40 mmol) was added. The suspension was heated to reflux for 6 h. The yellow precipitate was filtered to give **5·HCl** as yellow crystals (1.13 g, 85%). An analytical sample was obtained by crystallization from MeOH/Et_2O, mp 248−249 °C (dec.). IR (KBr) ν 3468, 3410, 3327, 3135, 3047, 3025, 2997, 2948, 2880, 2414, 1669, 1620, 1527, 1470, 1434, 1374, 1363, 1281, 1169, 1085, 1045, 1015, 973, 854, 819, 766, 710, 645 cm^{-1}. ^{1}H NMR (400 MHz, CD_3OD) δ 0.15−0.23 (complex signal, 2 H, 9-H_2), 1.02 [m, 2 H, 8(10)-H], 2.81 [m, 2 H, 2(6)-H], 2.92 [broad s, 2 H, 1(7)-H], 3.12 [dd, J = 10.8 Hz, J' = 3.4 Hz, 2 H, 3(5)-H_a], 3.52 [m, 2 H, 3(5)-H_b], 5.85 [m, 2 H, 11(12)-H]. ^{13}C NMR (100.6 MHz, CD_3OD) δ 4.7 (CH_2, C9), 10.7 [CH, C8(10)], 37.0 [CH, C1(7)], 45.1 [CH, C2(6)], 52.4 [CH_2, C3(5)], 130.1 [CH, C11(12)], 155.5 (C, $\underline{C}$NH). MS (DI), m/e (%). Main ions: 203 ($M^{\bullet+}$, 15), 126 (13), 125 (32), 124 (28), 115 (15), 114 (16), 113 (50), 112 (78), 111 (55), 110 (14), 92 (25), 91 (70), 77 (14), 69 (43), 68 (100), 67 (18), 65 (13).

4-Amidino-4-azatetracyclo[5.3.2.0^{2,6}.0^{8,10}]dodecane Hydrochloride, 7·HCl. To a solution of **6·HCl** (377 mg, 1.57 mmol) in absolute EtOH (35 mL), Pd on charcoal (78 mg, ca. 10% Pd) was added, and the resulting suspension was hydrogenated at room temperature and at 150 psi of H_2 overnight. The black suspension was filtered to furnish **7·HCl** as an off-white powder (290 mg, 77%). An analytical sample was obtained by crystallization from MeOH/Et_2O, mp 208−209 °C. IR (KBr) ν 3311, 3124, 3007, 2993, 2949, 2924, 2907, 1653, 1602, 1529, 1484, 1465, 1378, 1352, 1337, 1299, 1283, 1208, 1185, 1171, 1136, 1071, 1024, 936, 805, 642, 539, 487 cm^{-1}. ^{1}H NMR (400 MHz, CD_3OD) δ 0.51 [dt, J = 6.2 Hz, J' = 7.8 Hz, 2 H, 9(10)-H_a], 0.87 [dt, J = 6.2 Hz, J' = 3.6 Hz, 2 H, 9(10)-H_b], 1.02 [m, 2 H, 8(10)-H], 1.18 [broad d, J = 10.0 Hz, 2 H, 11(12)-H_a], 1.29 [broad d, J = 10.0 Hz, 2 H, 11(12)-H_b], 1.92 [broad s, 2 H, 1(7)-H], 2.70 [m, 2 H, 2(6)-H], 3.48 [m, 2 H, 3(5)-H_a], 3.54 [dt, J = 11.2 Hz, J' = 2.0 Hz, 2 H, 3(5)-H_b]. ^{13}C NMR (100.6 MHz, CD_3OD) δ 5.4 (CH_2, C9), 15.8 [CH, C8(10)], 18.4 [CH_2, C11(12)], 30.4 [CH, C1(7)], 40.9 [CH, C2(6)], 51.0 [CH_2, C3(5)], 156.1 (C, $\underline{C}$NH). MS (DI), m/e (%). Main ions: 205 ($M^{\bullet+}$, 46), 204 (29), 138 (11), 112 (100), 111 (36), 110 (30), 91 (19), 79 (17), 72 (17), 68 (42).

dx.doi.org/10.1021/jm5005804 | J. Med. Chem. 2014, 57, 5738−5747

4-Azatetracyclo[5.4.2.0^{2,6}.0^{8,11}]trideca-9,12-diene Hydrochloride, 11·HCl. From a solution of imide **10** (1.46 g, 7.25 mmol) and sodium bis(2-methoxyethoxy)aluminum hydride (15.8 mL, 65% solution in toluene, 51.7 mmol) in dry and degassed toluene (45 mL) and following the same procedure that the one reported for compound **4**, diene **11** was obtained as an oil (876 mg, 70%). An analytical sample of **11·HCl** was obtained by solubilization of **9** in diethyl ether and addition of an excess of a 1.2 N ethereal solution followed by filtration of the solid, mp 206−207 °C. IR (ATR) ν 2924, 2482, 2340, 2158, 2016, 1716, 1540, 1049, 878, 824, 617 cm^{-1}. ^{1}H NMR (400 MHz, CD_3OD) δ 2.55 [m, 2 H, 2(6)-H], 2.74 [broad d, J = 11.6 Hz, 2 H, 1(7)-H], 2.76 [broad s, 2 H, 8(11)-H], 2.88 [m, 2 H, 3(5)-H$_a$], 3.43 [m, 2 H, 3(5)-H$_b$], 5.87 [s, 2 H, 9(10)-H], 6.04 [dd, 2 H, J = 4.4 Hz, J' = 3.2 Hz, 12(13)-H]. ^{13}C NMR (100.6 MHz, CD_3OD) δ 39.2 [CH, C1(7)], 42.9 [CH, C2(6)], 46.2 [CH, C8(11)], 51.5 [CH_2, C3(5)], 131.4 [CH, C12(13)], 138.9 [CH, C9(10)]. MS (DI), m/e (%). Main ions: 173 ($M^{\bullet+}$, 13), 128 (20), 120 (37), 115 (16), 106 (31), 91 (29), 80 (19), 78 (22), 68 (100), 67 (15).

4-Azatetracyclo[5.4.2.0^{2,6}.0^{8,11}]tridecane Hydrochloride, 12·HCl. To a solution of **11·HCl** (2.39 g, 11.4 mmol) in absolute EtOH (170 mL), Pd on charcoal (240 mg, ca. 10% Pd) was added and the resulting suspension was hydrogenated at room temperature and at atmospheric pressure until the addition of hydrogen stopped. The black suspension was filtered to furnish **12·HCl** as an off-white powder (2.30 g, 94%). An analytical sample was obtained by crystallization from MeOH/Et_2O, mp 266−269 °C. IR (ATR) ν 2897, 2769, 1568, 1489, 879, 640 cm^{-1}. ^{1}H NMR (400 MHz, CD_3OD) δ 1.55−1.59 [complex signal, 4 H, 12(13)-H$_a$ and 1(7)-H], 1.98 [dm, 2 H, J = 8.0 Hz, 12(13)-H$_b$], 2.10−2.25 [complex signal, 4 H, 9(10)-H_2], 2.28 [m, 2 H, 2(6)-H], 2.46 [m, 2 H, 8(11)-H], 3.18 [m, 2 H, 3(5)-H$_a$], 3.48 [m, 2 H, 3(5)-H$_b$], 4.86 (broad s, 2 H, NH_2). ^{13}C NMR (100.6 MHz, CD_3OD) δ 15.5 [CH_2, C12(13)], 21.3 [CH_2, C9(10)], 30.2 [CH, C1(7)], 38.1 [CH, C8(11)], 39.6 [CH, C2(6)], 49.0 [CH_2, C3(5)]. MS (DI), m/e (%). Main ions: 177 ($M^{\bullet+}$, 38), 176 (16), 149 (100), 91 (23), 79 (23), 77 (16), 70 (82), 68 (35), 67 (13).

4-Amidino-4-azatetracyclo[5.4.2.0^{2,6}.0^{8,11}]trideca-9,12-diene Hydrochloride, 13·HCl. To a suspension of **11·HCl** (1.0 g, 4.76 mmol) in acetonitrile (20 mL), 1*H*-pyrazole-1-carboxamidine monohydrochloride (838 mg, 5.74 mmol), and triethylamine (1.22 mL) were added. The suspension was heated to reflux for 6 h. The precipitate was filtered and washed with cold acetonitrile to give **13·HCl** as white crystals (816 mg, 68%), mp 234−237 °C; IR (ATR) ν 3120, 2926, 1657, 1644, 1593, 1534, 1475, 1294, 1195, 1030, 788, 742, 703, 624 cm^{-1}; ^{1}H NMR (400 MHz, CD_3OD) δ 2.63 [m, 2 H, 2(6)-H], 2.70 [m, 2 H, 1(7)-H], 2.74 [broad s, 2 H, 8(11)-H], 3.20 [dd, 2 H, J = 10.8 Hz, J = 3.6 Hz, 3(5)-H$_a$], 3.60 [m, 2 H, 3(5)-H$_b$], 5.86 [s, 2 H, 9(10)-H], 5.99 [dd, 2 H, J = 4.4 Hz, J' = 3.2 Hz, 12(13)-H]; ^{13}C NMR (100.6 MHz, CD_3OD) δ 40.9 [CH, C1(7)], 43.5 [CH, C2(6)], 46.0 [CH, C8(11)], 53.6 [CH_2, C3(5)], 130.8 [CH, C12(13)], 138.9 [CH, C9(10)]. MS (DI), m/e (%); main ions: 215 ($M^{\bullet+}$, 10), 214 (18), 128 (21), 120 (17), 115 (15), 111 (100), 110 (18), 91 (24), 78 (17), 77 (15), 68 (79).

4-Amidino-4-azatetracyclo[5.4.2.0^{2,6}.0^{8,11}]tridecane Hydrochloride, 14·HCl. To a solution of **12·HCl** (1.0 g, 4.68 mmol) in acetonitrile (20 mL), 1*H*-pyrazole-1-carboxamidine monohydrochloride (823 mg, 5.64 mmol), and triethylamine (1.19 mL) were added. The suspension was heated to reflux for 6 h. The precipitate was filtered and washed with cold acetonitrile to give **14·HCl** as white crystals (1.18 g, 98%), mp 299−301 °C. IR (ATR) ν 3308, 3112, 2938, 2899, 1659, 1644, 1590, 1536, 1487, 1188, 1157, 1030, 647, 627 cm^{-1}. ^{1}H NMR (400 MHz, CD_3OD) δ 1.47−1.60 [complex signal, 4 H, 12(13)-H$_a$ and 1(7)-H], 1.96 [broad d, 2 H, J = 8.4 Hz, 12(13)-H$_b$], 2.12−2.25 [complex signal, 4 H, 9(10)-H_2], 2.42−2.46 [complex signal, 4 H, 2(6)-H and 8(11)-H], 3.58 [m, 4 H, 3(5)-H_2]. ^{13}C NMR (100.6 MHz, CD_3OD) δ 15.9 [CH_2, C12(13)], 21.6 [CH_2, C9(10)], 32.5 [CH, C1(7)], 37.5 [CH, C8(11)], 39.9 [CH, C2(6)], 51.6 [CH_2, C3(5)]. MS (DI), m/e (%). Main ions: 219 ($M^{\bullet+}$, 41), 218 (21), 191 (38), 137 (24), 112 (57), 111 (100), 110 (19), 91 (20), 79 (18), 72 (15), 68 (39).

3,4,8,9-Tetramethyl-11,13-dioxo-12-azatricyclo[4.4.3]deca-3,8-diene (16). A mixture of known diacid **15** (200 mg, 0.72 mmol)[20,21] and urea (216 mg, 3.59 mmol) was heated slowly to 135 °C. When the mixture melted, it was heated to 180 °C for 30 min and cooled. Water (5 mL) was added, and the suspension was extracted with CH_2Cl_2 (6 × 4 mL). The combined organic extracts were washed with brine (1 × 5 mL), dried with anhyd Na_2SO_4, filtered and concentrated in vacuo to dryness to give imide **16** as a white solid (193 mg, 75% yield). An analytical sample of **16** was obtained by crystallization from CH_2Cl_2/pentane, mp 197−198 °C. IR (ATR) ν 3202, 3072, 2983, 2928, 2859, 1775, 1706, 1659, 1439, 1364, 1322, 1186, 1106, 982, 829, 739, 677 cm^{-1}. ^{1}H NMR (400 MHz, $CDCl_3$) δ 1.63 [d, J = 1.2 Hz, 12 H, 3(4,8,9)-CH_3], 2.07 [d, J = 14.2 Hz, 4 H, 2(5,7,10)-H$_a$], 2.35 [d, J = 14.2 Hz, 4 H, 2(5,7,10)-H$_b$], 8.23 (broad s, 1H, NH). ^{13}C NMR (100.6 MHz, $CDCl_3$) δ 19.1 [CH_3, C3(4,8,9)-CH_3], 38.7 [CH_2, C2(5,7,10], 52.9 [C, C1(6)], 127.4 [CH, C3(4,8,9)], 182.8 [C=O, C11(13)]. GC/MS, m/z (%). Main ions: 259 ($M^{\bullet+}$, 49), 188 (24), 17467 (25), 173 (15), 162 ($C_{12}H_{18}^{\bullet+}$, 100), 144 (13), 133 (16), 132 (10), 119 (18), 91 (13). HRMS-ESI+ m/z [M + H]$^+$ calcd for [$C_{16}H_{21}NO_2$ + H$^+$], 260.1645; found, 260.1649.

7,8,9,10-Tetramethyl-2,4-dioxo-3-azapentacyclo-[7.2.1.1^{5,8}.0^{1,5}.0^{7,10}]tridecane (17). A solution of **16** (630 mg, 2.43 mmol) and dry and degassed acetone (70 mL) in a quartz reactor was irradiated with a 125 W Hg lamp for 2 days under Ar atmosphere. The dark-yellow solution was concentrated under vacuo to give a yellow paste (1.08 g). The paste was purified by column chromatography (silica gel, hexane/EtOAc mixtures). With hexane/EtOAc (85/15) was recovered starting material (190 mg), while with hexane/EtOAc (80/20) imide **17** was obtained (160 mg, 36% brsm) as a white solid, mp 272−273 °C. IR (ATR) ν 3167, 3054, 2953, 2919, 2868, 1770, 1704, 1452, 1374, 1345, 1312, 1268, 1173, 1154, 1108, 1052, 1018, 842, 739, 628 cm^{-1}. ^{1}H NMR (400 MHz, $CDCl_3$) δ 1.01 [s, 12 H, 7(8,9,10)-C$\underline{H}_3$], 1.32 [d, J = 11.4 Hz, 4 H, 6(11,12,13)-H$_a$], 1.83 [d, J = 11.4 Hz, 4 H, 6(11,12,13)-H$_b$], 8.58 (broad s, 1H, NH). ^{13}C NMR (100.6 MHz, $CDCl_3$) δ 15.2 [CH_3, C14(15,16,17)], 40.5 [CH_2, C2(6,8,10)], 46.1 [C, C7(8,9,10)], 50.6 [C, C1(5)], 180.9 [C=O, C2(4)]. GC/MS, m/z (%). Main ions: 259 ($M^{\bullet+}$, 74), 188 [($C_{14}H_{20}$)$^{\bullet+}$, 39], 177 (36), 173 (17), 162 [($C_{12}H_{18}$)$^{\bullet+}$, 100], 145 (13), 133 (14), 119 (17), 91 (17). HRMS-ESI+ m/z [M + H]$^+$ calcd for [$C_{16}H_{21}NO_2$ + H$^+$], 260.1645; found, 260.1643.

7,8,9,10-Tetramethyl-3-azapentacyclo[7.2.1.1^{5,8}.0^{1,5}.0^{7,10}]-tridecane Hydrochloride (18·HCl). From **17** (210 mg, 0.81 mmol) in dry toluene (7 mL) and sodium bis(2-methoxyethoxy)aluminum hydride (1.2 mL, 70% solution in toluene, 4.05 mmol) and following the same procedure as reported for **4·HCl**, amine **18** as its hydrochloride was obtained as an off-white solid (154 mg, 71% yield). An analytical sample was obtained by crystallization from CH_2Cl_2/*n*-pentane, mp >300 °C (dec). IR (ATR) ν 2918, 2907, 2869, 2824, 2734, 2696, 2675, 2559, 2533, 2471, 1612, 1594, 1454, 1435, 1364, 1314, 1282, 1240, 1201, 1159, 1134, 1124, 1090, 1037, 1002, 979, 916 cm^{-1}. ^{1}H NMR (400 MHz, CD_3OD) δ 0.95 [d, J = 11.0 Hz, 4 H, 6(11,12,13)-H], 1.00 [s, 12 H, C7(8,9,10)-CH_3], 1.84 [d, J = 11.0 Hz, 4 H, 6(11,12,13)-H], 3.35 [s, 4 H, 2(4)-H]. ^{13}C NMR (100.6 MHz, CD_3OD) δ 15.7 [CH_3, C7(8,9,10)−CH3], 42.7 [CH_2, C6(11,12,13)], 46.7 [C, C7(8,9,10)], 48.8 [C1(5)], 52.7 [CH_2, C2(4)]. MS, m/z (%). Main ions: 231 [(M-HCl)$^{\bullet+}$, 100], 230 (58), 216 (25), 201 (14), 188 (36), 187 (31), 186 (60), 185 (19), 173 (20), 172 (17), 171 (65), 160 (14), 159 (23), 157 (16), 149 (26), 148 (94), 146 (47), 145 (34), 134 (20), 132 (23), 119 (40), 105 (21), 93 (17), 91 (36), 79 (18), 77 (21).

3-Amidino-7,8,9,10-tetramethyl-3-azapentacyclo-[7.2.1.1^{5,8}.0^{1,5}.0^{7,10}]tridecane Hydrochloride (19·HCl). From a suspension of **18·HCl** (187 mg, 0.70 mmol), Et_3N (0.15 mL, 1.05 mmol), and 1*H*-pyrazole-1-carboxamidine hydrochloride (123 mg, 0.84 mmol) in CH_3CN (7.5 mL) and following the same procedure as reported for **5·HCl**, guanidine **19·HCl** was obtained as a white solid (142 mg, 66% yield). An analytical sample was obtained by crystallization from *t*-butanol, mp >300 °C (dec). IR (ATR) ν 3178, 2854, 2914, 2868, 1771, 1704, 1697, 1651, 1555, 1455, 1374, 1347, 1312, 1269, 1173, 1154, 1052, 842, 739, 628 cm^{-1}. ^{1}H NMR (400

dx.doi.org/10.1021/jm5005804 | J. Med. Chem. 2014, 57, 5738−5747

MHz, CD_3OD) δ 0.95 [d, J = 11.0 Hz, 4 H, 6(11,12,13)-H], 1.00 [s, 12 H, C7(8,9,10)-CH_3], 1.87 [d, J = 11.0 Hz, 4 H, 6(11,12,13)-H], 3.59 [s, 4 H, 2(4)-H]. ^{13}C NMR (100.6 MHz, CD_3OD) δ 15.8 [CH_3, C7(8,9,10)-CH_3], 43.9 [CH_2, C6(11,12,13)], 46.6 [C, C7(8,9,10)], 49.5 [C1(5)], 54.6 [CH_2, C2(4)], 156.6 (C=NH). MS, m/z (%). Main ions: 273 [$(M - HCl)^{\bullet+}$, 85), 272 (18), 192 (25), 191 (100), 190 (76), 176 (15), 171 (65), 148 (15), 132 (12), 119 (11), 105 (10), 91 (17), 72 (26).

Molecular Modeling. The binding mode of Amt and compound **18** to the wt M2 channels and its V27A variant embedded on a model bilayer of 1-palmitoyl-2-oleoyl-*sn*-glycero-3-phosphocholine (POPC) was studied by molecular dynamics simulations. The M2 channel was modeled from the solid-state NMR structure obtained by Sharma et al.[28] (PDB entry 2L0J), and it was oriented using as template the solid state NMR structure with PDB entry 2KQT[23] as deposited in the Orientations of Proteins in Membranes (OPM) database.[29] The X-ray crystallographic structure 3LBW from the Protein Data Bank was used to model the position of water molecules inside the channel.[30] The initial position of the ligands was chosen to resemble the orientation of Amt in the 2KQT structure.

The CHARMM-GUI web server was used to build up the initial systems.[31−33] Briefly, the complex formed by the protein, the inner lumen water molecules, and the ligand was embedded on a 100 Å × 100 Å POPC bilayer patch. A 25 Å layer of TIP3P[34] water molecules was set up at both sides of the bilayer, and K^+ cations and Cl^- anions were added to achieve an ionic strength of 150 mM. The Parm99SB force field was used for the protein,[35] the ligands were parametrized using the gaff force field[36] in conjunction with RESP (HF/6-31G(d)) charges[37] as implemented in the Antechamber module of AMBER12 software package,[38] and the POPC molecules were parametrized according to the GAFF-lipid force field.[39] Joung and Cheatham parameters were used to model the counterions.[40] Each system comprised around 97000 atoms, including the protein ligand complex, 265 POPC molecules, around 58000 waters and 108 (51 K^+; 57 Cl^-) counterions in a simulation box of 100000 Å^3.

The geometry of the system was minimized in five cycles that combined 3500 steps of steepest descent algorithm followed by 4500 of conjugate gradient. Thermalization of the system was performed in 5 steps of 1 ns, where the temperature was gradually increased from 50 K to 298 K, while the protein, ligand, and POPC molecules were restrained with a force constant of 1 kcal mol^{-1} Å^{-2}. Prior to the production runs, a set of 20 ns simulations was performed to smoothly equilibrate the systems by gradually reducing the restraints first for the POPC molecules (restraints reduced by 0.1 kcal mol^{-1} Å^{-2} at each step) and then for the protein (restraints reduced by 0.2 kcal mol^{-1} Å^{-2} at each step). At this point, three different replicas were generated for each ligand−protein complex (accounting for a total of 12 different simulation systems).

We took advantage of the GPU-accelerated PMEMD module from AMBER12 software package for the production runs,[41] which consisted of 50 ns trajectories (accounting for a global simulation time of 600 ns) using SHAKE for bonds involving hydrogen atoms, a time step of 2 fs, periodic boundary conditions using anisotropic constant pressure and temperature (298 K; Langevin thermostat with a collision frequency of 3 ps^{-1}), particle mesh Ewald for long-range electrostatic interactions, and a cutoff of 10 Å for nonbonded interactions.

■ ASSOCIATED CONTENT

Supporting Information

Elemental analysis data of the new compounds; modeling studies. This material is available free of charge via the Internet at http://pubs.acs.org.

■ AUTHOR INFORMATION

Corresponding Author

*Phone: +34 934024533. Fax: +34 934035941. E-mail: svazquez@ub.edu.

Author Contributions

The manuscript was written through contributions of all authors. All authors have given approval to the final version of the manuscript.

Notes

The authors declare no competing financial interest.

■ ACKNOWLEDGMENTS

E.T., J.J.-J., and S.V. thank the Spanish Ministerio de Ciencia e Innovación (FPU and FIS fellowships to E.T. and J.J.-J., respectively; grant CTQ2011-22433 to S.V.; grant SAF2011-27642) and the Generalitat de Catalunya (FI fellowship to S.L.; grant 2014SGR1189) for financial support. M.R.-C. acknowledges a predoctoral grant from the Government of Andorra (ATCR2012/2013-00XX-AND). L.N. acknowledges financial support from the Geconcerteerde Onderzoeksacties (GOA/10/014), and the technical assistance from W. van Dam. F.J.L. is grateful to Icrea Academia for financial support. W.F.D. acknowledges support from GM56423 from the NIH. The Barcelona Supercomputer Center is acknowledged for computational facilities.

■ ABBREVIATIONS USED

Amt, amantadine; brsm, based on recovered starting material; BSA, bovine serum albumin; CPE, cytopathic effect; DMEM, Dulbecco's Modified Eagle Medium; DMPC, dimyristoylphosphatidylcholine; DPC, dodecylphosphocholine; MDCK, Madin−Darby canine kidney; MD, molecular dynamics; MTS, 3-(4,5-dimethylthiazol-2-yl)-5-(3-carboxymethoxyphenyl)-2-(4-sulfophenyl)-2*H*-tetrazolium; PBS, phosphate buffered saline; PDB, Protein Data Bank; qRT-PCR, quantitative real-time reverse transcription polymerase chain reaction; Rmt, rimantadine; ssNMR, solid state nuclear magnetic resonance; TEV, two-electrode voltage clamps; TM, transmembrane; wt, wild-type

■ REFERENCES

(1) Bright, R. A.; Shay, D. K.; Shu, B.; Cox, N. J.; Klimov, A. I. Adamantane resistance among influenza A viruses isolated early during the 2005−2006 influenza season in the United States. *JAMA, J. Am. Med. Assoc.* **2006**, *295*, 891−894.

(2) Fiore, A. E.; Shay, D. K.; Haber, P.; Iskander, J. K.; Uyeki, T. M.; Mootrey, G.; Bresee, J. S.; Cox, N. J. Prevention and control of influenza. Recommendations of the Advisory Committee on Immunization Practices (ACIP), 2007. *MMWR Recomm. Rep.* **2007**, *56*, 1−54.

(3) Lamb, R. A.; Zebedee, S. L.; Richardson, C. D. Influenza virus M2 protein is an integral membrane protein expressed on the infected-cell surface. *Cell* **1985**, *40*, 627−633.

(4) Hong, M.; DeGrado, W. F. Structural basis for proton conduction and inhibition by the influenza M2 protein. *Protein Sci.* **2012**, *21*, 1620−1633.

(5) Wang, J.; Qiu, J. X.; Soto, C. S.; DeGrado, W. F. Structural and dynamic mechanisms for the function and inhibition of the M2 proton cannel from influenza A virus. *Curr. Opin. Struct. Biol.* **2011**, *21*, 68−80.

(6) Balannik, V.; Carnevale, V.; Fiorin, G.; Levine, B. G.; Lamb, R. A.; Klein, M. L.; DeGrado, W. F.; Pinto, L. H. Functional studies and modeling of pore-lining residue mutants of the influenza a virus M2 ion channel. *Biochemistry* **2010**, *49*, 696−708.

(7) Furuse, Y.; Suzuki, A.; Oshitani, H. Large-scale sequence analysis of M gene of influenza A viruses from different species: mechanisms for emergence and spread of amantadine resistance. *Antimicrob. Agents Chemother.* **2009**, *53*, 4457−4463.

(8) Balannik, V.; Wang, J.; Ohigashi, Y.; Jing, X.; Magavern, E.; Lamb, R. A.; DeGrado, W. F.; Pinto, L. H. Design and pharmacological

characterization of inhibitors of amantadine-resistant mutants of the M2 ion channel of influenza A virus. *Biochemistry* **2009**, *48*, 11872−11882.
(9) Wang, J.; Ma, C.; Fiorin, G.; Carnevale, V.; Wang, T.; Hu, F.; Lamb, R. A.; Pinto, L. H.; Hong, M.; Klein, M. L.; DeGrado, W. F. Molecular dynamics simulation directed rational design of inhibitors targeting drug-resistant mutants of influenza A virus M2. *J. Am. Chem. Soc.* **2011**, *133*, 12834−12841.
(10) Wang, J.; Ma, C.; Wu, Y.; Lamb, R. A.; Pinto, L. H.; DeGrado, W. F. Exploring organosilane amines as potent inhibitors and structural probes of influenza A virus M2 proton channel. *J. Am. Chem. Soc.* **2011**, *133*, 13844−13847.
(11) Rey-Carrizo, M.; Torres, E.; Ma, C.; Barniol-Xicota, M.; Wang, J.; Wu, Y.; Naesens, L.; DeGrado, W. F.; Lamb, R. A.; Pinto, L. H.; Vázquez, S. 3-Azatetracyclo[5.2.1.1^{5,8}.0^{1,5}]undecane derivatives: from wild-type inhibitors of the M2 ion channel of influenza A virus to derivatives with potent activity against the V27A mutant. *J. Med. Chem.* **2013**, *56*, 9265−9274.
(12) Camps, P.; Duque, M. D.; Vázquez, S.; Naesens, L.; De Clercq, E.; Sureda, F. S.; López-Querol, M.; Camins, A.; Pallàs, M.; Prathalingam, S. R.; Kelly, J. M.; Romero, V.; Ivorra, D.; Cortés, D. Synthesis and pharmacological evaluation of several ring-contracted amantadine analogs. *Bioorg. Med. Chem.* **2008**, *16*, 9925−9936.
(13) Duque, M. D.; Ma, C.; Torres, E.; Wang, J.; Naesens, L.; Juárez-Jiménez, J.; Camps, P.; Luque, F. J.; DeGrado, W. F.; Lamb, R. A.; Pinto, L. H.; Vázquez, S. Exploring the size limit of templates for inhibitors of the M2 ion channel of influenza A virus. *J. Med. Chem.* **2011**, *54*, 2646−2657.
(14) Torres, E.; Vanderlinden, E.; Fernández, R.; Miquet, S.; Font-Bardia, M.; Naesens, L.; Vázquez, S. Synthesis and anti-influenza activity of 2,2-dialkylamantadines and related compounds. *ACS Med. Chem. Lett.* **2012**, *3*, 1065−1069.
(15) Torres, E.; Duque, M. D.; Vanderlinden, E.; Ma, C.; Pinto, L. H.; Camps, P.; Froeyen, M.; Vázquez, S.; Naesens, L. Role of the viral hemagglutinin in the anti-influenza virus activity of newly synthesized polycyclic amine compounds. *Antiviral Res.* **2013**, *99*, 281−291.
(16) Abou-Gharbia, M.; Patel, U. R.; Webb, M. B.; Moyer, J. A.; Andree, T. H.; Muth, E. A. Polycyclic aryl- and heteroarylpiperazinyl imides as 5-HT$_{1A}$ receptor ligands and potential anxiolytic agents: synthesis and structure−activity relationship studies. *J. Med. Chem.* **1988**, *31*, 1382−1392.
(17) Pielak, R. M.; Chou, J. J. Solution NMR structure of the V27A drug resistant mutant of influenza A M2 channel. *Biochem. Biophys. Res. Commun.* **2010**, *401*, 58−63.
(18) Gu, R.-X.; Liu, L. A.; Wang, Y.-H.; Xu, Q.; Wei, D. Q. Structural comparison of the wild-type and drug-resistant mutants of the influenza A M2 proton channel by molecular dynamics simulations. *J. Phys. Chem. B* **2013**, *117*, 6042−6051.
(19) Gu, R.-X.; Liu, L. A.; Wang, Y.-H.; Wei, D.-Q. Structural and energetic analysis of drug inhibition of the influenza A M2 proton channel. *Trends Pharmacol. Sci.* **2013**, *34*, 571−580.
(20) Mousseron-Canet, M.; Mousseron, M.; Brown, G. *Rev. Chim., Acad. Rep. Populaire Roumaine* **1962**, *7*, 1089−1101.
(21) Avila, W. B.; Silva, R. A. 3,4,8,9-Tetramethyltetracyclo-[4.4.0.0^{3,9}.0^{4,8}]decane-1,6-dioic anhydride. A Photosensitized π^2_s + π^2_s intramolecular cycloaddition. *Chem. Commun.* **1970**, 94−95.
(22) Wang, J.; Wu, Y.; Ma, C.; Fiorin, G.; Wang, J.; Pinto, L. H.; Lamb, R. A.; Klein, M. L.; DeGrado, W. F. Structure and Inhibition of the Drug-Resistant S31N Mutant of the M2 Ion Channel of Influenza A Virus. *Proc. Natl. Acad. Sci. U. S. A.* **2013**, *110*, 1315−1320.
(23) Cady, S. D.; Schmidt-Rohr, K.; Wang, J.; Soto, C. S.; DeGrado, W. F.; Hong, M. Structure of the amantadine binding site of influenza M2 proton channels in lipid bilayers. *Nature* **2010**, *463*, 689−692.
(24) Kolocouris, A.; Tzitzoglaki, C.; Johnson, F. B.; Zell, R.; Wright, A. K.; Cross, T. A.; Tietjen, I.; Fedida, D.; Busath, D. D. Aminoadamantanes with persistent in vitro efficacy against H1N1 (2009) influenza A. *J. Med. Chem.* **2014**, *57*, 4629−4639.
(25) Stevaert, A.; Dallocchio, R.; Dessì, A.; Pala, N.; Rogolino, D.; Sechi, M.; Naesens, L. Mutational analysis of the binding pockets of the diketo acid inhibitor L-742,001 in the influenza virus PA endonuclease. *J. Virol.* **2013**, *87*, 10524−10538.
(26) Ma, C.; Soto, C. S.; Ohigashi, Y.; Taylor, A.; Bournas, V.; Glawe, B.; Udo, M. K.; DeGrado, W. F.; Lamb, R. A.; Pinto, L. H. Identification of the pore-lining residues of the BM2 ion channel protein of influenza B virus. *J. Biol. Chem.* **2008**, *283*, 15921−15931.
(27) Vanderlinden, E.; Göktas, F.; Cesur, Z.; Froeyen, M.; Reed, M. L.; Russell, C. J.; Cesur, N.; Naesens, L. Novel inhibitors of influenza virus fusion: structure−activity relationship and interaction with the viral hemagglutinin. *J. Virol.* **2010**, *84*, 4277−4288.
(28) Sharma, M.; Yi, M.; Dong, H.; Qin, H.; Peterson, E.; Busath, D. D.; Zhou, H. X.; Cross, T. A. Insight into the mechanism of the influenza A proton channel from a structure in a lipid bilayer. *Science* **2010**, *330*, 509−512.
(29) Lomize, M. A.; Lomize, A. L.; Pogozheva, I. D.; Mosberg, H. I. OPM: Orientations of Proteins in Membranes Database. *Bioinformatics* **2006**, *22*, 623−625.
(30) Acharya, R.; Carnevale, V.; Florin, G.; Levine, B. G.; Polishchuk, A. L.; Balannik, V.; Samish, I.; Lamb, R. A.; Pinto, L. H.; DeGrado, W. F.; Klein, M. L. Structure and mechanism of proton transport through the transmembrane tetrameric M2 protein bundle of the influenza A virus. *Proc. Natl. Acad. Sci. U. S. A.* **2010**, *107*, 15075−15080.
(31) Jo, S.; Kim, T.; Iyer, V. G.; Im, W. CHARMM-GUI: A Web-based Graphical User Interface for CHARMM. *J. Comput. Chem.* **2008**, *29*, 1859−1865.
(32) Jo, S.; Lim, J. B.; Klauda, J. B.; Im, W. CHARMM-GUI Membrane Builder for Mixed Bilayers and Its Application to Yeast Membranes. *Biophys. J.* **2009**, *97*, 50−58.
(33) Jo, S.; Kim, T.; Im, W. Automated Builder and Database of Protein/Membrane Complexes for Molecular Dynamics Simulations. *PLoS One* **2007**, *2*, e880.
(34) Jorgensen, W. L.; Chandrasekhar, J.; Madura, J. D.; Impey, R. W.; Klein, M. L. Comparison of simple potential functions for simulating liquid water. *J. Chem. Phys.* **1983**, *79*, 926−935.
(35) Hornak, V.; Abel, R.; Okur, A.; Strockbine, B.; Roitberg, A.; Simmerling, C. Comparison of multiple Amber force fields and development of improved protein backbone parameters. *Proteins* **2006**, *65*, 712−725.
(36) Wang, J. M.; Wolf, R. M.; Caldwell, J. W.; Kollman, P. A.; Case, D. A. Development and testing of a general amber force field. *J. Comput. Chem.* **2005**, *26*, 1157−1174.
(37) Bayly, C. I.; Cieplak, P.; Cornell, W.; Kollman, P. A. A well-behaved electrostatic potential based method using charge restraints for deriving atomic charges: the RESP model. *J. Phys. Chem.* **1993**, *97*, 10269−10280.
(38) Case, D. A.; Darden, T. A.; Cheatham, T. E., III; Simmerling, C. L.; Wang, J.; Duke, R. E.; Luo, R.; Walker, R. C.; Zhang, W.; Merz, K. M.; Roberts, B.; Hayik, S.; Roitberg, A.; Seabra, G.; Swails, J.; Goetz, A. W.; Kolossváry, I.; Wong, K. F.; Paesani, F.; Vanicek, J.; Wolf, R. M.; Liu, J.; Wu, X.; Brozell, S. R.; Steinbrecher, T.; Gohlke, H.; Cai, Q.; Ye, X.; Wang, J.; Hsieh, M.-J.; Cui, G.; Roe, D. R.; Mathews, D. H.; Seetin, M. G.; Salomon- Ferrer, R.; Sagui, C.; Babin, V.; Luchko, T.; Gusarov, S.; Kovalenko, A.; Kollman, P. A. *AMBER 12*; University of California: San Francisco, 2012.
(39) Callum, J. D.; Rosso, L.; Betz, R. M.; Walker, R. C.; Gould, I. R. GAFFlipid: a General Amber Force Field for the accurate molecular dynamics simulation of phospholipid. *Soft Matter* **2012**, *8*, 9617−9627.
(40) Joung, I. S.; Cheatham, T. E. Molecular dynamics simulations of the dynamic and energetic properties of alkali and halide ions using wáter-model-specific ion parameters. *J. Phys. Chem. B* **2009**, *113*, 13279−13290.
(41) Salomon-Ferrer, R.; Goetz, A. W.; Poole, D.; Le Grand, S.; Walker, R. C. Routine microsecond molecular dynamics simulations with AMBER on GPUs. 2. Explicit solvent Particle Mesh Ewald. *J. Chem. Theory Comput.* **2013**, *9*, 3878−3888.

Supporting Information

Easily Accessible Polycyclic Amines that Inhibit the Wild-Type and Amantadine-Resistant Mutants of the M2 Channel of Influenza A Virus

Matias Rey-Carrizo,[ǂ] Marta Barniol-Xicota,[ǂ] Chunlong Ma,[#,§] Marta Frigolé-Vivas,[ǂ] Eva Torres,[ǂ] Lieve Naesens,[⊥] Salomé Llabrés,[Δ] Jordi Juárez-Jiménez,[Δ] Francisco J. Luque,[Δ] William F. DeGrado,[†] Robert A. Lamb,[§,∫] Lawrence H. Pinto,[#] Santiago Vázquez[ǂ]*

Table of contents

Elemental analysis data:

Compound	**Molecular Formula**	**Calculated**				**Found**			
		C	H	N	X	C	H	N	X
4·HCl	$C_{11}H_{15}N$·HCl	66.83	8.16	7.08	19.93	66.55	8.13	7.00	17.81
6·HCl·0.33H_2O	$C_{11}H_{17}N$·HCl·0.33H_2O	64.24	9.14	6.81	17.24	64.43	8.96	6.54	17.55
8·2.15HCl·H_2O	$C_{16}H_{24}N_2$·2.15HCl·H_2O	56.39	8.33	8.22	22.37	56.39	8.33	8.42	22.37
9·2HCl·0.5H_2O	$C_{16}H_{26}N_2$·2HCl·0.5H_2O	58.53	8.90	8.53	21.60	58.57	8.67	8.48	21.53
5·HCl·0.25H_2O	$C_{12}H_{17}N_3$·HCl·0.25H_2O	59.01	7.63	17.20	14.51	59.03	7.62	17.45	14.57
7·HCl·0.33H_2O	$C_{12}H_{19}N_3$·HCl·0.33H_2O	58.17	8.41	16.96	14.31	58.17	8.23	17.09	14.58
11·HCl·0.33H_2O	$C_{12}H_{15}N$·HCl·0.33H_2O	66.83	7.79	6.49	16.44	66.65	7.82	6.51	16.10
12·HCl·0.5H_2O	$C_{12}H_{19}N$·HCl·0.5H_2O	64.70	9.50	6.29	15.92	64.85	9.72	6.27	15.78
13·1.1HCl	$C_{13}H_{17}N_3$·1.1HCl	61.14	7.14	16.45	nd	61.40	7.48	16.47	nd
14·HCl	$C_{13}H_{21}N_3$·HCl	61.04	8.67	16.43	13.86	60.99	8.96	16.15	13.62
18·HCl·0.6H_2O	$C_{16}H_{25}N$·HCl·0.6 H_2O	68.70	9.84	5.01	nd	68.98	9.70	4.79	nd
19·1.1HCl·0.6H_2O	$C_{17}H_{27}N_3$·1.1HCl·0.6H_2O	62.75	9.11	12.91	11.98	62.47	8.84	13.06	11.72

Figure S1. Selected geometrical parameters (distances in Å; tilt angle in degrees) for the binding of compound **18** to the wt M2 channel along the trajectories sampled for the three 50 ns MD replicas.
Left: Distance from the amine N to the His37 plane and tilt angle (defined as the angle between amine N, COM of ligand, and COM of His37 Cα atoms). Right: distances from the COM of ligand to the plane formed by tetrads of residues along the pore.

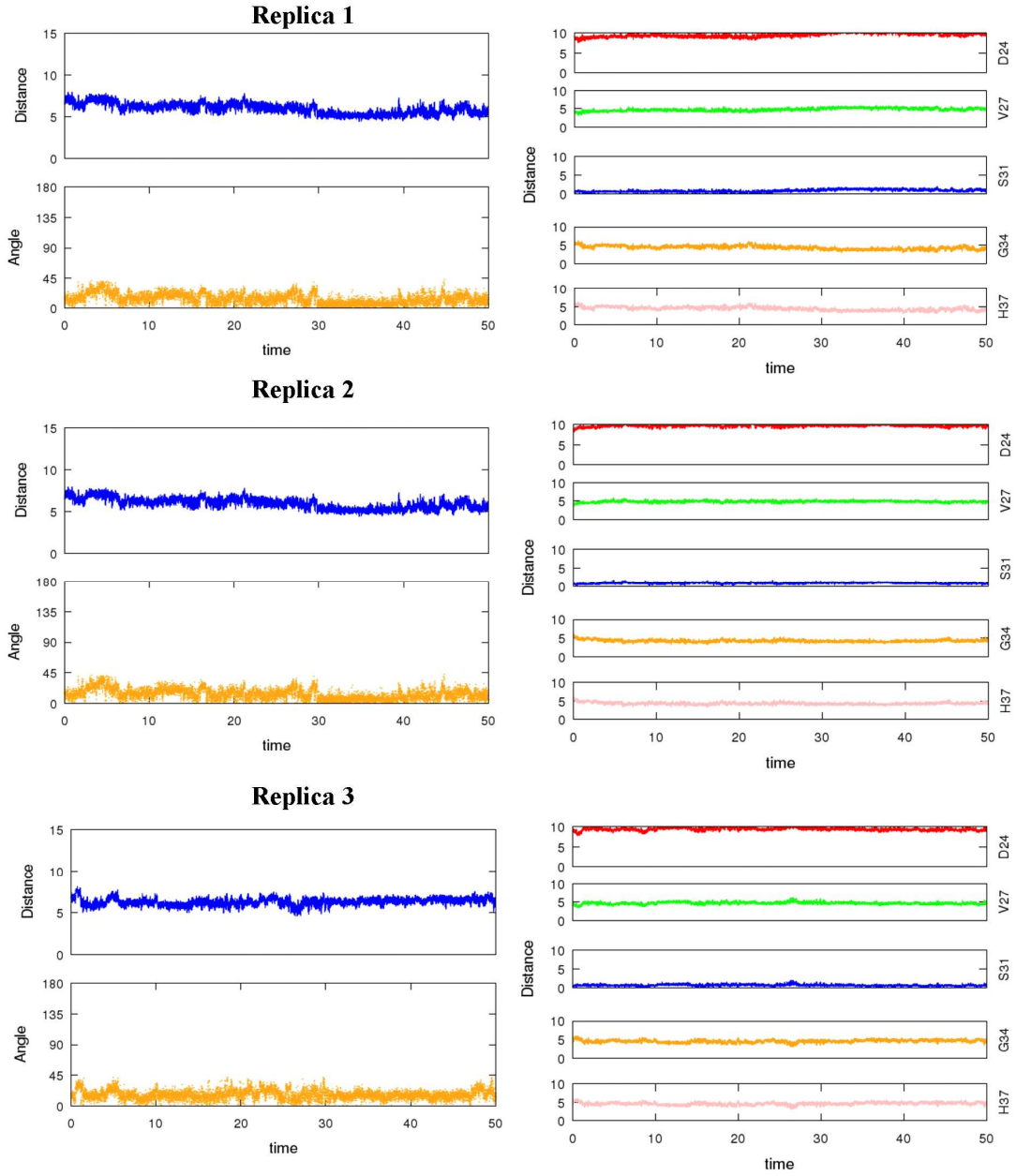

Replicas 1-3 show a stable arrangement of compound **18** in the pore, which is characterized by a distance from the amine nitrogen to the plane formed by the His37 residues close to 6.1 Å, and a tilt angle close to 16 degrees. Finally, the COM of the ligand is located close to the plane defined by the tetrad of Ser31 residues.

Figure S2. Selected geometrical parameters (distances in Å; tilt angle in degrees) for the binding of Amt to the wt M2 channel along the trajectories sampled for the three 50 ns MD replicas.
Left: Distance from the amine N to the His37 plane and tilt angle (defined as the angle between amine N, COM of ligand, and COM of His37 Cα atoms). Right: distances from the COM of ligand to the plane formed by tetrads of residues along the pore.

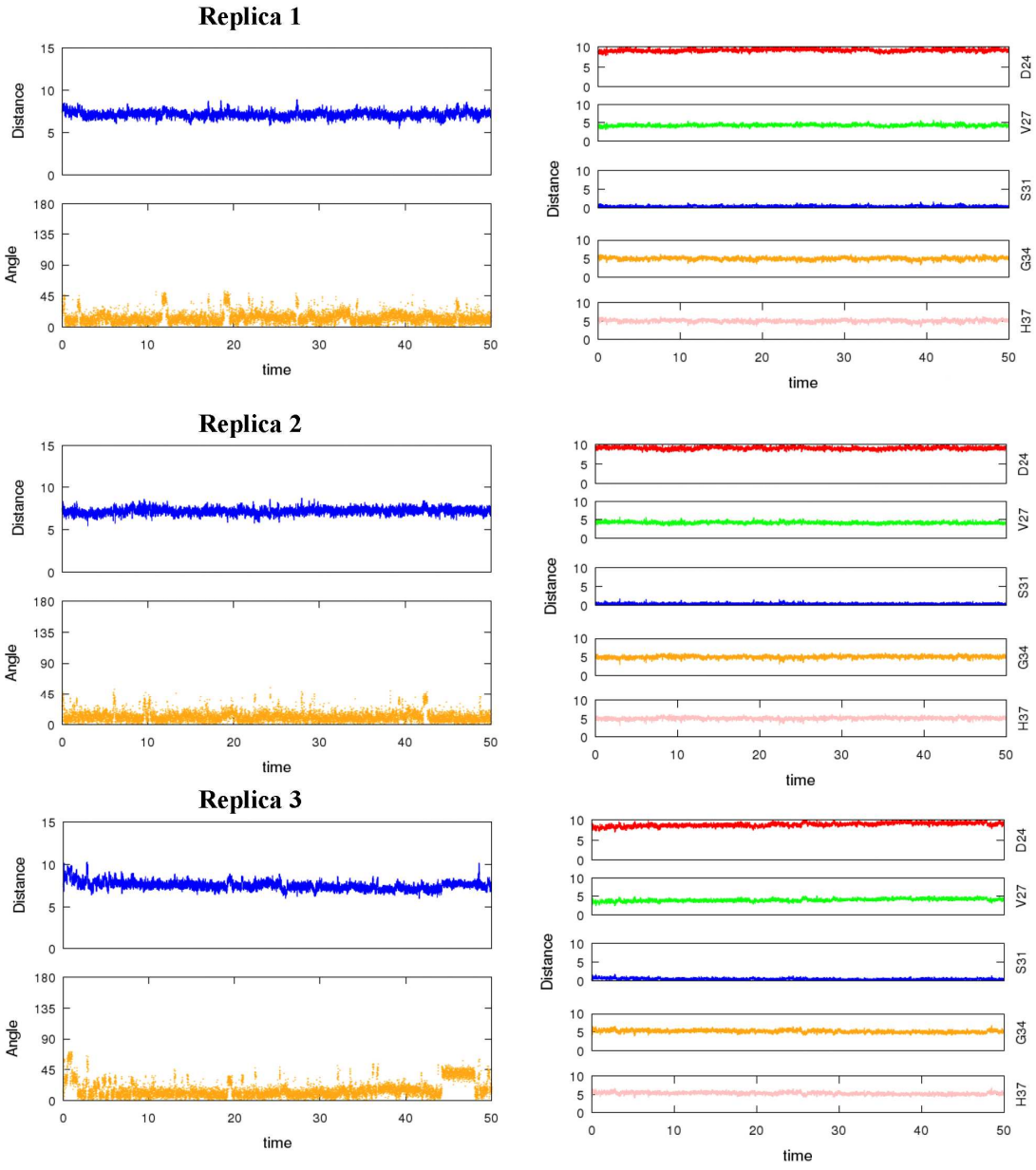

Replicas 1-3 show a stable arrangement of Amt in the pore, which is characterized by a distance from the amine nitrogen to the plane formed by the His37 residues close to 6.1 Å, and a tilt angle close to 16 degrees. Finally, the COM of the ligand is located close to the plane defined by the tetrad of Ser31 residues.

Figure S3. Selected geometrical parameters (distances in Å; tilt angle in degrees) for the binding of compound **18** to the V27A variant of the M2 channel along the trajectories sampled for the three 50 ns MD replicas.
Left: Distance from the amine N to the His37 plane and tilt angle (defined as the angle between amine N, COM of ligand, and COM of His37 Cα atoms). Right: distances from the COM of ligand to the plane formed by tetrads of residues along the pore.

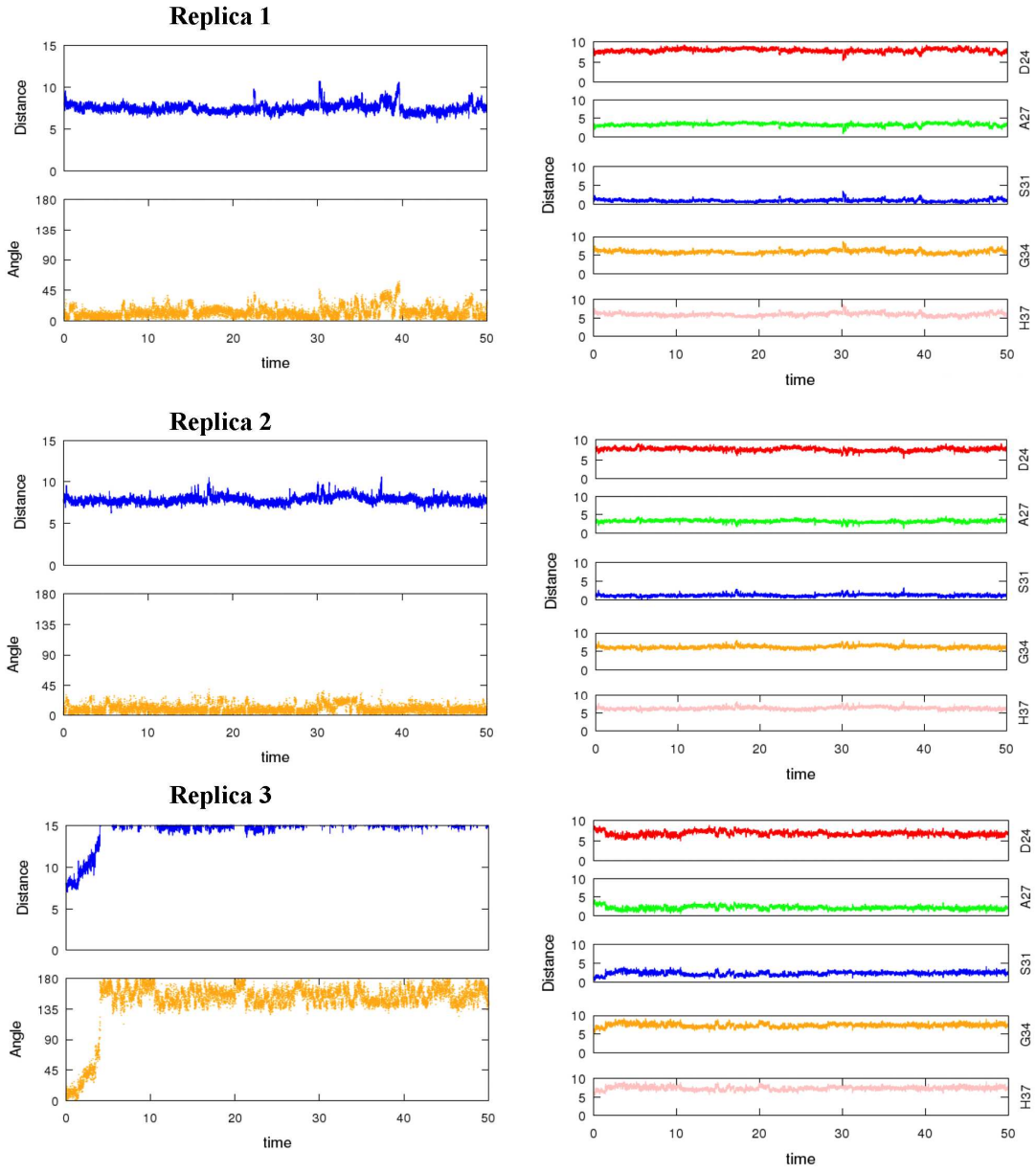

Replicas 1 and 2 exhibit a common arrangement of compound **18** in the pore, which is characterized by a distance from the amine nitrogen to the plane formed by the His37 residues close to 7.5 Å, and a tilt angle close to 12 degrees. Moreover, the COM of the ligand is shifted 1.1 Å from the plane formed by the tetrad of Ser31 residues.
Replica 3 differs due to the rearrangement of the inhibitor in the pore, as the amine nitrogen is now pointing toward the entrance to the channel. Thus, the distance from the amine nitrogen to the plane formed by the His37 residues is close to 15 Å, and the tilt

angle is close to 145 degrees. Finally, the COM of the ligand is further displaced toward the mouth of the channel, as the distance of the ligand COM to the plane formed by the tetrad of Ser31 residues is 2.3 Å.

Figure S4. Selected geometrical parameters (distances in Å; tilt angle in degrees) for the binding of Amt to the V27A variant of the M2 channel along the trajectories sampled for the three 50 ns MD replicas.
Left: Distance from the amine N to the His37 plane and tilt angle (defined as the angle between amine N, COM of ligand, and COM of His37 Cα atoms). Right: distances from the COM of ligand to the plane formed by tetrads of residues along the pore.

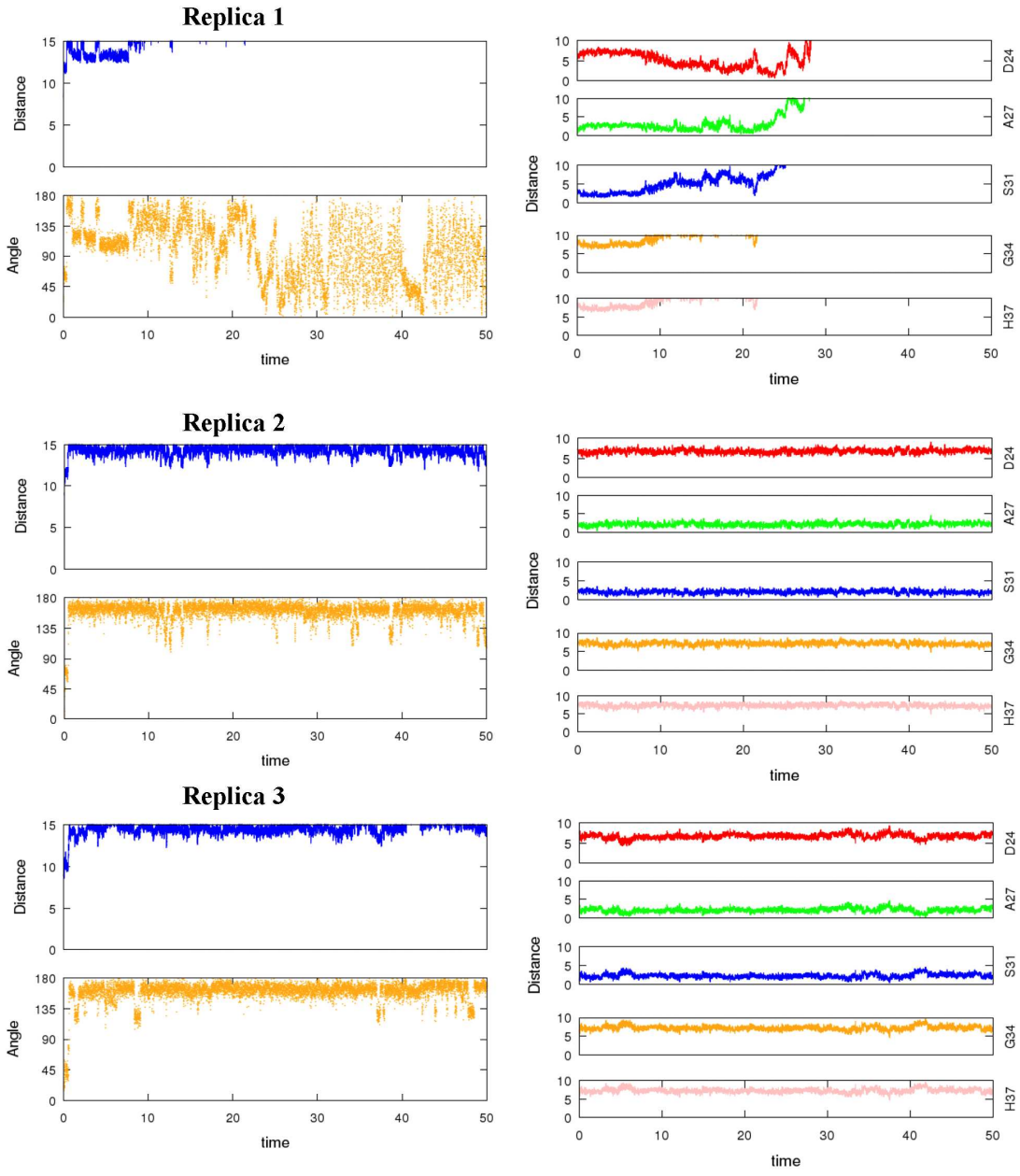

Replicas 2 and 3 exhibit a common arrangement of Amt in the pore, which is characterized by a distance from the amine nitrogen to the plane formed by the His37 residues close to 14.5 Å, and a tilt angle close to 159 degrees. Therefore, the arrangement of Amt is opposite to that found in the wt M2 channel. Furthermore, the COM of the ligand is located between the planes defined by tetrads of Val27 and Ser31 residues, as the distance to these planes is 2.2 and 2.1 Å, respectively.

Replica 1 exhibits a different behaviour, because the inhibitor was released from the pore to the bulk solution after the first 10 ns of the trajectory

Figure S5. Cross-diagonals between transmembrane helices in the M2 channel.

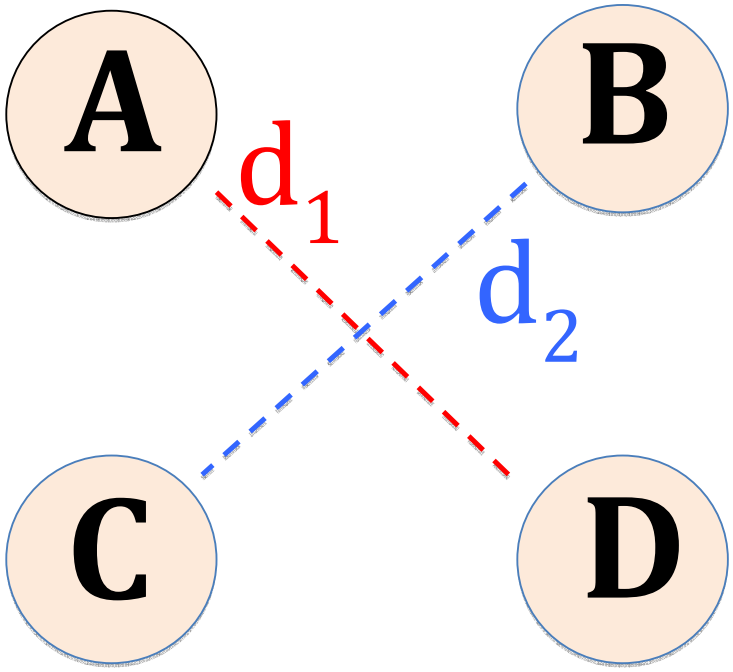

Figure S6. (A) Superposition of the NMR-derived structure obtained for the complex between the S31N channel and the 5-thienyl isoxazole derivative (PDB entry 2LY0; orange) and a representative snapshot of the complex between wt M2 channel and compound **18** (green). (B) Representation of the relative alignment of the 5-thienyl isoxazole derivative and compound 18 bound to S31N and wt channels, respectively.

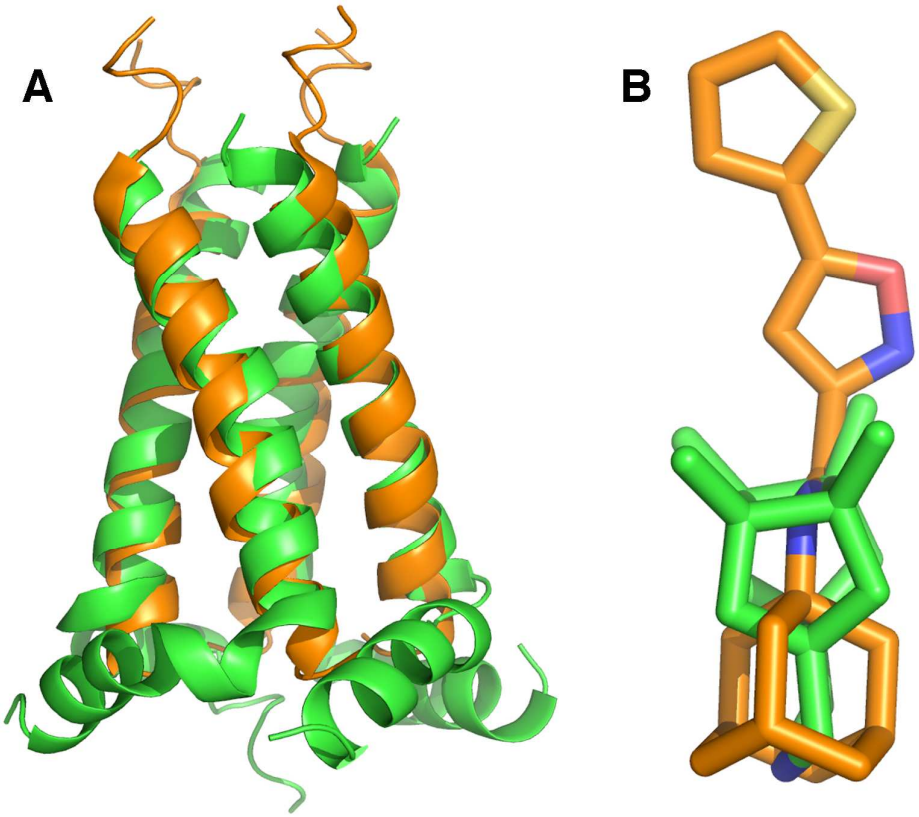

Table S1. Root-mean square deviations (Å) between the backbone atoms of the transmembrane helices of the wt M2 channel and its V27A variant in both apo and holo forms. Values determined for the averaged structure sampled in the last 10 ns of the trajectories.

Wild type		Holo(Amt)			Holo(**18**)		
		1	*2*	*3*	*1*	*2*	*3*
Apo		1.4	1.7	1.3	1.5	1.6	1.3
Holo(Amt)	*1*		1.2	1.0	1.2	1.6	1.2
	2			1.4	1.1	1.6	1.5
	3				1.2	1.4	1.2
Holo(**18**)	*1*					1.2	1.2
	2						1.4

V27A		Holo(Amt)			Holo(**18**)		
		1	*2*	*3*	*1*	*2*	*3*
Apo		1.5	1.3	1.8	1.5	1.3	1.4
Holo(Amt)	*1*		1.8	1.3	1.7	1.7	1.8
	2			1.8	1.2	1.2	1.4
	3				1.5	1.7	1.9
Holo(**18**)	*1*					1.3	1.4
	2						1.4

PART B

Dimerization of pyramidalized alkenes to a hydrocarbon featuring four cyclohexane rings in boat conformations

4B.1 Rationale and previous work

As previously mentioned (see Chapter 4-Part A, section 4A.3) this project arouse from our anti-influenza A research. The structural uniqueness of the prepared antivirals containing the scaffold **XVIII**, presented to us as an appealing scaffold to further investigate. The polycyclic core of this scaffold (in blue) was featuring an interesting combination of 2 cyclohexane rings in a boat conformation, 2 cyclopentane rings in envelope conformation and 1 planar cyclobutane ring.

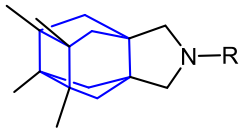

XVIII

wt IC_{50}= 18.0 μM
V27A IC_{50}= 0.7 μM
L26F IC_{50}= 8.6 μM

Figure 60. 7,8,9,10-tetramethyl-3-azapentacyclo[7.2.1.1^{5,8}.0^{1,5}.0^{7,10}]tridecane, triple inhibitor of the wt, V27A and L26F mutant channels of influenza A[1].

Taking into account the expertise of our group in polycyclic chemistry, specifically in highly pyramidalized alkenes[2,3], we could not miss the opportunity to further investigate this aesthetically pleasant polycyclic structure. For this, taking the opposite way of our usual route, we moved from a bioactive compound to the preparation of a compound of pure theoretical interest, the highly pyramidalized alkene **XII**. Besides this, the product of dimerization, **XIII**, featuring three planar cyclobutane rings, four cyclopentane rings and four cyclohexane rings in *frozen* boat conformation, caught our attention as we envisaged its cyclohexane methylenic hydrogen atoms, would display a H-H flagpole interaction[4]. This type of interactions are extremely rare to find, as sterically disfavoured, and are almost unreported in the literature[5,6,7].

---

[1] Rey-Carrizo, M., Torres, E., Ma, C., Barniol-Xicota, M., Wang, J., Wu, Y., Naesens, L., DeGrado, W.F., Lamb, R. A., Pinto, L. H. & S. Vázquez. 3-Azatetracyclo [5.2.1.15,8.01,5]undecane derivatives: from wild-type inhibitors of the M2 ion channel of influenza A virus to derivatives with potent activity against the V27A mutant. *J. Med. Chem*., **2013**, 56, 9265–9274.

[2] Camps, P., Muñoz, M. R. & Vázquez, S. Generation and trapping of tricyclo[3.3.0.0 3,7]oct-1(5)-ene derivatives containing carbonyl functionalities. *Tetrahedron* **2006**, 62, 7645.

[3] Camps, P., Pérez, F., Vázquez, S., Font-Bardia, M. & Solans, X. Synthesis, Chemical Trapping, and Dimerization of 3,7-Dimethyltricyclo[3.3.0.03, 7]oct-1(5)-ene: [2 + 2] Retrocycloaddition of the Cyclobutane Dimer. *Angew. Chem. Int. Ed. Engl*. **1995**, 34, 912.

[4] Sauers, R. R. Cyclohexane: Boat Form Revisited. *Journal of Chemical Education*. **2000**, 77(3), 332.

[5] Biethan, U., Gizycki, U. V. & Musso, H. Asterane. *Tetrahedron Lett*. **1965**, 6, 1477.

[6] Hamon, D. P. G. & Taylor, G. F. A synthesis of tetracyclo [5.3.1.12,6^{0}4,9] dodecane (iceane). *Tetrahedron Lett*. **1974**, 15, 155.

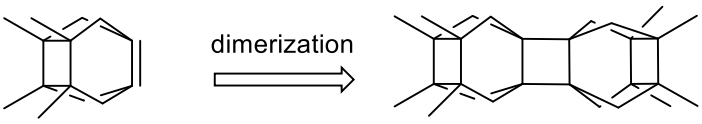

XII **XIII**

Chart 3. Highly pyramidalized alkene **XII** envisaged. The alkene **XII** was theoretically predicted to be synthetically accessible: (B3LYP/6-31G) pyramidalization angle Φ = 47.5º, 1.360 Å C-C double bond length of (e.g. 1.333 Å for ethylene) and HOMO-LUMO gap of 5.64 eV (e.g. 8.0 eV for ethylene).

For a deeper understanding of the project reported herein, it is worth clarifying that highly pyramidalized alkenes[8] are defined as olefins, which double-bond-forming atoms (either one or both) are out of the plane defined by the three atoms adjacent to it. Hence, this double bond presents a distorted geometry that triggers the 2s orbital into the π bond. As a consequence of this mixed hybridization the π* molecular orbital has a lowered antibonding overlap, hence the LUMO becomes less energetic and more stable. Contrarily, the π orbital energy remains unaffected, as the increased 2s character and the reduced overlap effects counteract.

The final outcome is the reduction of the HOMO-LUMO gap responsible for the unusual high reactivity[9,10] of the so called highly pyramidalized alkenes and their characteristic spectroscopic features, consisting in a deshielding in the ^{13}C NMR of the C-C double bond to 142 ppm (typical alkene values 150-170 ppm) and an increase of their UV absorption maximum towards longer wavelengths[11].

Of note, the main parameter that defines this double bond distortion is the pyramidalization angle Φ[12], which measures the angle between the plane containing one of the doubly bonded carbon atoms and the two substituents attached to it, as well as the extension of the double bond.

$$cos\varphi = -\frac{\cos\ (<RCC)}{\cos(\frac{1}{2}<RCR)}$$

Formula 1. Pyramidalization angle determination.

[7] Cupas, C. A. & Hodakowski, L. Iceane. *J. Am. Chem. Soc*. **1974**, 96, 4668.
[8] Borden, W. T. Pyramidalized Alkenes. *Chem. Rev.* **1989**, 89, 1095–1109.
[9] Ioannou, S., Krassos, H. & Nicolaides, A. V. Synthesis of a novel diene from a cyclobutane precursor: an entry to 2,9-disubstituted [2]diadamantanes. *Tetrahedron*. **2013**, 69, 8064.
[10] Vázquez, S. & Camps, P. Chemistry of Pyramidalized Alkenes. *Tetrahedron* **2005**, 61, 5147.
[11] Vázquez, S. GIAO-DFT study of 13C NMR chemical shifts of highly pyramidalized alkenes. *J. Chem. Soc. Perkin Trans.* **2002**, *2*, 2100.
[12] Volland, W. V., Davidson, E. R. & Borden, W. T. Effect of carbon atom pyramidalization on the bonding in ethylene. *J. Am. Chem. Soc*. **1979**, 101, 533.

As a final clarification, the cyclohexanes in boat conformation are almost free of angle strain but in contrast have torsional strain, associated with eclipsed bonds at four of the C atoms. The flagpole interaction is defined as the destabilizing steric interaction of the H atoms inside the bow and the stern, in the aforementioned conformation.

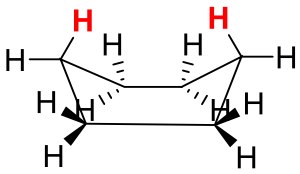

Figure 61. Cyclohexane in boat conformation, the flagpole hydrogens are shown in red.

4B.2 Theoretical discussion

In the present Thesis the preparation of **XII,** the obtainment of its dimer **XIII** and the crystal structures of **48**, **XI**, **51** and **XIII**, were carried out, as shown in Scheme 10.

The synthetic route, as well as the results, are reported in the journal article that follows. In short, the synthesis starts with the preparation of the known anhydride **47**[13] through two thermal Diels-Alder [4+2] cycloadditions of acetylenedicarboxylic acid and 1,3-butadiene. After irradiation with a 400 W mercury lamp, a third cycloaddition, this time a photochemical [2+2][14], furnished the anhydride **48**. A basic hydrolysis gave the diacid **49**, from which the key iododecarboxylation reaction, using 1,3-diiodo-5,5-dimethylhydantoin (DIH)[15] as initiator and source of iodine, yielded the pyramidalized alkene iodinated precursor **XI**.

[13] Torres, E., Leiva, R., Gazzarrini, S., Rey-Carrizo, M., Frigole, M., Moroni, A., Naesens, L. & Vázquez, S. Azapropellanes with Anti-Influenza A Virus Activity. *ACS Med. Chem. Lett*. **2014**, 5, 831–836.
[14] Ashkenazi, P. & Ginsburg, D. Propellanes—XLVIII:Intramolecular [2+2] photocycloadditions of various [4.4.3]propella-3,8-dienes. *Tetrahedron.* **1979**, 35, 1317.
[15] Virgil, S. C. & Wenderski, T. A. 1,3-Diiodo-5,5-dimethylhydantoin. *e-EROS Encyclopedia of Reagents for Organic Synthesis*. **2014** 1–3.

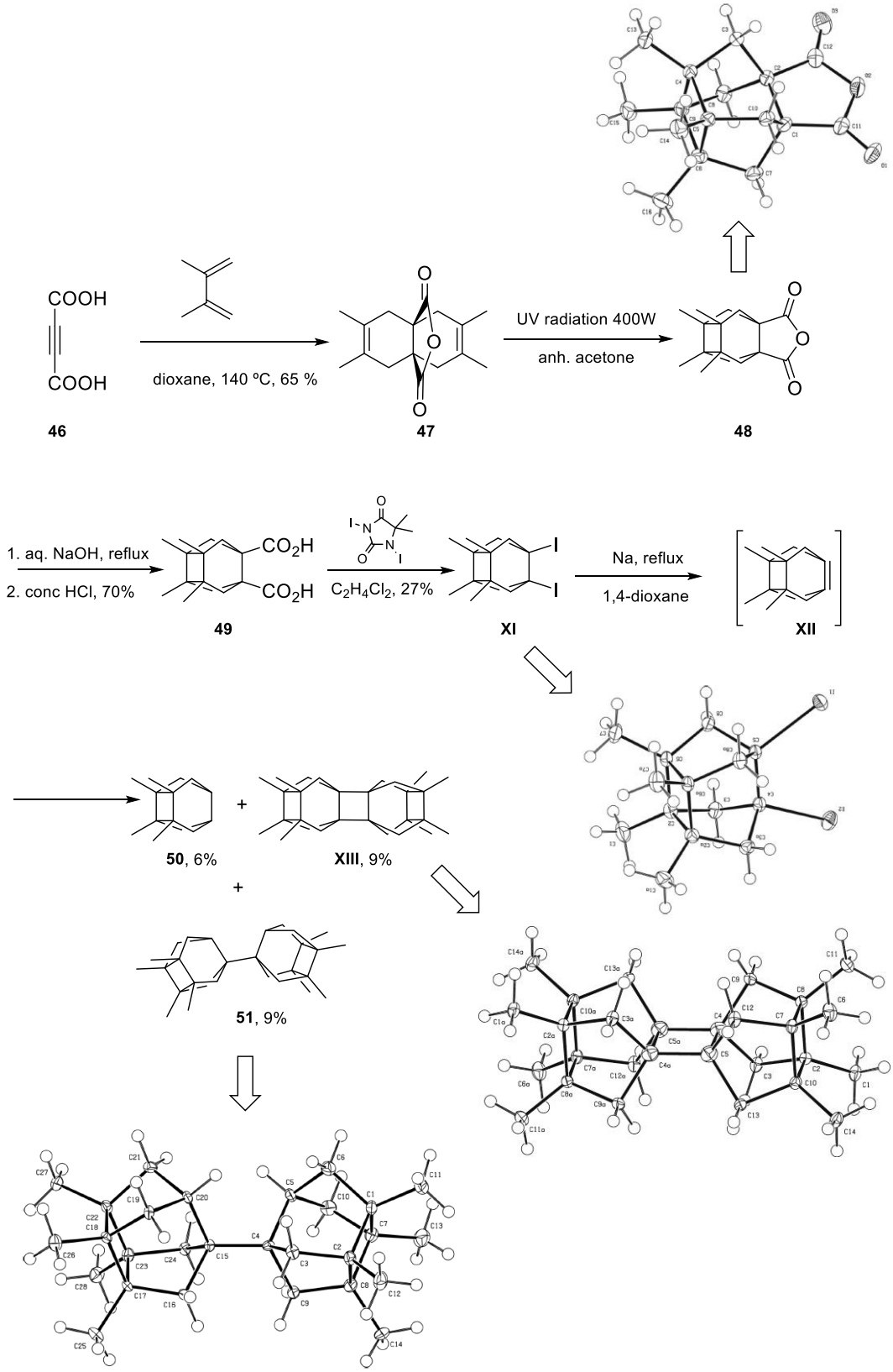

Scheme 10. Synthetic route for the preparation of the dimer **XIII.** The crystal structures solved of the compounds involved in this route are shown.

Of note, the photochemical cycloaddition and iododecarboxylation step, previously studied in the thesis of Dr. Matías Rey-Carrizo, were highly optimized in this thesis. The prior cycloaddition was carried out with a 125 W mercury lamp; after tuning up the potency to 400 W, the yield increased in a 50%, allowing the obtainment of **48** in a multigram scale. In the case of the iodination the use of DIH instead of the previous lead(IV) tetracetate[16] and iodine mixture, overcame the problems encountered in the previous procedure, which furnished mixtures of the diiodine product enriched in unreacted starting material. The mechanism through this optimized iododecarboxylation occurs is depicted in scheme 11.

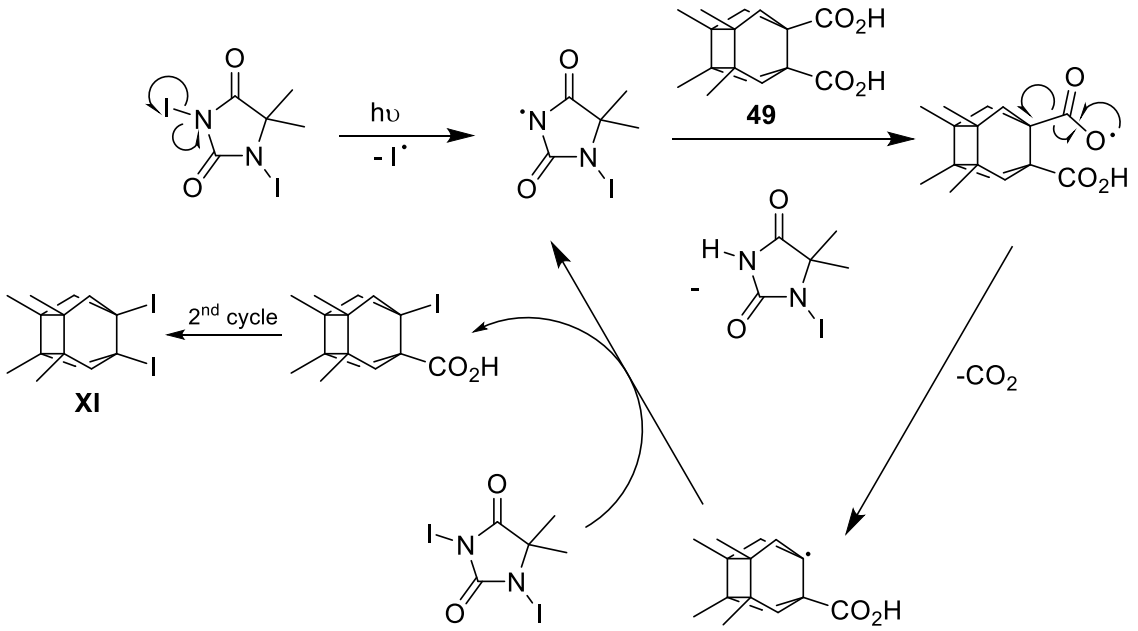

Scheme 11. Radical chain reaction of **49** with 1,3-diiodo-5,5-dimethylhydantoin (DIH).

After the photochemical homolytic cleavage of the N-I bond of the 1,3-diiodo-5,5-dimethylhydantoin, the radical-chain reaction starts when this generated DIH radical abstracts one hydrogen atom from the diacid. The formed acyloxy radical undergoes a spontaneous decarboxylation, which furnishes an intermediate polycyclic derivative bearing a radical on the sp^3 carbon atom that will be iodinated by another molecule of DIH, completing the cycle.

Taking into account the expertise of our group in the generation of highly pyramidalized alkenes using molten sodium as a non-nucleophilic reagent[3], the diiodinated intermediate **XI** was treated under these conditions. Prior single electron transfer from sodium to the starting diiodide and subsequent loss of an iodide by the radical-anion intermediate, the

[16] Krassowska-Řwiebocka, B., Luliński, P. & Skulski, L. Aromatic Iodination of Activated Arenes and Heterocycles with Lead Tetraacetate as the Oxidant. *Synthesis.* **1995**, 926.

alkyl radical was formed. This species followed two different paths. The first consisted in the reduction to the diradical, which collapsed to give the desired pyramidalized alkene **XII** and readily dimerized via a [2+2] cycloaddition to the dimer **XIII**. Alternatively it abstracted one hydrogen atom from the reaction media to finally undergo a reduction to the tertiary alkyl radical. This radical intermediate gave the reduction product **50**, via further hydrogen abstraction, and the alternative dihydrodimer **51**, prior dimerization. (Scheme 12)

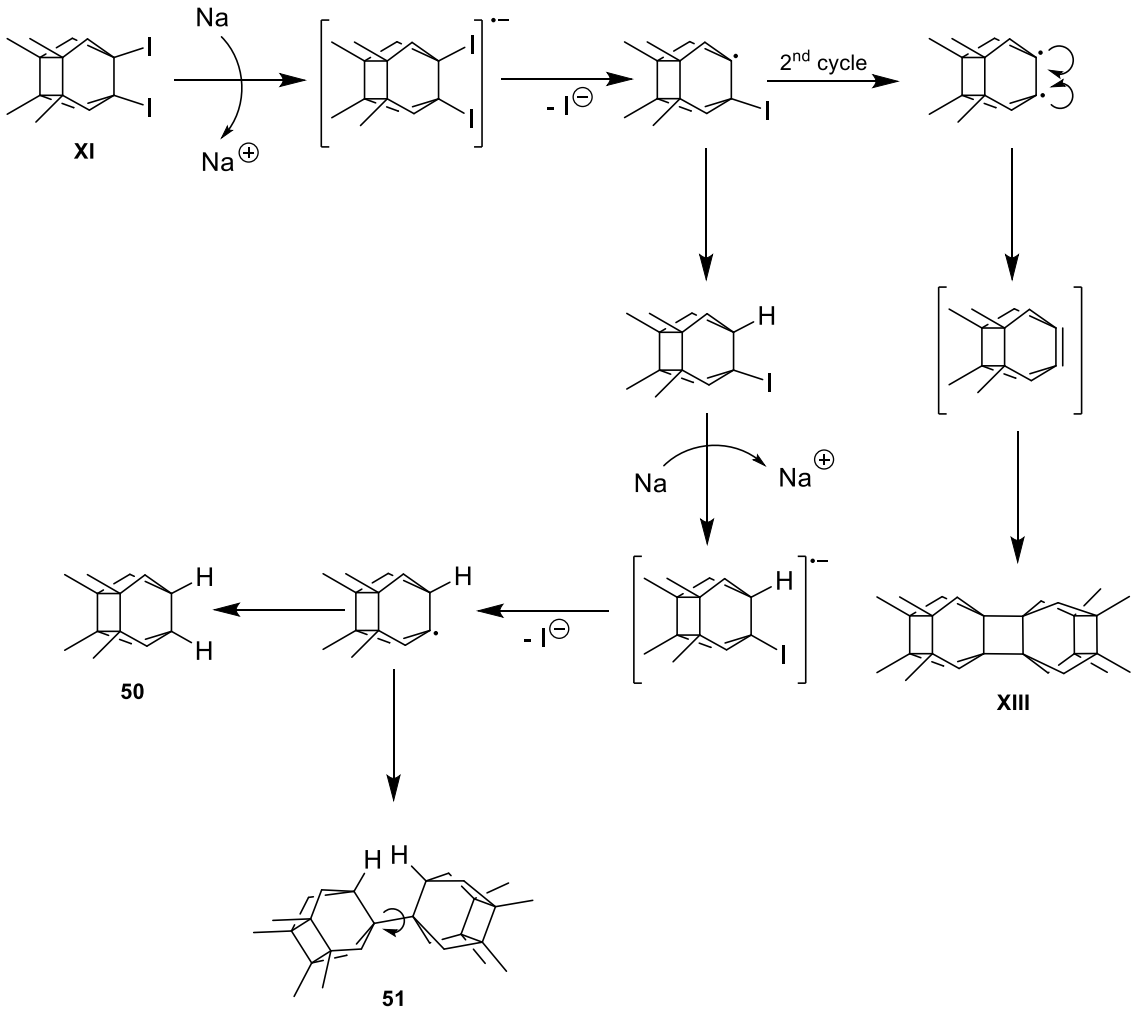

Scheme 12. Diiodoradical **XI** alternative paths of products formation.

Polycycles

DOI: 10.1002/anie.201403985

Dimerization of Pyramidalized 3,4,8,9-Tetramethyltetracyclo [4.4.0.0^{3,9}.0^{4,8}]dec-1(6)-ene to a Hydrocarbon Featuring Four Cyclohexane Rings in Boat Conformations**

*Matias Rey-Carrizo, Marta Barniol-Xicota, Mercè Font-Bardia, and Santiago Vázquez**

Dedicated to Professor Pelayo Camps

Abstract: *The synthesis, chemical trapping, and dimerization of a highly pyramidalized alkene is reported. Its dimer is a unique nonacycle featuring three planar cyclobutane rings, four cyclopentane rings, and four cyclohexane rings in boat conformations. The X-ray diffraction analysis showed a H–H distance between the flagpole hydrogen atoms of 1.999 Å and a separation of 2.619 Å between the two flagpole carbon atoms. The three cyclobutane rings of the dimer were thermally stable.*

Pyramidalized alkenes are compounds containing carbon–carbon double bonds in which one or both of the sp^2-carbon atoms do not lie in the same plane as the attached atoms.[1] We have reported the generation, trapping, and dimerization of several highly pyramidalized alkenes and the first cross-coupling of two different pyramidalized alkenes leading to a tetrasecododecahedradiene derivative.[1c,2,3] Herein, we report the generation of **4** (Scheme 1), a novel highly pyramidalized alkene, its trapping with 1,3-diphenylisobenzofuran, and its dimerization to a unique polycyclic hydrocarbon, **7**, which features three planar cyclobutane rings, four cyclopentane rings, and four cyclohexane rings in a boat conformations.

Theoretical calculations using B3LYP/6-31G(d) showed us that the alkene **4** should be an accessible target.[4] Its calculated pyramidalization angle ($\Phi = 47.5°$),[5] carbon–carbon double bond length (1.360 Å), heat of hydrogenation

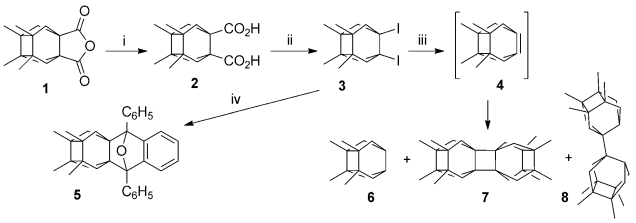

Scheme 1. Synthesis, trapping, and dimerization of alkene **4**. a) aq. NaOH, reflux, then conc HCl, 70% yield; b) 1,3-diiodo-5,5-dimethylhydantoin, 1,2-dichloroethane, 27% yield; c) Na, 1,4-dioxane, reflux, 4 h; d) *t*BuLi, 1,3-diphenylisobenzofuran, THF, −67 °C, 37% yield.

(−63.7 kcal mol^{-1}), HOMO–LUMO gap (5.64 eV), and predicted ^{13}C NMR chemical shift ($\delta = 148.4$ ppm) were in line with the values calculated for previously synthesized highly pyramidalized alkenes.[1c,6]

It is known that vicinal diiodo compounds are suitable precursors of highly pyramidalized alkenes, so the generation of **4** was envisioned from the diiodo derivative **3** (Scheme 1), whose preparation from the known anhydride **1**[7] was carried out in just two steps. Saponification of **1** gave the dicarboxylic acid **2** in 70% yield. The diiodo compound **3** was obtained in 27% yield by using a iododecarboxylation procedure recently reported by Gandelman and co-workers.[8] Previous attempts to carry out the iododecarboxylation of **2** using iodosobenzene diacetate or lead tetraacetate gave even lower yields of **3**. Reaction of **3** with *tert*-butyllithium in THF at −67 °C in the presence of 1,3-diphenylisobenzofuran furnished the expected Diels–Alder adduct **5** in 37% yield. Finally, reaction of **3** with a large excess of molten sodium in 1,4-dioxane at reflux for 4 hours gave a mixture of three products (GC/MS): the reduced product **6**, the expected dimer **7**, and the dihydrodimer **8**. From this mixture, **6** was isolated by sublimation (100 °C at 1 Torr), **7** was obtained by crystallization from *n*-pentane, and **8** was obtained from the mother liquors. X-Ray diffraction analysis unequivocally established the structures of **7** and **8**.[9]

The X-ray diffraction analysis of **7** revealed several interesting features. Firstly, **7** has three planar cyclobutanes, two of them with four eclipsed methyl groups. While the central cyclobutane is not a fully perfect square, as it has two newly formed carbon–carbon bonds being slightly shorter than the other two bonds, the other two cyclobutanes are nearly perfect squares (see Figure 1). Secondly, the compound

[*] M. Rey-Carrizo, M. Barniol-Xicota, Prof. Dr. S. Vázquez
Laboratori de Química Farmacèutica (Unitat Associada al CSIC), Facultat de Farmàcia, and Institute of Biomedicine (IBUB), Universitat de Barcelona
Av. Joan XXIII, s/n, 08028 Barcelona (Spain)
E-mail: svazquez@ub.edu
Homepage: http://www.ub.edu/farmaco/ca/farmaceutica/recerca/novel_polycyclic_compounds_with_biological_activity/8/
Dr. M. Font-Bardia
Unitat de Difracció de RX, Centres Científics i Tecnològics (CCiTUB), Universitat de Barcelona
Solé i Sabarís 1-3, 08028 Barcelona (Spain)

[**] S.V. thanks Ministerio de Ciencia e Innovación (project CTQ2011-22433) and the Generalitat de Catalunya (grant SCG-2009-294) for financial support. M.R.-C. thanks the Govern d'Andorra for a PhD grant (ATCR2012/2013-00XX-AND). We thank Prof. F. J. Luque for helping us with the theoretical calculations.

Supporting information for this article is available on the WWW under http://dx.doi.org/10.1002/anie.201403985.

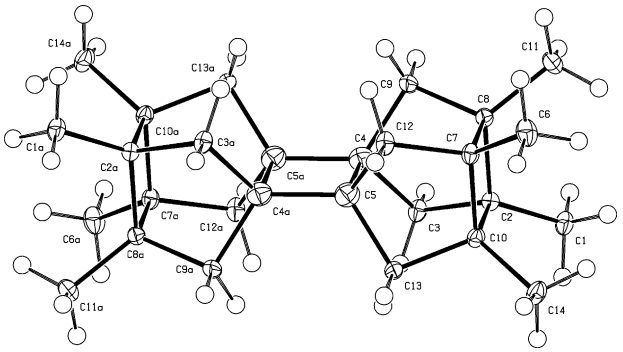

Figure 1. Crystal structure (ORTEP) of **7**. Thermal ellipsoids shown at 50% probability. Selected distances [Å] and angles [°]: C2–C8 1.5844(19), C7–C8 1.5841(19), C4–C5 1.589(2), C4–C5a 1.542(2), C8–C9 1.5376(19), C4–C9 1.543(2); C3-C2-C10 109.44(11), C3-C2-C8 105.41(11), C10-C2-C8 90.01(10), C2-C3-C4 99.61(11), H3a-C3-H3b 110.1 (15), C5a-C4-C5 90.05(11), C3-C4-C5 109.78(12), C4a-C5-C12 122.30(13), C12-C5-C13 101.86(12), C4a-C5-C4 89.95(11).

has four cyclopentane rings in a "frozen" envelope conformation. Finally, the structure features four cyclohexane rings in a boat conformation. Although there are several precedents of cyclohexane rings in boat conformations,[10] most of the known examples lack the typical H–H flagpole interaction of the boat conformation (e.g. camphor and other norbornane derivatives).[11] Some notable exceptions with frozen boat cyclohexanes, featuring a H–H flagpole interaction, are the asteranes, such as tetracyclo [3.3.1.$0^{2,8}$.$0^{4,6}$]nonane (triasterane; **9**)[12] tricyclo[3.1.1.$1^{2,4}$]octane (diasterane; **10**),[12d,13] and pentacyclo[6.4.0.$0^{2,7}$.$0^{4,11}$.$0^{5,10}$] dodecane (tetraasterane; **11**),[12a,d,14,15] and tetracyclo[5.3.1.$1^{2,6}$.$0^{4,9}$]dodecane (iceane; **12**),[16] a polycyclic compound featuring two chair and three boat cyclohexane rings (Figure 2). Interestingly, the cyclobutane rings of these polycyclic compounds can be either planar, as in **7** and **11**, or puckered as in **10**.

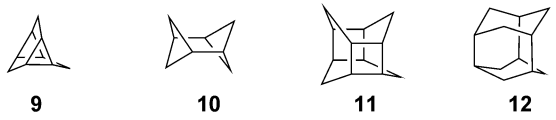

Figure 2. Known polycyclic compounds featuring boat cyclohexane rings.

According to a seminal paper by Hassel and Ottar,[17] the boat conformer of the cyclohexane ring with fixed C-C-C angles of 109.5° would have a distance between the flagpole hydrogen atoms of 1.8–1.83 Å and a separation of 2.57 Å would be expected between the flagpole carbon atoms. These distances should induce severe steric congestion given the van der Waals radius of hydrogen and carbon, 1.1–1.2 Å and 1.7–1.8 Å, respectively.[18] In fact, Sauers has found, using density functional calculations at the B3LYP/6-311 ++ G(2d,p) level of theory, that the boat conformer of cyclohexane suffers from significant distortions from pure sp^3 hybridization, thus relieving the flagpole H–H interaction at an interatomic separation of 2.353 Å and with a distance of 2.736 Å between the two flagpole carbon atoms.[11a] In this work, for the boat conformer of cyclohexane, we have found smaller distances using MP2/6-31G(d): 2.289 Å and 2.710 Å for the flagpole H–H and C–C interatomic distances, respectively.[4]

However, in the polycyclic compounds shown in Scheme 1 the ability of the boat cyclohexanes to relieve the flagpole H–H interaction is severely limited. Thus, the X-ray diffraction analysis of **7** revealed a distance between the flagpole hydrogen atoms of only 1.999 Å and a separation of 2.619 Å between the flagpole carbon atoms. We have optimized the structure of **7** at the MP2/6-31G(d) level of theory and found distances of 2.042 Å and 2.668 Å for the flagpole H–H and C–C distances, respectively, and they are in reasonable agreement with the experimental values. At this level, these distances are shorter than the corresponding values found in **9**, **11**, and **12**, but longer that those of **10** (Table 1).[4]

Table 1: H–H and C–C distances between the flagpole hydrogen atoms and the flagpole carbon atoms in boat cyclohexane and hydrocarbons **6**–**7** and **9**–**12**.

Compound	H–H distance [Å]		C–C distance [Å]	
	B3LYP/ 6-31G(d)	MP2/ 6-31G(d)	B3LYP/ 6-31G(d)	MP2/ 6-31G(d)
Cyclohexane	2.349	2.289	2.739	2.710
6	2.035	2.027	2.655	2.639
7[a]	2.054	2.042	2.684	2.668
9[b]	3.252	3.238	2.990	2.979
10	1.861	1.856	2.625	2.610
11	2.505	2.488	2.814	2.800
12	2.126	2.120	2.668	2.652

[a] The H–H and the C–C distances in the crystal structure of **7** were 1.999(2) Å and 2.619(1) Å, respectively. [b] The C–C distance obtained for **9** by gas-phase electron diffraction was 2.973(6).[12d]

Regarding the X-ray diffraction analysis of **8** two features are worthy of comment. Firstly, values between 1.93 and 2.03 Å were found for the distance between the flagpole hydrogen atoms, while an average value of 2.64 Å was found between the flagpole carbon atoms, very similar to the values found for **7**. These values are also very similar in the X-ray diffraction structures found for **1**, **3**, and **5**.[9] Secondly, the exocyclic intercage C–C bond length of **8** is 1.539(3) Å, the normal length for a C–C single bond, midway between the very short intercage C–C bond found in tetrahedranyltetrahedrane and bicubyl derivatives, which feature significantly shorter distances (around 1.44–1.46 Å),[19] and that of the 1-(1-adamantyl)adamantine (1.578(2) Å).[20]

Previously, we had observed that several cyclobutane dimers of highly pyramidalized alkenes underwent an exothermic [2+2] retrocycloaddition process to their corresponding diene isomers.[1,3d] However, the three cyclobutane rings in **7** were thermally stable. In fact, the only process that was observed when a sample of **7** was heated up to 500 °C was the melting process at 380 °C. MP2/6-311 ++ G(d,p)//MP2/6-31G(d) calculations carried out on **7** and its three theoretical diene isomers, **13**, **14**, and **15**, predicted endothermic processes for all the ring-opening reactions, with the transformation of **7** into **13** being more endothermic, 17.8 kcal mol^{-1}, than the

opening to **14** or **15**, 11.5 and 11.4 kcal mol^{-1}, respectively, thus probably reflecting the increase in the strain in **13** as a consequence of the approaching of the eclipsed methyl groups (Scheme 2).[4]

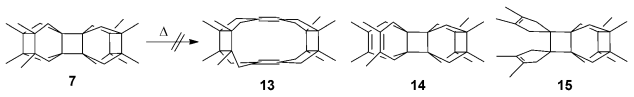

Scheme 2. Hypothetical [2+2] cycloreversion of **7** into the dienes **13**, **14**, and **15**.

In summary, we have presented here the synthesis, chemical trapping, and dimerization of a highly pyramidalized alkene. Its dimer features three planar cyclobutane rings and four cyclohexane rings in boat conformations. X-ray structural studies and theoretical calculations showed that the distances between the flagpole hydrogen atoms and the flagpole carbon atoms are smaller than the sum of the van der Waals radius of the involved atoms. Finally, in spite of the three cyclobutane rings, and in sharp contrast with the behavior of previously described dimers of highly pyramidalized alkenes, the nonacycle **7** is thermally stable.

Experimental Section

3,4,8,9-Tetramethyltetracyclo[4.4.0.0^{3,9}.0^{4,8}]decane-1,6-dicarboxylic acid (**2**): A solution of the anhydride **1** (270 mg, 1.03 mmol) in 1N NaOH (10 mL) was heated to reflux for 18 h. The suspension was allowed to cool down to room temperature, was acidified with 6N HCl, and extracted with EtOAc (3 × 50 mL). The organic phase was dried over anhydrous Na_2SO_4 and concentrated under reduced pressure to give **2** (203 mg, 70% yield) as a colorless solid, m.p. 209–210°C. ^{1}H NMR (400 MHz, [D$_6$]DMSO): $\delta = 0.92$ (s, 12H, 3(4,8,9)-CH$_3$], 0.98 [d, $J = 11.6$ Hz, 4H, 2(5,7,10)-H$_a$], 1.97 ppm [d, $J = 11.6$ Hz, 4H, 2(5,7,10)-H$_b$]; ^{13}C NMR (100.6 MHz, CD$_3$OD): $\delta =$ 15.7 [CH$_3$, 3(4,8,9)-CH$_3$], 43.5 [CH$_2$, 2(5,7,10)-CH$_2$], 46.4 [C, 3(4,8,9)-C], 53.7 [C, 1(6)-C], 179.1 ppm (C, CO$_2$H); IR (KBr): $\nu = 3000$–2400 (2953, 2921, 2867, 2673, 2570), 1717, 1429, 1299, 1218, 1176, 1116, 1061, 1030, 1013, 877, 771, 720 cm^{-1}; GC/MS (70 eV): *m*/*z* (%): 260 [(*M*−H$_2$O)$^{\cdot+}$, 5], 232 (51), 187 (100), 173 (73), 163 (19), 159 (15), 145 (34), 131 (23), 119 (37), 105 (17), 91 (36), 82 (37), 77 (31), 67 (17); Accurate mass [ESI(−)]: *m*/*z* calcd for $C_{16}H_{21}O_4$: 277.1445 [*M*−H]$^-$; found: 277.1448.

1,6-Diiodo-3,4,8,9-tetramethyltetracyclo[4.4.0.0^{3,9}.0^{4,8}]decane (**3**): 1,3-Diiodo-5,5-dimethylhydantoin (7.17 g, 18.9 mmol) was added to a solution of the diacid **2** (2.10 g, 7.54 mmol). The resulting orange solution was irradiated (2 × 60 W tungsten bulb) at reflux for 24 h. The suspension was cooled to room temperature and washed with 10% aqueous $NaHSO_3$ (50 mL). The aqueous layer was extracted with CH_2Cl_2 (25 mL) and the combined organic layers were washed with saturated aqueous solution of $NaHCO_3$ (2 × 25 mL), dried over Na_2SO_4, filtered, and concentrated under vacuum to obtain 1.4 g of a mixture of starting **2**, **3** and the corresponding iodoacid. Purification by column chromatography (silica gel, *n*-hexane) gave **3** as a colorless solid (900 mg, 27% yield), m.p. 234–235°C. ^{1}H NMR (400 MHz, CDCl$_3$): $\delta = 0.92$ (s, 12H, 3(4,8,9)-CH$_3$], 1.62 [d, $J = 12.0$ Hz, 4H, 2(5,7,10)-H$_a$], 2.69 ppm [d, $J = 12.0$ Hz, 4H, 2(5,7,10)-H$_b$]; ^{13}C NMR (100.6 MHz, CDCl$_3$): $\delta = 14.3$ [CH$_3$, 3(4,8,9)-CH$_3$], 47.0 [C, 3(4,8,9)-C], 48.7 [C, 1(6)-C], 53.7 ppm [CH$_2$, 2(5,7,10)-CH$_2$]; IR (KBr): $\nu =$ 2923, 2859, 1717, 1448, 1384, 1369, 1298, 1270, 1208, 1187, 1102, 935, 820, 790, 708, 654 cm^{-1}; GC/MS (70 eV): *m*/*z* (%): 442 (*M*$^{\cdot+}$, 2), 315 (46), 187 (100), 173 (46), 159 (13), 145 (34), 131 (16), 119 (23), 105 (11), 91 (20), 77 (12); Anal calcd for $C_{14}H_{20}I_2$: C 38.94%; H 4.49%; calcd for $C_{14}H_{20}I_2$·0.1 hexane: C: 38.91%, H 4.79%; found C: 38.94, H 4.49%.

12,13,14,17-Tetramethyl-2,9-diphenyl-19-oxaheptacyclo-[10.3.2.1^{2,9}.1^{10,13}.0^{1,10}.0^{3,8}.0^{14,17}]nonadec-3,5,7-triene (**5**). A solution of *tert*-butyllithium (1.6M in pentane, 0.61 mL, 0.97 mmol) was slowly added, under stirring, to a cold (−67°C) solution of **3** (252 mg, 0.6 mmol) and 1,3-diphenylisobenzofuran (186 mg, 0.68 mmol) in anhydrous THF (10 mL). The reaction mixture was kept at this temperature for 30 min and then it was allowed to warm to room temperature. Methanol (5 mL) and water (10 mL) were added dropwise and the mixture was extracted with diethyl ether (3 × 50 mL). The combined organic extracts were dried over Na_2SO_4, filtered, and concentrated in vacuo to dryness to give a yellow oil. Purification by column chromatography (EtOAc/*n*-hexane mixtures) gave **5** (96 mg, 37% yield) as a pale yellow solid, m.p. 182–183°C. ^{1}H NMR (500 MHz, CDCl$_3$): $\delta = 0.42$ [d, $J = 11.5$ Hz, 2H, 11(16)-H$_a$], 0.80 (s, 6H) and 0.85 (s, 6H) [C12(17)-C*H*$_3$ and C13(14)-C*H*$_3$], 0.94 [dd, $J = 11.0$ Hz, $J' = 2.5$ Hz, 2H, 15(18)-H$_b$], 1.06 [d, $J = 11.0$ Hz, 2H, 15(18)-H$_a$], 1.51 [dd, $J = 11.5$ Hz, $J' = 2.5$ Hz, 2H, 11(16)-H$_b$], 7.15 [m, 2H, 5(6)-H], 7.32 [m, 2H, 4(7)-H], 7.37 (tt, 2H, $J = 7.5$ Hz, $J' =$ 1.5 Hz, Ar-H$_{para}$), 7.49 (broad t, $J = 7.5$ Hz, 4H, Ar-H$_{meta}$), 7.78 ppm (d, $J = 8.0$ Hz, $J' = 1.5$ Hz, 4H, Ar-H$_{ortho}$); ^{13}C NMR (125.7 MHz, CDCl$_3$): $\delta = 15.6$ (CH$_3$) and 15.8 (CH$_3$) [C12(17)-CH$_3$ and C13(14)-CH$_3$], 39.2 [CH$_2$, C11(16)], 41.0 [CH$_2$, C15(18)], 44.6 [C, C12(17)], 45.4 [C, C13(14)], 55.3 [C, C1(10)], 88.8 [C, C2(9)], 119.6 [CH, C4(7)], 125.0 (CH, C$_{ortho}$-C$_6$H$_5$), 126.1 [CH, C5(6)], 127.0 (CH, C$_{para}$-C$_6$H$_5$), 128.2 (CH, C$_{meta}$-C$_6$H$_5$), 138.3 (C, C$_{ipso}$-C$_6$H$_5$), 146.7 ppm [C, C3(8)]; IR (KBr): $\nu = 3061$, 3024, 2943, 2913, 2860, 1597, 1457, 1446, 1370, 1342, 1302, 1272, 1217, 1178, 1155, 1119, 1021, 1001, 975, 936, 839, 745, 712, 698, 674 cm^{-1}; GC/MS (70 eV): *m*/*z* (%): 458 (*M*$^{\cdot+}$, 1), 353 (36), 270 (100), 241 (13), 193 (5), 165 (8), 105 (5), 77 (4); Accurate mass [ESI(+)]: *m*/*z* calcd for $C_{34}H_{35}O$: 459.2682 [*M*+H]$^+$; found: 459.2680; Anal calcd for $C_{34}H_{34}O$: C 89.04%; H 7.47%; calcd for $C_{34}H_{34}O$·0.05CH_2Cl_2: C: 88.35%, H 7.43%; found C: 88.10, H 7.63%.

3,4,8,9-Tetramethyltetracyclo[4.4.0.0^{3,9}.0^{4,8}]decane (**6**), 4,5,6,7,12,-13,16,17-octamethylnonacyclo[8.4.4.1^{2,5}.1^{6,9}.0^{1,10}.0^{2,9}.0^{4,7}.0^{12,17}.0^{13,16}]-eicosane (**7**), and 3,4,8,9-tetramethyl-1-[3,4,8,9-tetramethyltetracyclo[4.4.0.0^{3,9}.0^{4,8}]dec-1-yl]-tetracyclo[4.4.0.0^{3,9}.0^{4,8}]decane (**8**). Finely cut sodium (0.49 g, 21.5 mmol) was added to boiling anhydrous 1,4-dioxane (25 mL) and the mixture was heated with stirring under an argon atmosphere until the metal melted. Then, solid **3** (0.95 g, 2.15 mmol) was added and the mixture was heated under reflux for 4 h. The reaction mixture was cooled to room temperature and filtered through Celite®. The solid residue was washed with diethyl ether and *n*-pentane, and the combined filtrate and washings were concentrated under reduced pressure to give a solid white residue (151 mg, aprox. 35% yield). GC/MS spectrometry showed the presence of three main components with the following retention times, *m*/*z* of the molecular ions and relative areas (12.3 min, 190, 20.8%; 24.2 min, 376, 11.5%; 25.1 min, 378, 45.6%). By sublimation (100°C/1 atm), pure tetracycle **6** was obtained (19 mg, 5% yield), m.p. 189–190°C. ^{1}H NMR (400 MHz, CDCl$_3$): $\delta = 0.56$ [d, $J = 11.0$ Hz, 4H, 2(5,7,10)-H$_a$], 0.93 (s, 12H, 3(4,8,9)-CH$_3$], 1.70 [d, $J = 11.0$ Hz, 4H, 2(5,7,10)-H$_b$], 2.24 ppm [s, 2H, 1(6)-H]; ^{13}C NMR (100.6 MHz, CDCl$_3$): $\delta = 15.8$ (CH$_3$), 32.9 (CH), 38.1 (CH$_2$), 45.3 ppm (C); IR (KBr): $\nu = 3447$, 2946, 2864, 1458, 1381, 1369, 1323, 1116, 1096, 1028, 927 cm^{-1}; GC/MS (70 eV): *m*/*z* (%): 190 (*M*$^{\cdot+}$, 43), 120 (100), 119 (30), 108 (31), 107 (34), 105 (51), 95 (16), 93 (39), 91 (34), 77 (19). By recrystallization of the remaining mixture from *n*-pentane, pure dimer **7** (36 mg, 9% yield) was isolated by filtration, m.p. > 300°C. ^{1}H NMR (400 MHz, CDCl$_3$): $\delta = 0.64$ [d, $J = 13.5$ Hz, 8H, 3(8,11,14,15,18,19,20)-H$_a$], 0.91 (s, 24H, 4(5,6,7,12,13,16,17)-CH$_3$], 1.97 ppm [d, $J = 13.5$ Hz, 8H, 3(8,11,14,15,18,19,20)-H$_b$]; ^{13}C NMR (100.6 MHz, CDCl$_3$): $\delta = 15.8$ (CH$_3$), 38.9 (CH$_2$), 45.3 [C, 4(5,6,7,12,13,16,17)-C], 47.0 ppm [C, 1(2,9,10)-C]; IR (KBr): $\nu =$

2945, 2860, 1699, 1445, 1382, 1297, 1215, 1115 cm^{-1}; GC/MS (70 eV): *m/z* (%): 376 ($M^{\bullet+}$, 12), 190 (24), 189 (17), 188 (69), 187 (100), 186 (55), 185 (15), 173 (71), 171 (34), 145 (21), 131 (16), 119 (42), 105 (17), 91 (19), 79 (15); Anal calcd for $C_{28}H_{40}$: C 89.29%; H 10.71%; found C: 89.07, H 10.71%. The solid remaining after concentration of the mother liquors was washed with dichloromethane to give the pure dihydrodimer **8** (37 mg, 9% yield), m.p. 199–200 °C. ^{1}H NMR (400 MHz, $CDCl_3$): $\delta = 0.62$ [d, $J = 11.6$ Hz, 4H, 2(2′,10,10′)-H_a], 0.69 [dd, $J = 11.2$ Hz, $J' = 2.8$ Hz, 4H, 5(5′,7,7′)-H_a], 0.91 (s, 12H) and 0.93 (s, 12H) [3(3′,9,9′)-CH_3, and 4(4′,8,8′)-CH_3], 1.62 [d, $J = 11.2$ Hz, 4H, 2(2′,10,10′)-H_b], 1.71 [dd, $J = 11.2$ Hz, $J' = 1.4$ Hz, 4H, 5(5′,7,7′)-H_b], 2.31 ppm [m, 2H, 6(6′)-H]; ^{13}C NMR (100.6 MHz, $CDCl_3$): $\delta =$ 15.8 (CH_3), 16.1 (CH_3), 36.9 [CH, 6(6′)-C], 39.2 [CH_2, 2(2′,10,10′)-C], 39.4 [CH_2, 5(5′,7,7′)-C], 44.8 (C), and 45.3 (C) [3(3′,9,9′)-C and 4(4′,8,8′)-C], 47.5 ppm [C, 1(1′)-C]; IR (KBr): $\nu = 2943$, 2861, 1457, 1381, 1371, 1324, 1258, 1224, 1095, 1061, 1033, 799 cm^{-1}; GC/MS (70 eV): *m/z* (%): 378 ($M^{\bullet+}$, 21), 296 (49), 214 (18), 189 (65), 188 (68), 187 (20), 173 (33), 133 (21), 120 (25), 119 (100), 107 (50), 105 (29), 95 (54), 93 (16), 91 (34), 80 (19), 67 (20); Anal calcd for $C_{28}H_{42}$: C 88.82%; H 11.18%; calcd for $C_{28}H_{42}\cdot 0.1CH_2Cl_2$: C 87.18%; H 10.99%; found C: 87.43, H 11.11%.

Received: April 4, 2014
Published online: June 16, 2014

Keywords: ab initio calculations · dimerization · hydrocarbons · polycycles · strained molecules

[1] a) W. T. Borden, *Chem. Rev.* **1989**, *89*, 1095 – 1109; b) H. Hopf, *Classics in Hydrocarbon Chemistry: Syntheses, Concepts, Perspectives*, Wiley-VCH, Weinheim, **2000**, pp. 122 – 137; c) S. Vázquez, P. Camps, *Tetrahedron* **2005**, *61*, 5147 – 5208; d) A. Nicolaides in *Strained Hydrocarbons* (Ed: H. Dodziuk), Wiley-VCH, Weinheim, **2009**, pp. 112 – 121; e) S. P. Gavrish, *J. Comput. Chem.* **2012**, *33*, 2173 – 2179.

[2] For recent examples: a) P. Camps, M. R. Muñoz, S. Vázquez, *Tetrahedron* **2006**, *62*, 7645 – 7652; b) P. Camps, G. Colet, S. Delgado, M. R. Muñoz, M. A. Pericàs, L. Solà, S. Vázquez, *Tetrahedron* **2007**, *63*, 4669 – 4679.

[3] For recent works by other groups: a) F. A. Theophanous, A. J. Tasiopoulos, A. Nicolaides, X. Zhou, W. T. G. Johnson, W. T. Borden, *Org. Lett.* **2006**, *8*, 3001 – 3004; b) M. A. Forman, C. Moran, J. P. Herres, J. Stairs, E. Chopko, A. Pozzessere, M. Kerrigan, C. Kelly, L. Lowchyj, K. Salandria, A. Gallo, E. Loutzenhiser, *J. Org. Chem.* **2007**, *72*, 2996 – 3005; c) M. Pillekamp, W. Alachraf, I. M. Oppel, G. Dyker, *J. Org. Chem.* **2009**, *74*, 8355 – 8358; d) S. Ioannou, H. Krassos, A. V. Nicolaides, *Tetrahedron* **2013**, *69*, 8064 – 8068.

[4] Gaussian 09 (Revision A.1): M. J. Frisch et al., see the Supporting Information for details about the calculations.

[5] For a definition of the pyramidalization angle, see: W. V. Volland, E. R. Davidson, W. T. Borden, *J. Am. Chem. Soc.* **1979**, *101*, 533 – 537. For fullerenes and related compounds, pyramidalizations are typically reported as POAV angles. The POAV angle of **4** is 17.9°. For a definition of the POAV angle, see: a) R. C. Haddon, *J. Phys. Chem.* **1987**, *91*, 3719 – 3720; b) R. C. Haddon, *J. Am. Chem. Soc.* **1990**, *112*, 3385 – 3389; c) R. C. Haddon, *J. Phys. Chem. A* **2001**, *105*, 4164 – 4165.

[6] a) P. Camps, M. Font-Bardia, N. Méndez, F. Pérez, X. Pujol, X. Solans, S. Vázquez, M. Vilalta, *Tetrahedron* **1998**, *54*, 4679 – 4696; b) S. Vázquez, *J. Chem. Soc. Perkin Trans. 2* **2002**, 2100 – 2103.

[7] W. B. Avila, R. A. Silva, *J. Chem. Soc. Chem. Commun.* **1970**, 94 – 95.

[8] K. Kulbitski, G. Nisnevich, M. Gandelman, *Adv. Synth. Catal.* **2011**, *353*, 1438 – 1442.

[9] a) Crystal structure analysis of **7**: a translucent colorless prism-like specimen of **7**, approximate dimensions 0.071 mm × 0.093 mm × 0.109 mm, was used for the X-ray crystallographic analysis. The X-ray intensity data were measured on a D8 Venture system equipped with a Multilayer monochromator and a Mo microfocus ($\lambda = 0.71073$ Å). A total of 1473 frames were collected. The total exposure time was 4.09 h. The frames were integrated with the Bruker SAINT software package using a narrow-frame algorithm. The integration of the data using a monoclinic unit cell yielded a total of 34804 reflections to a maximum θ angle of 28.57° (0.74 Å resolution), of which 2683 were independent (average redundancy 12.972, completeness = 100.0%, $R_{int} = 5.79\%$) and 2224 (82.89%) were greater than $2\sigma(F^2)$. The final cell constants of $a = 6.978(6)$, $b = 11.110(10)$, $c = 14.848(13)$ Å, $\beta = 113.90(4)°$, volume = 1052.4(16) Å^3, are based upon the refinement of the XYZ-centroids of 87 reflections above 20 σ(I) with $7.348° < 2\theta < 54.87°$. Data were corrected for absorption effects using the multi-scan method (SADABS). The ratio of minimum to maximum apparent transmission was 0.955. The structure was solved and refined using the Bruker SHELXTL Software Package, with $Z = 2$ for the formula unit, $C_{28}H_{40}$. The final anisotropic full-matrix least-squares refinement on F^2 with 155 variables converged at $R1 = 5.13\%$, for the observed data and $wR2 = 14.36\%$ for all data. The goodness-of-fit was 1.065. The largest peak in the final difference electron density synthesis was 0.571 e$^-$ Å^{-3} and the largest hole was −0.444 e$^-$ Å^{-3} with an RMS deviation of 0.068 e$^-$ Å^{-3}. On the basis of the final model, the calculated density was 1.188 g cm^{-3} and F(000), 416 e$^-$. 8 H atoms were located from a difference synthesis and refined with an isotropic temperature factor equal to 1.2 time the equivalent temperature factor of the atom which are linked and 12 H atoms were computed and refined, using a riding model, with an isotropic temperature factor equal to 1.2 time the equivalent temperature factor of the atom which are linked; b) crystal structure analysis of **8**: a colorless Prism-like specimen of **8**, approximate dimensions 0.090 mm × 0.209 mm × 0.623 mm, was used for the X-ray crystallographic analysis. The X-ray intensity data were measured on a D8 Venture system equipped with a multilayer monochromator and a Mo microfocus ($\lambda = 0.71073$ Å). A total of 1064 frames were collected. The total exposure time was 17.73 h. The frames were integrated with the Bruker SAINT software package using a narrow-frame algorithm. The integration of the data using a monoclinic unit cell yielded a total of 40995 reflections to a maximum θ angle of 28.33° (0.75 Å resolution), of which 5377 were independent (average redundancy 7.587, completeness = 98.8%, $R_{int} = 5.79\%$, $R_{sig} = 3.37\%$) and 5037 (93.23%) were greater than $2\sigma(F^2)$.The final cell constants of $a = 22.792(3)$, $b = 7.8099(8)$, $c = 12.4331(15)$ Å, $\beta = 100.517(4)°$, volume = 2176.0.(4) Å^3, are based upon the refinement of the XYZ-centroids of 143 reflections above 20 σ(I) with $7.142° < 2\theta < 52.43°$. Data were corrected for absorption effects using the multi-scan method (SADABS). The ratio of minimum to maximum apparent transmission was 0.775. The structure was solved and refined using the Bruker SHELXTL Software Package, with $Z = 4$ for the formula unit, $C_{28}H_{42}$.The final anisotropic full-matrix least-squares refinement on F^2 with 322 variables converged at $R1 = 8.25\%$, for the observed data and $wR2 = 21.75\%$ for all data. The goodness-of-fit was 1.071. The largest peak in the final difference electron density synthesis was 0.426 e$^-$ Å^{-3} and the largest hole was −0.428 e$^-$ Å^{-3} with an RMS deviation of 0.099 e$^-$ Å^{-3}. On the basis of the final model, the calculated density was 1.156 g cm^{-3} and $F(000)$, 840 e$^-$. 22 H atoms were located from a difference synthesis and refined with an isotropic temperature factor equal to 1.2 time the equivalent temperature factor of the atom which are linked and 20 H atoms were computed and refined, using a riding model, with an

isotropic temperature factor equal to 1.2 time the equivalent temperature factor of the atom which are linked; c) the structures of **1**, **3** and **5** were also established by X-Ray diffraction analysis. See supporting information for details. CCDC 994900, 994901, 994902, 994903 and 994904 contain the supplementary crystallographic data for this paper. These data can be obtained free of charge from The Cambridge Crystallographic Data Centre via www.ccdc.cam.ac.uk/data_request/cif.

[10] M. Balasubramanian, *Chem. Rev.* **1962**, *62*, 591 – 598.

[11] a) R. R. Sauers, *J. Chem. Educ.* **2000**, *77*, 332 – 332; b) K. Kakhiani, U. Lourderaj, W. Hu, D. Birney, W. L. Hase, *J. Phys. Chem. A* **2009**, *113*, 4570 – 4580.

[12] a) U. Biethan, U. v. Gizycki, H. Musso, *Tetrahedron Lett.* **1965**, *6*, 1477 – 1482; b) H. Musso, U. Biethan, *Chem. Ber.* **1967**, *100*, 119 – 131; c) H. Musso, H. Klusacek, *Chem. Ber.* **1970**, *103*, 3076 – 3086; d) B. Ahlquist, A. Almenningen, B. Benterud, M. Traetteberg, P. Bakken, W. Lüttke, *Chem. Ber.* **1992**, *125*, 1217 – 1225.

[13] A. Otterbach, H. Musso, *Angew. Chem.* **1987**, *99*, 588 – 590; *Angew. Chem. Int. Ed. Engl.* **1987**, *26*, 554 – 555.

[14] a) H.-M. Hutmacher, H.-G. Fritz, H. Musso, *Angew. Chem.* **1975**, *87*, 174 – 175; *Angew. Chem. Int. Ed. Engl.* **1975**, *14*, 180 – 181; b) H.-G. Fritz, H.-M. Hutmacher, H. Musso, G. Ahlgren, B. Åkermark, R. Karlsson, *Chem. Ber.* **1976**, *109*, 3781 – 3792; c) G. Kaiser, H. Musso, *Chem. Ber.* **1985**, *118*, 2266 – 2281.

[15] Several double tetraasteranes are also known: a) V. T. Hoffmann, H. Musso, *Angew. Chem.* **1987**, *99*, 1036 – 1037; *Angew. Chem. Int. Ed. Engl.* **1987**, *26*, 1006 – 1007; b) V. T. Hoffmann, H. Musso, *Chem. Ber.* **1991**, *124*, 103 – 109.

[16] a) C. A. Cupas, L. Hodakowski, *J. Am. Chem. Soc.* **1974**, *96*, 4668 – 4669; b) D. P. G. Hamon, G. F. Taylor, *Tetrahedron Lett.* **1974**, *15*, 155 – 158; c) D. P. G. Hamon, G. F. Taylor, *Aust. J. Chem.* **1976**, *29*, 1721 – 1734.

[17] O. Hassel, B. Ottar, *Acta Chem. Scand.* **1947**, *1*, 929 – 943.

[18] a) R. Chauvin, *J. Phys. Chem.* **1992**, *96*, 9194 – 9197; b) R. S. Rowland, R. Taylor, *J. Phys. Chem.* **1996**, *100*, 7384 – 7391.

[19] a) R. Gilardi, M. Maggini, P. E. Eaton, *J. Am. Chem. Soc.* **1988**, *110*, 7232 – 7234; b) M. Tanaka, A. Sekiguchi, *Angew. Chem.* **2005**, *117*, 5971 – 5973; *Angew. Chem. Int. Ed.* **2005**, *44*, 5821 – 5823.

[20] R. A. Alden, J. Kraut, T. G. Traylor, *J. Am. Chem. Soc.* **1968**, *90*, 74 – 82.

Angewandte Chemie
Eine Zeitschrift der Gesellschaft Deutscher Chemiker

Supporting Information

69451 Weinheim, Germany

Dimerization of Pyramidalized 3,4,8,9-Tetramethyltetracyclo [4.4.0.0^{3,9}.0^{4,8}]dec-1(6)-ene to a Hydrocarbon Featuring Four Cyclohexane Rings in Boat Conformations**

*Matias Rey-Carrizo, Marta Barniol-Xicota, Mercè Font-Bardia, and Santiago Vázquez**

anie_201403985_sm_miscellaneous_information.pdf

TABLE OF CONTENTS

Full reference for [4]:

Gaussian 09, Revision **A.1**, Frisch, M. J.; Trucks, G. W.; Schlegel, H. B.; Scuseria, G. E.; Robb, M. A.; Cheeseman, J. R.; Scalmani, G.; Barone, V.; Mennucci, B.; Petersson, G. A.; Nakatsuji, H.; Caricato, M.; Li, X.; Hratchian, H. P.; Izmaylov, A. F.; Bloino, J.; Zheng, G.; Sonnenberg, J. L.; Hada, M.; Ehara, M.; Toyota, K.; Fukuda, R.; Hasegawa, J.; Ishida, M.; Nakajima, T.; Honda, Y.; Kitao, O.; Nakai, H.; Vreven, T.; Montgomery, Jr., J. A.; Peralta, J. E.; Ogliaro, F.; Bearpark, M.; Heyd, J. J.; Brothers, E.; Kudin, K. N.; Staroverov, V. N.; Kobayashi, R.; Normand, J.; Raghavachari, K.; Rendell, A.; Burant, J. C.; Iyengar, S. S.; Tomasi, J.; Cossi, M.; Rega, N.; Millam, N. J.; Klene, M.; Knox, J. E.; Cross, J. B.; Bakken, V.; Adamo, C.; Jaramillo, J.; Gomperts, R.; Stratmann, R. E.; Yazyev, O.; Austin, A. J.; Cammi, R.; Pomelli, C.; Ochterski, J. W.; Martin, R. L.; Morokuma, K.; Zakrzewski, V. G.; Voth, G. A.; Salvador, P.; Dannenberg, J. J.; Dapprich, S.; Daniels, A. D.; Farkas, Ö.; Foresman, J. B.; Ortiz, J. V.; Cioslowski, J.; Fox, D. J. Gaussian, Inc., Wallingford CT, **2009**.

^{1}H and ^{13}C NMR spectra

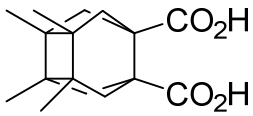

2

^{1}H NMR (400 MHz) DMSO-d_6

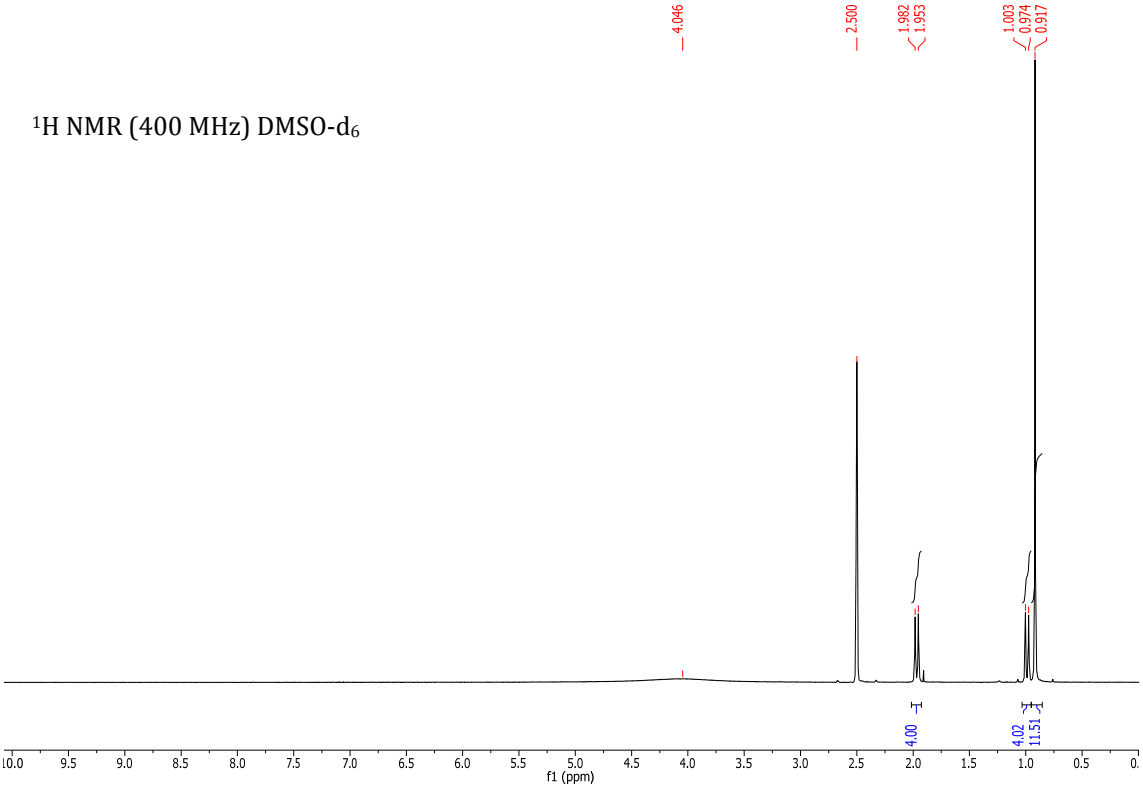

^{1}H NMR (400 MHz) DMSO-d_6

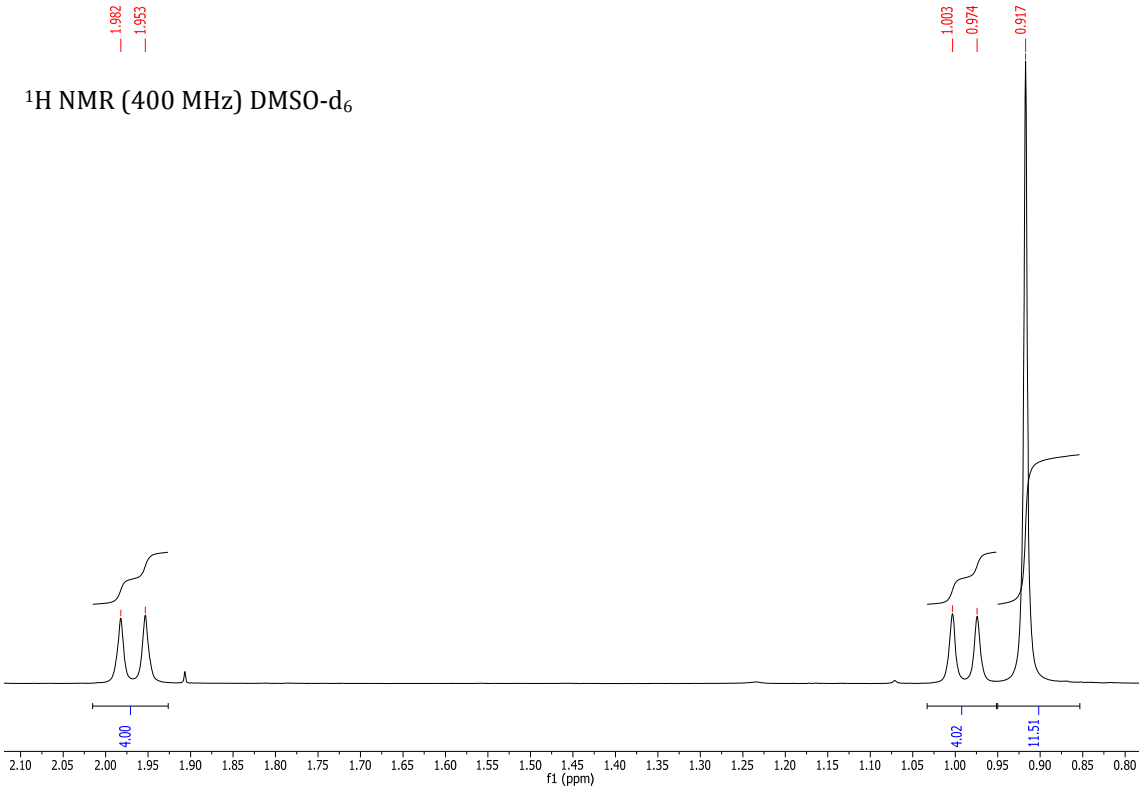

^{13}C NMR (400 MHz) CD_3OD

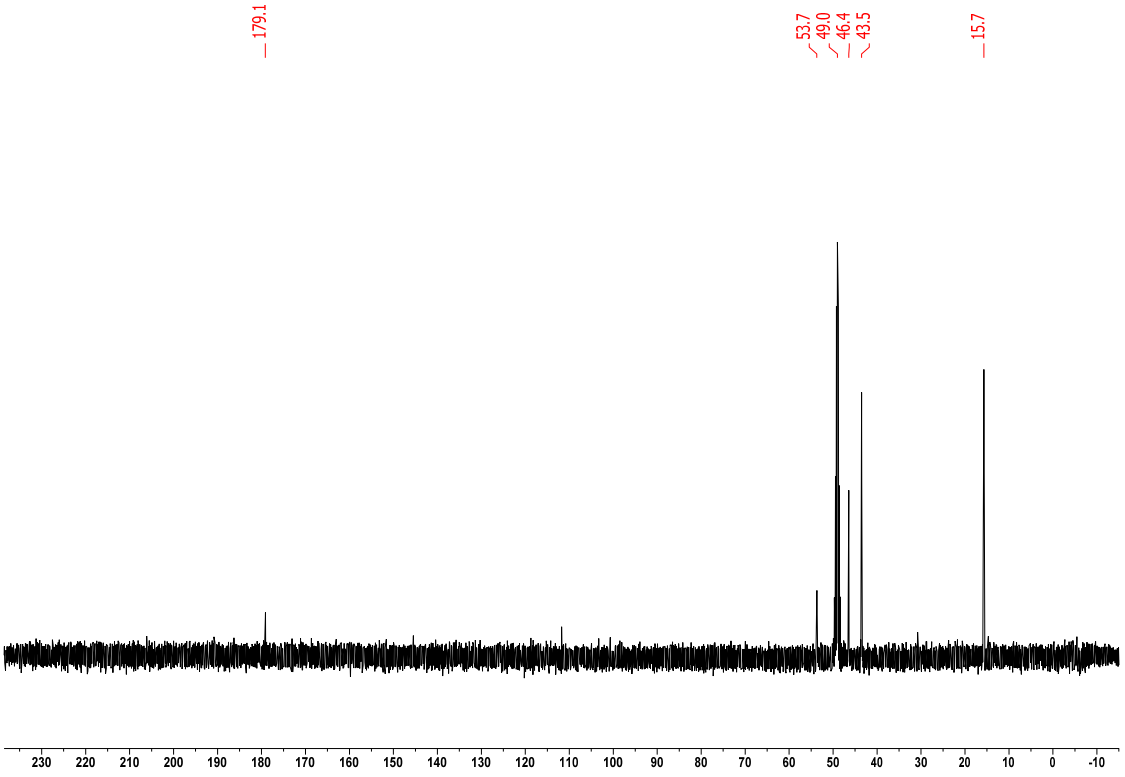

gHSQC NMR (400 MHz) CD_3OD

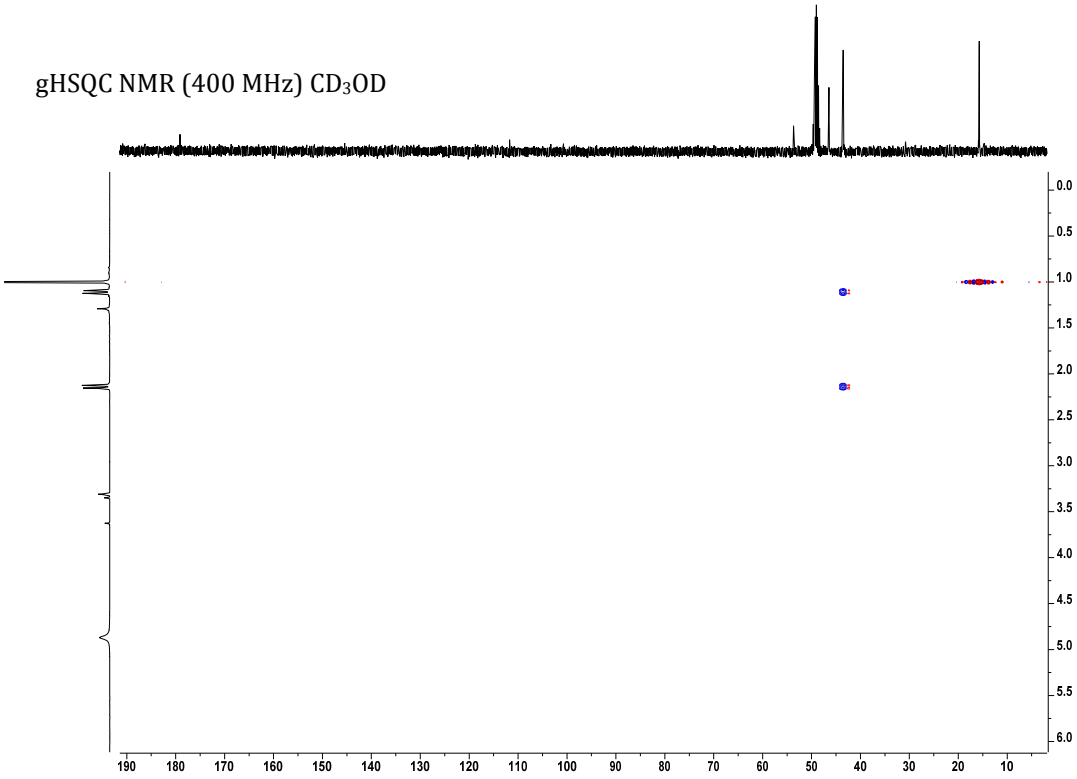

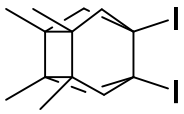

3

^{1}H NMR (400 MHz) $CDCl_3$

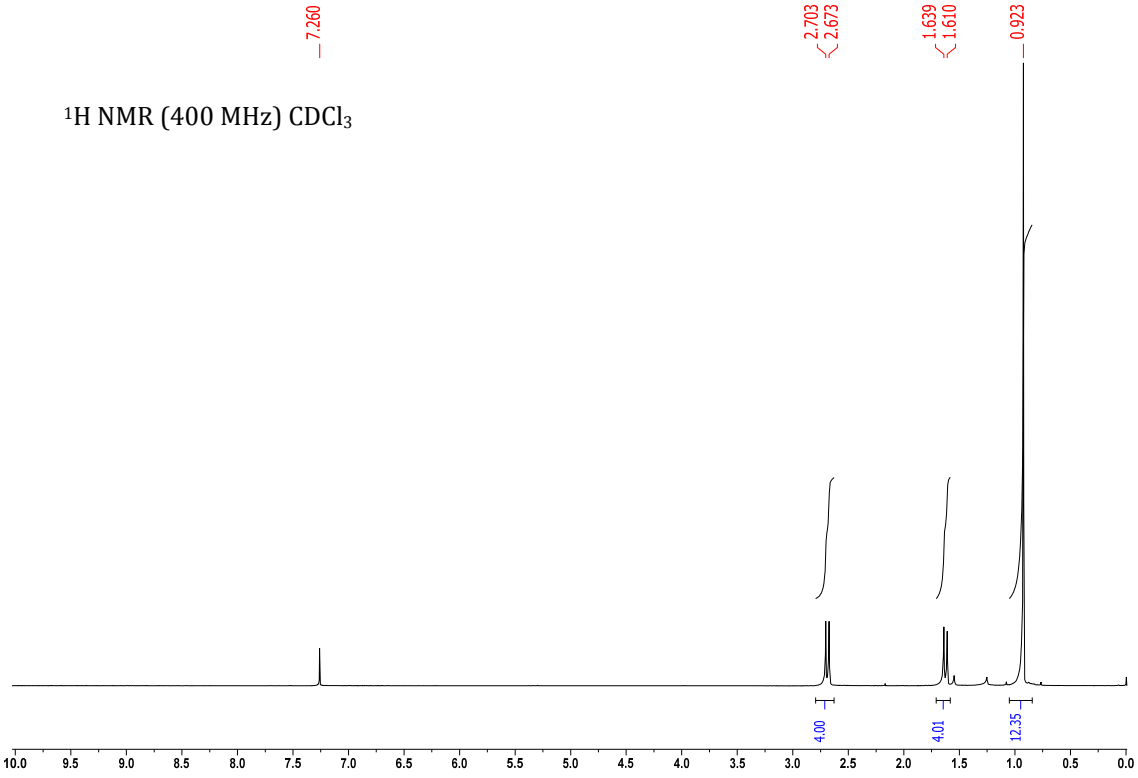

^{13}C NMR (400 MHz) $CDCl_3$

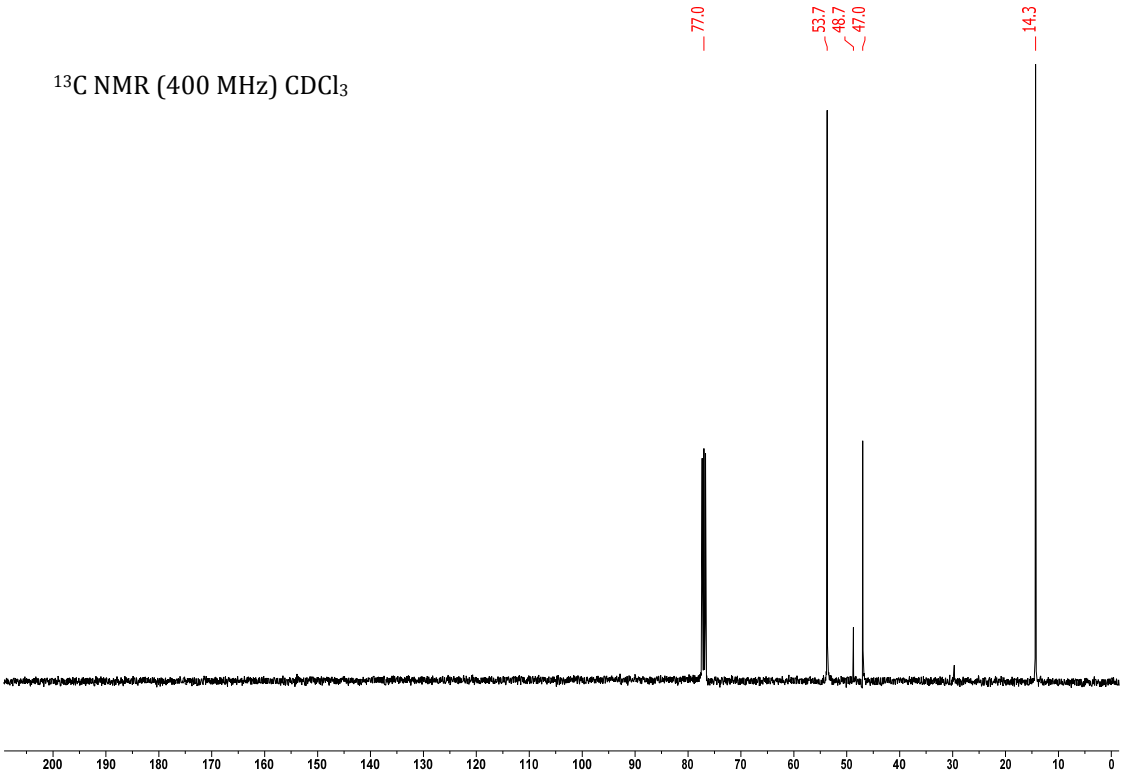

gHSQC NMR (400 MHz) $CDCl_3$

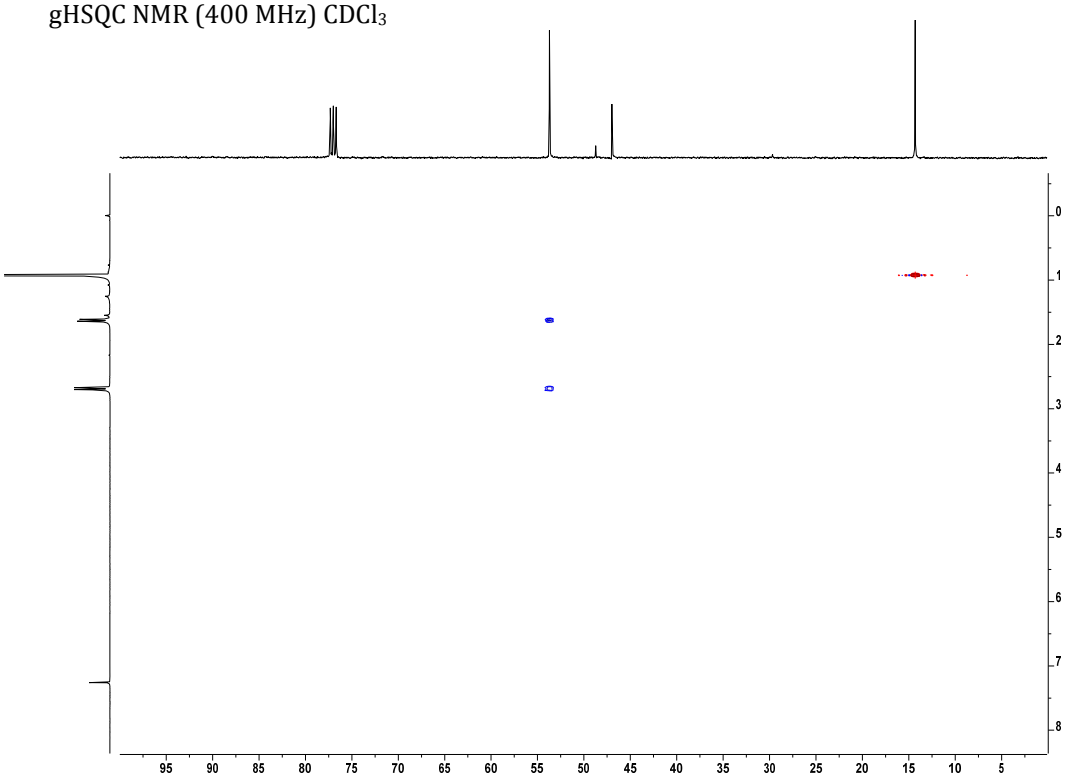

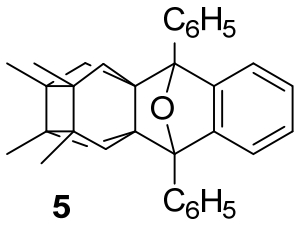

5

^{1}H NMR (500 MHz) $CDCl_3$

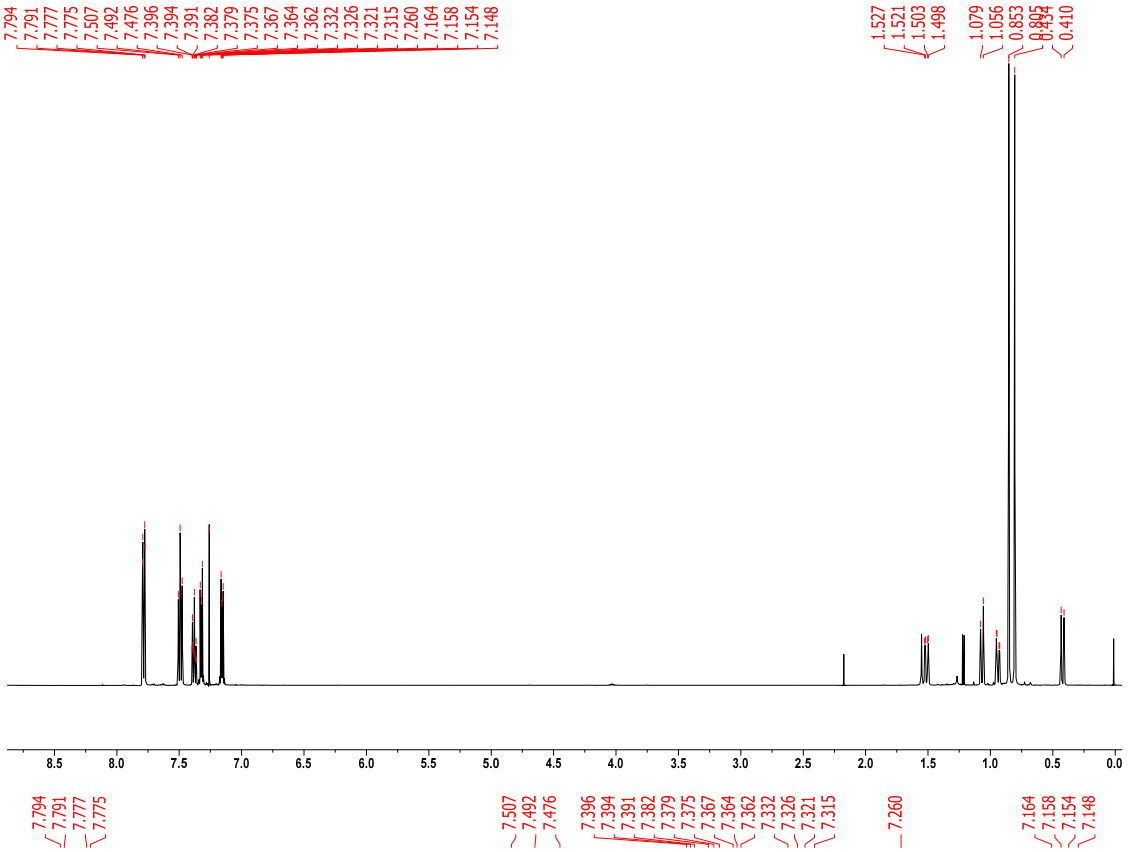

^{1}H NMR (500 MHz) $CDCl_3$

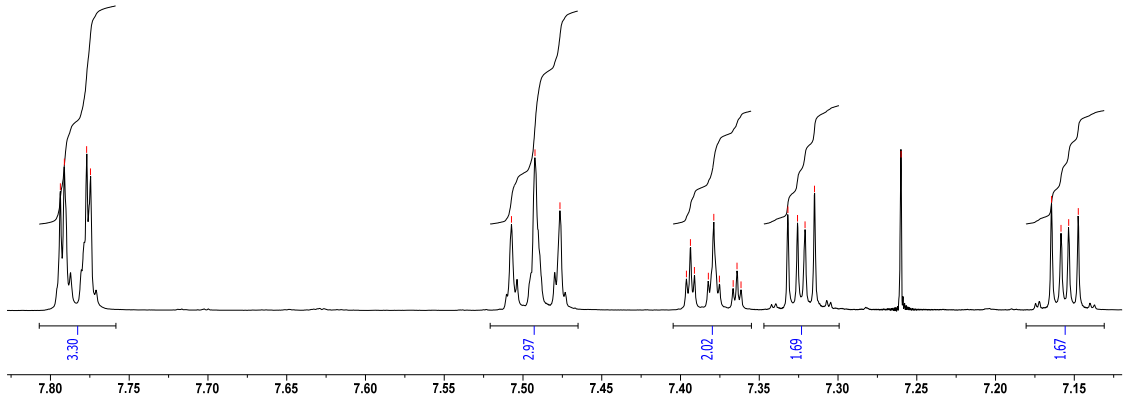

^{1}H NMR (500 MHz) $CDCl_3$

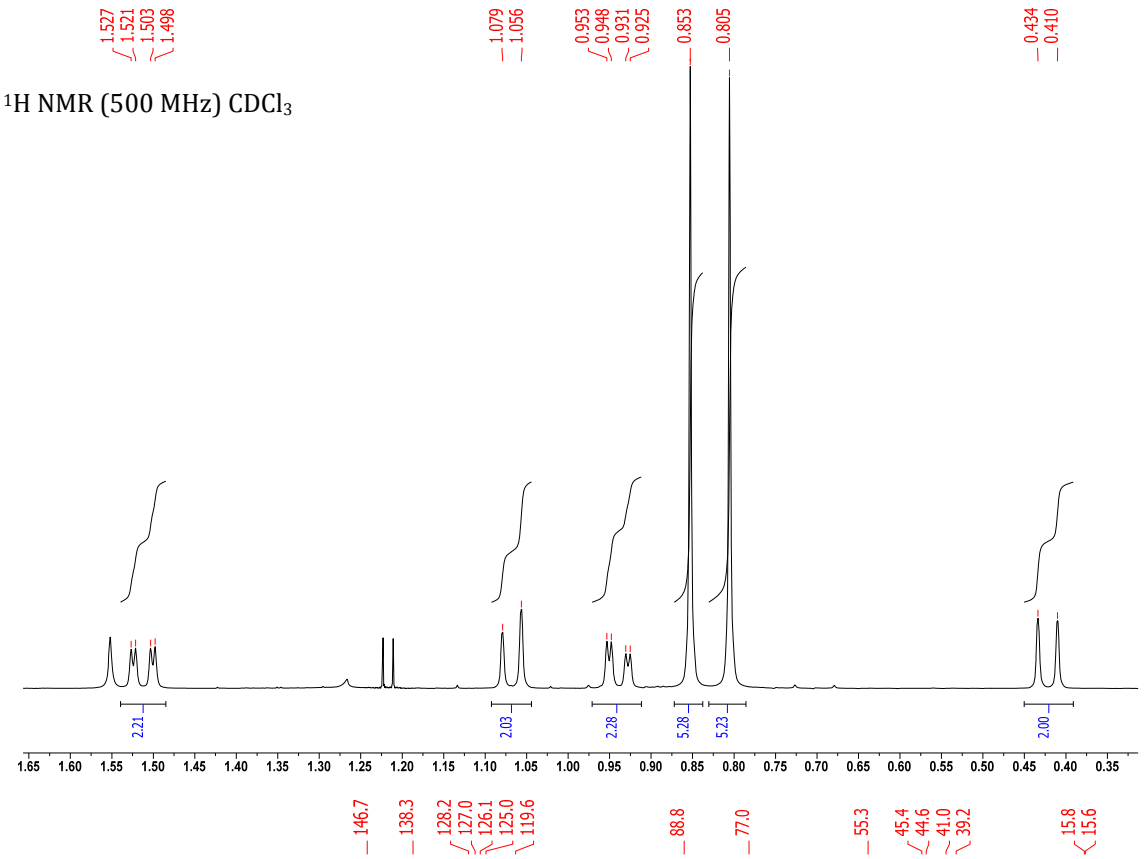

^{13}C NMR (500 MHz) $CDCl_3$

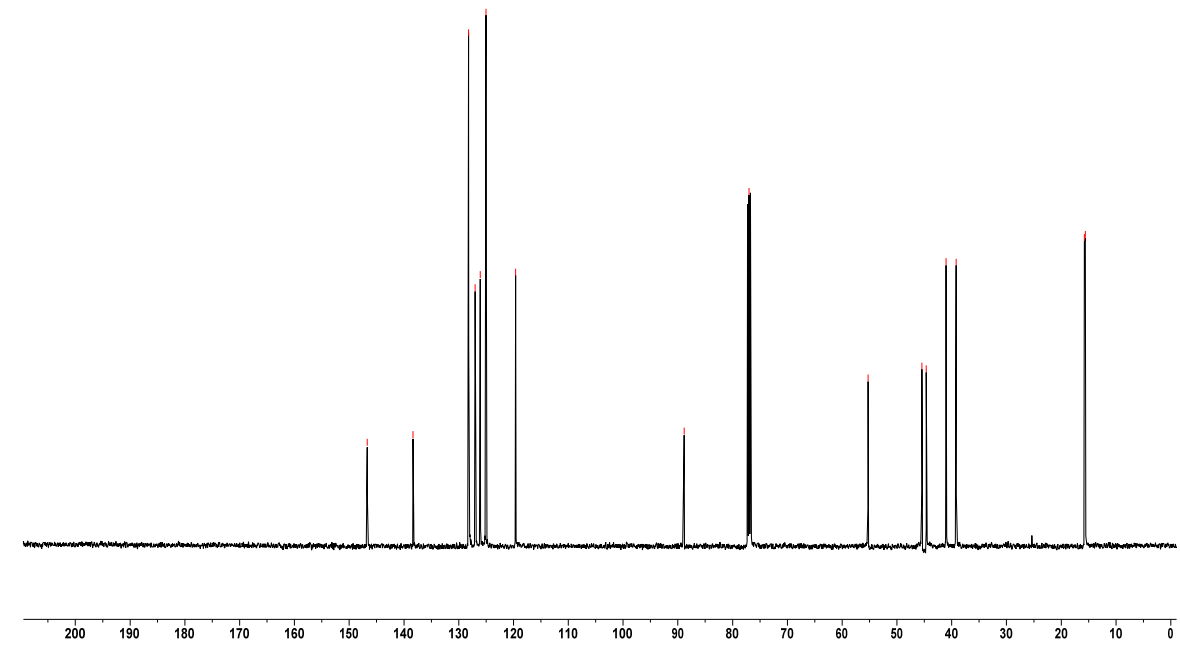

gCOSY NMR (500 MHz) $CDCl_3$

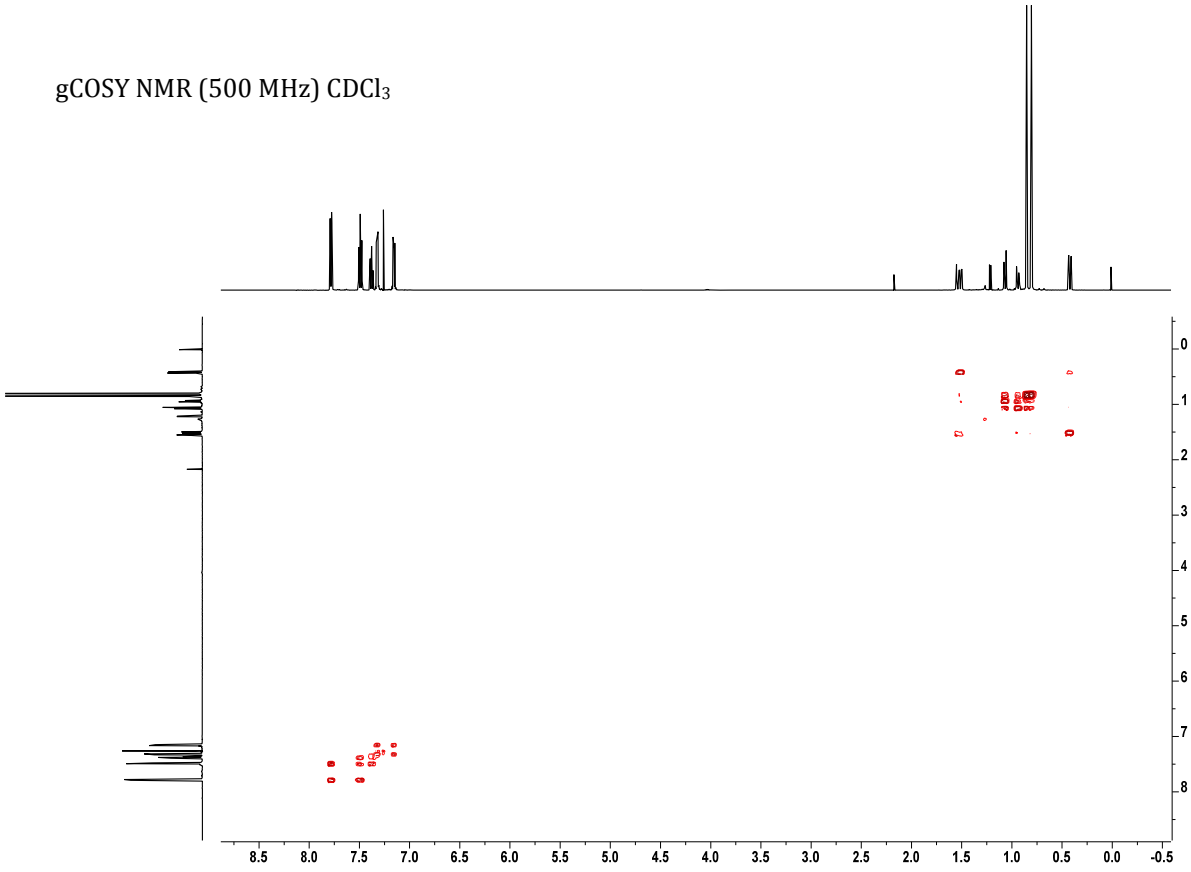

gCOSY NMR (500 MHz) $CDCl_3$

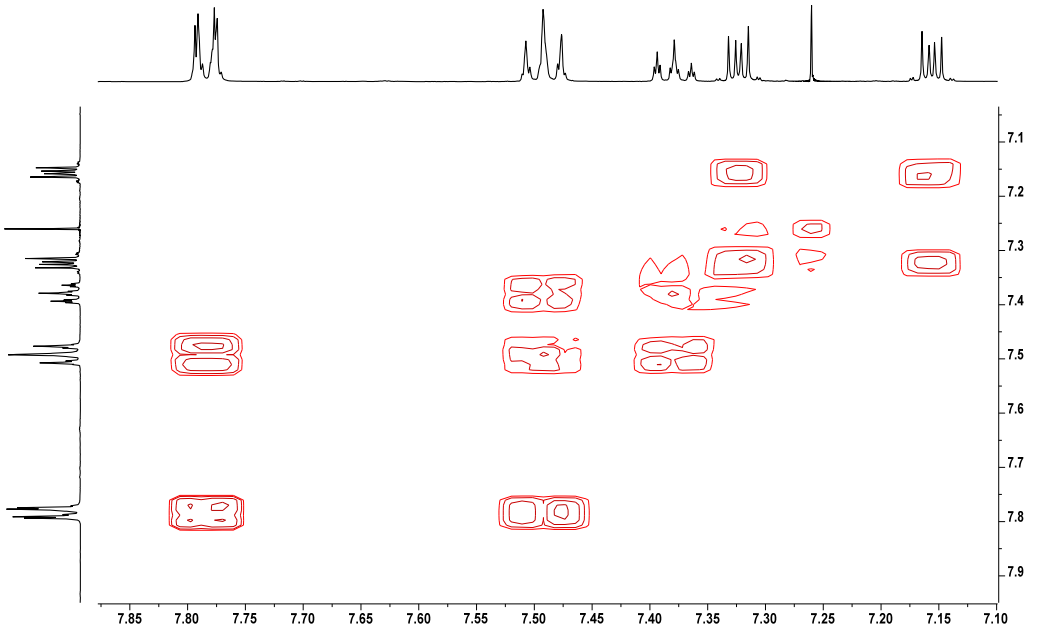

gCOSY NMR (500 MHz) $CDCl_3$

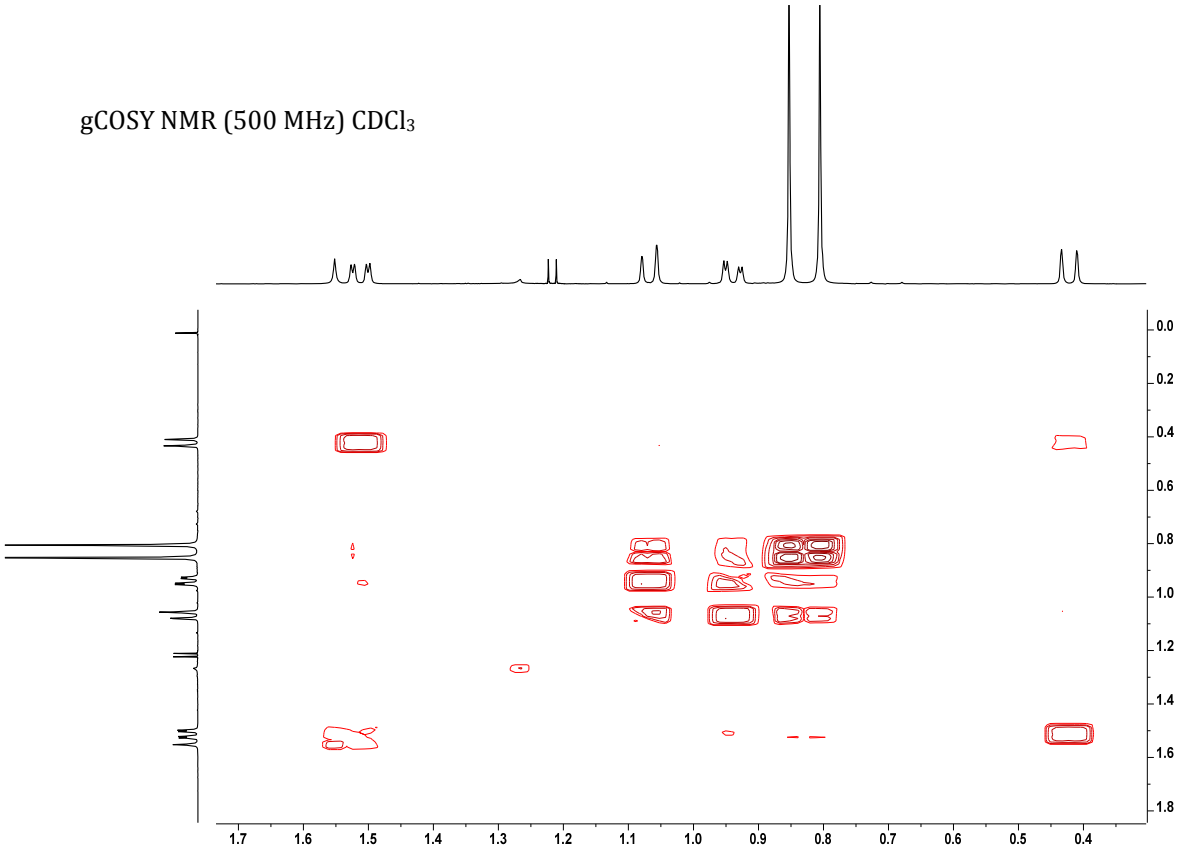

gHSQC NMR (500 MHz) $CDCl_3$

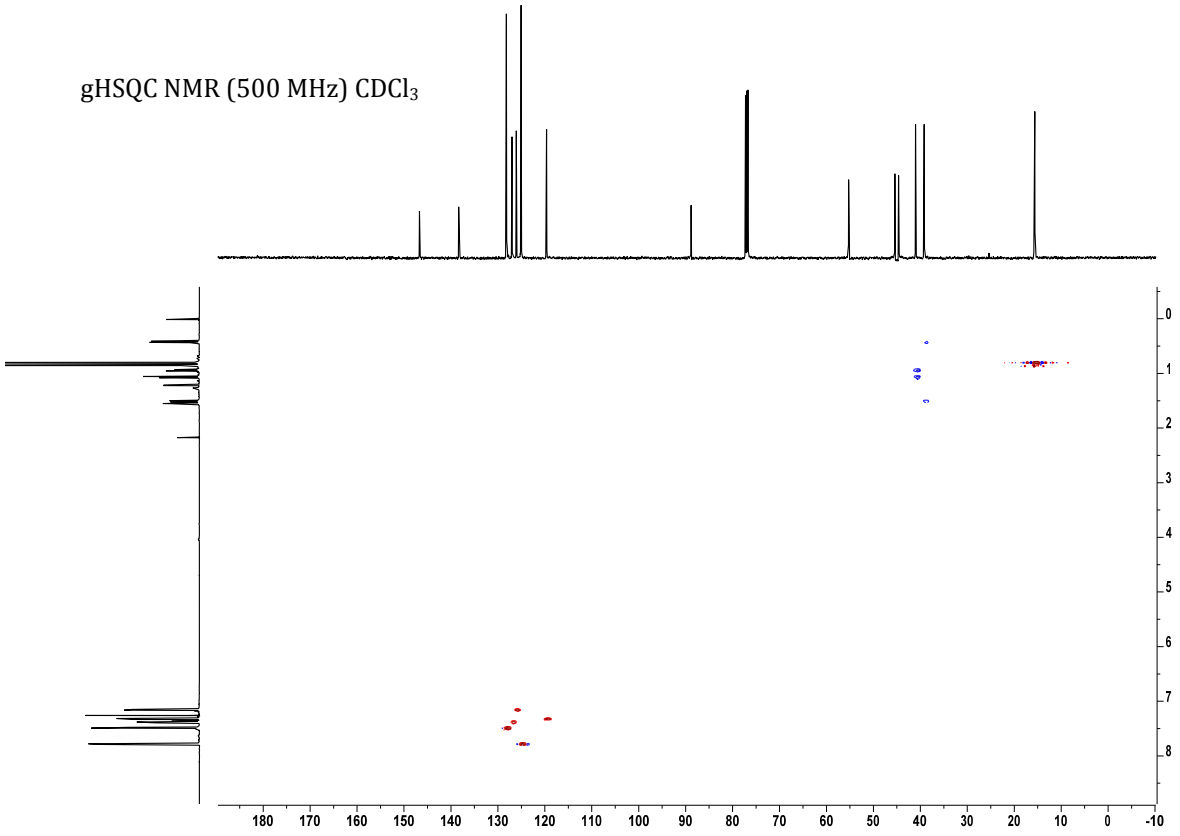

gHSQC NMR (500 MHz) $CDCl_3$

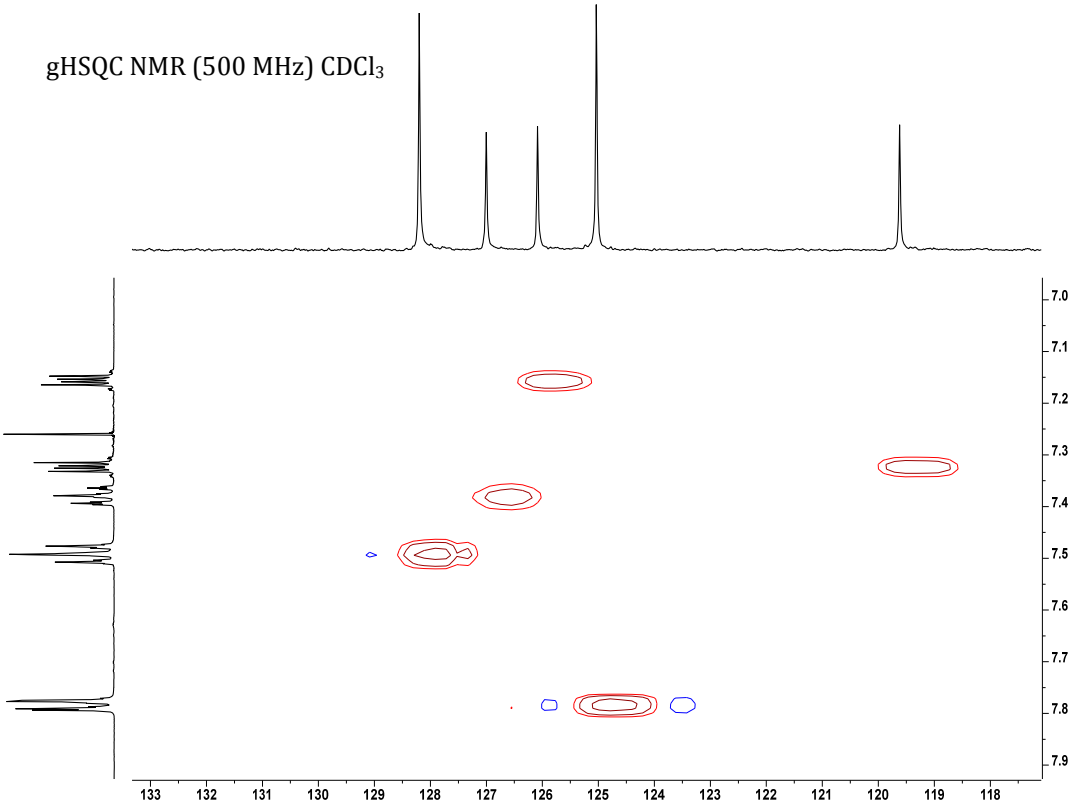

gHSQC NMR (500 MHz) $CDCl_3$

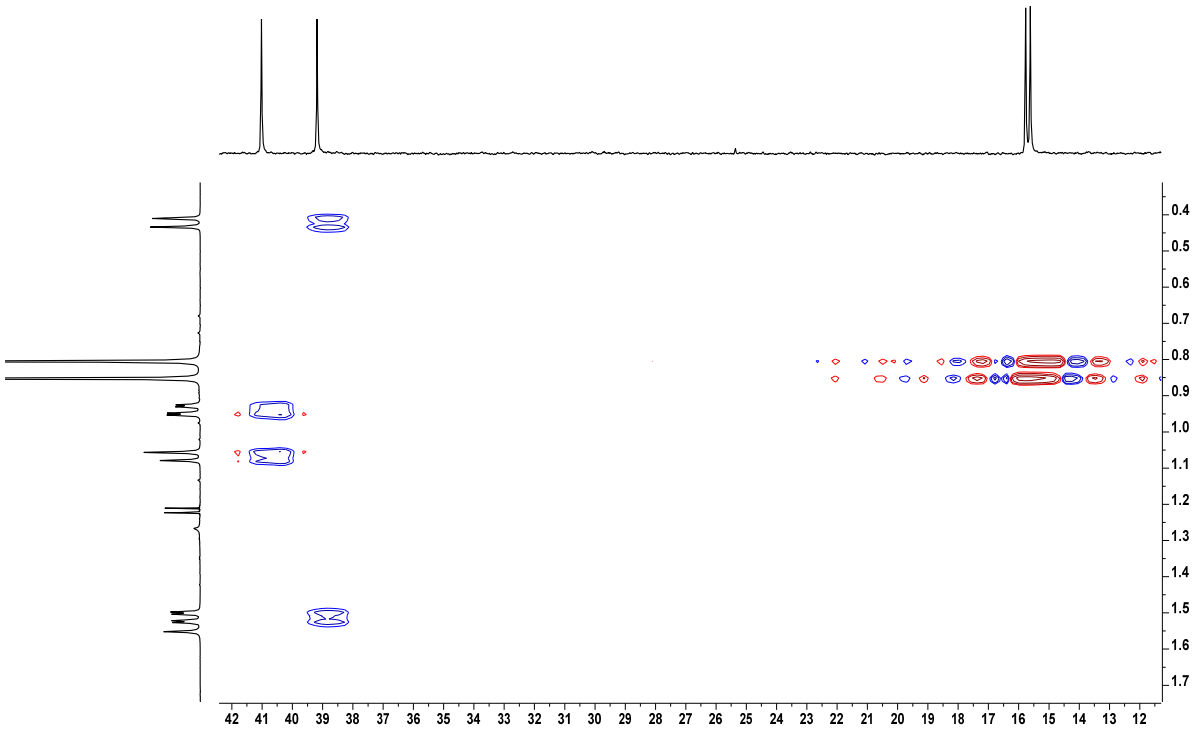

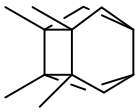

6

^{1}H NMR (400 MHz) $CDCl_3$

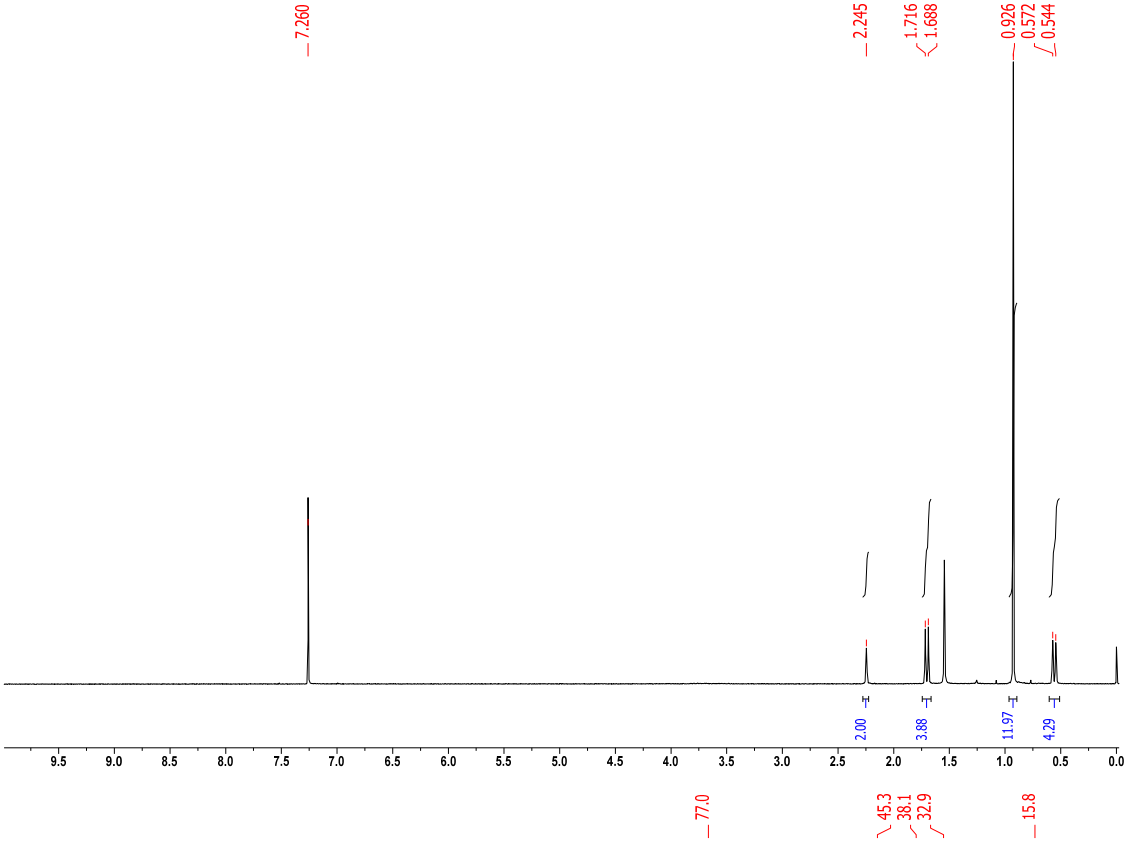

^{13}C NMR (400 MHz) $CDCl_3$

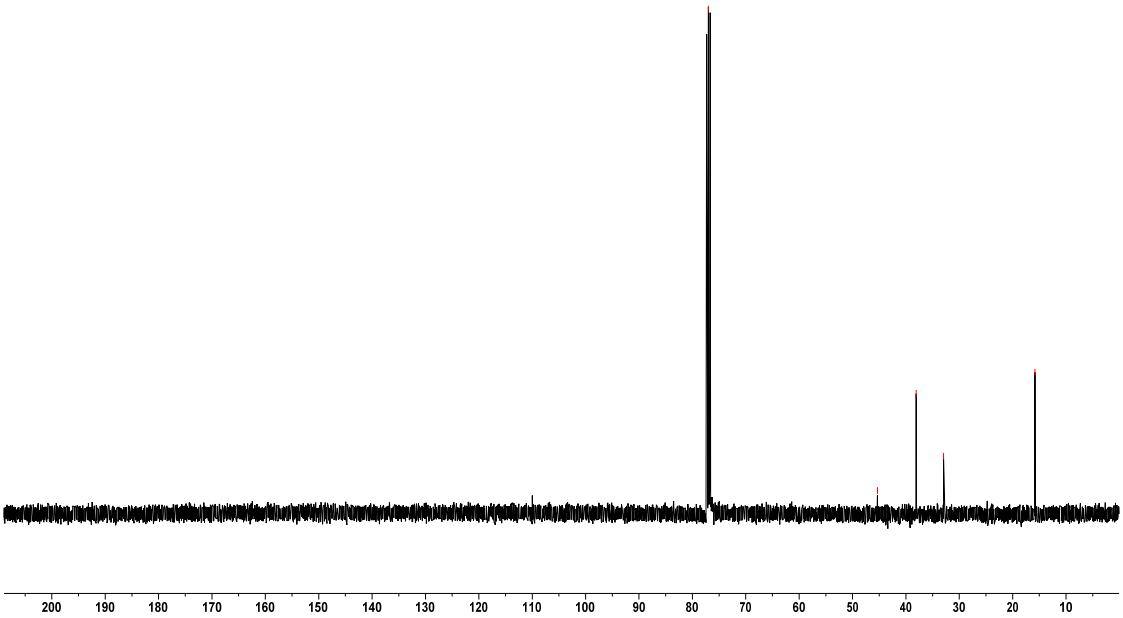

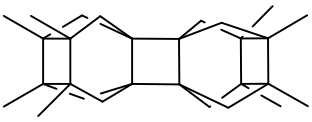

7

^{1}H NMR (400 MHz) $CDCl_3$

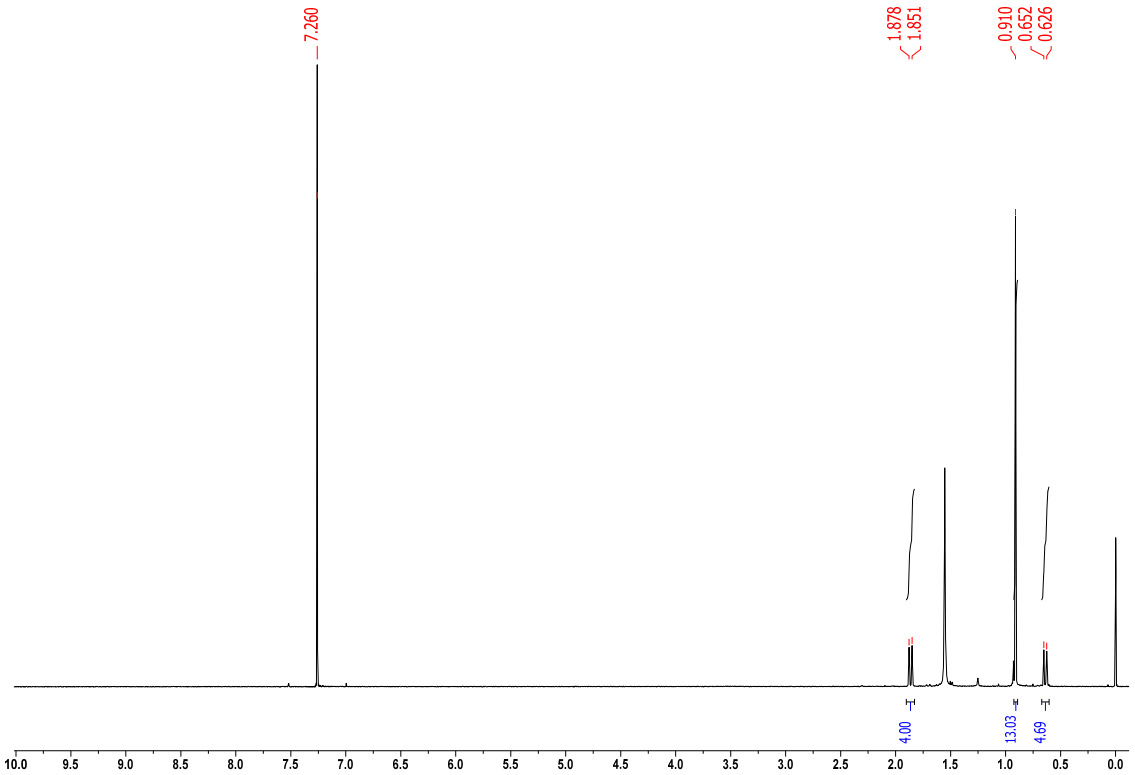

^{13}C NMR (400 MHz) $CDCl_3$

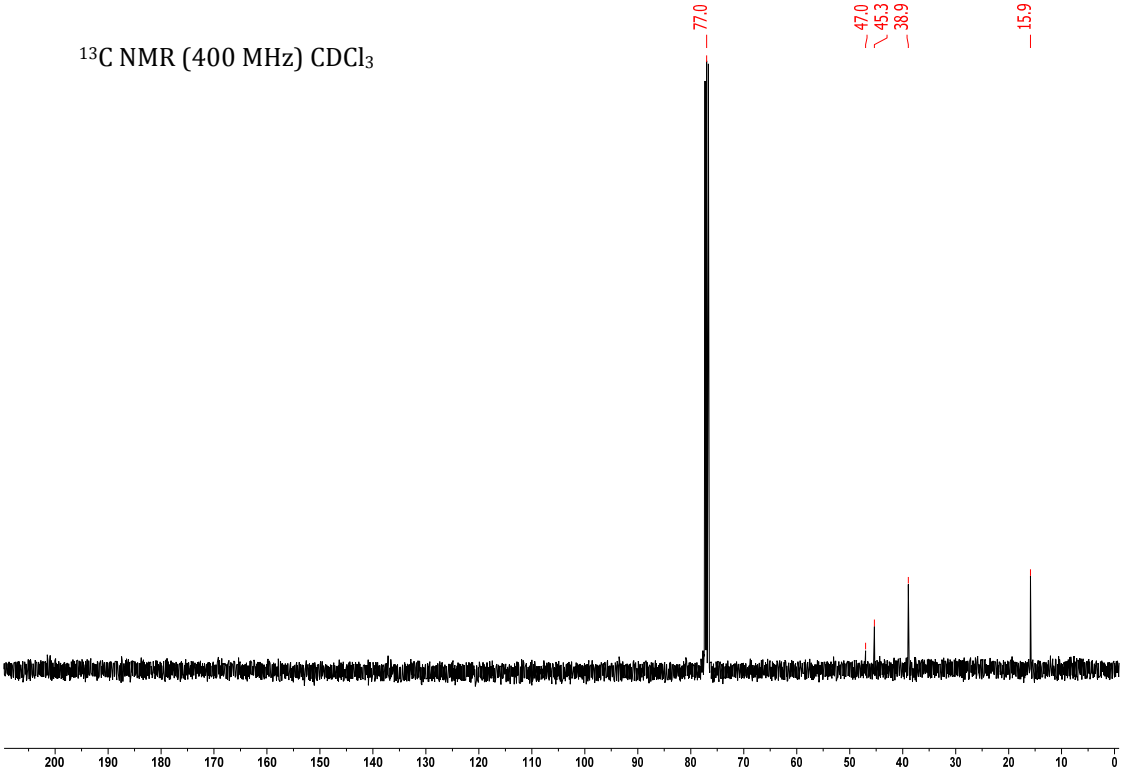

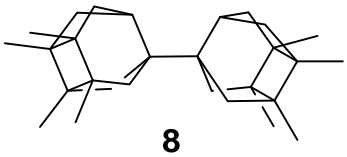

8

^{1}H NMR (400 MHz) $CDCl_3$

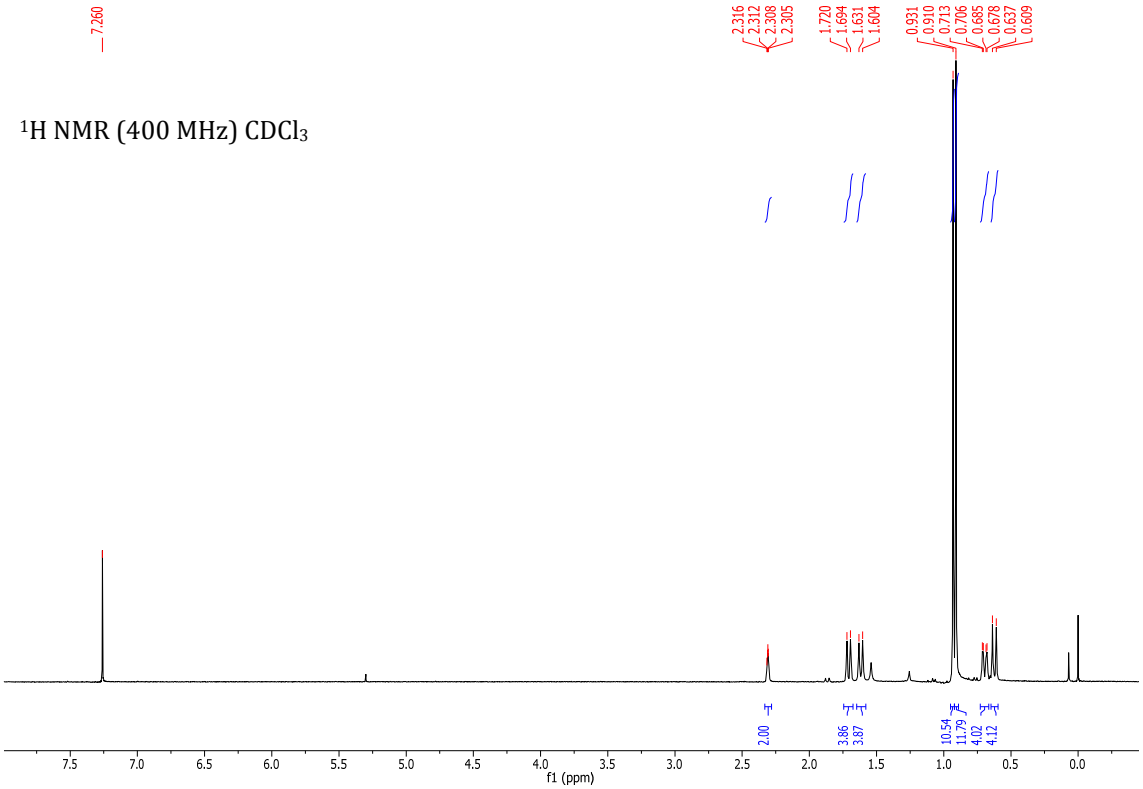

^{1}H NMR (400 MHz) $CDCl_3$

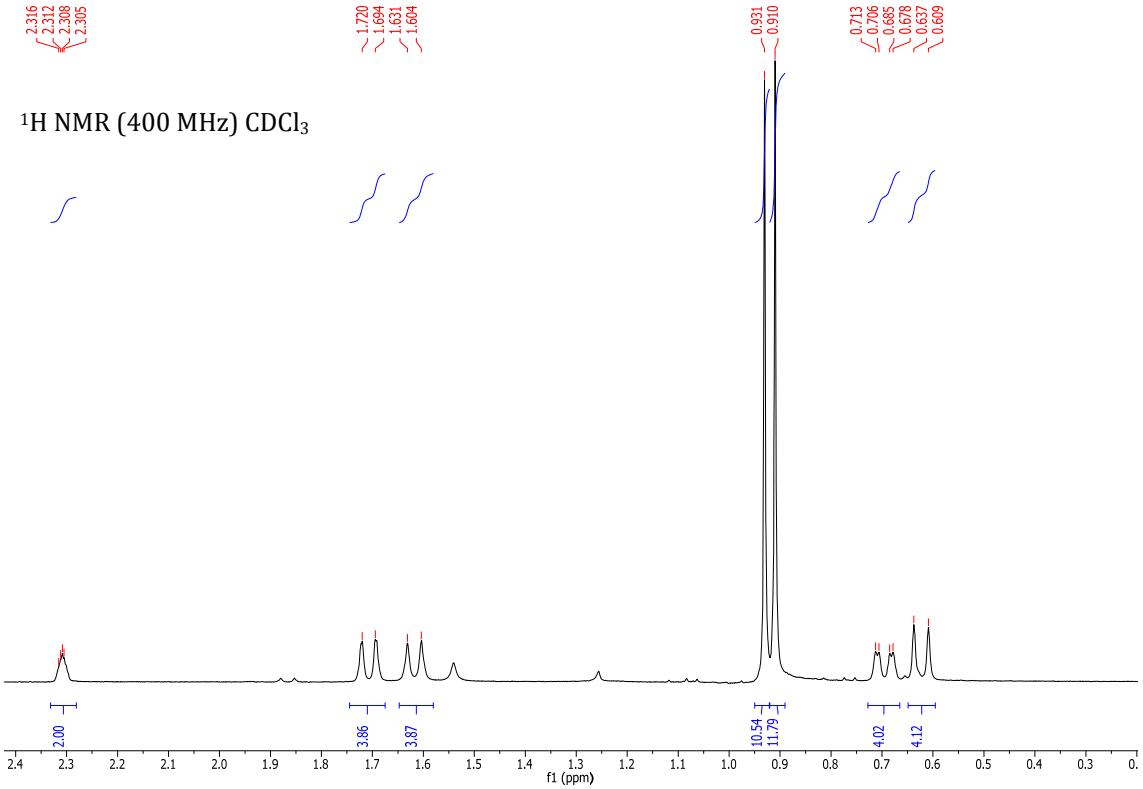

^{13}C NMR (400 MHz) $CDCl_3$

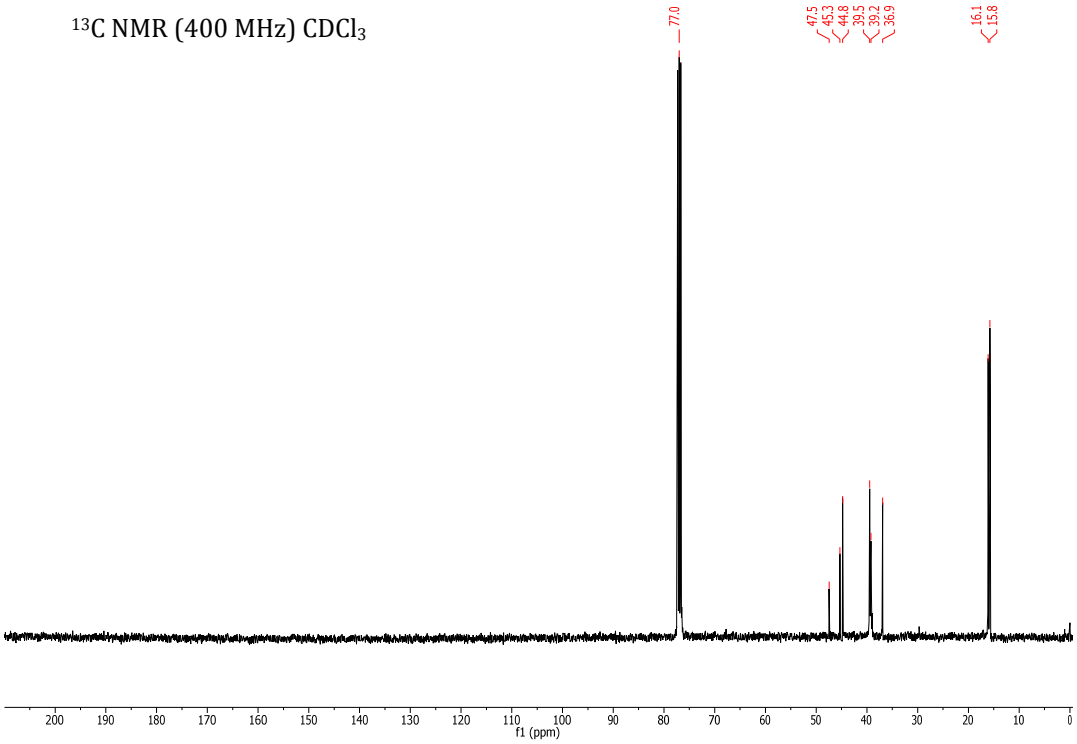

^{13}C NMR (400 MHz) $CDCl_3$

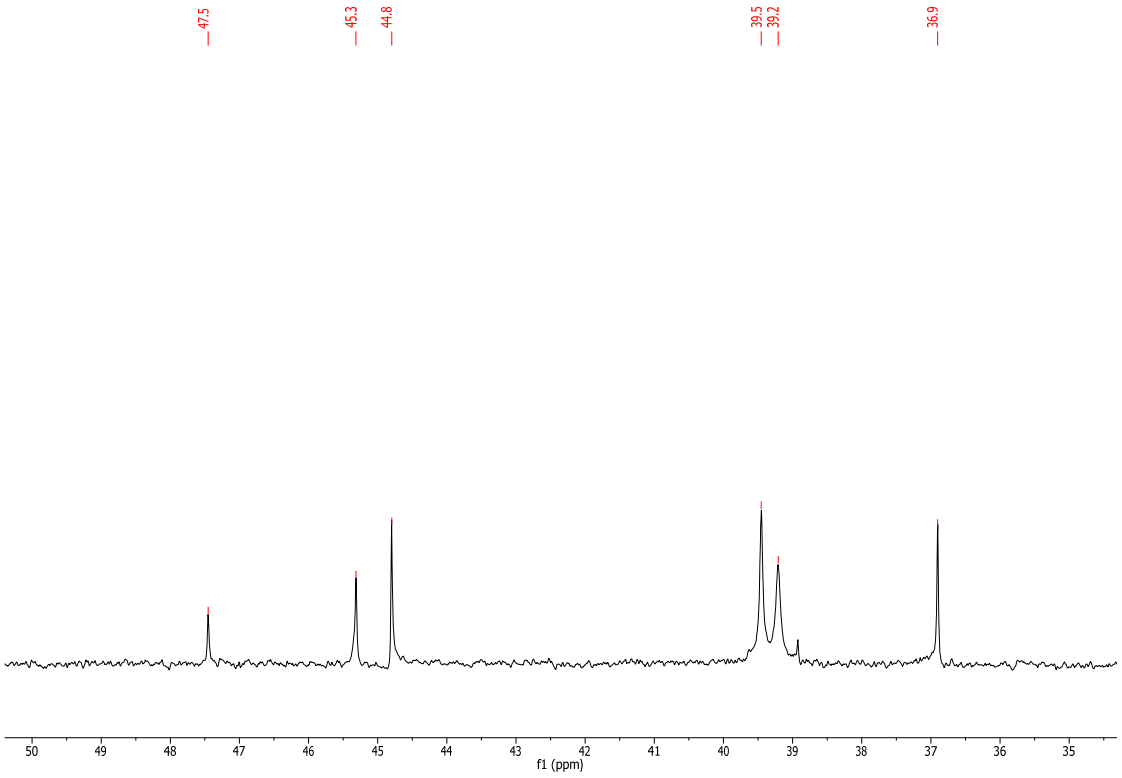

gHSQC NMR (400 MHz) $CDCl_3$

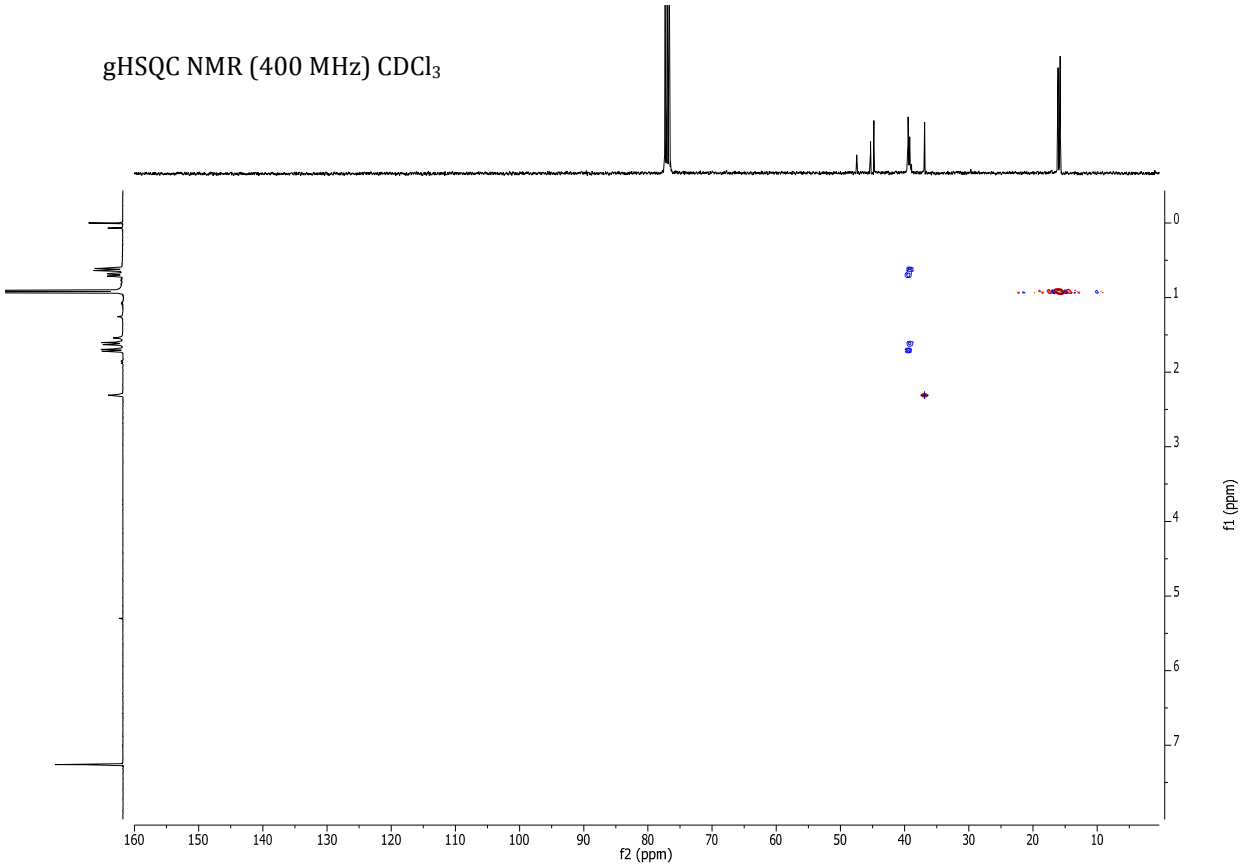

gHSQC NMR (400 MHz) $CDCl_3$

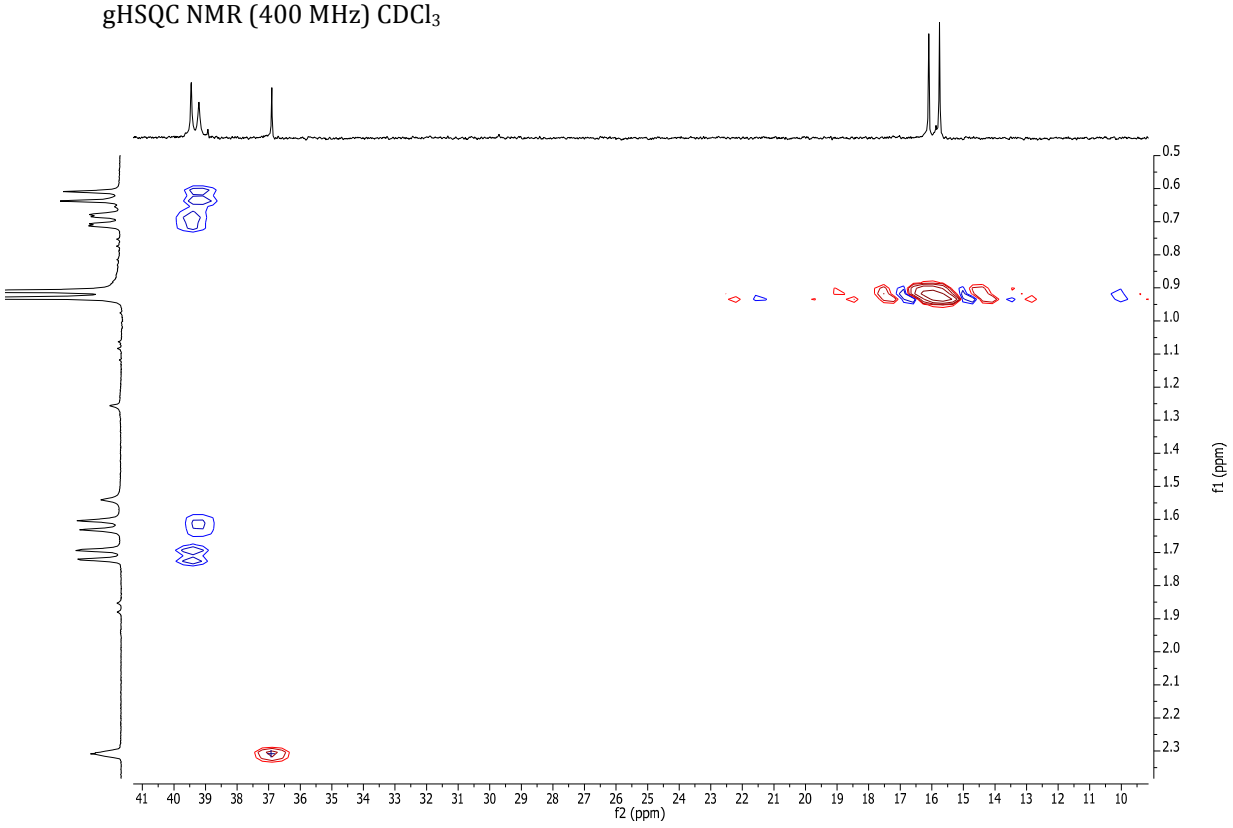

X-Ray crystallographic data

Crystal Structure Report for **1**

A translucent colourless plate-like specimen of $C_{16}H_{20}O_3$, approximate dimensions 0.127 mm x 0.199 mm x 0.572 mm, was used for the X-ray crystallographic analysis. The X-ray intensity data were measured on a D8 Venture system equipped with a Multilayer monochromator and a Mo microfocus (λ = 0.71073 Å).

A total of 996 frames were collected. The total exposure time was 2.77 hours. The frames were integrated with the Bruker SAINT software package using a narrow-frame algorithm. The integration of the data using a monoclinic unit cell yielded a total of 30388 reflections to a maximum θ angle of 32.27° (0.67 Å resolution), of which 4221 were independent (average redundancy 7.199, completeness = 88.5%, R_{int} = 5.54%) and 3149 (74.60%) were greater than $2\sigma(F^2)$. The final cell constants of a = 10.719(8) Å, b =11.141(8) Å, c = 11.248(10) Å, β = 91.317(3)°, volume = 1342.8(18) $Å^3$, are based upon the refinement of the XYZ-centroids of 117 reflections above 20 σ(I) with 5.306° < 2θ < 46.95°. Data were corrected for absorption effects using the multi-scan method (SADABS). The ratio of minimum to maximum apparent transmission was 0.850.

The structure was solved and refined using the Bruker SHELXTL Software Package, with Z = 4 for the formula unit, $C_{16}H_{20}O_3$. The final anisotropic full-matrix least-squares refinement on F^2 with 200 variables converged at R1 = 4.69%, for the observed data and wR2 = 12.18% for all data. The goodness-of-fit was 1.059. The largest peak in the final difference electron density synthesis was 0.407 $e^-/Å^3$ and the largest hole was -0.263 $e^-/Å^3$ with an RMS deviation of 0.058 $e^-/Å^3$. On the basis of the final model, the calculated density was 1.288 g/cm^3 and F(000), 560 e^-.

8 H atoms were located from a difference synthesis and refined with an isotropic temperature factor equal to 1.2 time the equivalent temperature factor of the atom which are linked and 12 H atoms were computed and refined, using a riding model, with an isotropic temperature factor equal to 1.2 time the equivalent temperature factor of the atom which are linked.

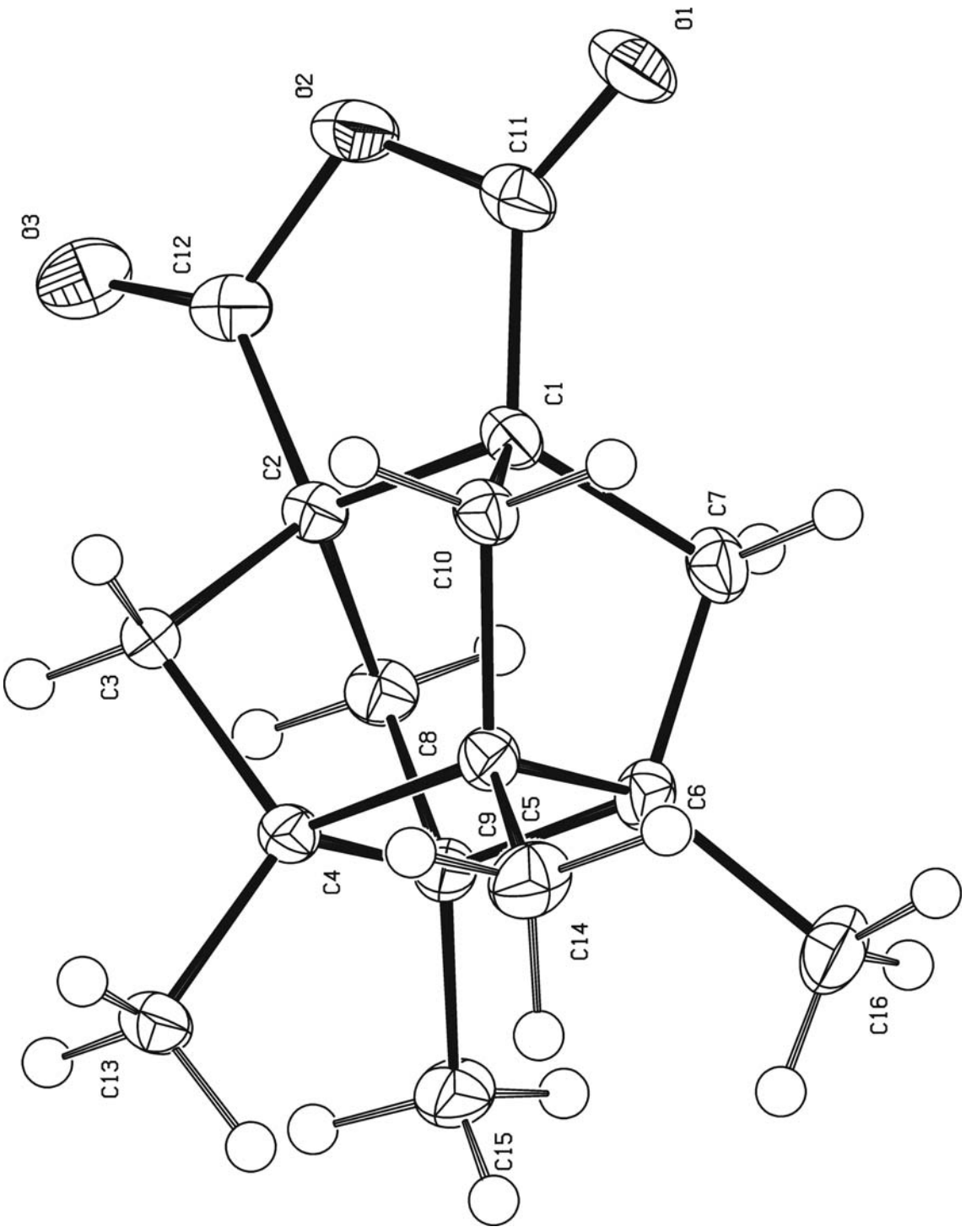
O1
O2
C11
O3
C12
C1
C2
C7
C10
C3
C8
C6
C9
C5
C4
C14
C16
C13
C15

Crystal Structure Report for **3**

A colourless prism-like specimen of $C_{14}H_{20}I_2$, approximate dimensions 0.128 mm x 0.233 mm x 0.445 mm, was used for the X-ray crystallographic analysis. The X-ray intensity data were measured on a D8 Venture system equipped with a multilayer monochromator and a Mo microfocus (λ = 0.71073 Å).

The frames were integrated with the Bruker SAINT software package using a narrow-frame algorithm. The integration of the data using an orthorhombic unit cell yielded a total of 20838 reflections to a maximum θ angle of 36.46° (0.60 Å resolution), of which 3683 were independent (average redundancy 5.658, completeness = 99.2%, R_{int} = 4.90%) and 2963 (80.45%) were greater than $2\sigma(F^2)$.The final cell constants of a = 13.9848(17) Å, b = 10.6099(13) Å, c = 9.7845(12) Å, volume = 1451.8(3) $Å^3$, are based upon the refinement of the XYZ-centroids of reflections above 20 σ(I).Data were corrected for absorption effects using the multi-scan method (SADABS). The ratio of minimum to maximum apparent transmission was 0.723. The calculated minimum and maximum transmission coefficients (based on crystal size) are 0.5401 and 0.7471.

The structure was solved and refined using the Bruker SHELXTL Software Package, using the space group P n m a, with Z = 4 for the formula unit, $C_{14}H_{20}I_2$.The final anisotropic full-matrix least-squares refinement on F^2 with 93 variables converged at R1 = 4.82%, for the observed data and wR2 = 9.80% for all data. The goodness-of-fit was 1.119. The largest peak in the final difference electron density synthesis was 2.474 $e^-/Å^3$ and the largest hole was -2.274 $e^-/Å^3$ with an RMS deviation of 0.229 $e^-/Å^3$. On the basis of the final model, the calculated density was 2.023 g/cm^3 and F(000), 840 e^-.

4 H atoms were located from a difference synthesis and refined with an isotropic temperature factor equal to 1.2 time the equivalent temperature factor of the atom which are linked and 12 H atoms were computed and refined, using a riding model, with an isotropic temperature factor equal to 1.2 time the equivalent temperature factor of the atom which are linked.

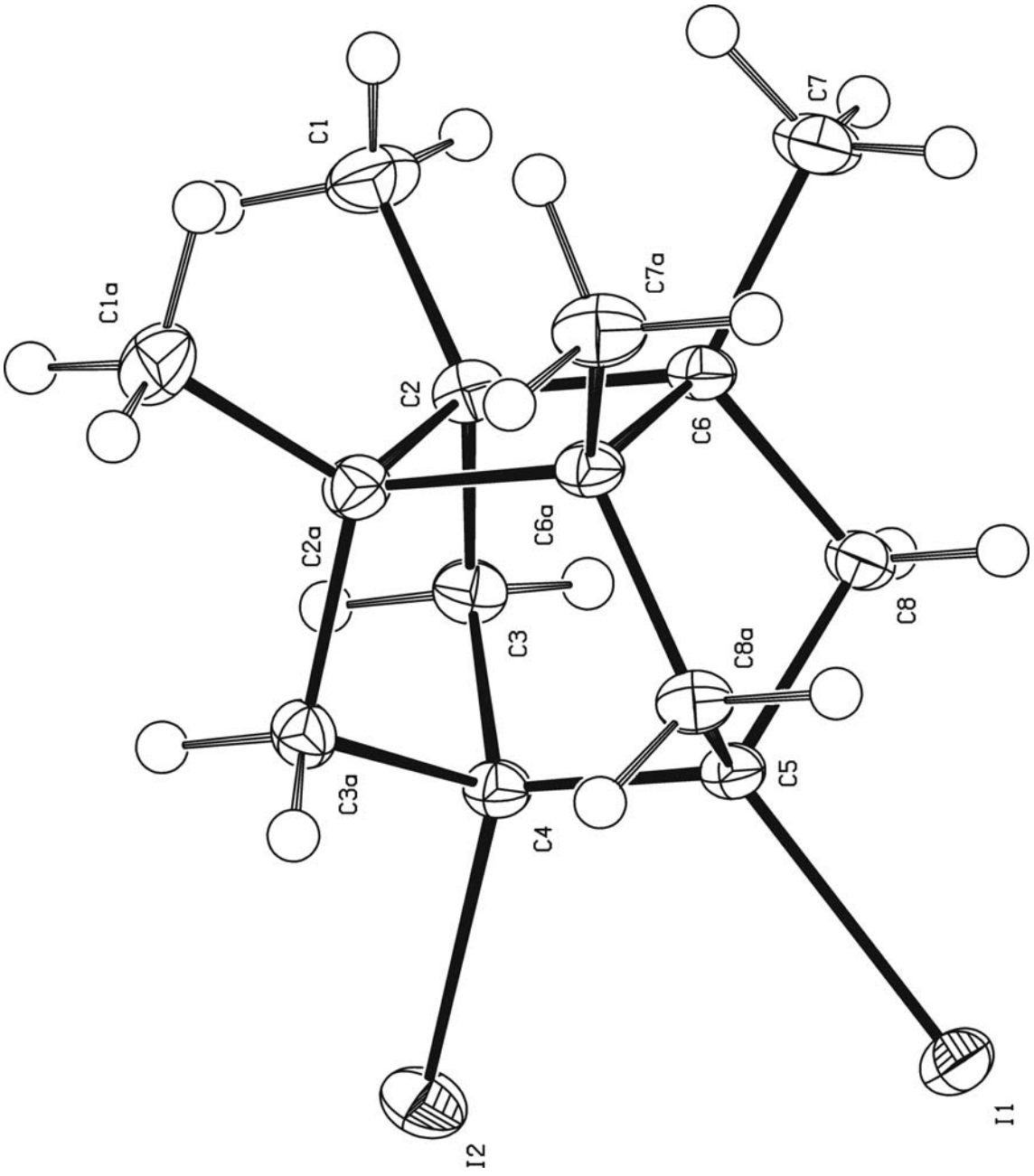
C1
C7
C1a
C7a
C2
C6
C2a
C6a
C8
C3
C8a
C3a
C5
C4
I2
I1

Crystal Structure Report for **5**

A colourless prism-like specimen of $C_{69}H_{70}Cl_2O_2$, approximate dimensions 0.222 mm x 0.298 mm x 0.984 mm, was used for the X-ray crystallographic analysis.The X-ray intensity data were measured on a D8 Venture system equipped with a multilayer monochromator and a Mo microfocus (λ = 0.71073 Å).

The frames were integrated with the Bruker SAINT software package using a narrow-frame algorithm. The integration of the data using a triclinic unit cell yielded a total of 113338 reflections to a maximum θ angle of 28.40° (0.75 Å resolution), of which 13323 were independent (average redundancy 8.507, completeness = 99.1%, R_{int} = 6.14%) and 10532 (79.05%) were greater than $2\sigma(F^2)$.The final cell constants of a = 10.8026(17) Å, b = 13.731(2) Å, c = 20.089(3) Å, α = 78.918(7)°, β = 74.852(7)°, γ = 69.502(7)°, volume = 2677.5(7) $Å^3$, are based upon the refinement of the XYZ-centroids of reflections above 20 σ(I).Data were corrected for absorption effects using the multi-scan method (SADABS). The ratio of minimum to maximum apparent transmission was 0.899. The calculated minimum and maximum transmission coefficients (based on crystal size) are 0.6706 and 0.7457.

The structure was solved and refined using the Bruker SHELXTL Software Package, using the space group P -1, with Z = 2 for the formula unit, $C_{69}H_{70}Cl_2O_2$.The final anisotropic full-matrix least-squares refinement on F^2 with 836 variables converged at R1 = 5.14%, for the observed data and wR2 = 12.87% for all data. The goodness-of-fit was 1.028. The largest peak in the final difference electron density synthesis was 1.465 $e^-/Å^3$ and the largest hole was -1.517 $e^-/Å^3$ with an RMS deviation of 0.062 $e^-/Å^3$. On the basis of the final model, the calculated density was 1.243 g/cm^3 and F(000), 1068 e^-.

58 H atoms were located from a difference synthesis and refined with an isotropic temperature factor equal to 1.2 time the equivalent temperature factor of the atom which are linked and 12 H atoms were computed and refined, using a riding model, with an isotropic temperature factor equal to 1.2 time the equivalent temperature factor of the atom which are linked.

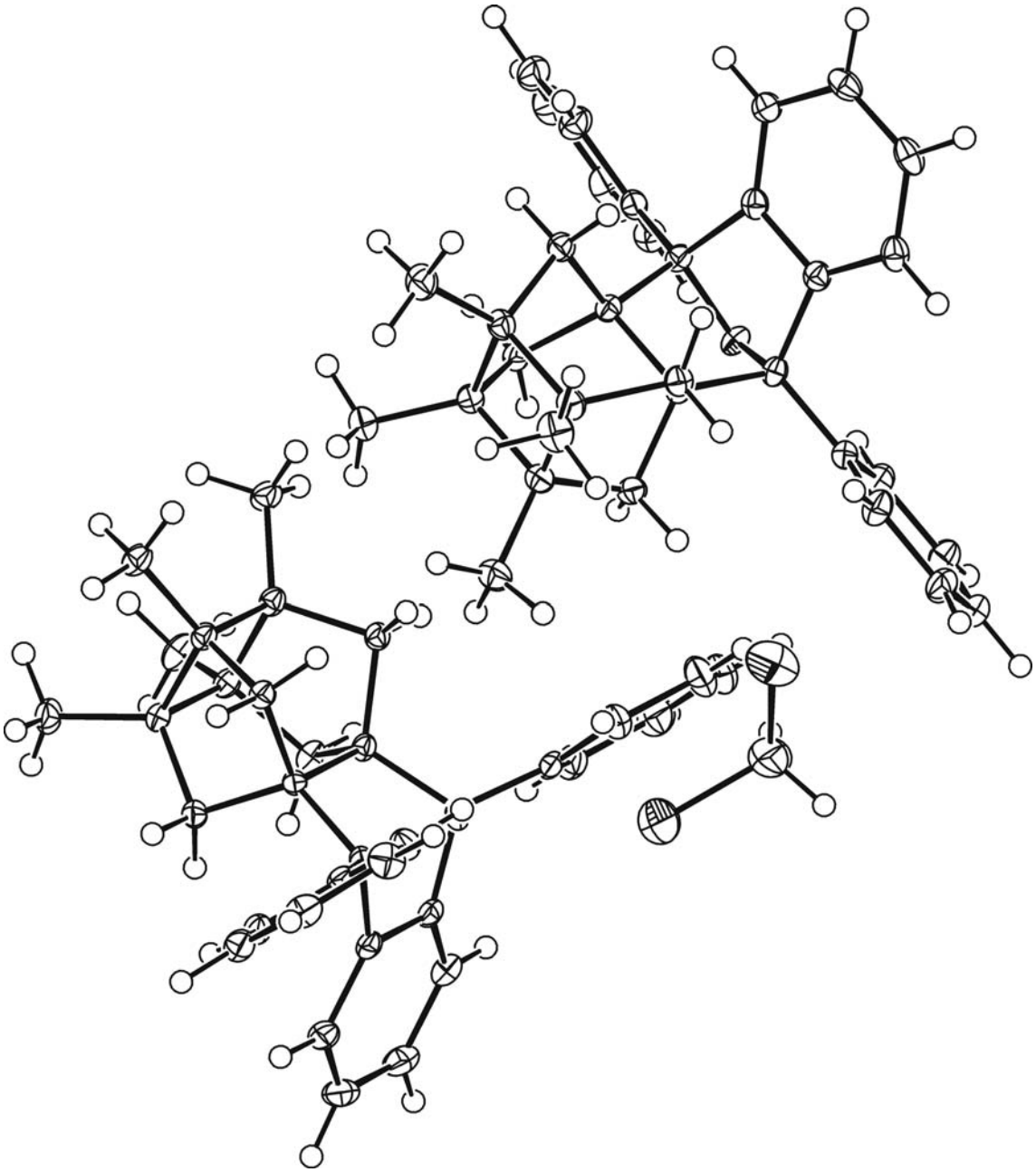

Crystal Structure Report for **7**

A translucent colourless prism-like specimen of $C_{28}H_{40}$, approximate dimensions 0.071 mm x 0.093 mm x 0.109 mm, was used for the X-ray crystallographic analysis. The X-ray intensity data were measured on a D8 Venture system equipped with a Multilayer monochromator and a Mo microfocus (λ = 0.71073 Å).

A total of 1473 frames were collected. The total exposure time was 4.09 hours. The frames were integrated with the Bruker SAINT software package using a narrow-frame algorithm. The integration of the data using a monoclinic unit cell yielded a total of 34804 reflections to a maximum θ angle of 28.57° (0.74 Å resolution), of which 2683 were independent (average redundancy 12.972, completeness = 100.0%, R_{int} = 5.79%) and 2224 (82.89%) were greater than $2\sigma(F^2)$. The final cell constants of $\underline{a}$ = 6.978(6) Å, $\underline{b}$ = 11.110(10) Å, $\underline{c}$ = 14.848(13) Å, β = 113.90(4)°, volume = 1052.4(16) $Å^3$, are based upon the refinement of the XYZ-centroids of 87 reflections above 20 σ(I) with 7.348° < 2θ < 54.87°. Data were corrected for absorption effects using the multi-scan method (SADABS). The ratio of minimum to maximum apparent transmission was 0.955.

The structure was solved and refined using the Bruker SHELXTL Software Package, with Z = 2 for the formula unit, $C_{28}H_{40}$. The final anisotropic full-matrix least-squares refinement on F^2 with 155 variables converged at R1 = 5.13%, for the observed data and wR2 = 14.36% for all data. The goodness-of-fit was 1.065. The largest peak in the final difference electron density synthesis was 0.571 $e^-/Å^3$ and the largest hole was -0.444 $e^-/Å^3$ with an RMS deviation of 0.068 $e^-/Å^3$. On the basis of the final model, the calculated density was 1.188 g/cm^3 and F(000), 416 e^-.

8 H atoms were located from a difference synthesis and refined with an isotropic temperature factor equal to 1.2 time the equivalent temperature factor of the atom which are linked and 12 H atoms were computed and refined, using a riding model, with an isotropic temperature factor equal to 1.2 time the equivalent temperature factor of the atom which are linked.

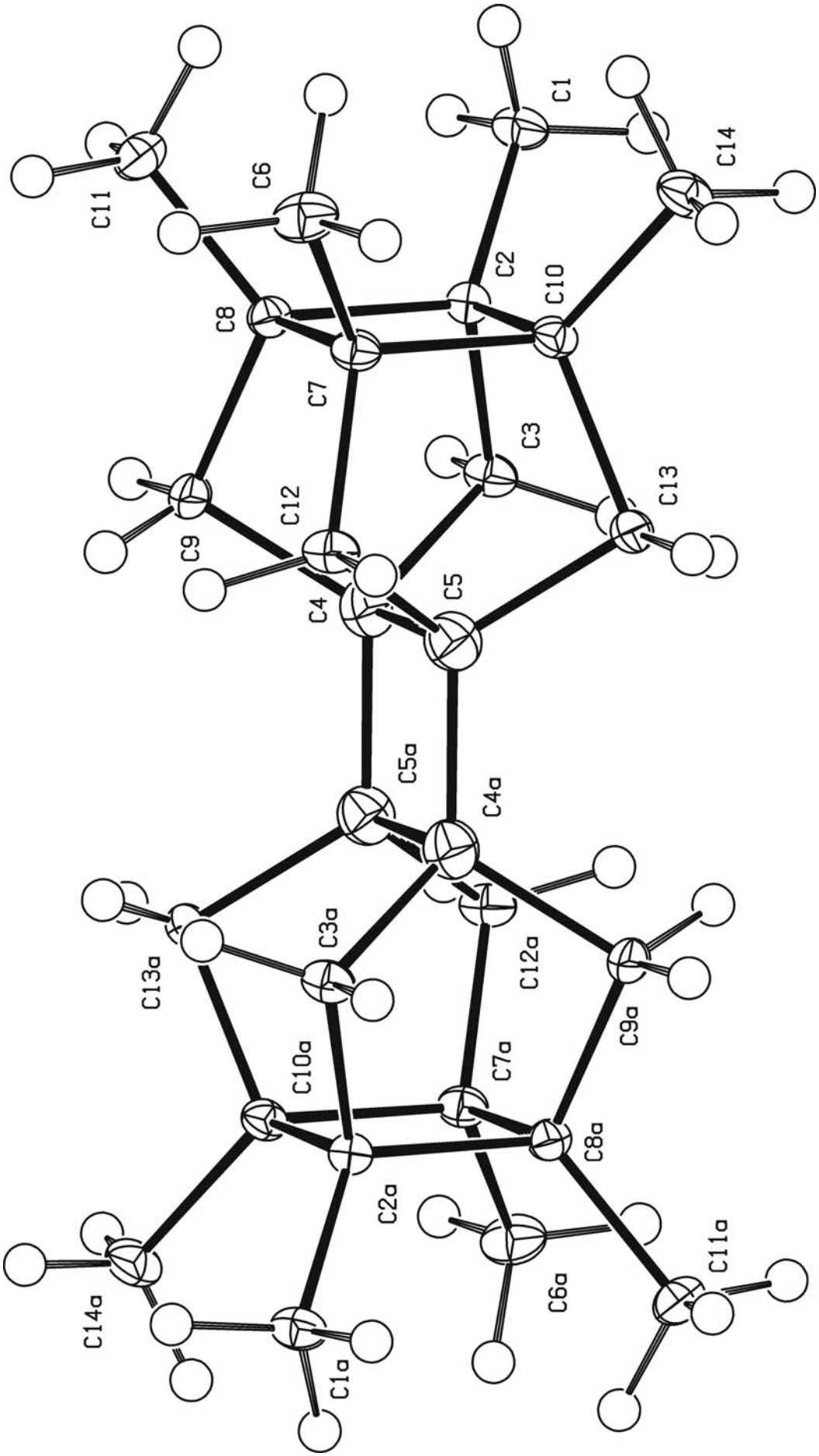
C1
C14
C6
C11
C2
C10
C8
C7
C3
C12
C13
C9
C4
C5
C5a
C4a
C3a
C13a
C12a
C9a
C10a
C7a
C8a
C2a
C6a
C11a
C14a
C1a

Crystal Structure Report for **8**

A colorless Prism-like specimen of $C_{28}H_{42}$, approximate dimensions 0.090 mm x 0.209 mm x 0.623 mm, was used for the X-ray crystallographic analysis.The X-ray intensity data were measured on a D8 Venture system equipped with a multilayer monochromator and a Mo microfocus (λ = 0.71073 Å).

A total of 1064 frames were collected. The total exposure time was 17.73 hours. The frames were integrated with the Bruker SAINT software package using a narrow-frame algorithm. The integration of the data using a monoclinic unit cell yielded a total of 40995 reflections to a maximum θ angle of 28.33° (0.75 Å resolution), of which 5377 were independent (average redundancy 7.587, completeness = 98.8%, R_{int} = 5.79%, R_{sig} = 3.37%) and 5037 (93.23%) were greater than $2\sigma(F^2)$.The final cell constants of a = 22.792(3) Å, b = 7.8099(8) Å, c = 12.4331(15) Å, β = 100.517(4)°, volume = 2176.0.(4) $Å^3$, are based upon the refinement of the XYZ-centroids of 143 reflections above 20 σ(I) with 7.142° < 2θ < 52.43°.Data were corrected for absorption effects using the multi-scan method (SADABS). The ratio of minimum to maximum apparent transmission was 0.775.

The structure was solved and refined using the Bruker SHELXTL Software Package, with Z = 4 for the formula unit, $C_{28}H_{42}$.The final anisotropic full-matrix least-squares refinement on F^2 with 322 variables converged at R1 = 8.25%, for the observed data and wR2 = 21.75% for all data. The goodness-of-fit was 1.071. The largest peak in the final difference electron density synthesis was 0.426 $e^-/Å^3$ and the largest hole was -0.428 $e^-/Å^3$ with an RMS deviation of 0.099 $e^-/Å^3$. On the basis of the final model, the calculated density was 1.156 g/cm^3 and F(000), 840 e^-.

22 H atoms were located from a difference synthesis and refined with an isotropic temperature factor equal to 1.2 time the equivalent temperature factor of the atom which are linked and 20 H atoms were computed and refined, using a riding model, with an isotropic temperature factor equal to 1.2 time the equivalent temperature factor of the atom which are linked.

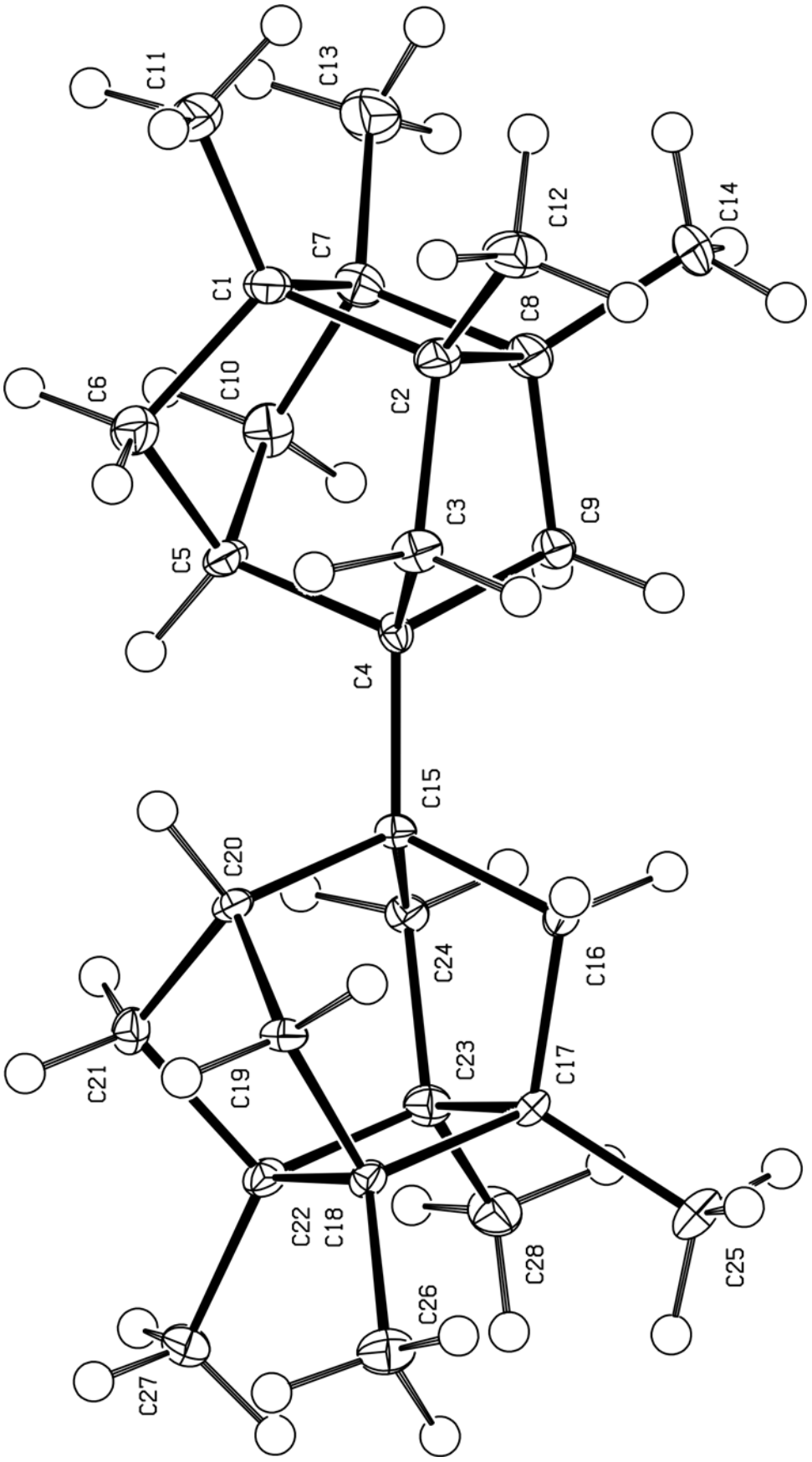
C11
C13
C12
C14
C7
C1
C8
C6
C10
C2
C3
C9
C5
C4
C15
C20
C24
C16
C21
C19
C23
C17
C22
C18
C28
C25
C26
C27

Optimized geometries, energies and thermal corrections

Optimized geometry of pyramidalized alkene 4 at B3LYP/6-31G(d)

Standard orientation:

Center Number	Atomic Number	Atomic Type	Coordinates (Angstroms) X	Y	Z
1	6	0	-1.155315	-1.183049	1.320693
2	6	0	-1.853652	-0.000032	0.679863
3	6	0	-1.155357	1.183009	1.320692
4	6	0	0.278466	0.801106	0.794841
5	6	0	0.278466	0.801106	-0.794841
6	6	0	-1.155357	1.183009	-1.320692
7	6	0	-1.853652	-0.000032	-0.679863
8	6	0	-1.155315	-1.183049	-1.320693
9	6	0	0.278494	-0.801097	-0.794841
10	6	0	0.278494	-0.801097	0.794841
11	6	0	1.401922	1.539580	1.511067
12	6	0	1.401922	1.539580	-1.511067
13	6	0	1.401976	-1.539532	-1.511066
14	6	0	1.401976	-1.539532	1.511066
15	1	0	-1.477397	-2.175813	1.001227
16	1	0	-1.186870	-1.157428	2.416119
17	1	0	-1.477472	2.175762	1.001223
18	1	0	-1.186912	1.157389	2.416118
19	1	0	-1.186912	1.157389	-2.416118
20	1	0	-1.477472	2.175762	-1.001223
21	1	0	-1.477397	-2.175813	-1.001227
22	1	0	-1.186870	-1.157428	-2.416119
23	1	0	1.326946	2.621955	1.347485
24	1	0	1.350975	1.368280	2.593227
25	1	0	2.396714	1.225506	1.175987
26	1	0	1.326946	2.621955	-1.347485
27	1	0	2.396714	1.225506	-1.175987
28	1	0	1.350975	1.368280	-2.593227
29	1	0	1.327037	-2.621911	-1.347484
30	1	0	1.351023	-1.368234	-2.593226
31	1	0	2.396755	-1.225423	-1.175983
32	1	0	1.327037	-2.621911	1.347484
33	1	0	2.396755	-1.225423	1.175983
34	1	0	1.351023	-1.368234	2.593226

E(RB+HF-LYP) = -545.433711877
Zero-point correction= 0.307673
Thermal correction to Energy= 0.319705
Thermal correction to Enthalpy= 0.320649
Thermal correction to Gibbs Free Energy= 0.272147

Optimized geometry of pyramidalized alkene 4 at MP2/6-31G(d)

```
 C   1.3154755473 -1.4179137675 -1.1792570971
 C   0.6871257158 -2.1169449244 -0.0000276887
 C   1.3154748896 -1.4179349751 1.1792146053
 C   0.7877922124 0.0026459853 0.793991584
 C   -0.7877921922 0.0026459882 0.793991584
 C   -1.3154748746 -1.4179349703 1.1792146053
 C   -0.6871257034 -2.1169449219 -0.0000276887
 C   -1.3154755323 -1.4179137627 -1.1792570971
 C   -0.7877922469 0.0026601462 -0.7940090304
 C   0.7877922672 0.0026601433 -0.7940090304
 C   1.497738565 1.1253042621 1.5267637132
 C   -1.4977385406 1.1253042676 1.5267637132
 C   -1.4977385363 1.1253316125 -1.5267610012
 C   1.4977385607 1.125331607 -1.5267610012
 H   0.9955226063 -1.7384998915 -2.173148746
 H   2.411570663 -1.4431905208 -1.1521785846
 H   0.9955210601 -1.7385387915 2.1731002973
 H   2.4115700153 -1.4432114728 1.1521364316
 H   -2.4115700005 -1.4432114639 1.1521364316
 H   -0.9955210463 -1.7385387878 2.1731002973
 H   -0.9955225925 -1.7384998878 -2.173148746
 H   -2.4115706481 -1.4431905118 -1.1521785846
 H   1.3334071281 1.0445761859 2.6072845091
 H   2.5775107567 1.0709883639 1.3490935246
 H   1.1561825542 2.1150608198 1.2091147281
 H   -1.333407104 1.0445761909 2.6072845091
 H   -1.1561825261 2.115060824 1.2091147281
 H   -2.5775107325 1.0709883735 1.3490935246
 H   -1.333407278 1.0446228329 -2.6072832695
 H   -2.5775107148 1.0710127182 -1.3490916238
 H   -1.1561823119 2.115082431 -1.2090943636
 H   1.3334073021 1.0446228279 -2.6072832695
 H   1.15618234 2.1150824267 -1.2090943636
 H   2.577510739 1.0710127086 -1.3490916238

E (MP2/6-31G(d))  =    -0.54354032447853D+03
Zero-point correction=                         0.312607
Thermal correction to Energy=                  0.324528
Thermal correction to Enthalpy=                0.325472
Thermal correction to Gibbs Free Energy=       0.277111
E (MP2/6-311++G(d,p))  =    -0.54389638607665D+03
```

Optimized geometry of boat cyclohexane at B3LYP/6-31G(d)

Standard orientation:

Center Number	Atomic Number	Atomic Type	Coordinates (Angstroms) X	Y	Z
1	6	0	0.000017	-1.369630	0.423247
2	6	0	1.271224	-0.779461	-0.209110
3	1	0	-1.351089	1.147659	-1.240506
4	6	0	1.271208	0.779485	-0.209113
5	6	0	-0.000009	1.369630	0.423247
6	6	0	-1.271231	0.779523	-0.209118
7	6	0	-1.271215	-0.779547	-0.209121
8	1	0	-0.000009	-1.174529	1.504123
9	1	0	0.000066	-2.461361	0.312285
10	1	0	2.153868	-1.162544	0.317235
11	1	0	1.351074	-1.147614	-1.240501
12	1	0	1.351046	1.147636	-1.240505
13	1	0	2.153846	1.162588	0.317228
14	1	0	-0.000029	1.174529	1.504123
15	1	0	0.000019	2.461361	0.312285
16	1	0	-2.153855	1.162556	0.317279
17	1	0	-1.351061	-1.147681	-1.240510
18	1	0	-2.153833	-1.162601	0.317271

1 imaginary frequencies (negative Signs): -100.3339
E(RB+HF-LYP) = -235.868769921
Zero-point correction= 0.170935
Thermal correction to Energy= 0.176204
Thermal correction to Enthalpy= 0.177148
Thermal correction to Gibbs Free Energy= 0.142406

Optimized geometry of boat cyclohexane at MP2/6-31G(d)

Standard orientation:

Center Number	Atomic Number	Atomic Type	Coordinates (Angstroms) X	Y	Z
1	6	0	-0.000032	1.355232	0.432083
2	6	0	-1.260579	0.775203	-0.212813
3	1	0	1.322076	-1.146559	-1.242862
4	6	0	-1.260541	-0.775260	-0.212820
5	6	0	0.000029	-1.355232	0.432083
6	6	0	1.260581	-0.775205	-0.212803
7	6	0	1.260542	0.775262	-0.212810
8	1	0	-0.000028	1.144519	1.507954
9	1	0	-0.000059	2.447233	0.334953
10	1	0	-2.148352	1.159121	0.302040
11	1	0	-1.322065	1.146559	-1.242873
12	1	0	-1.321998	-1.146610	-1.242884
13	1	0	-2.148300	-1.159226	0.302021
14	1	0	0.000017	-1.144519	1.507954
15	1	0	0.000052	-2.447233	0.334953
16	1	0	2.148350	-1.159121	0.302058
17	1	0	1.322008	1.146610	-1.242874
18	1	0	2.148298	1.159226	0.302038

1 imaginary frequencies (negative Signs): -120.7387
E (MP2/6-31G(d)) = -0.23497949815224D+03
Zero-poi nt correction= 0.174735
Thermal correction to Energy= 0.179884
Thermal correction to Enthalpy= 0.180829
Thermal correction to Gibbs Free Energy= 0.146296

Optimized geometry of 3,4,8,9-tetramethyl[4.4.0.0^{3,9}.0^{4,8}] decane, 6, at B3LYP/6-31G(d)

Standard orientation:

Center Number	Atomic Number	Atomic Type	Coordinates (Angstroms) X	Y	Z
1	6	0	1.064515	-1.327544	1.170094
2	6	0	1.918711	-0.792914	0.000000
3	6	0	1.064515	-1.327544	-1.170094
4	6	0	-0.335749	-0.794227	-0.795816
5	6	0	-0.335749	0.794228	-0.795816
6	6	0	1.064515	1.327544	-1.170094
7	6	0	1.918711	0.792914	0.000000
8	6	0	1.064515	1.327544	1.170094
9	6	0	-0.335749	0.794228	0.795816
10	6	0	-0.335749	-0.794227	0.795816
11	6	0	-1.465902	-1.504701	-1.531135
12	6	0	-1.465902	1.504701	-1.531135
13	6	0	-1.465902	1.504701	1.531135
14	6	0	-1.465902	-1.504701	1.531135
15	1	0	1.399556	-1.017647	2.164987
16	1	0	1.067715	-2.425484	1.162348
17	1	0	2.941408	-1.183857	0.000000
18	1	0	1.067715	-2.425484	-1.162348
19	1	0	1.399556	-1.017647	-2.164987
20	1	0	1.399556	1.017647	-2.164987
21	1	0	1.067716	2.425484	-1.162348
22	1	0	2.941409	1.183857	0.000000
23	1	0	1.399556	1.017647	2.164987
24	1	0	1.067716	2.425484	1.162348
25	1	0	-1.391586	-1.345674	-2.614501
26	1	0	-1.421435	-2.586963	-1.357014
27	1	0	-2.458270	-1.163588	-1.217607
28	1	0	-1.391586	1.345674	-2.614501
29	1	0	-2.458269	1.163588	-1.217607
30	1	0	-1.421434	2.586963	-1.357014
31	1	0	-1.421434	2.586963	1.357014
32	1	0	-2.458269	1.163588	1.217607
33	1	0	-1.391586	1.345674	2.614501
34	1	0	-1.421435	-2.586963	1.357014
35	1	0	-1.391586	-1.345674	2.614501
36	1	0	-2.458270	-1.163588	1.217607

E(RB+HF-LYP) = -546.722156232
Zero-point correction= 0.332382
Thermal correction to Energy= 0.344499
Thermal correction to Enthalpy= 0.345443
Thermal correction to Gibbs Free Energy= 0.296752

Optimized geometry of 3,4,8,9-tetramethyl[4.4.0.$0^{3,9}$.$0^{4,8}$] decane, 6, at MP2/6-31G(d)

Standard orientation:

Center Number	Atomic Number	Atomic Type	Coordinates (Angstroms) X	Y	Z
1	6	0	-1.058081	-1.319413	-1.164023
2	6	0	-1.908116	-0.786644	-0.000003
3	6	0	-1.058085	-1.319416	1.164017
4	6	0	0.331627	-0.787333	0.789059
5	6	0	0.331625	0.787331	0.789062
6	6	0	-1.058087	1.319411	1.164020
7	6	0	-1.908118	0.786640	-0.000001
8	6	0	-1.058084	1.319414	-1.164019
9	6	0	0.331626	0.787333	-0.789058
10	6	0	0.331629	-0.787330	-0.789061
11	6	0	1.459613	-1.492857	1.518325
12	6	0	1.459610	1.492855	1.518329
13	6	0	1.459614	1.492860	-1.518322
14	6	0	1.459616	-1.492852	-1.518326
15	1	0	-1.389006	-1.013584	-2.161806
16	1	0	-1.057142	-2.417807	-1.150741
17	1	0	-2.932037	-1.178886	-0.000005
18	1	0	-1.057146	-2.417811	1.150732
19	1	0	-1.389011	-1.013591	2.161800
20	1	0	-1.389012	1.013580	2.161802
21	1	0	-1.057151	2.417805	1.150738
22	1	0	-2.932039	1.178880	-0.000001
23	1	0	-1.389007	1.013587	-2.161803
24	1	0	-1.057148	2.417808	-1.150734
25	1	0	1.379850	-1.333230	2.599844
26	1	0	1.410378	-2.572592	1.337561
27	1	0	2.447363	-1.146433	1.201174
28	1	0	1.379847	1.333223	2.599848
29	1	0	2.447362	1.146434	1.201177
30	1	0	1.410372	2.572591	1.337566
31	1	0	1.410375	2.572595	-1.337558
32	1	0	2.447364	1.146437	-1.201169
33	1	0	1.379854	1.333232	-2.599841
34	1	0	1.410381	-2.572588	-1.337565
35	1	0	1.379856	-1.333222	-2.599845
36	1	0	2.447366	-1.146431	-1.201172

E (MP2/6-31G(d)) = -0.54479329461707D+03
Zero-point correction= 0.338127
Thermal correction to Energy= 0.350108
Thermal correction to Enthalpy= 0.351052
Thermal correction to Gibbs Free Energy= 0.302536

Optimized geometry of triasterane, 9, at B3LYP/6-31G(d)

Standard orientation:

Center Number	Atomic Number	Atomic Type	Coordinates (Angstroms) X	Y	Z
1	6	0	-1.260857	0.844880	-0.226801
2	6	0	0.000003	1.667125	-0.446955
3	6	0	1.260860	0.844877	-0.226800
4	6	0	1.260914	-0.618577	-0.618268
5	6	0	-0.000002	-1.221268	-1.219566
6	6	0	-1.260915	-0.618574	-0.618268
7	6	0	-1.261085	-0.225768	0.844702
8	6	0	-0.000001	-0.446666	1.667108
9	6	0	1.261084	-0.225771	0.844702
10	1	0	-2.189297	1.393883	-0.374493
11	1	0	0.000005	2.077160	-1.467817
12	1	0	0.000006	2.532141	0.232674
13	1	0	2.189301	1.393879	-0.374490
14	1	0	2.189421	-1.020634	-1.020072
15	1	0	-0.000005	-2.310194	-1.062928
16	1	0	-0.000002	-1.067133	-2.308800
17	1	0	-2.189423	-1.020626	-1.020076
18	1	0	-2.189609	-0.372444	1.393808
19	1	0	0.000000	0.232529	2.532593
20	1	0	-0.000004	-1.467662	2.076669
21	1	0	2.189608	-0.372452	1.393807

E(RB+HF-LYP) = -350.134438886
Zero-point correction= 0.189932
Thermal correction to Energy= 0.196213
Thermal correction to Enthalpy= 0.197157
Thermal correction to Gibbs Free Energy= 0.159805

Optimized geometry of triasterane, 9, at MP2/6-31G(d)

Standard orientation:

Center Number	Atomic Number	Atomic Type	Coordinates (Angstroms) X	Y	Z
1	6	0	-1.252890	0.812200	-0.315862
2	6	0	-0.000003	1.603188	-0.623456
3	6	0	1.252887	0.812204	-0.315863
4	6	0	1.252898	-0.679636	-0.545467
5	6	0	0.000000	-1.341547	-1.076629
6	6	0	-1.252897	-0.679638	-0.545465
7	6	0	-1.252907	-0.132561	0.861313
8	6	0	0.000003	-0.261650	1.700105
9	6	0	1.252909	-0.132558	0.861311
10	1	0	-2.187463	1.332969	-0.518383
11	1	0	-0.000005	1.897346	-1.682846
12	1	0	-0.000004	2.535747	-0.041082
13	1	0	2.187456	1.332974	-0.518387
14	1	0	2.187459	-1.115380	-0.895263
15	1	0	0.000002	-2.406060	-0.801588
16	1	0	0.000000	-1.303572	-2.175441
17	1	0	-2.187459	-1.115384	-0.895259
18	1	0	-2.187454	-0.217557	1.413612
19	1	0	0.000002	0.508726	2.484553
20	1	0	0.000005	-1.232277	2.216554
21	1	0	2.187457	-0.217551	1.413607

E (MP2/6-31G(d)) = -0.34892020158234D+03
Zero-point correction= 0.194141
Thermal correction to Energy= 0.200269
Thermal correction to Enthalpy= 0.201214
Thermal correction to Gibbs Free Energy= 0.164086

Optimized geometry of diasterane, 10, at B3LYP/6-31G(d)

Standard orientation:

Center Number	Atomic Number	Atomic Type	Coordinates (Angstroms) X	Y	Z
1	6	0	1.039307	0.796490	0.000000
2	6	0	0.000000	1.312316	1.044739
3	6	0	0.000000	1.312316	-1.044739
4	6	0	-1.039307	0.796490	0.000000
5	6	0	-1.039307	-0.796490	0.000000
6	6	0	0.000000	-1.312316	1.044739
7	6	0	1.039307	-0.796490	0.000000
8	6	0	0.000000	-1.312316	-1.044739
9	1	0	2.052722	1.210087	0.000000
10	1	0	0.000000	0.930458	2.065942
11	1	0	0.000000	2.406170	1.090059
12	1	0	0.000000	2.406171	-1.090059
13	1	0	0.000000	0.930459	-2.065942
14	1	0	-2.052722	1.210087	0.000000
15	1	0	-2.052722	-1.210087	0.000000
16	1	0	0.000000	-0.930458	2.065942
17	1	0	0.000000	-2.406170	1.090059
18	1	0	2.052722	-1.210087	0.000000
19	1	0	0.000000	-0.930459	-2.065942
20	1	0	0.000000	-2.406171	-1.090059

E(RB+HF-LYP) = -311.973697537
Zero-point correction= 0.184154
(Hartree/Particle)
Thermal correction to Energy= 0.189605
Thermal correction to Enthalpy= 0.190549
Thermal correction to Gibbs Free Energy= 0.155711

Optimized geometry of diasterane, 10, at MP2/6-31G(d)

Standard orientation:

Center Number	Atomic Number	Atomic Type	Coordinates (Angstroms) X	Y	Z
1	6	0	0.685278	0.463792	-1.004548
2	6	0	1.646452	-0.270045	-0.028784
3	6	0	0.632313	1.539967	0.115056
4	6	0	0.695378	0.305627	1.056818
5	6	0	-0.685278	-0.463792	1.004548
6	6	0	-0.632313	-1.539967	-0.115056
7	6	0	-0.695378	-0.305627	-1.056818
8	6	0	-1.646452	0.270045	0.028784
9	1	0	1.042125	0.742990	-2.001863
10	1	0	1.815562	-1.343177	-0.111951
11	1	0	2.620352	0.228264	0.004676
12	1	0	1.568271	2.105993	0.153900
13	1	0	-0.195454	2.246041	0.173286
14	1	0	1.062132	0.429683	2.081528
15	1	0	-1.042125	-0.742990	2.001863
16	1	0	0.195454	-2.246041	-0.173286
17	1	0	-1.568271	-2.105993	-0.153900
18	1	0	-1.062132	-0.429683	-2.081528
19	1	0	-1.815562	1.343177	0.111951
20	1	0	-2.620352	-0.228264	-0.004676

E (MP2/6-31G(d)) = -0.31087079793650D+03
Zero-point correction= 0.187428
Thermal correction to Energy= 0.192785
Thermal correction to Enthalpy= 0.193729
Thermal correction to Gibbs Free Energy= 0.158355

Optimized geometry of tetraasterane, 11, at B3LYP/6-31G(d)

Standard orientation:

Center Number	Atomic Number	Atomic Type	Coordinates (Angstroms) X	Y	Z
1	6	0	0.793491	-0.774617	1.254743
2	6	0	0.774616	0.793492	1.254743
3	6	0	1.424148	-1.389611	0.000001
4	6	0	1.389611	1.424148	0.000000
5	6	0	0.793492	-0.774617	-1.254742
6	6	0	0.774617	0.793491	-1.254743
7	6	0	-0.793491	0.774617	-1.254743
8	6	0	-1.424148	1.389611	-0.000001
9	6	0	-0.793492	0.774617	1.254742
10	6	0	-0.774617	-0.793492	1.254743
11	6	0	-1.389611	-1.424148	0.000000
12	6	0	-0.774616	-0.793492	-1.254743
13	1	0	1.234856	-1.205608	2.160029
14	1	0	1.205608	1.234857	2.160028
15	1	0	1.284192	-2.479816	0.000001
16	1	0	2.510278	-1.220895	0.000001
17	1	0	1.220896	2.510278	0.000000
18	1	0	2.479817	1.284190	0.000000
19	1	0	1.234857	-1.205609	-2.160028
20	1	0	1.205609	1.234856	-2.160028
21	1	0	-1.234856	1.205608	-2.160029
22	1	0	-1.284191	2.479816	-0.000001
23	1	0	-2.510278	1.220896	-0.000001
24	1	0	-1.234857	1.205609	2.160028
25	1	0	-1.205609	-1.234856	2.160028
26	1	0	-2.479817	-1.284190	0.000000
27	1	0	-1.220897	-2.510278	0.000000
28	1	0	-1.205608	-1.234857	-2.160028

E(RB+HF-LYP) = -466.876546090
Zero-point correction= 0.256651
Thermal correction to Energy= 0.264007
Thermal correction to Enthalpy= 0.264951
Thermal correction to Gibbs Free Energy= 0.225184

Optimized geometry of tetraasterane, 11, at MP2/6-31G(d)

Standard orientation:

Center Number	Atomic Number	Atomic Type	Coordinates (Angstroms) X	Y	Z
1	6	0	-0.804373	-0.753873	1.247912
2	6	0	0.753873	-0.804373	1.247912
3	6	0	-1.444552	-1.353957	0.000000
4	6	0	1.353957	-1.444552	0.000000
5	6	0	-0.804373	-0.753873	-1.247912
6	6	0	0.753873	-0.804373	-1.247912
7	6	0	0.804373	0.753873	-1.247912
8	6	0	1.444552	1.353957	0.000000
9	6	0	0.804373	0.753873	1.247912
10	6	0	-0.753873	0.804373	1.247912
11	6	0	-1.353957	1.444552	0.000000
12	6	0	-0.753873	0.804373	-1.247912
13	1	0	-1.254404	-1.175669	2.154667
14	1	0	1.175668	-1.254403	2.154667
15	1	0	-2.526702	-1.163224	-0.000001
16	1	0	-1.323909	-2.446150	0.000000
17	1	0	2.446150	-1.323908	0.000000
18	1	0	1.163225	-2.526702	0.000000
19	1	0	-1.254403	-1.175669	-2.154667
20	1	0	1.175670	-1.254404	-2.154667
21	1	0	1.254404	1.175669	-2.154667
22	1	0	2.526702	1.163224	0.000001
23	1	0	1.323909	2.446150	0.000000
24	1	0	1.254403	1.175669	2.154667
25	1	0	-1.175670	1.254404	2.154667
26	1	0	-1.163225	2.526702	0.000000
27	1	0	-2.446150	1.323908	0.000000
28	1	0	-1.175668	1.254403	-2.154667

E (MP2/6-31G(d)) = -0.46526360192596D+03
Zero-point correction= 0.260960
Thermal correction to Energy= 0.268220
Thermal correction to Enthalpy= 0.269164
Thermal correction to Gibbs Free Energy= 0.229531

Optimized geometry of iceane, 12, at B3LYP/6-31G(d)

Standard orientation:

Center Number	Atomic Number	Atomic Type	Coordinates (Angstroms) X	Y	Z
1	6	0	-1.334130	-0.988736	-1.046027
2	6	0	-0.790776	-1.411559	0.335670
3	6	0	-1.334484	-0.411930	1.378824
4	6	0	-0.790904	0.996314	1.054211
5	6	0	-1.334199	1.400639	-0.332887
6	6	0	-0.790955	0.415096	-1.389637
7	6	0	0.790777	-1.411559	0.335670
8	6	0	1.334130	-0.988736	-1.046027
9	6	0	0.790955	0.415097	-1.389637
10	6	0	0.790904	0.996314	1.054211
11	6	0	1.334198	1.400639	-0.332887
12	6	0	1.334485	-0.411930	1.378824
13	1	0	-2.432164	-0.963203	-1.018895
14	1	0	-1.063652	-1.717576	-1.818442
15	1	0	-1.152225	-2.419197	0.575127
16	1	0	-1.065768	-0.715712	2.396841
17	1	0	-2.432474	-0.400724	1.341340
18	1	0	-1.152241	1.707206	1.807473
19	1	0	-1.062488	2.433525	-0.578056
20	1	0	-2.432334	1.365208	-0.324220
21	1	0	-1.152193	0.711520	-2.382097
22	1	0	1.152226	-2.419197	0.575127
23	1	0	2.432165	-0.963203	-1.018895
24	1	0	1.063652	-1.717576	-1.818442
25	1	0	1.152193	0.711521	-2.382097
26	1	0	1.152241	1.707206	1.807472
27	1	0	2.432333	1.365209	-0.324221
28	1	0	1.062486	2.433525	-0.578056
29	1	0	1.065769	-0.715712	2.396841
30	1	0	2.432475	-0.400723	1.341339

E(RB+HF-LYP) = -468.125555002
Zero-point correction= 0.282155
Thermal correction to Energy= 0.289684
Thermal correction to Enthalpy= 0.290628
Thermal correction to Gibbs Free Energy= 0.250575

Optimized geometry of iceane, 12, at MP2/6-31G(d)

Standard orientation:

Center Number	Atomic Number	Atomic Type	Coordinates (Angstroms) X	Y	Z
1	6	0	1.325842	1.251672	-0.692617
2	6	0	0.784349	1.235091	0.743350
3	6	0	1.325864	-0.026009	1.430279
4	6	0	0.784350	-1.261302	0.697950
5	6	0	1.325843	-1.225662	-0.737668
6	6	0	0.784349	0.026210	-1.441293
7	6	0	-0.784347	1.235091	0.743351
8	6	0	-1.325842	1.251673	-0.692615
9	6	0	-0.784350	0.026210	-1.441293
10	6	0	-0.784349	-1.261302	0.697951
11	6	0	-1.325846	-1.225661	-0.737667
12	6	0	-1.325862	-0.026009	1.430281
13	1	0	2.423774	1.213911	-0.671722
14	1	0	1.059920	2.181655	-1.207231
15	1	0	1.146981	2.123110	1.277808
16	1	0	1.059988	-0.045342	2.492985
17	1	0	2.423792	-0.025227	1.387083
18	1	0	1.146981	-2.168164	1.199773
19	1	0	1.059922	-2.136320	-1.285752
20	1	0	2.423775	-1.188689	-0.715416
21	1	0	1.146977	0.045060	-2.477570
22	1	0	-1.146978	2.123110	1.277810
23	1	0	-2.423773	1.213912	-0.671719
24	1	0	-1.059920	2.181656	-1.207230
25	1	0	-1.146979	0.045060	-2.477569
26	1	0	-1.146980	-2.168162	1.199774
27	1	0	-2.423777	-1.188689	-0.715413
28	1	0	-1.059924	-2.136320	-1.285750
29	1	0	-1.059985	-0.045341	2.492986
30	1	0	-2.423790	-0.025225	1.387086

E (MP2/6-31G(d)) = -0.46648323304069D+03
Zero-point correction= 0.287078
Thermal correction to Energy= 0.294485
Thermal correction to Enthalpy= 0.295430
Thermal correction to Gibbs Free Energy= 0.255537

Optimized geometry of dimer 7 at MP2/6-31G(d)

C	1.5950331359	1.3344024296	1.1666740664
C	0.7692126617	0.7914376605	0.
C	1.5950331359	1.3344024296	-1.1666740664
C	2.9825494824	0.7892429813	-0.7902215572
C	2.9825494824	-0.7892429813	-0.7902215572
C	1.5950331359	-1.3344024296	-1.1666740664
C	0.7692126617	-0.7914376605	0.
C	1.5950331359	-1.3344024296	1.1666740664
C	2.9825494824	-0.7892429813	0.7902215572
C	2.9825494824	0.7892429813	0.7902215572
C	-0.7692126617	0.7914376605	0.
C	-0.7692126617	-0.7914376605	0.
C	-1.5950331359	1.3344024296	1.1666740664
C	-2.9825494824	0.7892429813	0.7902215572
C	-2.9825494824	-0.7892429813	0.7902215572
C	-1.5950331359	-1.3344024296	1.1666740664
C	-1.5950331359	-1.3344024296	-1.1666740664
C	-2.9825494824	-0.7892429813	-0.7902215572
C	-2.9825494824	0.7892429813	-0.7902215572
C	-1.5950331359	1.3344024296	-1.1666740664
C	4.1148087449	1.4904503393	-1.5180822053
C	4.1148087449	-1.4904503393	-1.5180822053
C	4.1148087449	-1.4904503393	1.5180822053
C	4.1148087449	1.4904503393	1.5180822053
C	-4.1148087449	1.4904503393	1.5180822053
C	-4.1148087449	-1.4904503393	1.5180822053
C	-4.1148087449	-1.4904503393	-1.5180822053
C	-4.1148087449	1.4904503393	-1.5180822053
H	1.259591644	1.0207807888	2.1609951457
H	1.5994115596	2.4341982231	1.159667846
H	1.259591644	1.0207807888	-2.1609951457
H	1.5994115596	2.4341982231	-1.159667846
H	1.5994115596	-2.4341982231	-1.159667846
H	1.259591644	-1.0207807888	-2.1609951457
H	1.259591644	-1.0207807888	2.1609951457
H	1.5994115596	-2.4341982231	1.159667846
H	-1.5994115596	2.4341982231	1.159667846
H	-1.259591644	1.0207807888	2.1609951457
H	-1.5994115596	-2.4341982231	1.159667846
H	-1.259591644	-1.0207807888	2.1609951457
H	-1.5994115596	-2.4341982231	-1.159667846
H	-1.259591644	-1.0207807888	-2.1609951457
H	-1.5994115596	2.4341982231	-1.159667846
H	-1.259591644	1.0207807888	-2.1609951457
H	4.034014565	1.3327674852	-2.5998383846
H	4.0701407697	2.5700322641	-1.3355106746
H	5.1011002893	1.1392436591	-1.2015168112
H	4.034014565	-1.3327674852	-2.5998383846
H	5.1011002893	-1.1392436591	-1.2015168112
H	4.0701407697	-2.5700322641	-1.3355106746
H	4.0701407697	-2.5700322641	1.3355106746
H	5.1011002893	-1.1392436591	1.2015168112
H	4.034014565	-1.3327674852	2.5998383846
H	4.0701407697	2.5700322641	1.3355106746
H	4.034014565	1.3327674852	2.5998383846

```
 H    5.1011002893 1.1392436591 1.2015168112
 H    -4.034014565 1.3327674852 2.5998383846
 H    -4.0701407697 2.5700322641 1.3355106746
 H    -5.1011002893 1.1392436591 1.2015168112
 H    -4.034014565 -1.3327674852 2.5998383846
 H    -5.1011002893 -1.1392436591 1.2015168112
 H    -4.0701407697 -2.5700322641 1.3355106746
 H    -4.0701407697 -2.5700322641 -1.3355106746
 H    -5.1011002893 -1.1392436591 -1.2015168112
 H    -4.034014565 -1.3327674852 -2.5998383846
 H    -5.1011002893 1.1392436591 -1.2015168112
 H    -4.0701407697 2.5700322641 -1.3355106746
 H    -4.034014565 1.3327674852 -2.5998383846

E(MP2/6-31G(d)) =    -0.10872497875164D+04
Zero-point correction=                          0.629650
Thermal correction to Energy=                   0.653840
Thermal correction to Enthalpy=                 0.654784
Thermal correction to Gibbs Free Energy=        0.583508
E (MP2/6-311++G(d,p))  =    -0.10879576861984D+04
```

Optimized geometry of diene 13 at MP2/6-31G(d)

C	1.5237426222	1.4253373032	1.2203914387
C	0.6381559781	1.4662831703	0.
C	1.5237426222	1.4253373032	-1.2203914387
C	2.8470168108	0.7613214925	-0.7873713098
C	2.892475232	-0.8191276584	-0.7877763177
C	1.600283427	-1.5461494006	-1.2101239762
C	0.703134692	-1.5289849329	0.
C	1.600283427	-1.5461494006	1.2101239762
C	2.892475232	-0.8191276584	0.7877763177
C	2.8470168108	0.7613214925	0.7873713098
C	-0.703134692	1.5289849329	0.
C	-0.6381559781	-1.4662831703	0.
C	-1.600283427	1.5461494006	1.2101239762
C	-2.892475232	0.8191276584	0.7877763177
C	-2.8470168108	-0.7613214925	0.7873713098
C	-1.5237426222	-1.4253373032	1.2203914387
C	-1.5237426222	-1.4253373032	-1.2203914387
C	-2.8470168108	-0.7613214925	-0.7873713098
C	-2.892475232	0.8191276584	-0.7877763177
C	-1.600283427	1.5461494006	-1.2101239762
C	4.0152719077	1.4521215101	-1.4841337556
C	4.0913031123	-1.4479690292	-1.4896725526
C	4.0913031123	-1.4479690292	1.4896725526
C	4.0152719077	1.4521215101	1.4841337556
C	-4.0913031123	1.4479690292	1.4896725526
C	-4.0152719077	-1.4521215101	1.4841337556
C	-4.0152719077	-1.4521215101	-1.4841337556
C	-4.0913031123	1.4479690292	-1.4896725526
H	1.0535761116	0.9329158131	2.0792628475
H	1.7417855206	2.4540795013	1.5485998437
H	1.0535761116	0.9329158131	-2.0792628475
H	1.7417855206	2.4540795013	-1.5485998437
H	1.8579876761	-2.5889836807	-1.4570171646
H	1.1377693008	-1.1290180283	-2.1115668589
H	1.1377693008	-1.1290180283	2.1115668589
H	1.8579876761	-2.5889836807	1.4570171646
H	-1.8579876761	2.5889836807	1.4570171646
H	-1.1377693008	1.1290180283	2.1115668589
H	-1.7417855206	-2.4540795013	1.5485998437
H	-1.0535761116	-0.9329158131	2.0792628475
H	-1.7417855206	-2.4540795013	-1.5485998437
H	-1.0535761116	-0.9329158131	-2.0792628475
H	-1.8579876761	2.5889836807	-1.4570171646
H	-1.1377693008	1.1290180283	-2.1115668589
H	3.95170737	1.3100176395	-2.5693166042
H	3.9816275987	2.5294995651	-1.2892909413
H	4.9910102055	1.0880582836	-1.1556207257
H	4.0177842262	-1.3071064942	-2.5744650671
H	5.0486078246	-1.0361398455	-1.1631548808
H	4.1128829945	-2.5261833138	-1.297488297
H	4.1128829945	-2.5261833138	1.297488297
H	5.0486078246	-1.0361398455	1.1631548808
H	4.0177842262	-1.3071064942	2.5744650671
H	3.9816275987	2.5294995651	1.2892909413
H	3.95170737	1.3100176395	2.5693166042
H	4.9910102055	1.0880582836	1.1556207257

```
 H    -4.0177842262 1.3071064942 2.5744650671
 H    -4.1128829945 2.5261833138 1.297488297
 H    -5.0486078246 1.0361398455 1.1631548808
 H    -3.95170737 -1.3100176395 2.5693166042
 H    -4.9910102055 -1.0880582836 1.1556207257
 H    -3.9816275987 -2.5294995651 1.2892909413
 H    -3.9816275987 -2.5294995651 -1.2892909413
 H    -4.9910102055 -1.0880582836 -1.1556207257
 H    -3.95170737 -1.3100176395 -2.5693166042
 H    -5.0486078246 1.0361398455 -1.1631548808
 H    -4.1128829945 2.5261833138 -1.297488297
 H    -4.0177842262 1.3071064942 -2.5744650671

E (MP2/6-31G(d))  =    -0.10872132575967D+04
Zero-point correction=                          0.627397
Thermal correction to Energy=                   0.652838
Thermal correction to Enthalpy=                 0.653783
Thermal correction to Gibbs Free Energy=        0.577931
E (MP2/6-311++G(d,p))  =    -0.10879237996083D+04
```

Optimized geometry of diene 14 at MP2/6-31G(d)

C	-1.0992782901	1.40378049	1.5436448768
C	0.0094326363	0.7882190603	0.6766241698
C	1.2241930647	1.262372371	1.4783856399
C	0.8380367866	0.7429628427	2.8836693654
C	0.7362216733	-0.8314751797	2.9116098934
C	1.0992782901	-1.40378049	1.5436448768
C	-0.0094326363	-0.7882190603	0.6766241698
C	-1.2241930647	-1.262372371	1.4783856399
C	-0.8380367866	-0.7429628427	2.8836693654
C	-0.7362216733	0.8314751797	2.9116098934
C	-0.0963381089	0.7744515407	-0.8800713542
C	0.0963381089	-0.7744515407	-0.8800713542
C	-1.5030223071	1.1198958945	-1.3957323369
C	-1.7264674303	0.5332301073	-2.7682820799
C	-1.4568563081	-0.7832626906	-2.907766152
C	-0.9767776563	-1.5364176561	-1.683446842
C	1.5030223071	-1.1198958945	-1.3957323369
C	1.7264674303	-0.5332301073	-2.7682820799
C	1.4568563081	0.7832626906	-2.907766152
C	0.9767776563	1.5364176561	-1.683446842
C	1.6322164072	1.4158853593	3.9884289762
C	1.4008828403	-1.5552314439	4.0678267718
C	-1.6322164072	-1.4158853593	3.9884289762
C	-1.4008828403	1.5552314439	4.0678267718
C	-2.2665187713	1.4556016407	-3.823912225
C	-1.6246993857	-1.5942579974	-4.1599331168
C	2.2665187713	-1.4556016407	-3.823912225
C	1.6246993857	1.5942579974	-4.1599331168
H	-2.1264214753	1.1687868827	1.2527526179
H	-1.010075408	2.5004849763	1.5444901931
H	2.1922279102	0.8810931511	1.1356641261
H	1.2948523278	2.3599328139	1.4894596421
H	1.010075408	-2.5004849763	1.5444901931
H	2.1264214753	-1.1687868827	1.2527526179
H	-2.1922279102	-0.8810931511	1.1356641261
H	-1.2948523278	-2.3599328139	1.4894596421
H	-1.6451577186	2.209444291	-1.3993545088
H	-2.2579636696	0.7119348823	-0.7108976627
H	-0.5880838646	-2.5220242704	-1.9763978379
H	-1.8391765332	-1.7396179287	-1.0300492629
H	1.6451577186	-2.209444291	-1.3993545088
H	2.2579636696	-0.7119348823	-0.7108976627
H	0.5880838646	2.5220242704	-1.9763978379
H	1.8391765332	1.7396179287	-1.0300492629
H	2.7014164943	1.198229722	3.8822482407
H	1.5085224596	2.5034615964	3.9362444185
H	1.322690926	1.092434964	4.9862275719
H	2.4910900786	-1.4584103191	4.0085412218
H	1.0832400174	-1.1734936325	5.0425535274
H	1.1589070554	-2.6234307918	4.0325357005
H	-1.5085224596	-2.5034615964	3.9362444185
H	-1.322690926	-1.092434964	4.9862275719
H	-2.7014164943	-1.198229722	3.8822482407
H	-1.1589070554	2.6234307918	4.0325357005
H	-2.4910900786	1.4584103191	4.0085412218
H	-1.0832400174	1.1734936325	5.0425535274

```
 H    -2.3033087949 1.0001262575 -4.8154839766
 H    -1.6530134485 2.3617747424 -3.8912924017
 H    -3.2821354044 1.7832279673 -3.566284092
 H    -2.0375287287 -1.0194632289 -4.9911398898
 H    -0.6603121612 -2.0074474019 -4.478108837
 H    -2.2925989957 -2.44541739 -3.9778023772
 H    2.3033087949 -1.0001262575 -4.8154839766
 H    1.6530134485 -2.3617747424 -3.8912924017
 H    3.2821354044 -1.7832279673 -3.566284092
 H    2.0375287287 1.0194632289 -4.9911398898
 H    0.6603121612 2.0074474019 -4.478108837
 H    2.2925989957 2.44541739 -3.9778023772

E (MP2/6-31G(d))  =    -0.10872197916641D+04
Zero-point correction=                          0.626243
Thermal correction to Energy=                   0.653020
Thermal correction to Enthalpy=                 0.653964
Thermal correction to Gibbs Free Energy=        0.575018
E (MP2/6-311++G(d,p))  =    -0.10879309072664D+04
```

Optimized geometry of diene 15 at MP2/6-31G(d)

C	-0.8861855865	1.54046248	1.5668048497
C	0.1297614507	0.776765603	0.7066313474
C	1.3975650178	1.0744272356	1.5076989433
C	0.9373478929	0.6157572953	2.9123270759
C	0.610268783	-0.9277249695	2.9368305588
C	0.8861855865	-1.54046248	1.5668048497
C	-0.1297614507	-0.776765603	0.7066313474
C	-1.3975650178	-1.0744272356	1.5076989433
C	-0.9373478929	-0.6157572953	2.9123270759
C	-0.610268783	0.9277249695	2.9368305588
C	0.0009696988	0.7928885305	-0.8378420307
C	-0.0009696988	-0.7928885305	-0.8378420307
C	-1.3185157816	1.4246958295	-1.323085156
C	-1.0848014341	1.6388235446	-2.7978607123
C	-0.2422240156	-1.6976621008	-3.0371802486
C	-1.0118238031	-1.5060210587	-1.7476083341
C	1.3185157816	-1.4246958295	-1.323085156
C	1.0848014341	-1.6388235446	-2.7978607123
C	0.2422240156	1.6976621008	-3.0371802486
C	1.0118238031	1.5060210587	-1.7476083341
C	1.8141910513	1.1664942237	4.0221781858
C	1.1662187047	-1.7430328631	4.0895311199
C	-1.8141910513	-1.1664942237	4.0221781858
C	-1.1662187047	1.7430328631	4.0895311199
C	-2.2252460112	1.8508579197	-3.7420547033
C	-0.9559386903	-1.9540989639	-4.3245168234
C	2.2252460112	-1.8508579197	-3.7420547033
C	0.9559386903	1.9540989639	-4.3245168234
H	-1.9312057393	1.4409375302	1.2588829525
H	-0.6516297127	2.6155151858	1.5678020884
H	2.3021718263	0.5645856461	1.1578538358
H	1.6172392636	2.1519356279	1.5173421018
H	0.6516297127	-2.6155151858	1.5678020884
H	1.9312057393	-1.4409375302	1.2588829525
H	-2.3021718263	-0.5645856461	1.1578538358
H	-1.6172392636	-2.1519356279	1.5173421018
H	-1.4592750936	2.3982344826	-0.8260532228
H	-2.2118550143	0.8320808053	-1.0923844666
H	-1.2839094817	-2.4848238723	-1.3151916373
H	-1.950293849	-0.9599958518	-1.8904702683
H	1.4592750936	-2.3982344826	-0.8260532228
H	2.2118550143	-0.8320808053	-1.0923844666
H	1.2839094817	2.4848238723	-1.3151916373
H	1.950293849	0.9599958518	-1.8904702683
H	2.8413445165	0.7968757225	3.9214817297
H	1.8490717183	2.260567145	3.9704221293
H	1.4558972801	0.8909827993	5.0180881264
H	2.2588801592	-1.804034171	4.0273929031
H	0.9092268476	-1.3225419508	5.0661855866
H	0.7729745058	-2.7652195247	4.0520821648
H	-1.8490717183	-2.260567145	3.9704221293
H	-1.4558972801	-0.8909827993	5.0180881264
H	-2.8413445165	-0.7968757225	3.9214817297
H	-0.7729745058	2.7652195247	4.0520821648
H	-2.2588801592	1.804034171	4.0273929031
H	-0.9092268476	1.3225419508	5.0661855866

```
 H    -2.9304375182 1.0121844594 -3.6962548711
 H    -2.7893742618 2.7535798324 -3.474958632
 H    -1.8913170172 1.957022542 -4.7777457108
 H    -1.6081452765 -1.1078830516 -4.5715374002
 H    -0.2659458366 -2.1069928642 -5.1587434065
 H    -1.5952748848 -2.8421824688 -4.2467840759
 H    2.7893742618 -2.7535798324 -3.474958632
 H    1.8913170172 -1.957022542 -4.7777457108
 H    2.9304375182 -1.0121844594 -3.6962548711
 H    0.2659458366 2.1069928642 -5.1587434065
 H    1.5952748848 2.8421824688 -4.2467840759
 H    1.6081452765 1.1078830516 -4.5715374002

E (MP2/6-31G(d))  =    -0.10872197588458D+04
Zero-point correction=                          0.625686
Thermal correction to Energy=                   0.652590
Thermal correction to Enthalpy=                 0.653535
Thermal correction to Gibbs Free Energy=        0.573953
E (MP2/6-311++G(d,p))  =    -0.10879300686580D+04
```

Chapter 5

A/M2 *wt* and V27A blockade dissimilarities amongst structurally related adamantyl piperidines. Insights on drug resistance.

5.1 Rationale and previous work

Regardless our previous efforts in the anti-influenza research line had been mainly oriented to replace the adamantane scaffold by a more suitable polycycle[1,2,3], the disclosure of several M2 channel structures with bound amantadine[4,5,6] or adamantane containing compounds[7], provided new detailed insights of the binding mode of adamantane-like molecules. Hence, we decided to take advantage of this recent knowledge to, building up on our expertise, design adamantane related compounds with improved features to display an upgraded inhibition profile.

In line with this, DeGrado's group disclosed in 2011 the spirocompound **52**, which shows an outstanding activity against the V27A, the L26F mutant and the *wt* M2 channels[8]. Worthy of note, Kolocouris et al. had previously reported the synthesis of **54**, an adamantyl piperidine related to **52**[9], which failed to show activity against an Influenza strain carrying an Amt-resistant S31N mutant M2 channel (A/X-31H3N2), and its isomeric piperidine **53**[10,11] that was found to be active against an strain containing a *wt* M2 channel (A/HongKong/7/87/H3N2). They also showed that the lowest energy conformation of **54**, resulted in a geometry quite different that the one shown by the amines **52** and **53**. These facts made us question the importance of the basic centre position in the molecule; hence, in our new designs we orientated this polar group towards the terminal histidines and perpendicular to the protein backbone, analogously to **52** (Chart 4).

[1] Duque, M. D., Ma, C., Torres, E., Wang, J., Naesens, L., Juárez-Jiménez, J., Camps, P., Luque, F. J., DeGrado, W. F., Lamb, R. A., Pinto, L. H. & Vázquez, S. *J. Med. Chem.* **2011**, 54, 2646–2657.

[2] Rey-Carrizo, M., Torres. E., Ma, C., Barniol-Xicota, M., Wang, J., Wu, Y., Naesens, L., Degrado, W. F., Lamb, R. A., Pinto, L. H. & Vázquez S. *J. Med. Chem.* **2013**, 56, 9265-74.

[3] Rey-Carrizo, M., Barniol-Xicota, M., Ma, C., Frigolé-Vivas, M., Torres, E., Naesens, L., Llabrés, S., Juárez-Jiménez, J., Luque, F. J., DeGrado, W. F., Lamb, R. A., Pinto, L. H. & Vázquez, S. *J Med Chem*. **2014**, 57(13):5738-47.

[4] Cady, S.D., Schmidt-Rohr, K., Wang, J., Soto, C., DeGrado, W.F. & Hong, M. *Nature*. **2010**, 463, 689-692

[5] Cady, S.D., Mishanina, T.V. & Hong, M. *J. Mol. Biol.* **2009**, 385, 1127-1141.

[6] Stouffer, A. L., Acharya, R., Salom, D., Levine, A. S., Costanzo, L. D., Soto, C. S., Tereshko, V., Nanda, V., Stayrook, S. & DeGrado, W.F. *Nature*. **2008**, 451, 596-600.

[7] Wu, Y., Canturk, B., Jo, H., Ma, C., Gianti, E., Klein, M. L., Pinto, L. H., Lamb, R. A., Fiorin, G., Wang, J. & DeGrado, W.F. *J.Am.Chem.Soc.* **2014**, 136, 17987-17995.

[8] Wang, J., Ma, C., Fiorin, G., Carnevale, V., Wang, T., Hu, F., Lamb, R. A., Pinto, L. H., Hong, M., Klein, M. L. & DeGrado, W. F. *J. Am. Chem. Soc*. **2011**, 133, 12834-12841.

[9] Kolocouris, A., Tataridis, D., Fytas, G., Mavromoustakos, T., Foscolos, G. B., Kolocouris, N. & De Clercq, E. Synthesis of 2-(2-adamantyl)piperidines and structure anti-influenza virus A activity relationship study using a combination of NMR spectroscopy and molecular modeling. *Bioorg. Med. Chem. Lett*. **1999**, 9, 3465-3470.

[10] Kolocouris, N., Zoidis, G., Foscolos, G. B., Fytas, G., Prathalingham, S. R., Kelly, J. M., Naesens, L. & De Clercq, E. Design and synthesis of bioactive adamantane spiro heterocycles. *Bioorg. Med. Chem. Lett.* **2007**, 17(15), 4358–4362.

[11] Kolocouris, A., Spearpoint, P., Martin, S. R., Hay, A. J., Lopez-Querol, M., Sureda, F. X., Padalko, E., Neyts, J. & De Clercq, E. Comparisons of the influenza virus A M2 channel binding affinities, anti-influenza virus potencies and NMDA antagonistic activities of 2-alkyl-2-aminoadamantanes and analogues. *Bioorg. Med. Chem. Lett*. **2008**, 18 (23), 6156–6160.

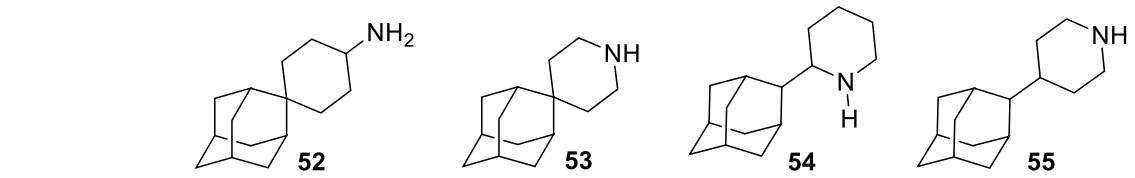

A/M2 wt IC_{50}	= 18.7 μM	= ND	= NA
A/M2 V27A IC_{50}	= 0.3 μM	= ND	= NA
A/M2 L26F IC_{50}	= 5.6 μM	= ND	= NA
		EC_{50}[a]= 0.16 μM	

Chart 4. Anti-influenza adamantyl compounds: spiro compound **52**, piperidines **53** and **54** and the novel envisaged analogue **55**. [a]EC_{50} determined in the influenza A/HongKong/7/87/H3N2 strain, which carries a *wt* channel.

To further address the basic centre orientation remark, besides modifying the position of the nitrogen atom in the piperidine ring, we decided to investigate which was the most suitable anchoring point for this ring, in the adamantane scaffold. For this we prepared two series of adamantyl piperidine analogues bearing the heterocycle in the adamantane C1 (as in amantadine) or C2 (as in the triple inhibitor **52**) positions. Our designs were first studied *in silico* by Prof. Javier Luque's group. Their theoretical calculations indicated that our compounds were very similar to **52**, so their increased length with respect to Amt could provide an improvement of the inhibitory activity (Table 5).

Compound	Length	Frontal view	Side View
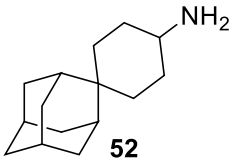 **52**	7,8 Å		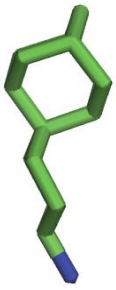
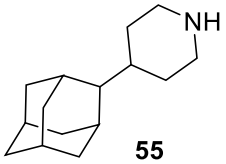 **55**	7,6 Å	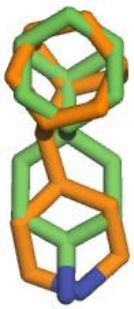	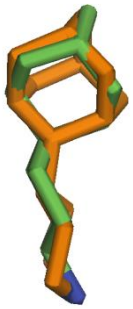

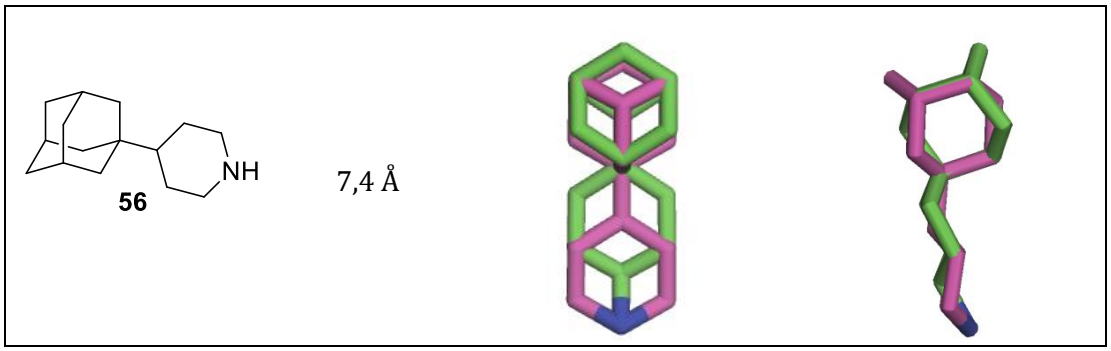

Table 5. Calculated 3-D structures of selected adamantane derivatives.

In light of those predictions we decided to prepare an extra series of C-1 analogues featuring a methylene group between the lipophilic core and the ring, displaying even longer scaffolds.

5.2 Theoretical discussion

While compound **56** and a few related compounds were synthesized in the Thesis of Eva Torres (see manuscript for details), in the present Thesis the compounds belonging to the C-2 series were prepared. The synthetic route to access the derivatives prepared is detailed in the manuscript and shown in scheme 13.

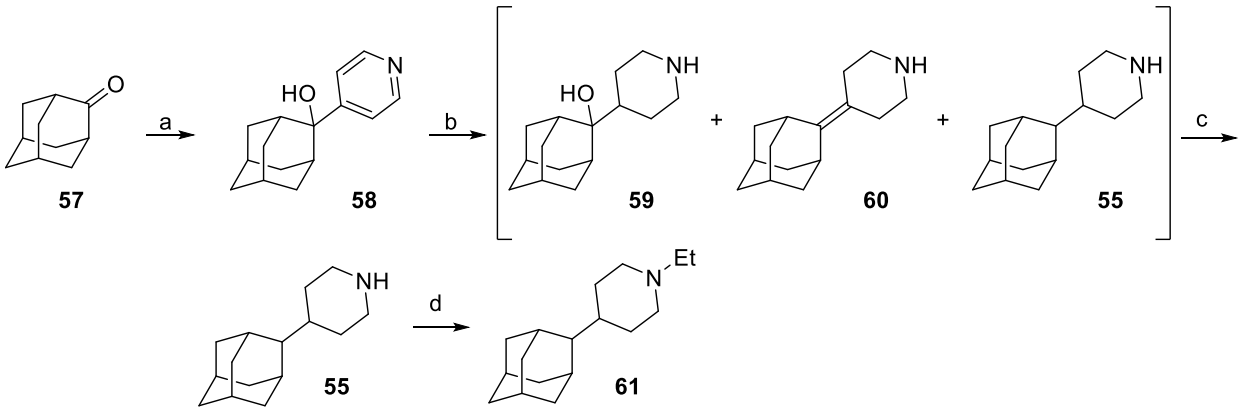

(continues in the next page)

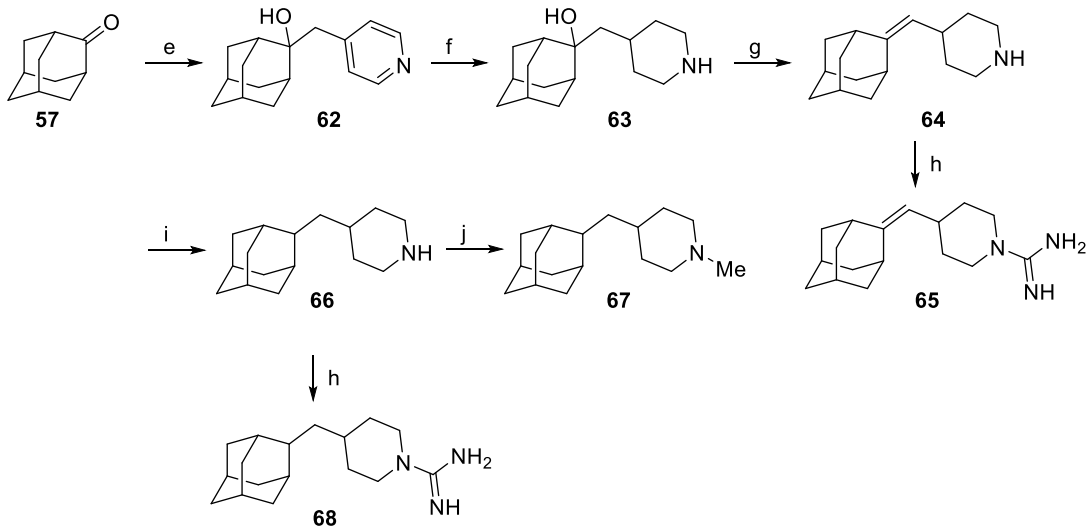

Scheme 13. Synthetic route for the preparation of the adamantyl piperidine C-2 series**.** Reagents and conditions: **a**: 4-pyridyl lithium; Et_2O/THF, -65 °C to rt, 70% yield; **b**: 1 atm H_2, PtO_2, ethanol, rt, 24 h, 93% yield of a mixture of **55**, **59** and **60**; **c**: 1) $SOCl_2$, pyridine, anh. CH_2Cl_2, -60 °C, 30 min, 2) 1 atm H_2, Pd/C, methanol, HCl, rt, 2 h, 63% overall yield; **d**: acetaldehyde, $NaCNBH_3$, AcOH, methanol, rt, 24 h, 76% yield; **e**: 4-picoline, anh THF, *n*-BuLi, 2 h, rt, 90% yield; **f**: 1 atm H_2, PtO_2, HCl, methanol, 5 days, > 99% yield; **g**: $SOCl_2$, pyridine, anh. CH_2Cl_2, -60 °C, 30 min, > 99% yield; **h**: 1*H*-pyrazole-1-carboxamidine hydrochloride, anh Et_3N, acetonitrile, 70 °C, 6 h, 88% yield for **65**, 64% yield for **68**; **i:** 1 atm H_2, Pd/C, methanol, HCl, rt, 2 h, 68% yield; **j**: formaldehyde (37% aqueous solution), $NaCNBH_3$, AcOH, rt, 18 h, 73% yield.

The preparation of both series was envisaged through the same synthetic sequence starting with the addition to 2-adamantanone of the corresponding in situ generated pyridyl lithiate, 4-pyridil lithium or 4-picolinyl lithium, respectively. The formed adamantyl pyridine species was then hydrogenated using platinum oxide as catalyst, to give the first bioactive compound (**59** and **63**). Prior treatment with thionyl chloride and pyridine, the tertiary hydroxyl group was eliminated to yield the corresponding olefin (**60** and **64**) that was on one side, reacted with 1*H*-pyrazole-1-carboxamidine hydrochloride furnishing the guanidine derivative (**65**) and on the other, further hydrogenated using 10% palladium over active charcoal as catalyst to give the saturated analogue (**55** and **66**). This saturated compounds were modified, as previously mentioned, to their guanidine derivatives (**68**) and converted to tertiary amines through a reductive alkylation reaction with acetaldehyde or formaldehyde (**61** and **67**, respectively).

Of note, the catalytic hydrogenation of the adamantyl pyridine **58** in the presence of PtO_2 and hydrochloric acid, instead of the pure piperidine **55**, gave a mixture of the piperidine alcohol **59**, the alkene **60** and the alkane **55**. Presumably this is due to two reaction paths

that simultaneously occur during the pyridine ring hydrogenation: In the first one, the hydroxyl group is protonated in the acid media and readily dehydrates to the olefinic derivative, which is further reduced under catalytic hydrogenation conditions, to the alkane **55.** The alternative route is explained by isomerization or rearrangement events[9], which eventually furnish the alkane **55.**

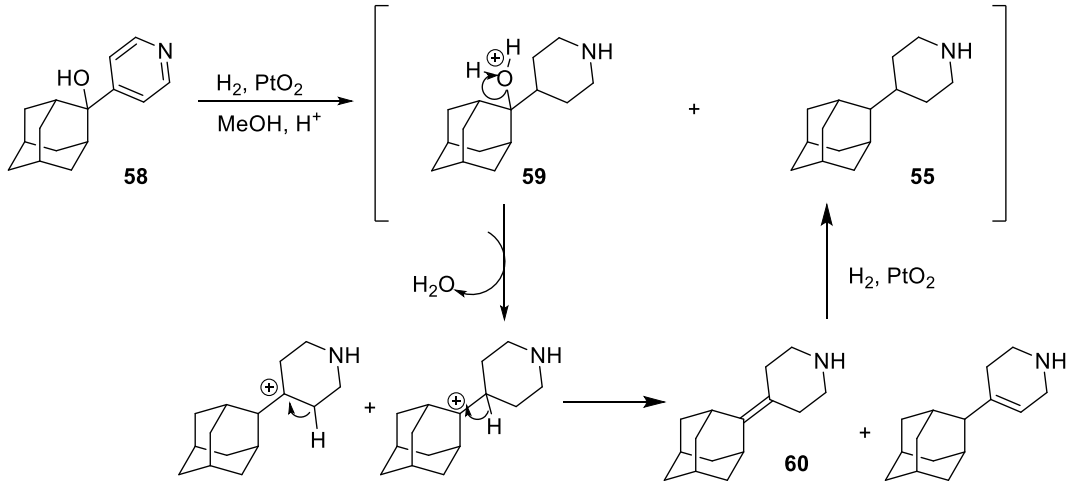

Scheme 14. Hydrogenation of **58** and proposed mechanism for the formation of the products.

The (2-adamantyl)piperidines were evaluated as M2 channel blockers by the group of Prof. Anna Moroni (University of Milan, Italy), who carried further TEVC assays, to assess the kinetics of the M2 channel inhibitors. As in previous series, the antiviral activities were assessed by the group of L. Naesens, for viruses carrying the *wt* or the S31N mutant M2 channels, and by the group of Dr. Jun Wang (Arizona State University, US) for a virus strain carrying the V27A mutant M2 channel.

From their evaluation results and steaming from the lack of correlation observed between those coming from the isochronic inhibition assays, in which several compounds displayed potent M2 blockade, and the antiviral activity assays, in which a reduced number of our molecules were identified as antivirals, we could experimentally prove the V27A resistance mechanism previously proposed *in silico* and through NMR studies. Being that despite the M2 antagonists are able to bind the channel, reason why we could see M2 blockade, this is only maintained for a short time, shown by prolonged electrophysiology experiments, after which the blocker is released from the channel that becomes functional again, observed with the lack of activity in the antiviral assays.

Influenza A *wt*			
Structure	**IC_{50}[a]**	**Kinetics[b]**	**EC_{50}[c]**
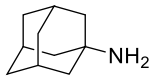 **Amt**	16.0 µM	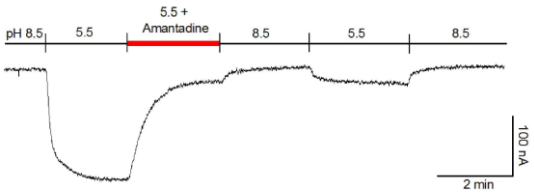	0.2 µM 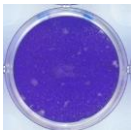
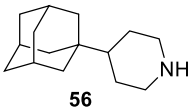 **56**	4.1 µM	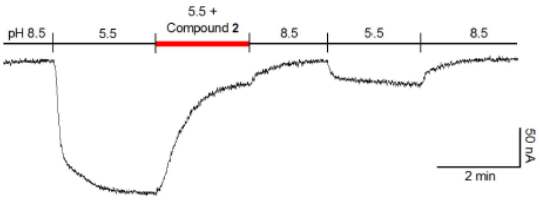	0.2 µM 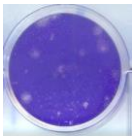
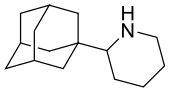 **69**	ND	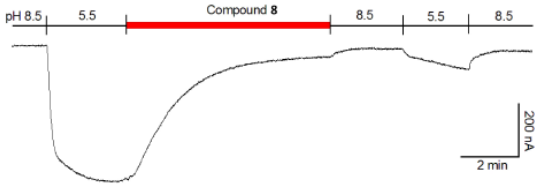	0.8 µM 
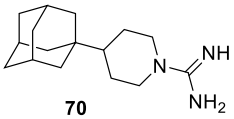 **70**	1.9 µM	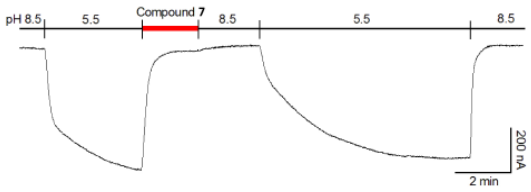	>50 µM

Table 6. Pharmacological assays in M2/wt wrap up. [a]Isochronic (2 min) values for IC_{50} are given.[b] TEV technique in *Xenopus* oocytes. [c] EC_{50} based on 72-h compound exposure time.

In table 5 it can be seen that only the compounds with slow K_{off} (as Amt, **56** and **69**) display antiviral activity, regardless their channel blocking ability. The importance of slowly leaving the channel before the rate of binding to it, can be seen when comparing **70**, which displays M2 blockade at 2 min but not antiviral activity, and **69**, that does not block the channel upon short exposure, due to a slow K_{on}, but displays antiviral activity.

Influenza A V27A			
Structure	**IC_{50}[a]**	**Kinetics[b]**	**EC_{50}[c]**
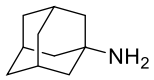 **Amt**	> 500	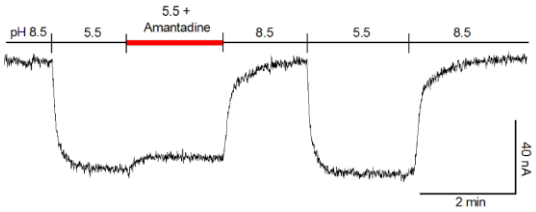	NA 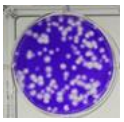
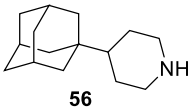 **56**	3.6 µM	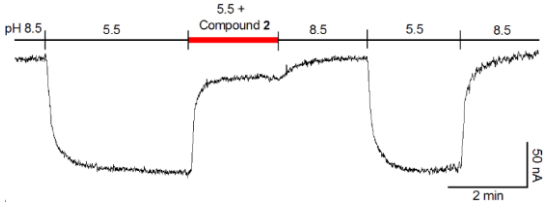	ND 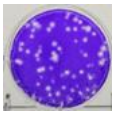
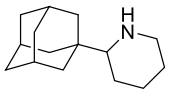 **69**	> 500	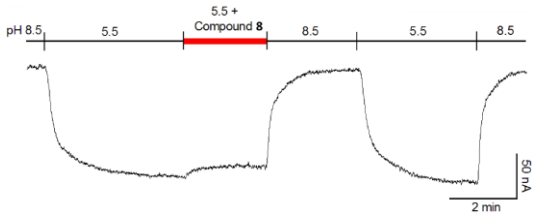	NA 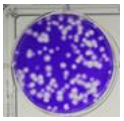
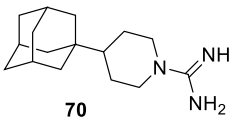 **70**	16.2 µM	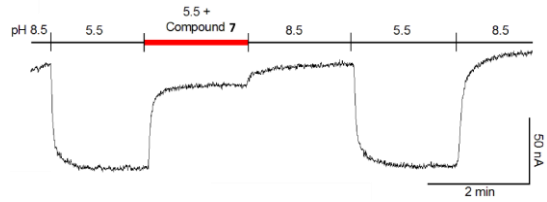	NA 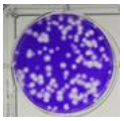

Table 7. Pharmacological assays in M2/V27A wrap up. [a]Isochronic (2 min) values for IC_{50} are given.[b] TEV technique in *Xenopus* oocytes. [c] EC_{50} based on 72-h compound exposure time. [c] EC_{50} based on 72-h compound exposure time. NA = Not active. ND = EC_{50} not determined.

Reassuring our findings in M2/*wt* (table 6) as the kinetics of our compounds revealed a fast K_{off} in M2/V27A, none of the compounds displayed M2 antiviral activity against a virus strain carrying this V27A M2 mutant channel. Note that some of the compounds (**56**, **70**) have the ability to block the M2/V27A channel.

Our new experimental evidence for V27A drug resistance reinforces the previous hypothesis and may lead to a more profound comprehension on how Influenza A virus acquires resistance, to eventually shed light to drug design.

5.3. Follow-up work

In the present Thesis the noradamantane analogues of the 4-(1-adamantyl) piperidine (**56**) and its 2-isomer, prepared by Dr. Eva Torres (see manuscript), were synthesized in a parallel way by decarboxylation of noradamantane carboxylic acid (Scheme 15).

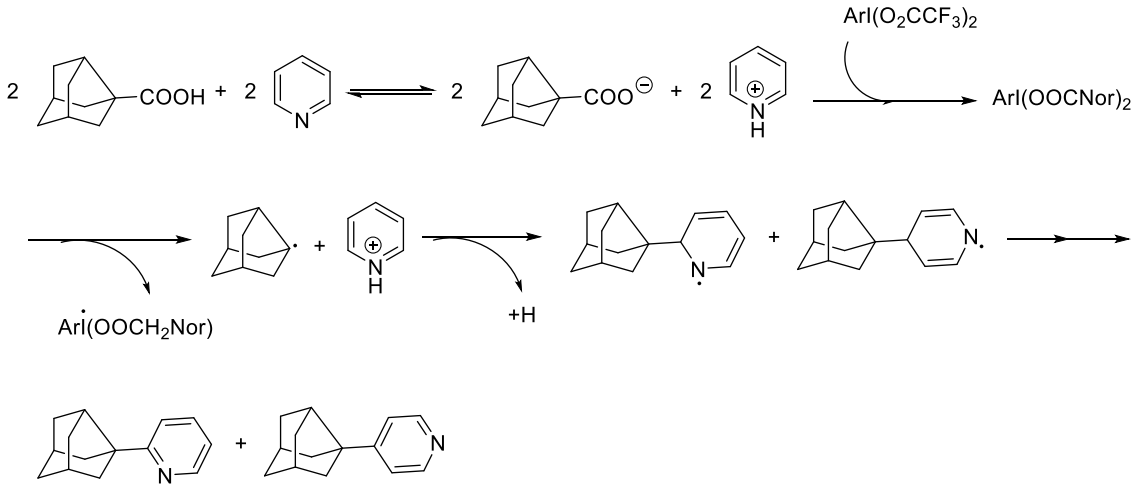

Scheme 15. Radical decarboxylation mechanism of noradamantane carboxylic acid.

Following the work of Togo and co-workers[12], the noradamantane carboxylic acid was reacted with pyridine in the presence of [bis(trifluoroacetoxy)iodo]benzene. The first step in this reaction is the acid-base exchange between noradamantane carboxylic acid and pyridine. Then, the [bis(trifluoroacetoxy)iodo]benzene changes anions, coordinating with the noradamantane carboxylate and displacing the trifluoroacetate moieties, in order to generate [bis(noradamantanecarboxyl)iodo]benzene. This specie undergoes a radical decarboxylation to generate a noradamantyl radical. This radical adds to the pyridinium cation that finally, rearomatizes to yield the desired addition products.

Despite the 4-pyridyl and 2-pyridyl noradamantane analogues were successfully prepared and isolated by means of column chromatography, the low yields obtained in this first step made us abandon this route.

[12] Togo, H., Aoki, M., Kuramochi, M. & Yokoyama, M. *J. Chem. Soc. Perkin Trans. 1*. **1993**, 2417-2427.

Slow but steady wins the race: dissimilarities among new dual inhibitors of the wild-type and the V27A mutant M2 channels of influenza A virus.

Marta Barniol-Xicota,[‡] *Sabrina Gazzarrini,*[#] *Eva Torres,*[‡] *Yanmei Hu,*[⊥,†] *Jun Wang,*[⊥,†] *Lieve Naesens,*[§] *Anna Moroni,*[#] *and Santiago Vázquez**[,‡]

[‡]Laboratori de Química Farmacèutica (Unitat Associada al CSIC), Facultat de Farmàcia i Ciències de l'Alimentació, and Institute of Biomedicine (IBUB), Universitat de Barcelona, Av. Joan XXIII, 27-31, Barcelona, E-08028, Spain

[#]Department of Biosciences and National Research Council (CNR) Biophysics Institute (IBF), University of Milan, Via Celoria 26, 20133 Milan, Italy

[⊥]Department of Pharmacology and Toxicology, College of Pharmacy, The University of Arizona, Tucson, Arizona 85721, United States

[†]BI05 Institute, The University of Arizona, Tucson, Arizona 85721, United States

[§]Rega Institute for Medical Research, KU Leuven, B-3000 Leuven, Belgium

KEYWORDS. Amantadine, drug design, influenza A virus, M2 proton channel, electrophysiology.

ABSTRACT. New insights on the amantadine resistance mechanism of the V27A mutant were obtained through the study of novel, easily accessible 4-(1- and 2-adamantyl)piperidines, identified as dual binders of the wild-type and V27A mutant M2 channels of influenza A virus. Their antiviral activity and channel blocking ability were determined using cell-based assays and two-electrode voltage clamp (TEVC) technique on M2 channels, respectively. In addition, electrophysiology experiments revealed that these inhibitors display a different behaviour against the wild-type *versus* V27A mutant A/M2 channels. This finding provides experimental evidence of the resistance mechanism of the V27A mutation to wild-type inhibitors, previously predicted in silico, and may help design new and more effective drugs.

Introduction

The target of amantadine (Amt) and rimantadine, two well-known clinically approved anti-influenza drugs,[1] is the M2 protein of influenza A virus (A/M2), a 97-residue integral membrane protein that forms an homotetrameric proton selective transmembrane channel with a critical role in the virus replication cycle.[2-11] Unfortunately, most of the circulating strains are Amt-resistant,[12] which has compelled the Centers for Disease Control and Prevention to deter its use.[13] Amt-resistant influenza strains possess one or more mutations in the M2 channel protein.[14,15] Although several mutations appear to be viable *in vitro*,[16] a recent analysis of 31,251 M2 protein sequences revealed that the most frequent Amt-resistant mutations in the circulating strains occur at position 31 (S31N) (~ 95%), followed by position 27 (V27A), while other mutations (L26F, A30T, G34E and L38F) were rare.[12] Although in this analysis the second most prevalent mutant, V27A, was only observed in about 1% of the sequences, other reports have pointed out that the V27A mutant occurred in 10-77% of influenza virus isolates, depending on the viral strain and season.[17,18] Several findings add functional relevance to the V27A mutation: (i) among the most prevalent mutations, V27A is the only one proven to originate from drug selection pressure;[19] (ii) while the S31N and L26F mutants are sensitive, to some extent, to Amt, this

drug is completely ineffective against the V27A mutant M2 channel;[16] (iii) recent studies have noticed an increased frequency of the Amt-resistant V27A/S31N double mutant;[20] and, (iv) finally, a virus harboring this V27A/S31N double mutant form of M2 displayed significantly higher mortality compared to wild-type (wt) virus in a mouse model.[21]

The design of new M2 inhibitors that address the problem of drug resistance is currently of utmost importance. Accordingly, efforts have been recently made to design small molecule inhibitors that target the drug-resistant forms of the influenza A/M2 proton channel.[22,23] While numerous compounds targeting the wt channel have been synthesized,[24-29] few dual inhibitors of the wt and either the V27A,[30-34] or the S31N mutants,[35-41] were only recently identified.

In 2011, Wang *et al.* used a computationally-driven design for the synthesis and pharmacological evaluation of the spiroadamante **1**, a triple inhibitor of the wt, V27A and L26F mutant channels, that features a primary amine.[31] Taking into account that the synthesis of **1** involves six steps from 2-adamantanone and that potent inhibition of the wt and V27A mutant channels was also achieved with secondary amines,[32-34] we wondered whether the synthetically more accessible analogs of **1**, such as the piperidine derivatives **2** and **3** described herein, would have similar channel blockage and antiviral activity as compound **1**. Of note, it is known that Amt (1-aminoadamantane) is, in some influenza A strains, more potent than its 2-isomer (2-aminoadamantane).[42-43] Specifically, the comparison of **2** and **3** would shed light on which position of the adamantane scaffold is more suitable for designing potent V27A inhibitors (Chart 1).

Chart 1. Structures of Amt, rimantadine, spiroadamantane **1** and novel analogs **2-3**.

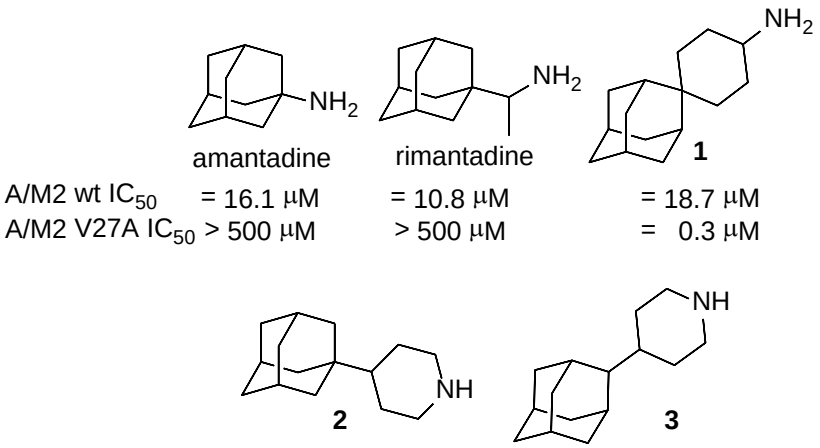

Herein we describe the synthesis and pharmacological evaluation of the aforementioned piperidine derivatives **2** and **3** and some related amines and guanidines. The activity of the compounds has been tested against the wt M2 channel as well as the V27A and S31N mutant forms in the two-electrode voltage clamp (TEVC) assay. Several novel compounds were low micromolar blockers of the wt A/M2 channel and/or the V27A A/M2 variant. Surprisingly, while their blocking abilities in the wt M2 channel nicely correlated with their antiviral activity in a wt-containing influenza A virus, there was a lack of correlation between their V27A channel blockage and antiviral activity of a V27A-containing influenza A virus. Only the 1-adamantyl substituted derivative **2** showed minimal antiviral activity against a virus carrying the V27A A/M2 mutant channel, despite its potent channel blockage. Interestingly, electrophysiology experiments revealed that our dual inhibitors display distinct channel affinities, which translate in two opposite binding patterns,[44] explaining the puzzling antiviral activities observed. Overall, these findings add valuable insights into the drug-resistance mechanism postulated for the V27A mutation.[45-46]

Chemistry

First, we undertook the synthesis of the 4-(1-adamantyl)piperidine, **2**, and its related compounds. Togo and coworkers had previously reported the synthesis of a mixture of the (1-adamantyl)pyridines **5** and **6** by radical decarboxylation of 1-adamantanecarboxylic acid, **4**, in the presence of pyridine.[47] In our hands, compounds **5** and **6** were obtained in a ratio 3 : 1 in 36% overall yield. Both isomers were easily separated by column chromatography. Catalytic hydrogenation of **5** and **6** gave the corresponding piperidines **2** and **8** in 97 and 99% yield, respectively. Kolocouris and coworkers previously reported the synthesis of **8** through a different route, and reported its activity against an H2N2 strain with a wt A/M2 channel.[48] For this reason, we also evaluated compound **8** for M2 channel inhibition (see below), although its basic nitrogen atom must adopt a different orientation in the channel compared to known inhibitors.[49]

While the reaction of amine **2** with 1*H*-pyrazole-1-carboxamide furnished guanidine **7** in 76% yield, several attempts directed towards the synthesis of the corresponding guanidine derived from **8** were unsuccessful, probably reflecting the greater steric congestion around this nitrogen atom (Scheme 1).

Scheme 1. Synthesis of (1-adamantyl)piperidines **2** and **8** and guanidine **7**.[a]

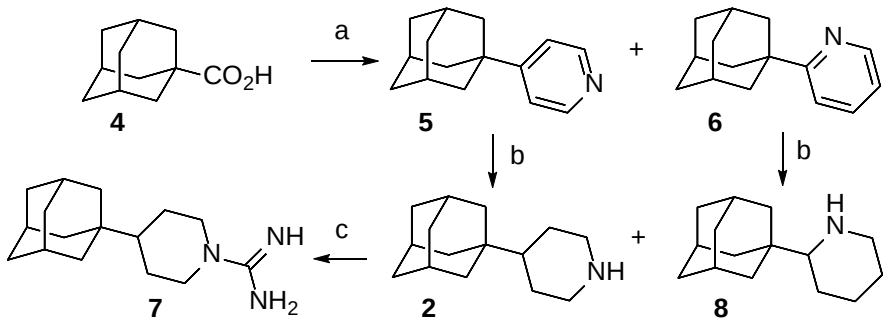

[a]Reagents and conditions: a: pyridine, [bis(trifluoroacetoxy)iodo]benzene, anh. benzene, reflux, overnight, **5**, 9%; **6**, 27%; b: H_2, PtO_2, MeOH, 30 atm, 97% yield for **2**; 99% yield for **8**; c: 1*H*-pyrazole-1-carboxamide hydrochloride, anh. Et_3N, acetonitrile, reflux, 6 h, 76% yield.

In order to synthesize piperidines **3** and **12**, we followed the pioneering work of Kolocouris *et al.* for the synthesis of the related 2-(2-adamantyl)piperidine,[50] but starting from 4-pyridyl lithium instead of 2-pyridyl lithium. The addition of 4-pyridyl lithium –synthesized *in situ* from air and light sensitive 4-bromopyridine–, to 2-adamantone, **9**, furnished the expected tertiary alcohol **10** in 70% yield. Catalytic hydrogenation of **10** or its hydrochloride under several conditions did not gave the pure alcohol **11**, but a complex mixture of **3**, **11** and **12** along with other minor impurities, presumably arising from isomerization or rearrangement.[50] By crystallization from CH_2Cl_2, we were able to isolate the pure alcohol **11** from **3** and **12**. Several unsuccessful attempts were made to elicit **3** and **12** from the mother liqueurs (containing **3**, **12** and remaining **11**) by crystallization or column chromatography, but without success. Therefore, we decided to proceed directly to piperidine **3** by treating the mixture with a dehydrating agent, securing the conversion of **11** to **12**, followed by catalytic hydrogenation to solely yield the compound **3**. Of note, after several fruitless dehydration trials with the acknowledged Burgess' reagent or anhydrous oxalic acid, which was successfully applied to a very related alcohol,[51] we finally were able to dehydrate the tertiary alcohol in very high yields using an extremely inexpensive, facile and fast procedure reported by Álvarez-Manzaneda *et al.*,[52] which involves the use of a mixture of $SOCl_2$ and pyridine in CH_2Cl_2. The catalytic hydrogenation of the remaining mixture of **3** and **12,** furnished the piperidine **3** in nearly quantitative yield (Scheme 2).

Since water molecules in the M2 channel are believed to play an important role in assisting the binding of the amino group of the putative inhibitor,[9,15,53] we decided to check the effect of introducing a tertiary amine in compound **3**. This was accomplished through the reductive alkylation of **3**, the assumption being that the ethyl derivative **13** should be less potent as M2 channel inhibitor than the secondary amine **3**. The reductive alkylation of **3** with acetaldehyde and $NaBH_3CN$ in methanol in the presence of acetic acid led to **13**.

Scheme 2. Synthesis of 4-(2-adamantyl)piperidines and related compounds from 2-adamantanone, **9**.[a]

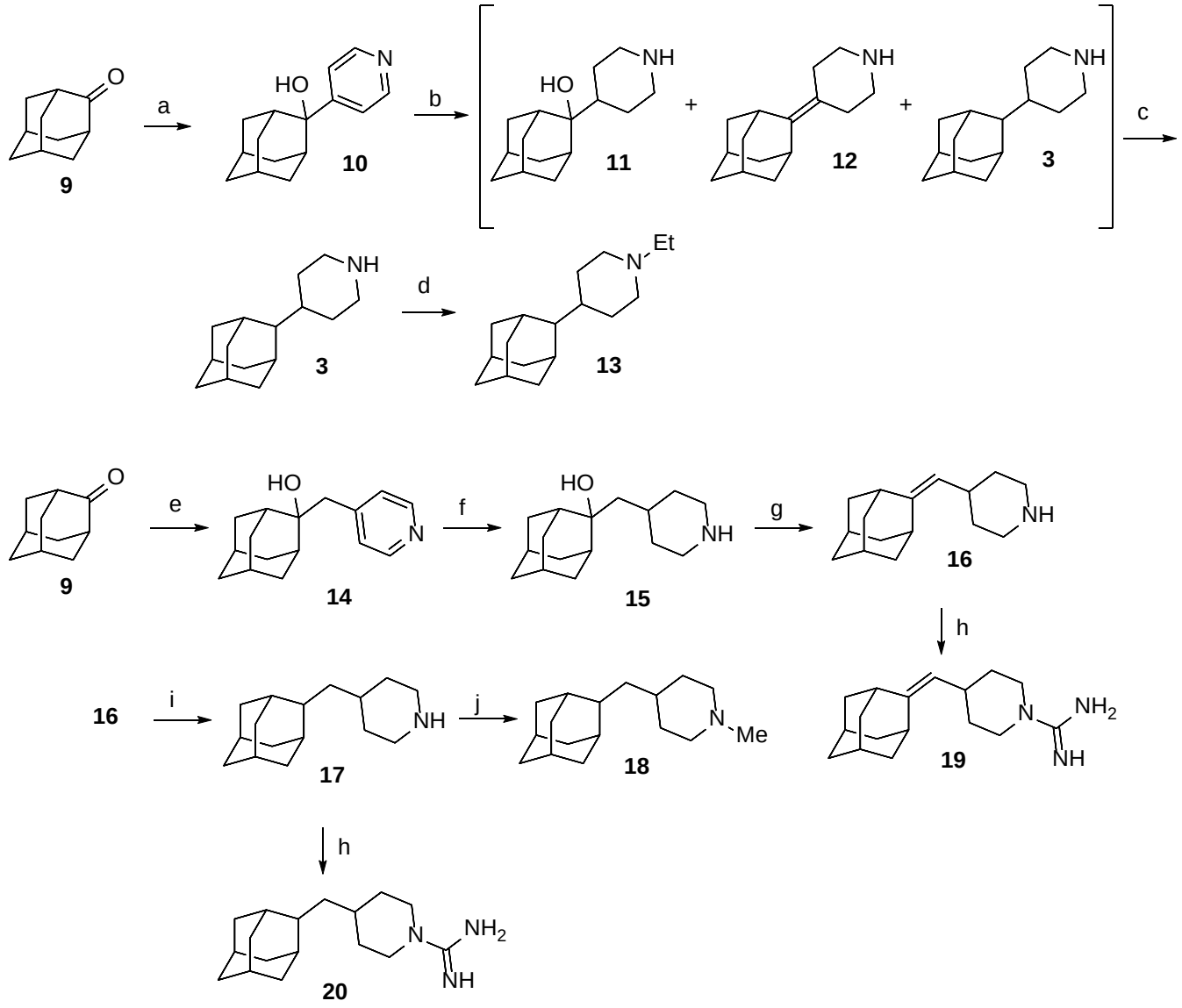

[a]Reagents and conditions: **a**: 4-pyridyl lithium; Et_2O/THF, −65 °C to rt, 70% yield; **b**: 1 atm H_2, PtO_2, ethanol, rt, 24 h, 93% yield of a mixture of **3**, **11** and **12**; **c**: 1) $SOCl_2$, pyridine, anh. CH_2Cl_2, -60 °C, 30 min, 2) 1 atm H_2, Pd/C, methanol, HCl, rt, 2 h, 63% overall yield; **d**: acetaldehyde, $NaCNBH_3$, AcOH, methanol, rt, 24 h, 76% yield; **e**: 1) 4-picoline, anh THF, *n*-BuLi; 2) **9**, 2 h, rt, 90% yield; **f**: 1 atm H_2, PtO_2, HCl, methanol, 5 days, > 99% yield; **g**: $SOCl_2$, pyridine, anh. CH_2Cl_2, -60 °C, 30 min, > 99% yield; **h**: 1*H*-pyrazole-1-carboxamidine hydrochloride, anh Et_3N, acetonitrile, 70 °C, 6 h, 88% yield for **19**, 64% yield for **20**; **i:** 1 atm H_2, Pd/C, methanol, HCl, rt, 2 h, 68% yield; **j**: formaldehyde (37% aqueous solution), $NaCNBH_3$, AcOH, rt, 18 h, 73% yield.

On the other hand, since the lumen of the V27A M2 protein is wider than that of the wt channel,[54-55] size-expanded Amt derivatives should lead to better inhibition of the V27A mutant channel.[31-34] Taking into account the poor inhibitory activity displayed by the first series (see discussion of inhibitory activity of **3** and **13** below), a second group of piperidine derivatives was envisaged from 2-adamantanone, **9**. The second series featured an increased length thanks to the introduction of an additional carbon atom between the piperidine and the adamantyl group. The addition of the organolithium derivative of 4-picoline to 2-adamantanone furnished alcohol **14** in 90% yield. The subsequent catalytic hydrogenation to the piperidine hydrochloride **15** elapsed in excellent yields. The dehydration of **15** using Alvarez-Manzaneda's procedure[52] led to alkene **16** in quantitative yield. Upon catalytic hydrogenation, **16** smoothly furnished **17** in 79% yield. Finally, guanidines **19** and **20** were synthesized from **16** and **17**, respectively, by reaction with 1*H*-pyrazole-carboxamidine hydrochloride. The tertiary amine **18** was prepared through a reductive alkylation of **17** with formaldehyde in 84% yield (Scheme 2).

Inhibition of the wt A/M2 ion channel and amantadine-resistant mutant forms

The inhibitory activity of the compounds was tested on A/M2 channels expressed in *Xenopus laevis* oocytes, using the TEVC technique. All inhibitors were initially tested at 100 µM. In the next step, the IC_{50} values for the compounds that inhibited the V27A channel by more than 60% were obtained using an isochronic (2 min) inhibition assay. The results are given in Table 1. As reference, Amt inhibited the wt A/M2 channel with an IC_{50} of 16.0 µM, while displaying much lower activity against the S31N mutant channel (IC_{50} of 200 µM),[56] and being totally inactive against the V27A mutant.[32]

For the wt M2 channel and any given scaffold, the guanidine derivative was more potent than the corresponding amine for the pairs **19** *versus* **16**, and **20** *versus* **17**, although such a difference was less apparent for the pair of compounds **7** *versus* **2**. Similar trends were also observed from the inhibitory data determined against the V27A mutant. Thus, the presence of the guanidinium fragment presumably

offers a better anchoring to the inhibitors in the interior of the wt M2 channel, though this effect is more relevant for compounds with a non-linear structural scaffold, as found in **16** and **17**. These results are in line with those previously reported for other sets of molecules.[32-33]

Moving the adamantane ring from position 2, as found in **8** and in the family of compounds reported by Kolocouris *et al*.,[48,50] to position 4 of the piperidine, as in the rest of our new inhibitors, had a clear incremental effect on the inhibitory activity for both wt and V27A channels. Indeed, the inhibitory effect increases from 48.1 (**8**) to 92% (**2**) in the wt M2 channel, and from 10.1 (**8**) to 85.7% (**2**) in the V27A mutant M2 channel. On the other hand, the insertion of an extra carbon atom between the adamantane and piperidine rings (**3** *versus* **17**) seemed to have little influence on the inhibitory potency. A larger effect, however, was achieved in both channels when moving the anchoring point of the piperidine ring from the C-2 position of adamantane, as in **3**, to the C-1 position, as in **2** and **7**. This change triggered a substantial increase of the inhibitory activity against both wt and V27A channels, as noted in the 11- and 17-fold reduction of the IC_{50} observed between compounds **3** and **2**. Unluckily, none of the tested molecules had activity against the S31N channel (<10%) (data not shown).

The electrophysiological inhibition assay for wt and mutant channels routinely uses a fixed time of 2 min to calculate the isochronical inhibitory constant (IC_{50}). As the amino alcohols **11** and **15** showed to be very poor inhibitors under these conditions, together with the fact that the bindings were far from saturated at 2 min, additional experiments were performed at longer times, taking **11** as a representative example. Even after 10 min, **11** inhibited only 30% of the wt channel current (data not shown). This observation suggests that the introduction of a hydroxyl group in the middle part of the molecule is deleterious for activity (**11** *versus* **3** or **15** *versus* **17**). Nevertheless, after incubation for 6 min compound **8** led to more than 90% inhibition of the *wt* channel (Figure 1D). This potent inhibition by compound **8** agrees with its activity in the cell-based antiviral assay (see below), in which the compound is applied for longer incubation times to achieve equilibrium.

Table 1. Inhibitory effect of the synthesized compounds on proton channel function of wt or V27A mutant A/M2.[a,b]

Compound	A/M2 wt (mean ± SE)		A/M2 V27A (mean ± SE)	
	Inhibition by 100 μM for 2 min (%)	IC_{50} (μM)	Inhibition by 100 μM for 2 min (%)	IC_{50} (μM)
Amantadine	91.0 ± 2.1	16.0 ± 1.2	8.9 ± 1.0	>500[32]
2	92.0 ± 1.4	4.1 ± 0.5	85.7 ± 1.5	3.6 ± 0.6
3	70.7 ± 2.4	45.3 ± 2.3	61.9 ± 2.3	60.6 ± 5.1
7	91.8 ± 1.0	1.9 ± 0.2	79.3 ± 2.8	16.2 ± 1.7
8	48.1 ± 3.4[c]	ND	10.1 ± 0.6	>500
11	10.9 ± 0.8[d]	ND	13.1 ± 0.6	ND
13	43.9 ± 1.0	ND	23.5 ± 2.1	ND
15	18.4 ± 2.8	ND	14.6 ± 1.9	ND
16	64.0 ± 4.3	ND	44.2 ± 1.9	ND
17	76.7 ± 4.0	ND	47.3 ± 3.5	ND
18	48.9 ± 10.7	ND	29.2 ± 0.9	ND
19	89.9 ± 0.9	6.8 ± 1.4	63.0 ± 0.9	46.0 ± 1.1
20	94.7 ± 1.2	4.2 ± 0.1	77.8 ± 1.5	21.7 ± 2.6

[a]The activity of the inhibitors was measured using the TEVC technique on A/M2 channels expressed in Xenopus oocytes; percentage of inhibition was the mean of at least three experiments. For IC_{50} experiments, 7-9 concentrations were measured, and, at each concentration, experiments were run at least three times. [b]Isochronic (2 min) values for IC_{50} are given. [c]The inhibition for 4 min was ca 75% and > 90% after 6 min of treatment. [d]The inhibition for 7 min was ca 25% and ca 30% after 10 min. See text and supporting information for details. ND, Not determined.

Antiviral activity and cytotoxicity in cell culture

The anti-influenza virus activity of the compounds was determined in MDCK cells using two different assays, i.e. a 24-h virus yield assay (based on RT-qPCR quantification of virus in the supernatant), and a 72-h virus plaque reduction assay (PRA), both with the A/HK/7/87 virus (H3N2 subtype), which carries a wt M2 protein (Table 2). Guanidine derivatives **7**, **19** and **20** did not display antiviral activity (data not shown). In the PRA (Figure 1), amines **2** and **8** and amino alcohol **15** were found to be active, with **2** being equally potent as Amt (EC_{50} = 0.14 μM for the two compounds in the PRA assay). Considering that compound **15** did not inhibit the wt M2 channel in the TEVC assay, its antiviral activity in cell culture suggests the involvement of another mechanism of action, an observation that we previously made for other adamantane derivatives.[43,57-58] In the case of compound **8**, its greater potency in the PRA compared to the electrophysiological method relates to its slow A/M2 binding kinetics (see Figure 2 and Table 3). Of note, the antiviral activity determined for **8** (EC_{50} = 1.0 μM) is very similar to the EC_{50} value of 3.3 μM that was reported for this compound by Kolocouris *et al*. in an assay with an H2N2 virus strain.[48] In addition, the antiviral activity of **2** and **8** (but not compound **15**) was confirmed in our virus yield assay (Table 2). This antiviral effect was seen at concentrations well below the cytotoxic concentrations, since compound **2** had a selectivity index (ratio of CC_{50} to EC_{50} based on 72-h compound exposure time) of 128, and compound **8** was devoid of cytotoxicity at 100 μM, the highest concentration tested.

The anti-influenza virus activity of compounds **2**, **3**, **7** and **19**, that inhibited the V27A channel (Table 1), was also determined in MDCK cells using a 46-h virus PRA with the A/WSN/33 virus (H1N1 subtype), which carries a N31S/V27A M2 protein. Compound **8**, that did not inhibit the V27A channel but showed antiviral activity against the A/HK/7/87, was also assayed. Surprisingly, in addition to **8**, compounds **3**, **7** and **19** were inactive and only a weak activity was found for compound **2** that clearly did not match its high potency in the TEVC assay (Table 1 and Figure S1).

Table 2. Antiviral activity in influenza virus-infected MDCK cells.[a]

Compound	Antiviral activity (μM) against A/HK/7/87 (wt M2)		Cytotoxicity (μM)
	EC_{50} (PRA)[b]	EC_{99} (Virus yield)[c]	CC_{50}[d]
2	0.14	≥1.7	18
3	ND	≥50	>100
7	>50	>2	10
8	1.0	3.5	>100
11	>100	76	>100
13	>10	>10	25
15	10	>50	>50
16	>5	>10	25
17	>10	>2	15
18	>10	>2	6.2
19	>5	>2	19
20	>10	>2	3.8
Amantadine	0.14	0.51	>500
Rimantadine	0.016	1.1	>500

[a]MDCK: Madin-Darby canine kidney cells; virus strain: A/HK/7/87 (A/H3N2 carrying wt M2). [b]EC_{50} in the virus plaque reduction assay (PRA): concentration at which the plaque number is reduced by 50% compared to untreated virus control. [c]EC_{99}: compound concentration giving 2-$\log_{10}$ reduction in virus yield, as determined by quantifying the virus in the supernatant at 24 h post infection, using an RT-qPCR based method.[59] [d]CC_{50}: 50% cytotoxic concentration, as determined by the MTS cell viability test in uninfected cells exposed to the compounds during 72 h. Values shown are the mean of 2-3 determinations. ND, not determined.

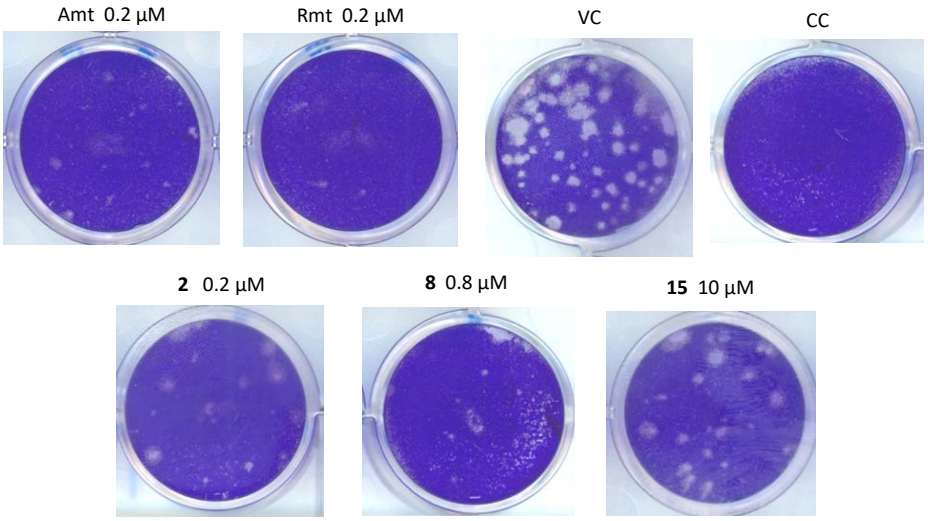

Figure 1. Activity of the compounds in the influenza virus plaque reduction assay. MDCK cells were infected with influenza virus (strain A/HK/7/87; 30 PFU per well) in the presence of the test compounds. After 72 h incubation, plaques were visualized by crystal violet staining. VC: mock-treated virus control; CC: uninfected cell control.

Inhibition kinetics of the wt A/M2 ion channel and amantadine-resistant mutant forms

To further characterize the inhibitory effects on wt and V27A channels and rationalize the antiviral results, the current kinetics of the most potent channel blockers **2**, **7**, **8**, **19** and **20** were determined and compared with the profile obtained for Amt (Figure 2 and Table 3; see also results for **19** and **20** in SI). Analysis of the curves for the wt channel (left panels in Figure 2) showed that the forward rate constant (k_{on}) for association and inhibition by compound **7** (654 $\pm$ 51 M^{-1} s^{-1}) was around 2.3-fold faster than the values obtained for compound **2** (259 ± 29 M^{-1} s^{-1}) and Amt (293 ± 37 M^{-1} s^{-1}). At saturating compound concentrations (100 µM), the slow k_{off} rate found for compounds **2** and **8** identified them as strong binders, thus resembling the behavior of Amt, which has a k_{off} rate of 3×10^{-4} s^{-1} (Figure 2A-B).[44] Contrarily, compound **7** dissociated from the channel after 5 min, an observation that may explain the failure to display antiviral activity in the PRA despite being able to block the channel (Figure 2C). This

result is consistent with the 33-fold slower k_{off} found for Amt ($3x10^{-4}$ s^{-1})[44] relative to compound **7** (10^{-2} s^{-1}) (Table 3). Compounds **19** and **20**, with rapid k_{on} and k_{off} values, displayed the same weak binding affinity as **7** (see Figures S2 and S3).

In the case of the V27A mutant channel (right panels in Figure 2), compounds **2** and **7** had higher affinity (IC_{50} of 3.6 ± 0.6 and 16.2 ± 1.7 μM, respectively) compared with Amt (IC_{50} > 500 μM)[32] and compound **8** (IC_{50} > 500 μM) (Table 1). Despite **2** and **7** showed greater k_{on} rate constants compared to Amt and **8**, which allowed them to display channel blockade at the 2 min assay (unlike Amt or **8**), all four compounds were weak (**2**, **8**) to very weak (Amt, **7**) affinity binders of the V27A mutant channel, exemplified with the faster k_{off} displayed. Hence, although these compounds can bind the V27A channel, and both **2** and **7** even show a fast association that allows to follow the inhibition of the proton current, the weak binding affinity facilitates dissociation during washing at pH 8.5, rendering the channel functional again (Figure 2E-H and Table 3),[44] noted in the dissociation constant (K_d) of 4.4 × 10^{-5} for compound **2**. This behavior agrees with the resistance mechanism proposed for Amt in the V27A mutant.[46] Interestingly, the case of compound **2** clearly exemplifies the different outcomes in the wt and V27A channels: although this compound has similar IC_{50} values (4.1 and 3.6 μM, respectively), the faster k_{off} in the mutated channel, probably reflecting a worse fitting to the wider pore,[54-55] allows the compound to be washed away, revoking the channel blockade. This fact correlates with the antiviral activity assays (see above), justifying that some compounds with promising V27A mutant M2 channel blockade activities fail to behave as good antivirals likely due to fast dissociation (fast k_{off} rate).

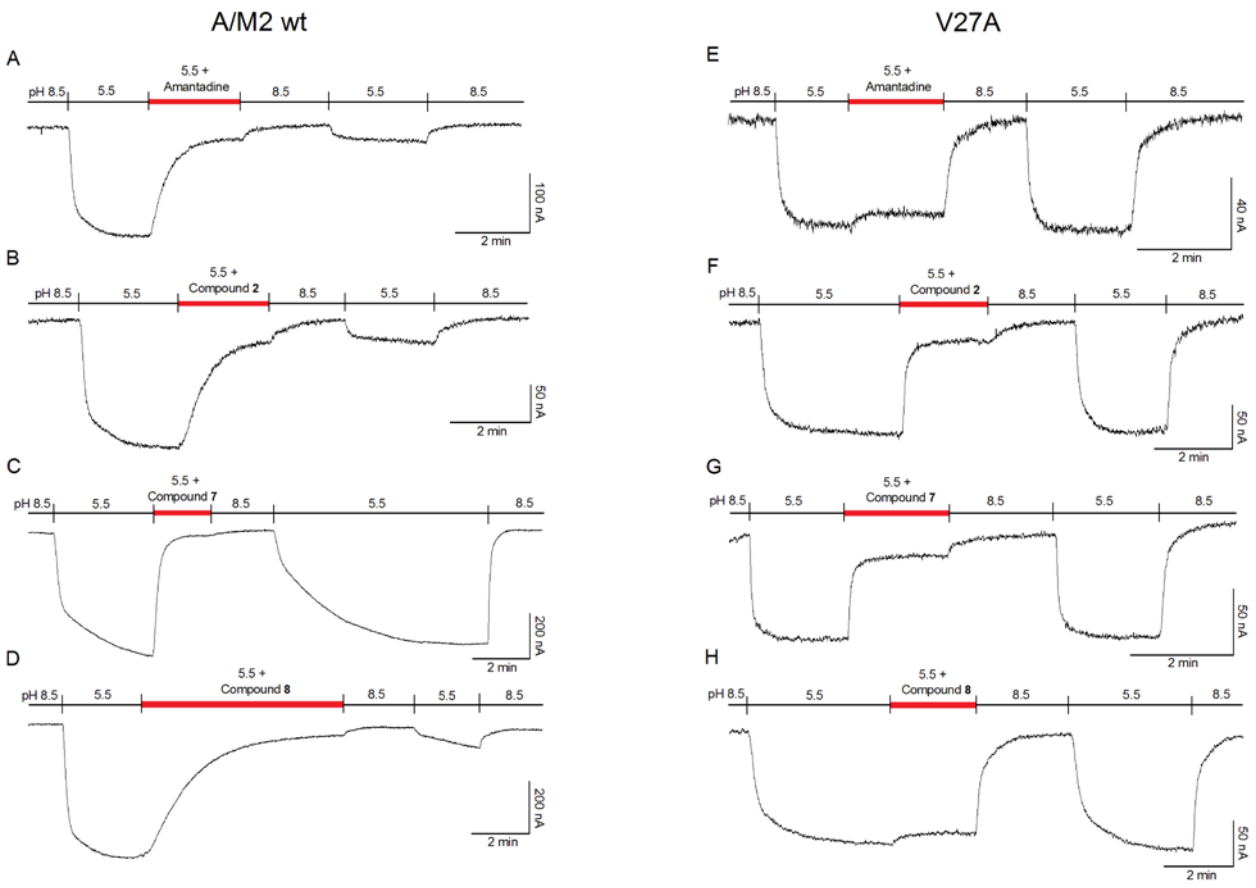

Figure 2. Inhibition of the A/M2 wt channel (derived from the A/Udorn/307/72 H3N2 virus strain) and V27A mutant form, using the TEVC technique in *Xenopus* oocytes. Oocytes were bathed in Barth solution at pH = 8.5 and pH = 5.5. Current was clamped at -20 mV and the indicated compounds were applied at 100 μM in pH 5.5 solution once the inward current reached maximum amplitude in A/M2 wt channel (A-D) and V27A mutant channel (E-H).

Table 3. Rate constants for association (k_{on}) and dissociation (k_{off}) of the compounds to/from the A/M2 wt or V27A mutant channels.[a]

Compound	A/M2 wt (mean ± SE)		V27A (mean ± SE)	
	k_{on} (M^{-1} s^{-1})	k_{off} (s^{-1})	k_{on} (M^{-1} s^{-1})	k_{off} (s^{-1})
Amantadine	293 ± 37 (4)	$3x10^{-4}$ (ref 44)	360 ± 18 (4)	$16x10^{-2}$ (1)
2	259 ± 29 (4)	ND	1369 ± 149 (9)	$6x10^{-2}$ ± 0.006 (5)
7	654 ± 51 (5)	10^{-2} ± 0.001 (3)	1028 ± 167 (9)	$14x10^{-2}$ ± 0.041 (3)
8	119 ± 11 (3)	ND	595 ± 48 (4)	$4x10^{-2}$ (1)

[a]Currents from Figure 1 were fitted to a single exponential function ($y=e^{-t/\tau}$ + constant with $r>0.94$) and the time constant τ was used to calculate the forward rate constant after addition of compound ($k_{on} = 1/[\text{compound}]\ \tau$) and the reverse rate constant during the washout at pH 5.5 ($k_{off} = 1/\tau$).[44] Number of tested oocytes in brackets. ND, not determined.

Conclusions

Several adamantane derivatives have been synthesized and tested as potential inhibitors of the influenza A virus. The novel 4-(1-adamantyl)piperidine **2** and its guanidine derivative **7**, were low micromolar blockers of the wt and V27A mutant M2 channels. The following SAR trends were observed: (i) alkylation of a secondary amine to a tertiary amine reduced the activity (**3** vs **13** and **17** vs **18**); (ii) switching the adamantane ring from position 2 to position 4 of the piperidine, triggered faster association rate to the channel (**8** vs **2**); (iii) moving the piperidine ring from the C-2 position of the adamantane, as in **3**, to the C-1 position, as in **2**, led to an increase in the inhibitory activity on both channels. The inhibitory activity of **2** was confirmed in cell-based antiviral (virus plaque reduction and virus yield) assays. Of note, the most potent compound in the antiviral assays, amine **2**, is synthetically accessible in just two steps from commercially available precursors and has a selectivity index of 128 (Table 2).

Remarkably our electrophysiological experiments have revealed some unexpected differences among structurally very similar compounds. Namely, amine **2** is a slow but strong binder of the wt channel, (Figure 2B), while its binding being fast and weak in the V27A (Figure 2F). Its guanidine derivative, **7**, behaves in both channels as a fast and weak binder (Figures 2C and 2G), meanwhile the compound **8**, its 2-piperidine isomer, shows a very slow but strong binding with the wt M2 channel (Figure 2D) and no remarkable binding at all with the V27A mutant channel (Figure 2H).

Building up from these findings we can conclude that: (1) M2 channel blockers with potent influenza A antiviral activity usually show slow but steady binding to the channel,[44] (2) caution has to be taken when defining M2 inhibitors solely by isochronic inhibition assays, M2 channel blockers are very slow binders, so the IC_{50} depends on the amount of time the drug is exposed to the target. In our case a good correlation between the TEVC and the antiviral activity for the amine **2** (IC_{50} = 4.1μM and EC_{50} = 0.14 μM, respectively) was observed in inhibiting wt M2. Nevertheless, while all the guanidine derivatives were pointed out to be potent dual inhibitors of the M2 and V27A channels by TEVC assays, their inactivity in the plaque reduction assays proved the TEVC predictions to be completely wrong. On top of that, the TEVC assay failed to identify **8**, shown to be one of the most promising antivirals synthesized (see Tables 1 and 2). (3) The fast (rapid k_{on}) but weak affinity (rapid k_{off}) behavior observed in our compounds for the V27A A/M2 mutant channel, goes in line with the proposed drug resistance mechanism by in silico[11,55,60-61] and structural[54] approaches. This is the first time the drug resistance mechanism is experimentally evidenced. Hence, our findings not only reinforce the previous in silico hypothesis but also lead to a more profound understanding of the influenza A virus resistance mechanism and to potential avenues for M2 inhibitor design.

Experimental section[62]

Plasmid, mRNA synthesis, and microinjection of oocytes. The cDNA encoding the influenza A/Udorn/72 (A/M2) was inserted into pSUPER vector for the expression on oocyte plasma membrane. A/M2 S31N and A/M2 V27A mutants were generated by QuikChange site-directed mutagenesis kit (Agilent Technologies). The synthesis of mRNA and microinjection of oocytes have been described previously.[63]

Two-electrode voltage clamp analysis. Macroscopic membrane current was recorded 24-72 hours after injection as described previously.[30] Oocytes were perfused at room temperature in Barth's solution containing (in mM) 88 NaCl, 1 KCl, 2.4 $NaHCO_3$, 0.3 $NaNO_3$, 0.71 $CaCl_2$, 0.82 $MgCl_2$, and 15 HEPES for pH 8.5 or 15 MES for pH 5.5 at a rate of 2 mL/min. The tested compounds were dissolved in DMSO and applied (100 μM) at pH 5.5 when the inward current reaches maximum. The compounds were applied for 2 min, and residual membrane current was compared with the membrane current before the application of compounds. The compounds were typically applied for 2 min, and residual membrane current was compared with the membrane current before the application of compounds. Membrane currents were recorded at −20 mV and analyzed with pCLAMP 10.0 software package (Axon Instruments, Sunnyvale, CA).

Antiviral assays. The anti-influenza virus activity in Madin-Darby canine kidney (MDCK) cells was determined by plaque reduction (PRA) and virus yield assays. For the PRA, influenza virus A/HK/7/87 (A/H3N2) was incubated (1 h at 4°C) with different concentrations of the compounds, and then added to confluent MDCK cells in 12-well plates. After 1 h incubation at 35°C, excess virus was removed and replaced by fresh medium containing the compounds and 0.8% agarose. After 72 h incubation, plaques were visualized by cell fixation with 3.7%

formaldehyde and staining with 0.1% crystal violet. For the virus yield assay, MDCK cells grown in 96-well plates were infected with influenza virus A/HK/7/87, and at the same time the test compounds were added in serial dilutions. After 24 h incubation at 35 ºC, supernatants were harvested to determine the virus yield by RT-qPCR.[59,64] In parallel, mock-infected cell cultures were used to determine the compounds' cytotoxicity. After 72 h incubation at 35 °C, cell viability was measured by the formazan-based MTS assay and the OD values were used to calculate the compound concentrations causing 50% cytotoxicity (CC_{50}).[64]

The PRA with A/WSN/33 N31S/V27A (H1N1) virus was carried out similarly as previously described.[31] Briefly, MDCK cells monolayers in 6-well plates were infected with virus (~100 PFU/well). After adding the inoculums, cells were kept in 4 °C for 1 h to synchronize the infection, then cells were moved to 37 °C incubator for 1 h. The inoculums were removed, and the cells were washed with phosphate buffered saline (PBS). The cells were then overlaid with DMEM containing 1.2% Avicel microcrystalline cellulose (FMC BioPolymer, Philadelphia, PA) and NAT (2.0 µg/ml). To examine the effect of the drugs on plaque formation, at 46 h after infection, the monolayers were fixed and stained with 0.2% crystal violet in 20% methanol.

Synthesis of 4-(1-adamantyl)piperidine hydrochloride, 2·HCl. A solution of compound **6** (830 mg, 3.9 mol) and PtO_2 at 10% (83 mg) in methanol (100 mL) containing few drops of HCl was hydrogenated at room temperature, at a pressure of 30 atm until no more hydrogen absorption was observed. The resulting suspension was filtered and the residue washed with methanol. The solvent was removed under vacuo to obtain amine **2·HCl** (970 mg, 97% yield) as a white solid. The analytical sample was obtained by crystallization from 2-propanol, mp 272-273 ºC (dec). IR (KBr) 3674, 2900, 2846, 2728, 2671, 2503, 1597, 1446, 1396, 1344, 1075, 1023, 960 cm^{-1}. ^{1}H-RMN (500 MHz, CD_3OD) δ 1.20 (tt, *J* = 12.3 Hz, *J*' = 3.2 Hz, 1 H, 4-H),

1.49 [qd, *J* = 14.0 Hz, *J*' = 4.0 Hz, 2 H, 3(5)-H_{ax}], 1.57 [d, *J* = 2.6 Hz, 6 H, 2'(8', 9')], 1.68 (d, *J* = 11.3 Hz, 3 H) and 1.77 (d, *J* = 12.1 Hz, 3 H) [4'(6', 10')-H_{exo} and H_{endo}], 1.94 [bs, 2 H, 3(5)-H_{eq}], 1.99 [bs, 3 H, 3'(5', 7')-H], 2.91 [dt, *J* = 13.1 Hz, *J*' = 2.9 Hz, 2 H, 2(6)-H_{ax}], 3.42 [dt, *J* = 12.4 Hz, *J*' = 2.2 Hz, 2 H, 2(6)-H_{eq}]. ^{13}C-RMN (125.7 MHz, CD_3OD) δ 23.6 [CH_2, C3(5)], 30.1 [CH, C3'(5', 7')], 35.0 (C, 1'), 38.3 [CH_2, C4'(6', 10')], 40.3 [CH_2, C2'(8', 9')], 45.8 (CH, C4), 46.0 [CH_2, C2(6)]. MS (EI), m/e (%); main ions: 219 ($M^{\cdot+}$, 100), 218 (21), 205 (60), 163 (15), 135 ($C_{10}H_{15}^+$, 83), 93 (27), 91 (19), 85 (83), 84 (50), 83 (21), 79 (33), 77 (16), 58 (18), 57 (48), 56 (25), 55 (21).

Synthesis of 2-(1-adamantyl)piperidine hydrochloride, 8·HCl. From a solution of compound **6** (2.25 g, 10.5 mol) and PtO_2 at 10% (225 mg) in MeOH (100 mL) containing few drops of HCl and following the same procedure than the previously mentioned for the synthesis of **2·HCl**, amine **8·HCl** (2.67 g, 99% yield) was obtained as a white solid, 262-265 ºC (dec). IR (ATR) 3392, 2911, 2855, 2754, 2698, 2481, 1585, 1431, 1413, 1375, 1342, 1304, 1276, 1054, 1016, 971, 814 cm-1. cm^{-1}. ^{1}H-RMN (400 MHz, CD_3OD) δ 1.40-2.04 [complex signal, 18 H, 3-H_2, 4-H_2, 5-H_2, 2'(8',9')-H_2, 4'(6',10')-H_2], 2.06 [broad s, 3 H, 3'(5',7')-H], 2.71 (dd, *J* = 11.6 , *J*' = 2.4 Hz, 1 H, 2-H), 3.00 (dt, *J* = 13.0 Hz, *J*' = 3.2 Hz, 1 H, 6-H_{ax}), 3.41 (dm, *J* = 13.0 Hz, 1 H, 6-H_{eq}). ^{13}C-RMN (100.6 MHz, CD_3OD) δ 23.6 (CH_2), 23.8 (CH_2) and 23.9 (CH_2) (C3, C4 and C5), 29.6 [CH, C3'(5', 7')], 36.0 (C, 1'), 37.6 [CH_2, C4'(6', 10')], 39.1 [CH_2, C2'(8', 9')], 47.6 (CH_2, C6), 46.0 (CH, C2). HRMS-ESI$^+$ m/z $[M+H]^+$ calcd for [C15H25N+H+]: 220.2060, found: 220.2061.

Synthesis of *N*-amidyl-4-(1-adamantyl)piperidine hydrochloride, 7·HCl. In a 10 mL round-bottomed flask equipped with a condenser and a magnetic stirrer, a suspension of amine **2·HCl** (484 mg, 1.9 mmol), 1*H*-pyrazole-1-carboxamidine hydrochloride (333 mg, 2.3 mmol),

anhydrous triethylamine (0.47 mL) in acetonitrile (5 mL) was prepared. The reaction was heated at 70 °C for 6 hours. The reaction was cooled down and stored at 4ºC overnight. The suspension was filtered out and the filtrate washed with cold acetonitrile obtaining the guanidine **7·HCl** as a beige solid (428 mg, 76% yield). The analytical sample was obtained by crystallization from 2-propanol, mp > 300 (dec.). IR (KBr) 3112, 2898, 2845, 1639, 1597, 1526, 1446, 1345, 1195, 1160, 967, 743 cm^{-1}. ^{1}H-RMN (400 MHz, CD_3OD) δ 1.18 (tt, *J* = 12.4 Hz, *J'* = 3.2 Hz, 1 H, 4-H), 1.31 [qd, *J* = 13.2 Hz, *J'* = 3.6 Hz, 2 H, 3(5)-H_{ax}], 1.57 [d, *J* = 2.4 Hz, 6 H, 2'(8', 9')], 1.68 (d, *J* = 12.0 Hz, 3 H) and 1.76 (d, *J* = 12.0 Hz, 3 H) [4'(6', 10')-H_{exo} and H_{endo}], 1.83 [dd, *J* = 13.2 Hz, *J'* = 1.6 Hz, 2 H, 3(5)-H_{eq}], 1.98 [bs, 3 H, 3'(5', 7')-H], 2.98 [td, *J* = 13.2 Hz, *J'* = 2.0 Hz, 2 H, 2(6)-H_{ax}], 3.93 [dt, *J* = 13.2 Hz, *J'* = 2.4 Hz, 2 H, 2(6)-H_{eq}]. ^{13}C-RMN (100.6 MHz, CD_3OD) δ 26.1 [CH_2, C3(5)], 30.1 [CH, C3'(5', 7')], 35.0 (C, 1'), 38.3 [CH_2, C4'(6', 10')], 40.5 [CH_2, C2'(8', 9')], 47.5 (CH, C4), 47.6 [CH_2, C2(6)], 157.4 (C, C=NH). MS (EI), m/e (%); main ions: 261 ($M^{\cdot+}$, 2), 219 (13), 135 ($C_{10}H_{15}^{+}$, 30), 129 (96), 128 (100), 127 (38), 101 (11), 93 (17), 91 (16), 88 (16), 87 (17), 86 (15), 85 (15), 79 (23), 77 (12), 75 (13), 74 (14), 67 (11), 57 (24), 56 (18), 55 (16).

2-(4-Piperidinyl)adamantan-2-ol, 11. A solution of the aminoalcohol **10** (980 mg, 4.27 mmol) in absolute ethanol, was hydrogenated over PtO_2 (100 mg) at room temperature and 1 atm pressure for 24 hours. After filtration in order to remove the catalyst, it was concentrated under reduced pressure and the white solid obtained, washed with pentane, giving 930 mg (aprox. 93%) of a mixture of **11**, **3** and **12**. An analytical sample of **11** was obtained by crystallization from dichloromethane, mp > 231 °C (dec.); IR (ATR) 3427, 2906, 2850, 2794, 2729, 2663, 2501, 1694, 1590, 1451, 1433, 1410, 1357, 1327, 1287, 1137, 1054, 1034, 991, 950, 928, 756 cm^{-1}. ^{1}H NMR (400 MHz, $CDCl_3$) δ 1.44-1.94 (complex signal, 16 H, adamantanyl-H and

3'(5´)-H_2], 2.08 (tt, *J* = 11.6 Hz, *J'* = 3.6 Hz, 1 H, 4'-H), 2.13 [d, *J* = 12.4 Hz, 2 H, adamantanyl-H), 2.4-2.7 (very broad signal, 2 H, NH and OH), 2.67 [td, 2 H, *J* = 12.4 Hz, *J'* = 2.8 Hz, 2'(6')-H_{ax}], 3.37 [broad d, 2 H, *J* = 12.4 Hz, 2'(6')-H_{eq}]. ^{13}C NMR (100.6 MHz, $CDCl_3$) δ 24.2 [CH_2, C3'(5')], 26.9 (CH) and 27.2 (CH) (C5 and C7), 33.0 [CH_2, C4(9) or C8(10)], 33.6 [CH, C1(3)], 33.7 [CH_2, C8(10) or C4(9)], 38.1 (CH, C4'), 38.2 (CH_2, C6), 46.4 [CH_2, C2'(6')], 75.0 (C, C2). GC/MS (EI), m/e (%); main ions: 235 ($M^{\cdot+}$, 9), 234 (42), 219 (18), 218 (100), 216 (28), 151 (24). HRMS-ESI$^+$ m/z $[M+H]^+$ calcd for [$C_{15}H_{25}NO+H^+$]: 236.2009, found: 236.2011.

4-(Adamantan-2-yl)piperidine hydrochloride, 3·HCl. $SOCl_2$ (0.42 mL, 5.8 mmol) was slowly added to a mixture of **3**, **11** and **12** (850 mg; ca 3.9 mmol) and pyridine (0.84 mL) in anhydrous CH_2Cl_2 (8 mL) at -60 °C. The reaction mixture was stirred at this temperature under argon atmosphere for 30 min and quenched with sat. aq. Solution of $NaHCO_3$ (1 mL) and the cooling bath was removed. The mixture was poured into diethyl ether-water (90 mL : 20 mL) and the phases were shaken and separated. The organic phases were reunited, washed with brine, dried over Na_2SO_4 and concentrated to dryness under reduced pressure. The yellow solid residue (a mixture of **3** and **12**, GC/MS) was solved in methanol containing few drops of conc. HCl and hydrogenated with Pd/C (460 mg) at room temperature and 1 atm pressure of H_2, for 2 hours. After filtration of the catalyst, the solvent was concentrated under reduced pressure and the white solid obtained was washed with pentane, giving 183 mg (21% yield) of the piperidine **3·HCl**. An analytical sample was obtained by crystallization from dichloromethane, mp 252-254 ºC. IR (ATR) 3311, 2931, 2911, 2850, 2820, 2785, 2724, 2501, 1598, 1451, 1423, 1302, 1279, 1041, 983 cm^{-1}. ^{1}H NMR (400 MHz, $CDCl_3$) δ 1.21-2.02 (complex signal, 20 H, adamantanyl-H and 3(5)-H_2], 2.91 [td, *J* = 12.4 Hz, *J'* = 3.2 Hz, 2 H, 2'(6')-H_{ax}], 3.34 [broad d, 2 H, *J* = 12.4 Hz, 2'(6')-H_{eq}]. ^{13}C NMR (100.6 MHz, $CDCl_3$) δ 28.6 [CH_2, C3(5)], 29.1 (CH) and 29.5 (CH) (C5'

and C7'), 29.7 [CH, C1'(3')], 32.7 [CH_2, C4'(9') or C8'(10')], 34.6 (CH, C4), 39.3 (CH_2, C6'), 40.2 [CH_2, C8'(10') or C4'(9')], 45.8 [CH_2, C2(6)], 50.4 (CH, C2'). GC/MS (EI), m/e (%); main ions: 219 ($M^{\cdot+}$, 17), 204 (100), 174 (20), 162 (93), 84 (32), 82 (18), 79 (20), 57 (22), 56 (27). HRMS-ESI+ m/z $[M+H]^+$ calcd for $[C_{15}H_{25}N+H^+]$: 220.2060, found: 220.2059.

Synthesis of 4-(adamantan-2-yl)-1-ethylpiperidine hydrochloride, 13·HCl. To a solution of **3·HCl** (100 mg, 0.39 mmol) in water (5 mL) was added a 10 N aqueous solution of NaOH. It was then extracted with EtOAc (3 x 5mL) and the organic phase was dried over Na_2SO_4, filtered and concentrated under vacuo (yellowish oil, 85 mg, quantitative yield). This oil was dissolved in MeOH (5 mL) and sodium cyanoborohydride (73.5 mg, 1.17 mmol), acetaldehyde (21 mg, 0.48 mmol) and glacial acetic acid (0.1 mL) were added to the solution. The solution was stirred at room temperature for 8 hours and a second portion of sodium cyanoborohydride (73.5 mg, 1.17 mmol) and acetaldehyde (21 mg, 0.48 mmol) were added. The yellow solution was further stirred at room temperature overnight. It was concentrated under vacuo and the yellow oil was solved in water (5 mL) and extracted with EtOAc (3 x 5 mL). The organic phase was dried over Na_2SO_4, filtered and concentrated under vacuo. Column chromatography of the solid (silica gel, hexane/EtOAc mixtures) gave the pure amine as an off-white solid (84 mg, 76%). An analytical sample of the hydrochloride was obtained by adding an excess of Et_2O·HCl to a solution of **13** in EtOAc followed by filtration of the obtained solid, mp > 300 °C (dec.); IR (ATR) 3336, 2911, 2850, 2643, 2531, 1648, 1453, 1433, 1393, 1244, 1107, 976 cm^{-1}. ^{1}H NMR (400 MHz, CD_3OD) δ 1.35 (t, *J*= 7.4 Hz, 3 H, $NCH_2C\underline{H}_3$), 1.58 [d, *J* = 12.4 Hz, 2 H, 4'(9')-H_a or 8'(10')-H_a], 1.74 [d, *J* = 10.4 Hz, 2 H, 8'(10')-H_a or 4'(9')-H_a], 1.76-1.95 [complex signal, 13 H, 3(5)-H_2 and 9-adamantyl-H], 2.09 (m, 1 H) and 2.12 (m, 1 H) (1'-H and 3'-H), 2.93 [td, *J* = 12.6 Hz, *J*' = 2.4 Hz, 2 H, 2(6)-H_{ax}], 3.15 (q, *J* = 7.4 Hz, 2 H, $N\underline{C}H_2CH_3$), 3.58 [dm, *J* = 12.6 Hz, 2 H, 2(6)-

H_{eq}]. ^{13}C NMR (100.6 MHz, CD_3OD) δ 9.6 (CH_3, $NCH_2\underline{C}H_3$), 28.9 [(CH_2, C3(5)], 29.1 (CH) and 29.4 (CH) (C5' and C7'), 29.9 [CH, C1'(3')], 32.7 [CH_2, C4'(9') or C8'(10')], 34.2 (CH, C4), 39.2 (CH_2, C6'), 40.1 [CH_2, C8'(10') or C4'(9')], 50.2 (CH, C2'), 53.3 (CH_2, $N\underline{C}H_2CH_3$), 53.7 [CH_2, C2(6)]. GC/MS (EI), m/e (%); main ions: 247 ($M^{\cdot+}$, 10), 233 (18), 232 (100), 58 (23). HRMS-ESI$^+$ m/z $[M+H]^+$ calcd for $[C_{17}H_{29}N+H^+]$: 248.2373, found: 248.2374.

Synthesis of 2-(piperidin-4-ylmethyl)adamantan-2-ol hydrochloride, 15·HCl. A solution of **14** (3.0 g, 12.3 mmol) and conc HCl (6 mL, 72 mmol) in methanol (50 mL), was hydrogenated over PtO_2 (50 mg) at room temperature and 1 atm for 5 days in which H_2 was recharged. After filtration in order to remove the catalyst, it was concentrated under reduced pressure, obtaining the desired product **15·HCl** as a white solid in quantitative yield. mp > 300 °C (dec.) IR (ATR) 3407, 2901, 2845, 2789, 2729, 2516, 2156, 1595, 1448, 1350, 1282, 1254, 1127, 1044, 1019, 1006, 958, 930 cm^{-1}. ^1H NMR (400 MHz, $CDCl_3$) δ 1.47 [m, 2 H, 3'(5')-H_{ax}], 1.54 [m, 2 H, 4(9)-H_a or 8(10)-H_a], 1.68 (d, *J* = 5.6 Hz, 2 H, 2C-C$\underline{H}_2$), 1.70-1.94 (complex signal, 11 H, 5-H, 7-H, 4'-H, 1(3)-H, 6-H_2 and C8(10)-H_2 or C4(9)-H_2], 2.02 [dm, *J* = 13.2 Hz, 2 H, 3'(5')-H_{eq}], 2.29 [dm, *J* = 12.0 Hz, 2 H, 4(9)-H_b or 8(10)-H_b], 2.98 [td, *J* = 12.4 Hz, *J'* = 3.2 Hz, 2 H, 2'(6')-H_{ax}], 3.34 [broad d, 2 H, *J* = 12.4 Hz, 2'(6')-H_{eq}]. ^{13}C NMR (100.6 MHz, $CDCl_3$) δ 28.9 (CH) and 29.9 (CH) (C5 and C7), 30.1 (CH, C4'), 32.0 [CH_2, C3'(5')], 33.8 [CH_2, C4(9) or C8(10)], 35.6 [CH_2, C8(10) or C4(9)], 38.4 [CH, C1(3)], 39.5 (CH_2, C6), 45.1 (CH_2, C2-$\underline{C}H_2$), 45.4 [CH_2, C2'(6')], 76.4 (CH, C2). HRMS-ESI$^+$ m/z $[M+H]^+$ calcd for [C16H27NO+H^+]: 250.2165, found: 250.2170.

Synthesis of 4-[(adamantan-2-ylidene)methyl]piperidine hydrochloride, 16·HCl. $SOCl_2$ (0.42 mL, 5.78 mmol) was slowly added to a solution of **15·HCl** (1.0 g, 3.50 mmol) and pyridine (0.84 mL) in dry CH_2Cl_2 (8 mL) at -60 °C. The reaction mixture was stirred at this temperature

under argon atmosphere for 30 min and quenched with saturated aqueous solution of $NaHCO_3$ (1 mL) and the cooling bath was removed. The mixture was poured into diethyl ether-water (90 mL : 20 mL) and the phases were shaken and separated. The aqueous layer was further extracted with diethyl ether twice. The organic phases were joined, washed with brine, dried over Na_2SO_4 and evaporated to give **16** as a white solid in quantitative yield. An analytical sample of the hydrochloride was obtained by adding an excess of $Et_2O{\cdot}HCl$ to a solution of **16** in diethyl ether, mp > 300 °C (dec.). IR (ATR) 3397, 2921, 2845, 2718, 2658, 2541, 2506, 1663, 1625, 1595, 1527, 1469, 1443, 1421241, 1100, 1077, 976, 930, 849, 806 cm^{-1}. 1H-NMR (400 MHz, CD3OD) δ: 1.44 [dq, 2 H, *J* = 4.0 Hz, *J'* = 12.6 Hz, 3(5)-H_{ax}], 1.68-1.82 (complex signal, 6 H, 3(5)-H_{eq}, 4'(10')-Ha and 8'(9')-H_a], 1.87 [broad s, 2 H, 5'(7')-H], 1.88-1.96 (complex signal, 6 H, 6'-H_2, 4'(10')-Hb and 8'(9')-H_b], 2.30 (broad s, 1 H, 1'-H), 2.51 (m, 1 H, 4-H), 2.85 (broad s, 1 H, 3'-H), 2.88 [dt, 3 H, *J* = 12.8 Hz, *J* = 2.8 Hz, 2(6)-H_{ax}], 3.26 [dm, 2 H, *J* = 12.8 Hz, 2(6)-H_{eq}], 4.90 (d, 1 H, *J* = 8.8 Hz, C2'=CH). ^{13}C-NMR (100.6 MHz, CD_3OD) δ: 29.9 [CH, C5´(7´)], 31.8 [CH_2, C3(5)], 33.2 (CH, C4), 34.1 (CH, C3'), 38.2 (CH2, C6'), 40.2 [CH_2, C4'(10') or C8'(9')], 40.9 [CH_2, C8'(9)' or C4'(10')], 41.9 (CH, C1'), 45.4 [CH_2, C2(6)], 121.1 (CH, C2'=CH), 149.8 (C, C2'). GC/MS (EI), m/e (%); main ions: 231 ($M^{\cdot+}$, 5), 83 (10), 82 (100), 57 (12). HRMS-ESI^+ m/z $[M+H]^+$ calcd for [$C_{16}H_{25}N+H^+$]: 232.2060, found: 232.2062.

Synthesis of 4-[(adamantan-2-yl)methyl]piperidine hydrochloride, 17·HCl. A solution of **16** (230 mg; 1 mmol) in methanol containing few drops of conc HCl, was hydrogenated over Pd/C (5% Pd, 23 mg) at room temperature and 1 atm pressure, for 2 hours. After filtration in order to remove the catalyst, it was concentrated under reduced pressure and the white solid obtained, washed with pentane, giving **17·HCl** (183 mg, 68% yield), mp > 278 °C (dec.). IR (ATR) 3397, 2906, 2845, 2718, 2496, 1595, 1448, 1385, 1271, 1100, 1072, 973, 953 cm^{-1}. ^{1}H-

NMR (400 MHz, CD_3OD) δ: 1.35 [m, 2 H, 3(5)-H_{ax}], 1.45 (t, 2 H, *J* = 7.6 Hz, Ad-CH_2-piperidine), 1.56 [d, 2 H, *J* = 12.8 Hz, 4'(9')-Ha or 8'(10')-H_a], 1.64 (m, 1 H, 4-H), 1.67 [s, 2 H, 1'(3')-H], 1.75-1.98 (complex signal, 14 H, 2'-H, 5'-H, 7'-H, 3(5)-H_{eq}, 8(10)-H_b or 4(9')-H_b, 6'-H_2, C8(10)-H_2 or C4(9)-H_2], 2.97 [tm, 2 H, *J* = 12.8 Hz, 2(6)-H_{ax}], 3.37 [dm, 2 H, *J* = 12.8 Hz, 2(6)-H_{eq}]. ^{13}C-NMR (100.6 MHz, CD_3OD) δ: 29.5 (CH) and 29.7 (CH) (C5' and C7'), 30.4 [CH_2, C3(5)], 32.4 (CH, C4), 32.6 [CH_2, C4'(9) or C8'(10')], 33.4 [CH, C1'(3')], 39.4 (CH_2, C6'), 40.2 (CH_2, Ad-CH_2-piperidine), 40.3 [CH_2, C8'(10') or C4'(9')], 41.9 (CH, C2'), 45.4 [CH_2, C2(6)]. GC/MS (EI), m/e (%); tr 20.5 min: 233 ($M^{\cdot+}$, 11), 219 (16), 218 (100), 98 (31), 85 (95), 84 (77), 82 (22), 79 (20), 67 (18), 57 (39), 56 (30), 55 (18). HRMS-ESI^+ m/z $[M+H]^+$ calcd for [$C_{16}H_{27}N+H^+$]: 234.2216, found: 234.2215.

4-[(adamantan-2-yl)methyl]-*N*-methylpiperidine, 18·HCl. In a 250 mL round bottom flask was added **17·HCl** (123 mg, 0.5 mmol), $NaBH_3CN$ (94.2 mg, 1.5 mmol), formaldehyde (37% aqueous solution, 0.13 mL, 1.5 mmol) and glacial acetic acid (0.1 mL) and left stirring, covered with a $CaCl_2$ tube at 30 °C overnight. The mixture was concentrated in vacuo, the residue was suspended in water (10 mL) and the solution was made basic with aqueous solution of 2 N NaOH and extracted with EtOAc (1×50 mL) and dichloromethane (2 x 50 mL). The combined organic extracts were dried, filtered and concentrated under vacuum. The corresponding hydrochloride, **18·HCl**, was made by adding an ethereal solution of HCl to a solution of the residue in EtOAc and purified by crystallization from diethyleter (104 mg, 73% yield), mp 265-267 °C. IR (ATR) 3417, 3362, 2906, 2850, 2663, 2546, 1615, 1464, 1451, 1256, 1067, 955 cm^{-1}. ^{1}H-NMR (400 MHz, CD_3OD) δ: 1.44 (t, 2 H, *J* = 6.8 Hz, Ad-C$\underline{H}_2$-piperidine), 1.45 [m, 2 H, 3(5)-H_{ax}], 1.55 [broad d, 2 H, *J* = 12.8 Hz, 4'(9')-H_a or 8'(10')-H_a], 1.59 (m, 1 H, 4-H), 1.66 [s, 2 H, 1'(3')-H], 1.74-1.82 (complex signal, 6 H, 2'-H, 5'-H or 7'-H, 8(10)-H_a or 4(9')-H_a, 6'-H_2],

1.84-2.00 (complex signal, 7 H, 8(10)-H_2 or C4(9)-H_2], 7'-H or 5'-H, 3(5)-H_{eq}], 2.83 (s, 3 H, NCH_3), 2.70 [broad t, 2 H, *J* = 12.8 Hz, 2(6)-H_{ax}], 3.47 [broad d, 2 H, *J* = 12.8 Hz, 2(6)-H_{eq}]. ^{13}C-NMR (100.6 MHz, CD_3OD) δ: 29.5 (CH) and 29.6 (CH) (C5' and C7'), 31.3 [CH_2, C3(5)], 31.8 (CH, C4), 32.5 [CH_2, C4'(9) or C8'(10')], 33.3 [CH, C1'(3')], 39.4 (CH_2, C6'), 39.9 (CH_2, Ad-$\underline{C}H_2$-piperidine), 40.3 [CH_2, C8'(10') or C4'(9')], 42.0 (CH, C2'), 44.1 (CH_3, N-$\underline{C}H_3$), 56.0 [CH_2, C2(6)]. HRMS-ESI$^+$ m/z [*M*+H]$^+$ calcd for [$C_{17}H_{29}N+H^+$]: 248.2373, found: 248.2374.

Synthesis of 4-[(adamantan-2-ylidene)methyl]piperidine-1-carboximidamide hydrochloride, 19·HCl. In a 10 mL round-bottomed flask equipped with a condenser and a magnetic stirrer, a suspension of amine **16** (131 mg, 0.56 mmol), 1*H*-pyrazole-1-carboxamidine hydrochloride (86.3 mg, 0.59 mmol), anhydrous triethylamine (0.12 mL, 0.86 mmol) in acetonitrile (3 mL) was prepared. The reaction was heated at 70 °C for 6 hours. The reaction was cooled down and stored at 4 °C overnight. The suspension was filtered out and the filtrate washed with cold pentane obtaining the guanidine **19·HCl** as a white solid (131 mg, 88% yield). mp 266-272 °C (dec.). IR (ATR) 3245, 3139, 2901, 2850, 1648, 1614, 1512, 1441, 1342, 1168, 1122, 960 cm^{-1}. ^{1}H-NMR (400 MHz, CD_3OD) δ: 1.35 [m, 2 H, 3(5)-H_{ax}], 1.65-1.79 (complex signal, 6 H, 3(5)-H_{eq}, 4'(10')-H_a and 8'(9')-H_a], 1.88 [broad s, 2 H, 5'(7')-H], 1.88-1.96 (complex signal, 6 H, 6'-H_2, 4'(10')-H_b and 8'(9')-H_b], 2.29 (broad s, 1 H, 1'-H), 2.58 (m, 1 H, 4-H), 2.87 (broad s, 1 H, 3'-H), 3.12 [dt, 3 H, *J* = 13.6 Hz, *J* = 2.8 Hz, 2(6)-H_{ax}], 3.85 [dm, 2 H, *J* = 13.6 Hz, 2(6)-H_{eq}], 4.90 (d, 1 H, *J* = 8.8 Hz, C2'=C$\underline{H}$). ^{13}C-NMR (100.6 MHz, CD_3OD) δ: 30.0 [CH, C5'(7')], 33.4 [CH_2, C3(5)], 34.1 (CH, C3'), 34.2 (CH, C4), 38.2 (CH_2, C6'), 40.2 [CH_2, C4'(10') or C8'(9')], 40.9 [CH_2, C8'(9)' or C4'(10')], 41.9 (CH, C1'), 46.9 [CH_2, C2(6)],

121.0 (CH, C2'=CH), 149.7 (C, C2'), 157.5 (C, C=NH). HRMS-ESI$^+$ m/z [*M*+H]$^+$ calcd for [$C_{17}H_{27}N_3$+H^+]: 274.2278, found: 274.2275.

4-[(adamantan-2-yl)methyl]piperidine-1-carboximidamide hydrochloride, 20·HCl. In a 10 mL round-bottomed flask equipped with a condenser and a magnetic stirrer, a suspension of amine **17·HCl** (83 mg, 0.3 mmol), 1*H*-pyrazole-1-carboxamidine hydrochloride (54.2 mg, 0.37 mmol), anhydrous triethylamine (0.1 mL) in acetonitrile (3 mL) was prepared. The reaction was heated at 70 °C for 6 hours. The reaction was cooled down and stored at 4 °C overnight. The suspension was filtered out and the filtrate washed with cold acetonitrile obtaining the guanidine **20·HCl** as a white solid (60 mg, 64% yield). mp 268-270 °C (dec.). IR (ATR) 3306, 3220, 3103, 2906, 2845, 1633, 1453, 1347, 1160, 1092, 963, 821, 723 cm^{-1}. ^{1}H-NMR (400 MHz, CD_3OD) δ: 1.19 [dq, 2 H, *J* = 13.6 Hz, *J'* = 4.0 Hz, 3(5)-H_{ax}], 1.32 (t, 2 H, *J* = 7.6 Hz, Ad-CH_2-piperidine), 1.55 [broad d, 2 H, *J* = 12.4 Hz, 4'(9')-H_a or 8'(10')-H_a], 1.64 (m, 1 H, 4-H), 1.67 [broad s, 2 H, 1'(3')-H], 1.75-1.98 [complex signal, 13 H, 3(5)-H_{eq}, 2'-H, 5'-H, 6'-H_2, 7'-H, 4'(9')-H_b or 8'(10')-H_b, 4'(9')-H_2 or 8'(10')-H_2], 3.06 [td, 2 H, *J* = 13.6 Hz, *J'* = 2.8 Hz, 2(6)-H_{ax}], 3.87 [dm, 2 H, *J* = 13.6 Hz, 2(6)-H_{eq}]. ^{13}C-NMR (100.6 MHz, CD_3OD) δ: 29.5 (CH) and 29.7 (CH) (C5' and C7'), 32.6 [CH_2, C4'(9) or C8'(10')], 33.1 [CH_2, C3(5)], 33.4 [CH, C1'(3')], 33.9 (CH, C4), 39.4 (CH_2, C6'), 40.3 (CH_2, Ad-CH_2-piperidine), 40.4 [CH_2, C8'(10') or C4'(9')], 42.0 (CH, C2'), 47.2 [CH_2, C2(6)], 157.5 (C, C=N). HRMS-ESI$^+$ m/z [*M*+H]$^+$ calcd for [$C_{17}H_{29}N_3$+H^+]: 276.2434, found: 276.2437.

ASSOCIATED CONTENT

Supporting Information. Descriptions of the synthesis and characterization of intermediate compounds and elemental analysis data of the new compounds. Additional electrophysiological

experiments. Plaque reduction assay with A/WSN/33 N31S/V27A (H1N1) virus. This material is available free of charge via the Internet at http://pubs.acs.org.

AUTHOR INFORMATION

Corresponding Author

*Phone: +34 934024533. E-mail: svazquez@ub.edu.

ACKNOWLEDGMENT

M.B.-X. thanks the Institute of Biomedicine of the Universitat de Barcelona (IBUB) for a PhD grant. The authors thank the Spanish *Ministerio de Ciencia e Innovación* (FPU fellowship to E.T.; grant SAF2014-57094-R to S.V.). L.N. acknowledges financial support from the Geconcerteerde Onderzoeksacties (GOA/15/019/TBA), and technical assistance from W. van Dam. J. W. acknowledges the support from NIH grant AI119187. We thank Prof. W. F. DeGrado for his expert advice.

ABBREVIATIONS

Amt, amantadine; ATR, Attenuated Total Reflectance; MDCK, Madin-Darby Canine Kidney; MTS, 3-(4,5-dimethylthiazol-2-yl)-5-(3-carboxymethoxyphenyl)-2-(4-sulfophenyl)-2*H*-tetrazolium; RT-qPCR, quantitative real-time reverse transcription polymerase chain reaction; TEVC, two-electrode voltage clamp; wt, wild-type.

REFERENCES

(1) Vanderlinden, E.; Naesens, L. Emerging Antiviral Strategies to Interfere with Influenza Virus Entry. *Med. Res. Rev.* **2014**, *34*, 301–339

(2) Pinto, L. H.; Lamb, R. A. The M2 proton channels of influenza A and B viruses. *J. Biol. Chem.* **2006**, *281*, 8997–9000.

(3) Wang, J.; Qiu, J. X.; Soto, C. S.; DeGrado, W. F. Structural and dynamic mechanisms for the function and inhibition of the M2 proton channel from influenza A virus. *Curr. Opin. Struct. Biol.* **2011**, *21*, 68-80.

(4) Hong, M.; DeGrado, W. F. Structural basis for proton conduction and inhibition by the influenza M2 protein. *Protein Sci.* **2012**, *21*, 1620-1633.

(5) Wei, C.; Pohorille, A. Activation and proton transport mechanism in influenza A M2 channel. *Biophys J.* **2013**, *105*, 2036-2045.

(6) Kawano, K.; Yano, Y.; Matsuzaki, K. A dimer is the minimal proton-conducting unit of the influenza A virus M2 channel. *J. Mol. Biol.* **2014**, *426*, 2679-2691.

(7) Georgieva, E. R.; Borbat, P. P.; Norman, H. D.; Freed, J. H. Mechanism of influenza A M2 transmembrane domain assembly in lipid membranes. *Sci. Rep.* **2015**, *5*, 11757.

(8) Andreas, L. B.; Reese, M.; Eddy, M. T.; Gelev, V.; Ni, Q. Z.; Miller, E. A.; Emsley, L.; Pintacuda, G.; Chou, J. J.; Griffin, R. G. Structure and mechanism of the influenza-A $M2_{18-60}$ dimer of dimers. *J. Am. Chem. Soc.* **2015**, *137*, 14877-14886.

(9) Thomaston, J. L.; Alfonso-Prieto, M.; Woldeyes, R. A.; Fraser, J. S.; Klein, M. L.; Fiorin, G.; DeGrado, W. F. High-resolution structures of the M2 channel from influenza A virus reveal dynamic pathways for proton stabilization and transduction. *Proc. Natl. Acad. Sci. USA* **2015**, *112*, 14260-14265.

(10) Wei, C.; Pohorille, A. M2 proton channel: toward a model of a primitive proton pump. *Orig. Life Evol. Biosph.* **2015**, *45*, 241-248.

(11) Gu, R.; Liu, L. A.; Wei, D. Drug inhibition and proton conduction mechanisms of the influenza A M2 proton channel. *Adv. Exp. Med. Biol.* **2015**, *827*, 205-226.

(12) Dong, G.; Peng, C.; Luo, J.; Wang, C.; Han, L.; Wu, B.; Ji, G.; He, H. Adamantane-resistant influenza A viruses in the world (1902-2013): frequency and distribution of M2 gene mutations. *PLoS One* **2015**, *10*, e0119115.

(13) Fiore, A. E.; Fry, A. M.; Shay, D. K.; Gubareva, L. V.; Bresee, J. S.; Uyeki, T. M. Antiviral agents for the treatment and chemoprophylaxis of influenza - recommendations of the Advisory Committee on Immunization Practices (ACIP). *MMWR Recomm. Rep.* **2011**, *60*, 1–28

(14) Gleed, M. L.; Busath, D. D. Why bound amantadine fails to inhibit proton conductance according to simulations of the drug-resistant influenza A M2 (S31N). *J. Phys. Chem. B* **2015**, *119*, 1225-1231.

(15) Gleed, M. L.; Ioannidis, H.; Kolocouris, A.; Busath, D. D. Resistance-mutation (N31) effects on drug orientation and channel hydration in amantadine-bound influenza A M2. *J. Phys. Chem. B* **2015**, *119*, 11548-11559.

(16) Balannik, V.; Carnevale, V.; Fiorin, G.; Levine, B. G.; Lamb, R. A.; Klein, M. L.; DeGrado, W. F.; Pinto, L. H. Functional studies and modeling of pore-lining residue mutants of the influenza A virus M2 ion channel. *Biochemistry* **2010**, *49*, 696–708.

(17) Suzuki, H.; Saito, R.; Masuda, H.; Oshitani, H.; Sato, M.; Sato, I. Emergence of amantadine-resistant influenza A viruses: Epidemiological study. *J. Infect. Chemother.* **2003**, *9*, 195–200.

(18) Saito, R.; Sakai, T.; Sato, I.; Sano, Y.; Oshitani, H.; Sato, M.; Suzuki, H. Frequency of amantadine-resistant influenza A viruses during two seasons featuring cocirculation of H1N1 and H3N2. *J. Clin. Microbiol.* **2003**, *41*, 2164–2165.

(19) Furuse, Y.; Suzuki, A.; Oshitani, H. Large-scale sequence analysis of M gene of influenza A viruses from different species: Mechanisms for emergence and spread of amantadine resistance. *Antimicrob. Agents Chemother*. **2009**, *53*, 4457–4463.

(20) Durrant, M. G.; Eggett, D. L.; Busath, D. D. Investigation of a recent rise of dual amantadine-resistance mutations in the influenza A M2 sequence. *BMC Genetics* **2015**, *16*(Suppl 2), S3.

(21) Abed, Y.; Goyette, N.; Boivin, G. Generation and characterization of recombinant influenza A (H1N1) viruses harboring amantadine resistance mutations. *Antimicrob. Agents Chemother*. **2005**, *49*, 556-559.

(22) Duque, M. D.; Valverde, E.; Barniol, M.; Guardiola, S.; Rey, M.; Vázquez, S. Inhibitors of the M2 channel of the influenza A virus, in *Recent Advances in Pharmaceutical Sciences*, Transworld Research Network, **2011**, 35-64.

(23) Wang, J.; Li, F.; Ma, C. Recent progress in designing inhibitors that target the drug-resistant M2 proton channels from the influenza A viruses. *Biopolymers (Pept. Sci.)*, **2015**, *104*, 291-309.

(24) Wang, J.; Cady, S. D.; Balannik, V.; Pinto, L. H.; DeGrado, W. F.; Hong, M. Discovery of spiro-piperidine inhibitors and their modulation of the dynamics of the M2 proton channel from influenza A virus. *J. Am. Chem. Soc.* **2009**, *131*, 8066-8076.

(25) Hu, W.; Zeng, S.; Li, C.; Jie, Y.; Li, Z.; Chen, L. Identification of hits as matrix-2 protein inhibitors through the focused screening of a small primary amine library. *J. Med. Chem.* **2010**, *53*, 3831-3834.

(26) Duque, M. D.; Ma, C.; Torres, E.; Wang, J.; Naesens, L.; Juárez-Jiménez, J.; Camps, P.; Luque, F. J.; DeGrado, W. F.; Lamb, R. A.; Pinto, L. H.; Vázquez, S. Exploring the size

limit of templates for inhibitors of the M2 ion channel of influenza A virus. *J. Med. Chem.* **2011**, *54*, 2646–2657.

(27) Wang, J.; Ma, C.; Balannik, V.; Pinto, L. H.; Lamb, R. A.; DeGrado, W. F. Exploring the requirements for the hydrophobic scaffold and polar amine in inhibitors of M2 from influenza A virus. *ACS Med. Chem. Let.* **2011**, *2*, 307-312.

(28) Zhao, X.; Zhang, Z.-W.; Cui, W.; Chen, S.; Zhou, Y.; Dong, J.; Jie, Y.; Wan, J.; Xu, Y.; Hu, W. Identification of camphor derivatives as novel M2 ion channel inhibitors of influenza A virus. *Med. Chem. Commun.* **2015**, *6*, 727-731.

(29) Wu, S.; Huang, J.; Gazzarrini, S.; He, S.; Chen, L.; Li, J.; Xing, L.; Li, C.; Chen, L.; Neochoritis, C. G.; Liao, G. P.; Zhou, H.; Dömling, A.; Moroni, A.; Wang, W. Isocyanides as influenza A virus subtype H5N1 wild-type M2 channel inhibitors. *ChemMedChem* **2015**, *10*, 1837-1845.

(30) Balannik, V.; Wang, J.; Ohigashi, Y.; Jing, X.; Magavern, E.; Lamb, R. A.; DeGrado, W. F.; Pinto, L. H. Design and pharmacological characterization of inhibitors of amantadine-resistant mutants of the M2 ion channel of influenza A virus. *Biochemistry* **2009**, *48*, 11872-11882.

(31) Wang, J.; Ma, C.; Fiorin, G.; Carnevale, V.; Wang, T.; Hu, F.; Lamb, R. A.; Pinto, L. H.; Hong, M.; Klein, M. L.; DeGrado, W. F. Molecular dynamics simulation directed rational design of inhibitors targeting drug-resistant mutants of influenza A virus M2. *J. Am. Chem. Soc.* **2011**, *133*, 12834-12841.

(32) Rey-Carrizo, M.; Torres, E.; Ma, C.; Barniol-Xicota, M.; Wang, J.; Wu, Y.; Naesens, L.; DeGrado, W. F.; Lamb, R. A.; Pinto, L. H.; Vazquez, S. Azatetracyclo[5.2.1.1^{5,8}.0^{1,5}]undecane derivatives: from wild-type inhibitors of the M2 ion

channel of influenza A virus to derivatives with potent activity against the V27A mutant. *J. Med. Chem.* **2013**, *56*, 9265–9274.

(33) Rey-Carrizo, M.; Barniol-Xicota, M.; Ma, C.; Frigolé-Vivas, M.; Torres, E.; Naesens, L.; Llabrés, S.; Juárez-Jiménez, J.; Luque, F. J.; DeGrado, W. F.; Lamb, R. A.; Pinto, L. H.; Vázquez, S. Easily accessible polycyclic amines that inhibit the wild-type and amantadine-resistant mutants of the M2 channel of influenza A virus. *J. Med. Chem.* **2014**, *57*, 5738–5747.

(34) Rey-Carrizo, M.; Gazzarrini, S.; Llabrés, S.; Frigolé-Vivas, M.; Juárez-Jiménez, J.; Font-Bardia, M.; Naesens, L.; Moroni, A.; Luque, F. J.; Vázquez, S. New polycyclic dual inhibitors of the wild type and the V27A mutant M2 channel of the influenza A virus with unexpected binding mode. *Eur. J. Med. Chem.* **2015**, *96*, 318-329.

(35) Wang, J.; Wu, Y.; Ma, C.; Fiorin, G. ; Wang, J. ; Pinto, L. H. ; Lamb, R. A.; Klein, M: L.; DeGrado, W. F. Structure and inhibition of the drug-resistant S31N mutant of the M2 ion channel of influenza A virus. *Proc. Natl. Acad. Sci. USA* **2013**, *110*, 1315-1320.

(36) Wang, J.; Ma, C.; Wang, J.; Jo, H.; Canturk, B.; Fiorin, G.; Pinto, L. H.; Lamb, R. A.; Klein, M. L.; DeGrado, W. F. Discovery of novel dual inhibitors of the wild-type and the most prevalent drug-resistant mutant, S31N, of the M2 proton channel from influenza A virus. *J. Med. Chem.* **2013**, *56*, 2804-2812.

(37) Williams, J. K.; Tietze, D.; Wang, J.; Wu, Y.; DeGrado, W. F.; Hong, M. Drug-induced conformational and dynamical changes of the S31N mutant of the influenza M2 proton channel investigated by solid-state NMR. *J. Am. Chem. Soc.* **2013**, *135*, 9885-9897.

(38) Wu, Y.; Canturk, B.; Jo, H.; Ma, C.; Gianti, E.; Fiorin, G.; Pinto, L. H.; Lamb, R. A.; Klein, M. L.; Wang, J.; DeGrado, W. F. Flipping in the pore: Discovery of dual inhibitors

that bind in different orientations to the wild-type versus the amantadine-resistant S31N mutant of the influenza A virus M2 proton channel. *J. Am. Chem. Soc.* **2014**, *136*, 17987–17995.

(39) Li, F.; Ma, C.; DeGrado, W. F.; Wang, J. Discovery of highly potent inhibitors targeting the predominant drug-resistant S31N mutant of the influenza A virus M2 proton channel. *J. Med. Chem.* **2016**, *59*, 1207-1216.

(40) Li, F.; Ma, C.; Hu, Y.; Wang, Y.; Wang, J. Discovery of potent antivirals against amantadine-resistant influenza A viruses by targeting the M2-S31N proton channel. *ACS Infect. Dis.* **2016**, *2*, 726-733.

(41) Jalily, P. H.; Eldstrom, J.; Miller, S. C.; Kwan, D. C.; Tai, S. S.-H.; Chou, D.; Niikura, M.; Tietjen, I.; Fedida, D. Mechanisms of action of novel influenza A/M2 viroporin inhibitors derived from hexamethylene amiloride. *Mol. Pharmacol.* **2016**, *90*, 80-95.

(42) Zoidis, G.; Kolocouris, N.; Foscolos, G. B.; Kolocouris, A.; Fytas, G.; Karayannis, P.; Padalko, E.; Neyts, J.; De Clercq, E. Are the 2-isomers of the drug rimantadine active anti-influenza A agents? *Antivir. Chem. Chemother.* **2003**, *14*, 153-164.

(43) Kolocouris, A.; Tzitzoglaki, C.; Johnson, F. B.; Zell, R.; Wright, A. K.; Cross, T. A.; Tietjen, I.; Fedida, D.; Busath, D. D. Aminoadamantanes with persistent in vitro efficacy against H1N1 (2009) influenza A. *J. Med. Chem.* **2014**, *57*, 4629-4639.

(44) Wang, C.; Takeuchi, K.; Pinto, L. H. Ion channel activity of influenza A virus M2 protein: characterization of the amantadine block. *J. Virol.* **1993**, *67*, 5585–5594.

(45) Astrahan, P.; Kass, I.; Cooper, M. A.; Arkin, I. T. A novel method of resistance for influenza against a channel-blocking antiviral drug. *Proteins* **2004**, 55, 251–257.

(46) Leonov, H.; Astrahan, P.; Krugliak, M.; Arkin, I. T. How do aminoadamantanes block the influenza M2 channel, and how does resistance develop? *J. Am. Chem. Soc.* **2011**, 133, 9903–9911.

(47) Togo, H.; Aoki, M.; Kuramochi, M.; Yokoyama, M. Radical decarboxylative alkylation onto heteroaromatic bases with trivalent iodine compounds. *J. Chem. Soc., Perkin Trans. 1* **1993**, 2417-2427.

(48) Stamatiou, G.; Foscolos, G. B.; Fytas, G.; Kolocouris, A.; Kolocouris, N.; Pannecouque, C.; Witvrouw, M.; Padalko, E.; Neyts, J.; De Clercq, E. Heterocyclic rimantadine analogues with antiviral activity. *Bioorg. Med. Chem.* **2003**, *11*, 5485-5492.

(49) Cady, S. D.; Schmidt-Rohr, K.; Wang, J.; Soto, C. S.; DeGrado, W. F.; Hong, M. Structure of the amantadine binding site of influenza M2 proton channels in lipid bilayers. *Nature* **2010**, *463*, 689-692.

(50) Kolocouris, A.; Tataridis, D.; Fytas, G.; Mavromoustakos, T. ; Foscolos, G. B. ; Kolocouris, N. ; De Clercq, E. Synthesis of 2-(2-adamantyl)piperidines and structure anti-influenza virus A activity relationship study using a combination of NMR spectroscopy and molecular modeling. *Bioorg. Med. Chem. Lett.* **1999**, *9*, 3465-3470.

(51) Mariani, E.; Schenone, P.; Bondavalli, F.; Lampa, E:; Marmo, E. (±)-1-(Adamantan-2-yl)-2-propanamine and other amines derived from 2-adamantanone. *Il Farmaco* **1980**, *35*, 430-440.

(52) Álvarez-Manzaneda, E.; Chahboun, R.; Álvarez, E.; Tapia, R.; Álvarez-Manzaneda, R. Enantioselective total synthesis of cytotoxic taiwaniaquinones A and F. *Chem. Commun.* **2010**, *46*, 9244-9246.

(53) Hydrogen-bonded water molecules in the M2 channel of the influenza A virus guide the binding preferences of ammonium-based inhibitors. Gianti, E.; Carnevale, V.; DeGrado, W. F.; Klein, M. L.; Fiorin, G. *J. Phys. Chem. B* **2015**, *119*, 1173-1183.

(54) Pielak, R. M.; Chou, J. J. Solution NMR structure of the V27A drug resistant mutant of influenza A M2 channel. *Biochem. Biophys. Res. Commun.* **2010**, *401*, 58-63.

(55) Gu, R.-X.; Liu, L. A.; Wang, Y.-H.; Xu, Q.; Wei, D.-Q. Structural comparison of the wild-type and drug-resistant mutants of the influenza A M2 proton channel by molecular dynamics simulations. *J. Phys. Chem. B* **2013**, *117*, 6042-6051.

(56) Jing, X.; Ma, C.; Ohigashi, Y.; Oliveira, F. A.; Jardetzky, T. S.; Pinto, L. H.; Lamb, R. A. Functional studies indicate amantadine binds to the pore of the influenza A virus M2 proton-selective ion channel. *Proc. Natl. Acad. Sci. USA* **2008**, *105*, 10967-10972.

(57) Torres, E.; Duque, M. D.; Vanderlinden, E.; Ma, C.; Pinto, L. H.; Camps, P.; Froeyen, M.; Vázquez, S.; Naesens, L. Role of the viral hemagglutinin in the anti-influenza virus activity of newly synthesized polycyclic amine compounds. *Antiviral Res.* **2013**, *99*, 281-291.

(58) For a recent set of compounds that seem to behave similarly, see: Dong, J.; Chen, S.; Li, R.; Cui, W.; Jiang, H.; Ling, Y. ; Yang, Z. ; Hu, W. Imidazole-based pinanamine derivatives: discovery of dual inhibitors of the wild-type and drug-resistant mutant of the influenza A virus. *Eur. J. Med. Chem.* **2016**, *108*, 605-615.

(59) Stevaert, A.; Dallocchio, R.; Dessì, A.; Pala, N.; Rogolino, D.; Sechi, M.; Naesens, L. Mutational analysis of the binding pockets of the diketo acid inhibitor L-742,001 in the influenza virus PA endonuclease. *J. Virol.* **2013**, *87*, 10524-10538.

(60) Gu, R.-X.; Liu, L. A.; Wei, D.-Q. Structural and energetic analysis of drug inhibition of the influenza A M2 proton channel. *Trends Pharm. Sci.* **2013**, *34*, 571-580.

(61) Van Nguyen, H.; Nguyen, H. T.; Le, L. T. Investigation of the free energy profiles of amantadine and rimantadine in the AM2 binding pocket. *Eur. Biophys. J.* **2016**, 45(1), 63–70.

(62) For general experimental methods, see the Supporting Information.

(63) Ma, C.; Soto, C. S.; Ohigashi, Y.; Taylor, A.; Bournas, V.; Glawe, B.; Udo, M. K.; DeGrado, W. F.; Lamb, R. A.; Pinto, L. H. Identification of the pore-lining residues of the BM2 ion channel protein of influenza B virus. *J. Biol. Chem.* **2008**, *283*, 15921-15931.

(64) Vanderlinden E.; Göktas F.; Cesur Z.; Froeyen M.; Reed M. L.; Russell, C. J.; Cesur, N.; Naesens L. Novel inhibitors of influenza virus fusion: structure-activity relationship and interaction with the viral hemagglutinin. *J. Virol.* **2010**, *84*, 4277-4288.

Table of Contents Graphic

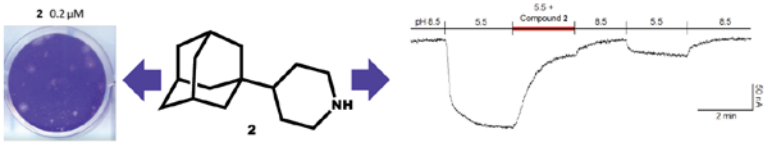

Supporting Information

Slow but steady wins the race: dissimilarities among new dual inhibitors of the wild-type and the V27A mutant M2 channels of influenza A virus

Marta Barniol-Xicota,[‡] *Sabrina Gazzarrini,*[#] *Eva Torres,*[‡] *Yanmi Hu,*[⊥,†] *Jun Wang,*[⊥,†]

Lieve Naesens,[§] *Anna Moroni,*[#] *and Santiago Vázquez**[,‡]

Table of contents

Chemical Synthesis. **General Methods**. Melting points were determined in open capillary tubes with a MFB 595010M Gallenkamp. 400 MHz ^{1}H/100.6 MHz ^{13}C NMR spectra, and 500 MHz ^{1}H NMR spectra were recorded on Varian Gemini 300, Varian Mercury 400, and Varian Inova 500 spectrometers, respectively. The chemical shifts are reported in ppm (δ scale) relative to internal tetramethylsilane, and coupling constants are reported in Hertz (Hz). Assignments given for the NMR spectra of the new compounds have been carried out on the basis of DEPT, COSY ^{1}H/^{1}H (standard procedures), and COSY ^{1}H/^{13}C (gHSQC and gHMBC sequences) experiments. IR spectra were run on Perkin-Elmer Spectrum RX I spectrophotometer. Absorption values are expressed as wave-numbers (cm^{-1}); only significant absorption bands are given. The GC/MS analysis was carried out in an inert Agilent Technologies 5975 gas chromatograph equipped with an Agilent 122-5532 DB-5MS 1b (30 m × 0.25 mm) capillary column with a stationary phase of phenylmethylsilicon (5% diphenyl – 95% dimethylpolysiloxane), using the following conditions: initial temperature of 50 ºC (1 min), with a gradient of 10 ºC / min up to 300 ºC, and a temperature in the source of 250 ºC. *Solvent Delay* (SD) of 4 minutes and a pressure of 7,35 psi. Column chromatography was performed on silica gel 60 AC.C (35–70 mesh, SDS, ref 2000027). Thin-layer chromatography was performed with aluminum-backed sheets with silica gel 60 F_{254} (Merck, ref 1.05554), and spots were visualized with UV light and 1% aqueous solution of $KMnO_4$. The analytical samples of all of the new compounds which were subjected to pharmacological evaluation possessed purity ≥95% as evidenced by their elemental analyses.

2-(4-Pyridyl)adamantan-2-ol, 10. To a 2.5 M solution of *n*-butyllithium in hexane (11.7 ml, 29.25 mmol) was added dropwise with stirring at −75 °C, a solution of the released base, 4-bromopyridine (5.048 g, 31.95 mmol) in anhydrous ether (80 mL) under argon atmosphere, giving a fuchsia light solution that was further stirred at -65 °C for 20 min. Afterwards a solution of 2-adamantanone (4 g, 26.6 mmol) in anhydrous ether (60 mL) and THF (2 mL) was added dropwise. The stirring was continued for 3 hours, after which the pink mixture was then allowed to gradually warm to ambient temperature and left stirring overnight. The reaction mixture was quenched with water (40 mL) and poured into a 5 N HCl solution (40 ml) under ice-cooling. The solution was stirred for 20 minutes and the acidic aqueous phase were separated (2 x 40mL) and basified with NaOH 5N (100 mL) over an ice bath. The resultant solid was filtered while cold under vacuum and washed with cold pentane and dried to give **10** was obtained (4.3 g, 70% yield) as a white solid, 184-186 ºC. IR (ATR) 2906, 2860, 1686, 1600, 1539, 1451, 1410, 1345, 1276, 1241, 983, 842 cm^{-1}. ^{1}H NMR (400 MHz, CD_3OD) δ 1.56 (broad d, *J* = 12.8 Hz, 2 H, 6-H_2), 1.74-1.93 [complex signal, 8 H, 4(9)-H_2 and 8(10)-H_2], 2.48 [d, J = 12.4 Hz, 2 H, 5(7)-H], 2.61 [broad s, 2 H, 1(3)-H], 8.20 [d, *J* = 6.6 Hz, 2 H, 3'(5')-H], 8.82 [d, *J* = 6.6 Hz, 2'(6')-H]. ^{13}C NMR (100.6 MHz, CD_3OD) δ 28.1 (CH) and 28.6 (CH) (C5 and C7), 33.5 (CH_2) and 35.5 (CH_2) [C4(9) and C8(10)], 35.9 [CH, C1(3)], 38.3 (CH_2, C6), 75.8 (C, C2), 125.9 [CH, C3'(5')], 143.1 [CH, C2'(6')], 168.3 (C, C4'). MS (EI), m/e (%); main ions: 229 ($M^{\cdot+}$, 29), 212 (14), 211 [$(M-H_2O)^{\cdot+}$, 72], 151 (100), 109 (20), 106 (32), 93 (20), 91 (16), 81 (30), 80 (50), 79 (93), 78 (23), 77 (16), 67 (17).

Synthesis of 2-(pyridin-4-ylmethyl)adamantan-2-ol, 14. To a solution of 4-picoline (3.1 g, 33.3 mmol) in anhydrous THF (25 mL) at -20 °C, *n*-butyllithium (13.4 mL, 2.5 N in hexanes, 33.5 mmol) was added dropwise. When the addition was over, the

mixture was allowed to reach room temperature and a solution of 2-adamantanone (5.0 g, 33.3 mmol) in anhydrous THF (18 mL) was added dropwise during 15 minutes and left stirring for 2 hours. After quenching with water (5 mL), the THF was evaporated. Diethyl ether was added, layers were separated and the aqueous one was washed with water (1 x 15 mL) and extracted with HCl 5N (3 x 15 mL). The aqueous extract was basified with solid Na_2CO_3. A white solid precipitated that was filtered, washed with water and dried to give pure **14** (7.3 g, 90% yield), mp 202-203 °C (dec.). IR (ATR) 3721, 3215, 2906, 1691, 1603, 1423, 1345, 1236, 1170, 1001, 958, 829, 753 cm^{-1}. ^1H NMR (400 MHz, CD_3OD) δ 1.53 [d, *J* = 12.6 Hz, 2 H, 4(9)-H_a or 8(10)-H_a], 1.62 [broad s, 2 H, 1(3)-H], 1.74-1.85 (complex signal, 5 H, 6-H_2, 8(10)-H_a or 4(9)-H_a and 5-H or 7-H], 1.91 (m, 1 H, 7-H or 5-H), 2.15 [broad d, *J* = 10.8 Hz, 2 H, 8(10)-H_b or 4(9)-H_b], 2.24 (broad d, *J* = 12.6 Hz, 2 H, 4(9)-H_b or 8(10)-H_b], 3.04 (s, 2 H, 2C-C$\underline{H}_2$), 7.34 [m, 2 H, 3'(5')-H], 8.39 [m, 2 H, 2'(6')-H]. ^{13}C NMR (100.6 MHz, CD_3OD) δ 28.8 (CH) and 28.9 (CH) (C5 and C7), 33.9 (CH_2) and 35.5 (CH_2) [C4(9) and C8(10)], 38.0 [CH, C1(3)], 39.6 (CH_2, C6), 44.6 (CH_2, 2C-$\underline{C}H_2$), 76.1 (C, 2C), 128.0 [CH, C3'(5')], 149.1 [CH, C2'(6')], 150.4 (C, C4'). HRMS-ESI^+ m/z $[M+H]^+$ calcd for [$C_{16}H_{21}NO+H^+$]: 244.1696, found: 244.1693.

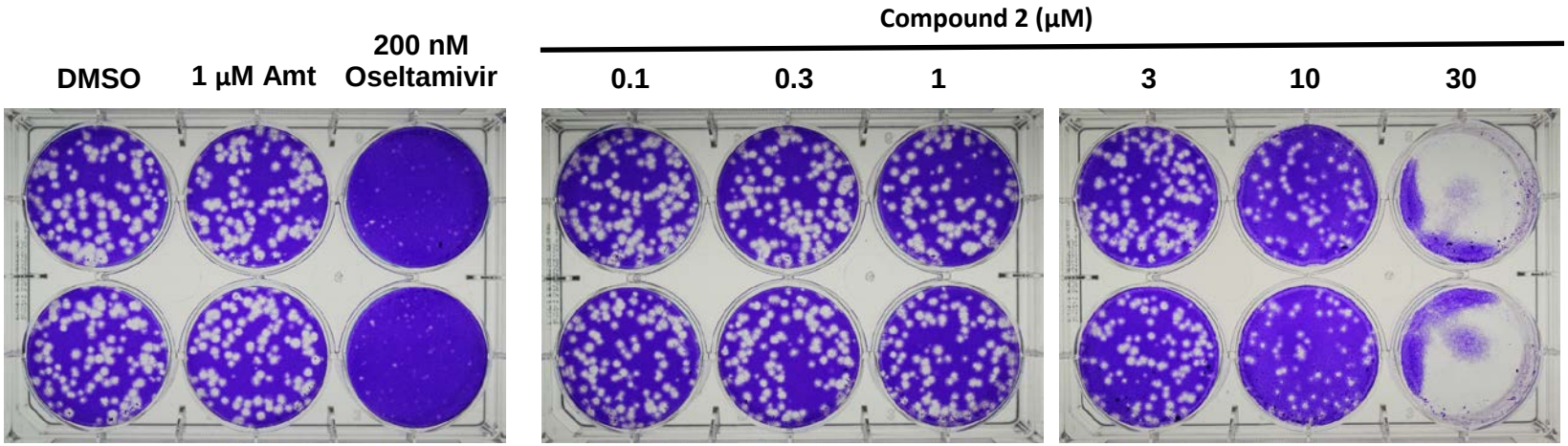

Figure S1. Activity of compound **2** in the influenza virus plaque reduction assay. MDCK cells were infected with influenza virus (strain N31S/V27A A/WSN/33) in the presence of the test compounds. After 46 h incubation, plaques were visualized by crystal violet staining.

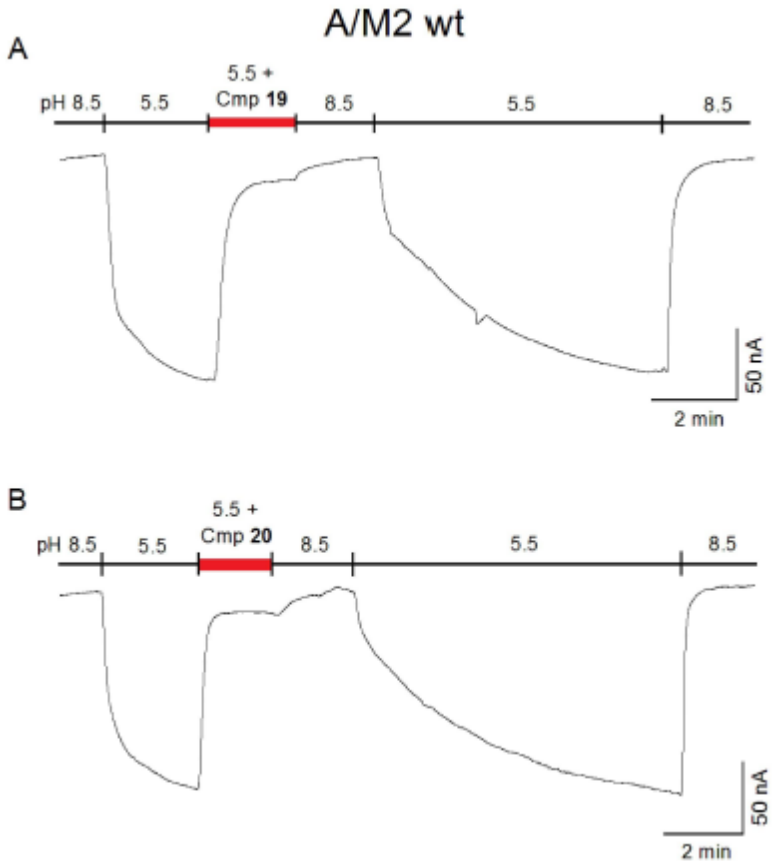

Figure S2. Inhibition of the A/M2 wt channel (derived from the A/Udorn/307/72 H3N2 virus strain) using the TEV technique in Xenopus oocytes. Oocytes were bathed in Barth solution at pH = 8.5 and pH = 5.5. Current was clamped at -20 mV and the indicated compounds were applied at 100 μM in pH 5.5 solution once the inward current reached maximum amplitude in M2 wt channel (A-B).

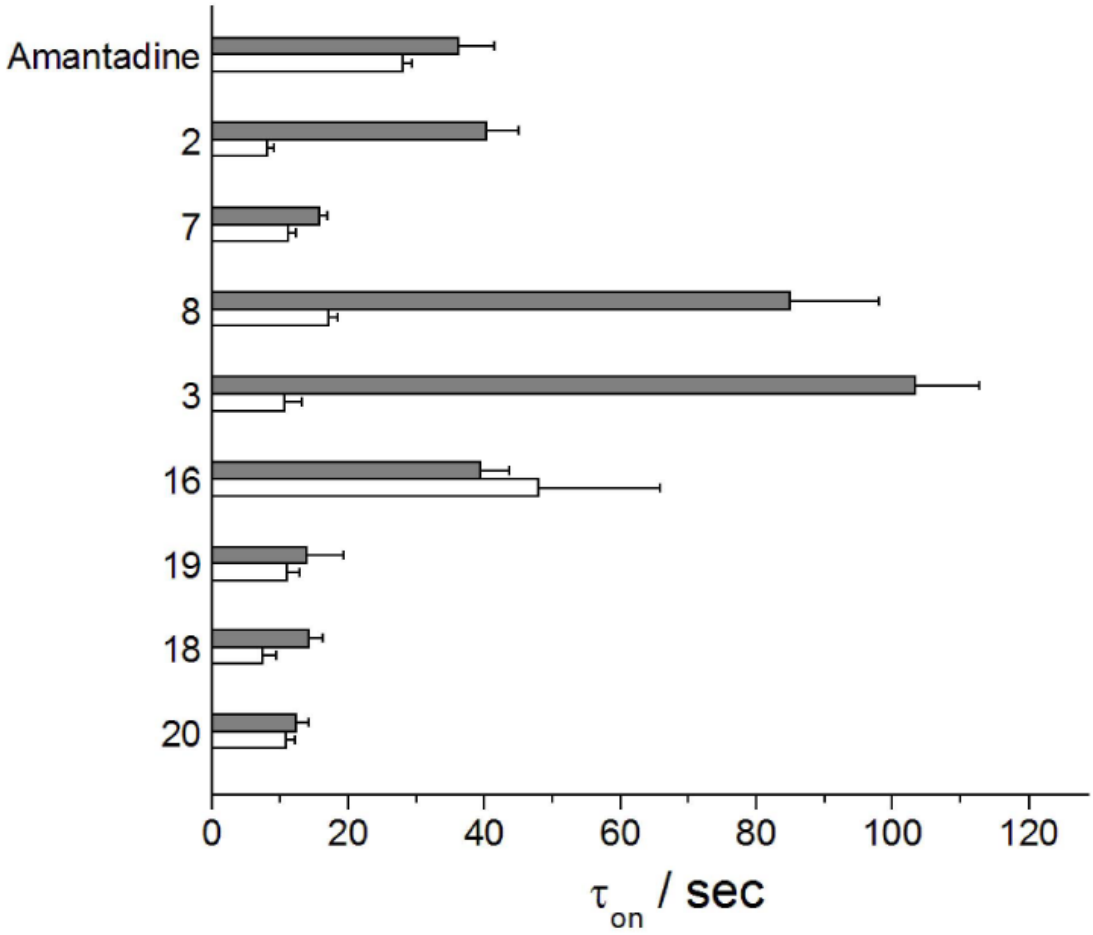

Figure S3. Time constant for inhibition measured in *Xenopus* oocytes expressing A/M2 wt and V27A mutant and TEVC technique. Histogram representing the time constant of inhibition after the addition of different compounds at 100 μM. Current traces were fitted with a single exponential ($y=e^{-t/\tau}$ + constant wit r>0.94).

Elemental analysis data:

Compound	**Molecular Formula**	**Calculated**				**Found**			
		C	H	N	Cl	C	H	N	X
2·HCl	$C_{15}H_{25}N$·HCl	70.42	10.24	5.48	13.86	70.30	10.42	5.53	13.90
7·HCl	$C_{16}H_{27}N_3$·HCl	64.52	9.47	14.11	11.90	64.32	9.63	13.93	12.01
8·HCl	$C_{15}H_{25}N$·HCl	70.42	10.24	5.48	13.86	70.24	10.29	5.60	13.93
11·0.3CH_2Cl_2	$C_{15}H_{25}NO$·0.3CH_2Cl_2	70.45	9.89	5.37	8.15	70.60	10.21	5.27	n.d.
15·1HCl·0.4CH_2Cl_2	$C_{16}H_{27}NO$·HCl·0.4CH_2Cl_2	61.59	9.08	4.38	19.95	61.62	9.28	4.41	n.d.
16·HCl·0.4H_2O	$C_{16}H_{25}N$·HCl·0.4H_2O	69.87	9.82	5.09	12.89	69.80	9.39	4.85	n.d.
17·3HCl	$C_{16}H_{27}N$·3HCl	56.06	8.82	4.09	31.03	56.19	8.44	4.08	n.d.
18·2.15HCl	$C_{17}H_{29}N$·2.15HCl	62.67	9.64	4.30	23.39	62.60	9.71	4.45	n.d.
19·2.2HCl	$C_{17}H_{27}N_3$·2.2HCl	57.74	8.32	11.88	22.06	57.82	8.06	11.99	n.d.
20·2.7HCl	$C_{17}H_{29}N_3$·2.7HCl	54.61	8.55	11.24	25.60	54.56	8.34	11.33	n.d.

Chapter 6

Adamantyl benzyl amines and aromatic piperidines as promising scaffolds with anti-hemagglutinin activity.

6.1 Rationale and previous work

The Hemagglutinin (HA) is an antigenic globular surface protein inserted in the membrane of the Influenza A virus[1]. Its importance relies on its responsibility to recognize the target sialic acids in the membranes of the respiratory tract cells and the posterior virus binding to them[2]. In addition to this, the HA also triggers the fusion of the viral envelope with the endosome membrane[3] after the M2 channel has lowered the pH. Consequently, its correct function is essential for the virus viability, therefore any compound able to target and disrupt its activity would behave as an anti-Influenza agent[4]. The therapeutic potential of the HA has raised substantial interest during the last years among the scientific community, giving place to numerous structural[5,6] and activity studies[7] which, in its turn have catalysed the flourishing of new HA inhibitors in the literature[8,9]. (See Chapter 1, section 1.4).

During the past years our group has been devoted to the preparation of M2 channel blockers as anti-influenza A compounds[10,11,12]. Great success has been achieved on that

[1] Böttcher-Friebertshäuer, E., Garten, W., Matrosovich, M. & Klenk, H. D. *The Hemagglutinin: A Determinant of Pathogenicity*. Influenza Pathogenesis and Control I. Current Topics in Microbiology and Immunology. **2015**, 3-34. Publisher: (Springer GmbH,) CODEN:CTMIA3 ISSN:2196-9965.

[2] Cross, K.J., Burleigh, L.M. & Steinhauer, D.A. Mechanisms of cell entry by influenza virus. *Expert Rev. Mol. Med.* **2001**, 3, (21), 1- 18.

[3] Harrison, S.C. Viral membrane fusion. *Nat. Struct. Mol. Biol.* **2008**, 15, (7), 690-698.

[4] Kido, H. Influenza virus pathogenicity regulated by host cellular proteases, cytokines and metabolites, and its therapeutic options. *Proc. Jpn. Acad. Ser. B Phys. Biol. Sci*. **2015**, 91, (8), 351-368.

[5] Russell, R. J., Kerry, P. S., Stevens, D. J., Steinhauer, D. A., Martin, S. R., Gamblin, S. J. & Skehel, J. J. Structure of influenza hemagglutinin in complex with an inhibitor of membrane fusion. *Proc. Nat. Acad. Sci. USA*. **2008**, 105 (46), 17736–41.

[6] Yusuf, M., Konc, J., Sy Bing, C., Trykowska Konc, J., Ahmad Khairudin, N. B., Janezic, D. & Wahab, H. A. Structurally conserved binding sites of hemagglutinin as targets for influenza drug and vaccine development. *J. Chem. Inf. Model*. **2013**, 53(9), 2423–2436.

[7] Carr, C. M. & Kim, P. S. A spring-loaded mechanism for the conformational change of influenza hemagglutinin. *Cell*. **1993**, 73(4), 823–832.

[8] Li, F., Ma, C. & Wang, J. Inhibitors Targeting the Influenza Virus Hemagglutinin. *Curr. Med. Chem.* **2015**, 1361–1382.

[9] Van, T.D., Tran, N., Le, L. & Eisenhaber, F. A Perspective on Rational Designs of a Hemagglutinin Based Universal Influenza Vaccine. *Curr. Pharm. Des.* **2016**, 22, (23), 3547-3554.

[10] Rey-Carrizo, M., Barniol-Xicota, M., Ma, C., Frigolé-Vivas, M., Torres, E., Naesens, L., Llabrés, S., Juárez-Jiménez, J., Luque, F. J., DeGrado, W. F., Lamb, R. A., Pinto, L. H. & Vázquez S. Easily Accessible Polycyclic Amines that Inhibit the Wild-Type and Amantadine-Resistant Mutants of the M2 Channel of Influenza A Virus. *J. Med. Chem*. **2014**, 57 (13), 5738-47.

[11] Rey-Carrizo, M., Torres, E., Ma, C., Barniol-Xicota, M., Wang, J., Wu, Y., Naesens, L., Degrado, W. F., Lamb, R. A., Pinto, L. H. & Vázquez, S. 3-Azatetracyclo[5.2.1.1(5,8).0(1,5)]undecane Derivatives: From Wild-Type Inhibitors of the M2 Ion Channel of Influenza A Virus to Derivatives with Potent Activity against the V27A Mutant. *J. Med. Chem*. **2013**, 56 (22), 9265-74.

[12] Duque, M. D., Ma, C., Torres, E., Wang, J., Naesens, L., Juárez-Jiménez, J., Camps, P., Luque, F. J., DeGrado, W. F., Lamb, R. A., Pinto, L. H. &Vázquez, S. Exploring the size limit of templates for inhibitors of the M2 ion channel of influenza A virus. *J. Med. Chem.* **2011**, 54(8), 2646–2657.

side by synthesizing several polycyclic Amt analogues, including ring-contracted[13], ring-rearranged[12] and 2,2-dialkyl[14] derivatives of Amt (Chart 5). It is worth noting that in our previous routine assays the antiviral activity was only determined for the most potent M2 channel blockers, leaving the weak channel inhibitors untested. With the raise of HA relevance as a therapeutic target, together with the disclosure of anti-HA compounds with adamantanic structure –related to ours- in the bibliography[15], we wondered if our compounds could function as HA inhibitors. In 2013 we decided to determine the antiviral activity for all our analogues to investigate if they were also able to target this protein. This change of strategy made us discover that strikingly, **71** and a series of 2,2-dialkylamantadines[14] (as **72**), previously characterized as weak blockers of the M2 protein, were displaying low micromolar activity against the influenza A/PR/8/34 (A/H1N1), carrying a S31N, Amt-resistant M2 channel, but not against A/H3N2 viruses, carrying a *wt* M2 channel. This finding promoted the preparation of several derivatives of **71** and to perform a broad anti-influenza virus testing, and selection and characterization of resistant viruses. The results indicated that our polycyclic amines were interfering with the HA-mediated fusion by causing subtle increases in the endosomal pH, so this is, they were HA fusion inhibitors[16]. After this point our HA research line started bearing promising results[17].

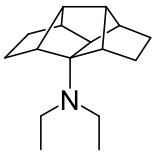

71
H1N1 EC_{50}= 0.80 μM
wt M2 inh= 0%

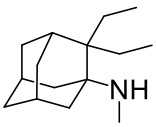

72
H1N1 EC_{50}= 4.0 μM
wt M2 inh= 15%

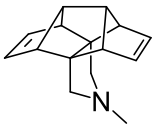

73
H1N1 EC_{50}= 0.40 μM
wt M2 inh= ND

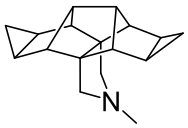

74
H1N1 EC_{50}= 4.6 μM
wt M2 inh= 27%

Chart 5. Previous HA fusion inhibitors prepared in the group.

[13] Camps, P., Duque, M. D., Vázquez, S., Naesens, L., Clercq, E. De, Sureda, F. X., López-Querol, M., Camins, A., Pallàs, M., Prathalingam, S. R., Kelly, J. M., Romero, V., Ivorra, M. D. & Cortés, D. Synthesis and pharmacological evaluation of several ring-contracted amantadine analogs. *Bioorg. Med. Chem.* **2008**, 16(23), 9925–9936.

[14] Torres, E., Fernández, R., Miquet, S., Font-Bardia, M., Vanderlinden, E., Naesens, L. & Vázquez, S. Synthesis and Anti-influenza A Virus Activity of 2,2-Dialkylamantadines and Related Compounds. *ACS Med Chem Lett*. **2012**, 3 (12), 1065–1069.

[15] Kolocouris, A., Tzitzoglaki, C., Johnson, F. B., Zell, R., Wright, A. K., Cross, T. A., Tietjen, I., Fedida, D. & Busath, D. D. Aminoadamantanes with persistent in vitro efficacy against H1N1 (2009) influenza A. *J. Med. Chem*. **2014**, 12(57), 4629-4639.

[16] Torres, E., Duque, M.D., Vanderlinden, E., Ma, C., Pinto, L.H., Camps, P., Froeyen, M., Vázquez, S. & Naesens, L. Role of the viral hemagglutinin in the anti-influenza virus activity of newly synthesized polycyclic amine compounds. *Antiviral Res*. **2013**, 99, 281-291.

[17] Torres, E., Leiva, R., Gazzarrini, S., Rey-carrizo, M., Frigole, M., Moroni, A., Naesens, L. & Vázquez, S. Azapropellanes with Anti-In fl uenza A Virus Activity. *ACS Med. Chem. Lett.* **2014**, 5, 831–836.

More recently and with the disclosure of Roche of RO5464466 and RO5487624[18], based on Bristol-Myers Squibb potent HA fusion inhibitor BMS-199945[19,20,21] and Wyeth-Ayerst, CL385319[22], we considered their shared structure, consisting in a hydrophobic moiety connected to an aromatic head group through a linker, as an attractive starting point to further develop HA inhibitors.

In this project we have synthesized a large batch of compounds, the driving force being to obtain strong SAR information to reinforce our future designs in this recently started line. The compounds presented in this work consisted in a lipophilic scaffold linked to an aromatic moiety and can be broadly classified in two series, either piperidines of general structure **XIX**, or adamantanes, of general structure **XX**. Herein we have studied the suitability of the adamantane versus carbon monocycles in the aliphatic moiety, the optimal substitution in the aromatic moiety, the effects of the heteroatom present in the linker and the chemical space in the pocket, by varying the size of the hydrophobic moiety (Chart 6).

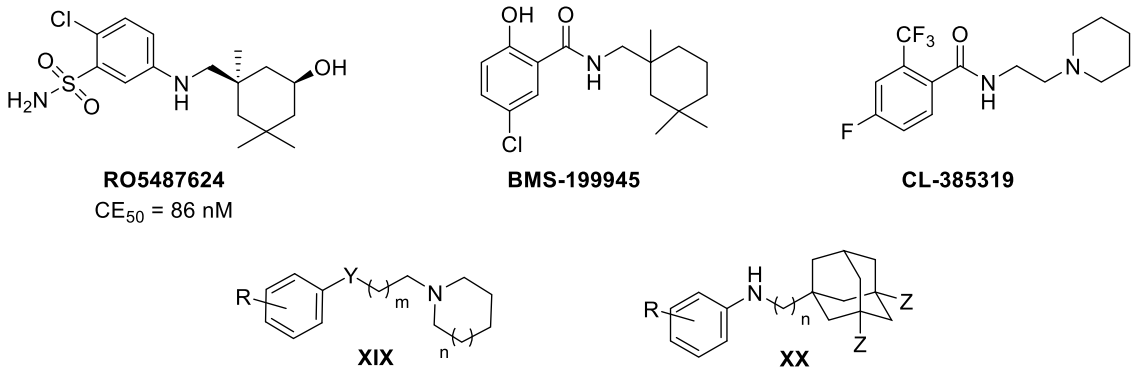

Chart 6. Previous HA fusion inhibitors disclosed in the bibliography and general structures of the new HA inhibitors designed.

[18] Tang, G., Lin, X., Qiu, Z., Li, W., Zhu, L., Wang, L., Li, S., Li, H., Lin, W., Yang, M., Guo, T., Chen, L., Lee, D., Wu, J. & Yang, W. Design and Synthesis of Benzenesulfonamide Derivatives as Potent Anti-Influenza Hemagglutinin Inhibitors. *ACS Med. Chem. Lett*. **2011**, 2, 603-607.

[19] Luo, G., Colonno, R. & Krystal, M. Characterization of a hemagglutinin-specific inhibitor of influenza A virus. *Virology*. **1996**, 226, 66-76.

[20] Cianci, C., Yu, K.-L., Dischino, D. D., Harte, W., Deshpande, M., Luo, G., Colonno, R. J., Meanwell, N. A. & Krystal, M. J. pH-Dependent changes in photoaffinity labelling patterns of the H1 influenza virus hemagglutinin by using an inhibitor of viral fusion. *Virology*. **1999**, 73, 1785-1794.

[21] Deshpande, M. S., Wei, J., Luo, G., Cianci, C., Danetz, S., Torri, A., Tiley, L., Krystal, M., Yu, K.-L., Huang, S., Gao, Q. & Meanwell, N. A. An approach to the identification of potent inhibitors of influenza. *Bioorg Med Chem Lett*. **2001**, 11 (17), 2393-6.

[22] Plotch, S.J., O'Hara, B., Morin, J., Palant, O., LaRocque, J., Bloom, J.D., Lang Jr., S.A., DiGrandi, M.J., Bradley, M., Nilakantan, R. & Gluzman, Y. Inhibition of influenza A virus replication by compounds interfering with the fusogenic function of the viral hemagglutinin. *J. Virol*. **1999**, 73, 140–151.

6.2 Theoretical discussion

In this Thesis context the preparation of the adamantyl and adamantane-related series, has been carried out. This is the synthesis of the final compounds **78a** to **78y**, **82a** and **82b**, as well as all the intermediates involved in the process.

Of note, the preparation of **78e** has been carried out by Sandra Codony in her first year of PhD.

In order to access the scaffolds type **78** a three-step route, was followed (Scheme 16). From 1-adamantanecarboxilic acid, the acid chloride was prepared upon treatment with thionyl chloride. The subsequent addition of this intermediate to a solution of the corresponding aniline in dry acetone yielded the precursor amide as a precipitate. As a final step, the amide was treated either with sodium bis(2-methoxyethoxy)aluminum hydride (Red-Al®) or with borane in THF to furnish the desired aniline in moderate to good yields. Prior to pharmacological evaluation the hydrochloride derivatives were prepared with hydrochloric acid in ether solution.

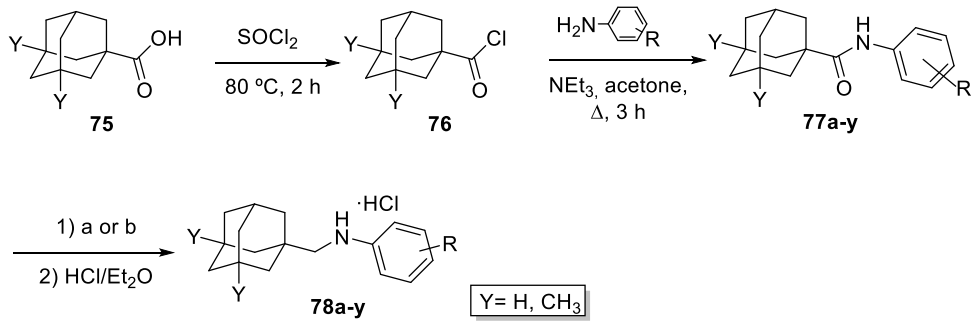

Scheme 16. Route to access to the first series of bioactive compounds prepared in this Thesis. **a**: $NaAlH_2(OCH_2CH_2OCH_3)_2$, toluene, 95 ºC, 24 h; **b**: BH_3·THF, 0 ºC to rt, 24 h.

Of note, meanwhile the vast majority of reductions elapsed with no further complications, the reaction of the amides bearing a trifluoromethyl group in either *ortho* or *para* positions, lead to the reduced amines bearing methyl groups in the aforementioned positions instead of the desired trifluoromethyl substituted ones. This dehalogenation phenomena, not observed in the case that the trifluoromethyl group was in *meta* position, has its origin in the Red-Al® mechanism of action (Scheme 17).

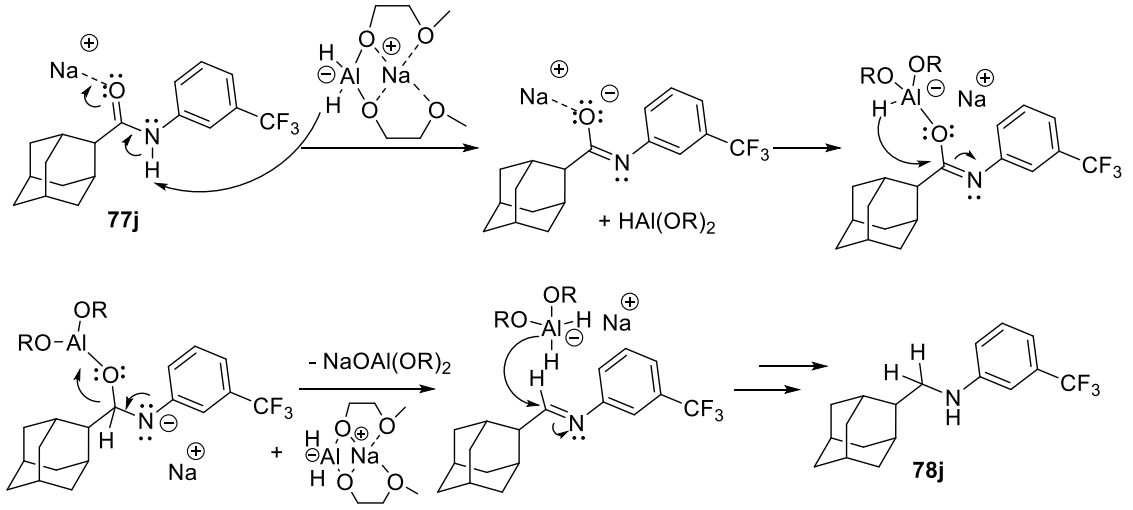

Scheme 17. Red-Al® reduction mechanism

The bis(2-methoxyethoxy)aluminum or Red-Al® is a strong hydride donor widely used as reducing agent. In an analogous way to lithium aluminium hydride, the reaction starts when the metallic cation coordinates with the carbonyl group of the compound prone to be reduced. This coordination step triggers the activation of the carbonyl group which will be the recipient of a hydride from the reagent. The process of hydride transfer keeps occurring until the most reduced specie is formed. Nevertheless, Red-Al® can also act as a base, deprotonating the amide's nitrogen in the molecule. This negative charge will delocalize from the nitrogen towards the aromatic ring through resonance intermediates. This can lead to the expulsion of a fluorine molecule, giving place to a non-aromatic intermediate, which upon a second hydride attack to the difluoromethyl group, will rearomatize. The process keeps occurring until the molecule has lost all the fluorine atoms. Hence, the observed methyl substituted aromatic rings are formed due to the competition between both mechanisms: reduction and dehalogenation (Schemes 17-18).

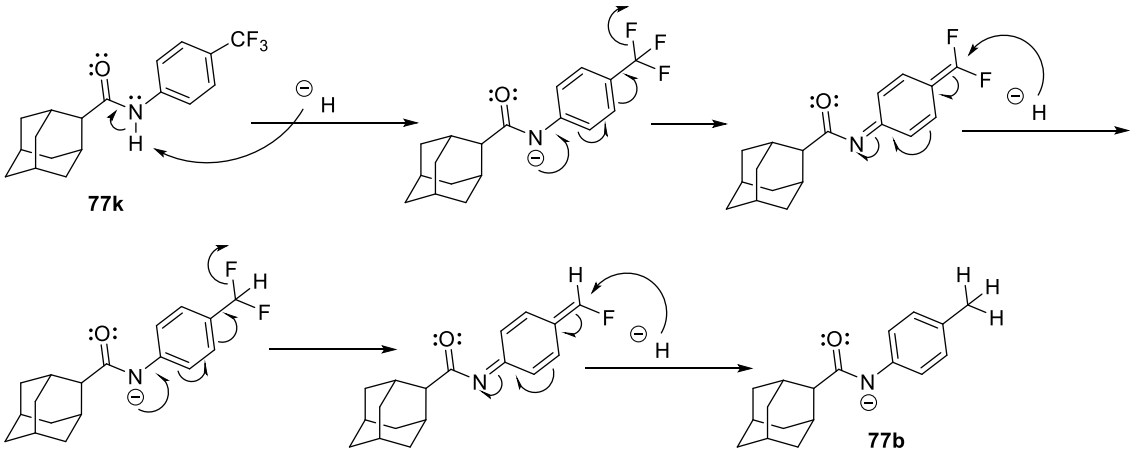

Scheme 18. Red-Al® dehalogenation mechanism

In order to overcome this setback and access the desired amines, we carried out the reaction using borane as a reducing agent. The borane shows a different mechanism than RedAl®; its electrophilic character does not trigger the amide deprotonation upon reacting, but instead it is attacked by the carbonyl group of the molecule prone to be reduced. This change of strategy yielded the desired amines in good yields (Scheme 19).

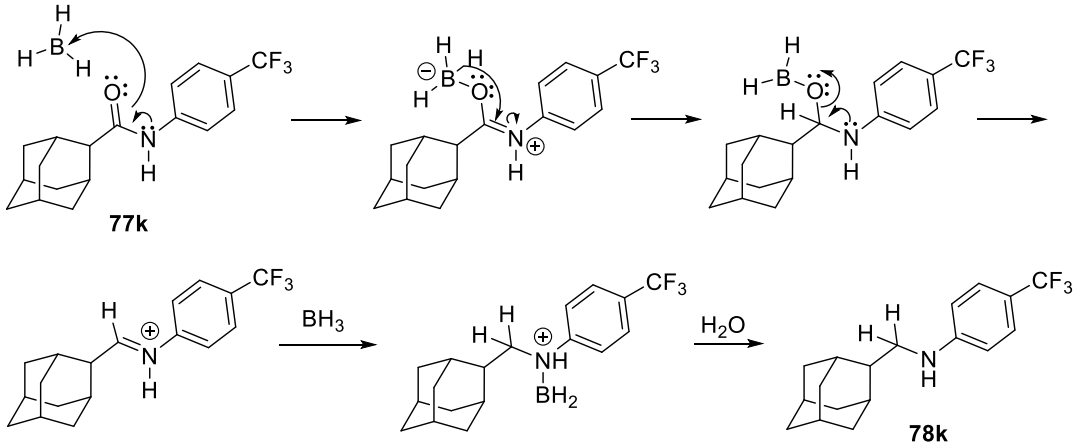

Scheme 19. Borane reduction mechanism.

A modified synthetic route was used for the preparation of the hydroxyadamantane series, starting from the same precursor. The 1-adamantane carboxylic acid was first reacted with a mixture of sulphuric and nitric acid to yield the hydroxyacid derivative. Following, **80** was coupled with the corresponding aniline using EDC and, upon reduction with RedAl®, the desired amine was obtained (Scheme 20).

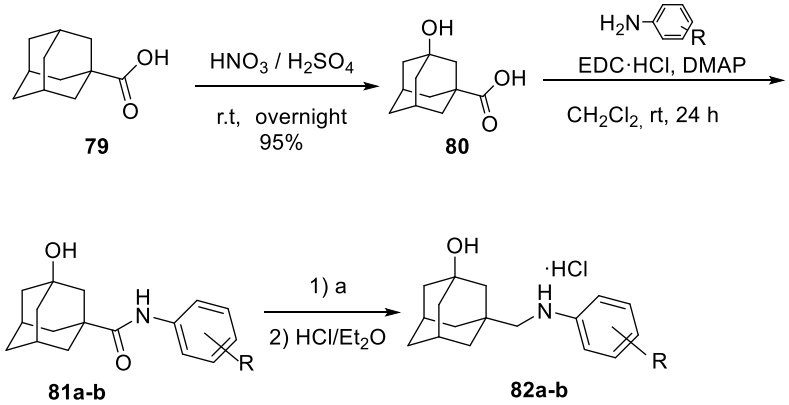

Scheme 20. Route to access to the hydroxyadamantane series of bioactive compounds prepared in this Thesis. **a**: $NaAlH_2(OCH_2CH_2OCH_3)_2$, toluene, 95 ºC, 24 h.

Of note, the transformation of the 1-adamantanecarboxilic acid to its hydroxylated derivative, was described in the bibliography[23], however its mechanism is unknown. Putatively the strong acid media conditions trigger the formation of a non-classical carbocation[24,25], in which 2 electrons are delocalized in between 3 atoms. Following, the nitric acid will rapidly attack the adamantyl carbocation, giving place to an intermediate specie, which after hydrolysis will yield the hydroxyadamantanic acid (Scheme 21). Despite we applied these conditions over the final amines and their amide precursors with the aim to gain access to this family in only one step, no success came from this side. In the case of amides, the hydrolysis products were observed, due to the strong acidic conditions. In the case of the amines a complex mixture was obtained; despite not further studied, it presumably contained products of aromatic substitution, as it is a more reactive position than the one in adamantane ring, as well as *N*-oxide derivatives.

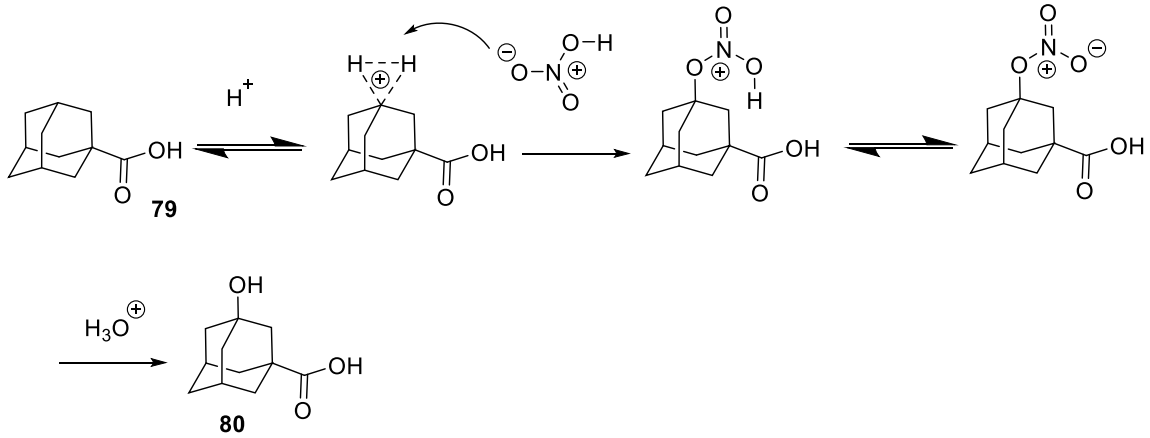

Scheme 21. Proposed mechanism for the adamantane hydroxylation.

Finally it is worth noting that the coupling step used for this family, could also be used for the preparation of the previous one, **78**. While this change reduced in one step the synthetic route, in our hands the overall yields were markedly reduced, being 21-48% in front of the overall 93-99% for the longer route.

The structures of the final compounds prepared and pharmacologically evaluated by the group of Prof. Lieve Naesens are gathered in table 8. The results of these compounds, together with the series **XIX** are discussed in the manuscript that follows.

[23] Wanka, L., Cabrele, C., Vanejews, M. & Schreiner, P. R. γ-Aminoadamantanecarboxylic Acids Through Direct C–H Bond Amidations. *Eur. J. Org. Chem.* **2007**, 1474–1490.

[24] Schleyer, P. R., Fort, R. C. & Watts, W. E. Stable Carbonium Ions. VIII. The 1-Adamantyl Cation. *J. Am. Chem. Soc*. **1964**, 86 (19), 4195–4197.

[25] Saunders, M., Schleyer, P. R. & Olah, G. A. Stable Carbonium Ions. XI.1 The Rate of Hydride Shifts in the 2-Norbornyl Cation. *J. Am. Chem. Soc*. **1964**, 86 (24), 5680–5681.

Structure		Structure		Structure	
78a	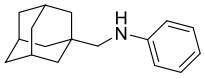	**78k**	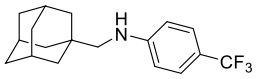	**78t**	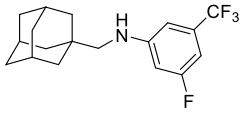
78b	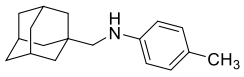	**78l**	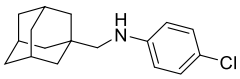	**78u**	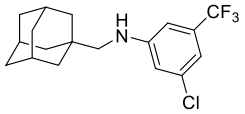
78c	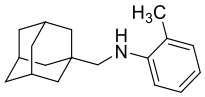	**78m**	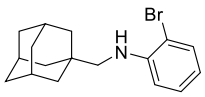	**78v**	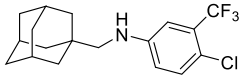
78d	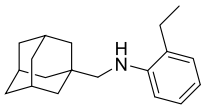	**78n**	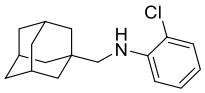	**78w**	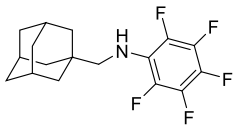
78f	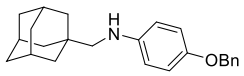	**78o**	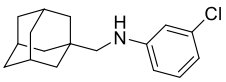	**78y**	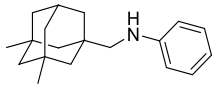
78g	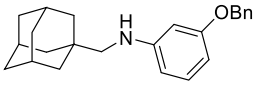	**78p**	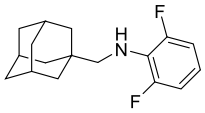	**82a**	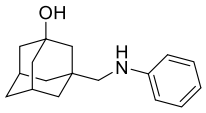
78h	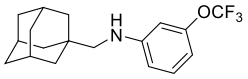	**78q**	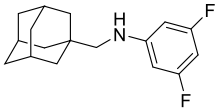	**82b**	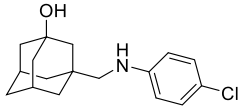
78i	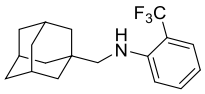	**78r**	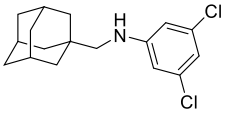		
78j	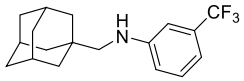	**78s**	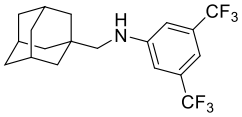		

Table 8. Anti-HA compounds prepared in this Thesis

6.3 Follow-up work

In order to unequivocally identify HA as the target of our compounds further experiments are being carried out with **83**, prepared for this project in the Thesis of Rosana Leiva, being:

- NMR titration and binding experiments (WaterLOGSY and STD-NMR) with HA (Dr. Michael Caffrey, University of Arizona, US), which will determine the site and stoichiometry of binding of our compounds.

- Resistance studies (Prof. L. Naesens), which besides identifying the target will also reveal the inhibitors mechanism of action.

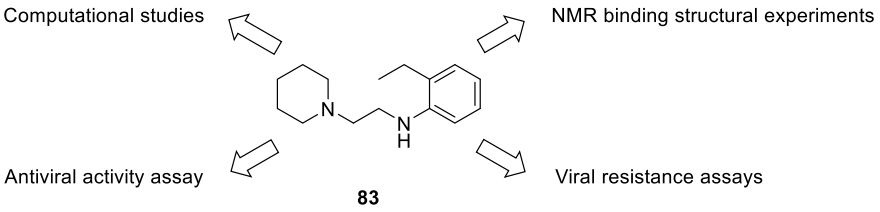

Chart 7. Studies over compound **83**.

Redesigning old anti-influenza compounds: synthesis and evaluation of novel anilines with activity against the 2009 H1N1 influenza virus

Rosana Leiva,[∫] *Marta Barniol-Xicota,*[∫,ǁ] *Sandra Codony,*[∫,ǁ] *Tiziana Ginex,*[#,ǁ] *Evelien Vanderlinden,*[§] *Marta Montes,*[∫] *Michael Caffrey,*[†] *F. Javier Luque,*[#] *Lieve Naesens,*[§] *and Santiago Vázquez**[∫]

[∫]Laboratori de Química Farmacèutica (Unitat Associada al CSIC), Facultat de Farmàcia i Ciències de l'Alimentació, and Institute of Biomedicine (IBUB), Universitat de Barcelona, Av. Joan XXIII, s/n, Barcelona, E-08028, Spain

[#]Department of Nutrition, Food Science and Gastronomy, Faculty of Pharmacy and Food Sciences, and Institute of Biomedicine (IBUB), Universitat de Barcelona, Av. Prat de la Riba 171, Santa Coloma de Gramanet, E-08921, Spain

[§]Rega Institute for Medical Research, KU Leuven, B-3000 Leuven, Belgium

[†]Department of Biochemistry & Molecular Genetics, University of Illinois at Chicago, 900 South Ashland Avenue, Chicago, Illinois 60607, United States

KEYWORDS. Antivirals, drug design, hemagglutinin, influenza A virus, molecular dynamics.

ABSTRACT. Two new series of easily accessible anilines were identified as anti-influenza A virus agents. The antiviral activity of these molecules was confirmed in cell-based assays. Several lines of evidence strongly suggest that the target of these compounds is the protein hemagglutinin of the virus.

Introduction

Influenza, commonly known as "the flu", is caused by the Influenza A virus, a single stranded RNA enveloped virus which infects the respiratory tract of human beings. Every year the flu translates in a huge economy burden and human loss worldwide.[1] Besides the concerns raised by seasonal epidemic outbreaks morbidity and mortality, the influenza A capacity to generate periodic pandemics, poses public health at risk. Several pandemics have been reported over the centuries, being the so called *Spanish flu*, which infected one third of the world population and terminated 100 million of lives, an obvious warning to its deadly potential.[2]

Nowadays the five available drugs for the prevention and treatment of Influenza A virus fall in two categories: M2 proton channel (M2) blockers or neuraminidase (NA) inhibitors.[3-4] However, the rapid mutation rate of this virus has triggered the current circulating strains to be resistant to M2 inhibitors, rendering these drugs obsolete.[3] The same faith is predicted for the NA inhibitors, as resistance is continuously on the raise.[5] Therefore, there is an urgent need to develop new antiviral drugs. Taking into account that strains that are resistant to both classes of drugs have been identified, it will be especially desirable to develop compounds that block other stages of the viral replication.[6-11]

In the last few years, the research effort made in this line has validated the previously undrugged influenza A proteins hemagglutinin (HA), RNA polymerase and NS1 protein, as targets.[12-14] Among those, the viral coat protein HA stands out as, arguably,

the most promising one. This protein of roughly 550 amino acids long is the most abundant glycoprotein on the surface of the virion and its correct function is essential for the viral infectivity. HA is synthesized as a polypeptide precursor, HA0 which is cleaved extracellularly, as a first step of the infection, by host proteases. This process gives places to two subunits: HA1 and HA2. HA1 contains the receptor-binding pocket for sialic acids located on the surface of host epithelial cells, allowing the virus to be recognized and internalized in the endosome. In a complementary manner HA2, mediates the fusion of the viral envelope and the endosome membrane, upon acidic pH exposure. The fusion allows the release of the virus genome within the cell cytoplasm and the following transfer into the cell nucleus, where the viral RNA replication can occur, making the viral infection progress.[15-17]

In this light, a compound able to block the HA function, either inhibiting the HA0 glycosylation or cleavage, the HA1-mediated attachment to host cells or the HA2-mediated membrane fusion, would avoid influenza A replication, hence virus infection. Besides this large opportunity of therapeutic intervention at each maturation stage of HA, choosing HA as a target, also opens a door to a future combination therapy with currently approved drugs. Moreover, inhibitors targeting the most conserved region of HA might have a higher genetic barrier for drug resistance. Recently, the disclosure of high-resolution structures of HA, has boosted the anti-HA therapeutics research.[18-21]

Research on this field has mostly revolved around the development of neutralizing antibodies to be used in prophylactic vaccines.[22-23] Despite the remarkable success on this endeavour, placing several candidates in clinical trials,[24] these vaccines are not completely effective. On the top of that, the vaccines will not provide a solution in the case of pandemics. The rapid transmission of this pathogen demands a readily available treatment, that is, a stockpiling drug.

To date, there are no anti HA drugs approved by the FDA,[25] however research on this field has already reported some encouraging results. The most promising molecules fall in the category of fusion inhibitors, this is peptide- and small molecule–based inhibitors targeting the HA-mediated membrane fusion. Despite the use of peptide-based antivirals is a well-established strategy for antiviral drug discovery,[26] as the recent entry of flufirvitide (FF-3) in phase II trials demonstrates,[27-28] the small molecule inhibitors are still more desirable as they can be orally bioavailable.

One of the earliest examples was *tert*-butylhydroquinone (TBHQ), which inhibits HA conformational change and viral infectivity at concentrations around 10 μM.[29] Of note, the structure of HA in complex with TBHQ showed that the inhibitor binds in a hydrophobic pocket formed at an interface between HA monomers.[18] The structure-activity relationship (SAR) analysis of TBHQ derivatives has very recently been revisited.[30]

In 1996, Bristol-Myers Squibb identified BMY-27709, BMS-199945 and related compounds as effective and potent HA fusion inhibitors, however the therapeutic interest was lost as they were only able to inhibit two of the 18 HA serotypes.[31-34] Several years later, BMS-199945 was used as lead compound by Roche, who identified several related HA inhibitors. Among the compounds developed, RO5464466 and its 2-chloro derivative, RO5487624, were active against the influenza A/Weiss/43 strain (H1N1) in cytopathic effect assays, with EC_{50} values of 210 nM and 86 nM, respectively. Noteworthy, in *in vivo* mouse studies, RO5487624 was shown to improve the survival rate up to 60%.[35-36]

On the other hand, CL385319, a benzamide first reported by Wyeth-Ayerst in 1999 as an inhibitor of the H1 and H2-subtypes of influenza virus type A,[37] was recently shown

to inhibit H5N1 avian influenza A virus infection by interfering with the fusogenic function of the viral hemagglutinin.[38-40]

Chart 1. Structures of Influenza A Hemagglutinin small molecule inhibitors.

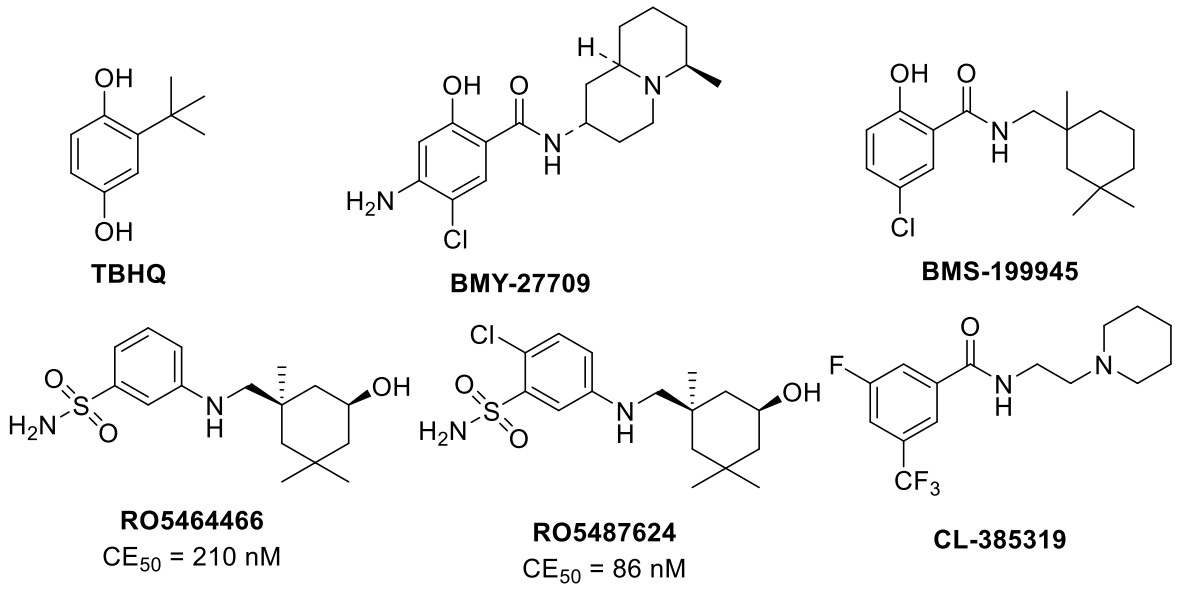

All of these data makes BMS-199945 and CL385319, consisting in a hydrophobic moiety connected to an aromatic headgroup through a linker, attractive to further characterize and develop HA inhibitors. Herein we describe the synthesis and pharmacological evaluation of two series of novel anilines derivatives and related compounds of general structures **I** and **II**.

First, taking into account that the benzamide group of BMS-199945 can be replaced by an aniline group, as in RO5464466 and RO5487624, we reasoned that, starting from CL-385317, compounds of general structure **I**, may also display anti-influenza activity.

Second, considering the well-known antiviral activity of several adamantane derivatives,[41] the large experience of our group in the synthesis of adamantane-related polycyclic antiviral compounds,[42-46] and the antiviral activity found for several members of the family of compounds of general structure **I** (see below), we next fully replaced

the cyclohexyl or piperidyl moiety of RO546666 or **I**, respectively, by the bulkier adamantane. Our vision was this polycyclic group may occupy the space that the 1,3,3-trimethylcyclohexyl does in BMS199945 and that of the piperidine ring in **I**.

For this, and in order to exploit the aforementioned lead scaffolds potential, we have developed a series of analogues with which explore: a) the optimal substitution in the aromatic moiety in both series of compounds, b) the effects of the heteroatom present in the linker of **I** and c) the chemical space in the pocket, by varying the size of the hydrophobic moiety.

The antiviral activity of the compounds has been tested in influenza strains carrying type 1 or type 3 HA. In addition a broad antiviral test has been carried out, testing the compounds against diverse relevant virus including, HIV, vesicular stomatitis virus, herpes simplex and vaccinia virus.

Scheme 1. General structures of the new HA inhibitors designed. Y = NH, O, S; m = 1 or 2; n = 0, 1 or 2; Z = H or CH_3.

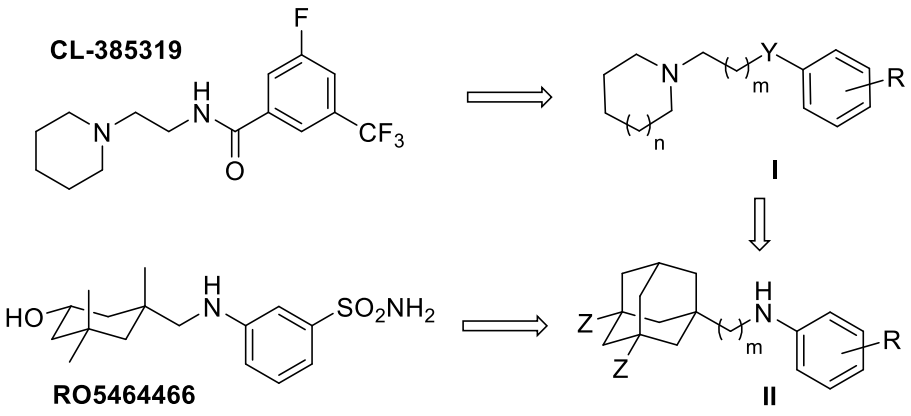

Chemistry

First, we undertook the synthesis of the piperidines with the general structure **I** (n = 1) and related ring expanded (n = 2) and ring contracted analogues (n = 0) (Scheme 2). The desired bioactive compounds could be accessed in just one facile synthetic step from commercially available starting materials. For the aromatic moiety, several commercially available anilines, phenols or thiophenols bearing the desired substitution were used, as well as a range of diverse chloroalkyl compounds. Thus, the attack of the nucleophilic group in the aromatic moiety to the desired chloroalkyl derivative upon heating, yielded the desired products in low (for the less reactive anilines) to very good (for the phenols and thiophenols) yields. While a few of the alkylated anilines were obtained in high yield (ca 80%) by heating a neat mixture of the aniline and *N*-(2-chloroethyl)piperidine hydrochloride at 120 ºC overnight,[47] the less reactive anilines (e.g., bearing electronwithdrawing groups) needed the addition of base, either K_2CO_3 or NaH, KI catalyst and extending (30 hours) heating, furnishing the products in only moderate to low yield. The corresponding alkylation of phenols and thiophenols proceeded in medium to very high yields by using NaOH in refluxing ethanol. All the tested compounds were fully characterized as the corresponding hydrochloride derivatives, prepared upon addition of an excess of hydrochloric acid in ether or 1,4-dioxane to a solution of the free base in ethyl acetate.

Scheme 2. Synthesis of the general scaffold **I** derivatives **1-7**.[a]

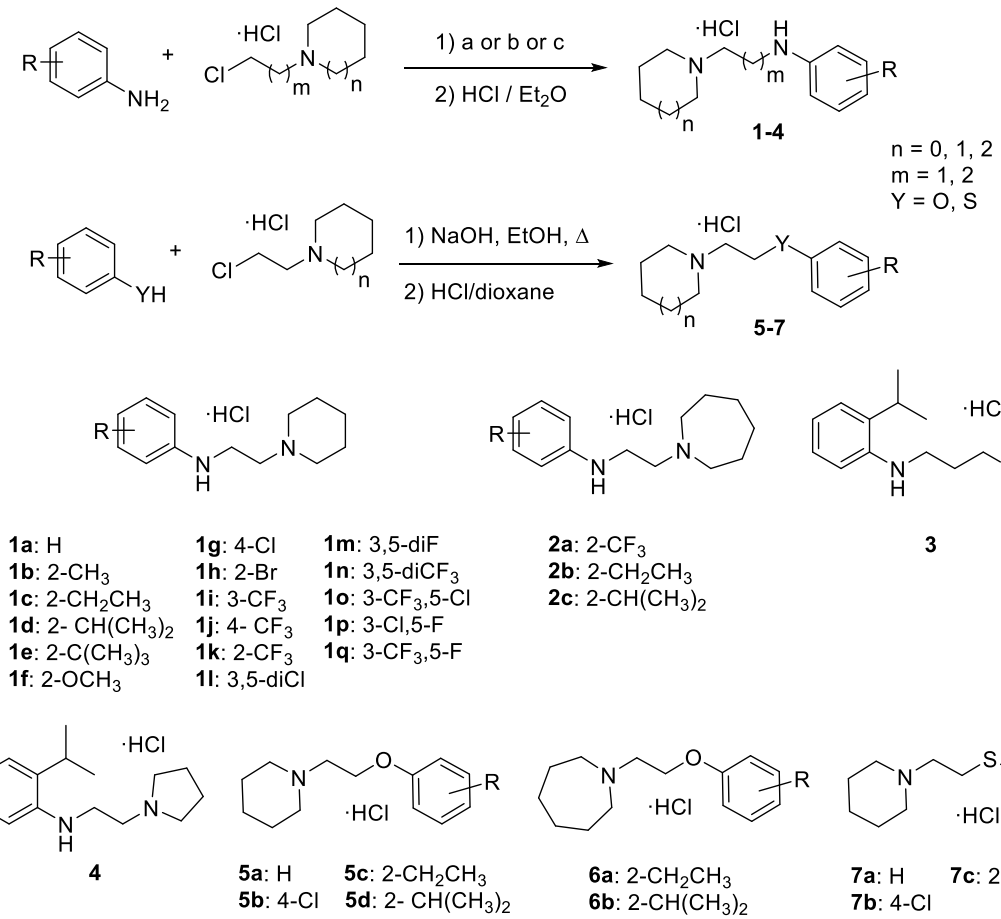

a. Reagents and conditions: a. heat; b. K_2CO_3, KI, DMF, heat; c. NaH, KI, dry DMF, heat. n = 0, 1, 2; m = 1, 2; Y = O, S.

A different synthetic strategy was undertaken for the preparation of the (adamantylmethyl)anilines of general structure **II** (Scheme 3). In this case the desired compounds of structure **11a-w** were prepared via a three-step route, starting from the commercially available 1-adamantanecarboxilic acid. Using thionyl chloride the corresponding acid chloride was readily obtained and added to a solution of the corresponding aniline in dry acetone. Upon continuous heating the desired amide **10a-w** did precipitate in a good yield. Without further purification, this precipitate was treated with sodium bis-(2-methoxyethoxy)aluminum hydride to furnish the corresponding

aniline in moderate to good yields. Aniline **11x** was synthesized in a similar way, starting from commercially available 3,5-dimethyl-1-adamantanecarboxylic acid.

Scheme 3. Synthesis of anilines **11a-x**, **14a-b** and **17**.[a]

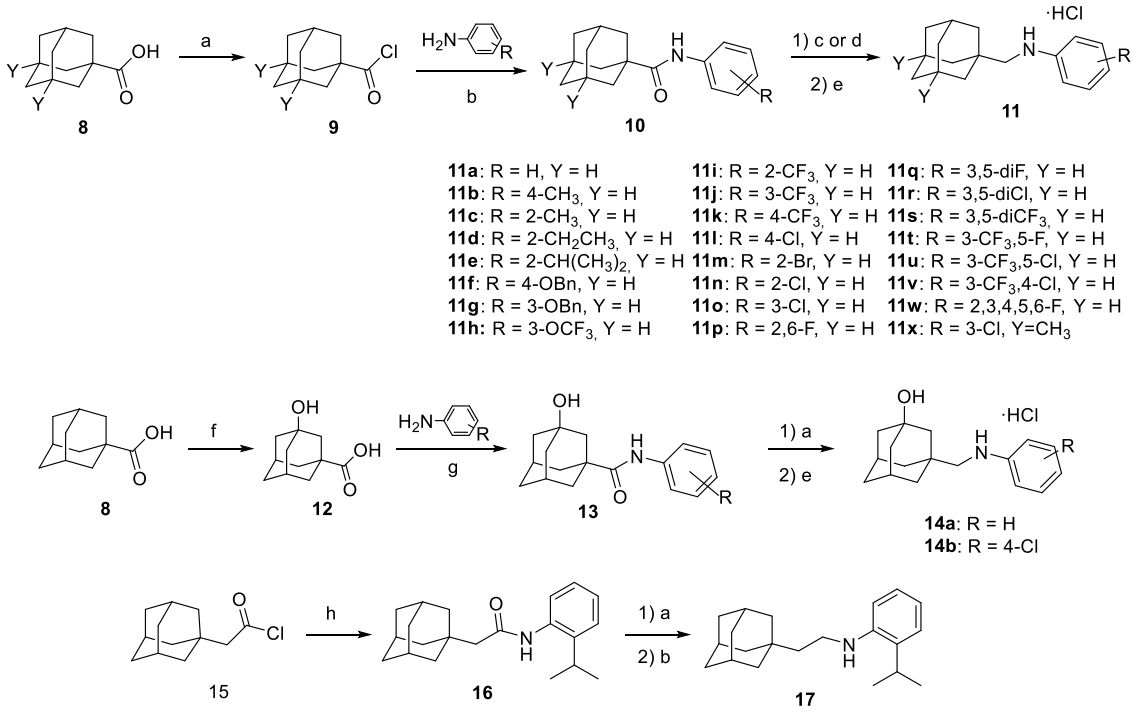

[a]Reagents and conditions: a) $SOCl_2$, 80 ºC, 2 h; trimethylamine, acetone, reflux, 3 h; c) $NaAlH_2(OCH_2CH_2OCH_3)_2$, toluene, 95 ºC, 24 h; d. BH_3·THF, 0ºC to rt, 24 h; e) HCl/Et2O; f) HNO_3, H_2SO_4, rt, overnight, 95%; g) EDC·HCl, DMAP, dichloromethane, rt, 24 h; h) 2-isopropylaniline, trimethylamine, acetone, reflux.

The preparation of the 3-hydroxyadamantane derivatives **14a-b** was first envisaged as a direct step, through the direct low-temperature hydroxylation with HNO_3 / H_2SO_4 of the required aniline **11**. Unfortunately, several attempts led to complex mixtures of products, probably arising from competitive oxidation of the aniline. Alternatively, the derivatives **14a-b** were accessed from known 3-hydroxyadamantanecarboxylic acid, **12**.[48] Thus, the reaction of **12** with the required aniline using EDC as a coupling agent furnished amides **13a-b** that were reduced with sodium bis-(2-

methoxyethoxy)aluminum hydride to yield **14a-b**. Finally, aniline **17**, featuring an additional methylene unit in the linker, was prepared in an analogous manner than the **11** series. All the novel amines were fully characterized as their corresponding hydrochlorides.

Of note, while the reduction of **10j**, featuring a trifluoromethyl group in the meta position proceeded as expected to furnish aniline **11j**, the reduction of its *ortho* and *para* isomers, **10i** and **10j**, did not furnished the expected anilines, but **11c** and **11b**, respectively (Scheme 4). The formation of **11b** and **11c** can be easily explained taking into account the strong basicity of the hydride used, which triggers a dehalogenation reaction that competes with the reduction. In order to avoid this problem, we switched ti borane, an electrophilic reductor agent, that smoothly furnished anilines **11i** and **11k**.

Overall, from this work, 47 compounds were synthesized and fully characterized and were subsequently tested.

Scheme 4. Reduction of amides **10i-k** with sodium bis-(2-methoxyethoxy)aluminum hydride.[a]

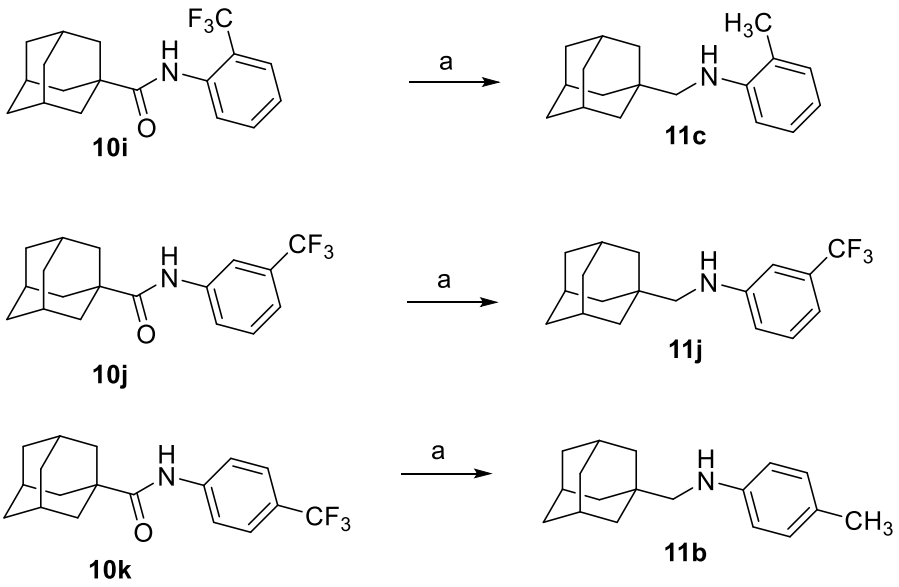

[a]Reagents and conditions: a) $NaAlH_2(OCH_2CH_2OCH_3)_2$, toluene, 95 ºC, 24 h.

Antiviral activity and cytotoxicity in cell culture

The anti-influenza virus activity of the compounds was determined in MDCK cells infected with three influenza A strains, A/HongKong/7/87 (H3N2 subtype), A/PueroRico/8/34 (H1N1 subtype) and A/Virginia/ATCC3/2009 (H1N1 subtype), and the influenza B strain (B/HongKong/5/1972). Of note, the A/HongKong/7/87 carries an amantadine sensitive, wild-type M2 protein, meanwhile the other strains carry a S31N mutant M2 channel, resistant to amantadine. The compounds' inhibitory effect on virus replication, as well as their cytotoxicity, were monitored by microscopical examination of cellular morphology change (CPE) at 3 days post-infection and confirmed by the colorimetric MTS cell viability assay (Table 1).[49]

These assays revealed that the compounds evaluated were inactive against the influenza A/H3N2 subtype and the influenza B strain (results not shown). Nevertheless several compounds displayed good activities against the influenza A/H1N1 subtypes, which revealed interesting SAR trends.

Regarding the aromatic moiety it is evident that ring-substitution is required for activity, the unsubstituted **1a**, **5a**, **7a** and **11a** rendered inactive. Moreover it can also be affirmed that the *ortho* position is the more appropriate for good anti-influenza potency; meanwhile *para*-, *meta*- or full ring substitution, e.g. **1g**, **1i**, **11w** respectively, are deleterious for this endeavour. More specifically the ideal substituent in the aforementioned position, poises to be the isopropyl group, yielding the most potent compounds reported: **1d**, **5d**, **11e** and **17.** Within the series of 2-alkyl-*N*-[2-(piperidin-1-yl)ethyl]anilines **1a-d**, the progressive chain increase from hydrogen, **1a**, methyl, **1b**, ethyl, **1c**, to isopropyl, **1d,** increased the antiviral activity against both H1N1 strains. In addition, the slight loss of activity in the *tert*-butyl substituted **1e**, sets the length limit of this trend.

Table 1. Antiviral activity of the synthesized compounds in influenza virus-infected MDCK cells.[a] For the sake of clarity, only active compounds are shown.

Compd	Antiviral EC_{50} (μM)[b,c] Influenza A H1N1				Cytotoxicity (μM)	
	A/PuertoRico/8/34		A/Virginia/ATCC3/2009		CC_{50}[d]	MCC[e]
	CPE	MTS	CPE	MTS		
1c	21	21	13	9.6	>100	>100
1d	4.6	5.5	1.6	1.6	>56	>100
1e	29	32	36	26	>100	>100
1f	>100	>100	5.1	3.4	>100	>100
1h	25	42	15	34	>100	>100
1k	14	10	5.4	5.6	61	100
2a	>100	>100	0.8	0.8	11	20
2b	>100	>100	1.7	1.5	14	20
2c	>100	>100	1.6	<1.3	54	>100
3	>100	>100	18	7.9	74	60
4	23	39	17	8.0	>100	>100
5c	8.9	11	8.0	5.7	>100	>100
5d	30	15	<20	<1.6	>100	>100
6a	>100	>100	4.0	0.8	10	>4
6b	>100	>100	1.4	1.9	31	20
10f	>100	>100	52	39	>100	>100
11d	>100	>100	0.19	0.15	0.97	<2
11e	>100	>100	0.8	>100	3.4	4.0
11p	>100	>100	0.2	>100	2.1	≥2.0
14a	5.6	5.2	>100	>100	23	>20
17	>100	>100	0.8	>100	1.6	4
Amt	85	178	>500	>500	>500	>500

[a]MDCK: Madin-Darby canine kidney cells; virus strains: A/HongKong/7/87, A/PuertoRico/8/34, A/Virginia/ACC3/2009 and B/HongKong/5/72. [b]50% Effective concentration, or concentration producing 50% inhibition of virus-induced cytopathic effect, as determined by visual scoring of the CPE or by measuring the cell viability with the colorimetric formazan-based MTS assay. [c]All the compounds showed EC50 > 100 mM against the A/HK/7/87 and the B/HongKong/5/1972 strains. [d]50% Cytotoxic concentration, as determined by measuring the cell viability with the colorimetric formazan-based MTS assay. [e]Minimum compound concentration that causes a microscopically detectable alteration of normal cell morphology. Values shown are the mean of 2-3 determinations.

In the case of the linker between the aromatic ring and the piperidine, an optimal length of 3 atoms was found (e.g., **1d** vs **3**). Regarding the linker's heteroatom nature, a nitrogen atom was slightly better than oxygen (compare **1c** *vs* **5c**, **1d** *vs* **5d**, **2b** *vs* **6a** and **2c** *vs* **6b**), with the sulfur analogues being always inactive (**7a-c**).

Drawing our attention to the heterocyclic ring, the piperidine ring seems to be the best for activity. Ring-contraction from piperidine to pyrrolidine reduced the antiviral activity in the two A/H1N1 strains (e.g., **1d** vs **4**). On the other hand, ring-expansion from piperidine to the azepane ring was very deleterious for the activity against the A/PR/8/34 strain and also increased the cytotoxicity.

Remarkably, **10f** and **14a** seemed not to follow the previous activity trends. The amide **10f** that displayed antiviral activity against A/Virginia/ATCCE/2009 standed out for two reasons: it is the only amide from the series **10a-x** endowed with anti-influenza activity, and it bears a *para*-benzyloxy group in the aromatic moiety, being the only active compound with an electron donating group. Very interesting is the case of **14a**, which bears a hydroxyl group in the adamantane moiety and poises not only as the sole compound to show antiviral activity with an unsubstituted aromatic moiety, but also to inhibit A/PuertoRico/8/34 and not A/Virginia/ATCCE/2009. Taking into account the presence of a hydroxyl group in RO5464466 and RO5487624, further derivatives of **14a** should be explored.

Selection and characterization of 1d-resistant virus mutants

There are strong hints that pointed to the viral hemagglutinin (HA) as the likely antiviral target of the compounds. First of all, they share an important structural similarity with HA inhibitors reported in the past, e.g. RO5464466. Second, only the strains carrying a type 1 hemagglutinin protein are inhibited. Moreover despite A/PR/8/34 and A/VR/ACCC/2009 are both H1N1 strains, their HA differ in a 20% of

their amino acids, fact that may help explain the different inhibition patterns observed (see below, molecular modeling section). Importantly, one of these structural mismatches is found at the entrance of the protein's binding site. There the threonine in A/PR/8/34 is replaced by a smaller serine in A/VR/ACCC/2009, easing the access to its binding site. This observation correlates with the fact that the bulkier azepanes can target A/VR/ACCC/2009 but fail inhibiting A/PR/8/31 (compare series **1** *vs* **2** and **5** *vs* **6**). Finally, while this work was in progress, Basu et al. reported that MBX-2329, a ring expanded analog to **5c**, was a potent entry inhibitor targeting the hemagglutinin-mediated influenza A virus fusion, thus validating our predictions.[50]

To further confirm that the target of our compounds was HA, we serially passed the influenza A/PR/8/34 virus in the presence of the aniline **1d**, which was chosen because of its superior activity and selectivity, making it possible to apply compound very high concentrations. A control condition in which the virus was passed in the absence of test compound was included, to identify which HA mutations appear as the virus, produced in eggs, is adapted to cell culture. After three passages, sequencing analysis of resistant A/PR/8 viruses in infected MDCK cells treated with compound **1d** allowed to localize the Thr107→Ile mutation in the HA2 monomer of HA.

WaterLOGSY NMR experiments

Specific inhibition of influenza viruses with group 1 HA by several of our anilines suggest that they interact with group 1 HA, but not with group 2 HA (see above). To verify that HA is the target of the compounds, we investigated the binding of **1d** to recombinant H5 HA (a group 1 HA) using WaterLOGSY NMR spectroscopy, which is designed to detect binding of small molecules to high-molecular-mass targets. These experiments indicated that **1d** binds to H5 HA. We further examined the binding epitopes of **1d** for H5 HA by an STD NMR experiment, which identifies ^{1}H in closest

proximity to the protein surface. This experiment revealed that the contact is relatively uniform, with the aromatic ring and the isopropyl group of **1d** in closest contact.

Molecular modeling studies

A potential strategy against influenza consists of the stabilization of the pre-fusogenic form of HA and prevention of its pH-mediated refolding by fusion inhibitors.[16,36] Identifying the binding site of these inhibitors is of utmost relevance for understanding their mechanism of action and to develop more effective potent drugs. In this regard, two putative binding sites have been proposed (Figure 1; see also Figure S1 in Supporting Information). Plotch and co-workers reported docking studies on the A/HK/8/68 (H3N2) strain for the CL series of compounds and suggested a possible site in the middle of the HA trimer, near the buried fusion peptide.[37] Later, Skehel and co-workers reported the X-ray structure of the HA complex with an hydroquinone inhibitor, TBHQ, selective for the H3 X31 subtype, unveiling the existence of a distinct pocket,[18] and the binding mode has been recently explored by MD simulations.[30] This latter pocket has been proposed to be the binding site of *N*-(1-thia-4-azaspiro[4.5]decan-4-yl)carboxamide inhibitors, which are also selective for the H3 strain.[49]

Currently, only two crystallographic structures of HA (H3 and H14 subtypes) bound to TBHQ are available in the Protein Data Bank (entries 3EYM, 3EYK and 3EYJ). In these structures the binding site adopts the "open" form, which is characterized by the unfolding of the C-terminal region of the helix A (Figure 1A). No similar structural information is available for the binding of fusion peptide inhibitors on the H1 subtypes, and all the X-ray structures are found in a "closed" state, where residues 56-59 adopt a full helical arrangement (Figure 1B).

Homology modeling. In order to examine the binding of compound **1d** to both H1 and H3 subtypes, homology modeling was used to build up a 3D model of the H1-subtype

HA in the "open" form. To this end, a multiple alignment of the amino acid sequences of A/PuertoRico/8/1934 (H1N1 subtype), A/Virginia/ATCC3/2009 (H1N1 subtype) and A/HongKong/7/1987 (H3N2 subtype) was performed. The sequence identity of the two former strains amounts to 81%, but drops to 42% when they are compared to the H3 subtype. However, if the analysis is restricted to the HA2 chain, which contains the TBHQ binding site (Figure 1), the sequence similarity increases up to 92% between the two H1 strains and 61% with the H3 subtype (Figure S2 of Supplementary Material). This supports the usage of the H3-subtype X-ray structures to build up the "open" form of the H1 HA. This was accomplished by using the PDB code 3EYM of H3 X31 strain, and the 3D models generated for A/HK/7/1987, A/Virginia/ATCC3/2009 and A/PR/8/1934 were subjected to a preliminary minimization using Sybyl X2.1 (Tripos). Inspection of the energy-minimized structures revealed the absence of incorrect structural arrangements or steric clashes in the binding site.

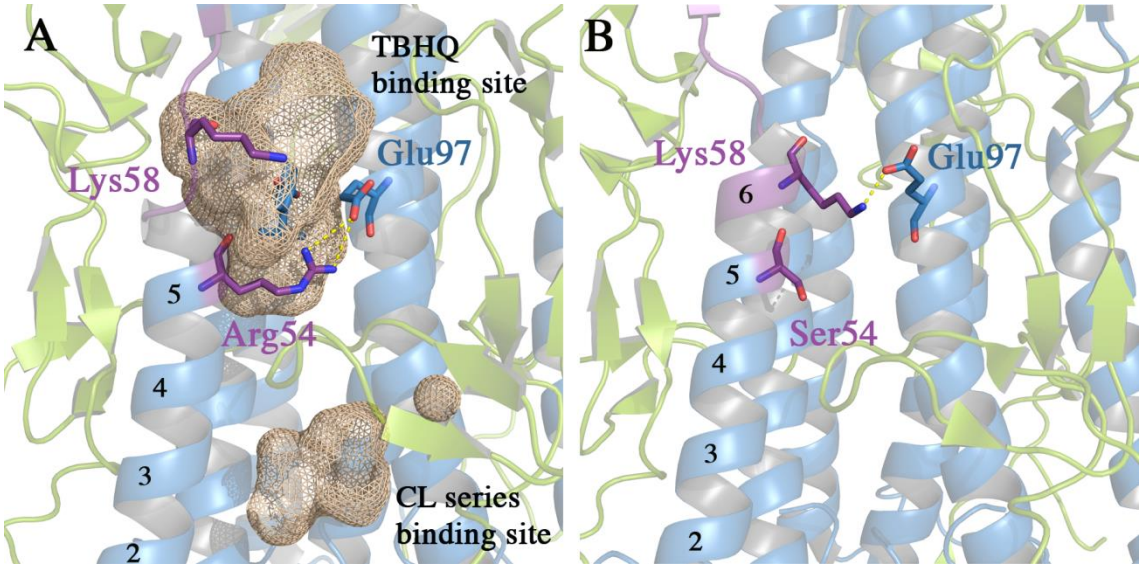

Figure 1. Representation of the (A) *open* and (B) *closed* conformations for the two HA subtypes, H3N2 (PDB ID: 3EYM) and H1N1 (PDB ID: 1RU7). Binding sites for fusion inhibitors pertaining to the CL and TBHQ series of compounds are also shown (brown mesh).

For the sake of clarity, the two monomers of HA are shown in green/blue. Protein regions implicated in the conformational change responsible for cavity opening (primarily affecting the sixth helical turn) are highlighted in pink.

A preliminary docking analysis was performed into the binding site proposed by Plotch and co-workers,[37] but no suitable poses able to explain the SAR profile of our inhibitors were found (data not shown). Moreover, experimental data about H3-subtype selectivity[18] for the TBHQ binding site makes this region of HA more interesting for the design of selective inhibitors, as recently suggested by Yusuf and co-workers.[51] Therefore, we limit ourselves to discuss the results concerning the TBHQ pocket.

The residues that shape this binding site are generally conserved between H1 and H3 substypes (see Figure 2), although subtle differences can be identified. In the interior of the cavity, Tyr308 of A/PR/8/1934 is replaced by Phe in both A/Virginia/ATCC3/2009 and A/HK/7/1987, thus reducing the polarity within the cavity. At the entrance of the binding site, Thr54 in A/PR/8/1934 is mutated to Ser in A/Virginia/ATCC3/2009, and to Arg54 in A/HK/7/1987. These mutations may alter the accessibility to the binding site, especially due to the formation of a salt bridge between Arg54 and Glu97 that could stabilize the long α-helix on HA2, while enabling the partial "opening" of its C-terminal part.[18] Instead, replacement of Arg54 with Ser and Thr in the H1 subtypes may favor the electrostatic interaction between Glu97 and Lys58, which would rigidify the terminal helical turn of the helix A, thus impeding the helical rearrangement that opens the binding site. Other mutations involve the change of Val36 (H1 subtype) by Ile45 (H3 subtype), and Leu101 (H1 subtype) by Ala101 (H3 subtype), which would generate local differences in the shape and hydrophobicity of the subpocket filled by the *t*-butyl moiety of TBHQ.

Adaptive Poisson-Boltzmann solver (APBS) calculations[52] were performed to examine the effect of these changes on the solvent-screened electrostatic potential at the

binding site. A clear difference emerges between H1 and H3 subtypes (Figure 2): while the ligand-binding site for A/PR/8/1934 and A/Virginia/ATCC3/2009 shows a pronounced negative potential, which can stabilize positively charged ligands, the pocket in A/HK/7/1987 is less polar and more prone to accommodate hydrophobic ligands.

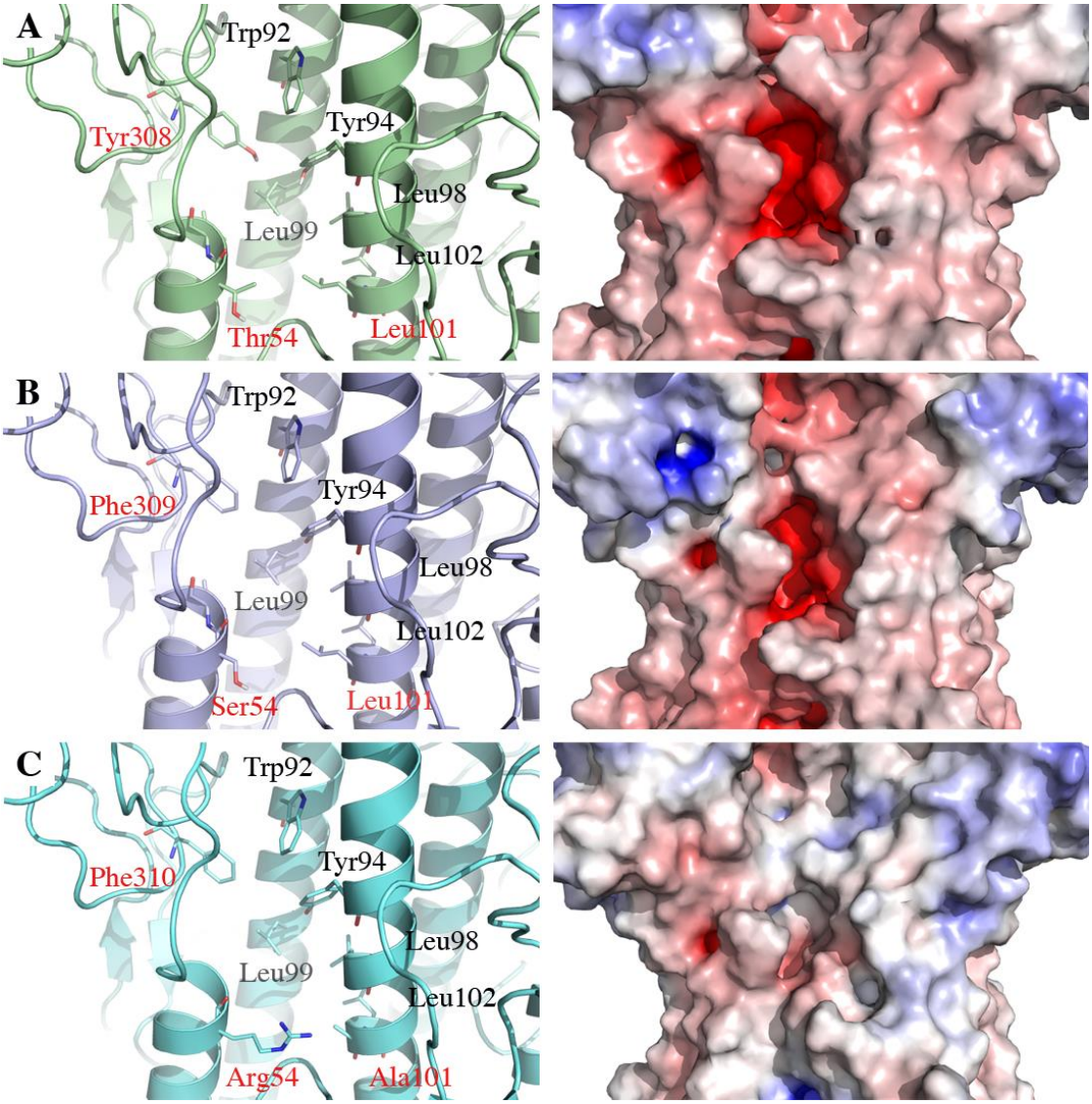

Figure 2. Comparison of (*left*) the binding sites for (A) A/PR/8/1934, (B) A/Virginia/ATCC3/2009 and (C) A/HK/7/87 obtained by homology modelling. Mutations at the binding site among the three strains are highlighted in red. (*Right*) Representation of the solvent-screened electrostatic potential for A/PR/8/1934 (A), A/Virginia/ATCC3/2009 (B) and A/HK/7/1987 (C): Level -15/+5 kT/e).

Docking calculations. Surflex-Dock tool was then used to dock compound **1d** within the TBHQ binding site of these structural models. No suitable docking poses were identified for A/HK/7/1987, an effect that can be ascribed to the reduced accessibility caused by the Arg54 side chain and the unfavourable electrostatic stabilization for a positively charged compound (see above), in agreement with the H1 selectivity profile determined experimentally for this compound. In contrast, similar interaction patterns were found for the binding of **1d** to both A/PR/8/1934 and A/Virginia/ATCC3/2009 binding sites (Figure 3A,B). Next, MD simulations were carried out examine the structural integrity of this binding mode, leading to a stable accommodation of the ligand after the first 25 ns of simulation.

In the binding mode, the 2-isopropylaniline moiety is stably placed in a subpocket delimited by Leu98, Leu99, and Leu101, matching most of the region filled by TBHQ in the X-ray structure. The size of the pocket occupied by the aniline moiety tolerates the accommodation of relatively small hydrophobic substituents, such as ethyl (**1c**) and *t*-butyl (**1e**), and bromine (**1h**). However, compounds with hydrogen (**1a**) or an *o*-methyl (**1b**) group are inactive, an effect that may reflect either a poorer binding of the compound or the geometrical influence of the *ortho*-substituent on the conformational preferences of the aliphatic linker. Moreover, *meta*- (see **1l-q**) or *para*-substitutions (see **1g**, **1j**, **5b** or **7b**) seems to be not allowed, as are also associated to loss of antiviral activity, likely due to steric clashes with residues in the binding pocket.

The piperidine ring occupies the inner part of the cavity, facing Tyr308 in A/PR/8/1934) and Phe309 in A/Virginia/ATCC3/2009). This arrangement is assisted by stable hydrogen-bonding interactions formed by the charged piperidine and aniline nitrogen atoms with the backbone carbonyl groups of Glu57 and Thr54 in A/PR/8/1934, and with Val55 and Ser54 in A/Virginia ATCC3/2009 (Figure 3C,D). This is noted in

average distances close to 2.8 Å (piperidine N) and 3.5 Å (aniline N), and O···H-N angles in the range 130°-160°. In this regard, a more stable interaction pattern is found for the complex with A/Virginia ATCC3/2009, as deduced from the larger stability of these interactions along the MD simulations (Figure S3 in Supporting Information), in agreement with the larger inhibitory potency found for this HA subtype. On the other hand, the replacement of N with S (**7c**), which suppresses the inhibitory activity on the two subtypes, may be ascribed to the loss of the hydrogen bond formed with the backbone oxygen of Ser/Thr54. This could probably explain the differences in inhibitory activity among the N-(O/S) series.

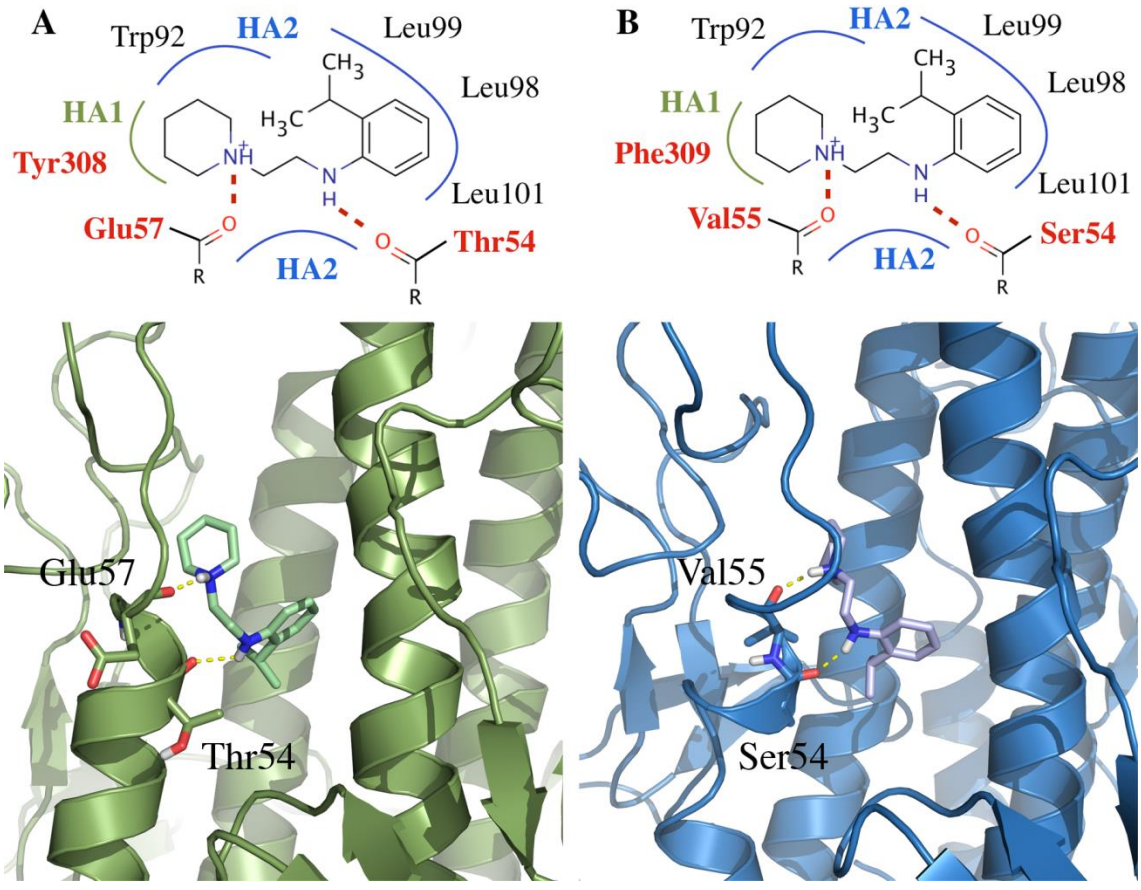

Figure 3. (*Top*) 2D representation of the binding modes for compound RL-007 (**1d**) on A/PR/8/1934 (A) and A/Virginia/ATCC3/2009 (B). (*Bottom*) Protein-inhibitor complexes for compound **1d** (in light green for A/PR and in violet for A/Virginia) within A/PR/8/1934 (A) and A/Virginia/ATCC3/2009 (B) obtained after 50 ns of MD simulations.

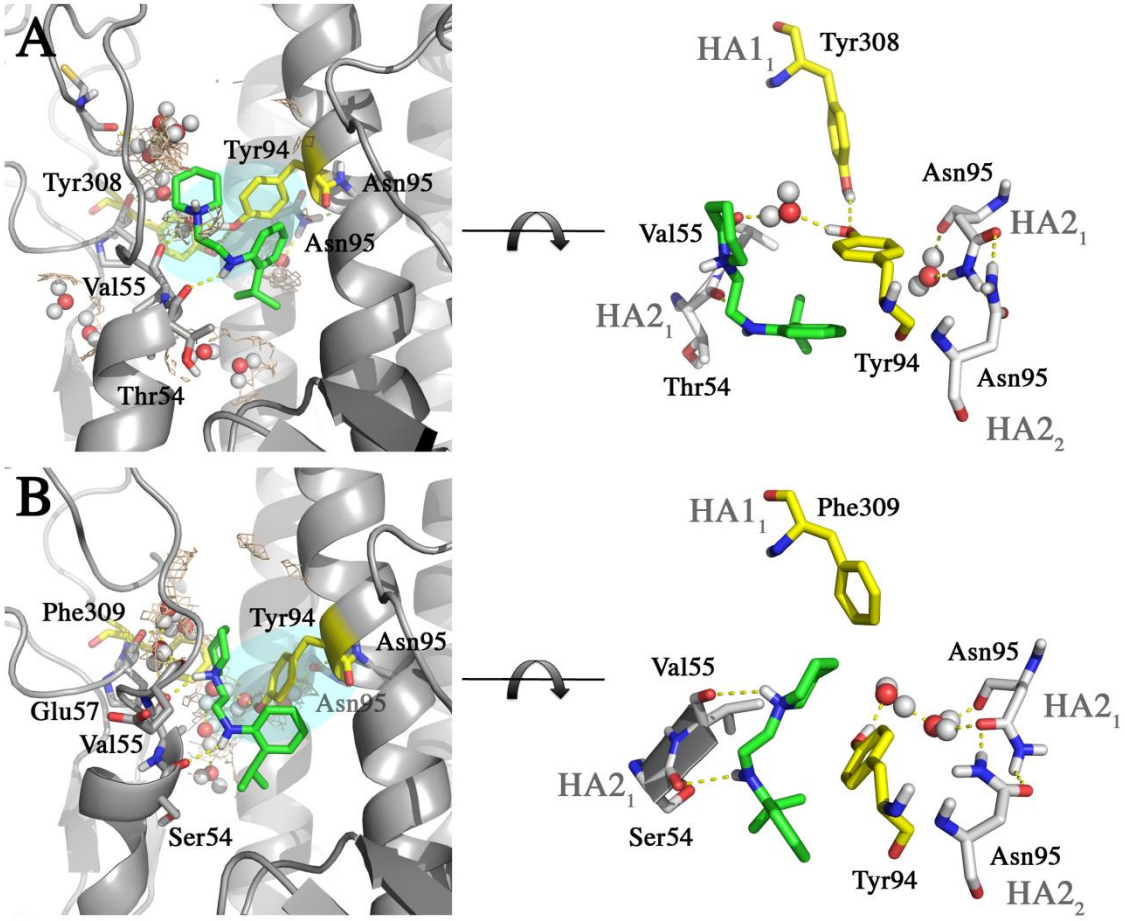

Figure 4. Analysis of water electron density contours (in wheat dashes) for the complexes of **1d** (green) with (A) A/PR/8/1934 and (B) A/Virginia/ATCC3/2009. Solvated trajectories obtained from the last 15 ns of MD simulation were used for the analysis.

Finally, the expansion of the piperidine ring to a seven-membered cycle (**2c**) reduces the inhibitory activity in A/PR/8/1934, even though this change does not impair the inhibitory activity in A/Virginia/ATCC3/2009. We hypothesize that this effect may be attributed to the impact of the ring expansion on the network of water molecules present in the binding pocket, a relevant feature highlighted by other researchers.[53-54] The electron density map for the crystal structure of H3 X31 co-crystallized with TBHQ reveals the presence of water molecules near Tyr94 (Figure S4 of Supporting Material). Indeed, the analysis of the MD trajectories shows the presence of a "stable" water

network in front of Tyr94 (Figure 4A) that facilitates water-mediated interactions with Val55, and may contribute to stabilize the hydrogen bond between Tyr308 and Tyr94. Going to the A/Virginia-**1d** complex, mutation of Tyr94 to Phe causes the loss of the water-assisted Val-Tyr-Tyr interaction, which permits the phenol moiety of Tyr94 to adopt a distinct orientation within the pocket. This change reduces the conformational constraint within the cavity, thus allowing the piperidine moiety of the ligand to stack against Tyr94 (Figure 4B), and facilitates the formation of a polar interaction with the backbone oxygen of Val55. Overall, we suggest that the ring expansion is better fitted in A/Virginia/ATCC3/2009 due to the subtle rearrangement of the side chains of Phe309 and Tyr94, and the dehydration cost required to break the water-mediated interactions between Val55, Tyr308 and Tyr94 in A/PR/8/1934. Furthermore, the reduction in the local permittivity in the binding site linked to the disruption of the water network could also justify the larger stability observed for the polar interaction between the charged piperidine nitrogen and the backbone oxygen of Val55 in A/Virginia ATCC3/2009 during MD simulations (Figure S3 of Supporting Material).

Ligand-induced mutations for A/PR. Three passages of A/PR/8 virus with **1d** leads to drug resistance (see above). Sequencing analysis of A/PR/8 viruses in infected MDCK cells treated with these compounds allowed to localize the Thr107→Ile mutation in the HA2 monomer of HA. This residue is located near the fusion peptide and contributes to stabilize the reciprocal orientation adopted by the three α-helixes that form the TBHQ binding site (Figure 5) through a water-assisted network of polar interactions involving Thr107, Arg106, Glu103, Lys51, and Thr54. The mutation could destabilize these interactions, particularly the electrostatic interaction between Lys51 and Glu103, which in turn interacts with Arg106 and water molecules below the ligand binding site. Such a

destabilization could weaken the binding affinity of the ligand, or facilitate the release of the fusion peptide, thus explaining the loss of its antiviral efficacy.

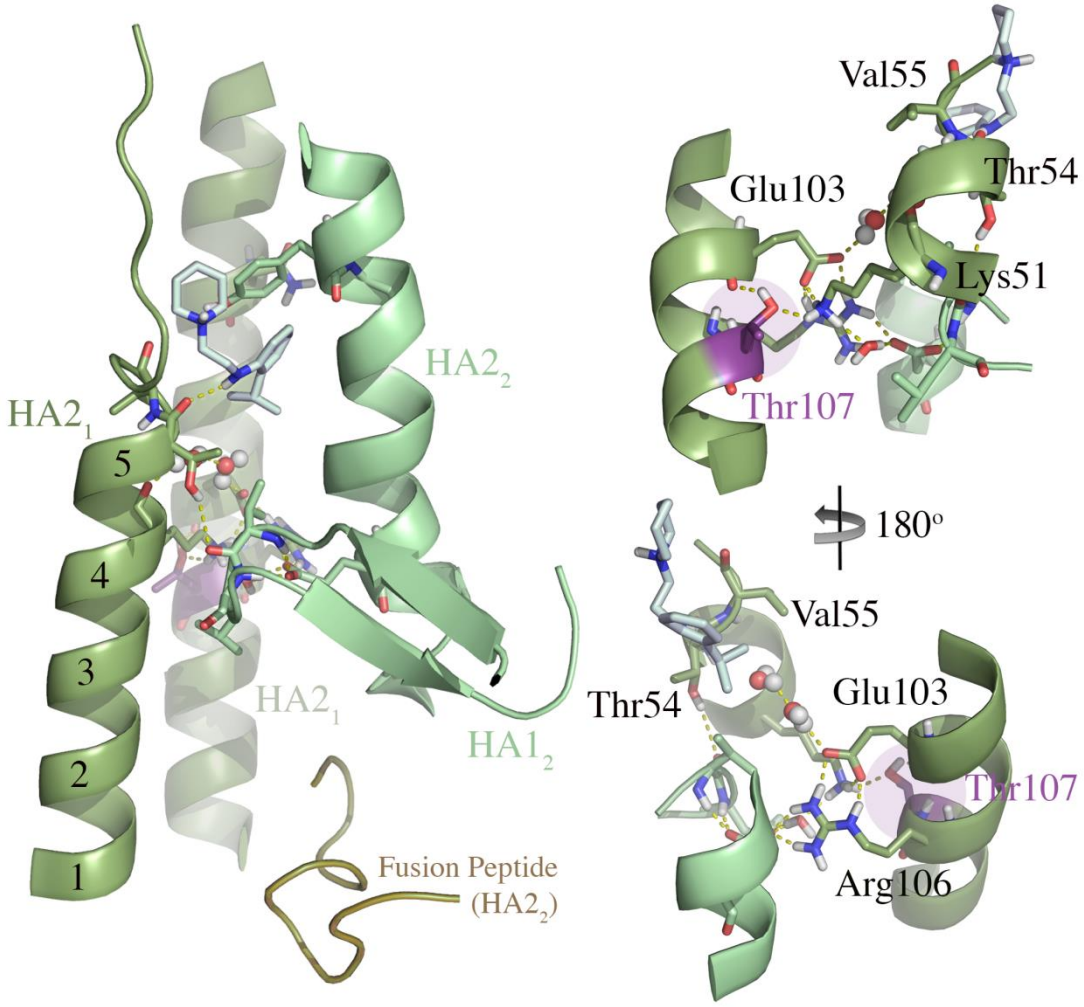

Figure 5. Effects of Thr107 →Ile mutation on water-assisted polar network generated by residues pertaining to (right-top) $HA2_1$, and (right-bottom) $HA2_1$ and $HA2_2$ helices for A/PR/8 virus in MDCK cells under **1d**. The Thr →Ile mutation not only breaks the interaction between the hydroxyl group of Thr107 and Lys51, but it also is expected to destabilize the electrostatic interaction between Lys51 and Glu103, which in turn interacts with Arg106 and water molecules below the ligand binding site. The net effect would promote structural instability, weakening ligand binding and leading to antiviral inefficacy.

Activity against other viruses

In addition to the influenza virus, for all the compounds, CPE (cytopathic effect) reduction assays were performed to determine the antiviral activity against a broad panel of DNA and RNA viruses, i.e. herpes simplex virus type 1 and type 2, and

vaccinia virus (evaluated in HEL cells); feline coronavirus and feline herpesvirus (in Crandell-Rees Feline Kidney cells); vesicular stomatitis virus (VSV), Coxsackie B4 virus and respiratory syncytium virus (tested in HeLa cells); and para-influenza-3 virus, reovirus-1, Sindbis virus and Punta Toro virus (tested in Vero cells).

Of note, three derivatives carrying the adamantyl scaffold poised as potent inhibitors of the VSV, which has a great relevance in veterinary and currently has no treatment (Table 2). Finally, **11i** revealed as a potent inhibitor of the virus Parainfluenza 3, (EC_{50} = 9 μM) and **11f** turned out as a good inhibitor of virus Coxsackie B4 (EC_{50} = 8.9 μM).

All this together makes stand out the usefulness of the general scaffolds **I** and **II**, when seeking for a range of antiviral compounds. Further SAR around the antiviral activity of these compounds against VSV, parainfluenza 3 and coxsackie B4 viruses will be reported in due course.

Table 2. Antiviral activity of the synthesized compounds in VSV infected HeLa cells.

Compd	Antiviral EC_{50} (μM)[a]	Cytotoxicity (CC_{50})[b]
6b	45	>100
11t	12	>100
11u	12	>100
Rivabirin	22	>250

[a]50% Effective concentration, or concentration producing 50% inhibition of virus-induced cytopathic effect, as determined by visual scoring of the CPE. [b]Minimum compound concentration that causes a microscopically detectable alteration of normal cell morphology

Conclusions

Two series of novel anilines have been synthesized, fully characterized and evaluated as antivirals. Several compounds displayed activity against A/H1N1 influenza strains, several of them at the low micromolar range. Our sequencing data strongly argued for a role of the HA protein in the antiviral mode of action of **1d**, and, most likely, the other

polycyclic amines studied here. NMR experiments also support the HA as the target of our compounds.

MD simulations suggest that ligand **1d** is able to fill the TBHQ binding site present in A/PR/8/1934 and A/Virginia/ATCC3/2009. In addition, the mayor inhibitory activity observed for **1d** on A/Virginia/ATCC3/2009 can be attributed to the different conformational constraints induced by the water network within A/PR/8/1934 and A/Virginia/ATCC3/2009 cavities.

The activity displayed by selected examples of the synthesized compounds against VSV, parainfluenza 3 virus and cosxackie B4 virus warrants further exploration of the SAR, a work that will be reported in due course.

Experimental Section

Chemical Synthesis. General Methods. Melting points were determined in open capillary tubes with a MFB 595010M Gallenkamp. 400 MHz ^{1}H/100.6 MHz ^{13}C NMR spectra, and 500 MHz ^{1}H NMR spectra were recorded on Varian Mercury 400, and Varian Inova 500 spectrometers, respectively. The chemical shifts are reported in ppm (δ scale) relative to internal tetramethylsilane, and coupling constants are reported in Hertz (Hz). Assignments given for the NMR spectra of the new compounds have been carried out on the basis of DEPT, COSY ^{1}H/^{1}H (standard procedures), and COSY ^{1}H/^{13}C (gHSQC and gHMBC sequences) experiments. IR spectra were run on Perkin-Elmer Spectrum RX I spectrophotometer. Absorption values are expressed as wave-numbers (cm^{-1}); only significant absorption bands are given. The GC/MS analysis was carried out in an inert Agilent Technologies 5975 gas chromatograph equipped with an Agilent 122-5532 DB-5MS 1b (30 m × 0.25 mm) capillary column with a stationary phase of phenylmethylsilicon (5% diphenyl – 95% dimethylpolysiloxane), using the following conditions: initial temperature of 50 ºC (1 min), with a gradient of 10 ºC / min up to 300 ºC, and a temperature in the source of 250 ºC. *Solvent Delay* (SD) of 4 minutes and a pressure of 7.35 psi. Column chromatography was performed on silica gel 60 AC.C (35−70 mesh, SDS, ref 2000027). Thin-layer chromatography was performed with aluminum-backed sheets with silica gel 60 F_{254} (Merck, ref 1.05554), and spots were visualized with UV light and 1% aqueous solution of $KMnO_4$. The analytical samples of all of the new compounds which were subjected to pharmacological evaluation possessed purity ≥95% as evidenced by their elemental analyses.

General Procedure A. To a solution of the required aniline (2 eq) in dry DMF at room temperature, the chloroalkyl derivative (1 eq), K_2CO_3 (2 eq) and KI (0.1 eq) were

sequentially added. The reaction mixture was stirred and heated at 90 ºC during 30 hours. After cooling down to room temperature, the resulting crude material was dissolved in DCM. The solution was washed with water, dried over anh. Na_2SO_4, filtered and concentrated *in vacuo* to obtain the desired product and some recovered starting materials. Column chromatography (Hexane/Ethyl acetate mixtures) gave the expected product. An analytical sample of its hydrochloride was prepared by adding an excess of HCl either in diethyl ether or 1,4-dioxane to a solution of the base in ethyl acetate.

General Procedure B. A solution of the required aniline (2 eq) and 1-(2-chloroethyl)piperidine hydrochloride (1 eq) was stirred and heated at 120 ºC overnight. After cooling down to room temperature, the resulting mixture was dissolved in water and solid sodium acetate was added to obtain pH 5.5. The excess of aniline was extracted with diethyl ether. The aqueous layer was alkalized with 2N NaOH aqueous solution and extracted with diethyl ether. The combined organic layers were dried over anh. Na_2SO_4, filtered and concentrated *in vacuo* to obtain the desired product. An analytical sample of its hydrochloride was prepared by adding an excess of HCl either in diethyl ether or 1,4-dioxane to a solution of the base in ethyl acetate.

General Procedure C. Sodium hydroxide (0.800 g, 20 mmol, 2 eq) was refluxed in ethanol (150 mL) for 30 min. To the resulting solution was added the corresponding phenol or tiophenol (10 mmol, 1 eq) and further refluxed for 1 hour. A solution in ethanol (35 mL) of either 1-(2-chloroethyl)piperidine hydrochloride or 1-(2-chloroethyl)azepane hydrochloride (10 mmol, 1 eq) was added to the basic solution and the reaction mixture refluxed for further 3 hours. After pouring into cold water (125 mL), the product was extracted with DCM (4 x 125 mL) and the joined extracts were washed with water (4 x 150 mL), dried over anh Na_2SO_4, filtered and concentrated *in*

vacuo to obtain the desired product. Its hydrochloride was prepared by adding an excess of HCl either in diethyl ether or 1,4-dioxane to a solution of the base in ethyl acetate.

***N*-[2-(piperidin-1-yl)ethyl]aniline hydrochloride, 1a**.[55] Following general procedure B, aniline (1.82 mL, 20 mmol) and 1-(2-chloroethyl)piperidine hydrochloride (1.83 g, 10 mmol) gave the product as an orange oil (2.06 g, 85.8% yield), that formed its hydrochloride salt as a white solid (904 mg). The analytical sample was obtained by crystallization from EtOAc/Pentane. mp= 185-186 ºC. IR (ATR) ν: 691, 747, 830, 851, 871, 902, 949, 988, 1013, 1027, 1075, 1125, 1155, 1178, 1194, 1243, 1268, 1290, 1324, 1356, 1405, 1433, 1472, 1497, 1534, 1602, 2575, 2537, 2639, 2848, 2948, 3026, 3273 cm^{-1}. ^{1}H-NMR (400 MHz, CD_3OD) δ: 1.60-1.78 (c. s., 2 H, 11-H_2), 1.80-1.94 [c. s., 4 H, 10(12)-H_2], 3.15-3.34 [c. s., 4 H, 9(13)-H_2], 3.27 (t, *J* = 6.4 Hz, 2 H, 8-H_2), 3.53 (t, *J* = 6.4 Hz, 2 H, 7-H_2), 6.68 (m, 1 H, 4-H), 6.70 [m, 2 H, 2(4)-H], 7.15 [m, 2 H, 3(5)-H]. ^{13}C-NMR (100.5 MHz, CD_3OD) δ: 22.8 (CH_2, C11), 24.2 [CH_2, C10(12)], 39.5 (CH_2, C7), 54.7 [CH_2, C9(13)], 57.1 (CH_2, C8), 114.1 [CH, C2(6)], 119.0 (CH, C4), 130.3 [CH, C3(5)], 149.1 (C, C1). Anal. Calcd for $C_{13}H_{20}N_2$·HCl: C 64.85, H 8.79, Cl 14.72, N 11.63. Found: C 64.66, H 8.98, Cl 14.55, N 11.41.

2-methyl-*N*-[2-(piperidin-1-yl)ethyl]aniline hydrochloride, 1b. Following the general procedure A, 2-methylaniline (1.07 mL, 10 mmol), 1-(2-chloroethyl)piperidine hydrochloride (920 mg, 5 mmol), K_2CO_3 (1.38 g, 10 mmol) and KI (83 mg, 0.5 mmol) in dry DMF (2 mL) were mixed to obtain a yellowish oil (1.38 g). After column chromatography, the product was obtained as a colourless oil (557 mg, 51.0% yield) that formed its hydrochloride salt as a white solid (600 mg). mp = 182-183 ºC. IR (ATR) ν: 665, 708, 753, 771, 804, 854, 930, 948, 963, 988, 1008, 1049, 1079, 1117, 1132, 1170, 1196, 1226, 1261, 1292, 1330, 1405, 1451, 1479, 1514, 1582, 1600, 1648, 2400, 2526, 2612, 2936, 3321 cm^{-1}. ^{1}H-NMR (400 MHz, CD_3OD) δ: 1.55 (m, 1 H, 11-

H_{ax}), 1.76-2.00 [c. s., 5 H, 11-H_{eq} and 10(12)-H_2], 2.30 (s, 3 H, CH_3), 3.04 [m, 2 H, 9(13)-H_{ax}], 3.45 (t, *J* = 6.8 Hz, 2H, 8-H_2), 3.62 (m, 2 H, 9(13)-H_{eq}), 3.72 (t, *J* = 6.8 Hz, 2 H, 7-H_2), 6.89 (dd, *J* = *J'* = 7.8 Hz, 1 H, 4-H), 6.97 (d, *J* = 7.8 Hz, 1 H, 6-H), 7.15 (d, *J* = 7.8 Hz, 1 H, 3-H), 7.18 (ddd, *J* = *J'* = 7.8 Hz, J'' = 1.2 Hz, 1 H, 5-H). ^{13}C-NMR (100.5 MHz, CD_3OD) δ: 17.8 (CH_3), 22.6 (CH_2, C11), 24.1 [CH_2, C10(12)], 41.2 (CH_2, C7), 54.8 [CH_2, C9(13)], 55.8 (CH_2, C8), 114.9 (CH, C6), 122.7 (CH, C4), 127.1 (CH, C5), 128.4 (CH, C3), 132.1 (C, C2), 142.9 (C, C1). HRMS-ESI+ m/z [*M*+H]$^+$ calcd for [$C_{14}H_{22}N_2$+H]$^+$: 219.1856, found: 219.1858.

2-Ethyl-*N*-[2-(piperidin-1-yl)ethyl]aniline hydrochloride, 1c. Following general procedure B, 2-ethylaniline (2.47 mL, 20 mmol) and 1-(2-chloroethyl)piperidine hydrochloride (1.83 g, 10 mmol) gave the product as a yellow oil (1.93 g, 83.1%), that formed its hydrochloride salt as a pale brown solid (818 mg). mp = 173-174 ºC. IR (ATR) ν: 728, 745, 799, 833, 902, 925, 947, 993, 1013, 1050, 1087, 1136, 1164, 1193, 1238, 1261, 1287, 1304, 1329, 1369, 1426, 1452, 1478, 1518, 1586, 1600, 2507, 2610, 2867, 2924, 2947, 3341 cm^{-1}. ^{1}H-NMR (400 MHz, CD_3OD) δ: 1.21 (t, *J* = 7.6 Hz, 3 H, -$CH_2C\underline{H}_3$), 1.56-1.68 (c. s., 2 H, 11-H_2), 1.76-1.86 [c. s., 4 H, 10(12)-H_2], 2.55 (q, *J* = 7.6 Hz, 2 H, -$C\underline{H}_2CH_3$), 2.98-3.12 [c. s., 4 H, 9(13)-H_2], 3.13 (t, *J* = 6.4 Hz, 2 H, 8-H_2), 3.51 (t, *J* = 6.4 Hz, 2 H, 7-H_2), 6.64-6.70 (c. s., 2 H, Ar), 7.01-7.10 (c. s., 2 H, Ar). ^{13}C-NMR (100.5 MHz, CD_3OD) δ: 13.8 (CH_3, -$CH_2\underline{C}H_3$), 23.4 (CH_2, C11), 24.8 (CH_2, $\underline{C}H_2CH_3$), 24.9 [CH_2, C10(12)], 40.2 (CH_2, C7), 55.0 [CH_2, C9(13)], 57.4 (CH_2, C8), 111.3 (CH, C6), 118.9 (CH, C4), 128.0 (CH, C5), 129.3 (CH, C3), 130.0 (C, C2), 146.2 (C, C1). HRMS-ESI+ m/z [*M*+H]$^+$ calcd for [$C_{15}H_{24}N_2$+H]$^+$: 233.2012, found: 233.2005.

2-isopropyl-*N*-[2-(piperidin-1-yl)ethyl]aniline hydrochloride, 1d. Following general procedure B, 2-isopropylaniline (2.83 mL, 20 mmol) and 1-(2-chloroethyl)piperidine hydrochloride (1.83 g, 10 mmol) gave the product as a brown oil

(2.02 g, 82.2%), that formed its hydrochloride salt as a pale brown solid (1.15 g). mp = 140-141 ºC. IR (ATR) ν: 760, 855, 948, 966, 1007, 1039, 1096, 1172, 1193, 1257, 1270, 1294, 1327, 1356, 1376, 1403, 1445, 1513, 1583, 1599, 2356, 2529, 2614, 2861, 2932, 3328 cm^{-1}. ^{1}H-NMR (400 MHz, CD_3OD) δ: 1.22 [d, *J* = 6.8 Hz, 6 H, -CH(C<u>H</u>$_3$)$_2$], 1.54-1.66 (c. s., 2 H, 11-H_2), 1.74-1.84 [c. s., 4 H, 10(12)-H_2], 2.94-3.05 [c. s., 5 H, 9(13)-H_2, and -C<u>H</u>$(CH_3)_2$], 3.07 (t, *J* = 6.4 Hz, 2 H, 8-H_2), 3.47 (t, *J* = 6.4 Hz, 2 H, 7-H_2), 6.68 (broad d, *J* = 8.0 Hz, 1 H, 6-H), 6.70 (dt, *J* = 7.2 Hz, *J'* = 1.2 Hz, 1 H, 5-H), 7.05 (dt, *J* = 7.6 Hz, *J'* = 1.6 Hz, 1 H, 4-H), 7.12 (dd, *J* = 7.6 Hz, *J'* = 1.6 Hz, 1 H, 3-H). ^{13}C-NMR (100.5 MHz, CD_3OD) δ: 23.1 [CH_3, -CH(<u>C</u>H$_3$)$_2$], 23.6 (CH_2, C11), 25.2 [CH_2, C10(12)], 27.9 [CH, -<u>C</u>H$(CH_3)_2$], 40.5 (CH_2, C7), 55.0 [CH_2, C9(13)], 57.5 (CH_2, C8), 111.9 (CH, C6), 119.1 (CH, C4), 126.1 (CH, C5), 127.7 (CH, C3), 134.6 (C, C2), 145.6 (C, C1). HRMS-ESI+ m/z [*M*+H]$^+$ calcd for [$C_{16}H_{26}N_2$+H]$^+$: 247.2169, found: 247.2166.

2-*t*-butyl-*N*-[2-(piperidin-1-yl)ethyl]aniline hydrochloride, 1e. Following the general procedure A, 2-*tert*-butylaniline (1.56 mL, 10 mmol), 1-(2-chloroethyl)piperidine hydrochloride (0.92 g, 5 mmol), K_2CO_3 (1.38 g, 10 mmol) and KI (83 mg, 0.5 mmol) in dry DMF (2.5 mL) were mixed to obtain a brown oil (0.99 g). After column chromatography, the product was obtained as a yellow oil (290 mg, 19.5% yield) that formed its hydrochloride salt as a white solid (234 mg). mp = 101-102 ºC. IR (ATR) ν: 747, 773, 847, 899, 987, 1054, 1108, 1147, 1173, 1194, 1232, 1256, 1287, 1305, 1367, 1387, 1444, 1504, 1576, 1594, 2346, 2537, 2661, 2950, 3379, 3416 cm^{-1}. ^{1}H-NMR (400 MHz, CD_3OD) δ: 1.42 (s, 9 H, C(C<u>H</u>$_3$)$_3$], 1.56 (m, 1 H, 11-H_{ax}), 1.76-2.00 [c. s., 5 H, 11-H_{eq} and 10(12)-H_2], 3.05 [td, *J* = 12.4 Hz, *J'* = 3.2 Hz, 2 H, 9(13)-H_{ax}], 3.37 (t, *J* = 6.8 Hz, 2 H, 8-H_2), 3.63 (dm, J = 12.4 Hz, 2 H, 9(13)-H_{eq}), 3.73 (t, *J* = 6.8 Hz, 2 H, 7-H_2), 6.77 (ddd, *J* = *J'* = 7.6 Hz, *J''* = 1.2 Hz, 1 H, 4-H), 6.84 (dd, *J*

= 8.0, *J'* = 1.2, 1 H, 6-H), 7.14 (ddd, *J* = 8.0 Hz, *J'* = 7.6 Hz, *J''* = 1.6 Hz, 1 H, 5-H), 7.28 (dd, *J* = 7.6 Hz, *J'* = 1.6 Hz, 1 H, 3-H). ^{13}C-NMR (100.5 MHz, CD_3OD) δ: 22.5 (CH_2, C11), 24.2 [CH_2, C10(12)], 30.7 [CH_3, C($\underline{C}H_3$)$_3$], 35.3 [C, $\underline{C}(CH_3)_3$], 42.1 (CH_2, C7), 55.0 [CH_2, C9(13)], 56.1 (CH_2, C8), 116.1 (CH, C6), 122.0 (CH, C4), 128.1 (CH, C5*), 128.5 (CH, C3*), 137.6 (C, C2), 143.6 (C, C1). HRMS-ESI+ m/z [*M*+H]$^+$ calcd for [$C_{17}H_{28}N_2$+H]$^+$: 261.2325, found: 261.2333.

2-methoxy-*N*-[2-(piperidin-1-yl)ethyl]aniline hydrochloride, 1f.[56] Following the general procedure A, 2-methoxyaniline (0.56 mL, 5 mmol), 1-(2-chloroethyl)piperidine hydrochloride (0.92 g, 5 mmol), K_2CO_3 (2.07 g, 15 mmol) and KI (83 mg, 0.5 mmol) in dry DMF (2.5 mL) were mixed to obtain a brown oil (0.94 g). After column chromatography, the product was obtained as a yellow oil (380 mg, 28.6% yield) that formed its hydrochloride salt as a yellow solid (291 mg). mp = 174-175 ºC. IR (ATR) ν: 638, 754, 798, 827, 853, 948, 971, 1023, 1039, 1098, 1121, 1163, 1186, 1263, 1289, 1325, 1413, 1439, 1501, 1578, 1612, 2341, 2532, 2651, 2940, 3328 cm^{-1}. ^{1}H-NMR (400 MHz, CD_3OD) δ: 1.55 (m, 1 H, 11-H_{ax}), 1.78-2.06 [c. s., 5 H, 11-H_{eq} and 10(12)-H_2], 3.06 [m, 2 H, 9(13)-H_{ax}], 3.51 (t, *J* = 6.8 Hz, 2 H, 8-H_2), 3.63 (m, 2 H, 9(13)-H_{eq}), 3.87 (t, *J* = 6.8 Hz, 2 H, 7-H_2), 4.00 (s, 3 H, OCH_3), 7.10 (ddd, *J* = *J'* = 7.6 Hz, *J''* = 1.2 Hz, 1 H, 5-H), 7.24 (dd, *J* = 8.4, *J'* = 1.2, 1 H, 3-H), 7.43 (ddd, *J* = 8.4 Hz, *J'* = 7.6 Hz, *J''* = 1.6 Hz, 1 H, 4-H), 7.51 (dd, *J* = 7.6 Hz, *J'* = 1.6 Hz, 1 H, 6-H). ^{13}C-NMR (100.5 MHz, CD_3OD) δ: 22.5 (CH_2, C11), 24.2 [CH_2, C10(12)], 44.5 (CH_2, C7), 53.8 (CH_2, C8), 55.0 [CH_2, C9(13)], 56.9 (CH_3, OCH_3), 113.8 (CH, C6), 122.6 (CH, C3), 123.0 (CH, C4), 126.2 (C, C1), 130.9 (CH, C5), 153.1 (C, C2). HRMS-ESI+ m/z [*M*+H]$^+$ calcd for [$C_{14}H_{22}N_2O$+H]$^+$: 235.1805, found: 235.1814.

4-chloro-*N*-[2-(piperidin-1-yl)ethyl]aniline hydrochloride, 1g.[57] Following general procedure B, 4-chloroaniline (2.55 g, 20 mmol) and 1-(2-chloroethyl)piperidine

hydrochloride (1.83 g, 10 mmol) gave a pale yellow oil (1.74 g). After column chromatography (Hexane/Ethyl acetate mixture) the product was obtained as a yellow oil (1.16 g, 72.9% yield) that formed its hydrochloride salt as a white solid (310 mg). mp= 198-199 ºC. IR (ATR) ν: 651, 704, 809, 829, 861, 957, 971, 1004, 1070, 1091, 1134, 1183, 1200, 1253, 1292, 1310, 1460, 1478, 1488, 1520, 1599, 2542, 2639, 2947, 3261 cm^{-1}. ^{1}H-NMR (400 MHz, CD_3OD) δ: 1.50-1.80 (c. s., 2 H, 11-H_2), 1.81-1.98 [c. s., 4 H, 10(12)-H_2], 3.00-3.42 [c. s., 4 H, 9(13)-H_2], 3.29 (t, *J* = 6.4 Hz, 2 H, 8-H_2), 3.53 (t, *J* = 6.4 Hz, 2 H, 7-H_2), 6.68 [m, 2 H, 2(6)-H], 7.11 [m, 2 H, 3(5)-H]. ^{13}C-NMR (100.5 MHz, CD_3OD) δ: 22.7 (CH_2, C11), 24.1 [CH_2, C10(12)], 39.4 (CH_2, C7), 54.6 [CH_2, C9(13)], 56.8 (CH_2, C8), 115.3 [CH, C2(6)], 123.4 (CH, C4), 130.1 [CH, C3(5)], 147.9 (C, C1). Anal. Calcd for $C_{13}H_{19}ClN_2 \cdot HCl$: C 56.73, H 7.33, Cl 25.76, N 10.18. Found: C 56.58, H 7.52, Cl 25.71%, N 10.10.

2-bromo-*N*-[2-(piperidin-1-yl)ethyl]aniline hydrochloride 1h. Following the general procedure A, 2-bromoaniline (1.13 mL, 10 mmol), 1-(2-chloroethyl)piperidine hydrochloride (0.92 g, 5 mmol), K_2CO_3 (1.38 g, 10 mmol) and KI (83 mg, 0.5 mmol) in dry DMF (2.5 mL) were mixed to obtain a brown oil (1.78 g). After column chromatography, the product was obtained as a yellow oil (134 mg, 8.4% yield) that formed its hydrochloride salt as a dark yellow solid (139 mg). mp = 161-162 ºC. IR (ATR) ν: 654, 752, 948, 964, 1018, 1090, 1173, 1194, 1222, 1271, 1297, 1336, 1405, 1452, 1504, 1589, 2485, 2614, 2940, 3317 cm^{-1}. ^{1}H-NMR (400 MHz, CD_3OD) δ: 1.47-1.61 (c. s., 2 H, 11-H_2), 1.78-2.00 [c. s., 4 H, 10(12)-H_2], 3.03 [td, *J* = 12.0 Hz, *J'* = 3.2 Hz, 2 H, 9(13)-H_{ax}], 3.35 (t, *J* = 6.4 Hz, 2 H, 8-H_2), 3.61 (dm, *J* = 12.0 Hz, 2 H, 9(13)-H_{eq}), 3.69 (t, *J* = 6.4 Hz, 2 H, 7-H_2), 6.65 (ddd, *J* = *J'* = 8.0 Hz, *J''* = 1.6 Hz, 1 H, 5-H), 6.85 (dd, *J* = 8.0, *J'* = 1.2, 1 H, 6-H), 7.24 (ddd, *J* = *J'* = 8.0 Hz, *J''* = 1.2 Hz, 1 H, 4-H), 7.44 (dd, *J* = 8.0 Hz, *J'* = 1.6 Hz, 1 H, 3-H). ^{13}C-NMR (100.5 MHz, CD_3OD) δ: 21.3

(CH_2, C11), 22.9 [CH_2, C10(12)], 38.2 (CH_2, C7), 53.6 [CH_2, C9(13)], 55.3 (CH_2, C8), 109.8 (C, C2), 111.8 (CH, C6), 119.0 (CH, C4), 128.6 (CH, C5), 132.7 (CH, C3), 144.0 (C, C1). HRMS-ESI+ m/z $[M+H]^+$ calcd for $[C_{13}H_{19}BrN_2+H]^+$: 283.0804, found: 283.0815.

***N*-[2-(piperidin-1-yl)ethyl]-3-(trifluromethyl)aniline hydrochloride, 1i**.[47] Following the general procedure A, 3-trifluoromethylaniline (2.5 mL, 20 mmol), 1-(2-chloroethyl)piperidine hydrochloride (1.830 g, 10 mmol), K_2CO_3 (2.76 g, 20 mmol) and KI (166 mg, 1 mmol) in dry DMF (4 mL) were mixed to obtain a brown oil (3.73 g). After column chromatography the product was obtained as a yellow oil (1.04 g, 38.4% yield) that formed its hydrochloride salt as a white solid (824 mg). mp = 169-170 ºC. IR (ATR) ν: 636, 658, 696, 737, 786, 802, 815, 860, 869, 897, 915, 959, 974, 993, 1000, 1037, 1067, 1116, 1168, 1226, 1247, 1319, 1340, 1455, 1477, 1545, 1617, 2262, 2543, 2639, 2944, 3061, 3251 cm^{-1}. ^{1}H-NMR (400 MHz, CD_3OD) δ: 1.58-1.78 (c. s., 2 H, 11-H_2), 1.82-1.96 [c. s., 4 H, 10(12)-H_2], 3.00-3.45 [c. s., 4 H, 9(13)-H_2], 3.31 (t, *J* = 6.4 Hz, 2 H, 8-H_2), 3.59 (t, *J* = 6.4 Hz, 2 H, 7-H_2), 6.90-6.98 (c. s., 3 H, Ar), 7.32 (t, *J* = 8.6 Hz, 1 H, 5-Ar). ^{13}C-NMR (100.5 MHz, CD_3OD) δ: 22.7 (CH_2, C11), 24.2 [CH_2, C10(12)], 39.1 (CH_2, C7), 54.7 [CH_2, C9(13)], 56.8 (CH_2, C8), 110.1 (q, *J* = 4 Hz, CH, C2), 114.9 (q, *J* = 4 Hz, CH, C4), 117.0 (m, CH, C5), 125.9 (q, *J* = 270 Hz, C, CF_3), 131.0 (CH, C6), 132.6 (q, *J* = 32 Hz, C, C3), 149.6 (C, C1). Anal. Calcd. for $C_{14}H_{19}F_3N_2 \cdot HCl$: C 54.46, H 6.53, Cl 11.48, F 18.46, N 9.0%. Found: C 54.45, H 6.66, Cl 11.27, F 18.23 N 8.99.

***N*-[2-(piperidin-1-yl)ethyl]-4-(trifluromethyl)aniline hydrochloride, 1j**. Following the general procedure A, 4-trifluoromethylaniline (2.5 mL, 20 mmol), 1-(2-chloroethyl)piperidine hydrochloride (1.83 g, 10 mmol), K_2CO_3 (2.76 g, 20 mmol) and KI (166 mg, 1 mmol) in dry DMF (4 mL) were mixed to obtain a brown oil (3.69 g).

After column chromatography, the product was obtained as a yellow oil (437 mg, 16.1% yield) that formed its hydrochloride salt as a white solid (421 mg). mp= 206-207 ºC. IR (ATR) ν: 634, 808, 836, 953, 970, 1007, 1073, 1096, 1121, 1158, 1195, 1267, 1321, 1461, 1492, 1538, 1615, 2547, 2639, 2930, 3261 cm^{-1}. ^{1}H-NMR (400 MHz, CD_3OD) δ: 1.45-1.1.63 (c. s., 2 H, 11-H_2), 1.78-2.00 [c. s., 4 H, 10(12)-H_2], 3.02 [td, *J* = 12.4 Hz, *J'* = 3.2 Hz, 2 H, 9(13)-H_{ax}], 3.33 (t, *J* = 6.4 Hz, 2 H, 8-H_2), 3.59 [m, 2 H, 9(13)-H_{eq}], 3.62 (t, *J* = 6.4 Hz, 2 H, 7-H_2), 6.79 [d, *J* = 8.8 Hz, 2 H, 2(6)-H], 7.41 [d, *J* = 8.8 Hz, 2 H, 3(5)-H]. ^{13}C-NMR (100.5 MHz, CD_3OD) δ: 22.6 (CH_2, C11), 24.1 [CH_2, C10(12)], 38.8 (CH_2, C7), 54.6 [CH_2, C9(13)], 56.6 (CH_2, C8), 113.2 [CH, C2(6)], 120.0 (q, *J* = 32 Hz, C, C4), 126.5 (q, *J* = 269 Hz, C, CF_3), 127.6 [q, *J* = 4 Hz, CH, C3(5)], 150.5 (C, C1). Anal. Calcd for $C_{14}H_{19}F_3N_2 \cdot HCl$: C 54.46, H 6.53, Cl 11.48, F 18.46, N 9.07. Found: C 54.25, H 6.56, Cl 11.63, F 18.23, N 8.99.

***N*-[2-(piperidin-1-yl)ethyl]-2-(trifluromethyl)aniline hydrochloride, 1k**. Following the general procedure A, 2-trifluoromethylaniline (2.51 mL, 20 mmol), 1-(2-chloroethyl)piperidine hydrochloride (1.83 g, 10 mmol), K_2CO_3 (2.76 g, 20 mmol) and KI (166 mg, 1 mmol) in dry DMF (4 mL) were mixed to obtain a brown oil (3.65 g). After column chromatography, the product was obtained as a yellowish oil (972 mg, 35.9% yield) that formed its hydrochloride salt as a white solid (787 mg). mp = 165-166 ºC. IR (ATR) ν: 648, 753, 762 856, 899, 950, 964, 1007, 1030, 1053, 1090, 1107, 1127, 1158, 1224, 1258, 1281, 1304, 1335, 1404, 1452, 1478, 1520, 1583, 1609, 2405, 2496, 2519, 2610, 2947, 3341 cm^{-1}. ^{1}H-NMR (400 MHz, CD_3OD) δ: 1.46-1.60 (c. s., 1 H, 11-H_{ax}), 1.76-2.00 [c. s., 5 H, 10(12)-H_2 and 11-H_{eq}], 3.05 [td, *J* = 12.0 Hz, *J'* = 2.8 Hz, 2 H, 9(13)-H_{ax}], 3.34 (t, *J* = 6.6 Hz, 2 H, 8-H_2), 3.62 (dm, *J* = 11.6 Hz, 2 H, 9(13)-H_{eq}), 3.75 (t, *J* = 6.4 Hz, 2 H, 7-H_2), 6.81 (t, *J* = 7.6 Hz, 1 H, 4-H), 6.98 (d, *J* = 8.4 Hz, 1 H, 6-H), 7.42-7.50 (c. s., 2 H, 3-H and 5-H). ^{13}C-NMR (100.5 MHz, CD_3OD) δ: 22.6 (CH_2,

C11), 24.2 [CH_2, C10(12)], 39.1 (CH_2, C7), 54.9 [CH_2, C9(13)], 56.3 (CH_2, C8), 113.2 (CH, C6), 115.3 (q, *J* = 29.1 Hz, C, C2), 117.9 (CH, C4), 126.4 (q, *J* = 271 Hz, C, CF_3), 127.8 (m, CH, C3), 134.7 (CH, C5), 145.8 (C, C1). Anal. Calcd for $C_{14}H_{19}F_3N_2 \cdot HCl$: C 54.46, H 6.53, Cl 11.48, F 18.46, N 9.07. Found: C 54.15, H 6.84, Cl 11.47, F 18.47, N 8.86.

3,5-dichloro-*N*-[2-(piperidin-1-yl)ethyl]aniline hydrochloride, 1l. Following the general procedure A, 3,5-dichloroaniline (1.62 g, 10 mmol), 1-(2-chloroethyl)piperidine hydrochloride (0.92 g, 5 mmol), K_2CO_3 (1.38 g, 10 mmol) and KI (83 mg, 0.5 mmol) in dry DMF (2 mL) were mixed to obtain a dark oil (1.67 g). After column chromatography, the product was obtained as a brown oil (465 mg, 34.0 % yield) that formed its hydrochloride salt as a brown solid (527 mg). mp = 195-196 ºC. IR (ATR) ν: 677, 771, 799, 854, 895, 930, 953, 973, 1016, 1077, 1102, 1130, 1168, 1246, 1319, 1365, 1383, 1426, 1443, 1469, 1524, 1565, 1590, 2040, 2162, 2546, 2632, 2850, 2951, 3265 cm^{-1}. ^{1}H-NMR (400 MHz, CD_3OD) δ: 1.54 (m, 1 H, 11-H_{ax}), 1.78-1.99 [c. s., 5 H, 11-H_{eq} and 10(12)-H_2], 3.01 [td, *J* = 12.0 Hz, *J'* = 4.0 Hz, 2 H, 9(13)-H_{ax}], 3.32 (t, *J* = 6.4 Hz, 2 H, 8-H_2), 3.57 (t, *J* = 6.4 Hz, 2 H, 7-H_2), 3.60 [m, 2 H, 9(13)-H_{eq}], 6.68-6.71 (c. s., 3 H, Ar-H). ^{13}C-NMR (100.5 MHz, CD_3OD) δ: 22.6 (CH_2, C11), 24.1 [CH_2, C10(12)], 39.1 (CH_2, C7), 54.6 [CH_2, C9(13)], 56.4 (CH_2, C8), 112.4 [CH, C2(6)], 118.2 (CH, C4), 136.7 [C, C3(5)], 150.8 (C, C1). HRMS-ESI+ m/z [*M*+H]$^+$ calcd for [$C_{13}H_{18}Cl_2N_2$+H]$^+$: 273.0920, found: 273.0917.

3,5-difluoro-*N*-[2-(piperidin-1-yl)ethyl]aniline hydrochloride, 1m. A mixture of 3,5-difluroroaniline (2.58 g, 20 mmol), 1-(2-chloroethyl)piperidine hydrochloride (1.84 g, 10 mmol), NaH (0.72 g, 30 mmol) and KI (166 mg, 1 mmol) in dry DMF (4 mL) were stirred under N_2 atmosphere at 90 ºC for 24 hours. The mixture was allowed to reach room temperature, poured into ice and extracted with DCM (3 x 10 mL). The

combined organics were dried over anh. Na_2SO_4, filtered and concentrated *in vacuo* to obtain a dark oil (2.66 g). After column chromatography, the product was obtained as a yellowish oil (232 mg, 11.4% yield) that formed its hydrochloride salt as a yellowish solid (250 mg). mp = 173-174 ºC. IR (ATR) ν: 670, 776, 801, 842, 882, 945, 960, 978, 993, 1039, 1084, 1107, 1132, 1180, 1201, 1216, 1239, 1307, 1327, 1362, 1385, 1426, 1443, 1469, 1512, 1542, 1618, 2470, 2546, 2668, 2946, 3032, 3225 cm^{-1}. ^{1}H-NMR (400 MHz, CD_3OD) δ: 1.54 (m, 1 H, 11-H_{ax}), 1.78-1.99 [c. s., 5 H, 11-H_{eq} and 10(12)-H_2], 3.02 [td, *J* = 12.0 Hz, *J'* = 3.2 Hz, 2 H, 9(13)-H_{ax}], 3.32 (t, *J* = 6.4 Hz, 2 H, 8-H_2), 3.54-3.62 (c. s., 2 H, 9(13)-H_{eq}), 3.58 (t, *J* = 6.4 Hz, 2 H, 7-H_2), 6.20 (m, 1 H, 4-H), 6.33 [m, 2 H, 2(6)-H]. ^{13}C-NMR (100.5 MHz, CD_3OD) δ: 22.6 (CH_2, C11), 24.1 [CH_2, C10(12)], 39.3 (CH_2, C7), 54.7 [CH_2, C9(13)], 56.4 (CH_2, C8), 93.5 (t, *J* = 27 Hz, CH, C4), 97.0 [m, CH, C2(6)], 151.3 (m, C, C1), 165.7 [dd, *J* = 243 Hz, *J'* = 16 Hz, C, C3(5)]. HRMS-ESI+ m/z $[M+H]^+$ calcd for $[C_{13}H_{18}F_2N_2+H]^+$: 241.1511, found: 241.1514.

***N*-[2-(piperidin-1-yl)ethyl]-3,5-bis(trifluoromethyl)aniline hydrochloride, 1n**. Following the general procedure A, 3,5-bis(trifluoromethyl)aniline (1.55 mL, 10 mmol), 1-(2-chloroethyl)piperidine hydrochloride (0.92 g, 5 mmol), K_2CO_3 (1.38 g, 10 mmol) and KI (83 mg, 0.5 mmol) in dry DMF (2 mL) were mixed to obtain a dark oil (2.20 g). After column chromatography, the product was obtained as a brown oil (515 mg, 30.3% yield) that formed its hydrochloride salt as a brown solid (175 mg). mp = 162-163 ºC. IR (ATR) ν: 680, 700, 730, 854, 882, 968, 991, 1011, 1122, 1165, 1178, 1274, 1317, 1362, 1383, 1405, 1433, 1471, 1562, 1615, 2536, 2622, 2860, 2941, 3093, 3265 cm^{-1}. ^{1}H-NMR (400 MHz, CD_3OD) δ: 1.55 (m, 1 H, 11-H_{ax}), 1.76-2.00 [c. s., 5 H, 11-H_{eq} and 10(12)-H_2], 3.04 [td, *J* = 12.2 Hz, *J'* = 3.2 Hz, 2 H, 9(13)-H_{ax}], 3.36 (t, *J* = 6.4 Hz, 2 H, 8-H_2), 3.61 [dm, *J* = 12.2 Hz, 2 H, 9(13)-H_{eq}], 3.66 (t, *J* = 6.4 Hz, 2 H, 7-H_2), 7.15 (m, 1 H, 4-H), 7.18 [m, 2 H, 2(6)-H]. ^{13}C-NMR (100.5 MHz, CD_3OD) δ: 22.6 (CH_2, C11),

24.1 [CH_2, C10(12)], 38.8 (CH_2, C7), 54.7 [CH_2, C9(13)], 56.5 (CH_2, C8), 110.7 (sept, J = 4 Hz, CH, C4), 113.2 [m, CH, C2(6)], 125.1 (q, J = 271.5 Hz, C, CF_3), 133.6 [q, J = 32.5 Hz, C, C3(5)], 150.5 (C, C1). HRMS-ESI+ m/z $[M+H]^+$ calcd for $[C_{15}H_{18}F_6N_2+H]^+$: 341.1447, found: 341.1449.

3-chloro-*N*-[2-(piperidin-1-yl)ethyl]-5-(trifluoromethyl)aniline hydrochloride, 1o. Following the general procedure A, 3-chloro-5-trifluoromethylaniline (1.38 mL, 10 mmol), 1-(2-chloroethyl)piperidine hydrochloride (0.92 g, 5 mmol), K_2CO_3 (1.38 g, 10 mmol) and KI (83 mg, 0.5 mmol) in dry DMF (2 mL) were mixed to obtain a dark oil (2.02 g). After column chromatography, the product was obtained as a brown oil (320 mg, 20.9% yield) that formed its hydrochloride salt as a brown solid (327 mg). mp = 191-192 ºC. IR (ATR) ν: 690, 703, 824, 837, 900, 971, 988, 1014, 1097, 1120, 1165, 1236, 1259, 1279, 1302, 1347, 1428, 1464, 1595, 1605, 2541, 2632, 2946, 3088, 3270 cm^{-1}. ^{1}H-NMR (400 MHz, CD_3OD) δ: 1.56 (m, 1 H, 11-H_{ax}), 1.72-2.04 [c. s., 5 H, 11-H_{eq} and 10(12)-H_2], 3.02 [m, 2 H, 9(13)-H_{ax}], 3.33 (t, J = 6.4 Hz, 2 H, 8-H_2), 3.50-3.70 [very broad signal, 2 H, 9(13)-H_{eq}], 3.60 (t, J = 6.4 Hz, 2 H, 7-H_2), 6.88 (complex signal, 2 H, 4-H and 6-H), 6.94 (m, 1 H, 2-H). ^{13}C-NMR (100.5 MHz, CD_3OD) δ: 22.6 (CH_2, C11), 24.1 [CH_2, C10(12)], 38.9 (CH_2, C7), 54.7 [CH_2, C9(13)], 56.5 (CH_2, C8), 109.0 (q, J = 3.8 Hz, CH, C6), 114.4 (q, J = 4.0 Hz, CH, C4), 116.2 (CH, C2), 125.0 (q, J = 272.0 Hz, C, CF_3), 133.9 (q, J = 32.5 Hz, C, C5), 136.9 (C, C3), 150.9 (C, C1). HRMS-ESI+ m/z $[M+H]^+$ calcd for $[C_{14}H_{18}ClF_3N_2+H]^+$: 307.1183, found: 307.1176.

3-chloro-5-fluoro-*N*-[2-(piperidin-1-yl)ethyl]aniline hydrochloride, 1p. Following the general procedure A, 3-chloro-5-fluoroaniline (0.54 mL, 5 mmol), 1-(2-chloroethyl)piperidine hydrochloride (0.46 g, 2.5 mmol), K_2CO_3 (691 mg, 5 mmol) and KI (42 mg, 0.25 mmol) in dry DMF (2 mL) were mixed to obtain a dark oil (1.10 g). After column chromatography, the product was obtained as a yellow oil (210 mg,

32.7% yield) that formed its hydrochloride salt as a white solid (199 mg). mp = 194-195 ºC. IR (ATR) ν: 670, 776, 804, 849, 885, 938, 963, 981, 1001, 1036, 1079, 1110, 1135, 1170, 1198, 1218, 1246, 1269, 1319, 1360, 1385, 1426, 1451, 1476, 1509, 1534, 1603, 2359, 2546, 2587, 2632, 2951, 3012, 3048, 3255 cm^{-1}. ^{1}H-NMR (400 MHz, CD_3OD) δ: 1.54 (m, 1 H, 11-H_{ax}), 1.78-1.99 [c. s., 5 H, 11-H_{eq} and 10(12)-H_2], 3.02 [td, *J* = 12.0 Hz, *J'* = 3.6 Hz, 2 H, 9(13)-H_{ax}], 3.32 (t, *J* = 6.2 Hz, 2 H, 8-H_2), 3.52-3.62 [c. s., 2 H, 9(13)-H_{eq}], 3.58 (t, *J* = 6.2 Hz, 2 H, 7-H_2), 6.44 [c. s., 2 H, 2-H and 6-H], 6.58 (m, 1 H, 4-H). ^{13}C-NMR (100.5 MHz, CD_3OD) δ: 22.6 (CH_2, C11), 24.1 [CH_2, C10(12)], 39.2 (CH_2, C7), 54.6 [CH_2, C9(13)], 56.4 (CH_2, C8), 99.3 (d, *J* = 26 Hz, CH, C6), 105.8 (d, *J* = 26 Hz, CH, C4), 110.2 (d, *J* = 3 Hz, CH, C2), 136.7 (d, *J* = 14 Hz, C, C3), 151.2 (d, *J* = 12 Hz, C, C1), 165.3 (d, *J* = 244 Hz, C, C5). HRMS-ESI+ m/z $[M+H]^+$ calcd for $[C_{13}H_{18}ClFN_2+H]^+$: 257.1215, found: 257.1218.

3-fluoro-*N*-[2-(piperidin-1-yl)ethyl]-5-(trifluoromethyl)aniline hydrochloride, 1q. Following the general procedure A, 3-fluoro-5-trifluoromethylaniline (0.64 mL, 5 mmol), 1-(2-chloroethyl)piperidine hydrochloride (460 mg, 2.5 mmol), K_2CO_3 (691 mg, 5 mmol) and KI (42 mg, 0.25 mmol) in dry DMF (2 mL) were mixed to obtain a brown oil (1.10 g). After column chromatography, the product was obtained as a yellow oil (71 mg, 9.8% yield) that formed its hydrochloride salt as a white solid (38 mg). mp = 193-194 ºC. IR (ATR) ν: 698, 720, 806, 829, 857, 887, 917, 948, 963, 988, 1011, 1082, 1100, 1122, 1165, 1203, 1211, 1264, 1307, 1332, 1362, 1378, 1453, 1481, 1529, 1603, 1623, 1651, 2354, 2556, 2637, 2936, 3255 cm^{-1}. ^{1}H-NMR (400 MHz, CD_3OD) δ: 1.54 (m, 1 H, 11-H_{ax}), 1.78-2.00 [c. s., 5 H, 11-H_{eq} and 10(12)-H_2], 3.02 [td, *J* = 12.4 Hz, *J'* = 3.2 Hz, 2 H, 9(13)-H_{ax}], 3.33 (t, *J* = 6.4 Hz, 2 H, 8-H_2), 3.56-3.64 [c. s., 2 H, 9(13)-H_{eq}], 3.60 (t, *J* = 6.4 Hz, 2 H, 7-H_2), 6.64 (dm, *J* = 8.4 Hz, 1 H, 4-H), 6.68 (dt, *J* = 11.6, *J'* = 2.4 Hz, 1 H, 2-H), 6.78 (m, 1 H, 6-H). ^{13}C-NMR (125.7 MHz, CD_3OD) δ: 22.6

(CH_2, C11), 24.1 [CH_2, C10(12)], 38.9 (CH_2, C7), 54.7 [CH_2, C9(13)], 56.5 (CH_2, C8), 101.5 (dq, *J* = 25.6 Hz, J'=3.8 Hz, CH, C4), 103.0 (d, *J* = 25.7 Hz, CH, C2), 106.8 (m, CH, C6), 125.0 (dq, *J* = 2.4 Hz, *J'* = 271.3 Hz, C, $\underline{C}F_3$), 134.1 (dq, *J* = 10.6 Hz, *J'* = 32.6 Hz, C, C5), 151.7 (d, *J* = 11.2 Hz, C, C1), 165.4 (d, *J* = 243.5 Hz, C, C3). HRMS-ESI+ m/z $[M+H]^+$ calcd for $[C_{14}H_{18}ClF_4N_2+H]^+$: 291.1479, found: 291.1488.

***N*-[2-(azepan-1-yl)ethyl]-2-(trifluoromethyl)aniline hydrochloride, 2a**. Following the general procedure A, 2-(trifluoromethyl)aniline (1.26 mL, 10 mmol), 1-(2-chloroethyl)azepane hydrochloride (0.99 g, 5 mmol), K_2CO_3 (1.38 g, 10 mmol) and KI (83 mg, 0.5 mmol) in dry DMF (2.5 mL) were mixed to obtain a brown oil (1.86 g). After column chromatography, the product was obtained as an orange oil (351 mg, 21.7% yield) that formed its hydrochloride salt as a yellow solid (376 mg). mp = 138-139 ºC. IR (ATR) ν: 646, 742, 801, 855, 938, 1031, 1093, 1132, 1165, 1240, 1258, 1292, 1336, 1470, 1522, 1581, 1612, 2625, 2935, 3359 cm^{-1}. ^{1}H-NMR (400 MHz, CD_3OD) δ: 1.76-1.84 [c. s., 4 H, 11(12)-H_2], 1.86-2.04 [c. s., 4 H, 10(13)-H_2], 3.30 [m, 2 H, 9(14)-H_a], 3.39 (t, *J* = 6.8 Hz, 2 H, 8-H_2), 3.54 (m, 2 H, 9(13)-H_b), 3.73 (t, *J* = 6.8 Hz, 2 H, 7-H_2), 6.81 (tt, *J* = 7.2 Hz, *J'* = 0.8 Hz, 1 H, Ar), 6.96 (d, J = 8.8 Hz, 1 H, 6-H), 7.42-7.50 (c. s., 2 H, Ar). ^{13}C-NMR (100.5 MHz, CD_3OD) δ: 24.7 [CH_2, C11(12)], 27.3 [CH_2, C10(13)], 39.4 (CH_2, C7), 56.5 [CH_2, C9(14)], 56.7 (CH_2, C8), 113.3 (CH, C6), 115.7 (q, *J* = 29.5 Hz, C, C2), 118.1 (CH, C4), 126.4 (q, *J* = 260 Hz, C, CF_3), 127.8 (q, *J* = 5.5 Hz, CH, C3), 134.7 (CH, C5), 145.9 (C, C1). HRMS-ESI+ m/z $[M+H]^+$ calcd for $[C_{15}H_{21}F_3N_2+H]^+$: 287.1730, found: 287.1739.

***N*-[2-(azepan-1-yl)ethyl]-2-ethylaniline hydrochloride, 2b**. Following general procedure B, 2-ethylaniline (0.92 mL, 7.5 mmol) and 1-(2-chloroethyl)azepane hydrochloride (0.99 g, 5 mmol) were mixed to obtain a yellow oil (665 mg). After column chromatography (Hexane/Ethyl acetate mixture), the product was obtained as a

yellow oil (541 mg, 38.4% yield) that formed its hydrochloride salt as a white solid (615 mg). mp = 156-157 ºC. IR (ATR) ν: 654, 705, 718, 770, 793, 876, 915, 948, 990, 1015, 1101, 1271, 1315, 1449, 1485, 1594, 2423, 2459, 2583, 2620, 2857, 2930, 3167, 3240 cm^{-1}. ^{1}H-NMR (400 MHz, CD_3OD) δ: 1.33 (t, *J* = 7.6 Hz, 3 H, $CH_2C\underline{H}_3$), 1.66-1.86 [c. s., 4 H, 10(13)-H_2], 1.92-2.06 [c. s., 4 H, 11(12)-H_2], 2.83 (q, *J* = 7.6 Hz, 2 H, $C\underline{H}_2CH_3$), 3.30 [m, 2 H, 9(14)-H_a], 3.54-3.64 [c. s., 2 H, 9(14)-H_b], 3.69 (t, *J* = 6.8 Hz, 2 H, 8-H_2), 3.89 (t, *J* = 6.8 Hz, 2 H, 7-H_2), 7.33-7.40 (complex signal, 2 H, Ar), 7.44 (m, 1 H, Ar), 7.49 (m, 1 H, Ar). ^{13}C-NMR (100.5 MHz, CD_3OD) δ: 14.9 (CH_3, $CH_2\underline{C}H_3$), 24.2 (CH_2, $\underline{C}H_2CH_3$), 24.9 [CH_2, C11(12)], 27.2 [CH_2, C10(13)], 45.8 (CH_2, C7), 54.5 (CH_2, C8), 56.7 [CH_2, C9(14)], 121.9 (CH, Ar), 128.8 (CH, Ar), 129.3 (CH, Ar), 131.4 (C, Ar), 136.1 (C, C2), 137.3 (C, C1). HRMS-ESI+ m/z $[M+H]^+$ calcd for $[C_{16}H_{26}N_2+H]^+$: 247.2169, found: 247.2176.

***N*-[2-(azepan-1-yl)ethyl]-2-isopropylaniline hydrochloride, 2c**. Following general procedure B, 2-isopropylaniline (1.42 mL, 10 mmol) and 1-(2-chloroethyl)azepane hydrochloride (0.99 g, 5 mmol) were mixed to obtain a brown oil (1.52 g). After column chromatography (Hexane/Ethyl acetate mixture), the product was obtained as a brown oil (680 mg, 46.0% yield) that formed its hydrochloride salt as a dark green solid (742 mg). mp = 155-156 ºC. IR (ATR) ν: 618, 757, 873, 917, 951, 1044, 1181, 1312, 1364, 1442, 1452, 1573, 1635, 1997, 2149, 2196, 2361, 2496, 2594, 2863, 2925, 3193, 3312, 3374, 3447, 3509 cm^{-1}. ^{1}H-NMR (400 MHz, CD_3OD) δ: 1.33 [d, *J* = 6.8 Hz, 6 H, -$CH(C\underline{H}_3)_2$], 1.64-1.90 [c. s., 4 H, 11(12)-H_2], 1.94-2.06 [c. s., 4 H, 10(13)-H_2], 3.23 [sept, *J* = 6.8 Hz, 1 H, -$C\underline{H}(CH_3)_2$], 3.33 [m, 2 H, 9(14)-H_a], 3.60 [m, 2 H, 9(14)-H_b], 3.70 (t, *J* = 6.8 Hz, 2 H, 8-H_2), 3.86 (t, *J* = 6.8 Hz, 2 H, 7-H_2), 7.35 (dt, *J* = 7.8 Hz, *J'* = 1.6 Hz, 1 H), 7.40 (dt, J = 7.8 Hz, J' = 1.2 Hz, 1 H), 7.48 (dd, *J* = 7.8 Hz, *J'* = 1.2 Hz, 1 H), 7.53 (dd, *J* = 7.8 Hz, *J'* = 1.6 Hz, 1 H) (Ar-H). ^{13}C-NMR (100.5 MHz, CD_3OD) δ:

24.4 [CH_3, -CH($\underline{C}H_3)_2$], 24.9 [CH_2, C11(12)], 27.2 [CH_2, C10(12)], 28.7 [CH, -$\underline{C}H(CH_3)_2$], 46.4 (CH_2, C7), 54.5 (CH_2, C8), 56.7 [CH_2, C9(14)], 122.1 (CH), 128.8 (CH), 129.1 (CH) and 129.7 (CH) (4 CH-Ar), 135.1 (C, C2), 142.3 (C, C1). HRMS-ESI+ m/z [*M*+H]$^+$ calcd for [$C_{17}H_{28}N_2$+H]$^+$: 261.2325, found: 261.2334.

2-isopropyl-*N*-[3-(piperidin-1-yl)propyl]aniline hydrochloride, 3. Following the general procedure A, 2-isopropylaniline (0.70 mL, 5 mmol), 1-(3-chloropropyl)piperidine hydrochloride (0.49 g, 2.5 mmol), K_2CO_3 (0.69 g, 5 mmol) and KI (42 mg, 0.25 mmol) in dry DMF (2 mL) were mixed to obtain a dark oil (1.65 g). After column chromatography, **3** was obtained as a grey oil (106 mg, 16.3% yield) that formed its hydrochloride salt as a grey solid (95 mg). mp = 220-221 ºC. IR (ATR) ν: 720, 773, 801, 854, 877, 945, 855, 963, 1014, 1029, 1077, 1092, 1168, 1213, 1228, 1259, 1282, 1302, 1322, 1360, 1383, 1410, 1443, 1466, 1499, 1582, 1595, 2354, 2405, 2501, 2612, 2643, 2668, 2881, 2946 cm^{-1}. ^{1}H-NMR (400 MHz, CD_3OD) δ: 1.35 [d, *J* = 6.8 Hz, 6 H, -CH($C\underline{H}_3)_2$], 1.53 (m, 1 H, 12-H_{ax}), 1.78-2.02 [c. s., 5 H, 12-H_{eq} and 11(13)-H_2], 2.35 (m, 2 H, 8-H_2), 2.99 [td, *J* = 12.4 Hz, *J'* = 3.2 Hz, 2 H, 10(14)-H_{ax}], 3.18 [sept, *J* = 6.8 Hz, 1 H, -C$\underline{H}(CH_3)_2$], 3.26 (t, *J* = 8.0 Hz, 2 H, 9-H_2), 3.47 (t, *J* = 8.0 Hz, 2 H, 7-H_2), 3.57 [m, 2 H, 10(14)-H_{eq}], 7.39 (m, 1 H, Ar), 7.49-7.56 (c. s., 2 H, Ar), 7.60 (dd, *J* = 8.0 Hz, *J'* = 1.6 Hz, 1 H, Ar). ^{13}C-NMR (100.5 MHz, CD_3OD) δ: 22.2 (CH_2, C12), 22.6 (CH_2, C8), 24.2 (CH_3, -CH($\underline{C}H_3)_2$], 24.6 [CH_2, C11(13)], 28.8 [CH, -$\underline{C}H(CH_3)_2$], 50.6 (CH_2, C7), 54.6 [CH_2, C10(14)], 54.8 (CH_2, C9), 124.4 (CH, C6), 128.9 (CH, C4), 129.6 (CH, C5), 131.6 (CH, C3), 133.3 (C, C2), 143.7 (C, C1). HRMS-ESI+ m/z [*M*+H]$^+$ calcd for [$C_{17}H_{28}N_2$+H]$^+$: 261.2325, found: 261.2330.

2-isopropyl-*N*-[2-(pyrrolidin-1-yl)ethyl]aniline hydrochloride, 4. Following the general procedure A, 2-isopropylaniline (1.41 mL, 10 mmol), 1-(2-chloroethyl)pyrrolidine hydrochloride (0.85 g, 5 mmol), K_2CO_3 (1.38 g, 10 mmol) and

KI (83 mg, 0.5 mmol) in dry DMF (2 mL) were mixed to obtain a dark oil (1.88 g). After column chromatography, the product was obtained as a brown oil (307 mg, 26.4% yield) that formed its hydrochloride salt as a brown solid (380 mg). mp = 160-161 ºC. IR (ATR) ν: 758, 806, 864, 910, 928, 960, 1008, 1034, 1067, 1082, 1115, 1183, 1218, 1287, 1314, 1362, 1385, 1423, 1451, 1494, 1537, 1585, 1598, 2389, 2475, 2592, 2683, 2860, 2967, 3291 cm^{-1}. ^{1}H-NMR (400 MHz, CD_3OD) δ: 1.33 [d, *J* = 6.8 Hz, 6 H, -CH($C\underline{H}_3$)$_2$], 2.00-2.28 [c. s., 4 H, 10(11)-H_2], 3.12-3.28 [c. s., 2 H, 9(13)-H_a], 3.22 [sept, *J* = 6.8 Hz, 1 H, -$C\underline{H}$(CH_3)$_2$], 3.70-3.86 (c. s., 6 H, 9(13)-H_b, 8-H_2 and 7-H_2), 7.31-7.42 (c. s., 2 H, 4-H and 5-H), 7.44 (dd, *J* = 8 Hz, *J'* = 1.6 Hz, 1 H, 6-H), 7.53 (m, 1 H, 3-H). ^{13}C-NMR (100.5 MHz, CD_3OD) δ: 24.0 [CH_3, -CH($\underline{C}H_3$)$_2$], 24.3 [CH_2, C10(11)], 28.7 [CH, -$\underline{C}$H(CH_3)$_2$], 47.0 (CH_2, C7), 51.8 (CH_2, C8), 55.6 [CH_2, C9(12)], 121.8 (CH, C6), 128.7 (CH, C4), 129.0 (CH, C5), 129.4 (CH, C3), 135.3 (C, C2), 142.1 (C, C1). HRMS-ESI+ m/z [*M*+H]$^+$ calcd for [$C_{15}H_{24}N_2$+H]$^+$: 233.2012, found: 233.2008.

1-(2-phenoxyethyl)piperidine hydrochloride, 5a. Following general procedure C, from phenol (0.94 g, 10 mmol) and 1-(2-chloroethyl)piperidine hydrochloride (1.83 g, 10 mmol), an orange oil (1.85 g) was obtained. Column chromatography (Hexane/Ethyl acetate mixture) gave the product as a yellow oil (1.43 g, 69.6% yield) that formed its hydrochloride salt as a yellowish solid (915 mg). The analytical sample was obtained by crystallization with EtOAc/Pentane. mp = 170-171 ºC. IR (ATR) ν: 691, 765, 791, 816, 845, 890, 913, 939, 953, 1002, 1016, 1027, 1087, 1153, 1175, 1227, 1290, 1386, 1412, 1432, 1452, 1472, 1489, 1586, 1595, 2490, 2610, 2856, 2941 cm^{-1}. ^{1}H-NMR (400 MHz, CD_3OD) δ: 1.60-1.80 (c. s., 2 H, 11-H_2), 1.82-1.98 [c. s., 4 H, 10(12)-H_2], 3.15-3.50 [c. s., 4 H, 9(13)-H_2], 3.55 (t, *J* = 4.8 Hz, 2 H, 8-H_2), 4.38 (t, *J* = 4.8 Hz, 2 H, 7-H_2), 6.97-7.06 (c. s., 3 H, 2(6)-H and 4-H), 7.32 [m, 2 H, 3(5)-H]. ^{13}C-NMR (100.5 MHz, CD_3OD) δ: 22.6 (CH_2, C11), 24.1 [CH_2, C10(12)], 54.9 [CH_2, C9(13)], 57.2 (CH_2, C8),

63.1 (CH_2, C7), 115.7 [CH, C2(6)], 122.9 (CH, C4), 130.7 [CH, C3(5)], 159.2 (C, C1). Anal. Calcd for $C_{13}H_{19}ClNO \cdot HCl$: C 64.59, H 8.34, Cl 14.66, N 5.79. Found: C 64.27, H 8.42, Cl 14.49, N 5.59.

1-[2-(4-chlorophenoxy)ethyl]piperidine hydrochloride, 5b. Following general procedure C, from 4-chlorophenol (1.29 g, 10 mmol) and 1-(2-chloroethyl)piperidine hydrochloride (1.83 g, 10 mmol), an orange oil (2.13 g) was obtained. Column chromatography (Hexane/Ethyl acetate mixture) gave the product as a yellow oil (1.40 g, 58.5% yield) that formed its hydrochloride salt as a white solid (1.40 g). mp = 199-200 ºC. IR (ATR) ν: 668, 802, 816, 828, 953, 967, 1007, 1039, 1070, 1093, 1175, 1244, 1284, 1386, 1429, 1458, 1472, 1489, 1578, 1597, 2513, 2622, 2941 cm^{-1}. ^{1}H-NMR (400 MHz, CD_3OD) δ: 1.50-1.60 (c. s., 2 H, 11-H_2), 1.81-2.05 [c. s., 4 H, 10(12)-H_2], 2.85-3.80 [c. s., 4 H, 9(13)-H_2], 3.56 (t, *J* = 4.8 Hz, 2 H, 8-H_2), 4.37 (t, *J* = 4.8 Hz, 2 H, 7-H_2), 7.01 [m, 2 H, 3(5)-H], 7.31 [m, 2 H, 2(6)-H]. ^{13}C-NMR (100.5 MHz, CD_3OD) δ: 22.6 (CH_2, C11), 24.1 [CH_2, C10(12)], 54.9 [CH_2, C9(13)], 57.1 (CH_2, C8), 63.5 (CH_2, C7), 117.3 [CH, C2(6)], 127.8 (C, C4), 130.6 [CH, C3(5)], 157.9 (C, C1). Anal. Calcd for $C_{13}H_{18}ClNO \cdot HCl$: C 56.53, H 6.93, Cl 25.67, N 5.07. Found: C 56.72, H 7.17, Cl 25.73, N 4.96.

1-[2-(2-ethylphenoxy)ethyl]piperidine hydrochloride, 5c. Following general procedure C, from 2-ethylphenol (1.18 mL, 10 mmol) and 1-(2-chloroethyl)piperidine hydrochloride (1.83 g, 10 mmol), an orange oil (2.20 g) was obtained. Column chromatography (Hexane/Ethyl acetate mixture) gave the product as a yellow oil (1.42 g, 60.9% yield) that formed its hydrochloride salt as a white solid (1.18 g). mp = 136-137 ºC. IR (ATR) ν: 614, 734, 751, 810, 868, 905, 927, 947, 967, 996, 1013, 1053, 1061, 1096, 1127, 1190, 1235, 1295, 1332, 1398, 1426, 1452, 1478, 1495, 1600, 2473, 2507, 2861, 2941 cm^{-1}. ^{1}H-NMR (400 MHz, CD_3OD) δ: 1.20 (t, *J* = 7.6 Hz, 3 H,

$CH_2C\underline{H}_3$), 1.56-1.82 (c. s., 2 H, 11-H_2), 1.84-2.02 [c. s., 4 H, 10(12)-H_2], 2.68 (q, *J* = 7.6 Hz, 2 H, $C\underline{H}_2CH_3$), 3.00-3.85 [c. s., 4 H, 9(13)-H_2], 3.60 (t, *J* = 4.8 Hz, 2 H, 8-H_2), 4.40 (t, *J* = 4.8 Hz, 2 H, 7-H_2), 6.92-7.00 (c. s., 2 H, Ar-H), 7.15-7.22 (c. s., 2 H, Ar-H). ^{13}C-NMR (100.5 MHz, CD_3OD) δ: 15.0 (CH_3, $CH_2\underline{C}H_3$), 22.5 (CH_2, C11), 24.1 (CH_2, $\underline{C}H_2CH_3$), 24.2 [CH_2, C10(12)], 55.3 [CH_2, C9(13)], 57.5 (CH_2, C8), 64.0 (CH_2, C7), 112.7 (CH, C6), 122.9 (CH, C4), 128.2 (CH, C5), 130.3 (CH, C3), 133.7 (C, C2), 156.8 (C, C1). Anal. Calcd for $C_{15}H_{23}NO\cdot HCl$: C 66.77, H 8.97, Cl 13.14, N 5.19. Found: C 66.74, H 8.94, Cl 13.22, N 5.16.

1-[2-(2-isopropylphenoxy)ethyl]piperidine hydrochloride, 5d. Following general procedure C, from 2-isopropylphenol (0.67 mL, 5 mmol) and 1-(2-chloroethyl)piperidine hydrochloride (0.91 g, 5 mmol), a yellow oil (1.41 g) was obtained. Column chromatography (Hexane/Ethyl acetate mixture) gave the product as a yellow oil (0.70 g, 56.9% yield) that formed its hydrochloride salt as a white solid (793 mg). mp = 176-177 ºC. IR (ATR) ν: 744, 822, 855, 930, 969, 1010, 1044, 1080, 1111, 1155, 1196, 1240, 1292, 1343, 1356, 1444, 1493, 1597, 2475, 2604, 2956 cm^{-1}. ^{1}H-NMR (400 MHz, CD_3OD) δ: 1.22 [d, *J* = 6.8 Hz, 6 H, $CH(C\underline{H}_3)_2$], 1.45-2.10 [c. s., 6 H, 11-H_2 and 10(12)-H_2], 3.16 [m, 2 H, 9(13)-H_{ax}], 3.38 [sept, *J* = 6.8, 1 H, $C\underline{H}(CH_3)_2$], 3.56-3.80 [c. s., 2H, 9(13)-H_{eq}], 3.61 (t, J = 4.8 Hz, 2 H, 8-H_2), 4.40 (t, *J* = 4.8 Hz, 2 H, 7-H_2), 6.95-7.02 (c. s., 2 H, 5-H and 6-H), 7.17 (ddd, *J* = 8.8 Hz, *J'* = 7.2 Hz, *J''* = 1.6 Hz, 1 H, 4-H), 7.25 (dd, *J* = 8.0 Hz, *J'* = 1.6 Hz, 1 H, 3-H). ^{13}C-NMR (100.5 MHz, CD_3OD) δ: 22.5 (CH_2, C11), 23.4 [CH_3, $CH(\underline{C}H_3)_2$], 24.2 [CH_2, C10(12)], 27.4 [CH, $\underline{C}H(CH_3)_2$], 55.2 [CH_2, C9(13)], 57.5 (CH_2, C8), 64.1 (CH_2, C7), 112.9 (CH, C6), 123.0 (CH, C4), 127.2 (CH, C5), 127.9 (CH, C3), 138.1 (C, C2), 156.1 (C, C1). Anal. Calcd for $C_{16}H_{25}NO\cdot HCl$: C 67.71, H 9.23, N 4.93. Found: C 67.87, H 9.47, N 4.81.

1-[2-(2-ethylphenoxy)ethyl]azepane hydrochloride, 6a. Following general procedure C, from 2-ethylphenol (0.59 mL, 5 mmol) and 1-(2-chloroethyl)azepane hydrochloride (0.99 g, 5 mmol), a yellow oil (1.05 g) was obtained. Column chromatography (Hexane/Ethyl acetate mixture) gave the product as a yellow oil (0.44 g, 35.3% yield) that form its hydrochloride salt as a white solid (483 mg). mp = 101-102 ºC. IR (ATR) ν: 734, 749, 804, 881, 915, 951, 1023, 1054, 1067, 1126, 1160, 1186, 1232, 1289, 1395, 1449, 1475, 1491, 1594, 2527, 2594, 2863, 2930, 3410 cm^{-1}. ^{1}H-NMR (400 MHz, CD_3OD) δ: 1.20 (t, *J* = 7.6 Hz, 3 H, -$CH_2C\underline{H}_3$), 1.70-1.86 [c. s., 4 H, 11(12)-H_2], 1.90-2.05 [c. s., 4 H, 10(13)-H_2], 2.68 (q, *J* = 7.6 Hz, 2 H, -$C\underline{H}_2CH_3$), 3.40-3.60 [c. s., 4 H, 9(14)-H_2], 3.67 (t, *J* = 5.2 Hz, 2H, 8-H_2), 4.40 (t, *J* = 5.2 Hz, 2 H, 7-H_2), 6.92-7.02 (c. s., 2 H, H-Ar), 7.15-7.22 (c. s., 2 H, H-Ar). ^{13}C-NMR (100.5 MHz, CD_3OD) δ: 14.9 (CH_3, -$CH_2\underline{C}H_3$), 24.1 (CH_2, -$\underline{C}H_2CH_3$), 24.6 [CH_2, C11(12)], 27.5 [CH_2, C10(13)], 56.9 [CH_2, C9(14)], 57.7 (CH_2, C8), 64.3 (CH_2, C7), 112.7 (CH, C6), 122.9 (CH, C4), 128.2 (CH, C5), 130.3 (CH, C3), 133.7 (C, C2), 156.8 (C, C1). Anal. Calcd for $C_{16}H_{25}NO\cdot HCl$: C 67.71, H 9.23, N 4.93. Found: C 67.50, H 9.43, N 4.76.

1-[2-(2-isopropylphenoxy)ethyl]azepane hydrochloride, 6b. Following general procedure C, from 2-isopropylphenol (0.67 mL, 5 mmol) and 1-(2-chloroethyl)azepane hydrochloride (0.99 g, 5 mmol), a yellow oil (1.34 g) was obtained. Column chromatography (Hexane/Ethyl acetate mixture) gave the product as a yellow oil (0.34 g, 25.9% yield) that formed its hydrochloride salt as a white solid (316 mg). mp = 168-169 ºC. IR (ATR) ν: 742, 819, 922, 953, 1028, 1080, 1114, 1129, 1152, 1194, 1240, 1287, 1341, 1444, 1478, 1493, 1581, 1597, 2506, 2589, 2863, 2935 cm^{-1}. ^{1}H-NMR (400 MHz, CD_3OD) δ: 1.22 [d, *J* = 7.2 Hz, 6 H, -$CH(C\underline{H}_3)_2$], 1.68-1.86 [c. s., 4 H, 11(12)-H_2], 1.88-2.04 [c. s., 4 H, 10(13)-H_2], 3.37 [sept, *J* = 7.2 Hz, 1 H, -$C\underline{H}(CH_3)_2$], 3.43 [m, 2 H, 9(14)-H_a], 3.63 [m, 2 H, 9(14)-H_b], 3.68 (t, J = 5.2 Hz, 2 H, 8-H_2), 4.42 (t, *J* = 5.2

Hz, 2 H, 7-H_2), 6.95-7.04 (c. s., 2 H, 5-H and 6-H), 7.17 (ddd, *J* = 8.8 Hz, *J'* = 7.6 Hz, *J''* = 1.6 Hz, 1 H, 4-H), 7.25 (dd, *J* = 8.0 Hz, *J'* = 1.6 Hz, 1 H, 3-H). ^{13}C-NMR (100.5 MHz, CD_3OD) δ: 23.4 [CH_3, -CH($\underline{C}H_3$)$_2$], 24.6 [CH_2, C10(12)], 27.4 [CH, -$\underline{C}$H(CH_3)$_2$, and CH_2, C10(13)], 56.9 [CH_2, C9(14)], 57.7 (CH_2, C8), 64.5 (CH_2, C7), 113.0 (CH, C6), 123.1 (CH, C4), 127.2 (CH, C5), 127.9 (CH, C3), 138.2 (C, C2), 156.1 (C, C1). Anal. Calcd for $C_{17}H_{27}NO$·HCl: C 68.55, H 9.48, N 4.70. Found: C 68.52, H 9.72, N 4.54.

1-[2-(phenylthio)ethyl]piperidine hydrochloride, 7a. Following general procedure C, from thiophenol (1.0 mL, 10 mmol) and 1-(2-chloroethyl)piperidine hydrochloride (1.83 g, 10 mmol), the product was obtained as a pale yellow oil (1.94 g, 87.3% yield) that formed its hydrochloride salt as a white solid (821 mg). The analytical sample was obtained by crystallization from MeOH/diethyl ether. mp = 191-192 ºC. IR (ATR) ν: 690, 742, 835, 853, 897, 946, 961, 1021, 1059, 1095, 1147, 1188, 1209, 1325, 1439, 1452, 1480, 1578, 2516, 2620, 2940 cm^{-1}. ^{1}H-NMR (400 MHz, CD_3OD) δ: 1.50-1.78 (c. s., 2 H, 11-H_2), 1.79-1.98 [c. s., 4 H, 10(12)-H_2], 2.60-3.80 [c. s., 8 H, 9(13)-H_2, 7-H_2 and 8-H_2], 7.27 [tt, *J* = 7.4 Hz, *J'* = 1.6 Hz, 1 H, 4-H), 7.36 [tm, *J* = 7.4 Hz, 2 H, 3(5)-H], 7.46 (m, 2 H, 2(6)-H]. ^{13}C-NMR (100.5 MHz, CD_3OD) δ: 22.6 (CH_2, C11), 24.2 [CH_2, C10(12)], 28.5 (CH_2, C7), 54.4 [CH_2, C9(13)], 57.3 (CH_2, C8), 128.4 (CH, C4), 130.5 [CH, C2(6)], 131.4 [CH, C3(5)], 135.1 (C, C1). Anal. Calcd for $C_{13}H_{19}NS$·HCl: C 60.56, H 7.82, Cl 13.75, N 5.43, S 12.44. Found: C 60.80, H 7.75, Cl 13.97, N 5.28, S 12.17.

1-[2-((4-chlorophenyl)thio)ethyl]piperidine hydrochloride 7b. Following general procedure C, from 4-chlorothiophenol (1.45 g, 10 mmol) and 1-(2-chloroethyl)piperidine hydrochloride (1.83 g, 10 mmol), the product was obtained as a palid yellow oil (2.31 g, 90.6% yield) that formed its hydrochloride salt as a white solid

(1.003 g). mp = 206-207 ºC. IR (ATR) ν: 748, 813, 833, 853, 947, 962, 1007, 1047, 1067, 1093, 1113, 1153, 1270, 1292, 1327, 1349, 1386, 1429, 1458, 1472, 2525, 2542, 2599, 2633, 2941 cm^{-1}. ^{1}H-NMR (400 MHz, CD_3OD) δ: 1.55-1.75 (c. s., 2 H, 11-H_2), 1.80-1.94 [c. s., 4 H, 10(12)-H_2], 3.05-3.40 [c. s., 8 H, 9(13)-H_2, 7-H_2 and 8-H_2], 7.37 [dd, *J* = 9.2 Hz, *J'* = 2.0 Hz, 2 H, Ar-H], 7.45 [dd, *J* = 9.2 Hz, *J'* = 2.0 Hz, 2 H, Ar-H]. ^{13}C-NMR (100.5 MHz, CD_3OD) δ: 22.8 (CH_2, C11), 24.4 [CH_2, C10(12)], 28.7 (CH_2, C7), 54.5 [CH_2, C9(13)], 57.2 (CH_2, C8), 130.5 [CH, C3(5)], 132.8 [CH, C2(6)], 134.1 (C) and 134.3 (C) (C1 and C4). Anal. Calcd for $C_{13}H_{18}ClNS{\cdot}HCl$: C 53.43, H 6.55, N 4.79, S 10.97. Found: C 53.81, H 6.53, N 4.65, S 10.71.

1-[2-((2-ethylphenyl)thio)ethyl]piperidine hydrochloride 7c. Following general procedure C, from 2-ethylthiophenol (1.35 mL, 10 mmol) and 1-(2-chloroethyl)piperidine hydrochloride (1.83 g, 10 mmol), the product was obtained as a palid yellow oil (2.40 g, 96.4% yield) that formed its hydrochloride salt as a white solid (915 mg). mp = 164-165 ºC. IR (ATR) ν: 679, 742, 768, 793, 853, 902, 947, 964, 987, 1021, 1036, 1056, 1133, 1156, 1184, 1218, 1278, 1398, 1426, 1441, 1458, 1586, 2525, 2565, 2633, 2930, 2976, 3055 cm^{-1}. ^{1}H-NMR (400 MHz, CD_3OD) δ: 1.21 (t, *J* = 7.6 Hz, 3 H, $CH_2C\underline{H}_3$), 1.50-1.75 (c. s., 2 H, 11-H_2), 1.76-1.94 [c. s., 4 H, 10(12)-H_2], 2.81 (q, *J* = 7.6 Hz, 2 H, $C\underline{H}_2CH_3$), 3.00-3.40 [c. s., 8 H, 9(13)-H_2, 7-H_2 and 8-H_2], 7.18-7.30 (c. s., 3 H, Ar), 7.46 (m, 1 H, Ar). ^{13}C-NMR (100.5 MHz, CD_3OD) δ: 15.5 (CH_3, $CH_2\underline{C}H_3$), 22.6 (CH_2, C11), 24.3 [CH_2, C10(12)], 28.0 (CH_2, $\underline{C}H_2CH_3$), 28.3 (CH_2, C7), 54.4 [CH_2, C9(13)], 57.2 (CH_2, C8), 128.1 (CH, C4), 128.6 (CH, C5), 130.3 (CH, C6), 131.1 (CH, C3), 133.5 (C, C2), 146.1 (C, C1). Anal. Calcd for $C_{15}H_{23}NS{\cdot}HCl$: C 63.02, H 8.46, Cl 12.40, N 4.90, S 11.21. Found: C 63.11, H 8.45, Cl 12.42, N 4.78, S 11.09.

Preparation of 1-adamantanecarbonyl chloride, 9a. A mixture of thionyl chloride (6 eq) and 1-adamantanecarboxylic acid (1 eq) was stirred at 80°C for 2 h in a round

bottom flask provided with a tube of anhydrous $CaCl_2$. Then, the excess of thionyl chloride was removed in vacuo. Dry toluene (40 mL) was added to the residue, and the remaining thionyl chloride was azeotropically removed to give a white solid of 1-adamantanecarbonylchloride (quantitative yield). The spectroscopic data matched with the reported in the bibliography.[58]

Preparation of 3,5-dimethyl-1-adamantanecarbonyl chloride, 9b. A mixture of thionyl chloride (2.5 mL, 1.64 g/mL, 34.6 mmol) and 3,5-dimethyladamantane-1-carboxylic acid (1,2 g, 5.8 mmol) was stirred at 80°C for 2 h in a round bottom flask provided with a tube of anhydrous $CaCl_2$. Then, the excess of thionyl chloride was removed in vacuo. Dry toluene (40 mL) was added to the residue, and the remaining thionyl chloride was azeotropically removed to give a white solid of 3,5-dimethyladamantane-1-carbonyl chloride (0.9 g, quantitative yield). The compound was analyzed by IR and used for the next step without any further purification.

General Procedure D

A solution of 1-adamantanecarbonyl chloride (1.11 mmol, 1.2 eq) in anhydrous acetone (1.35 mL) was added dropwise into a solution of the corresponding aniline (0.92 mmol, 1 eq) and triethylamine (1.11 mmol, 1.2 eq), under a nitrogen atmosphere. The mixture was heated at 90°C for 3 h and allowed to cool to room temperature. Water (1 mL) was added to the suspension and the resulting solid was filtered and washed with a further amount of water (1 mL). The solid was dried *in vacuo* to give the desired product as a white pure solid.

***N*-phenyladamantane-1-carboxamide, 10a**. Following the general procedure E, aniline (0.75 mL, 1.02 g/mL, 8.3 mmol) and adamantane-1-carboxylic acid (1.50 g, 8.3 mmol) in CH_2Cl_2 (18.8 mL), with EDC·HCl (1.92 g, 10 mmol) and DMAP (1.22 g, 10 mmol), gave amide **10a** (1.01 g, 48%) as a white solid. mp = 196-197 °C (dec). IR

(ATR) ν: 3276, 2897, 2849, 1643, 1596, 1537, 1490, 1437, 1328, 1308, 1253, 1177, 925, 754, 695 cm^{-1}. ^{1}H-NMR, δ_H (400 MHz, $CDCl_3$): 1.72-1.80 [complex signal, 6H, 4'(6',10')-H_2], 1.97 [broad s, 6H, 2'(8',9')-H_2], 2.10 [broad s, 3H, 3'(5',7')-H], 7.09 (tt, *J* = 7.2 Hz, *J'* = 1.0 Hz, 1H, 4-H), 7.28-7.33 [complex signal, 3H, 3(5)-H and NH], 7.53 [dd, *J* = 8.4 Hz, *J'* = 1.2 Hz, 2H, 2(6)-H]. ^{13}C-NMR, δ_C (100.6 MHz, $CDCl_3$): 28.1 [CH, C3'(5',7')], 36.4 [CH_2, C4'(6',10')], 39.2 [CH_2, C2'(8',9')], 41.5 (C, C1'), 119.9 [CH, C2(6)], 124.0 (CH, C4), 128.9 [CH, C3(5)], 138.0 (C, C1), 176.0 (C, CO). HRMS-ESI$^+$ m/z [*M*+H]$^+$: calcd for [$C_{17}H_{21}NO$+H^+]: 256.1696, found: 256.1695.

***N*-(2-ethylphenyl)adamantane-1-carboxamide, 10d**. Following the general procedure E, 2-ethylaniline (1.03 mL, 0.98 g/mL, 8.3 mmol) and adamantane-1-carboxylic acid, 1, (1.50 g, 8.3 mmol) in CH_2Cl_2 (18.8 mL), with EDC·HCl (1.92 g, 10 mmol) and DMAP (1.22 g, 10 mmol), gave amide **10d** (0.50 g, 21%) as a white solid. mp = 162-163 ºC (dec). IR (ATR) ν 3252, 2901, 2847, 1637, 1513, 1447, 1289, 1264, 1178, 924, 745, 654 cm^{-1}. ^{1}H-NMR, δ_H (400 MHz, $CDCl_3$): 1.26 (t, *J* = 7.6 Hz, 3 H, $CH_2C\underline{H}_3$), 1.74-1.82 [complex signal, 6H, 4'(6',10')-H_2], 2.00 [broad s, 6H, 2'(8',9')-H_2], 2.11 [broad s, 3H, 3'(5',7')-H], 2.60 (q, *J* = 7.6 Hz, 2 H, $C\underline{H}_2CH_3$), 7.09 (td, *J* = 7.2 Hz, *J'* = 1.4 Hz, 1H, 5-H), 7.28-7.33 (complex signal), 3H, 3-H and 4-H), 7.28 (broad s, 1H, NH), 7.89 (dd, *J* = 8.4 Hz, *J'* = 0.8 Hz, 1H, 6-H).^{13}C-NMR, δ_C (100.6 MHz, $CDCl_3$): 13.9 (CH_3, $CH_2\underline{C}H_3$), 24.4 (CH_2, $\underline{C}H_2CH_3$), 28.2 [CH, C3'(5',7')], 36.5 [CH_2, C4'(6',10')], 39.4 [CH_2, C2'(8',9')], 41.6 (C, C1'), 123.2 (CH, C6*), 125.0 (CH, C3*), 126.7 (CH, C5), 128.4 (CH, C4), 134.3 (C, C2), 135.2 (C, C1), 175.9 (C, CO). HRMS-ESI$^+$ m/z [*M*+H]$^+$ calcd for [$C_{19}H_{25}NO$+H^+]: 284.2009, found: 284.2013.

***N*-(2-isopropylphenyl)adamantane-1-carboxamide, 10e**. Following the general procedure D, from 1-adamantanecarbonyl chloride (1.100 g, 5.5 mmol) in anh. acetone (6.5 mL), and a solution of 2-isopropylaniline (0.78 mL, 5.5 mmol) in triethylamine

(0.84 mL, 6.05 mmol), the product was obtained as a white solid (892 mg, 54.6% yield). Crystallization from hot acetone gave a white solid (615 mg). mp = 208-209 ºC. IR (ATR) ν: 675, 730, 751, 801, 925, 945, 976, 1031, 1079, 1100, 1178, 1259, 1342, 1367, 1443, 1466, 1499, 1544, 1638, 2349, 2496, 2845, 2896, 2951, 3301 cm^{-1}. ^{1}H-NMR (400 MHz, $CDCl_3$) δ: 1.27 [d, *J* = 6.8 Hz, 6 H, -CH(C<u>H</u>$_3$)$_2$], 1.72-1.84 [c. s., 6 H, 4'(6',10')-H_2], 1.94-2.04 [c. s., 6 H, 2'(8',9')-H_2], 2.11 [m, 3 H, 3'(5',7')-H], 2.98 [sept, *J* = 6.8 Hz, 1 H, -C<u>H</u>(CH$_3$)$_2$], 7.10-7.23 (c. s., 2 H, 4-H and 5-H), 7.27 (dm, *J* = 7.6 Hz, 1 H, 6-H), 7.30 (broad s, 1 H, NH), 7.78 (broad d, *J* = 7.6 Hz, 1 H, 3-H). ^{13}C-NMR (100.5 MHz, $CDCl_3$) δ: 22.8 [CH_3, -CH(<u>C</u>H$_3$)$_2$], 28.1 [CH, -<u>C</u>H(CH$_3$)$_2$], 28.2 [CH, C3'(5',7')], 36.5 [CH_2, C4'(6',10')], 39.4 [CH_2, C2'(8',9')], 41.6 (C, C1'), 124.2 (CH, C6), 125.3 (CH, C5), 125.4 (CH, C3), 126.4 (CH, C4), 134.3 (C, C1), 139.6 (C, C2), 176.0 (C, CO). HRMS-ESI+ m/z [*M*+H]$^+$ calcd for [$C_{20}H_{27}NO$+H]$^+$: 298.2165, found: 298.2167.

***N*-[4-(benzyloxy)phenyl]adamantane-1-carboxamide, 10f**. Following the general procedure D, 1-adamantanecarbonyl chloride (2 g, 10.1 mmol) in acetone (13.5 mL), and a solution of 4-(benzyloxy)aniline (1.7 g, 7.2 mmol) in triethylamine (2.4 mL, 0.73 g/mL, 17.3 mmol), gave amide **10f** (2.9 g, 94%) as a white solid. mp = 221-225 °C (dec). IR (ATR) ν: 3279, 2900, 2849, 1646, 1597, 1533, 1508, 1470, 1412, 1380, 1297, 1232, 1172, 1001, 825, 797, 746, 698 cm^{-1}. ^{1}H-NMR, δ_H (400 MHz, $CDCl_3$): 1.72-1.80 [complex signal, 6H, 4'(6',10')-H_2], 1.95 [broad s, 6H, 2'(8',9')-H_2], 2.10 [broad s, 3H, 3'(5',7')-H], 5.05 (s, 2H, C<u>H</u>$_2$C$_6$H$_5$), 6.92 (m, 2H, 3(5)-H), 7.20 (broad s, 1H, NH), 7.31 (tt, *J* = 7.2 Hz, *J'* = 1.6 Hz, 1H, phenyl-CH_{para}), 7.37 (t, *J* = 7.6 Hz, 2H, phenyl-CH_{meta}), 7.40-7.44 (complex signal, 4H, 2(6)-H, phenyl-CH_{ortho}). ^{13}C-NMR, δ_C (100.6 MHz, $CDCl_3$): 28.1 [CH, C3'(5',7')], 36.4 [CH_2, C4'(6',10')], 39.2 [CH_2, C2'(8',9')], 41.3 (C, C1'), 70.3 (CH_2, <u>C</u>H$_2$C$_6$H$_5$), 115.2 [CH, C3(5)], 121.7 [CH, C2(6)], 127.4 (CH, phenyl-C_{ortho}), 127.9 (CH, phenyl-C_{para}), 128.5 (CH, phenyl-C_{meta}), 131.4 (C, C1), 137.0 (C,

phenyl-C_{ipso}), 155.4 (C, C4), 175.8 (C, CO). GC/MS (EI), t_r = 36.4 min; m/e (%); main ions: 361 ($M^{\cdot+}$, 19), 136 (11), 135 (100), 93 (10), 91 (39), 79 (12). HRMS-ESI$^+$ m/z [*M*+H]$^+$: calcd for [$C_{24}H_{27}NO_2$+H^+]: 362.2115, found: 362.2117.

***N*-[3-(benzyloxy)phenyl]adamantane-1-carboxamide, 10g**. Following the general procedure D, 1-adamantanecarbonyl chloride (2.34 g, 11.8 mmol) in acetone (14.4 mL), and a solution of 3-(benzyloxy)aniline (1.97 g, 9.9 mmol) in triethylamine (1.6 mL, 0.73 g/mL, 11.8 mmol), gave amide **10g** (3.49 g, 97%) as a white solid. mp = 194-195 °C (dec). IR (ATR) ν: 3314, 2917, 2899, 2851, 1650, 1607, 1594, 1539, 1437, 1380, 1291, 1275, 1247, 1156, 1010, 858, 781, 737, 697, 688 cm^{-1}. ^{1}H-NMR, δ_H (400 MHz, $CDCl_3$): 1.72-1.81 [complex signal, 6H, 4'(6',10')-H_2], 1.97 [broad s, 6H, 2'(8',9')-H_2], 2.11 [broad s, 3H, 3'(5',7')-H], 5.07 (s, 2H, C$\underline{H_2}C_6H_5$), 6.73 (dd, *J* = 8.2 Hz, *J'* = 2.6 Hz, 1H, 4-H), 6.97 (d, *J* = 8.2 Hz, *J'* = 1.2 Hz, 1H, 6-H), 7.20 (t, *J* = 8.2 Hz, 1H, 5-H), 7.27-7.35 (complex signal, 2 H, NH and phenyl-CH_{para}), 7.38 (t, *J* = 7.5 Hz, 2H, phenyl-CH_{meta}), 7.43 (d, *J* = 7.5 Hz, 2H, phenyl-CH_{ortho}), 7.53 (t, *J* = 2.2 Hz, 1H, 2-H). ^{13}C-NMR, δ_C (100.6 MHz, $CDCl_3$): 28.1 [CH, C3'(5',7')], 36.4 [CH_2, C4'(6',10')], 39.2 [CH_2, C2'(8',9')], 41.5 (C, C1'), 69.9 (CH_2, $\underline{C}H_2C_6H_5$), 106.3 (CH, C6), 111.0 (CH, C4*), 112.1 (CH, C2*), 127.5 (CH, phenyl-C_{ortho}), 127.9 (CH, phenyl-C_{para}), 128.5 (CH, phenyl-C_{meta}), 129.5 (CH, C5), 136.9 (C, phenyl-C_{ipso}), 139.3 (C, C1), 159.3 (C, C3), 176.1 (C, CO). GC/MS (EI), t_r = 34.6 min; m/e (%); main ions: 361 ($M^{\cdot+}$, 14), 136 (10), 135 (100), 93 (13), 91 (81), 79 (15). HRMS-ESI$^+$ m/z [*M*+H]$^+$: calcd for [$C_{24}H_{27}NO_2$+H^+]: 362.2115, found: 362.2116.

N-[3-(trifluoromethoxy)phenyl]adamantane-1-carboxamide, 10h. Following the general procedure D, from 1-adamantanecarbonyl chloride (2.5 g, 12.4 mmol) In acetone (13 ml) and a solution of 3-trifluoromethoxyaniline (1.0 ml, 10.2 mmol) in triethylamine (1.7 ml, 12.4 mmol) amide **10h** was obtained (2.8 g, 67%) as a white

solid. Mp = 132-133 ºC (dec). IR (ATR) ν: 3290, 2899, 2850, 1806, 1651, 1602, 1531, 1488, 1445, 1248, 1214, 1150, 991, 974, 883, 786, 770, 701, 683 cm^{-1}. ^{1}H-NMR, δ_H (400 MHz, $CDCl_3$): 1.73-1.81 [complex signal, 6H, 4'(6',10')-H_2], 1.95 [cs, 6H, 2'(8',9')-H_2], 2.14 [m, 3H, 3'(5',7')-H], 7.95 (d, *J* = 8.0 Hz, 1H, 4-H), 7.29-7.39 (complex signal, 3H, Ar-H), 7.61 (bs, 1H, NH). ^{13}C-NMR, δ_C (100.6 MHz, $CDCl_3$): 28.1 [CH, C3'(5',7')], 36.4 [CH_2, C4'(6',10')], 39.2 [CH_2, C2'(8',9')], 41.6 (C, C1'), 112.7 (CH, Ar-CH), 116.2 (CH, Ar-CH), 117.8 (CH, Ar-CH), 129.9 [(CH, Ar-CH)(C, CF_3)], 139.5 (C, Ar-C), 149.6 (C, Ar-C-OCF_3), 176.2 (CO). HRMS-ESI$^+$ m/z [*M*+H]$^+$: calcd for [$C_{18}H_{20}F_3NO_2$+H^+]: 340.15, found: 340.1516

***N*-[2-(trifluoromethyl)phenyl]adamantane-1-carboxamide, 10i**. Following the general procedure D, 1-adamantanecarbonyl chloride (2.2 g, 11.1 mmol) in acetone (13.5 mL), and a solution of 2-(trifluoromethyl)aniline (1.16 mL, 1.28 g/mL, 9.2 mmol) in triethylamine (1.55 mL, 0.73 g/mL, 11.1 mmol), gave amide 10i (2.9 g, 97%) as a white solid. mp = 122-125 °C. IR (ATR) ν: 3323, 2904, 2851, 1646, 1605, 1584, 1503, 1487, 1452, 1315, 1276, 1252, 1155, 1131, 1110, 1056, 1037, 769, 732, 650 cm^{-1}. ^{1}H-NMR, δ_H (400 MHz, $CDCl_3$): 1.73-1.81 [complex signal, 6H, 4'(6',10')-H_2], 1.96 [s, 6H, 2'(8',9')-H_2], 2.11 [m, 3H, 3'(5',7')-H], 7.19 (d, *J* = 7.6 Hz, 1H, 4-H), 7.54 (t, *J* = 8.0 Hz, 1H, 5-H), 7.59 (d, *J* = 7.6 Hz, 1H, 3-H), 7.77 (bs, 1H, NH), 8.27 (t, *J* = 2.5 Hz, 1H, 6-H).^{13}C-NMR, δ_C (100.6 MHz, $CDCl_3$): 28.2 [CH, C3'(5',7')], 36.5 [CH_2, C4'(6',10')], 39.2 [CH_2, C2'(8',9')], 41.9 (C, C1'), 119.9 (C, q, *J* = 29.2 Hz, C2), 124.1 (CH, C6*), 124.3 (CH, C4*), 124.4 (C, q, *J* = 273.6 Hz, CF_3), 126.1 (CH, q, *J* = 5.0 Hz, C3), 133.0 (CH, C5), 135.9 (C, C1), 176.3 (CO). GC/MS (EI), t_r = 22.1 min; m/e (%); main ions: 323 ($M^{\cdot+}$, 5), 136 (12), 135 (100), 93 (13), 91 (8), 79 (16). HRMS-ESI$^+$ m/z [*M*+H]$^+$: calcd for [$C_{18}H_{20}F_3NO$+H^+]: 324.157, found: 324.1568.

***N*-[3-(trifluoromethyl)phenyl]adamantane-1-carboxamide, 10j**. Following the general procedure D, 1-adamantanecarbonyl chloride (2.2 g, 11.1 mmol) in acetone (13.5 mL), and a solution of 3-(trifluoromethyl)aniline (1.16 mL, 1.29 g/mL, 9.2 mmol) in triethylamine (1.55 mL, 0.73 g/mL, 11.1 mmol), gave amide **10j** (3 g, quantitative yield) as a white solid. mp = 174-176 °C. IR (ATR) ν: 3297, 2900, 2850, 1655, 1600, 1550, 1442, 1331, 1291, 1259, 1218, 1164, 1126, 1100, 1069, 897, 792, 697 cm^{-1}. ^{1}H-NMR, δ_H (400 MHz, $CDCl_3$): 1.72-1.81 [complex signal, 6H, 4'(6',10')-H_2], 1.98 [broad s, 6H, 2'(8',9')-H_2], 2.11 [m, 3H, 3'(5',7')-H], 7.34 (d, *J* = 8.0 Hz, 1H, 4-H), 7.40-7.44 (complex signal, 2H, 2-H and 5-H), 7.73 (d, *J* = 8.0 Hz, 1H, 6-H), 7.86 (bs, 1H, NH). ^{13}C-NMR, δ_C (100.6 MHz, $CDCl_3$): 28.2 [CH, C3'(5',7')], 36.5 [CH_2, C4'(6',10')], 39.4 [CH_2, C2'(8',9')], 41.8 (C, C1'), 116.8 (CH, C4), 120.7 (CH, C6*), 123.1 (CH, C2*), 124.0 (C, q, *J* = 271.6 Hz, CF_3), 129.6 (CH, C5), 131.5 (C, q, *J* = 32.2 Hz, C3), 138.7 (C, C1), 176.5 (CO). GC/MS (EI), t_r = 23.5 min; m/e (%); main ions: 323 ($M^{\cdot+}$, 4), 136 (12), 135 (100), 93 (13), 79 (16), 77 (8). HRMS-ESI$^+$ m/z $[M+H]^+$: calcd for $[C_{18}H_{20}F_3NO+H^+]$: 324.157, found: 324.1572.

***N*-[4-(trifluoromethyl)phenyl]adamantane-1-carboxamide, 10k**. Following the general procedure D, from 1-adamantanecarbonyl chloride (2.2 g, 11.1 mmol) in acetone (13.5 mL), and a solution of 4-(trifluoromethyl)aniline (1.16 mL, 1.28 g/mL, 9.2 mmol) in triethylamine (1.55 mL, 0.73 g/mL, 11.1 mmol), gave amide **10k** (1.7 g, 57%) as a white solid. mp = 192-194 °C (dec). IR (ATR) ν: 3302, 2901, 2849, 1660, 1603, 1530, 1407, 1318, 1309, 1258, 1184, 1156, 1128, 1112, 1061, 1016, 843, 699 cm^{-1}. ^{1}H-NMR, δ_H (400 MHz, DMSO): 1.69 [s, 6H, 4'(6',10')-H_2], 1.90 [s, 6H, 2'(8',9')-H_2], 2.00 [broad s, 3H, 3'(5',7')-H], 7.62 [d, *J* = 8.0 Hz, 2H, 2(6)-H], 7.87 [d, *J* = 8.0 Hz, 2H, 3(5)-H], 9.45 (bs, 1H, NH). ^{13}C-NMR, δ_C (100.6 MHz, DMSO): 27.8 [CH, C3'(5',7')], 36.1 [CH_2, C4'(6',10')], 38.3 [CH_2, C2'(8',9')], 41.3 (C, C1'), 120.1 [CH,

C2(6)], 125.8 [CH, C3(5)], 143.1 (C, C1), 176.8 (CO). The signals of the C4 and the CF_3 were not observed. GC/MS (EI), t_r = 23.7 min; m/e (%); main ions: 323 ($M^{\cdot+}$, 4), 136 (11), 135 (100), 93 (12), 79 (14). HRMS-ESI$^+$ m/z [*M*+H]$^+$: calcd for [$C_{18}H_{20}F_3NO$+H^+]: 324.157 , found: 324.1569.

***N*-(4-chlorophenyl)adamantane-1-carboxamide, 10l**. Following the general procedure E, 4-chloroaniline (0.7 g, 5.5 mmol) and adamantane-1-carboxylic acid (0.99 g, 5.5 mmol) in CH_2Cl_2 (6.25 mL), with EDC·HCl (1.26 g, 6.6 mmol) and DMAP (0.81 g, 6.6 mmol), gave amide **10l** (0.29 g, 19%) as a white solid.mp = 207-209 °C (dec). IR (ATR) ν: 3276, 2897, 2849, 1643, 1596, 1537, 1490, 1437, 1328, 1308, 1253, 754, 695 cm^{-1}. ^{1}H-NMR, δ_H (400 MHz, DMSO): 1.70 [broad s, 6H, 4'(6',10')-H_2], 1.90 [broad s, 6H, 2'(8',9')-H_2], 2.01 [broad s, 3H, 3'(5',7')-H], 7.32 [d, *J* = 8.8 Hz, 2H, 3(5)-H], 7.70 [d, *J* = 8.8 Hz, 2H, 2(6)-H], 9.22 (broad s, 1H, NH). ^{13}C-NMR, δ_C (100.6 MHz, DMSO): 27.6 [CH, C3'(5',7')], 36.0 [CH_2, C4'(6',10')], 38.2 [CH_2, C2'(8',9')], 40.9 (C, C1'), 121.6 [CH, C2(6)], 126.6 (C, C4), 128.2 [CH, C3(5)], 138.3 (C, C1), 176.0 (C, CO). GC/MS (EI), t_r = 28.9 min; m/e (%); main ions: 289 ($M^{\cdot+}$, 10), 136 (11), 135 (100), 93 (10), 79 (12). HRMS-ESI$^+$ m/z [*M*+H]$^+$ calcd for [$C_{17}H_{20}ClNO$+H^+]: 290.1306, found: 290.1313.

N-(2-bromophenyl)adamantane-1-carboxamide, 10m. Following the general procedure D, from 1-adamantanecarbonyl chloride (2.0 g, 10.1 mmol) In acetone (13 ml) and a solution of 2-bromoaniline (0.94 ml, 8.33 mmol) in triethylamine (1.41 ml, 10.1 mmol) amide **10m** was obtained (1.7 g, 50%) as a white solid. mp = 119-120 ºC. IR (ATR) ν: 1689, 1510, 1295, 754 cm^{-1}. ^{1}H-NMR, δ_H (400 MHz, $CDCl_3$): 1.74-1.81 [complex signal, 6H, 4'(6',10')-H_2], 1.96 [d, *J* = 2.4 Hz, 6H, 2'(8',9')-H_2], 2.11 [s, 3H, 3'(5',7')-H], 7.0 (dt, *J'*=1.6 Hz, *J* = 7.6 Hz, 1H, H_{AR}), 7.26 (t, *J* = 8.4 Hz, 1H, H_{AR}), 7.35 (dd, *J'*=1.6 Hz, *J* = 8 Hz, 1H, H_{AR}), 7.99 (bs, 1H, NH), 8.43 (dd, *J'*=1.2 Hz, *J* = 8.2

Hz, 1H, H_{AR}).^{13}C-NMR, δ_C (100.6 MHz, $CDCl_3$): 28.1 [CH, C3'(5',7')], 36.4 [CH_2, C4'(6',10')], 39.2 [CH_2, C2'(8',9')], 42.0 (C, C1'), 121.4 (C, q, C2), 122.9 (CH, C6*), 124.2 (CH, C4*), 127.7 (CH, C3), 128.8 (CH, C5), 134.7 (C, C1), 171.3 (CO). HRMS-ESI$^+$ m/z [*M*+H]$^+$: calcd for [$C_{17}H_{20}BrNO+H^+$]: 334.07, found: 334.0794.

N-(2-chlorophenyl)adamantane-1-carboxamide, 10n. Following the general procedure D, from 1-adamantanecarbonyl chloride (2.0 g, 10.1 mmol) In acetone (13 ml) and a solution of 2-chloroaniline (0.87 ml, 18.3 mmol) in triethylamine (1.41 ml, 10.1 mmol) amide **10n** was obtained (1.9 g, 65%) as a solid. Mp = 130-131 ºC. IR (ATR) ν: 3056, 2897, 1688, 1581, 1505, 1428, 1290, 1217, 1073, 1019, 753 cm^{-1}. ^{1}H-NMR, δ_H (400 MHz, $CDCl_3$): 1.74-1.81 [complex signal, 6H, 4'(6',10')-H_2], 2.00 [d, *J* = 2.8 Hz, 6H, 2'(8',9')-H_2], 2.12 [s, 3H, 3'(5',7')-H], 6.95 (dt, *J'*=1.6 Hz, *J* = 7.6 Hz, 1H, H_{AR}), 7.26 (t, *J* = 8.0 Hz, 1H, H_{AR}), 7.52 (dd, *J'*=1.2 Hz, *J* = 8 Hz, 1H, H_{AR}), 7.99 (bs, 1H, NH), 8.42 (dd, *J'*=1.2 Hz, *J* = 8.0 Hz, 1H, H_{AR}).^{13}C-NMR, δ_C (100.6 MHz, $CDCl_3$): 28.1 [CH, C3'(5',7')], 36.4 [CH_2, C4'(6',10')], 39.2 [CH_2, C2'(8',9')], 42.1 (C, C1'), 113.6 (C, C2), 121.6 (CH, C6*), 124.8 (CH, C4*), 128.4 (CH, C3), 132.1 (CH, C5), 135.9 (C, C1), 176.2 (CO). HRMS-ESI$^+$ m/z [*M*+H]$^+$: calcd for [$C_{17}H_{20}ClNO+H^+$]: 290.12, found: 290.1309.

***N*-(3-chlorophenyl)adamantane-1-carboxamide, 10o**. Following the general procedure D, from 1-adamantanecarbonyl chloride (2.2 g, 11.1 mmol) in acetone (13.5 mL), and a solution of 3-chloroaniline (0.98 mL, 1.21 g/mL, 9.3 mmol) in triethylamine (1.55 mL, 0.73 g/mL, 11.1 mmol), amide **10o** was obtained (2.6 g, 96%) as a white solid. mp 185-190 °C. IR (ATR) ν: 3267, 2899, 2849, 1651, 1587, 1523, 1479, 1401, 1299, 1245, 1185, 1096, 1076, 899, 874, 774, 683 cm^{-1}.^{1}H-NMR, δ_H (400 MHz, $CDCl_3$): 1.71-1.79 [complex signal, 6H, 4'(6',10')-H_2], 1.95 [s, 6H, 2'(8',9')-H_2], 2.09 [s, 3H, 3'(5',7')-H], 7.05 (ddd, *J* = 8.0 Hz, *J'* = 2.5 Hz, *J''* = 1.0 Hz, 1H, 4-H), 7.21 (t, *J*

= 8.0 Hz, 1H, 5-H), 7.32 (bs, 1H, NH), 7.36 (ddd, *J* = 8.0 Hz, *J'* = 2.5 Hz, *J''* = 1.0 Hz, 1H, 6-H), 7.69 (t, *J* = 2.5 Hz, 1H, 2-H).^{13}C NMR, δ_C (100.6 MHz, $CDCl_3$): 28.1 [CH, C3'(5',7')], 36.3 [CH_2, C4'(6',10')], 39.2 [CH_2, C2'(8',9')], 41.6 (C, C1'), 117.8 (CH, C6), 120.1 (CH, C2), 124.1 (CH, C4), 129.8 (CH, C5), 134.5 (C, C3), 139.2 (C, C1), 176.1 (C, CO). GC/MS (EI), t_r = 25.9 min; m/e (%); main ions: 289 ($M^{\cdot+}$, 100), 136 (11), 135 (100), 93 (12), 79 (14). HRMS-ESI$^+$ m/z [*M*+H]$^+$: calcd for [$C_{17}H_{20}ClNO+H^+$]: 290.1306, found: 290.1309.

N-(2,6-difluorophenyl)adamantane-1-carboxamide, 10p. Following the general procedure D, from 1-adamantanecarbonyl chloride (2.1 g, 10.8 mmol) In acetone (13 ml) and a solution of 2,6-difluoroaniline (1.5 ml, 8.8 mmol) in triethylamine (1.5 ml, 10.8 mmol) amide **10p** was obtained (2.612 g, 83.18 %) as a beige solid. Mp = 141-142 ºC (dec). IR (ATR) ν: 2903, 1644, 1495, 1256, 1138, 1079, 962, 848, 810 cm^{-1}. ^{1}H-NMR, δ_H (400 MHz, $CDCl_3$): 1.73-1.80 [complex signal, 6H, 4'(6',10')-H_2], 1.97 [d, *J* = 2.4 Hz, 6H, 2'(8',9')-H_2], 2.11 [broad s, 3H, 3'(5',7')-H], 6.86 (cs, 2H, Ar-H), 7.47 (s, 1H, NH), 8.30 (cs, 1H, Ar-H). ^{13}C-NMR, δ_C (100.6 MHz, $CDCl_3$): 28.0 [CH, C3'(5',7')], 36.3 [CH_2, C4'(6',10')], 39.2 [CH_2, C2'(8',9')], 41.8 (C, C1'), 103.3 (CH, t, *J* = 26.5 Hz, Ar-CH), 123.9 (CH, d, *J* = 21.4 Hz, Ar-CH), 122.8 (C, Ar-C), 155.4 (C, q, *J* = 577.4 Hz, Ar-C-F), 176.1 (C, CO). HRMS-ESI$^+$ m/z [*M*+H]$^+$: calcd for [$C_{17}H_{19}F_2NO+H^+$]: 292.15, found: 292.0915.

N-(3,5-difluorophenyl)adamantane-1-carboxamide, 10q. Following the general procedure D, from 1-adamantanecarbonyl chloride (2.5 g, 12.4 mmol) In acetone (13 ml) and a solution of 3,5-difluoroaniline (1.3g, 10.2 mmol) in triethylamine (1.7 ml, 12.4 mmol) amide **10q** was obtained (2.9 g, 81%) as a white solid. Mp = 196-197 ºC. IR (ATR) ν: 3279, 2902, 1658, 1602, 1530, 1415, 1248, 1113, 991, 828, 743, 668 cm^{-1}. ^{1}H-NMR, δ_H (400 MHz, $CDCl_3$): 1.70-1.80 [complex signal, 6H, 4'(6',10')-H_2], 1.94

[d, J = 2.8 Hz, 6H, 2'(8',9')-H_2], 2.92 [broad s, 3H, 3'(5',7')-H], 6.53 (tt, 2H, J''= 2.8 Hz, J'= 8.6, J''= 15,2 Hz, Ar-H), 7.17 (cs, 1H, Ar-H), 7.36 (s, 1H, NH). ^{13}C-NMR, δ_C (100.6 MHz, $CDCl_3$): 28.0 [CH, C3'(5',7')], 36.3 [CH_2, C4'(6',10')], 39.1 [CH_2, C2'(8',9')], 41.7 (C, C1'), 99.2 (CH, t, J' = 25.6, J = 51.4, Hz, Ar-CH), 102.8 (CH, dd, J' = 8.5, J = 21.0, Hz, Ar-CH), 140.2 (C, t, J' = 13.3, J = 26.5 Hz, Ar-C), 163.1 (C, dd, J' = 13.9, J = 246.5 Hz, Ar-C-F), 176.2 (C, CO). HRMS-ESI$^+$ m/z $[M+H]^+$: calcd for $[C_{17}H_{19}F_2NO+H^+]$: 292.15, found: 292.1508.

N-(3,5-dichlorophenyl)adamantane-1-carboxamide, 10r. Following the general procedure D, from 1-adamantanecarbonyl chloride (2.1 g, 10.9 mmol) In acetone (13 ml) and a solid of 3,5-dichloroaniline (1.4 g, 8.9 mmol) in triethylamine (1.5 ml, 10.9 mmol) amide **10r** was obtained (2.9 g, 84%) as a violet solid. mp=228-229ºC (dec). IR (ATR) ν: 2898, 1657, 1585, 797, 668 cm^{-1}.^{1}H-NMR, δ_H (400 MHz, $CDCl_3$): 1.70-1.80 [complex signal, 6H, 4'(6',10')-H_2], 1.95 [d, J = 2.8 Hz, 6H, 2'(8',9')-H_2], 2.10 [broad s, 3H, 3'(5',7')-H], 7.07 [t, J = 1.6 Hz, 1H, Ar-H] 7.32 (s, 1H, NH), 7.52 [d, J = 2 Hz, 2H, Ar-H]. ^{13}C-NMR, δ_C (100.6 MHz, $CDCl_3$): 28.0 [CH, C3'(5',7')], 36.3 [CH_2, C4'(6',10')], 39.1 [CH_2, C2'(8',9')], 41.7 (C, C1'), 118.1 (CH, C4), 123.9 (CH, C2), 135.1 (CH, C6), 139.8 (C, C3), 176.2 (C, CO). HRMS-ESI$^+$ m/z $[M+H]^+$: calcd for $[C_{17}H_{19}Cl_2NO+H^+]$: 324.08, found: 324.0918.

N-(3,5-bis(trifluoromethyl)phenyl)adamantane-1-carboxamide, 10s. Following the general procedure D, from 1-adamantanecarbonyl chloride (2.1g, 10.8 mmol) In acetone (13 ml) and a solution of 3,5-bis(trifluoromethyl)aniline (1.3 ml, 8.8 mmol) in triethylamine (1.5 ml, 10.8 mmol) amide 10s was obtained (3.0 g, 70%) as a white solid. Mp = 230-231 ºC. IR (ATR) ν: 3302, 2908, 2855, 1658, 1543, 1470, 1433, 1379, 1277, 1245, 1215, 1168, 1129, 1078, 944, 901, 886, 848, 680 cm^{-1}. ^{1}H-NMR, δ_H (400 MHz, $CDCl_3$): 1.72-1.82 [m, 6H, 4'(6',10')-H_2], 1.97 [d, J = 2.8 Hz, 6H, 2'(8',9')-H_2],

2.13 [broad s, 3H, 3'(5',7')-H], 7.58 (bs, 2H, Ar-H, NH), 8.1 (s, 1H, Ar-H). ^{13}C-NMR, δ_C (100.6 MHz, $CDCl_3$): 27.9 [CH, C3'(5',7')], 36.3 [CH_2, C4'(6',10')], 39.1 [CH_2, C2'(8',9')], 41.7 (C, C1'), 117.3 (C, t, J = 3.9 Hz, Ar-C_{para}), 119.6 (C, J = 3.1 Hz, Ar-C_{orto}), 123.1 (C, q, J = 525.4 Hz, CF_3), 132.6 (C, q, J = 66.9 Hz, Ar-C_{meta}), 139.5 (C, NH-Ar-C), 176.4 (CO). 176.5 (C, CO). HRMS-ESI$^+$ m/z $[M+H]^+$: calcd for $[C_{19}H_{19}F_6NO+H^+]$: 392.14, found: 392.1450.

***N*-[3-fluoro-5-(trifluoromethyl)phenyl]adamantane-1-carboxamide, 10t**. Following the general procedure D, 1-adamantanecarbonyl chloride (1.31 g, 6.6 mmol) in acetone (7.1 mL), and a solution of 3-fluoro-5-(trifluoromethyl)aniline (0.98 g, 5.5 mmol) in triethylamine (0.92 mL, 0.73 g/mL, 6.6 mmol), gave amide **10t** (1.7 g, 90%) as a white solid. mp = 178-180 °C (dec). IR (ATR) ν: 3281, 2901, 2850, 1657, 1610, 1547, 1439, 1356, 1234, 1144, 1091, 898, 871, 822, 695 cm^{-1}. ^{1}H-NMR, δ_H (400 MHz, $CDCl_3$): 1.72-1.82 [complex signal, 6H, 4'(6',10')-H_2], 1.97 [broad s, 6H, 2'(8',9')-H_2], 2.12 [broad s, 3H, 3'(5',7')-H], 7.05 (dm, J = 8.4 Hz, 1H, 4-H), 7.44 (broad s, 1H, 2-H), 7.46 (broad s, 1H, NH), 7.76 (dt, J = 10.4 Hz, J = 2.4 Hz, 1H, 6-H). ^{13}C-NMR, δ_C (100.6 MHz, $CDCl_3$): 28.2 [CH, C3'(5',7')], 36.5 [CH_2, C4'(6',10')], 39.3 [CH_2, C2'(8',9')], 41.9 (C, C1'), 176.1 (C, CO). The aromatic signals were not fully observed. GC/MS (EI), t_r = 22.9 min; m/e (%); main ions: 341 ($M^{\cdot+}$, 2), 322 (2), 136 (12), 135 (100), 93 (13), 79 (16). HRMS-ESI$^+$ m/z $[M+H]^+$: calcd for $[C_{18}H_{19}F_4NO+H^+]$: 342.1476, found: 342.1473.

***N*-[3-chloro-5-(trifluoromethyl)phenyl]adamantane-1-carboxamide, 10u**. Following the general procedure D, 1-adamantanecarbonyl chloride (1.25 g, 6.3 mmol) in acetone (6.75 mL), and a solution of 3-chloro-5-(trifluoromethyl)aniline (1.04 g, 5.3 mmol) in triethylamine (0.87 mL, 0.73 g/mL, 6.3 mmol), gave amide **10u** (1.7 g, 89%) as a white solid. mp = 199-201 °C (dec). IR (ATR) ν: 3285, 2899, 2850, 1655, 1596,

1537, 1451, 1427, 1330, 1277, 1219, 1168, 1138, 1123, 1099, 1083, 943, 875, 833, 695 cm^{-1}. ^{1}H-NMR, δ_H (400 MHz, $CDCl_3$): 1.72-1.81 [complex signal, 6H, 4'(6',10')-H_2], 1.96 [broad s, 6H, 2'(8',9')-H_2], 2.11 [broad s, 3H, 3'(5',7')-H], 7.32 (s, 1H, 4-H), 7.46 (broad s, 1H, NH), 7.68 (s, 1H, 6-H), 7.89 (s, 1 H, 2-H). ^{13}C-NMR, δ_C (100.6 MHz, $CDCl_3$): 28.2 [CH, C3'(5',7')], 36.5 [CH_2, C4'(6',10')], 39.3 [CH_2, C2'(8',9')], 41.9 (C, C1'), 114.9 (CH, C4), 120.9 (CH, C2), 123.1 (CH, C6), 123.2 (C, *J* = 272.9 Hz, CF_3), 132.63 (C, *J* = 33.2 Hz, C3), 135.5 (C, C5), 139.9 (C, C1), 176.6 (C, CO). GC/MS (EI), t_r = 24.7 min; m/e (%); main ions: 357 ($M^{\cdot+}$, 2), 338 (2), 136 (11), 135 (100), 93 (12), 79 (14). HRMS-ESI$^+$ m/z [*M*+H]$^+$: calcd for [$C_{18}H_{19}ClF_3NO$+H^+]: 358.118, found: 358.1183.

***N*-[4-chloro-3-(trifluoromethyl)phenyl]adamantane-1-carboxamide, 10v**. Following the general procedure D, 1-adamantanecarbonyl chloride (2.56 g, 12.9 mmol) in acetone (16.25 mL), and a solution of 4-chloro-3-(trifluoromethyl)aniline (2.1 g, 10.7 mmol) in triethylamine (1.8 mL, 0.73 g/mL, 12.9 mmol), gave amide **10v** (3.8 g, 99%) as a white solid. mp = 190-196 °C (dec). IR (ATR) ν: 3293, 2908, 2852, 1659, 1590, 1531, 1479, 1408, 1321, 1287, 1261, 1173, 1138, 1110, 1033, 894, 830, 812, 693 cm^{-1}. ^{1}H-NMR, δ_H (400 MHz, $CDCl_3$): 1.71-1.80 [complex signal, 6H, 4'(6',10')-H_2], 1.96 [broad s, 6H, 2'(8',9')-H_2], 2.10 [broad s, 3H, 3'(5',7')-H], 7.41 (d, *J* = 8.8 Hz, 1H, 6-H), 7.46 (broad s, 1H, NH), 7.74 (d, *J* = 8.8 Hz, 1H, 5-H), 7.87 (s, 1 H, 2-H). ^{13}C-NMR, δ_C (100.6 MHz, $CDCl_3$): 28.0 [CH, C3'(5',7')], 36.3 [CH_2, C4'(6',10')], 39.2 [CH_2, C2'(8',9')], 41.6 (C, C1'), 118.9 (CH, C2), 122.7 (C, *J* = 272.9 Hz, CF_3), 123.9 (CH, C5), 126.6 (C, C4), 128.5 (C, *J* = 31.7 Hz, C3), 131.8 (CH, C6), 136.9 (C, C1), 176.4 (CO). GC/MS (EI), t_r = 25.5 min; m/e (%); main ions: 357 ($M^{\cdot+}$, 2), 136 (12), 135 (100), 93 (12), 79 (15). HRMS-ESI$^+$ m/z [*M*+H]$^+$: calcd for [$C_{18}H_{19}ClF_3NO$+H^+]: 358.118, found: 358.1181.

N-(pentafluorophenyl)adamantane-1-carboxamide, 10w. Following the general procedure D, from 1-adamantanecarbonyl chloride (2.1 g, 10.8 mmol) In acetone (13 ml) and a solution of pentafluoroaniline (0.93 ml, 8.85 mmol) in triethylamine (1.5 ml, 10.8 mmol) amide **10w** was obtained (2.7g, 72%) as a white solid. mp=185-186°C (dec). IR (ATR) ν: 3295, 2907, 2853, 2156, 1664, 1650, 1487, 1367, 1245, 1183, 1157, 1103, 1074, 1050, 988, 834, 647, 622 cm^{-1}. ^{1}H-NMR, δ_H (400 MHz, $CDCl_3$): 1.72-1.81 [complex signal, 6H, 4'(6',10')-H_2], 1.89 [d, *J* = 2.8 Hz, 6H, 2'(8',9')-H_2], 2.11 [broad s, 3H, 3'(5',7')-H], 6.90 (broad s, 1H, NH). ^{13}C-NMR, δ_C (100.6 MHz, $CDCl_3$): 27.9 [CH, C3'(5',7')], 36.3 [CH_2, C4'(6',10')], 39.2 [CH_2, C2'(8',9')], 41.6 (C, C1'), 112.2 (CH, dt, *J'*=4.0 Hz, *J*=15.1 Hz, Ar-C), 136.3 (C, cs, Ar-CF), 138.8 (C, cs, Ar-CF), 141.2 (C, cs, Ar-CF), 141.8 (C, cs, Ar-CF), 144.3 (C, cs, Ar-CF), 176.3 (C, CO). HRMS-ESI$^+$ m/z $[M+H]^+$: calcd for $[C_{17}H_{16}F_5NO+H^+]$: 346.12, found: 346.1223.

N-(3-chlorophenyl)-3,5-dimethyladamantane-1-carboxamide, 10x. A solution of 3,5-dimethyladamantane-1-carbonyl chloride (0.89 g, 3.9 mmol) in acetone (7 mL) was added dropwise into a solution of 3-chloroaniline (0.35 mL, 1.21 g/mL, 3.3 mmol) and triethylamine (0.54 mL, 0.73 g/mL, 1.11 mmol), under a nitrogen atmosphere. The mixture was heated at 90°C for 3 h and allowed to cool to room temperature. Water (1 mL) was added to the suspension and the resulting solid was filtered and washed with a further amount of water (1 mL). The solid was dried under vacuum to give a white solid (1.0 g, quantitative yield). mp = 112-115 °C (dec). IR (ATR) ν: 3270, 2897, 2843, 1640, 1592, 1520, 1425, 1308, 1287, 1254, 1175, 924, 880, 791, 780, 750, 678 cm^{-1}. ^{1}H-NMR, δ_H (400 MHz, $CDCl_3$): 0.88 [s, 6H, C3'(5')-CH_3], 1.15-1.24 (complex signal, 2H, 6'-H_2), 1.35-1.43 [complex signal, 4H, 4'(10')-H_2], 1.52-1.61 [complex signal, 4H, 8'(9')-H], 1.75-1.79 (complex signal, 2H, 2'-H_2), 2.18 (m, 1 H, 7'-H), 7.05 (dd, *J* = 8.0 Hz, *J'* = 1.0 Hz, 1H, 4-H), 7.21 (t, *J* = 8.0 Hz, 1H, 5-H), 7.33 (bs, 1H, NH), 7.37 (dd, *J* = 8.0

Hz, J' = 1.0 Hz, 1H, 6-H), 7.67 (t, *J* = 2.0 Hz, 1H, 2-H). ^{13}C NMR, δ_C (100.6 MHz, $CDCl_3$): 29.2 (CH, C7'), 30.4 [CH_3, C3'(5')-$\underline{C}H_3$], 31.2 [C, C3'(5')], 37.9 (CH_2, C2'), 42.6 [CH_2, C8'(9')], 43.5 (C, C1'), 45.4 [CH_2, C4'(10')], 50.5 (CH_2, C6'), 117.9 (CH, C6), 120.1 (CH, C2), 124.1 (CH, C4), 129.9 (CH, C5), 134.6 (C, C3), 139.1 (C, C1), 175.9 (C, CO). HRMS-ESI$^+$ m/z [*M*+H]$^+$ calcd for [$C_{19}H_{24}ClNO+H^+$]: 318.1619, found: 318.1627.

3-hydroxyadamantane-1-carboxylic acid, 12. 1-adamantanecarboxylic acid (5 g, 27.7 mmol) was mixed with nitric acid 65% (2.8 mL, 66.6 mmol) and cooled to 0 °C with an ice bath. Concentrated H_2SO_4 (34.7 mL, 651 mmol) was added dropwise via an addition funnel so that the temperature was kept at 0 °C. Stirring at 0 °C was continued for another 3 h. Then, the mixture was poured over 65 g of ice and the white precipitate was filtered and dried with P_2O_5 in a dessicator at reduced pressure (5.4 g, 98%). The spectroscopic data of our compound matched with the reported in the bibliography.[48]

General procedure E.

To a solution of the required aniline, (5.1 mmol) and 3-hydroxyadamantane-1-carboxylic acid, 12, (5.1 mmol) in CH_2Cl_2 (12.5 mL) were added EDC·HCl (6.1 mmol) and DMAP (6.1 mmol), and the mixture was stirred overnight at room temperature. The reaction mixture was concentrated under reduced pressure and the residue was partitioned between ethyl acetate and 1 N HCl. The layers were separated and the organic layer was washed with water, saturated aqueous solution of $NaHCO_3$ and brine, dried over Na_2SO_4 and filtered. The solvent was removed under reduced pressure to give the amides 13 as a white solid.

3-hydroxy-*N*-phenyladamantane-1-carboxamide, 13a. Following the general procedure E, aniline (0.46 mL, 1.02 g/mL, 5.1 mmol) and 3-hydroxyadamantanecarboxylic acid, **6**, (1.0 g, 5.1 mmol) in CH_2Cl_2 (12.5 mL), with

EDC·HCl (1.16 g, 6.1 mmol) and DMAP (0.75 g, 6.1 mmol), gave amide **13a** (0.64 g, 46%) as a white solid. mp = 199-201 °C (dec). IR (ATR) ν: 3274, 2905, 2853, 1647, 1595, 1522, 1498, 1439, 1309, 1253, 1125, 1030, 763, 741, 689 cm^{-1}. ^{1}H-NMR, δ_H (400 MHz, DMSO): 1.53-1.63 (complex signal, 6H, adamantyl-CH_2), 1.73-1.81 (complex signal, 6H, adamantyl-CH_2), 2.18 [broad s, 2H, 5'(7')-H], 4.53 (s, 1H, OH), 7.02 (t, *J* = 7.6 Hz, 1H, 4-H), 7.27 [t, *J* = 7.6 Hz, 2H, 3(5)-H], 7.64 [dd, *J* = 8.4 Hz, *J'* = 1.0 Hz, 2H, 2(6)-H], 9.12 (s, 1H, NH). ^{13}C-NMR, δ_C (100.6 MHz, DMSO): 29.9 [CH, C3'(5',7')], 34.9 (CH_2, C6'), 37.4 [CH_2, C8(9)], 44.27 [CH_2, C4(10)], 44.3 (C, C1'), 46.3 (CH_2, C2'), 66.7 (C, C3'), 120.2 [CH, C2(6)], 123.1 (CH, C4), 128.4 [CH, C3(5)], 139.3 (C, C1), 175.1 (C, CO). HRMS-ESI$^+$ m/z [*M*+H]$^+$: calcd for [$C_{17}H_{21}NO_2$+H^+]: 272.1645, found: 272.1637.

***N*-(4-chlorophenyl)-3-hydroxyadamantane-1-carboxamide, 13b**. Following the general procedure E, 4-chloroaniline (0.65 g, 5.1 mmol) and 3-hydroxyadamantanecarboxylic acid, **6**, (1.0 g, 5.1 mmol) in CH_2Cl_2 (12.5 mL), with EDC·HCl (1.16 g, 6.1 mmol) and DMAP (0.75 g, 6.1 mmol), gave amide **7c** (0.8 g, 50%) as a white solid. mp = 214-215 °C (dec). IR (ATR) ν: 3328, 2904, 2851, 2361, 1648, 1594, 1534, 1490, 1396, 1306, 1251, 1123, 1090, 1026, 908, 829, 751, 688 cm^{-1}. ^{1}H-NMR, δ_H (400 MHz, DMSO): 1.59-1.75 (complex signal, 1H, adamantyl-CH_2), 2.17 [broad s, 2H, 5'(7')-H], 4.53 (s, 1H, OH), 7.32 [d, *J* = 8.0 Hz, 2H, 3(5)-H], 7.69 [d, *J* = 8.0 Hz, 2H, 2(6)-H], 9.26 (s, 1H, NH). ^{13}C-NMR, δ_C (100.6 MHz, DMSO): 29.9 [CH, C3'(5',7')], 34.8 (CH_2, C6'), 37.3 [CH_2, C8(9)], 44.2 [CH_2, C4(10)], 44.2 (C, C1'), 46.2 (CH_2, C2'), 66.6 (C, C3'), 121.7 [CH, C2(6)], 126.7 (C, C4), 128.2 [CH, C3(5)], 138.3 (C, C1), 175.2 (C, CO). GC/MS (EI), t_r = 27.3 min; m/e (%); main ions: 305 ($M^{\cdot+}$, 14), 152 (12), 151 (100), 127 (34), 95 (19), 93 (24). HRMS-ESI$^+$ m/z [*M*+H]$^+$: calcd for [$C_{17}H_{20}ClNO_2$+H^+]: 306.1255, found: 306.1253.

General Procedure F. Sodium bis-(2-methoxyethoxy)aluminum hydride (65% wt solution in toluene, 1.04 g/mL, 4 mmol) was added dropwise to a cool (5 ºC, ice bath) solution of the required amide (1 mmol) in dry toluene (15 mL). The resulting solution was heated to reflux and stirred for 2 days. The solution was allowed to cool down to room temperature and 30% aqueous KOH was added dropwise until basic pH. The organic phase was separated and the aqueous layer was extracted with dichloromethane (3 x 20 mL). The combined organic extracts were dried over anh. Na_2SO_4, filtered and concentrated under vacuo to give the corresponding amine as an oil. The analytical sample of the aniline, as its hydrochloride, was obtained by dissolving this oil in Et_2O and adding an excess of Et_2O/HCl. The resulting suspension was cooled down for 24 h at 0 °C and the precipitated solid was filtered and dried *in vacuo* to afford the corresponding amine hydrochloride. The analytical sample was obtained by crystallization from methanol.

General procedure G. A solution of amide (3.1 mmol) in dry THF (25 mL) was cooled 0 °C with an ice bath and BH_3·THF (1M in THF, 12.4 mmol) was added dropwise and stirred at room temperature overnight. Methanol (25 mL) and then water (25 mL) were carefully added. The organic phase was evaporated under vacuo. The aqueous phase was extracted with dichloromethane (3 x 25 mL). The combined organic extracts were dried over Na_2SO_4, filtered and concentrated under vacuo to give the corresponding amine as an oil. This oil was dissolved in Et_2O and treated with Et_2O/HCl (0.6 N). The resulting suspension was cooled down for 24 h at 0 °C and the precipitated solid was filtered and dried in vacuo to afford the corresponding amine hydrochloride. The analytical sample was obtained by crystallization from methanol.

***N*-[(adamant-1-yl)methyl]aniline hydrochloride, 11a**.[59] Following the general procedure F, the reduction of amide 10a (0.5 g, 1.96 mmol) with sodium bis-(2-

methoxyethoxy)aluminum hydride (65% solution in toluene, 2.34 mL, 7.84 mmol), gave the corresponding amine as an oil (0.41 g, 82%). The corresponding purified amine hydrochloride **11a** was obtained after a treatment with Et_2O/HCl (0.6 N) and a crystallization from methanol. mp = >193 ºC (dec). IR (ATR) ν: 2896, 2848, 2659, 2425, 1602, 1581, 1499, 1488, 1431, 1394, 1372, 1185, 1031, 993, 750, 690 cm^{-1}.^{1}H-NMR, δ_H (400 MHz, DMSO): 1.61-1.70 (complex signal, 12H, adamantyl-CH_2), 1.97 [broad s, 3H, 3'(5',7')-H], 2.89 (s, 2H, CH_2N), 7.15 (m, 1H, 4-H), 7.30 [m, 2H, 2(6)-H], 7.37 [m, 2 H, 3(5)-H].^{13}C-NMR, δ_C (100.6 MHz, DMSO): 27.6 [CH, C3'(5',7')], 33.0 (C, C1'), 36.2 [CH_2, C4'(6',10')], 39.4 [CH_2, C2'(8',9')], 129.4 (CH, Ar-C). Only an aromatic signal was observed and the CH2NH signal is a very broad band, difficult to see. MS-DIP (EI), m/e (%); main ions: 241 ($M^{\cdot+}$, 94), 106 (100), 79 (11), 77 (14). Anal. Calcd. for $C_{17}H_{23}ClN{\cdot}HCl$ (277.84): C 73.49, H 8.71, N 5.04, Cl 12.76. Calcd. for $C_{17}H_{23}ClN{\cdot}HCl{\cdot}0.15H_2O$ (280.54): C 72.78, H 8.73, N 4.99, Cl 12.64. Found: C 72.75, H 8.80, N 4.77, Cl 12.54.

***N*-[(adamant-1-yl)methyl]-4-methylaniline hydrochloride, 11b**.[60] Following the general procedure F, the reduction of amide 10k (1 g, 3.1 mmol) with sodium bis-(2-methoxyethoxy)aluminum hydride (65% solution in toluene, 3.7 mL, 12.4 mmol), gave the corresponding amine as an oil (0.75 g, 78%). The corresponding purified amine hydrochloride **11b** was obtained after a treatment with Et_2O/HCl (0.6 N) and a crystallization from methanol. mp > 226 °C (dec). IR (ATR) ν: 2904, 2846, 1595, 1513, 1430, 1369, 1106, 990, 813 cm^{-1}. ^{1}H-NMR, δ_H (400 MHz, DMSO): 1.62-1.71 (complex signal, 12H, adamantyl-CH_2), 1.98 [broad s, 3H, 3'(5',7')-H], 2.29 (s, 3H, Ar-C$\underline{H}_3$), 2.89 (s, 2H, CH_2N), 7.21 (d, J = 8.0 Hz, 2H, Ar-H), 7.29 (d, J = 8.0 Hz, 2H, Ar-H). ^{13}C-NMR, δ_C (100.6 MHz, DMSO): 20.2 (CH_3, Ar-$\underline{C}H_3$), 27.4 [CH, C3'(5',7')], 32.7 (C, C1'), 36.0 [CH_2, C4'(6',10')], 39.2 [CH_2, C2'(8',9')], 62.1 (CH_2, $\underline{C}H_2N$), 120.6 (CH,

Ar-C), 129.4 (CH, Ar-C), 134.9 (C, Ar-C), 137.9 (C, Ar-C). MS-DIP (EI), m/e (%); main ions: 255 ($M^{\cdot+}$, 84), 120 (100), 91 (13). Anal. Calcd. for $C_{18}H_{25}N{\cdot}HCl$ (291.86): C 74.08, H 8.98, N 4.80, Cl 12.15. Calcd. for $C_{18}H_{25}N{\cdot}HCl{\cdot}1/3H_2O$ (297.81): C 72.60, H 9.02, N 4.70, Cl 11.90. Found: C 72.64, H 8.75, N 4.68, Cl 12.09.

***N*-[(adamant-1-yl)methyl]-2-methylaniline hydrochloride, 11c**. Following the general procedure F, the reduction of amide 10i (1 g, 3.1 mmol) with sodium bis-(2-methoxyethoxy)aluminum hydride (65% solution in toluene, 3.7 mL, 12.4 mmol), gave the corresponding amine as an oil (0.82 g, 85%). The corresponding purified amine hydrochloride **11c** was obtained after a treatment with Et_2O/HCl (0.6 N) and a crystallization from methanol. mp > 193 °C (dec). IR (ATR) ν: 2905, 2844, 1580, 1441, 993, 761 cm^{-1}.^{1}H-NMR, δ_H (400 MHz, DMSO): 1.62-1.69 (complex signal, 12H, adamantyl-CH_2), 1.98 [broad s, 3H, 3'(5',7')-H], 2.36 (s, 3H, Ar-C$\underline{H}_3$), 2.87 (s, 2H, CH_2N), 3.77 (broad s, 1H, NH), 7.13 (t, *J* = 7.2 Hz, 1H, Ar-H), 7.22-7.27 (complex signal, 2H, Ar-H), 7.38 (d, *J* = 8.0 Hz, 1H, Ar-H). ^{13}C-NMR, δ_C (100.6 MHz, DMSO): 7.1 (CH_3, Ar-$\underline{C}H_3$), 27.7 [CH, C3'(5',7')], 33.2 (C, C1'), 36.2 [CH_2, C4'(6',10')], 39.3 [CH_2, C2'(8',9')], 61.5 (CH_2, $\underline{C}H_2N$), 120.3 (CH, Ar-CH), 125.6 (CH, Ar-CH), 127.2 (CH, Ar-CH), 128.9 (C, Ar-C), 131.7 (CH, Ar-CH), 138.8 (C, Ar-CH). MS-DIP (EI), m/e (%); main ions: 255 ($M^{\cdot+}$, 62), 135 (8), 120 (100), 91 (12). Anal. Calcd. for $C_{18}H_{25}N{\cdot}HCl$ (291.86): C 74.08, H 8.98, N 4.80, Cl 12.15. Calcd. for $C_{18}H_{25}N{\cdot}HCl{\cdot}1/2H_2O$ (300.87): C 71.86, H 9.04, N 4.66, Cl 11.78. Found: C 72.05, H 8.87, N 4.81, Cl 11.40.

***N*-[(adamant-1-yl)methyl]-2-ethylaniline hydrochloride, 11d**. Following the general procedure F, the reduction of amide **10d** (0.3 g, 1.06 mmol) with sodium bis-(2-methoxyethoxy)aluminum hydride (65% solution in toluene, 1.27 mL, 4.24 mmol), gave the corresponding amine as an oil (0.21 g, 72%). The corresponding purified

amine hydrochloride **11d** was obtained after a treatment with Et_2O/HCl (0.6 N) and a crystallization from methanol. mp > 178 ºC. IR (ATR) ν: 2900, 2848, 2684, 1583, 1499, 1434, 1372, 1105, 995, 750, 690 cm^{-1}. ^{1}H-NMR, δ_H (400 MHz, CD_3OD): 1.38 (t, *J* = 7.6 Hz, 3H, $CH_2C\underline{H}_3$), 1.79-1.86 (complex signal, 12H, adamantyl-CH_2), 2.10 [broad s, 3H, 3'(5',7')-H], 2.77 (q, *J* = 7.6 Hz, 2H, $C\underline{H}_2CH_3$), 3.03 (s, 2H, CH_2N), 4.86 (broad s, 2H, NH), 7.38-7.54 (complex signal, 4H, Ar-H).^{13}C-NMR, δ_C (100.6 MHz, CD_3OD): 14.5 (CH_3, $CH_2\underline{C}H_3$), 23.2 (CH_2, $\underline{C}H_2CH_3$), 29.4 [CH, C3'(5',7')], 34.2 (C, C1'), 37.4 [CH_2, C4'(6',10')], 40.5 [CH_2, C2'(8',9')], 66.8 (CH_2, CH_2N), 128.9 (CH, Ar-C), 131.6 (CH, Ar-C). Only two aromatic signal were observed. Anal. Calcd. for $C_{19}H_{27}N\cdot HCl$ (305.89): C 74.60, H 9.23, N 4.58, Cl 11.59. Calcd. for $C_{19}H_{27}N\cdot 1.05HCl\cdot 0.85H_2O$ (323.03): C 70.65, H 9.28, N 4.34, Cl 11.52. Found: C 70.66, H 9.02, N 4.07, Cl 11.52.

***N*-[(adamant-1-yl)methyl]-2-isopropylaniline hydrochloride, 11e**. Following the general procedure F, **10e** (0.55 g, 1.85 mmol) and sodium bis-(2-methoxyethoxy)aluminum hydride (65% wt solution in toluene, 1.76 mL, 9.00 mmol) in anhydrous toluene (14 mL), gave a yellow solid (483 mg, 83%). The pure product was obtained after crystallization from hot EtOAc as a white solid (195 mg, 37.2% yield). mp = 107-108 ºC. IR (ATR) ν: 733, 811, 925, 958, 986, 1039, 1059, 1100, 1117, 1140, 1249, 1256, 1282, 1309, 1352, 1448, 1507, 1582, 1605, 2329, 2349, 2840, 2901, 2967, 3037, 3448 cm^{-1}. ^{1}H-NMR (400 MHz, $CDCl_3$) δ: 1.29 [d, *J* = 6.8 Hz, 6 H, -CH($C\underline{H}_3$)$_2$], 1.62-1.65 [c. s., 6 H, 2'(8',9')-H_2], 1.66-1.82 [c. s., 6 H, 4'(6',10')-H_2], 2.03 [m, 3 H, 3'(5',7')-H], 2.83 (s, 2 H, 7-H_2), 2.88 [sept, *J* = 6.8 Hz, 1 H, -C$\underline{H}$(CH_3)$_2$], 3.72 (broad s, 1 H, NH), 6.66 (broad d, *J* = 8.0 Hz, 1 H, 6-H), 6.70 (td, *J* = 7.6 Hz, *J'* = 1.2 Hz, 1 H, 4-H), 7.08-7.17 (c. s., 2 H, 3-H and 5-H). ^{13}C-NMR (100.5 MHz, $CDCl_3$) δ: 22.2 [CH_3, -CH($\underline{C}H_3$)$_2$], 27.4 [CH, -$\underline{C}$H(CH_3)$_2$], 28.4 [CH, C3'(5',7')], 33.7 (C, C1'), 37.1 [CH_2, C4'(6',10')], 41.0 [CH_2, C2'(8',9')], 56.3 (CH_2, C7), 110.1 (CH, C6), 116.6 (CH, C4),

124.8 (CH, C5), 126.7 (CH, C3), 131.7 (C, C2), 145.6 (C, C1). HRMS-ESI+ m/z $[M+H]^+$ calcd for $[C_{20}H_{29}N+H]^+$: 284.2373, found: 284.2382.

***N*-[(adamant-1-yl)methyl]-4-(benzyloxy)aniline hydrochloride, 11f.** Following the general procedure F, the reduction of amide **10f** (2 g, 5.5 mmol) with sodium bis-(2-methoxyethoxy)aluminum hydride (65% solution in toluene, 6.58 mL, 22.0 mmol), gave the corresponding amine as an oil (1.5 g, 79%). The corresponding purified amine hydrochloride **11f** was obtained after a treatment with Et_2O/HCl (0.6 N) and a crystallization from methanol. mp = 199-200 °C. IR (ATR) ν: 2901, 2848, 2494, 2412, 1605, 1577, 1513, 1439, 1250, 1006, 838, 746, 697 cm^{-1}. ^{1}H-NMR, δ_H (400 MHz, DMSO): 1.58-1.70 (complex signal, 12H, adamantyl-CH_2), 1.97 [broad s, 3H, 3'(5',7')-H], 2.91 (s, 2H, CH_2N), 5.12 (s, 2H, CH_2O), 7.11 (d, J = 9.2 Hz, 2H, Ar-H), 7.33 (m, 1H, $CH_2C_6H_5$-H_{para}), 7.37 (t, J = 6.8 Hz, 2H, $CH_2C_6H_5$-H_{meta}), 7.42 (d, J = 6.8 Hz, 2H, $CH_2C_6H_5$-H_{ortho}), 7.43 (m, 2H, Ar-H). ^{13}C-NMR, δ_C (100.6 MHz, DMSO): 27.5 [CH, C3'(5',7')], 32.6 (C, C1'), 36.0 [CH_2, C4'(6',10')], 39.2 [CH_2, C2'(8',9')], 69.6 (CH_2, $\underline{C}H_2O$), 115.7 [C, C3(5)], 127.7 (CH, $CH_2C_6H_5$-C_{ortho}), 127.8 (CH, $CH_2C_6H_5$-C_{para}), 128.4 (CH, $CH_2C_6H_5$-C_{meta}), 136.7 (C, $CH_2C_6H_5$-C_{ipso}). No all the C signals were observed. MS-DIP (EI), m/e (%); main ions: 347 ($M^{\cdot+}$, 19), 256 (100), 149 (26), 93 (10), 91 (14). Anal. Calcd. for $C_{24}H_{29}NO\cdot HCl$ (383.96): C 75.08, H 7.88, N 3.65, Cl 9.23. Calcd. for $C_{24}H_{29}NO\cdot HCl\cdot 1/4\ H_2O$ (388.46): C 74.21, H 7.91, N 3.61, Cl 9.13. Found: C 74.49, H 7.94, N 3.60, Cl 8.90.

***N*-[(adamant-1-yl)methyl]-3-(benzyloxy)aniline hydrochloride, 11g**. Following the general procedure F, the reduction of amide **10g** (2.5 g, 6.93 mmol) with sodium bis-(2-methoxyethoxy)aluminum hydride (65% solution in toluene, 8.29 mL, 27.72 mmol), gave the corresponding amine as an oil (2.23 g, 92%). The corresponding purified amine hydrochloride **11g** was obtained after a treatment with Et_2O/HCl (0.6 N) and a

crystallization from methanol. mp = 188-193 °C. IR (ATR) ν: 2899, 2845, 2411, 1611, 1597, 1498, 1425, 1388, 1255, 1145, 1024, 860, 740, 695 cm^{-1}.^{1}H-NMR, δ_H (400 MHz, DMSO): 1.48-1.69 (complex signal, 12H, adamantyl-CH_2), 1.95 [broad s, 3H, 3'(5',7')-H], 2.84 (s, 2H, CH_2N), 5.08 (s, 2H, CH_2O), 6.65-6.82 (complex signal, 3H, 2-H, 4-H and 6-H), 7.20 (t, *J* = 8.0 Hz, 1H, 5H), 7.31 (t, *J* = 6.8 Hz, 1H, $CH_2C_6H_5$-H_{para}), 7.37 (t, *J* = 6.8 Hz, 2H, $CH_2C_6H_5$-H_{meta}), 7.42 (d, *J* = 6.8 Hz, 2H, $CH_2C_6H_5$-H_{ortho}).^{13}C-NMR, δ_C (100.6 MHz, DMSO): 27.6 [CH, C3'(5',7')], 33.2 (C, C1'), 36.3 [CH_2, C4'(6',10')], 39.5 [CH_2, C2'(8',9')], 69.2 (CH_2, $\underline{C}H_2O$), 127.5 (C, Ar-C), 127.7 (CH, $CH_2C_6H_5$-C_{ortho}), 127.8 (CH, $CH_2C_6H_5$-C_{para}), 128.6 (CH, $CH_2C_6H_5$-C_{meta}), 130.1 (CH, Ar-C), 136.9 (C, $CH_2C_6H_5$-C_{ipso}), 159.1 (C, C3). No all the C signals were observed. MS-DIP (EI), m/e (%); main ions: 347 ($M^{\cdot+}$, 100), 212 (97), 93 (11), 91 (37). Anal. Calcd. for $C_{24}H_{29}NO\cdot HCl$ (383.96): C 75.08, H 7.88, N 3.65, Cl 9.23. Calcd. for $C_{24}H_{29}NO\cdot HCl\cdot 0.1H_2O$ (385.76): C 74.74, H 7.89, N 3.63, Cl 9.19. Found: C 74.74, H 7.80, N 3.55, Cl 9.16.

N-[(adamantan-1-yl)methyl]-3-(trifluoromethoxy)aniline hydrochloride, 11h.[60] Following the general procedure F, the reduction of amide **10h** (0.5g, 1.47 mmol) with sodium bis-(2-methoxyethoxy)aluminum hydride (65% wt solution in toluene, 2.6 ml, 8.84 mmol), get the corresponding amine as an oil (0.41g, 87%) . The corresponding purified amine hydrochloride **11h** was obtained after treatment with Et_2O/HCl, mp = 195-196 ºC. IR (ATR) ν: 2902, 1428, 1251, 1213, 116, 864, 791, 681 cm^{-1}. HRMS-ESI^+ m/z $[M+H]^+$: calcd for $[C_{18}H_{23}F_3NO+H^+]$: 326.17, found: 326.1728.

***N*-[(adamant-1-yl)methyl]-2-(trifluoromethyl)aniline hydrochloride, 11i**. Following the general procedure G, the reduction of amide **10i** (0.3 g, 0.93 mmol) with $BH_3\cdot THF$ (1M in THF, 3.72 mmol), gave the corresponding amine as an oil (0.18 g, 62%). The purified amine hydrochloride **11i** was obtained after a treatment with

Et_2O/HCl (0.6 N) and a crystallization from methanol. mp = 71-72 °C. IR (ATR) ν: 3367, 2906, 2845, 1612, 1585, 1514, 1461, 1292, 1245, 1162, 1095, 1029, 741, 659 cm^{-1}. ^{1}H-NMR, δ_H (400 MHz, DMSO): 1.51 (bs, 6H, adamantyl-CH_2), 1.52-1.69 (m, 6H, adamantyl-CH_2), 1.94 [broad s, 3H, 3'(5',7')-H], 2.89 (s, 2H, C$\underline{H}_2$N), 4.72 (broad signal, 1H, NH), 6.65 (t, *J* = 7.5 Hz, 1H, Ar-H), 6.90 (d, *J* = 8.0 Hz, 1H, Ar-H), 7.37 (complex signal, 2H, Ar-H). ^{13}C-NMR, δ_C (100.6 MHz, DMSO): 27.7 [CH, C3'(5',7')], 34.2 (C, C1), 36.5 [CH_2, C4'(6',10')], 40.0 [CH_2, C2'(8',9')], 54.0 (CH_2, $\underline{C}H_2$N), 111.0 (C, q, J = 28.6 Hz, 2C), 112.1 (CH, 6C), 114.9 (CH, 4C), 125.3 (C, q, *J* = 272.1 Hz, CF_3), 126.1 (CH, q, *J* = 5.3 Hz, 3C), 133.4 (CH, 5C), 146.3 (C, q, *J* = 1.5 Hz, 1C). MS-DIP (EI), m/e (%); main ions: 309 ($M^{\cdot+}$, 100), 174 (64), 154 (33), 135 (58), 93 (12), 91 (7), 79 (13).

***N*-[(adamant-1-yl)methyl]-3-(trifluoromethyl)aniline hydrochloride, 11j**. Following the general procedure F, the reduction of amide **10j** (1 g, 3.1 mmol) with sodium bis-(2-methoxyethoxy)aluminum hydride (65% solution in toluene, 3.7 mL, 12.4 mmol), gave the corresponding amine as an oil (0.99 g, quantitative yield). The corresponding purified amine hydrochloride **11j** was obtained after a treatment with Et_2O/HCl (0.6 N) and a crystallization from methanol. mp = 193-197 °C. IR (ATR) ν: 2916, 2851, 2494, 2417, 1582, 1470, 1435, 1327, 1171, 1123, 1096, 797, 692 cm^{-1}. ^{1}H-NMR, δ_H (400 MHz, DMSO, 50°C): 1.56 (s, 6H, adamantyl-CH_2), 1.57-1.70 (complex signal, 6H, adamantyl-CH_2), 1.95 [broad s, 3H, 3'(5',7')-H], 2.75 (s, 2H, CH_2N), 4.38 (broad s, NH), 6.77 (d, *J* = 7.6 Hz, 1H, 6-H), 6.90 (dd, *J* = 8.0 Hz, *J* = 2.0 Hz, 1H, 4-H), 6.94 (broad s, 1 H, 2-H), 7.24 (t, *J* = 8.0 Hz, 1H, 5-H). ^{13}C-NMR, δ_C (100.6 MHz, DMSO, 50°C): 27.7 [CH, C3'(5',7')], 33.8 (C, C1'), 36.4 [CH_2, C4'(6',10')], 39.8 [CH_2, C2'(8',9')], 55.2 (CH_2, $\underline{C}H_2$N), 108.2 (CH, C2), 111.2 (CH, C4), 115.3 (CH, C6), 124.3 (C, q, *J* = 273.7 Hz, CF_3), 129.5 (CH, C5), 129.6 (C, q, *J* = 30.7 Hz, C3), 149.7

(C, C1). MS-DIP (EI), m/e (%); main ions: 309 ($M^{\cdot+}$, 80), 290 (9), 174 (82), 135 (100), 93 (19), 79 (21). Anal. Calcd. for $C_{18}H_{22}F_3N \cdot HCl$ (345.83): C 62.51, H 6.70, N 4.05, Cl 10.25, F 16.48. Found: C 62.71, H 6.72, N 3.99, Cl 10.12, F 16.28.

***N*-[(adamant-1-yl)methyl]-4-(trifluoromethyl)aniline hydrochloride, 11k**. Following the general procedure G, the reduction of amide **10k** (0.5 g, 1.6 mmol) with $BH_3 \cdot THF$ (1M in THF, 6.4 mmol), gave the corresponding amine as an oil (0.3 g, 61%). The corresponding purified amine hydrochlororide **11k** was obtained after a treatment with Et_2O/HCl (0.6 N) and a crystallization from methanol. mp = 168-171°C. IR (ATR) ν: 2912, 2849, 2499, 2414, 1617, 1518, 1452, 1414, 1319, 1168, 1129, 1070, 1020, 847, 647 cm^{-1}. ^{1}H-NMR, δ_H (400 MHz, CD_3OD): 1.67 (bs, 6H, adamantyl-CH_2), 1.71-1.81 (m, 6H, adamantyl-CH_2), 2.02 [broad s, 3H, 3'(5',7')-H], 2.95 (s, 2H, C$\underline{H_2}$N), 4.87 (broad signal, NH), 7.09 [d, *J* = 8.4 Hz, 2H, 2(6)-H], 7.53 [d, *J* = 8.4 Hz, 2H, 3(5)-H].^{13}C-NMR, δ_C (100.6 MHz, CD_3OD): 29.7 [CH, C3'(5',7')], 35.0 (C, C1), 37.9 [CH_2, C4'(6',10')], 41.2 [CH_2, C2'(8',9')], 60.2 (CH_2, $\underline{C}H_2$N), 117.1 [CH, C2(6)], 127.7 [CH, C3(5)], 149.3 (C, C1). The signal from CF_3 was not observed. Anal. Calcd. for $C_{18}H_{22}ClF_3N \cdot HCl$ (345.83): C 62.51, H 6.70, N 4.05, Cl 10.25, F 16.48. Calcd. for $C_{18}H_{22}ClF_3N \cdot HCl \cdot 1/2H_2O$ (354.84): C 60.93, H 6.82, N 3.95. Found: C 61.01, H 6.57, N 3.71.

***N*-[(adamant-1-yl)methyl]-4-chloroaniline hydrochloride, 11l**.[59] Following the general procedure F, the reduction of amide **10l** (0.25 g, 0.86 mmol) with sodium bis-(2-methoxyethoxy)aluminum hydride (65% solution in toluene, 1.03 mL, 3.44 mmol), gave the corresponding amine as an oil (0.21 g, 91%). The corresponding purified amine hydrochloride **11l** was obtained after a treatment with Et_2O/HCl (0.6 N) and a crystallization from methanol. mp = 186-190 °C. IR (ATR) ν: 2899, 2845, 2660, 1582, 1491, 1415, 1095, 818 cm^{-1}. ^{1}H-NMR, δ_H (400 MHz, DMSO): 1.58-1.69 (complex

signal, 12H, adamantyl-CH_2), 1.95 [broad s, 3H, 3'(5',7')-H], 2.77 (s, 2H, CH_2N), 6.94 [broad d, *J* = 7.6 Hz, 2H, 2(6)-H], 7.20 [d, J = 8.8 Hz, 2H, 3(5)-H].^{13}C-NMR, δ_C (100.6 MHz, DMSO): 27.7 [CH, C3'(5',7')], 33.6 (C, C1'), 36.4 [CH_2, C4'(6',10')], 39.7 [CH_2, C2'(8',9')], 58.3 (CH_2, $\underline{C}H_2N$), 136.7 (CH, Ar-C). Only an aromatic signal was observed. MS-DIP (EI), m/e (%); main ions: 277 ($M^{\cdot+}$, ^{37}Cl, 36), 275 ($M^{\cdot+}$, ^{35}Cl, 100), 142 (29), 140 (86), 139 (29), 135 (37), 93 (11), 91 (7), 79 (11). Anal. Calcd. for $C_{17}H_{22}ClN{\cdot}HCl$ (312.28): C 65.39, H 7.42, N 4.49, Cl 22.70. Calcd. for $C_{17}H_{22}ClN{\cdot}1.6HCl{\cdot}0.9H_2O$ (332.14): C 61.48, H 7.56, N 4.22, Cl 22.42. Found: C 61.66, H 7.15, N 4.03, Cl 22.01.

N-[(adamantan-1-yl)methyl]-2-bromoaniline hydrochloride, 11m. Following the general procedure F, the reduction of amide **10m** (0.9g, 2.69 mmol) with sodium bis(2methoxyethoxy)aluminum hydride (65% wt solution in toluene, 3.21ml, 10.76 mmol), get the corresponding amine **11m** as an oil (0.74g, 85.87%) . The corresponding purified amine hydrochloride was obtained after the working with Et_2O/HCl (0.6N). mp= 189-190 ºC. IR (ATR) ν: 2909, 2847, 2642, 1566, 1440, 1392, 1060, 989, 851, 757 cm^{-1}. ^{1}H-NMR, δ_H (400 MHz, DMSO): 1.54 [d, *J'*=2.8 Hz, 6H, 2'(8',9')-H_2], 1.60-1.67 [m, 6H, 4'(6',10')-H_2], 1.95 [s, 3H, 3'(5',7')-H], 2.87 (s, 2H, C$\underline{H_2}$N), 6.5 (dt, *J''*=1.5 Hz, *J'*=7.5 Hz, *J* = 7.6 Hz, 1H, H_{AR}), 6.79 (dd, *J'*=1.5 Hz, *J* = 8.31 Hz, 1H, H_{AR}), 7.10 (ddd, *J''*=1.5 Hz, *J'*=7.3 Hz, *J* = 8.6 Hz, 1H, H_{AR}), 7.23 (dd, *J'*=1.6 Hz, *J* = 7.9 Hz, 1H, H_{AR}). ^{13}C-NMR, δ_C (100.6 MHz, MeOD): 29.3 [CH, C3'(5',7')], 34.2 [CH_2, C4'(6',10')], 37.3 [CH_2, C2'(8',9')], 40.5 (C, C1'), 63.9 (CH_2, $\underline{C}H_2N$), 123.6 (C, C2), 126.6 (CH, C6*), 129.6 (CH, C4*), 129.8 (CH, C3), 131.9 (CH, C5), 136.6 (C, C1). Anal. Calcd. for $C_{17}H_{22}BrN$ (320.27): C 63.75, H 6.92, N 4.37. Calcd. for $C_{17}H_{22}BrN$ ·0.4 toluene (357.12): C 66.59, H 7.11, N 3.92. Found: C 66.56, H 7.52, N 4.39.

***N*-[(Adamantan-1-yl)methyl]-2-chloroaniline hydrochloride, 11n**.[59] Following the general procedure F, the reduction of amide **10n** (1g, 3.45 mmol) with sodium bis(2methoxyethoxy)aluminum hydride (65% wt solution in toluene, 4.11 ml, 13.8 mmol), get the corresponding amine **11n** as an oil (0.99g, 95%) . The corresponding purified amine hydrochloride was obtained after treatment with Et_2O/HCl (0.6N). Mp = 224-225 ºC. IR (ATR) ν: 2895, 2846, 2649, 1580, 1488, 1429, 1394, 1372, 1184, 1106, 992, 749, 717, 690 cm^{-1}. ^{1}H-NMR, δ_H (400 MHz, MeOD): 1.57-1.92 [cs, 12H, 2'(4',6',8',9',10')-H_2], 2.07 [s, 3H, 3'(5',7')-H], 3.12 (s, 2H, C$\underline{H_2}$N), 7.22-7.78 (cs, 4H, H_{AR}). ^{13}C-NMR, δ_C (100.6 MHz, MeOD): 28.0 [CH, C3'(5',7')], 32.5 (C, C1'), 36.0 [CH_2, C2'(8',9')], 39.2 [CH_2, C4'(6',10')], 65.4 (CH_2, $\underline{C}H_2$N), 122.5 (C, q, C2), 129.5 (CH, 2 C_{AR}), 130.2 (CH, 2 C_{AR}), 136.7 (C, C1). HRMS-ESI$^+$ m/z $[M+H]^+$: calcd for [$C_{17}H_{22}ClN+H^+$]: 276.14, found: 276.1521.

***N*-[(adamant-1-yl)methyl]-3-chloroaniline hydrochloride, 11o**.[59] Following the general procedure F, the reduction of amide **10o** (1 g, 3.46 mmol) with sodium bis-(2-methoxyethoxy)aluminum hydride (65% wt solution in toluene, 4.14 mL, 13.84 mmol), gave the corresponding amine as an oil (0.79 g, 83%). The corresponding purified amine hydrochloride **11o** was obtained after a treatment with Et_2O/HCl (0.6 N) and a crystallization from methanol. mp = 187-190 °C. IR (ATR) ν: 2901, 2846, 2682, 2416, 1597, 1578, 1481, 1426, 1098, 989, 878, 785, 678 cm^{-1}. ^{1}H-NMR, δ_H (400 MHz, DMSO): 1.53 (bs, 6H, adamantyl-CH_2), 1.63 (m, 6H, adamantyl-CH_2), 1.94 [broad s, 3H, 3'(5',7')-H], 2.70 (s, 2H, C$\underline{H_2}$N), 3.89 (broad signal, NH), 6.48 (dd, J = 8.0 Hz, J' = 1.5 Hz, 1H, 6-H), 6.59 (dd, J = 8.4 Hz, J' = 1.5 Hz, 1H, 4-H), 6.66 (t, J = 1.5 Hz, 1H, 2-H), 7.03 (t, J = 8.0 Hz, 1H, 5-H). ^{13}C-NMR, δ_C (100.6 MHz, DMSO): 27.8 [CH, C3'(5',7')], 34.0 (C, C1), 36.6 [CH_2, C4'(6',10')], 39.9 [CH_2, C2'(8',9')], 55.2 (CH_2, $\underline{C}H_2$N), 110.9 (CH, C6), 111.4 (CH, C2), 114.8 (CH, C4), 130.2 (CH, C5), 133.5 (C,

C3), 150.8 (C, C1). MS-DIP (EI), m/e (%); main ions: 275 ($M^{\cdot+}$, 100), 140 (100), 135 (69), 93 (17), 79 (18), 77 (12).

N-[(adamantan-1-yl)methyl]-2,6-difluoroaniline hydrochloride, 11p. Following the general procedure F, the reduction of amide **10p** (1g, 3.43 mmol) with sodium bis-(2-methoxyethoxy)aluminum hydride (65% wt solution in toluene, 6.15 ml, 20.59 mmol), get the corresponding amine as an oil (0.87g, 92%) . The corresponding purified amine hydrochloride **11p** was obtained after treatment with Et_2O/HCl (0.6N). mp = 188-189 ºC. IR (ATR) ν: 2894, 2846, 1509, 1428, 1262, 1096, 956, 795 cm^{-1}. ^{1}H-NMR, δ_H (400 MHz, MeOD): 1.67 [s, 6H, 2'(8',9')-H_2], 1.70-1.84 [m, 6H, 4'(6',10')-H_2], 2.02 [s, 3H, 3'(5',7')-H], 2.95 (s, 2H, C$\underline{H_2}$N), 6.96 21 (dddd, *J'''*= 1.6 Hz, *J''*= 2.9 Hz, *J'*=8.2 Hz, *J*=9.1, 1H, H_{AR}), 7.08 (ddd, *J''*= 2.8 Hz, *J'*=8.6 Hz, *J*=11.4 Hz, 1H, H_{AR}), 7.21 (td, *J* = 9.2 Hz, 1H, H_{AR}). ^{13}C-NMR, δ_C (100.6 MHz, MeOD): 28.2 [CH, C3'(5',7')], 33.3 (C, C1'), 36.3 [CH_2, C2'(8',9')], 39.5 [CH_2, C4'(6',10')], 60.2 (CH_2, $\underline{C}H_2$N), 104.3 (CH, Ar-C_{para}), 111.4 (CH, Ar-C_{meta}), 119.0 (C, Ar- C_{ortho}) 120.8 (C, dd, *J* = 284.7 Hz, Ar-C1). HRMS-ESI$^+$ m/z [*M*+H]$^+$: calcd for [$C_{17}H_{21}F_2N$+H^+]: 278.16, found: 278.1724.

N-[(adamantan-1-yl)methyl)-3,5-difluoroaniline hydrochloride, 11q.[61] Following the general procedure F, the reduction of amide **10q** (1g, 3.43 mmol) with sodium bis(2methoxyethoxy)aluminum hydride (65% wt solution in toluene, 6.15 ml, 20.59 mmol), get the corresponding amine as an oil (0.88g, 93%) . The corresponding purified amine hydrochloride **11q** was obtained after treatment with Et_2O/HCl (0.6N). mp = 207-209 ºC. IR (ATR) ν: 2905, 2661, 1616, 1426, 1129, 983, 862, 681 cm^{-1}. ^{1}H-NMR, δ_H (400 MHz, $CDCl_3$): 1.48 [s, 6H, 2'(8',9')-H_2], 1.56-1.69 [m, 6H, 4'(6',10')-H_2], 1.94 [s, 3H, 3'(5',7')-H], 2.68 (d, *J*=6.0 Hz, 2H, C$\underline{H_2}$N), 3.84 (s, N$\underline{H}$), 5.88-6.16 (m, 3H, H_{AR}). HRMS-ESI$^+$ m/z [*M*+H]$^+$: calcd for [$C_{17}H_{21}F_2N$+H^+]: 278.16, found: 278.1722.

N-[(adamantan-1-yl)methyl]-3,5-dichloroaniline hydrochloride, 11r.[61] Following the general procedure F, the reduction of amide **10r** (1g, 3.08 mmol) with sodium bis(2-methoxyethoxy) aluminum hydride 65% wt solution in toluene, 3.68 ml, 12.35 mmol), get the corresponding amine as an oil (0.85g, 89%) . The corresponding purified amine hydrochloride **11r** was obtained after treatment with Et_2O/HCl (0.6N). mp = 194-195 ºC. IR (ATR) ν: 2900, 2846, 2657, 1586, 1415, 1106, 914, 862, 802, 674 cm^{-1}. ^{1}H-NMR, δ_H (400 MHz, DMSO): 1.50 [d, *J*=1.8 Hz, 6H, 2'(8',9')-H_2], 1.62 [m, 6H, 4'(6',10')-H_2], 1.92 [s, 3H, 3'(5',7')-H], 2.69 (s, 2H, C$\underline{H_2}$N), 3.55 (s, N$\underline{H}$), $\underline{6}$.48 (t, *J'* = 1.8 Hz, *J* = 2.0 Hz, 1H, H_{Ar}), 6.60 (d, *J* = 1.8 Hz, 2H, H_{Ar}). HRMS-ESI$^+$ m/z [*M*+H]$^+$: calcd for [$C_{17}H_{21}Cl_2N$+H^+]: 310.11, found: 310.1131.

N-[(adamantan-1-yl)methyl]-3,5-bis(trifluoromethyl)aniline hydrochloride, 11s. Following the general procedure F, the reduction of amide **10s** (1g, 2.56 mmol) with sodium bis-(2-methoxyethoxy)aluminum hydride (65% wt solution in toluene, 3.05 ml, 10.24 mmol), get the corresponding amine as an oil (0.53g, 55%). The corresponding purified amine hydrochloride **11s** was obtained after treatment with Et_2O/HCl (0.6N). mp = 170-171 ºC. IR (ATR) ν: 2906, 2641, 1585, 1434, 1369, 1274, 1166, 1129, 886, 681 cm^{-1}. ^{1}H-NMR, δ_H (400 MHz, DMSO): 1.54 [s, 6H, 2'(8',9')-H_2], 1.63 [M, 6H, 4'(6',10')-H_2], 1.94 [s, 3H, 3'(5',7')-H], 2.79 (s, 2H, C$\underline{H_2}$N), 6.95 (s, 1H, H_{Ar}), 7.15 (s, 2H, H_{Ar}). ^{13}C-NMR, δ_C (100.6 MHz, MeOD): 29.2 [CH, C3'(5',7')], 35.1 (C, C1'), 37.8 [CH_2, C2'(8',9')], 41.3 [CH_2, C4'(6',10')], 57.4 (CH_2, $\underline{C}H_2$N), 110.1 (CH, Ar-C_{para}), 113.5 (CH, Ar-C_{ortho}), 125.9 (CH, d, *J* = 271.62, $\underline{C}F_3$), 133.1 (C, m, Ar-C_{meta}), 150.6 (C, C1). HRMS-ESI$^+$ m/z [*M*+H]$^+$: calcd for [$C_{19}H_{21}F_6N$+H^+]: 378.16, found: 378.1662.

***N*-[(adamant-1-yl)methyl]-3-fluoro-5-(trifluoromethyl)aniline hydrochloride, 11t**. Following the general procedure F, the reduction of amide **10t** (1 g, 3.03 mmol) with sodium bis-(2-methoxyethoxy)aluminum hydride (65% solution in toluene, 3.62 mL,

12.12 mmol), gave the corresponding amine as an oil (0.8 g, 83%). The corresponding purified amine hydrochloride **11t** was obtained after a treatment with Et_2O/HCl (0.6 N) and a crystallization from methanol. mp = 146-149 °C. IR (ATR) ν: 2898, 2852, 2488, 2414, 1610, 1581, 1434, 1348, 1180, 1139, 981, 867, 689 cm^{-1}. ^{1}H-NMR, δ_H (400 MHz, DMSO): 1.53-1.69 (complex signal, 12H, adamantyl-CH_2), 1.94 [broad s, 3H, 3'(5',7')-H], 2.74 (s, 2H, CH_2N), 5.65 (broad s, 1H, NH), 6.52 (broad d, *J* = 8.8 Hz, 1H, 4-H), 6.64 (dt, *J* = 12.4 Hz, *J* = 2Hz, 1H, 2-H), 6.80 (broad s, 1H, 6-H). ^{13}C-NMR, δ_C (100.6 MHz, DMSO): 27.7 [CH, C3'(5',7')], 34.0 (C, C1'), 36.5 [CH_2, C4'(6',10')], 39.8 [CH_2, C2'(8',9')], 54.7 (CH_2, $\underline{C}H_2N$), 97.3 (CH, d, *J* = 25.8 Hz, C4), 100.5 (CH, d, *J* = 26.0 Hz, C2), 104.9 (CH, C6), 131.1 (broad C, C5), 152.4 (C, C1), 163.3 (C, d, *J* = 240.9 Hz, C3). The signal from the CF_3 group is not clearly visible. MS-DIP (EI), m/e (%); main ions: 327 ($M^{\cdot+}$, 62), 309 (13), 192 (26), 135 (100), 93 (16), 91 (7), 79 (15). Anal. Calcd. for $C_{18}H_{21}F_4N$·HCl (363.82): C 59.42, H 6.10, N 3.85, Cl 9.74, F 20.89. Found: C 59.69, H 6.45, N 3.79, Cl 9.45, F 20.95.

***N*-[(adamant-1-yl)methyl]-3-chloro-5-(trifluoromethyl)aniline hydrochloride, 11u**. Following the general procedure F, the reduction of amide **10u** (1 g, 2.84 mmol) with sodium bis-(2-methoxyethoxy)aluminum hydride (65% solution in toluene, 3.40 mL, 11.36 mmol), gave the corresponding amine as an oil (0.91 g, 95%). The corresponding purified amine hydrochloride **11u** was obtained after a treatment with Et_2O/HCl (0.6 N) and a crystallization from methanol. mp = 132-138 °C. IR (ATR) ν: 2900, 2852, 2476, 2410, 1577, 1435, 1322, 1176, 1138, 1103, 867, 832, 686 cm^{-1}. ^{1}H-NMR, δ_H (400 MHz, DMSO): 1.53-1.69 (complex signal, 12H, adamantyl-CH_2), 1.94 [broad s, 3H, 3'(5',7')-H], 2.74 (s, 2H, CH_2N), 5.87 (broad s, 1H, NH), 6.72 (s, 1H, Ar-H), 6.88 (broad s, 2H, Ar-H).^{13}C-NMR, δ_C (100.6 MHz, DMSO): 27.7 [CH, C3'(5',7')], 34.0 (C, C1'), 36.5 [CH_2, C4'(6',10')], 39.8 [CH_2, C2'(8',9')], 54.5 (CH_2, $\underline{C}H_2N$), 107.0

(CH, C6), 109.9 (CH, C4), 113.6 (CH, C2), 123.7 (C, q, *J* = 272.7 Hz, CF_3), 131.1 (C, q, *J* = 31.6 Hz, C5), 134.5 (C, C3), 151.6 (C, C1). MS-DIP (EI), m/e (%); main ions: 343 ($M^{\cdot+}$, 63), 208 (25), 135 (100), 93 (15), 91 (7), 79 (14). Anal. Calcd. for $C_{18}H_{21}ClF_3N{\cdot}HCl$ (380.28): C 56.85, H 5.83, N 3.68, Cl 18.64, F 14.99. Found: C 57.01, H 5.95, N 3.60, Cl 18.53, F 14.79.

***N*-[(adamant-1-yl)methyl]-4-chloro-3-(trifluoromethyl)aniline hydrochloride, 11v**. Following the general procedure F, the reduction of amide **10v** (1 g, 3.46 mmol) with sodium bis-(2-methoxyethoxy)aluminum hydride (65% solution in toluene, 4.14 mL, 13.84 mmol), gave the corresponding amine as an oil (1.9 g, quantitative yield). The corresponding purified amine hydrochloride **11v** was obtained after a treatment with Et_2O/HCl (0.6 N) and a crystallization from methanol. mp = 159-164 °C. IR (ATR) ν: 2908, 2498, 2415, 1483, 1461, 1425, 1317, 1266, 1185, 1134, 1039, 834 cm^{-1}. ^{1}H-NMR, δ_H (400 MHz, DMSO): 1.53 (s, 6H, adamantyl-CH_2), 1.54-1.68 (complex signal, 6H, adamantyl-CH_2), 1.93 [broad s, 3H, 3'(5',7')-H], 2.72 (s, 2H, CH_2N), 4.75 (broad s, NH), 6.83 (dd, *J* = 8.8 Hz, *J'* = 2.8 Hz, 1H, 6-H), 7.06 (d, *J* = 2.8 Hz, 1H, 2-H), 7.27 (t, *J* = 9.2 Hz, 1H, 5-H).^{13}C-NMR, δ_C (100.6 MHz, DMSO): 27.8 [CH, C3'(5',7')], 34.0 (C, C1'), 36.6 [CH_2, C4'(6',10')], 39.9 [CH_2, C2'(8',9')], 54.9 (CH_2, $\underline{C}H_2N$), 110.7 (CH, C2), 114.2 (C, C4), 115.4 (CH, C6), 123.2 (C, q, *J* = 272.8 Hz, CF_3), 126.6 (C, q, *J* = 30.0 Hz, C3), 131.8 (CH, C5), 148.8 (C, C1). MS-DIP (EI), m/e (%); main ions: 343 ($M^{\cdot+}$, 90), 210 (15), 209 (11), 207 (22), 135 (100), 93 (16), 91 (8), 79 (15). Anal. Calcd. for $C_{18}H_{21}ClF_3N{\cdot}HCl$ (380.28): C 56.85, H 5.83, N 3.68, Cl 18.64, F 14.99. Calcd. for $C_{18}H_{21}ClF_3N{\cdot}HCl{\cdot}1/3MeOH$ (390.85): C 56.33, H 6.01, N 3.58, Cl 18.14, F 14.58. Found: C 56.25, H 5.99, N 3.54, Cl 17.89, F 14.93.

N-[(adamantan-1-yl)methyl]-2,3,4,5,6-pentafluoroaniline hydrochloride, 11w.[56] Following the general procedure F, the reduction of amide **10w** (1g, 2.9 mmol) with

sodium bis(2-methoxyethoxy) aluminum hydride (65% wt solution in toluene, 3.68 ml, 12.35 mmol), get the corresponding amine as an oil (0.65g, 68%) . The corresponding purified amine hydrochloride **11w** was obtained after treatment with Et_2O/HCl (0.6N). mp = 185-186 ºC. IR (ATR) ν: 2898, 2846, 2356, 1644, 1493, 1257, 1085, 870, 799 cm^{-1}. ^{1}H-NMR, δ_H (400 MHz, DMSO): 1.50 [s, 6H, 2'(8',9')-H_2], 1.62 [broad signal, 6H, 4'(6',10')-H_2], 1.92 [s, 3H, 3'(5',7')-H], 2.65 (s, 2H, C$\underline{H}_2$N). Anal. Calcd. for $C_{17}H_{19}ClF_5N$ (367.11): C 55.52, H 5.21, N 3.81. Calcd. for $C_{17}H_{19}ClF_5N$ ·0.1 toluene (376.99): C 56.39, H 5.29, N 3.72. Found: C 56.55, H 5.38, N 3.38.

N-[(3,5-dimethyladamantan-1-yl)methyl]-3-chloroaniline hydrochloride, 11x. Following the general procedure F, the reduction of amide **10x** (0.5 g, 1.6 mmol) with sodium bis-(2-methoxyethoxy)aluminum hydride (65% wt solution in toluene, 1.2 ml, 6.3 mmol), get the corresponding amine as an oil (0.44 g, 92%) . The corresponding purified amine hydrochloride **11x** was obtained after treatment with Et_2O/HCl (0.6N). mp = 157-160 ºC (dec). IR (ATR) ν: 2903, 2834, 2582, 2418, 2356, 1597, 1581, 1477, 1457, 1425, 1375, 1082, 1000, 984, 894, 873, 792, 704, 682 cm^{-1}. ^{1}H-NMR, δ_H (400 MHz, DMSO): 0.79 [s, 6 H, 3(5)-CH_3], 1.09 (m, 2H, adamantyl-CH_2), 1.17 (m, 4H, adamantyl-CH_2), 1.28 [m, 4H, adamantyl-CH_2], 1.37 (m, 2H, adamantyl-CH_2), 2.02 (m, 1 H, adamantyl-CH), 2.74 (s, 2H, C$\underline{H}_2$N), 5.27 (broad signal, NH), 6.49 (dd, *J* = 8.0 Hz, *J'* = 2.0 Hz, 1H, 6-H), 6.60 (dd, *J* = 8.0 Hz, *J'* = 2.0 Hz, 1H, 4-H), 6.67 (t, *J* = 2.0 Hz, 1H, 2-H), 7.03 (t, *J* = 8.0 Hz, 1H, 5-H). ^{13}C-NMR, δ_C (100.6 MHz, DMSO): 28.9 (CH, C7'), 30.5 [CH_3, C3(5)-$\underline{C}H_3$], 30.7 [C, C3(5)], 35.7 (CH_2, C4'), 38.5 [CH_2, C2'(9')]*, 42.8 [CH_2, C6'(10')]*, 46.2 (CH_2, C8'), 50.7 (CH_2, $\underline{C}H_2$N), 110.9 (CH, C6), 111.5 (CH, C2), 114.9 (CH, C4), 130.2 (CH, C5), 133.5 (C, C3), 150.7 (C, C1).

3-[(Phenylamino)methyl]adamantan-1-ol hydrochloride, 14a. Following the general procedure F, the reduction of amide **13a** (0.5 g, 1.8 mmol) with sodium bis-(2-methoxyethoxy)aluminum hydride (65% solution in toluene, 2.15 mL, 7.2 mmol), gave the corresponding amine as an oil (0.4 g, 85%). The corresponding purified amine hydrochloride **14a** was obtained after a treatment with Et_2O/HCl (0.6 N) and a crystallization from methanol. mp > 183 °C (dec). IR (ATR) ν: 3329, 2903, 2849, 2670, 2430, 1581, 1493, 1429, 1146, 1051, 755, 693 cm^{-1}.^{1}H-NMR, δ_H (400 MHz, DMSO): 1.49-1.54 (complex signal, 12H, adamantyl-CH_2), 2.12 [broad s, 2H, 5'(7')-H], 2.93 (s, 2H, CH_2N), 7.01-7.35 (complex signal, 5H, Ar-H).^{13}C-NMR, δ_C (100.6 MHz, DMSO): 29.7 [CH, C5'(7')], 35.1 (CH_2, C6'), 36.5 (C, C1'), 38.5 [CH_2, C8(9)], 44.4 [CH_2, C4(10)], 47.5 (CH_2, C2'), 59.7 (CH_2, $\underline{C}H_2N$), 66.6 (C, C3'), 129.5 (CH, Ar-C). Only an aromatic signal was observed. MS-DIP (EI), m/e (%); main ions: 257 ($M^{\cdot+}$, 50), 151 (6), 107 (20), 106 (100), 93 (12), 77 (11). Anal. Calcd. for $C_{17}H_{23}NO\cdot HCl$ (293.84): C 69.49, H 8.23, N 4.77, Cl 12.06. Calcd. for $C_{17}H_{23}NO\cdot HCl\cdot 1/3AcOEt$ (322.91): C 68.14, H 8.32, N 4.34, Cl 10.98. Found: C 67.81, H 7.96, N 4.28, Cl 11.18.

3-[((4-Chlorophenyl)amino)methyl]adamantan-1-ol hydrochloride, 14b. Following the general procedure F, the reduction of amide **13b** (0.33 g, 1.08 mmol) with sodium bis-(2-methoxyethoxy)aluminum hydride (65% solution in toluene, 1.30 mL, 4.32 mmol), gave the corresponding amine as an oil (0.24 g, 77%). The corresponding purified amine hydrochloride **14b** was obtained after a treatment with Et_2O/HCl (0.6 N) and a crystallization from methanol. mp > 172 °C (dec). IR (ATR) ν: 2913, 2844, 1575, 1489, 1457, 1414, 1339, 1146, 1093, 1052, 902, 823 cm^{-1}.^{1}H-NMR, δ_H (400 MHz, DMSO): 1.43-1.56 (complex signal, 12H, adamantyl-CH_2), 2.10 [broad s, 2H, 5'(7')-H], 2.81 (s, 2H, CH_2N), 6.61 (broad s, 1H, NH), 6.88 [d, J = 8.5 Hz, 2H, 2(6)-H], 7.17 [d, J = 8.5 Hz, 2H, 3(5)-H].^{13}C-NMR, δ_C (100.6 MHz, DMSO): 29.8 [CH,

C5'(7')], 35.3 (CH_2, C6'), 37.2 (C, C1'), 39.4 [CH_2, C8(9)], 44.6 [CH_2, C4(10)], 47.8 (CH_2, C2'), 56.6 (CH_2, $\underline{C}H_2N$), 66.7 (C, C3'), 128.7 (CH, Ar-C). Only an aromatic signal was observed. MS-DIP (EI), m/e (%); main ions: 293 ($M^{\cdot+}$, ^{37}Cl, 20), 291 ($M^{\cdot+}$, ^{35}Cl, 61), 142 (34), 141 (30), 140 (100), 139 (19), 95 (14), 93 (16). Anal. Calcd. for $C_{17}H_{22}ClNO\cdot HCl$ (328.28): C 62.20, H 7.06, N 4.27, Cl 21.60. Calcd. for $C_{17}H_{22}ClNO\cdot 1/10HCl\cdot 1/5H_2O$ (335.53): C 60.85, H 7.06, N 4.17, Cl 22.19. Found: C 60.74, H 6.80, N 4.06, Cl 22.00.

2-(Adamant-1-yl)-*N*-(2-isopropylphenyl)acetamide, 16. Following the general procedure D, from 2-(adamant-1-yl)acetyl chloride (0.50 g, 2.38 mmol) in anh. acetone (3 mL), and a solution of 2-isopropylaniline (0.34 mL, 2.38 mmol) in triethylamine (0.37 mL, 2.62 mmol), the product was obtained as a yellow semisolid (663 mg, 93.6% yield). Crystallization from hot acetone gave a white solid (440 mg). mp = 158-159 ºC. IR (ATR) ν: 670, 705, 725, 753, 920, 945, 966, 988, 1029, 1084, 1100, 1150, 1198, 1244, 1266, 1312, 1340, 1375, 1446, 1491, 1504, 1600, 1648, 2845, 2896, 2962, 3286 cm^{-1}. ^{1}H-NMR (400 MHz, $CDCl_3$) δ: 1.25 [d, *J* = 6.8 Hz, 6 H, -CH($C\underline{H}_3$)$_2$], 1.60-1.78 [c. s., 12 H, 2'(8',9')-H_2 and 4'(6',10')-H_2], 2.00 [m, 3 H, 3'(5',7')-H], 2.13 (s, 2 H, 7-H_2), 3.03 [sept, *J* = 6.8 Hz, 1 H, -C$\underline{H}$(CH_3)$_2$], 6.95 (broad s, 1 H, NH), 7.12-7.22 (c. s., 2 H, 4-H and 5-H), 7.28 (dd, 1 H, *J* = 7.2 Hz, *J'* = 2.0, 6-H), 7.72 (dd, *J* = 7.2 Hz, *J'* = 1.6 Hz, 1 H, 3-H). ^{13}C-NMR (100.5 MHz, $CDCl_3$) δ: 23.1 [CH_3, -CH($\underline{C}H_3$)$_2$], 28.0 [CH, -$\underline{C}$H(CH_3)$_2$], 28.6 [CH, C3'(5',7')], 33.2 (C, C1'), 36.7 [CH_2, C4'(6',10')], 42.7 [CH_2, C2'(8',9')], 52.7 (CH_2, C7), 124.6 (CH, C6), 125.5 (CH, C5), 125.8 (CH, C3), 126.3 (CH, C4), 134.2 (C, C1), 140.1 (C, C2), 169.6 (C, CO). HRMS-ESI+ m/z [*M*+H]$^+$ calcd for [$C_{21}H_{29}NO$+H]$^+$: 312.2322, found: 312.2328.

***N*-[2-(Adamant-1-yl)ethyl]-2-isopropylaniline hydrochloride, 17**. Following the general procedure F, amide **16** (0.370 g, 1.18 mmol) and sodium bis-(2-

methoxyethoxy)aluminum hydride (65% wt solution in toluene, 1.15 mL, 5.90 mmol) in anhydrous toluene (9.5 mL), gave **17** as a yellow oil (340 mg, 86.3%) that formed its hydrochloride salt as a yellow solid after the treatment with HCl/Et_2O (312 mg). mp = 70-71 ºC. IR (ATR) ν: 705, 720, 761, 816, 935, 978, 993, 1024, 1054, 1072, 1097, 1155, 1239, 1271, 1317, 1342, 1362, 1385, 1448, 1494, 1552, 1577, 1739, 2359, 2445, 2653, 2845, 2901, 2951, 3397 cm^{-1}. ^{1}H-NMR (400 MHz, CD_3OD) δ: 1.34 [d, *J* = 6.8 Hz, 6 H, -CH($C\underline{H}_3$)$_2$], 1.50-1.60 [c. s., 6 H, 2'(8',9')-H_2 and 8-H_2], 1.64-1.80 [c. s., 6 H, 4'(6',10')-H_2], 1.96 [m, 3 H, 3'(5',7')-H], 3.07 [sept, *J* = 6.8 Hz, 1 H, -C$\underline{H}$(CH_3)$_2$], 3.35 (m, 2 H, 7-H_2), 7.37-7.42 (c. s., 2 H, 4-H and 6-H), 7.53 (m, 1 H, 5-H), 7.60 (d, 1 H, *J* = 7.6 Hz, 3-H). ^{13}C-NMR (100.5 MHz, $CDCl_3$) δ: 24.5 [CH_3, -CH($\underline{C}H_3$)$_2$], 28.9 (C, C1'), 29.9 [CH, C3'(5',7') and -$\underline{C}$H(CH_3)$_2$], 32.8 (CH_2, C8), 37.8 [CH_2, C4'(6',10')], 40.6 (CH_2, C7), 43.0 [CH_2, C2'(8',9')], 124.5 (CH, C6), 128.9 (CH, C4), 129.6 (CH, C5), 131.6 (CH, C3), 133.1 (C, C2), 143.6 (C, C1). HRMS-ESI+ m/z [*M*+H]$^+$ calcd for [$C_{21}H_{31}N$+H]$^+$: 298.2529, found: 298.2524.

Molecular modeling

Homology modelling and electrostatic surface potential analysis. The PDB code 3EYM[18] of H3 X31 co-crystallized with TBHQ was used as template to generate the 3D models of A/PuertoRico/8/1934 H1N1 (UniprotKB code: I6TAG2), A/Virginia/ATCC3/2009 H1N1 (ATCC® VR-1736™, purchased from ATCC) and A/HongKong/7/1987 H3N2 (UniprotKB code: Q38TH2) variants of HA. This was accomplished taking advantage of a sequence identity higher than 50% between the template and target sequences. Internal sequence comparison for the three strains revealed a sequence identity that goes from 81% among A/PuertoRico/8/1934 and A/Virginia/ATCC3/2009 to about 42% for the previous two ones and A/HongKong/7/1987.

After their generation, all the three models were minimized with the staged minimization option on SYBYL (Tripos force field),[62] using the Powell optimization method with Gasteiger-Hückel point charges,[63] a non-bonded cutoff of 8.0 Å, a dielectric constant of 2.0, and a convergence of 0.001 kcal mol^{-1} $Å^{-1}$ or maximum number of 1,500 iterations. After visual inspection of the optimized structures, linearized Poisson-Boltzmann calculations as implemented in APBS (Adaptive Poisson-Boltzmann solver)[64-65] were performed to screen the solvent-dependent electrostatic properties of the previously minimized A/PR, A/Virginia and A/HK HA models. In this regards, a single-point multigrid PB calculation without focusing with a grid spacing of 0.70 Å/point was used. Default parameters of Amber force field were used to set the atomic partial charges and radii of the atoms. A dielectric constant of 2.0 and 78.5 was considered respectively for the biopolymer and the solvent.

Molecular Docking. Surflex-Dock[66] as implemented in Sybyl X2.1 – Tripos, was used to perform molecular docking of compounds RL-007 (**1d**), RL-010 (**7c**) and SCG007 (**2c**) (**Figure 4**) within the TBHQ binding site generated by homology modelling on A/PR, A/Virginia and A/HK models. The binding site was defined considering the area covered by a radius of 12 Å around the residue Tyr308 (for A/PR), Phe309 (for A/Virginia) and Phe310 (for A/HK). Docking-guided conformational exploration of the binding site was performed by molecular fragmentation. A maximum of 20 conformations per fragment were generated. The maximum number of poses per ligand was set to 20 with a minimum RMSD between final poses of 0.50 Å.

Molecular Dynamics simulations. Amber12[67] was used to perform MD simulations on the selected ligand–protein complexes previously generated by docking analysis. In this context, the general Amber force field (GAFF)[68] was used to parameterize the ligand, and the partial charges were derived at the B3LYP/6-31G(d) level,[69] after preliminary

optimization of the molecular structure, by using the restrained electrostatic potential (RESP)[70] fitting method implemented in Gaussian09 and Antechamber.

The conformational preferences of the ligand in water solution were explored by using the multilevel conformational sampling technique.[71-72] To this end, the ligand was immersed in a truncated octahedral (TIP3P) water box with a layer of 12 Å and neutralized by adding Cl^- ions. Before MD production, the solvated and neutralized ligand was minimized, heated in 200 ps by rising the temperature from 50 to 298 K at constant volume, and finally equilibrated in 200 ps MD simulation at constant pressure and temperature (1 bar, 298 K). 600 ns of classical MD simulation in PBC conditions at constant volume and temperature with an integration time step of 1 fs was carried out by using the CUDA-accelerated version of the PMEMD module of Amber12. Finally, sampling of conformational space to extract the most representative conformers obtained during classical MD simulation for the solvated ligand was realized following the original procedure reported in previous works. The relative stability of the conformational families was determined by combining single-point MP2/aug-cc-pVDZ calculations for representative conformers optimized at the B3LYP/6-31G(d) level taking into account solvent effects via the IEF-PCM/MST solvation model.[69]

MD simulations were carried out to analyse the conformational flexibility of compound RL007 within the protein environment formed by A/PR and A/Virginia HA models. Accordingly, the two RL007-A/PR and RL007-A/Virginia complexes were solvated with a truncated octahedral (TIP3P)[73] water box with a layer of 18 Å and neutralized by adding Na^+ ions. Complexes were subjected to three-stages of energy minimization that involved firstly all hydrogen atoms, then water molecules, and finally all the system with a maximum number of minimization cycles of 10000 for the latter stage. Before MD simulation, a preliminary heating of the system from 0 to 300 K was

accomplished in six steps, the first being performed at constant volume and the rest at constant pressure. The SHAKE algorithm[74] was applied to constrain bonds involving hydrogen atoms. Periodic boundary conditions at constant volume were imposed on the system during the MD simulations. Cut-off for the non-bonded interactions was set to 10 Å. The electrostatic interactions beyond the cut-off within the periodic box were computed by applying the Particle Mesh Ewald (PME) method.[75] Langevin dynamics with a collision frequency of 1.0 was applied for temperature regulation during the heating. Finally, 50 ns of MD simulation at constant volume and temperature (300 K) were run using the weak-coupling algorithm[76] (with a time constant of 10.0) to stabilize the temperature during the simulation. Time step for saving of trajectory was set to 2 ps. A total of 50,000 snapshots were collected for each complex.

ASSOCIATED CONTENT

Supporting Information. Descriptions of the synthesis and characterization of intermediate compounds, elemental analysis data of the new compounds. This material is available free of charge via the Internet at http://pubs.acs.org.

AUTHOR INFORMATION

Corresponding Author

*Phone: +34 934024533. E-mail: svazquez@ub.edu.

[I]These authors contributed equally to this work.

ACKNOWLEDGMENT

We thank financial support from *Ministerio de Economía y Competitividad* (Project SAF2014-57094-R to F. J. L. and S. V.) and the *Generalitat de Catalunya* (grants 2014-

SGR-00052 and 2014-SGR-1189) and the *Consorci de Serveis Universitaris de Catalunya* for computational resources. R. L. thanks the Spanish *Ministerio de Educación Cultura y Deporte* for a PhD Grant (FPU program). M.B.-X. thanks the Institute of Biomedicine of the Universitat de Barcelona (IBUB) for a PhD grant. F. J. L. acknowledges the support from ICREA Academia. L. N. acknowledges financial support from the Geconcerteerde Onderzoeksacties (GOA/15/019/TBA), and technical assistance from W. van Dam.

ABBREVIATIONS

ATR, Attenuated Total Reflectance; CPE, cytopathic effect; MDCK, Madin-Darby Canine Kidney; MTS, 3-(4,5-dimethylthiazol-2-yl)-5-(3-carboxymethoxyphenyl)-2-(4-sulfophenyl)-2*H*-tetrazolium; RT-qPCR, quantitative real-time reverse transcription polymerase chain reaction; VSV, vesicular stomatitis virus.

REFERENCES

(1) http://www.who.int/influenza/en/

(2) Taubenberger J. K.; Morens, D. M. 1918 Influenza: the mother of all pandemics. *Emerg. Infect. Dis.* **2006**, *12*, 15-22.

(3) Wang, J.; Li, F.; Ma, C. Recent progress in designing inhibitors that target the drug-resistant M2 proton channels from the influenza A viruses. *Biopolymers (Pept. Sci.)*, **2015**, *104*, 291-309.

(4) Jefferson, T.; Jones, M. A.; Doshi, P.; Del Mar, C. B.; Hama, R.; Thompson, M. J.; Spencer, E. A.; Onakpopya, I.; Mahtani, K. R:; Nuna, D.; Howick, J.; Heneghan, C. J. Neuraminidase inhibitors for preventing and treating influenza in healthy adults and children. *Cochrane Database Syst. Rev.* **2014**: CD008965.

(5) Samson, M.; Pizzorno, A.; Abed, Y.; Boivin, G. Influenza virus resistance to neuraminidase inhibitors. *Antiviral Res.* **2013**, *98*, 174-185.

(6) Das K, Aramini J, Ma L, Krug R, Arnold E, Structures of influenza A proteins and insights into antiviral drug targets. *Nat. Struct. Mol. Biol.,* **2010**, *17*, 530-538.

(7) Hayden, F. G.; Newer influenza antivirals, biotherapeutics and combinations. *Influenza Other Respir. Viruses* **2013**, *7(S1)*, 63-75.

(8) Loregian A, Mercorelli B, Nannetti G, Compagnin C, Palù G, Antiviral strategies against influenza virus: towards new therapeutic approaches. *Cell Mol. Life Sci.* **2014**, 1-25.

(9) Vanderlinden, E.; Naesens, L. Emerging antiviral strategies to interfere with influenza virus entry. *Med. Res. Rev.* **2014**, *34*, 301-339.

(10) Naesens, L.; Stevaert, A.; Vanderlinden, E. Antiviral therapies on the horizon for influenza. *Curr. Opin. Pharmacol.* **2016**, *30*, 106-115.

(11) Yen, H. L. Current and novel antiviral strategies for influenza infection. *Curr. Opin. Virol.* **2016**, *18*, 126-134.

(12) Li, F.; Ma, C.; Wang, J. Inhibitors targeting the influenza virus hemagglutinin. *Curr. Med. Chem.* **2015**, *22*, 1361-1382.

(13) Stevaert, A.; Naesens, L. The influenza virus polymerase complex: an update on its structure, functions, and significance for antiviral drug design. *Med. Res. Rev.* **2016**, *36*, 1127-1173.

(14) Engel, D. A. The influenza virus NS1 protein as a therapeutic target. *Antiviral Res.* **2013**, *99*, 409-416.

(15) Wiley, D. C.; Skehel, J. J.; The structure and function of the hemagglutinin membrane glycoprotein of influenza virus. *Annu. Rev. Biochem.* **1987**, *56*, 365-394.

(16) Skehel, J. J.; Wiley, D. C. Receptor binding and membrane fusion in virus entry: the influenza hemagglutinin. *Ann. Rev. Biochem.* **2000,** *69*, 531-569.

(17) Hamilton, B. S.; Whittaker, G. R.; Daniel, S. Influenza virus-mediated membrane fusion: determinants of hemagglutinin fusogenic activity and experimental approaches for assessing virus fusion. *Viruses* **2012**, *4*, 1144-1168.

(18) Russell R. J.; Kerry, P. S.; Stevens, D. J.; Steinhauer, D. A.; Martin, S. R.; Gamblin, S. J.; Skehel, J. J. Structure of influenza hemagglutinin in complex with an inhibitor of membrane fusion. *Proc. Natl. Acad. Sci. USA* **2008**, *105*, 17736-17741.

(19) Yang, H.; Chang, J. C.; Guo, Z.; Carney, P. J.; Shore, D. A.; Donis, R. O.; Cox, N. J.; Villanueva, J. M.; Klimov, A. I.; Stevens, J. Structural stability of influenza A(H1N1)pdm09 virus hemagglutinins. *J. Virol.* **2014**, *88*, 4828-4838.

(20) Yang, H.; Carney, P. J.; Chang, J. C.; Guo, Z.; Villanueva, J. M.; Stevens, J. Structure and receptor binding preferences of recombinant human A(H3N2) virus hemagglutinins. *Virology*, **2015**, *477*, 18-31.

(21) Zhang, W.; Shi, Y.; Lu, X.; Shu, Y. ; Qi, J. ; Gao, G. F. An airborne transmissible avian influenza H5 hemagglutinin seen at the atomic level. *Science* **2013**, *340*, 1463-1467.

(22) Laursen, N. S.; Wilson, I. A. Broadly neutralizing antibodies against influenza viruses. *Antiviral Res*. **2013**, *98*, 476-483.

(23) Cho, A.; Wrammert, J. Implications of broadly neutralizing antibodies in the development of a universal influenza vaccine. *Curr. Opin. Virol*. **2016**, *17*, 110-115.

(24) Zeng, L.-Y.; Yang, J.; Liu, S. Investigational hemagglutinin-targeted influenza virus inhibitors. *Expert Opin Investig. Drugs* (in press), DOI: 10.1080/13543784.2017.1269170.

(25) Arbidol, an HA inhibitor, is clinically used in Russia, China and other countries for prophylaxis and treatment of influenza and other respiratory viral infections. However, its detail mechanism of action is not limited to HA inhibition. See, for example: a) Blaising, J.; Polyak, S. J.; Pécheur, E. I. Arbidol as a broad-spectrum antiviral: an update. *Antiviral Res.* **2014**, *107*, 84-94; b) Pécheur, E. I.; Borisevich, V.; Halfmann, P.; Morrey, J. D.; Smee, D. F.; Prichard, M.; Mire, C. E.; Kawaoka, Y.; Gesibert, T. W.; Polyak, S. J. The synthetic antiviral drug arbidol inhibits globally prevalent pathogenic viruses. *J. Virol.* **2016**, *6*, 3086-3092.

(26) Zenilman, J. M.; Fuchs, E. J.; Hendrix, C. W.; Radebaugh, C.; Jurao, R.; Nayak, S. U.; Hamilton, R. G.; McLeod Griffiss, J. Phase 1 clinical trials of DAS181, an inhaled sialidase, in healthy adults. *Antiviral Res.* **2015**, *123*, 114-119.

(27) Badani, H.; Garry, R. F.; Wimley, W. C. Peptide entry inhibitors of enveloped viruses: the importance of interfacial hydrophobicity. *Biochim. Biophys. Acta*. **2014**, *1838*, 2180-2197.

(28) Badani, H.; Garry, R. F.; Voss, T. G.; Wilson, R. B.; Wimley, W. C. Mechanism and action of flufirvitide, a peptide inhibitor of influenza virus infection. *Biophys J.* **2014**, *106 (Suppl 1)*, 707a.

(29) Bodian, D.; Yamasaki, R.; Buswell, R.; Stearns, J.; White, J.; Kuntz, I. Inhibition of the fusion-inducing conformational change of influenza hemagglutinin by benzoquinones and hydroquinones. *Biochemistry* **1993**, 32, 2967-2978.

(30) Antanasijevic, A.; Hafeman, N. J.; Tundup, S.; Kingsley, C.; Mishra, R. K.; Rong, L.; Manicassamy, B.; Wardrop, D.; Caffrey, M. Stabilization and improvement of a promising influenza antiviral: making a PAIN PAINless. *ACS Infect. Dis.* **2016**, *2*, 608-615.

(31) Luo, G.; Colonno, R.; Krystal, M. Characterization of a hemagglutinin-specific inhibitor of influenza A virus. *Virology* **1996**, *226*, 66-76.

(32) Luo, G.; Torri, A.; Harte, W. E.; Danetz, S.; Cianci, C.; Tiley, L.; Say, S.; Mullaney, D.; Yu, K.-L.; Ouellet, C.; Dextraze, P.; Meanwell, N.; Colonno, R.; Kyrstal, M. Molecular mechanism underlying the action of a novel fusion inhibitor of influenza A virus. *J. Virol.* **1997**, *71*, 4062-4070.

(33) Cianci, C.; Yu, K.-L.; Dischino, D. D.; Harte, W. ; Deshpande, M. ; Luo, G. ; Colonno, R. J. ; Meanwell, N. A. ; Krystal, M. J. pH-Dependent changes in photoaffinity labelling patterns of the H1 influenza virus hemagglutinin by using an inhibitor of viral fusion. *Virology* **1999**, *73*, 1785-1794.

(34) Deshpande, M. S.; Wei, J.; Luo, G.; Cianci, C.; Danetz, S.; Torri, A. ; Tiley, L. ; Krystal, M. ; Yu, K.-L.; Huang, S.; Gao, Q.; Meanwell, N. A. An approach to the identification of potent inhibitors of influenza virus fusion using parallel synthesis methodology. *Bioorg. Med. Chem. Lett.* **2001**, *11*, 2393-2396.

(35) Tang, G.; Lin, X.; Qiu, Z.; Li, W.; Zhu, L.; Wang, L.; Li, S.; Li, H.; Lin, W.; Yang, M.; Guo, T.; Chen, L.; Lee, D.; Wu, J. ; Yang, W. *ACS Med. Chem. Lett.* **2011**, *2*, 603-607.

(36) Zhu, L.; Li, Y.; Li, S.; Li, H.; Qiu, Z.; Lee, C.; Lu, H.; Lin, X.; Zhao, R.; Chen, L.; Wu, J.; Tang, G.; Yang, W. Inhibition of Influenza A Virus (H1N1) Fusion by Benzenesulfonamide Derivatives Targeting Viral Hemagglutinin. *PLos One,* **2011**, *6*, e29120.

(37) Plotch, S. J.; O'Hara, B.; Morin, J.; Palant, O.; LaRocque, J.; Bloom, J. D.; Lang, Jr., S. A.; DiGrandi, M. J.; Bradley, M.; Nilakantan, R.; Gluzman, Y. Inhibition of influenza A virus replication by compounds interfering with the fusogenic function of the viral hemagglutinin. *J. Virology* **1999**, *73*, 140-151.

(38) Liu, S.; Li, R.; Zhang, R.; Chan, C. C. S.; Xi, B.; Zhu, Z.; Yang, J.; Poon, V. K. M. ; Zhou, J.; Münch, J.; Kirchhoff, F.; Pleschka, S.; Haarmann, T.; Dietrich, U.; Pan, C.; Du, L.; Jiang, S.; Zheng, B. CL-385319 inhibits H5N1 avian influenza A virus infection by blocking viral entry. *Eur. J. Pharm.* **2011**, *660*, 460-467.

(39) Li, R.; Song, D.; Zhu, Z.; Xu, H.; Liu, S. *PLoS One* **2012**, *7*, e41956.

(40) Zhu, Z.; Li, R.; Xiao, G.; Chen, Z.; Yang, J.; Zhu, Q.; Liu, S. Design, synthesis and structure-activity relationship of novel inhibitors against H5N1 hemagglutinin-mediated membrane fusion. *Eur. J. Med. Chem.* **2012**, *57*, 211-216.

(41) Wanka, L.; Iqbal, K.; Schreiner, P. R. The lipophilic bullet hits the targets: medicinal chemistry of adamantane derivatives. *Chem. Rev.* **2013**, 113, 3516-604.

(42) Duque, M. D.; Ma, C.; Torres, E.; Wang, J.; Naesens, L.; Juárez-Jiménez, J.; Camps, P.; Luque, F. J.; DeGrado, W. F.; Lamb, R. A.; Pinto, L. H.; Vázquez, S.

Exploring the size limit of templates for inhibitors of the M2 ion channel of influenza A virus. *J. Med. Chem.* **2011**, *54*, 2646–2657.

(43) Torres, E.; Duque, M. D.; Vanderlinden, E.; Ma, C.; Pinto, L. H.; Camps, P.; Froeyen, M.; Vázquez, S.; Naesens, L. Role of the viral hemagglutinin in the anti-influenza virus activity of newly synthesized polycyclic amine compounds. *Antiviral Res.* **2013**, *99*, 281-291.

(44) Rey-Carrizo, M.; Torres, E.; Ma, C.; Barniol-Xicota, M.; Wang, J.; Wu, Y.; Naesens, L.; DeGrado, W. F.; Lamb, R. A.; Pinto, L. H.; Vazquez, S. Azatetracyclo[5.2.1.$1^{5,8}$.$0^{1,5}$]undecane derivatives: from wild-type inhibitors of the M2 ion channel of influenza A virus to derivatives with potent activity against the V27A mutant. *J. Med. Chem.* **2013**, *56*, 9265–9274.

(45) Rey-Carrizo, M.; Barniol-Xicota, M.; Ma, C.; Frigolé-Vivas, M.; Torres, E.; Naesens, L.; Llabrés, S.; Juárez-Jiménez, J.; Luque, F. J.; DeGrado, W. F.; Lamb, R. A.; Pinto, L. H.; Vázquez, S. Easily accessible polycyclic amines that inhibit the wild-type and amantadine-resistant mutants of the M2 channel of influenza A virus. *J. Med. Chem.* **2014**, *57*, 5738–5747.

(46) Rey-Carrizo, M.; Gazzarrini, S.; Llabrés, S.; Frigolé-Vivas, M.; Juárez-Jiménez, J.; Font-Bardia, M.; Naesens, L.; Moroni, A.; Luque, F. J.; Vázquez, S. New polycyclic dual inhibitors of the wild type and the V27A mutant M2 channel of the influenza A virus with unexpected binding mode. *Eur. J. Med. Chem.* **2015**, *96*, 318-329.

(47) Boido, V.; Sparatore, F. *N*-Lupinilarilammine e *N*-amminoalchil-*m*-triflurometilaniline d'interesse farmacologico e microbiologico. *Farmaco Sci.* **1974**, *29*, 526-533.

(48) Wanka, L.; Cabrele, C.; Vanejews, M.; Schreiner, P.R. γ-Aminoadamantanecarboxylic acids through direct C-H bond amidations. *Eur. J. Org. Chem.* **2007**, 1474–1490.

(49) Vanderlinden E.; Göktas F.; Cesur Z.; Froeyen M.; Reed M. L.; Russell, C. J.; Cesur, N.; Naesens L. Novel inhibitors of influenza virus fusion: structure-activity relationship and interaction with the viral hemagglutinin. *J. Virol.* **2010**, *84*, 4277-4288.

(50) Basu, A.; Antanasijevic, A.; Wang, M.; Li, B.; Mills, D. M.; Ames, J. A.; Nash, P. J.; Williams, J. D.; Peet, N. P.; Moir, D. T.; Prichard, M. N.; Keith, K. A.; Narnard, D. L.; Caffrey, M.; Rong, L.; Bowlin, T. L. New small molecule entry inhibitors targeting hemagglutinin-mediated influenza A virus fusion. *J. Virology* **2014**, *88*, 1447-1460.

(51) Yusuf, M.; Konc, J.; Sy Bing, C.; Trykowska Konc, J.; Ahmad Khairudin, N. B.; Janezic, D.; Wahab, H. A. Structurally conserved binding sites of hemagglutinin as targets for influenza drug and vaccine development. *J. Chem Inf. Model.* **2013**, *53*, 2423-2436.

(52) Dolinsky, T. J.; Nielsen, J. E.; McCammon, J. A.; Baker, N. A. PDB2PQR: an automated pipeline for the setup of Poisson–Boltzmann electrostatics calculations. *Nucleic Acids Res.* 2004, 32, W665-W667.

(53) Klebe G. Applying thermodynamic profiling in lead finding and optimization. *Nat. Rev. Drug Discov*. **2015**, *14*, 95-110.

(54) Biela, A.; Sielaff, F.; Terwesten, F.; Heine, A.; Steinmetzer, T.; Klebe, G.; Ligand binding stepwise disrupts water network in thrombin: enthalpic and

entropic changes reveal classical hydrophobic effect. *J. Med. Chem.* **2012**, *55*, 6094-110.

(55) Wright, W. R.; Brabander, H. J.; Hardy, Jr., R. A. Synthetic analgesics. II. Basic anilides and carbanilates. *J. Org. Chem.* **1961**, *26*, 476-485.

(56) Sawa, Y.; Kawakami, Y.; Imai, S.; Kawarazaki, T. Synthesis of *N*-(2-picolyl)-*N*-phenyl-*N*-(2-piperidinoethyl)amine (TAT-3), its derivatives, and its organic acid salts. *Takeda Kenkyushoho* **1970**, *29*, 275-282.

(57) Van Gilse, J.; Paerels, G. B. Algicidal composition and method of preventing or controlling algae with said composition. GB 2026867 B.

(58) Molle, G.; Bauer, P.; Dubois, J. E. *J. Org. Chem*. **1982**, *47*, 4120-4128.

(59) Averin, A. D.; Ulanovskaya, M. A.; Bryak, A. K.; Savel'ev, E. N.; Orlinson, B. S.; Novakov, I. A.; Beletskaya, I. P. Arylation of adamantanamines: II. Palladium-catalyzed amination of dihalobenzenes with adamantylalkanamines. *Russ. J. Org. Chem.* **2010**, *46*, 1790-1811.

(60) Kadutskii, A. P.; Kozlov, N. G. A novel three-component reaction of anilines, formaldehyde and b-diketones: simple synthesis of 3-spirosubstituted 1,2,3,4-tetrahydroquinolines. *Synlett* **2006**, 3349-3351.

(61) DeGrado, W. F.; Wang, J.; Wang, J.; Jo, H.; Canturk, B. US 2015/091439 A1.

(62) Clark, M.; Cramer, R. D.; Van Opdenbosch, N. Validation of the general purpose Tripos 5.2 force field. *J. Comput. Chem*. **1989**, *10*, 982-1012.

(63) Fletcher, R.; Powell, M. J. A rapidly convergent descent method for minimization. *Comput. J.,* **1963**, *6*, 163-168.

(64) Baker, N. A.; Sept, D.; Joseph, S.; Holst, M. J.; McCammon, J. A. Electrostatics of nanosystems: application to microtubules and the ribosome. *Proc. Natl. Acad. Sci. USA* **2001**, *98*, 10037-10041.

(65) Dolinsky, T. J.; Czodrowski, P.; Li, H.; Nielsen, J. E.; Jensen, J. H.; Klebe, G.; Baker, N. A. PDB2PQR: Expanding and upgrading automated preparation of biomolecular structures for molecular simulations. *Nuc. Acids Res*. **2007**, *35*, W522-E525.

(66) Spitzer, R.; Jain, A. N. Surflex-Dock: Docking benchmarks and real-world application. *J. Comput. Aided Mol. Des*. **2012**, *26*, 687-699.

(67) Case, D. A.; Darden, T. A.; Cheatham, T. E.; Simmerling, C. L.; Wang, J.; Duke, R. E.; Luo, R.; Walker, R. C.; Zhang, W.; Merz, K. M.; Roberts, B.; Hayik, S.; Roitberg, A.; Seabra, G.; Swails, J.; Goetz, A. W.; Kolossváry, I.; Wong, K. F.; Paesani, F.; Vanicek, J.; Wolf, R. M.; Liu, J.; Wu, X.; Brozell, S. R.; Steinbrecher, T.; Gohlke, H.; Cai, Q.; Ye, X.; Wang, J.; Hsieh, M. J.; Cui, G.; Roe, D. R.; Mathews, D. H.; Seetin, M. G.; Salomon-Ferrer, R.; Sagui, C.; Babin, V.; Luchko, T.; Gusarov, S.; Kovalenko, A.; Kollman, P. A. AMBER 12, 2012.

(68) Wang, J.; Wolf, R. M.; Caldwell, J. W.; Kollman, P. A.; Case, D. A. Development and Testing of a General Amber Force Field. *J. Comput. Chem.* **2004**, *25*, 1157-1174.

(69) Gaussian 09, Revision E.01, Frisch, M. J.; Trucks, G. W.; Schlegel, H. B.; Scuseria, G. E.; Robb, M. A.; Cheeseman, J. R.; Scalmani, G.; Barone, V.; Mennucci, B.; Petersson, G. A.; Nakatsuji, H.; Caricato, M.; Li, X.; Hratchian, H. P.; Izmaylov, A. F.; Bloino, J.; Zheng, G.; Sonnenberg, J. L.; Hada, M.; Ehara, M.; Toyota, K.; Fukuda, R.; Hasegawa, J.; Ishida, M.; Nakajima, T.; Honda, Y.;

Kitao, O.; Nakai, H.; Vreven, T.; Montgomery, J. A., Jr.; Peralta, J. E.; Ogliaro, F.; Bearpark, M.; Heyd, J. J.; Brothers, E.; Kudin, K. N.; Staroverov, V. N.; Kobayashi, R.; Normand, J.; Raghavachari, K.; Rendell, A.; Burant, J. C.; Iyengar, S. S.; Tomasi, J.; Cossi, M.; Rega, N.; Millam, J. M.; Klene, M.; Knox, J. E.; Cross, J. B.; Bakken, V.; Adamo, C.; Jaramillo, J.; Gomperts, R.; Stratmann, R. E.; Yazyev, O.; Austin, A. J.; Cammi, R.; Pomelli, C.; Ochterski, J. W.; Martin, R. L.; Morokuma, K.; Zakrzewski, V. G.; Voth, G. A.; Salvador, P.; Dannenberg, J. J.; Dapprich, S.; Daniels, A. D.; Farkas, Ö.; Foresman, J. B.; Ortiz, J. V.; Cioslowski, J.; Fox, D. J. Gaussian, Inc., Wallingford CT, 2009.

(70) Wang, J.; Cieplak, P.; Kollman, P. A. How Well Does a Restrained Electrostatic Potential (RESP) Model Perform in Calculating Conformational Energies of Organic and Biological Molecules? *J. Comput. Chem.* **2000**, *21*, 1049-1074.

(71) Forti, F.; Cavasotto, C. N.; Orozco, M.; Barril, X.; Luque, F. J. A multilevel strategy for the exploration of the conformational flexibility of small molecules. *J. Chem. Theory Comput*. **2012**, *8*, 1808-1819.

(72) Juárez-Jiménez, J.; Barril, X.; Orozco, M.; Pouplana, R.; Luque, F. J. Assessing the suitability of the multilevel strategy for the conformational analysis of small ligands. *J. Phys. Chem. B* **2015**, *119*, 1164-1172.

(73) Jorgensen, W. L.; Chandrasekhar, J.; Madura, J. D.; Impey, R. W.; Klein, M. L. Comparison of Simple Potential Functions for Simulating Liquid Water. *J. Chem. Phys*. **1983**, *79*, 926.

(74) Ryckaert, J.-P.; Ciccotti, G.; Berendsen, H. J. C. Numerical Integration fo the Cartesian Equations of Motion of a System with Constraints: Molecular Dynamics of n-Alkanes. *J. Comput. Phys.* **1977**, *23*, 327-341.

(75) Darden, T.; York, D.; Pedersen, L. An N.log(N) Method for Ewald Sums in Large Systems. *J. Chem. Phys*. **1993**, *98*, 10089.

(76) Berendsen, H. J., Postma, J. V., van Gunsteren, W. F., DiNola, A. R. H. J., & Haak, J. R. Molecular dynamics with coupling to an external bath. *J. Chem. Phys*. **1984**, *81*, 3684-3690.

Redesigning old anti-influenza compounds: synthesis and evaluation of novel anilines with activity against the 2009 H1N1 influenza virus

Rosana Leiva,[∫] Marta Barniol-Xicota,[∫,ǁ] Sandra Codony,[∫,ǁ] Tiziana Ginex,[#,ǁ] Evelien Vanderlinden,[§] Marta Montes,[∫] Michael Caffrey,[†] F. Javier Luque,[#] Lieve Naesens,[§] and Santiago Vázquez[∫]*

TABLE OF CONTENTS

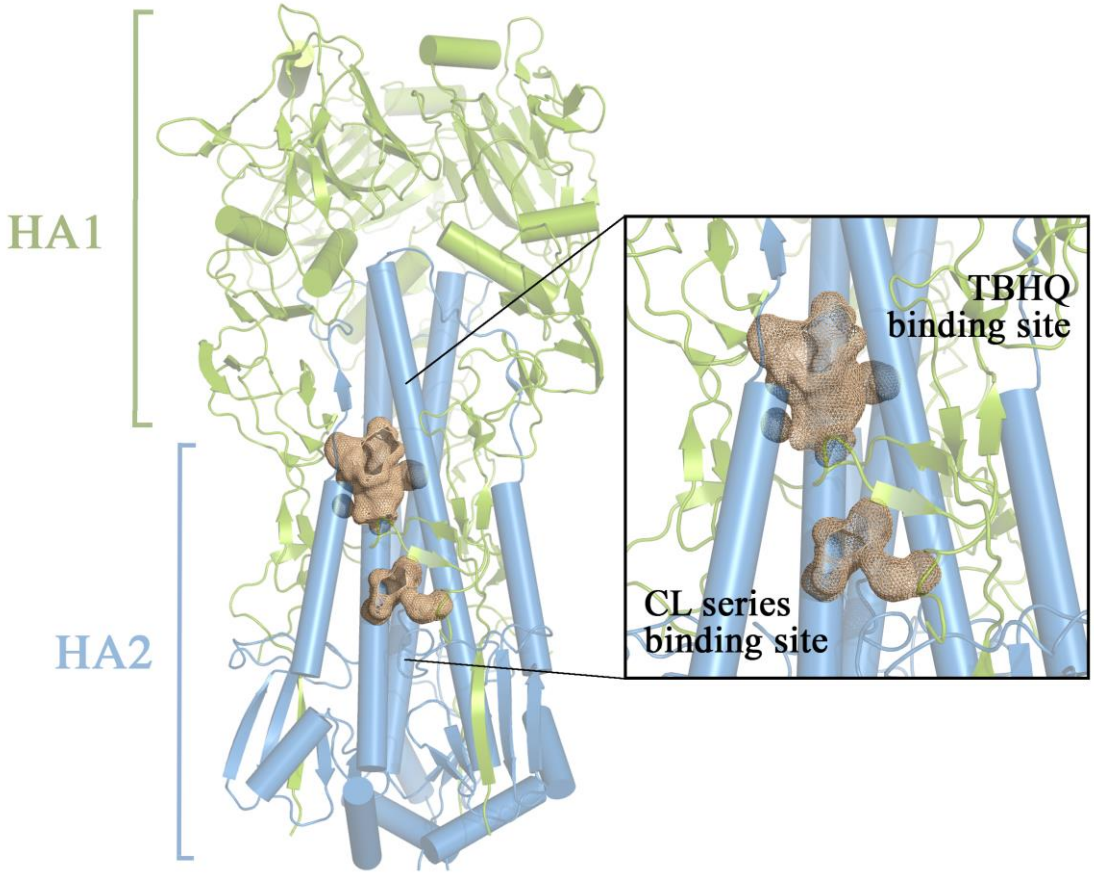

Figure S1. Representation of the two proposed binding sites for fusion inhibitors pertaining to the CL and TBHQ series of compounds. For the sake of clarity, the two monomers of HA are shown in green (HA1) and blue (HA2).

Figure S2. Multiple sequence alignment for HA1 (in green) and HA2 (in blue) monomers of A/PR/8/1934 (H1N1 subtype), A/Virginia/ATCC3/2009 (H1N1 subtype), A/HK/7/1987 (H3N2 subtype) and A/Aichi/2/1968 (H3N2 subtype; PDB code: 3EYM). This last structure was used as template for homology modelling. The cleavage region for the four strains was evidenced in yellow. Residues involved in ligand recognition pertaining to the HA1 and HA2 monomers are evidenced respectively in green and blue.

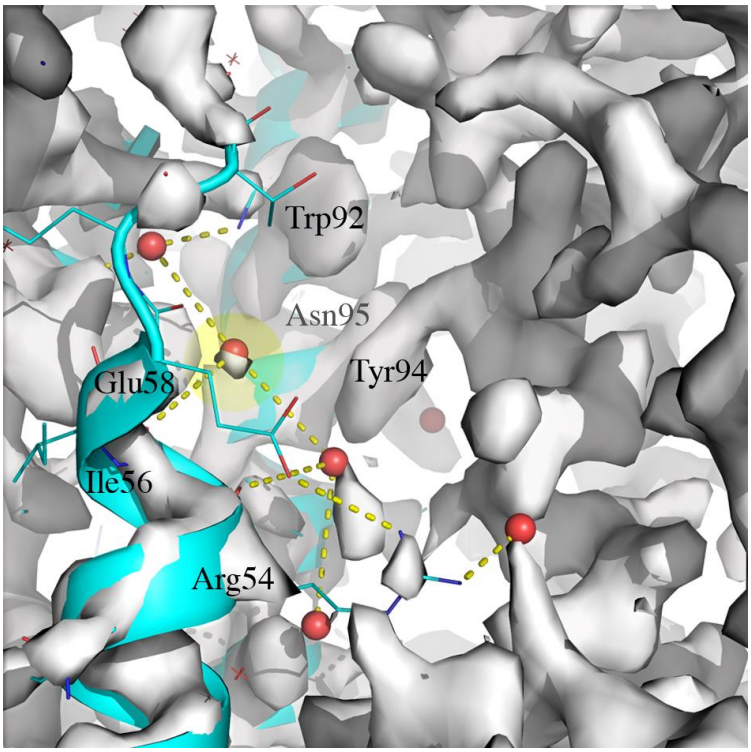

Figure S3. Electron density map for influenza A virus, strain A/Mallard/Astrakhan/244/1982 H14N6 (PDB ID: 3EYJ), strain A/Mallard/Astrakhan/244/1982 H14N6 (PDB ID: 3EYK) and strain A/Aichi/2/1968 H3N2 (PDB ID: 3EYM). A stable water molecule near Tyr94 ($HA2_2$) and Phe310 ($HA1_1$) is highlighted in a yellow circle.

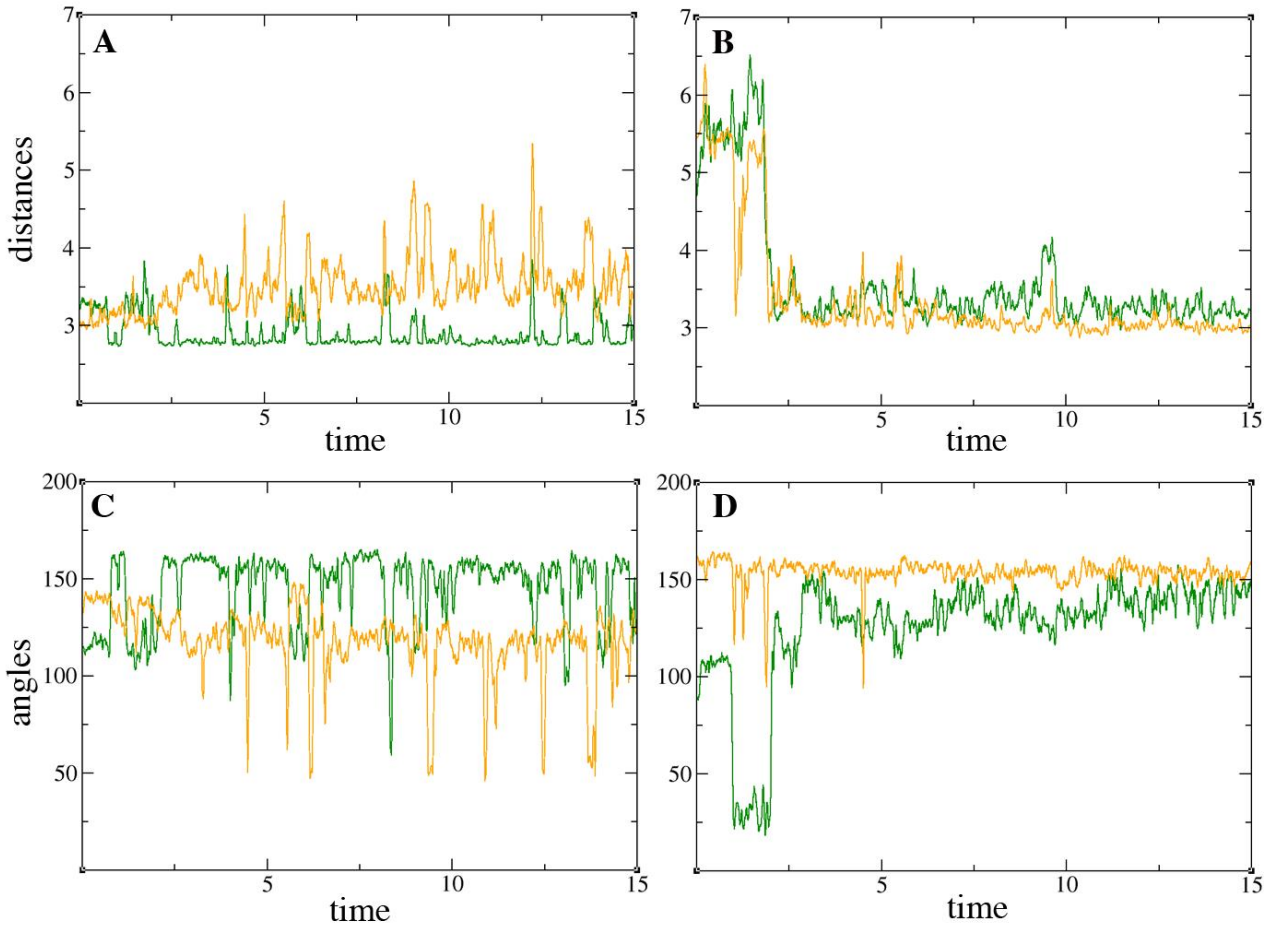

Figure S4. Time (ns) evolution of protein-inhibitor H-bonding interactions in the last 15 ns of MD simulation in (A, C) A/PR/8/1934 and (B, D) A/Virginia/ATCC3/2009. Distances (Å; A, B) and angles (degrees; C, D) between (i) the backbone oxygen of Glu58 (green) or Val55 (orange) and the charged piperazine nitrogen of the ligand, and (ii) the backbone oxygen of Thr54 (green) or Ser54 (orange) and the aniline nitrogen are shown.

Chapter 7

Adamantane scaffold optimization for the $P2X_7$ antagonists development.

7.1 Rationale and previous work

The P2X$_7$ receptor is a purinergic ligand gated ion channel that upon physiological activation by ATP, leads to cellular influx of ions Na^+ and Ca^{2+} and efflux of K^+. This receptor is widely distributed in the human body being involved in a handful of essential biological processes. Its identification as a key player in important and currently unhealable diseases is on the rise, including cancers, Parkinson's disease, mood disorders, osteoporosis, among others. The ample possibility of therapeutic intervention the P2X$_7$ offers, together with the fact that there are no commercial drugs approved for this target, has placed this receptor in the medicinal chemistry research spotlight (see introduction, section 1.5).

In the last decade, the research efforts in this direction have given place to the disclosure of numerous compounds displaying potent P2X$_7$ antagonistic activities and the entrance of some promising drug candidates to clinical trials. Nevertheless all this compounds failed in the process, therefore the search of the first P2X$_7$ drug is still a hot topic and on the go. Of special remark is the bloom of patent applications revolving this receptor[1], only in the period from 2008 to 2013 more than 50 new patents and patent applications have been published by more than 12 pharmaceutical companies and laboratories. There, more than 3500 novel compounds with diverse chemical scaffolds are described[2].

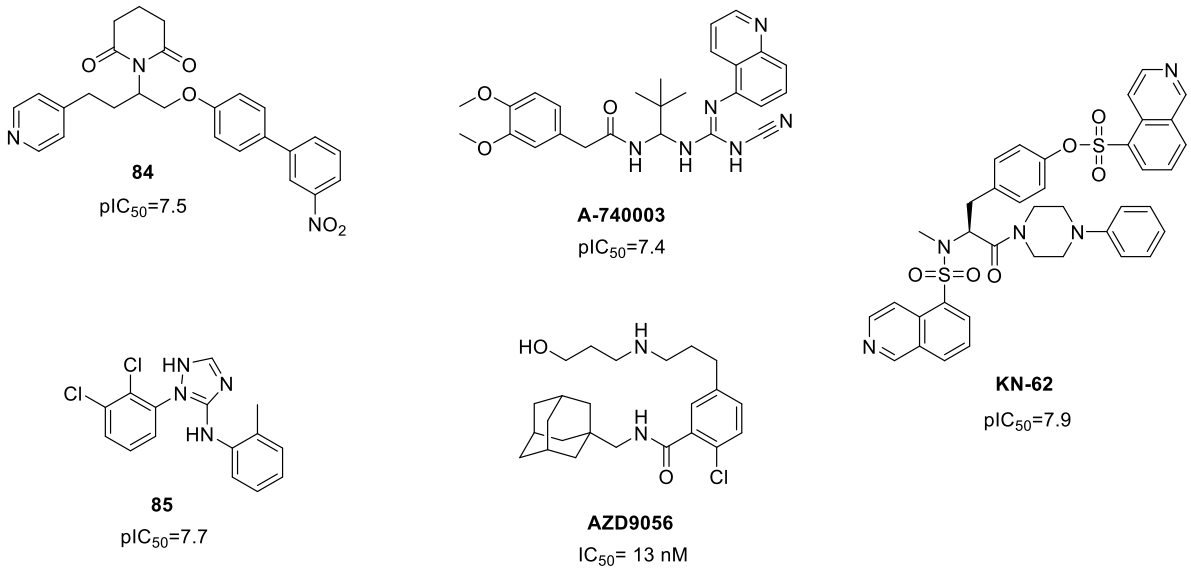

Figure 62. Chemical diversity in the P2X$_7$ antagonists.

[1] Friedle, S. A., Curet, M. A. & Watters, J. J. Recent patents on novel P2X$_7$ receptor antagonists and their potential for reducing central nervous system inflammation. *Recent Pat. CNS Drug Discov.* **2010**, 5 (1), 35–45.
[2] Nagy, J. Recent Patents on Novel P2X$_7$ Receptor Antagonists Potentially Effective for Treatment of Inflammatory Diseases. *Recent Pat. Biomark.* **2013**, 1–24.

Broadly, we can classify these molecules in the following chemical groups: arylamides and related structures[3], diverse amides[4], tetrazoles and related structures[5], cyclic imides and related structures[6], piperazines[7], amidines[8] and guanidines[9] and KN-62 derivatives[10] (Figure 60). Of special interest are the group of arylamides, which had its algid point with the entrance to phase IIb of AZD9056[11], developed by AstraZeneca. Despite the inability of AZD9056 to demonstrate efficacy in patients, its adamantylmethylamine scaffold was still further explored (e.g., AZ10606120, AZ11657312)[12,13], yielding novel and improved ligands of the receptor.

Even though several modifications upon this structure have been carried out, surprisingly, little to no effort has been made in order to replace the adamantane scaffold for other polycycles that may suit better the purpose. In fact, the few examples available in the literature trigger a dramatic drop of the activity in the receptor[14,15,16] (Figure 63).

[3] Baxter, A., Bent, J., Bowers, K., Braddock, M., Brough, S., Fagura, M., Lawson, M., McInally, T., Mortimore, M., Robertson, M., Weaver, R. & Webborn, P. Hit-to-lead studies: the discovery of potent adamantane amide $P2X_7$ receptor antagonists. *Bioorg. Med. Chem. Lett*. **2003**, 13, 4047–4050.

[4] Concepcion, A., Inoue, T., Mochizuki, Y., Muramatsu, A., Gantner, F., Nakashima, K., Urbahns, K. & Bacon, K. B. Preparation of Pyrazolylmethylbenzamides as $P2X_7$ Receptor Antagonists. WO 2005019182, **2005**.

[5] Chung, J., Gabel, C. & Jungbluth, G. Combination Therapies Utilizing Benzamide Inhibitors of the $P2X_7$ Receptor. WO2006003517, **2006**.

[6] Baxter, A., Kindon, N., Pairaudeau, G., Roberts, B. & Thom, S. Preparation of 1-(Piperidin-4-yl)-1,4-dihydro-2H-3,1-benzoxazin-2- ones as Purinoceptor $P2X_7$ Receptor Antagonists for Use in the Treatment of Inflammatory, Immune, or Cardiovascular Diseases. WO 2001044213, **2001.**

[7] Meghani, P. & Bennion, C. Synthesis and Use of Substituted Piperidine and Piperazine Derivatives (e.g. N-(Sulfonyl)aryl, N-Alkylcarboxa- mido Piperazines) as Antagonists of the $P2X_7$ Receptor. WO 2001046200, **2001**.

[8] Carroll, W. A., Perez-Medrano, A., Peddi, S. & Alan, S. Preparation of Aryl Cyanoamidines as $P2X_7$ Antagonists for the Treatment of Pain, Inflammation, and Neurodegeneration. US 20060025614, **2006**.

[9] Carroll, W. A., Medrano, A. P., Jarvis, M. F., Wang, Y. & Peddi, S. Preparation of (Acylaminomethyl)cyanoguanidines as $P2X_7$ Purinoceptor Antagonists for the Treatment of Neuropathic Pain. US 20050171195, **2005**.

[10] Gargett, C. E. & Wiley, J. S. The isoquinoline derivative KN-62 a potent antagonist of the P2Z-receptor of human lymphocytes. *Br. J. Pharmacol*. **1997**, 120, 1483–1490.

[11] Keystone, E. C., Wang, M. M., Layton, M., Hollis, S. & McInnes, I. B. Clinical evaluation of the efficacy of the P2X7 purinergic receptor antagonist AZD9056 on the signs and symptoms of rheumatoid arthritis in patients with active disease despite treatment with methotrexate or sulphasalazine. *Ann. Rheum. Dis.* **2012**. 71 (10), 1630–1635.

[12] Adinolfi, E., Raffaghello, L., Giuliani, A. L., Cavazzini, L., Capece, M., Chiozzi, P., Bianchi, G., Kroemer, G., Pistoia, V. & Di Virgilio, F. Expression of $P2X_7$ receptor increases in vivo tumor growth. *Cancer Res.* **2012**, 72 (12), 2957-69.

[13] Broom, D. C., Matson, D. J., Bradshaw, E., Buck, M. E., Meade, R., Coombs, S., Matchett, M., Ford, K. K., Yu, W., Yuan, J., Sun, S. H., Ochoa, R., Krause, J. E., Wustrow, D. J. & Cortright, D. N. Characterization of N-(adamantan-1-ylmethyl)-5-[(3R-amino-pyrrolidin-1-yl)methyl]-2-chloro-benzamide, a $P2X_7$ antagonist in animal models of pain and inflammation. *J. Pharmacol. Exp. Ther*. **2008**, 327 (3), 620-33.

[14] Lee, W.-G., Lee, S.-D., Cho, J.-H., Jung, Y., Kim, J., Hien, T. & Kim, Y.-C. Structure-activity relationships and optimization of 3,5-dichloropyridine derivatives as novel $P2X_7$ receptor antagonists. *J. Med. Chem.* **2012**, 55 (8), 3687–98.

[15] Gunosewoyo, H., Guo, J. L., Bennett, M. R., Coster, M. J. & Kassiou, M. Cubyl amides: novel $P2X_7$ receptor antagonists. *Bioorg. Med. Chem. Lett*. **2008**, 18(13), 3720–3.

[16] Wilkinson, S. M., Gunosewoyo, H., Barron, M. L., Boucher, A., McDonnell, M., Turner, P., Morrison, D. E., Bennett, M. R., McGregor, I. S., Rendina, L. M. & Kassiou, M. The first CNS-active carborane: a novel $P2X_7$ receptor antagonist with antidepressant activity. *ACS Med. Chem. Lett*. **2024**, 7–11.

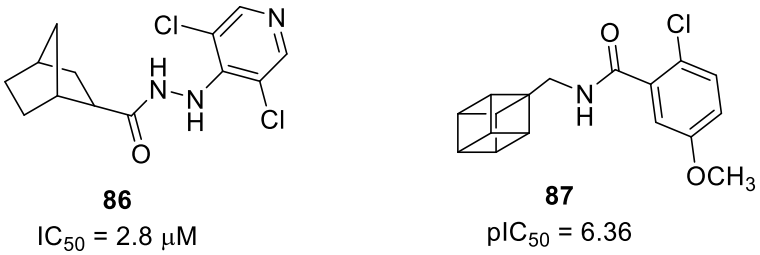

86
IC_{50} = 2.8 μM

87
pIC_{50} = 6.36

Figure 63. Reported adamantane replacements by polycyclic scaffolds.

For this, and taking into account the vast experience of our group in polycyclic chemistry and our previous success in replacing the adamantane scaffold by our tailor made polycyclic compounds[17,18]; we started the project covered in this chapter, aimed to find a scaffold which could substitute the adamantane, equaling or improving the antagonistic potencies of the lead compound.

In our first attempt the bisnoradamantane (**XXI**), the 4-azatetracyclo[5.3.2.0^{2,6}.0^{8,10}] dodecane (**XXII**) and the pentacyclo[6.4.0.0^{2,10}.0^{3,7}.0^{4,9}]dodecane scaffolds (**XXIII**, **XXIV**) were chosen in order to explore the size limits of the P2X$_7$ binding pocket, which due to the lack of a crystal structure of the receptor, is still unclear. As a reference compound we used an adamantane derivative reported by Abbott with an IC_{50} = 11.5 nM, shown in Chart 8.[19]

[17] Rey-Carrizo, M., Gazzarrini, S., Llabrés, S., Frigolé-Vivas, M., Juárez-Jiménez, J., Font-Bardia, M. & Vázquez, S. New polycyclic dual inhibitors of the wild type and the V27A mutant M2 channel of the influenza A virus with unexpected binding mode. *Eur. J. Med. Chem.* **2015**, 96, 318–329.

[18] Camps, P., Duque, M. D., Vázquez, S., Naesens, L., Clercq, E. De, Sureda, F. X., Cortés, D. Synthesis and pharmacological evaluation of several ring-contracted amantadine analogs. *Bioorg. Med. Chem.* **2008**, 16(23), 9925–9936.

[19] Nelson, D. W., Sarris, K., Kalvin, D. M., Namovic, M. T., Grayson, G., Donnelly-Roberts, D. L., Harris, H., Honore, P., Jarvis, M. F., Faltynek, C. R. & Carroll, W. A. Structure-activity relationship studies on N'-aryl carbohydrazide P2X7 antagonists. *J. Med. Chem.* **2008**, 51(10), 3030–4.

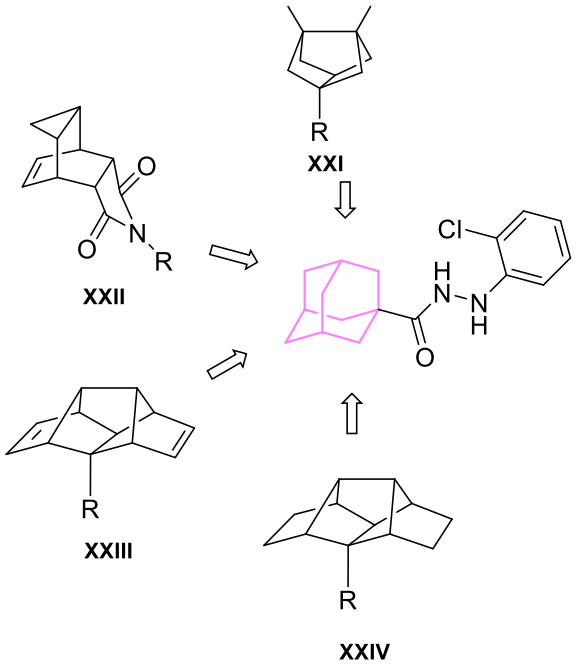

Chart 8. Adamantane replacements described in the manuscript.

7.2 Theoretical discussion

In the present Thesis the compounds featuring the scaffolds **XXIII** and **XXIV** were prepared. The synthetic route to access the pentacyclo[6.4.0.0^{2,10}.0^{3,7}.0^{4,9}]dodecane structure, already reported by the group[20], is depicted in scheme 22.

[20] Camps, P., Pujol, X., Rossi, R. A., Vázquez, S. Synthesis of Several 8-Halopentacyclo [6.4.0.02,10.03,7.04,9] dodecane Derivatives. *Synthesis* **1999**, 854-858.

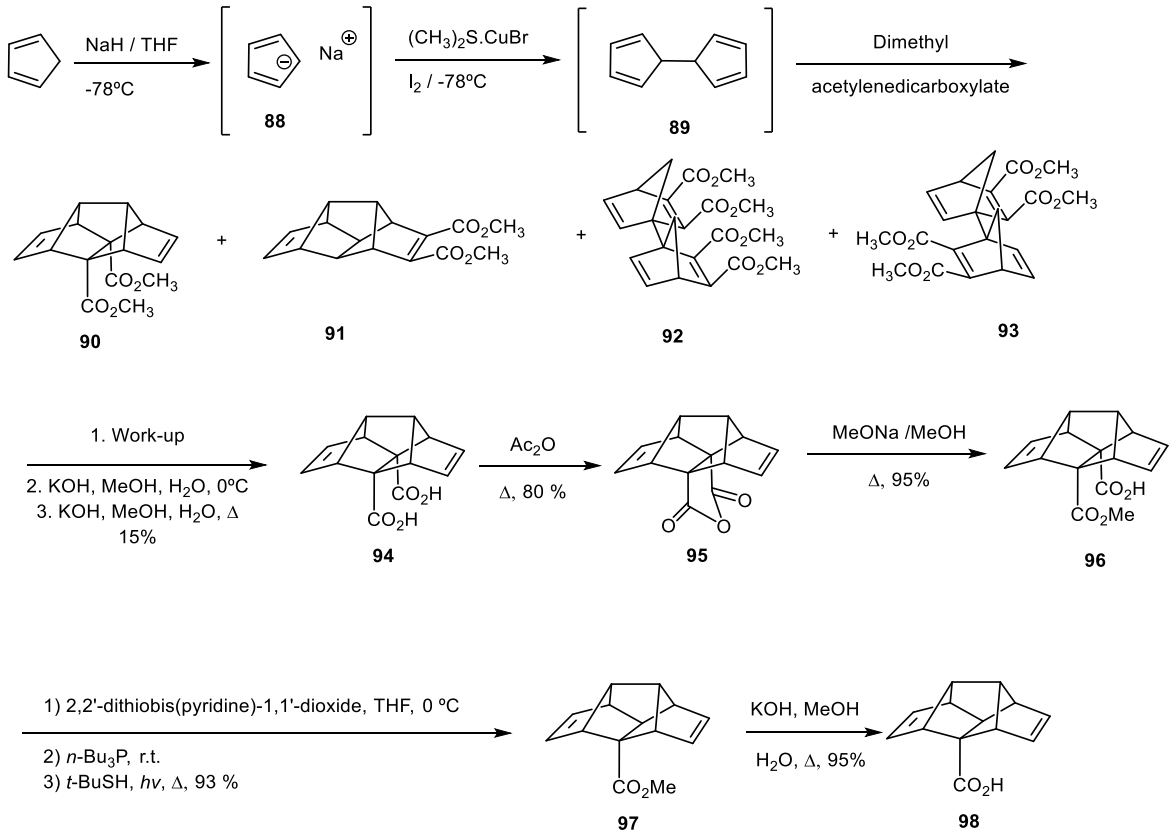

Scheme 22. Synthetic route for the obtention of the pentacyclic monoacid **98.**

The synthesis starts with a one-pot reaction consisting in the deprotonation of the cyclopentadiene by sodium hydride, followed by an oxidative coupling of the anion triggered by iodide under low temperature. The *in situ* generated 9,10-dihydrofulvalene is then reacted with dimethyl acetylenedicarboxylate through a double Diels-Alder reaction, leading to the diesters **90** and **91**, together with a complex mixture of polycyclic structures as side products (e.g. **92** and **93**). This procedure was simultaneously described by Hedaya's and Paquette's research groups in 1974[21,22] and optimized later on by Paquette[23]. The Diels-Alder by-products are discarded thanks a thorough work up, consisting in the suspension of the crude product in diethyl ether in which the tetraesters **92** and **93** are not soluble. Hence, a simple filtration allows the removal of the side-products. Next the mixture of the two isomers **90** and **91** is submitted to mild basic hydrolysis conditions,

[21] Paquette, L. A. & Wyvratt, M. J. Domino Diels-Alder reactions. I. Applications to the rapid construction of polyfused cyclopentanoid systems. *J. Am. Chem. Soc.* **1974**, *96*, 4671-4673.
[22] McNeil, D., Vogt, B. R., Sudol, J. J., Theodoropulos, S. & Hedaya, E. Multiple cycloaddition reaction of 9,10-dihydrofulvalene. New approach to 3,4,7-methenocyclopenta[a]pentalene derivatives. *J. Am. Chem. Soc.* **1974**, *96*, 4673-4674.
[23] Taylor, R. J., Welter, M. W., Paquette, L. A. *Org. Synth. Coll. VIII* **1993**, 298-302.

using KOH and MeOH at room temperature. Under this circumstances only **91** is reacted giving the corresponding diacid. The no-reaction of **90** may be due to the higher steric hinderance the ester groups confer to the structure. The mixture of the diacid and the diester **90** can be then treated with an acid-base wash to yield the pure isolated diester **90**. A second hydrolysis, with harshened conditions, furnishes the diacid **94**, which upon dehydration leads to **95**. This anhydride **95** is treated with sodium methoxide in anhydrous methanol to give the hemiester **96**, which is decarboxylated under Barton conditions[24,25] to **97.** The ester **97** via a hydrolysis yields the monoacid **98**.

As detailed in the manuscript the derivatives **100 - 103** were prepared upon reaction of the acid chloride derivative of **98** and the corresponding phenylhydrazine. These olefinic compounds upon treatment with hydrazine in an oxygen rich atmosphere[26], yielded the reduced derivatives **104 - 107** in quantitative yields. The seven derivatives that were pharmacologically evaluated were prepared as follow (Scheme 23).

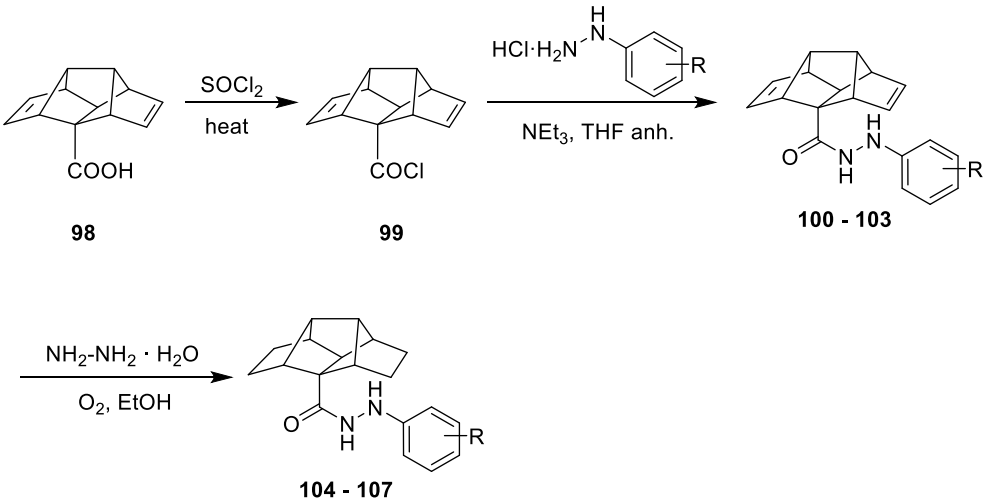

Scheme 23. Synthesis of the active compounds of general structure **XXIII** (**100**-**103**) and **XXIV** (**104**-**107**).

[24] Barton, D. H. R., Crich, D. & Motherwell, W. B. The invention of new radical chain reactions. Part VIII. Radical chemistry of thiohydroxamic esters; A new method for the generation of carbon radicals from carboxylic acids. *Tetrahedron.* **1985**, *41*, 3901-3924.

[25] Barton, D. H. R. & Samadi, M. The invention of radical reactions. Part XXV. A convenient method for the synthesis of the acyl derivatives of N-hydroxypyridine-2-thione. *Tetrahedron* **1992**, *48*, 7083-7090.

[26] Menges, N. & Balci, M. Catalyst-free hydrogenation of alkenes and alkynes with hydrazine in the presence of oxygen. *Synlett*. **2014**, 25(5), 671–676.

The compounds prepared and the results of the pharmacological evaluation by the group of Prof. Yong-Chul Kim (Gwangju Institute of Science and Technology, Republic of Korea) are gathered in Table 9.

Cmpd	Structure	IC_{50} (nM)[a]	Cmpd	Structure	IC_{50} (nM)[a]
100	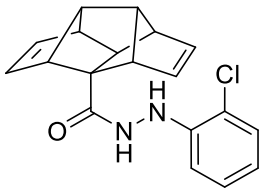	96	**104**	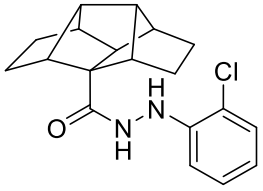	933
101	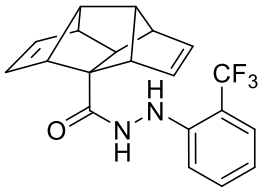	132	**105**	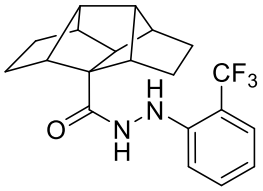	366
102	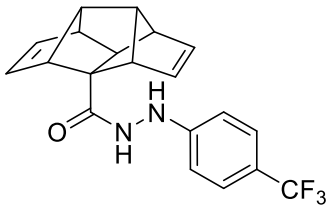	<20%[b]	**106**	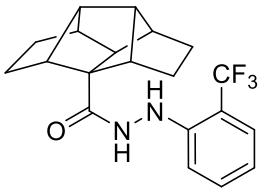	<20%[b]
103	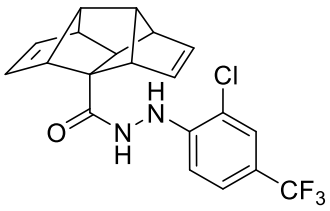	1557			

Table 9. [a] Number of determinations ≥ 3. [b] Percentage of inhibition at a concentration of 10 μM.

Of note the reduced analogue of **103** could not be accessed as it degraded under the reaction conditions (Scheme 24).

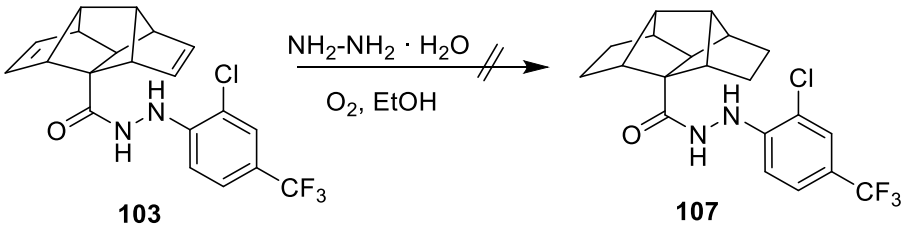

Scheme 24. Try-out to access the reduced derivative of **103.**

7.3 Follow-up work (unpublished results)

Although the compounds shown in the Table 8 were less potent than the adamantane derivative reported by Abbott, steaming from the aforementioned results, in the present Thesis an optimized polycyclic scaffold was designed and synthesized. Two examples containing this new nucleus were prepared and pharmacologically evaluated as $P2X_7$ antagonists (Table 10).

Cmpd	Structure	IC_{50} (nM)[a]	Cmpd	Structure	IC_{50} (nM)[a]
108	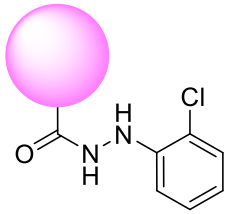	5.9±0.2	**109**	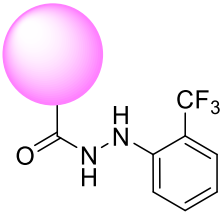	1.7±0.8

Table 10. [a] Number of determinations ≥ 3

The high potencies of both compounds, in the low nanomolar range and better than the corresponding adamantane analog, have given place to further pharmacological testing and the start of a patent application process. For this reason, the full structure of both compounds is not disclosed in the present Thesis.

Bioorganic & Medicinal Chemistry Letters
journal homepage: www.elsevier.com

Escape from adamantane: scaffold optimization of novel P2X$_7$ antagonists featuring complex polycycles

Marta Barniol-Xicota[a], Emily Caseley[b], Elena Valverde[a], Lin-Hua Jiang[b], Yong-Chul Kim[c,*], and Santiago Vázquez[a,*]

[a]*Laboratori de Química Farmacèutica (Unitat Associada al CSIC), Facultat de Farmàcia i Ciències de l'Alimentació, and Institute of Biomedicine (IBUB), Universitat de Barcelona, Av. Joan XXIII 27-31, Barcelona, E-08028, Spain*
[b]*School of Biomedical Sciences, University of Leeds, Leeds, United Kingdom*
[c]*School of Life Sciences, Gwangju Institute of Science and Technology (GIST), Gwangju 500-712, Republic of Korea*

ARTICLE INFO

Article history:
Received
Received in revised form
Accepted
Available online

Keywords:
Adamantane
Drug discovery
Homology models
P2X$_7$ antagonists
Scaffold replacement

ABSTRACT

The adamantane scaffold, despite being widely used in medicinal chemistry, is not devoid of problems. In the recent years we have developed new polycyclic scaffolds as surrogates of the adamantane group with encouraging results in multiple targets. As an adamantane scaffold is a common structural feature in several P2X$_7$ receptor antagonists, herein we report the synthesis and pharmacological evaluation of multiple replacement options which maintain a good activity profile. Molecular modeling studies support the binding of the compounds to a site close to the central pore, rather than to the ATP-binding site and shed light on the shape requirements for novel P2X$_7$ antagonists.

The P2X$_7$ receptor is an ionotropic ligand-gated purinergic receptor which is activated by extracellular ATP.[1] Upon the application of physiological concentrations of this messenger, the P2X$_7$ receptor acts as a cation selective ion channel, allowing the passage of Na^+, K^+ and Ca^{2+} through the plasma membrane, activating several signal transduction pathways for the correct function of the organism.[2] However, when this receptor is prolongedly exposed to high concentrations of ATP, in the high micromolar range, it induces the formation of a non-selective large pore[3] permeable to molecules up to 900 Da, which ultimately triggers cell apoptosis.[4]

This ion channel is present in virtually all tissues of the body, being especially abundant in cells of hematopoietic lineage.[5] Due to the widespread presence of the P2X$_7$ receptor in the mammalian organism, its malfunction has been linked to a vast number of pathological conditions,[6] including rheumatoid arthritis, osteoporosis, Parkinson's disease, multiple sclerosis and cancer, among other relevant inflammatory, immune or musculoskeletal disorders.[7] Taking into account the ample possibility of therapeutic intervention that the P2X$_7$ receptor offers, it is no surprise that in recent years several academic and non-academic groups have directed their research efforts to the development of potential P2X$_7$ antagonists.[8]

Resulting from this endeavour several structurally diverse small molecule inhibitors have come to light, placing the most promising ones into clinical trials (Figure 1). Unfortunately, all the candidates to date have failed in this process, resulting in a void in the P2X$_7$ therapeutic pipeline.

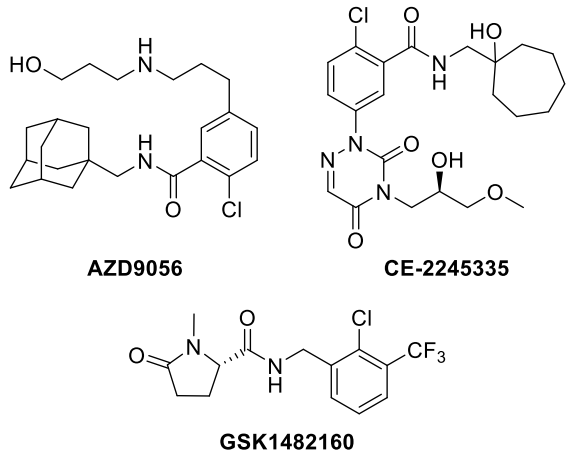

Figure 1. Structures of unsuccessful P2X$_7$ clinical candidates. Two additional drugs (AFC-5128 and EVT-401, of undisclosed structures, also failed in clinical trials).

* Corresponding author. Tel.: +34-934-024-533; e-mail: svazquez@ub.edu; Tel.: +82-627-152-502; e-mail: yongchul@gist.ac.kr

One of the most promising chemical classes of $P2X_7$ antagonists is found in the adamantyl derivatives. Indeed, this class of compounds had its most auspicious example in the AZ9056 (Figure 1), which successfully progressed to phase II clinical trials; regrettably it failed to show significant efficacy in several inflammatory diseases (osteoarthritis, rheumatoid arthritis, COPD and Chrohn's disease).[9] Unexpectedly after this failure, the adamantane core was not only not abandoned, but regained interest as a scaffold for $P2X_7$ antagonists. Proof of this are the several patents filled by AstraZeneca, Lundbeck, Renovis and Abbot.[10] Even more curious is the case of the academic groups that also resisted abandoning this scaffold, eagerly pursuing the preparation of adamantyl derivatives as $P2X_7$ antagonists. Worth mentioning are the compounds developed by Lee *et al.*,[11] such as **2**, and the C-2 substituted adamantanes developed by Battilocchio *et al.,* such as **3**.[12] Despite the aforementioned combination of industry and academic efforts, modifying other moieties of the adamantyl derivatives, has not met the expectation to overcome the drawbacks found in the past, to send a compound to clinic. Surprisingly, little to no effort has been dedicated to exploring the possibilities of the adamantane moiety replacement. Among the few examples reported so far, we find only weakly active compounds as the norbornane **4**,[11] and cubane **5** (Figure 2).[13]

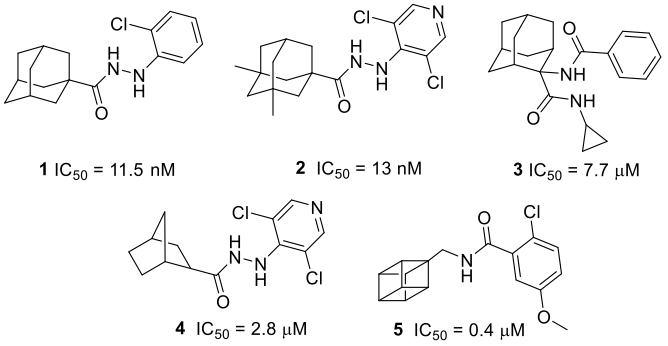

Figure 2. Selected adamantane derivatives (**1**-**3**) with potent activity as $P2X_7$ receptor antagonists and examples of adamantane replacements (**4**-**5**).

Taking into account the vast experience of our group in successfully replacing the adamantane with other tailor made polycyclic moieties and the capability of the aforementioned compounds to undergo structural modification we decided to explore this understudied path.[14]

For this we envisaged four types of suitable scaffolds to act as adamantane replacement and assessed their influence on the $P2X_7$ receptor activity. The aliphatic polycyclic scaffolds were judiciously chosen taking into account several factors, first of all the maintenance of the desirable drug-like properties shown by the adamantane compounds. Secondly, the fact that they already proved as suitable adamantane replacements in our hands, yielding to potent compounds. Finally, taking into account that no crystal structures of the $P2X_7$ are available nowadays, we aimed to explore the chemical space in the drug-binding site. To this aim, starting from the known nanomolar inhibitor **1**, the bulkier substitution possibilities were embodied by **I**, its saturated analogue **II**, which display a similar shape index as adamantyl compounds, and **III**, which poised as a greater length alternative with restricted free rotation of the phenylhydrazine moiety. On the other hand, taking into account that smaller analogs of adamantane such as the norbornane and the cubane scaffolds exemplified by **4** and **5** led to poor antagonists, just one smaller scaffold (**IV**) was envisaged (Figure 3).

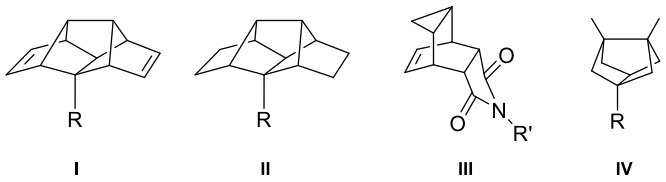

Figure 3. Adamantane replacement scaffolds. R = CONHNHAr, R' = NHAr.

Diene **6**, envisaged as a suitable precursor of **I** and **II**, was accessed through a concise 7-step synthetic route previously developed by our group.[15] Upon treatment of **6** with thionyl chloride, the resulting acid chloride **7** was obtained and readily reacted with the desired hydrazine, to yield hydrazides **8-11** in good yields. The saturated analogues **12-14** were successfully prepared through a double bond reduction with hydrazide monohydrate under oxygen atmosphere.[16] The compounds with the general structure **III** were easily accessed through the reaction of 1,3,5-cyclohepatriene with maleic anhydride, which furnished the polycyclic core in good yields.[17] Upon reaction of **15** with the corresponding phenylhydrazine, the compounds **16 - 18** were dehydrated under Dean-Stark conditions to yield the cyclized adducts **19 – 21** (Scheme 1).

As the pharmacology trends for the already tested series **I** and **II** placed the 2-Cl substitution among the preferred one (see below), for the scaffold **IV**, only **24** was prepared. The hydrazide **24** was accessed then from the known bisnoradamantane monoacid precursor[18] and, paralleling the procedure for the preparation of derivatives **I**, was treated with thionyl chloride and readily reacted with 2-chlorophenylhydrazine (Scheme 1).

The structure of all new compounds was confirmed by accurate mass measurement, IR, ^{1}H NMR and ^{13}C NMR spectroscopy.

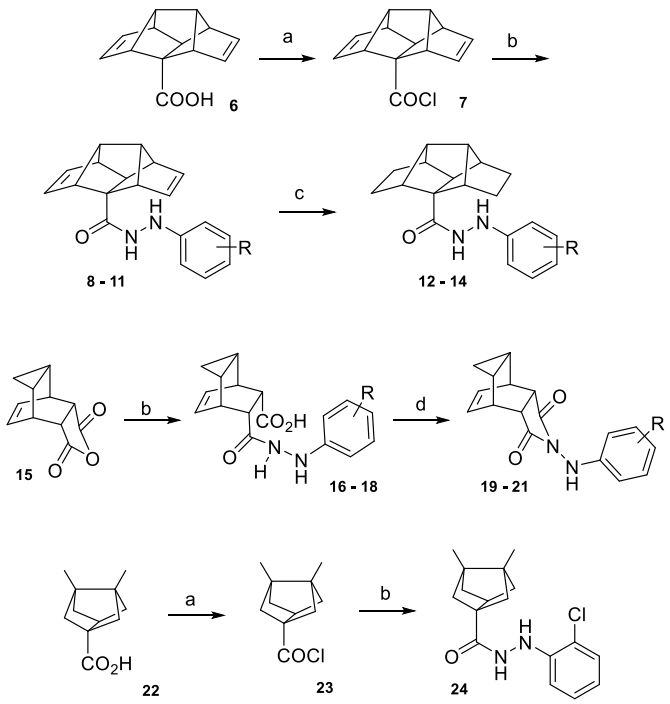

Scheme 1. Reagents and conditions: (a) $SOCl_2$, Δ; quantitative yield. (b) substituted phenylhydrazine hydrochloride, triethylamine, anh. THF, 2 h. (c) hydrazine monohydrate, O_2, ethanol, rt, 24 h. (d) toluene, Dean-Stark, Δ; quantitative yield. (e) 2-chlorophenylhydrazine hydrochloride, triethylamine, anh. THF, 95%. See supporting information for details.

All new compounds were evaluated for their antagonistic effects on 2'(3')-*O*-(4-benzoylbenzoyl)-ATP (BzATP)-induced ethidium bromide uptake in human embryonic kidney 293 (HEK 293) cells stably expressing the human $P2X_7$ receptor, using compound KN62 as a positive control (Table 1).[19]

In order to rationalize the results, the binding mode of all the compounds was analysed by docking in the extracellular domain of the homology models of the receptor $hP2X_7$ and $rP2X_7$, using AutoDock version 4.2.[20] In short, they supported the ability of the surrogate adamantane scaffolds to fill a cavity close to the central pore of human $P2X_7$, localized deeper in the receptor than the ATP binding site of human $P2X_7$ and provided some clues about the observed SAR (Figure 4A-B).

Regarding the aromatic moiety substitution, we took advantage of the SAR previously developed by Abbott around the adamantane derivative **1** that revealed electron withdrawing substitutents in the *ortho* position of the phenyl ring as the preferred group.[21] In fact, within our series, the *ortho* position clearly showed to be the preferred one for the activity (compare **9** *vs* **10** and **13** vs **14**). Interestingly, the introduction of a substituent in the *para* position was not only detrimental for the activity of the monosubstituted derivative (e.g., **10**), but was able to abolish the benefitial effect of the *ortho* group (e.g., **11**). This observation is explained by the steric clash of the *para*-trifluoromethyl group with the residue Phe95 of the receptor that has been previously shown to play a key role by forming pi-stacking interactions with distinct inhibitors (Figure 4C).[22]

Within this series, the most potent compound, **8** (IC_{50} = 96 nM), bearing a chlorine atom in *ortho*, was nearly 9 times less potent than its adamantane counterpart, **1** (IC_{50} = 11.5 nM). Notwithstanding, **8** was much more potent than previously studied replacements for adamantane (e.g., **4** and **5**). Moving from dienes **I** to alkanes **II** led to higher IC_{50} values (compare **8** *vs* **12** and **9** *vs* **13**), so full saturation of the structure is detrimental for the activity. This is rationalized as the diedral angle formed by the amide and the aromatic ring, suffers a slight tilt in the saturated compound, compared to its more active unsaturated analogue (Figure 4D).

As the hydrogen atom of the CONH group did not seem to play an essential role in the binding, we drew our attention to the conformationally restricted series **III**. Neither the unsubstituted phenyl derivative, **19**, nor the *ortho* substituted analogues **20** and **21**, displayed significant activity, a fact that indicates that a degree of conformational freedom in the aromatic moiety is required when designing $P2X_7$ inhibitors.

Fully unexpectedly, taking into account the weak inhibitory activity displayed by known smaller replacement of adamantane, such as **4** and **5** (see above), compound **24** was revealed as the most potent analog synthesized in this work, displaying an activity in the low nanomolar range (IC_{50} = 18 nM) which pairs the one displayed by its adamantane analogue **1** (IC_{50} = 11.5 nM).

Strikingly, upon docking in the receptor, **24**, showed to adopt a completey different orientation (Figure 4E-F) than the one shown by its adamantane analogue **1** and **8**, which parallels the adamantane compound in the binding site**.** Moreover, upon docking in the $rP2X_7$ receptor, no unfavourable interactions were observed for **24**, suggesting good antagonist potency. Taking into account that several clases of inhibitors display significantly reduced the binding affinity in $rP2X_7$ receptor, complicating further *in vivo* studies, our docking results further highlight the potential interest of bisnoradamantane derivatives as surrogates of adamantane.

Table 1. $P2X_7$ receptor antagonist activity of novel compounds.[a]

Compound	R	IC_{50} (nM)
8	2-Cl	96±0.8
9	2-CF_3	132±0.2
10	4-CF_3	<20%[b]
11	2-Cl, 4-CF_3	1557±1.3
12	2-Cl	933±0.8
13	2-CF_3	366±0.8
14	4-CF_3	<20%[b]
19	H	<20%[b]
20	2-Cl	<20%[b]
21	2-F	<20%[b]
24	2-Cl	18±0.5
KN-62	2-Cl	96

[a]Experiments were assessed in the ethidium accumulation assay using $hP2X_7R$-expressing HEK293 cells. The IC_{50} values were obtained from concentration-response curves. Data are expressed as the means SD. [b]Percent inhibition at concentration 10 μM. All experiments were repeated at least 3-6 times.

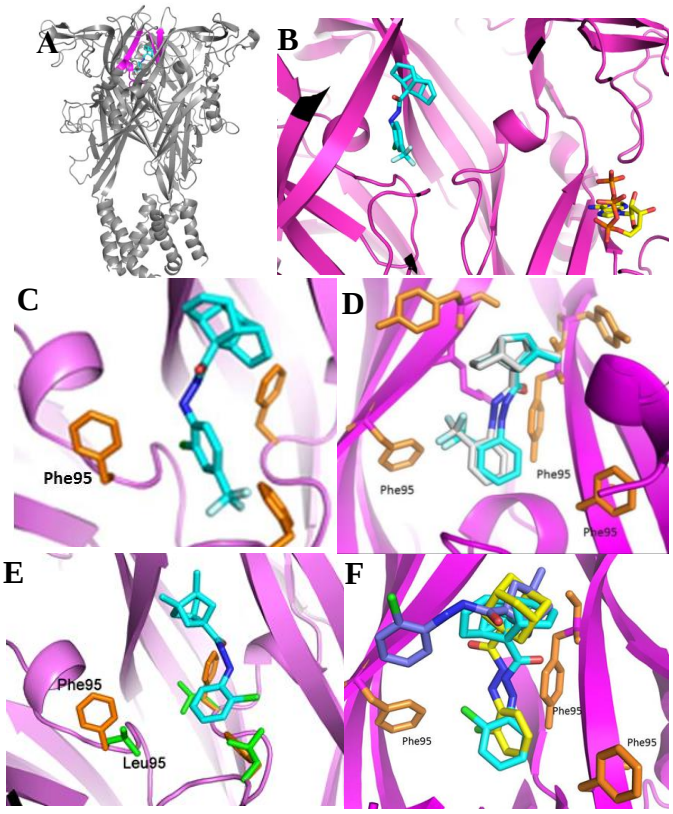

Figure 4. Docking of selected compounds and adamantane derivative **1** into the human $P2X_7$ receptor. **A**. Compounds binding site in the whole extracellular domain. **B**. Compounds binding site in relation with the ATP binding site. **C**. Steric clash of the trifluoromethyl group of **10**. **D**. Superposition of **8** and **12** in the binding site. **E**. Bisnoradamantane derivative **24** in the receptor binding pocket. Position 95 being Leu in the $rP2X_7$ and Phe in the $hP2X_7$. **F**. Superposition of **1** (yellow), **8** (light blue) and **24** (purple) in their binding site.

To further explore the suitability as an adamantane replacement we predicted their physicochemical properties using DataWarrior.[23] Of note, **24** and its isomer **1** displayed very similar physicochemical properties (Table 2). One of the main concerns when moving adamantane derivatives further into drug discovery programs is its easy metabolization by oxidation in the bridgehead positions. Taking into account that scaffold **IV** features two of the bridgehead positions substituted, it might be of interest for replacing adamantane when metabolic oxidation is an issue.[24]

Table 2. Relevant physicochemical properties for a representative example of each scaffold predicted by DataWarrior.[a]

Compound (scaffold)	mw	cLogP	H-A	H-D	PSA	SI[b]	MF[c]	sp^3 atoms
1	304.82	4.32	3	2	41.13	0.52	0.53	10
8 (I)	324.81	3.57	3	2	41.13	0.48	0.74	8
12 (II)	328.84	4.12	3	3	41.13	0.48	0.74	12
20 (III)	314.77	2.64	4	1	49.41	0.50	0.64	7
24 (IV)	304.82	4.29	3	2	41.13	0.52	0.73	10

[a]All the series were predicted not to be mutagenic or tumorogenic agents. [b]Shape index. [c]Molecular flexibility.

In conclusion, eleven new compounds have been synthesized from four available polycyclic compounds as putative $P2X_7$ antagonists. Several of these novel compounds displayed reasonable activity with **24**, being the most potent with low nanomolar potency. To the best of our knowledge this is the first time, within the $P2X_7$ antagonist context, that the adamantane scaffold has been successfully replaced by a different polycyclic structure. On top of that, **24** is predicted to have physicochemical properties that parallel those of adamantane, reinforcing its suitability as a scaffold to develop drug-like compounds. Taken together, we can conclude that the smaller bisnoradamantane scaffold **IV** revealed as a very promising surrogate of adamantane regarding $P2X_7$ inhibition, although a hit-to-lead study reported by AstraZeneca mentioned that no replacements for adamantane were found.[25]

Research towards the development of novel polycyclic scaffolds to function as adamantane replacement and the exploration of further analogues of **24** are in progress to reach derivatives with optimum $P2X_7$ activity and enhanced ADME properties.

Acknowledgments

M. B.-X. and E. V. thank the Institute of Biomedicine of the University of Barcelona (IBUB) for a PhD Grant. S. V. thanks financial support from *Ministerio de Economía y Competitividad* (Spain) (SAF2014-57094-R) and the *Generalitat de Catalunya* (2014-SGR-00052).

References and notes

1. Burnstock, G. *Pharmacol. Rev.* **1972**, *24*, 509–581.
2. (a) Burnstock, G. *Pharmacol Rev.* **2006**, *58*, 58–86. (b) Coddou, C.; Yan, Z.; Obsil, T.; Huidobro-Toro, J.P; Stojilkovic, S. S. *Pharmacol. Rev.* **2011**, *63*, 641–683.
3. Yan, Z; Li, S; Liang, Z; Tomic, M.; Stojilkovic, S. S. *J. Gen. Physiol.* **2008**, *132*, 563–573.
4. Khadra, A.; Tomic, Melanija; Y., Zonghe; Z., H.; Sherman, A.; Stojilkovic, S. S. *Biophys. J.* **2013**, *104*, 2612–2621.
5. Parvathenani, L. K.; Tertyshnikova, S.; Greco, C. R.; Roberts, S. B.; Robertson, B.; Posmantur, R. *J. Biol. Chem.* **2003**, *278*, 13309–13317.
6. (a) De Marchi, E.; Orioli, E.; Dal Ben, D.; Adinolfini, E. *Adv. Protein Chem. Struct. Biol*. **2016**, *104*, 39–79. (b) Tewari, M; Seth, P. *Ageing Res. Rev*. **2015**, *24*, 328–342. (c) Skaper, S. D.; Debetto, P.; Giusti, P. *FASEB J*. **2010**, *24*, 337–345. (d) North, R. A.; Jarvis, M. F. *Molec. Pharmacol*. **2003**, *83*, 759–69. (e) Roger, S.; Pelegrin, P. *Expert Opin. Investig. Drugs*. **2011**, *20*, 875–80.
7. (a) Arulkumaran, N.; Unwin, R. J.; Tam, F. W. *Expert Opin. Investig. Drugs*. **2011**, *20*, 897–915. (b) Di Virgilio, F.; Ceruti, S.; Bramanti, P.; Abbracchio, M. P. *Trends Neurosci*. **2009**, *32*, 79–87.
8. (a) Friedle, S. A.; Curet, M. A.; Watters, J. J. *Recent Pat. CNS Drug Discov.***2010**, *5*, 35–45. (b) Bartlett, R.; Stokes, L.; Sluyter, R. *Pharmacol. Rev*. **2014**, *66*, 638–75.
9. (a) Keystone, E.C.; Wang, M.M.; Layton, M.; Hollis, S.; McInnes, I. B. *Ann. Rheum. Dis*. **2012**. *71*, 1630–1635. (b) Eser, A.; Colombel, J. F.; Rutgeerts, P.; Vermeire, S.; Vogelsang, H.; Braddock, M.; Persson, T.; Reinisch, W. *Inflamm. Bowel Dis.* **2015**, *21*, 2247-2253. (c) https://openinnovation.astrazeneca.com/azd9056.html, accessed on Dec. 12th, 2016.
10. (a) Gunosewoyo, H.; Kassiou, M. *Expert Opin. Ther. Pat.* **2010**, *20*, 625–646. (b) Park, J.-H.; Kim, Y.-C. *Expert Opin. Ther. Pat.* doi: 10.1080/13543776.2017.1246538
11. Lee, W.-G.; Lee, S.-D.; Cho, J.-H.; Jung, Y.; Kim, J.-H.; Hien, T. T.; Kang, K.-W.; Ko, H.; Kim, Y.-C. *J. Med. Chem.* **2012**, *55*, 3687–3698.
12. Battilocchio, C.; Guetzoyan, L.; Cervetto, C.; Di Cesare Mannelli, L.; Frattaroli, D.; Baxendale, I. R.; Maura, G.; Rossi, A.; Sautebin, L.; Biava, M.; Ghelardini, C.; Marcoli, M.; Ley, S. V. *ACS Med. Chem. Lett.* **2013**, *4*, 704–709.
13. (a) Gunosewoyo, H.; Guo, J. L.; Bennett, M. R.; Coster, M. J.; Kassiou, M. *Bioorg. Med. Chem. Lett.* **2008**, *18*, 3720–3723. (b) Wilkinson, S. M.; Gunosewoyo, H.; Barron, M. L.; Boucher, A.; McDonnell, M.; Turner, P.; Morrison, D. E.; Bennett, M. R.; McGregor, I. S.; Rendina, L. M.; Kassiou, M. *ACS Chem. Neurosci.* **2014**, *5*, 335–339.
14. (a) Camps, P.; Duque, M. D.; Vázquez, S.; Naesens, L.; De Clercq, E.; Sureda, F. S.; López-Querol, M.; Camins, A.; Pallàs, M.; Prathalingam, S. R.; Kelly, J. M.; Romero, V.; Ivorra, D.; Cortés, D. *Bioorg. Med. Chem.* **2008**, *16*, 9925–9936. (b) Duque, M. D.; Camps, P.; Profire, L.; Montaner, S.; Vázquez, S.; Sureda, F. S.; Mallol, J.; López-Querol, M.; Naesens, L.; De Clercq, E.; Prathalingam, S. R.; Kelly, J. M. *Bioorg. Med. Chem.* **2009**, *17*, 3198–3206. (c) Duque, M. D.; Camps, P.; Torres, E.; Valverde, E.; Sureda, F. X.; López-Querol, M.; Camins, A.; Prathalingam, S. R.; Kelly, J. M.; Vázquez, S. *Bioorg. Med. Chem.* **2010**, *18*, 46–57. (d) Duque, M. D.; Ma, C.; Torres, E.; Wang, J.; Naesens, L.; Juárez- Jiménez, J.; Camps, P.; Luque, F. J.; DeGrado, W. F.; Lamb, R. A.; Pinto, L. H.; Vázquez, S. *J. Med. Chem*. **2011**, *54*, 2646−2657. (e) Torres, E.; Duque, M. D.; López-Querol, M.; Taylor, M. C.; Naesens, L.; Ma, C.; Pinto, L. H.; Sureda, F. X.; Kelly, J. M.; Vázquez, S. *Bioorg. Med. Chem.* **2012**, *20*, 942–948. (f) Rey-Carrizo, M.; Torres, E.; Ma, C.; Barniol-Xicota, M.; Wang, J.; Wu, Y.; Naesens, L.; DeGrado, W. F.; Lamb, R. A.; Pinto, L. H.; Vázquez, S. *J. Med. Chem.* **2013**, *56*, 9265–9274. (g) Torres, E.; Leiva, R.; Gazzarrini, S.; Rey-Carrizo, M.; Frigolé-Vivas, M.; Moroni, A.; Naesens, L.; Vázquez S. *ACS Med. Chem. Lett.* **2014**, *5*, 831–836. (h) Rey-Carrizo, M.; Barniol-Xicota, M.; Ma, C.; Frigolé-Vivas, M.; Torres, E.; Naesens, L.; Llabrés, S.; Juárez-Jiménez, J.; Luque, F. J.; DeGrado, W. F.; Lamb, R. A.; Pinto, L. H.; Vázquez, S. *J. Med. Chem.* **2014**, *57*, 5738–5747. (i) Valverde, E.; Sureda, F. X.; Vázquez, S. *Bioorg. Med. Chem.* **2014**, *22*, 2678–2683. (j) Rey-Carrizo, M.; Gazzarrini, S.; Llabrés, S.; Frigolé-Vivas, M.; Juárez-Jiménez, J.; Font-Bardia, M.; Naesens, L.; Moroni, A.; Luque, F. J.; Vázquez, S. *Eur. J. Med. Chem.* **2015**, *96*, 318–329. (k) Valverde, E.; Seira, C.; McBride, A.; Binnie, M.; Luque, F. J.; Webster, S. P.; Bidon-Chanal, A.; Vázquez, S. *Bioorg. Med. Chem.* **2015**, *23*, 7607–7617.
15. Camps, P., Pujol, X., Rossi, R. A., Vázquez, S. *Synthesis.* **1999**, 854–58.
16. Menges, N.; Balci, M. *Synlett.* **2014**, *25*, 671–676.
17. Abou-Gharbia, M.; Patel, U. R.; Webb, M. B.; Moyer, J. A.; Andree, T. H.; Muth, E. A. *J. Med. Chem.* **1988**, *31*, 1382−1392.
18. (a) Camps, P.; Iglesias, C.; Rodríguez, M. J.; Grancha, M. D.; Gregori, M. E.; Lozano, R.; Miranda, M. A.; Figueredo, M.; Linares, A. *A. Chem. Ber.* **1988**, *121*, 647–654. (b) Camps, P.; Font-Bardia, M.; Pérez, F.; Solans, X.; Vázquez, S. *Angew. Chem. Int. Ed. Engl*. **1995**, *34*, 912–914. (c) Camps, P.; Lukach, A. E.; Rossi, R. A. *J. Org. Chem.* **2001**, *66*, 5366–5373.

19. *$P2X_7$ receptor antagonist activity*. *Dye uptake using the ethidium ion assay*. HEK293 cells stably expressing $P2X_7$ receptor were maintained in Dulbecco's modified Eagle's medium (DMEM) supplemented with 10% fetal bovine serum (FBS), 2 mM L-glutamine, and antibiotics (50 U/mL penicillin and 50 mg/mL streptomycin) in a humidified 5% CO_2 atmosphere at 37 ºC. We used Lipofectamine as a transfection reagent with a pcDNA3.1 vector-based plasmid harbouring $hP2X_7$ receptor (Invitrogen). After diluting to 2.5 x 10^6 cells/mL, 80 mL of the cell suspension was added to each well of 96-well culture plates. The test compounds and 2'(3')-*O*-(4-benzoylbenzoyl)-ATP (BzATP) were then added, and the cells were incubated for 2 h in a humidified 5% CO_2 atmosphere at 37ºC. After incubation, a Bio-Tek FL600 fluorescence plate reader was used to measure the absorbance at an excitation wavelength of 530 nm and an emission wavelength of 590 nm. The inhibition (percent) of ethidium ion uptake was expressed as a relative value of the maximum accumulation when stimulated with BzATP only. To calculate the IC_{50} values, we calculated a series of dose-response data using nonlinear regression analysis (i.e., per-centage accumulation of ethidium bromide vs compound concentration).
20. *Homology modelling*. Structural models of the $P2X_7$ receptor were produced based on the zebrafish $P2X_4$ receptor crystal structure in the closed and ATP-bound states (Protein Data Bank code 4DW0 and 4DW1, respectively). [26] Modeller version 9.12 was used to generate one hundred versions of each model.[27] The five with the lowest energy were further analysed with MolProbity and those with the greatest percentage of residues in allowed regions of the Ramachandran plot were selected for use in this study.[28] The ModLoop server was used to model the non-conserved loop region between the β2 and β3 strands.[29] *Molecular docking simulations*. Molecular docking was carried out using AUTODOCK version 4.2.[30] The target cavity file for each docking simulation consisted of the $P2X_7$ receptor extracellular domain. The auxiliary program AutoGrid was used to generate the affinity grid files.
21. Nelson, D. W.; Sarris, K.; Kalvin, D. M.; Namovic, M. T.; Grayson, G.; Donnelly-Roberts, D. L.; Harris, R.; Honore, P.; Jarvis, M. F.; Faltynek, C. R.; Carroll, W. A. *J. Med. Chem.* **2008**, *51*, 3030–3034.
22. Caseley, E. A.; Muench, S. P.; Baldwin, S. A.; Simmons, K.; Fishwick, C. W.; Jiang, L.-H. *Bioorg. Med. Chem. Lett.* **2015**, *25*, 3164–2167.
23. DataWarrior version 4.4.4.
24. We have already found, working in other targets, that bisnoradamantane derivatives displayed higher microsomal stability than their adamantane counterparts (unpublished results).
25. Baxter, A.; Bent, J.; Bowers, K.; Braddock, M.; Brough, S.; Fagura, M.; Lawson, M.; McInally, T.; Mortimore, M.; Robertson, M.; Weaver, R.; Webborn, P. *Bioorg. Med. Chem. Lett.* **2003**, *13*, 4047–4050.
26. Hattori, M.; Gouaux, E. *Nature* **2012**, *485*, 207-212.
27. Webb, B.; Sali, A. *Curr. Protoc. Bioinformatics* **2006**, unit 5.6. DOI: 10.1002/cphi.3
28. Davis, I. W.; Leaver-Fay, A.; Chen, V. B.; Block, J. N.; Kapral, G. J.; Wang, X.; Murray, L. W.; Arendall, W. B.; Snoeyink, J.; Richardson, J. S. *Nucleic Acids Res.* **2007**, *35(suppl 2)*, W375-W383.
29. Fieser, A.; Do, R. K. G.; Šali, A. *Protein Sci.* **2000**, *9*, 1753-1773.
30. Morris, G.M.; Huey, R.; Lindstrom, W.; Sanner, M.F.; Belew, R.K.; Goodsell, D.S.; Olson, A.J. *J. Comput. Chem*. **2009**, *30*, 2785–2791.

Supplementary Material

Experimental procedures and characterization details for the new compounds.

Supporting information

Escape from adamantane: scaffold optimization of novel $P2X_7$ antagonists featuring complex polycycles

Marta Barniol-Xicota[a], Emily Caseley[b], Elena Valverde[a], Lin-Hua Jiang[b], Yong-Chul Kim[c,*], and Santiago Vázquez[a,*]

[a]*Laboratori de Química Farmacèutica (Unitat Associada al CSIC), Facultat de Farmàcia i Ciències de l'Alimentació, and Institute of Biomedicine (IBUB), Universitat de Barcelona, Av. Joan XXIII 27-31, Barcelona, E-08028, Spain*
[b]*School of Biomedical Sciences, University of Leeds, Leeds, United Kingdom*
[c]*School of Life Sciences, Gwangju Institute of Science and Technology (GIST), Gwangju 500-712, Republic of Korea*

Table of content:

∗ Corresponding author. Tel.: +34-934-024-533; e-mail: svazquez@ub.edu; Tel.: +82-627-152-502; e-mail: yongchul@gist.ac.kr

Chemical Synthesis. General Methods

Melting points were determined in open capillary tubes with a MFB 595010M Gallenkamp melting point apparatus. 400 MHz ^{1}H NMR and 100.6 MHz ^{13}C NMR spectra were recorded on a Varian Mercury 400 spectrometer. The chemical shifts are reported in ppm (δ scale) relative to internal tetramethylsilane, and coupling constants are reported in hertz (Hz). Assignments given for the NMR spectra of the new compounds are based on COSY $^{1}H/^{13}C$ (gHSQC sequence) experiments. IR spectra were run on a Perkin-Elmer Spectrum RX I spectrophotometer. Absorption values are expressed as wavenumbers (cm^{-1}). Column chromatography was performed on silica gel 60 Å (35-70 mesh, SDS, ref 2000027). Thin-layer chromatography was performed with aluminum-backed sheets with silica gel 60 F254 (Merck, ref 1.05554), and spots were visualized with UV light and 1% aqueous solution of $KMnO_4$.

General procedure A

The monoacid **6** or **22** (3 mmol, 1 eq) was solved in 6 mL of thionyl chloride (83.4 mmol, 27 eq) and stirred at 80 °C for 2 h in a round bottom flask provided with a tube of anhydrous $CaCl_2$. Then, the excess of thionyl chloride was removed under vacuum. Dry toluene (40 mL) was added to the residue, and the remaining thionyl chloride was azeotropically removed to give the acid chloride as a white wax in quantitative yield. The compound was analyzed by IR and used for the next step without any further purification.

General procedure B

Under nitrogen atmosphere the desired hydrazine (1.5 mmol, 1.1 eq) was solved in anhydrous THF (5 mL) and upon addition of anhydrous triethylamine (2.7 mmol, 2 eq), the mixture was stirred for 10 minutes. Upon addition of the corresponding acid chloride (1.4 mmol, 1 eq) in anhydrous THF (15 mL), the whole was left stirring overnight. The formed precipitate was filtered and subsequently washed with diethyl ether, yielding the pure product.

General procedure C

The corresponding alkene **8**-**11** (1.22 mmol, 1 eq) was solved in absolute ethanol (5 mL) and hydrazine monohydrate 98% (4.88 mmol, 4 eq) was added to the reaction media. The solution was left stirring overnight at room temperature under oxygen atmosphere. The solvent was removed under vacuo and the product was obtained by crystallization from ethyl acetate.

General procedure D

The corresponding hydrazine (2.00 mmol, 1 eq) was solved in absolute ethanol (2.5 mL) and the anhydride **15** (2.00 mmol, 1 eq) was added to the reaction media. The solution was left stirring overnight at room temperature under oxygen atmosphere. The reaction crude was filtered under vacuo and the resulting solid washed with absolute ethanol, to obtain the desired intermediates **16** - **18** which were readily used in the following step.

General procedure E

The intermediates **16** – **18** were dehydrated under Dean-Stark conditions overnight. Prior solvent removal and crystallization from isopropanol, the desired products **19** – **21** were obtained.

***N'*-(2-chlorophenyl)pentacyclo[6.4.0.0^{2,10}.0^{3,7}.0^{4,9}]dodeca-5,11-diene-8-carbohydrazide**, **8**.

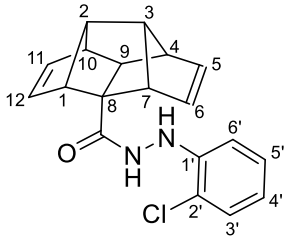

Following the general procedure B, 2-chlorophenylhydrazine hydrochloride (268.5 mg, 1.5 mmol), anhydrous triethylamine (0.4 mL, 2.7 mmol) and the acid chloride **7** (300 mg, 1.4 mmol) gave the desired product as a white solid in quantitative yield. IR (ATR) ν: 695, 748, 1049, 1115, 1132, 1249, 1302, 1486, 1592, 1648, 1654, 2977, 3286 cm^{-1}. ^{1}H-NMR (400 MHz, $CDCl_3$) δ: 2.19 (t, *J* = 2.4 Hz, 1 H, 9-H), 2.58 [m, 2 H, 2(3)-H], 3.09 [s, 2 H, 4(10)-H], 3.30 [s, 2 H, 1(7)-H], 6.03 [ddd, *J* = 6.0 Hz, *J'* = 2.8 Hz, *J''* = 1.0 Hz, 2 H, 6(12)-H], 6.08 [ddd, *J* = 6.0 Hz, *J'* = 2.8 Hz, *J''* = 1.0 Hz, 2 H, 6(12)-H], 6.42 (d, 1 H, *J* = 3.6 Hz, NH), 6.72 (dd, 1 H, *J'*= 8.0 Hz, *J* = 1.6 Hz, 6'-H), 6.81 (td, 1 H, *J''* = 8.0 Hz, *J'* = 1.6 Hz, 4'-H), 7.12 (td, 1 H, *J* = 8.0 Hz, *J'* = 1.6 Hz, 5'-H), 7.13 (d, J = 3.6 Hz, 1 H, NH), 7.25 (dd, *J* = 8.0 Hz, *J'* = 1.6 Hz, 3'-H). ^{13}C-NMR (100.6 MHz, $CDCl_3$) δ: 56.1 (CH, C9), 61.3 [CH, C(2)3], 61.5 [CH, C(4)10], 63.7 [CH, C1(7)], 64.0 (C, C8), 113.6 (CH, C6'), 119.7 (C, C2'), 121.3 (CH, C4'), 127.5 (CH, C5'), 129.4 (CH, C3'), 131.9 [CH, C(6)12], 134.0 [CH, C(5)11], 143.9 (C, C1'), 173.7 (C, CO). HRMS-ESI$^+$ m/z $[M+H]^+$: calcd for $[C_{19}H_{17}ClN_2O+H^+]$: 325.1102, found: 325.1112.

***N'*-(2-chlorophenyl)pentacyclo[6.4.0.0^{2,10}.0^{3,7}.0^{4,9}]dodecane-8-carbohydrazide**, **12**.

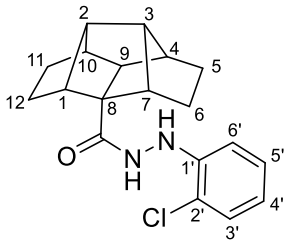

Following the general procedure C, **8** (397 mg, 1.22 mmol) and hydrazine monohydrate (0.24 mL, 4.88 mmol) gave the desired product as a white solid in quantitative yield. IR (ATR) ν: 758, 950, 1031, 1054, 1100, 1127, 1165, 1249, 1282, 1322, 1461, 1479, 1499, 1590, 1615, 1646, 1870, 2946, 3275, 3392 cm^{-1}. ^{1}H-NMR (400 MHz, $CDCl_3$) δ: 1.49-1.70 [complex signal, 8 H, 5(11)-H_2 and 6(12)-H_2], 1.98 (s, 1 H, 9-H), 2.28 [s, 2H,

4(10)-H], 2.36 [m, 2 H, 2(3)-H], 2.51 [m, 2 H, 1(7)-H], 6.55 (m, 1 H, NH), 6.82 (td, 1 H, *J* = 8.0 Hz, *J'* = 1.6 Hz, 4'-H), 6.88 (dd, 1 H, *J* = 8.0 Hz, *J'* = 1.6 Hz, , 6'-H), 7.15 (td, 1 H, *J* = 8.0 Hz, *J'* = 1.6 Hz, 5'-H), 7.24 (bs, 1 H, NH), 7.28 (dd, 1 H, *J* = 8.0 Hz, *J'* = 1.6 Hz, 3'-H). ^{13}C-NMR (100.6 MHz, $CDCl_3$) δ: 23.2 [CH_2, C6(12)], 24.1 [CH_2, C5(11)], 49.1 [CH, C2(3)], 50.1 (CH, C9), 53.4 [CH, C4(10)], 58.0 [CH, C1(7)], 58.2 (C, C8), 113.7 (CH, C6'), 121.4 (CH, C4'), 127.6 (CH, C5'), 129.5 (CH, C3'), 173.7 (C, CO), the signals from C1' and C2' were not observed. HRMS-ESI$^+$ m/z [*M*+H]$^+$: calcd for [$C_{19}H_{21}ClN_2O$+H^+]: 329.1415, found: 329.1411

_N'_-[(2-trifluoromethyl)phenyl]pentacyclo[6.4.0.0^{2,10}.0^{3,7}.0^{4,9}]dodeca-5,11-diene-8-carbohydrazide, **9**.

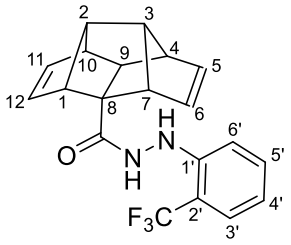

Following the general procedure B, 3-(trifluoromethyl)phenylhydrazine hydrochloride (320.8 mg, 1.5 mmol), anhydrous triethylamine (0.4 mL, 2.7 mmol) and **7** (300 mg, 1.4 mmol) gave the desired product as a brown solid (500 mg, 98% yield). IR (ATR) ν: 687, 756, 867, 971, 1031, 1054, 1107, 1163, 1246, 1279, 1319, 1471, 1494, 1590, 1613, 1651, 2967, 3270 cm^{-1}. ^{1}H-NMR (400 MHz, $CDCl_3$) δ: 2.22 (broad s, 1 H, 9-H), 2.61 [m, 2 H, 2(3)-H], 3.11 [s, 2 H, 4(10)-H], 3.32 [s, 2 H, 1(7)-H], 6.06 [ddd, *J* = 5.6 Hz, *J'* = 2.8 Hz, *J''* = 1.0 Hz, 2 H, 6(12)-H], 6.10 [ddd, *J* = 5.6 Hz, *J'* = 2.8 Hz, *J''* = 1.0 Hz, 2 H, 5(11)-H], 6.55 (broad s, 1 H, NH), 6.84 (d, *J* = 8.4 Hz, 1 H, 6'-H), 6.93 (broad t, *J* = 7.6 Hz, 1 H, 4'-H), 7.01 (broad s, 1 H, NH), 7.37 (broad t, *J* = 7.6 Hz, 1 H, 5'-H), 7.48 (d, *J* = 7.6 Hz, 1 H, 3'-H). ^{13}C-NMR (100.6 MHz, $CDCl_3$) δ: 56.2 (CH, C9), 61.4 [CH, C(2)3], 61.5 [CH, C(4)10], 63.9 [CH, (1)7], 64.0 (C, C8), 113.4 (CH, C6'), 115.1 (C, q, *J* = 30.6 Hz, C2'), 120.2 (CH, C4'), 124.5 (C, q, *J* = 272.6 Hz, CF_3), 126.5 (CH, q, *J* = 5.6 Hz, C3'), 132.0 [CH, C(6)12], 132.9 (CH, C5'), 134.1 [CH, C(5)11], 145.8 (C, C1'), 173.8 (C, CO). HRMS-ESI$^+$ m/z [*M*+H]$^+$: calcd for [$C_{20}H_{17}F_3N_2O$+H^+]: 359.1366, found: 359.1364

***N'*-[(2-trifluoromethyl)phenyl]pentacyclo[6.4.0.0^{2,10}.0^{3,7}.0^{4,9}]dodecane-8-carbohydrazide**, **13**.

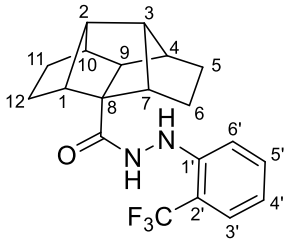

Following the general procedure C, **9** (370 mg, 1.03 mmol) and hydrazine monohydrate (0.20 mL, 4.13 mmol) gave **13** as a light yellow solid in quantitative yield. IR (ATR) ν: 730, 743, 786, 849, 910, 923, 1034, 1044, 1084, 1135, 1145, 1203, 1231, 1292, 1416, 1476, 1595, 1656, 1939, 2055, 2567, 2643, 2708, 2946, 3245 cm^{-1}. ^{1}H-NMR (400 MHz, $CDCl_3$) δ: 1.50-1.65 [complex signal, 8 H, 5(11)-H_2 and 6(12)-H_2], 1.99 (s, 1 H, 9-H), 2.27 [s, 2H, 4(10)-H], 2.35 [m, 2 H, 2(3)-H], 2.52 [m, 2 H, 1(7)-H], 6.67 (broad s, 1 H, N<u>H</u>), 6.94 (t, 1 H, *J* = 7.6 Hz, 4'-H), 7.0 (d, 1 H, *J* = 7.6 Hz, 6'-H), 7.32 (bs, 1 H, N<u>H</u>), 7.39 (t, 1 H, *J* = 8.0 Hz, 5'-H), 7.50 (d, 1 H, *J* = 7.6 Hz, 3'-H). ^{13}C-NMR (100.6 MHz, $CDCl_3$) δ: 23.2 [CH_2, C6(12)], 24.0 [CH_2, C5(11)], 49.1 [CH, C2(3)], 50.0 (CH, C9), 53.4 [CH, C4(10)], 58.0 [CH, 1(7)], 58.2 (C, C8), 113.4 (CH, C6'), 115.1 (C, q, *J* = 30.5 Hz, C2'), 120.2 (CH, C4'), 124.5 (C, q, *J* = 272.5 Hz, <u>C</u>F_3), 126.5 (CH, q, *J* = 5.5 Hz, C3'), 132.9 (CH, C5'), 146.1 (C, C1'), 173.9 (C, <u>C</u>O). HRMS-ESI^{+} m/z [*M*+H]$^{+}$: calcd for [$C_{20}H_{21}F_3N_2O$+H^{+}]: 363.1679, found: 363.1686.

***N'*-[(4-trifluoromethyl)phenyl]pentacyclo[6.4.0.0^{2,10}.0^{3,7}.0^{4,9}]dodeca-5,11-diene-8-carbohydrazide**, **10**.

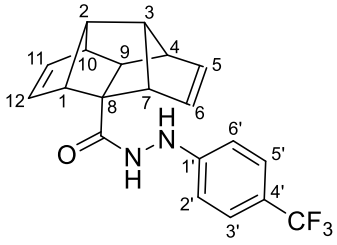

Following the general procedure B, 4-(trifluoromethyl)phenylhydrazine hydrochloride (160 mg, 0.75 mmol), anhydrous triethylamine (0.2 mL, 1.5 mmol) and **7** (150 mg, 0.69 mmol) gave **10** as a white solid in quantitative yield. IR (ATR) ν: 690, 743, 753,

829, 1006, 1062, 1102, 1115, 1158, 1180, 1254, 1325, 1486, 1613, 1651, 2977, 3063, 3301 cm^{-1}. ^{1}H-NMR (400 MHz, $CDCl_3$) δ: 2.19 (s, 1 H, 9-H), 2.62 (m, 2 H, 2(3)-H), 3.12 (s, 2 H, 4(10)-H), 3.31 (s, 2 H, 1(7)-H), 6.04 [ddd, *J* = 6.0 Hz, *J'* = 3.0 Hz, *J''* = 1.0 Hz, 2 H, 6(12)-H], 6.11 [ddd, *J* = 6.0 Hz, *J'* = 2.8 Hz, *J''* = 1.0 Hz, 2 H, 5(11)-H], 6.27 (broad s, 1H, NH), 6.76 [d, 2 H, *J* = 8.4 Hz, 2'(6')-H], 7.04 (s, 1H, NH), 7.44 [d, 2 H, *J* = 8.4 Hz, 3'(5')-H]. ^{13}C-NMR (100.6 MHz, $CDCl_3$) δ: 56.3 (CH, C9), 61.4 [CH, C2(3)], 61.5 [CH, 4(10)], 63.9 [CH, C1(7)], 64.0 (C, C8), 112.8 [CH, C2'(6')], 122.8 (C, q, *J* = 30.8 Hz, C4') 124.4 (C, q, *J* = 270.9 Hz, CF_3), 126.5 [CH, q, *J* = 3.8 Hz, C3'(5')], 131.9 [CH, C(6)12], 134.1 [CH, C(5)11], 151.0 (C, C1'), 174.0 (C, CO). HRMS-ESI$^+$ m/z $[M+H]^+$: calcd for $[C_{20}H_{17}F_3N_2O+H^+]$: 359.1366, found: 359.1367.

***N'*-[(4-trifluoromethyl)phenyl]pentacyclo[6.4.0.0^{2,10}.0^{3,7}.0^{4,9}]dodecane-8-carbohydrazide, 14.**

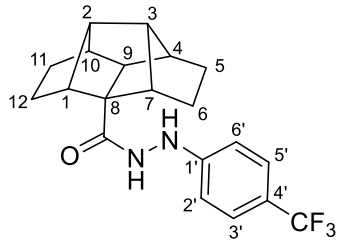

Following the general procedure C, **10** (300 mg, 0.83 mmol) and hydrazine monohydrate (0.16 mL, 3.34 mmol) gave **14** as a white solid in quantitative yield. IR (ATR) ν: 748, 826, 867, 1049, 1064, 1107, 1158, 1231, 1269, 1294, 1322, 1370, 1413, 1476, 1529, 1615, 1651, 2860, 2951, 3275 cm^{-1}. ^{1}H-NMR (400 MHz, $CDCl_3$) δ: 1.50-1.65 [complex signal, 8 H, 5(11)-H_2 and 6(12)-H_2], 1.98 (s, 1 H, 9-H), 2.28 (s, 2 H, 4(10)-H], 2.36 (m, 2 H, 2(3)-H], 2.51 (s, 2 H, 1(7)-H], 6.43 (s, 1 H, NH), 6.87 [d, 2 H, *J* = 8.6 Hz, 2'(6')-H], 7.34 (s, 1H, NH), 7.47 [d, 2 H, *J* = 8.6 Hz, 3'(5')-H]. ^{13}C-NMR (100.6 MHz, $CDCl_3$) δ: 23.2 [CH_2, C6(12)], 24.0 [CH_2, C5(11)], 49.1 [CH, C2(3)], 50.0 (CH, C9), 53.4 [CH, C(4)10], 58.0 [CH, C1(7)], 58.2 (C, C8), 112.9 [CH, C2'(6')], 122.7 (C, d, *J* = 30.8 Hz, C4'), 123.3 (C, d, *J* = 27.9 Hz, CF_3), 126.6 [CH, d, *J* = 3.8 Hz, C3'(5')], 151.4 (C, C1'), 174.2 (C, CO). HRMS-ESI$^+$ m/z $[M+H]^+$: calcd for $[C_{20}H_{21}F_3N_2O+H^+]$: 363.1679, found: 363.1688.

***N'*-[2-chloro-(4-trifluoromethyl)phenyl]pentacyclo[6.4.0.0^{2,10}.0^{3,7}.0^{4,9}]dodeca-5,11-diene-8-carbohydrazide**, **11.**

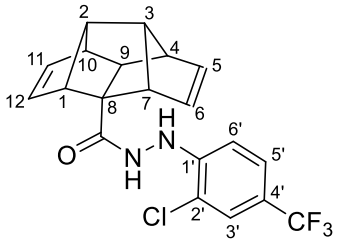

Following the general procedure B, [2-chloro-4-(trifluoromethyl)phenyl]hydrazine hydrochloride (322.6 mg, 1.3 mmol), anhydrous triethylamine (0.3 mL, 2.5 mmol) and **7** (250 mg, 1.2 mmol) gave the desired product as a white solid in quantitative yield. IR (ATR) ν: 690, 819, 882, 1049, 1115, 1135, 1168, 1259, 1314, 1421, 1474, 1494, 1732, 2815, 2992, 3346 cm^{-1}. ^{1}H-NMR (400 MHz, $CDCl_3$) δ: 2.20 (m, 1 H, 9-H), 2.63 [m, 2 H, 7(8)-H], 3.13 (s, 2 H, 4(10)-H), 3.33 (s, 2 H, 1(7)-H), 6.06 [dd, *J* = 6.0 Hz, *J'* = 2.8 Hz, 2 H, 6(12)-H], 6.12 [dd, *J* = 6.0 Hz, *J'* = 3.0 Hz, 2 H, 5(11)-H], 6.48 (broad s, 1 H, NH), 6.78 (d, 1 H, *J* = 8.8 Hz, 6'-H), 6.91 (broad d, 1H, NH), 7.34 (dd, 1 H, *J* = 8.8 Hz, *J'* = 2.4 Hz, 5'-H), 7.47 (d, 1 H, *J* = 2.4 Hz, 3'H). ^{13}C-NMR (100.6 MHz, $CDCl_3$) δ: 56.3 (CH, C9), 61.4 [CH, C2(3)], 61.5 [CH, C4(10)], 63.9 [CH, C178)], 64.0 (C, C8), 115.1 (CH, C6'), 125.3 (C, C2'), 126.5 (CH, d, *J* = 5.7 Hz, C3'), 131.9 [CH, C6(12)], 132.8 (CH, C5'), 134.2 [CH, C(5)11], 144.5 (C, C1'), 174.0 (C, CO), the signals of C4' and CF_3 were not observed. HRMS-ESI$^+$ m/z $[M+H]^+$: calcd for $[C_{20}H_{16}ClF_3N_2O+H^+]$: 392.0976, found: 393.0982.

***N*'-(2-chlorophenyl)-3,7-dimethyltricyclo[3.3.0.0^{3,7}]octane-1-carbohydrazide**, **24**.

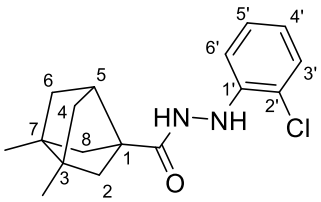

Following the general procedure B, 2-chlorophenylhydrazine hydrochloride (226 mg, 1.1 mmol), anhydrous triethylamine (0.2 mL, 1.4 mmol) and the acid chloride **7** (220 mg, 1.2 mmol) gave the desired product as a white solid in quantitative yield. ^{1}H NMR (500 MHz, DMSO) δ: 1.15 [s, 6 H, C3(7)-CH_3], 1.32 [dd, *J* = 8.0 Hz, *J'* = 3.5 Hz, 2 H, 4(6)-H_a], 1.58-1.63 [overlapped signal, 4 H, 4(6)-H_b and 2(8)-H_a], 1.73 [d, *J* = 7.5 Hz, 2 H, 2(8)-H_b], 3.06 (complex signal, 1 H, 5-H), 6.69-6.75 (overlapped signals, 2 H, 4'-H

and 6'-H), 7.16 (t, *J* = 8.0 Hz, 1 H, 5'-H), 7.27 (d, *J* = 7.5 Hz, 1 H, 3'-H), 7.34 (broad s, 1 H, CONHNH), 9.60 (broad s, 1 H, CONHNH). ^{13}C NMR (125.7 MHz, DMSO) δ: 16.3 [CH_3, C3(7)-CH_3], 45.4 (CH, C5), 47.1 [C, C3(7)], 52.8 [CH_2, C4(6)], 53.1 (C, C1), 56.1 [CH_2, C2(8)], 112.8 (CH, C6'), 117.2 (C, C2'), 119.3 (CH, C4'), 127.7 (CH, C5'), 129.1 (CH, C3'), 145.0 (C, C1'), 173.4 (CO). HRMS-ESI$^+$ m/z [*M*+H]$^+$: calcd for [$C_{17}H_{21}ClN_2O$+H^+]: 305.1415, found: 305.1416.

4-(Phenylamino)-4-azapentacyclo[5.3.2.0^{2,6}.0^{8,10}]dodec-11-ene-3,5-dione, **19.**

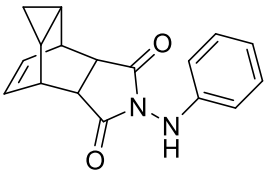

Following the general procedures D and E, phenylhydrazine (218 mg, 2.0 mmol) and the anhydride **15** (380 mg, 2.0 mmol) gave the desired product as an orange solid in a 47% overall yield. ^{1}H-NMR (400 MHz, DMSO) δ: 0.06 (dt, *J* = 4.8 Hz, *J'* = 3.6 Hz, 1 H, 9-H_a), 0.26 (dt, *J* = 7.2 Hz, *J'* = 5.6 Hz, 1 H, 9-H_b), 1.17 [broad s, 2 H, 8(10)-H], 3.17 [broad s, 2 H, 2(6)-H], 3.32 [broad s, 2 H, 1(7)-H], 5.86 [t, *J* = 3.6 Hz, 2 H, 11(12)-H], 6.59 [d, *J* = 8.0 Hz, 2 H, 2'(6')-H], 6.75 (t, *J* = 7.2 Hz, 1 H, 4'-H), 7.14 [t, *J* = 8.0 Hz, 2 H, 3'(5')-H], 8.33 (broad s, 1 H, NH). ^{13}C NMR (100.6 MHz, DMSO) δ: 4.0 (CH_2, C9), 9.2 [CH, C8(10)], 32.9 [CH, C1(7)], 43.1 [CH, C2(6)], 112.5 [CH, C2'(6') or C3'(5')], 119.5 (CH, C4'), 128.0 [CH, C11(12)], 128.7 [CH, C3'(5') or C2'(6')], 146.3 (C, C1'), 176.3 [C, C3(5)]. HRMS-ESI$^+$ m/z [*M*+H]$^+$: calcd for [$C_{17}H_{16}N_2O_2$+H^+]: 281.1285, found: 281.1288.

4-(2-Chlorophenylamino)-4-azapentacyclo[5.3.2.0^{2,6}.0^{8,10}]dodec-11-ene-3,5-dione, 20.

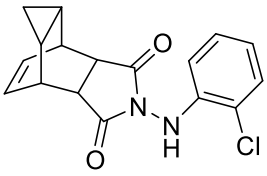

Following the general procedures D and E, 2-chlorophenylhydrazine (354 mg, 2.5 mmol) and the anhydride **15** (472 mg, 2.5 mmol) gave the desired product as a brown solid in an 81% overall yield. ^{1}H NMR (400 MHz, DMSO) δ: 0.01 (complex signal, 1 H, 9-H_a), 0.23 (m, 1 H, 9-H_b), 1.11 [complex signal, 2 H, 8(10)-H], 3.16 and 3.34 [t, *J* =

1.6 Hz, 2 H, 2(6)-H], 3.27 [broad s, 2 H, 1(7)-H], 5.80 and 5.84 [dd, J = 4.8 Hz, J' = 3.2 Hz, 2 H, 11(12)-H], 6.41 (dd, J = 8.0 Hz, J' = 1.6 Hz, 1 H, 6'-H), 6.75 (td, J = 7.6 Hz, J' = 1.6 Hz, 1 H, 4'-H), 7.07 (td, J = 8.0 Hz, J' = 1.2 Hz, 1 H, 5'-H), 7.27 (dd, J = 8.0 Hz, J' = 1.2 Hz, 1 H, 3'-H), 8.01 (broad s, 1 H, NH). ^{13}C NMR (100.6 MHz, DMSO) δ: 4.0 and 4.6 (CH_2, C9), 8.9 and 9.2 [CH, C8(10)], 32.9 and 33.1 [CH, C1(7)], 43.1 and 46.6 [CH, C2(6)], 112.8 (CH, C6'), 117.4 (C, C2'), 120.5 (CH, C4'), 127.7 (CH, C5'), 128.1 and 128.3 [CH, C11(12)], 129.4 (CH, C3'), 141.8 (C, C1'), 173.3 and 175.8 [C, C3(5)]. HRMS-ESI$^+$ m/z [M+H]$^+$: calcd for [$C_{17}H_{15}ClN_2O_2$+H^+]: 315.0900, found: 315.0895.

4-(2-Fluorophenylamino)-4-azapentacyclo[5.3.2.0^{2,6}.0^{8,10}]dodec-11-ene-3,5-dione, 21.

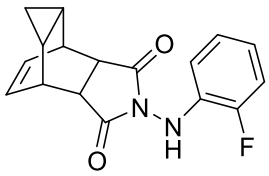

Following the general procedures D and E, 2-fluorophenylhydrazine (267 mg, 2.1 mmol) and the anhydride **15** (403 mg, 2.1 mmol) gave the desired product as a brown solid in an 81% overall yield. ^{1}H NMR (500 MHz, DMSO) δ: 0.05 (complex signal, 1 H, 9-H_a), 0.26 (m, 1 H, 9-H_b), 1.18 [complex signal, 2 H, 8(10)-H], 3.20 [t, J = 2.0 or 1.5 Hz, 2 H, 2(6)-H], 3.28 [complex signal, 2 H, 1(7)-H], 5.87 [m, 2 H, 11(12)-H], 6.50 (dd, J = 8.5 Hz, J' = 1.5 Hz, 1 H, 6'-H), 6.78 (complex signal, 1 H, 4'-H), 6.96 (td, J = 8.5Hz, J' = 1.0 Hz, 1 H, 5'-H), 7.11 (ddd, J = 12.0 Hz, J' = 8.0 Hz, J'' = 1.5 Hz, 1 H, 3'-H), 8.37 (broad s, 1 H, NH). ^{13}C NMR (125.7 MHz, DMSO) δ: 4.1 (CH_2, C9), 9.2 [CH, C8(10)], 32.9 [CH, C1(7)], 43.1 [CH, C2(6)], 113.7 (CH, d, $^3J_{C\text{-}F}$ = 2.3 Hz, C6'), 115.2 (CH, d, $^2J_{C\text{-}F}$ = 17.6 Hz, C3'), 119.9 (CH, d, $^3J_{C\text{-}F}$ = 6.8 Hz, C4'), 124.5 (CH, d, $^4J_{C\text{-}F}$ = 3.3 Hz, C5'), 128.1 [CH, C11(12)], 133.8 (C, $^2J_{C\text{-}F}$ = 11.1 Hz, C1'), 150.1 (C, d, $^1J_{C\text{-}F}$ = 239.8 Hz, C2'), 176.0 [C, C3(5)]. HRMS-ESI$^+$ m/z [M+H]$^+$: calcd for [$C_{17}H_{15}FN_2O_2$+H^+]: 299.1190, found: 299.1186.

Chapter 8

First MTDL to the NMDA and $P2X_7$ receptors, of potential interest for the treatment of Alzheimer's Disease.

8.1 Rationale and previous work

The presence of the P2X$_7$ receptor in the CNS is acknowledged nowadays, there, this purinergic ion channel participates in several physiological processes by initiating calcium dependent biological cascades, upon activation by the neurotransmitter ATP[1]. Depending on the concentration and the duration of the exposure to its ligand, the outcome of P2X$_7$ activation leads to opposite effects. On the one hand, upon low concentrations and/or low times of ligand exposure, the inflammatory response triggered by this receptor, helps reduce the secondary side effects of aggressions through specific mechanisms for survival of neural cells. On the other hand, when exposed to the typical chronic damage conditions, being either high concentrations of ATP or continued exposure to this neurotransmitter, the P2X$_7$ receptor up-regulates[2] or triggers the formation of a non-selective macropore, respectively. This non selective pore may then mediate the efflux of glutamate, γ-aminobutyric acid and other large molecules, up to 900 Da[3,4]. Under chronic inflammation conditions therefore, the P2X$_7$ contributes to excitotoxicity which eventually results in neuronal death[5].

A similar neurotoxic-neuroprotective double faced behaviour is displayed by the NMDA (N-methyl-D-aspartate) receptor[6]. When activated by its usual co-agonist, glycine, and a brief stimulation of glutamate, the RNMDA functions for normal synaptic transmission and plasticity. However the high levels of ambient glutamate, usually found in neurodegenerative disorders, cause excessive tonic activation of receptors inducing excitotoxicity. Consequently the RNMDA is believed to play a key role in the pathogenesis of these disorders and its modulation has been widely studied to avoid the progression of neurodegeneration[7,8,9,10].

[1] Tewari, M. & Seth, P. Emerging role of P2X$_7$ receptors in CNS health and disease. *Ageing Res. Rev*. **2015**, 24, 328–342.
[2] McLarnon, J. G., Ryu, J. K., Walker, D. G. & Choi, H. B. Upregulated expression of purinergic P2X$_7$ receptor in Alzheimer disease and amyloid-beta peptide-treated microglia and in peptide-injected rat hippocampus. *J. Neuropathol. Exp. Neurol*. **2006**, 65(11), 1090–7.
[3] Volonte, C. Apolloni, S. Skaper, S. D. & Burnstock, G. P2X$_7$ receptors: channels, pores and more. *CNS Neurol. Disord.: Drug Targets* **2012**, 11, 705.
[4] Duan, S. & Neary, J.T. P2X$_7$ receptors: properties and relevance to CNS function. *Glia*. **2006**, 54, 738-746.
[5] Burnstock, G. Physiopathological roles of P2X receptors in the central nervous system. *Curr. Med. Chem*. **2015**, 22(7), 819–844.
[6] Vyklicky, V., Korinek, M., Smejkalova, T., Balik, A., Krausova, B., Kaniakova, M. & Vyklicky, L. Structure, function, and pharmacology of NMDA receptor channels. *Physiolog. Res*. **2014**, 63 Suppl 1, S191-203.
[7] Gonda, X. Basic pharmacology of NMDA receptors. *Curr. Pharm. Des.* **2012**, 18, 1558.
[8] Malinow, R. New developments on the role of NMDA receptors in Alzheimer's disease. *Curr. Opin. Neurobiol.* **2012**, 22, 559.
[9] Lipton, S. Paradigm shift in neuroprotection by NMDA receptor blockade: memantine and beyond. *Nat. Rev. Drug Discov*. **2006**, 5(2), 160–170.

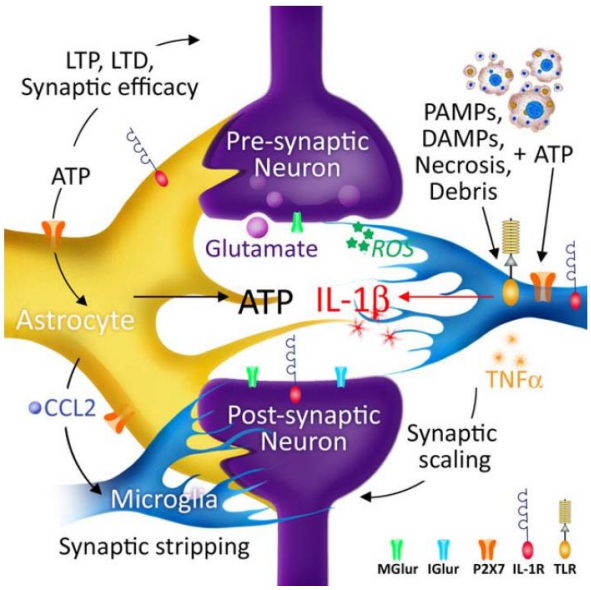

Figure 63. Schematic representation a tetrapartite synapse. It can be seen the close connections in glial $P2X_7$ (in orange) and NMDA (in blue, as iGluR).

In this light is no-surprise that these two receptors have been proposed to have a central role in the Alzheimer's disease (AD) pathophysiology. For this and taking into account:

1. The previous experience of the group in the preparation of NMDA antagonists[11,12,13].
2. $P2X_7$ antagonists (chapter 7) and NMDA antagonists (unpublished results) were already being developed in the current thesis.
3. Both receptors will require the same profile of antagonism, being the low-affinity antagonists the desired ones in order to preserve their physiological function, but inhibit the exocitotoxicity.
4. The complexity of AD pathophysiology has prompted the flourishment of the multitarget drug approach, which consists in simultaneously hitting two or more biological targets involved in the same disease with one sole compound[14,15,16.]

[10] Danysz, W. & Parsons, C. G. Alzheimer's disease,β-amyloid, glutamate, NMDA receptors and memantine - Searching for the connections. *Br. J. Pharmacol*. **2012,** 167(2), 324–352.
[11] Duque, M. D., Camps, P., Profire, L., Montaner, S., Vázquez, S., Sureda, F. X., Mallol, J., López-Querol, M., Naesens, L., De Clercq, E., Prathalingam, S. R. & Kelly, J. M. *Bioorg. Med. Chem*. **2009**, 17, 3198.
[12] Duque, M. D., Camps, P., Torres, E., Valverde, E., Sureda, F. X., López-Querol, M., Camins, A., Prathalingam, S. R., Kelly, J. M. & Vázquez, S. *Bioorg. Med. Chem*. **2010**, 18,46.
[13] Torres, E., Duque, M. D., López-Querol, M., Taylor, M. C., Naesens, L., Ma, C., Pinto, L. H., Sureda, F. X., Kelly, J. M. & Vázquez, S. *Bioorg. Med. Chem*. **2012**, 20, 942.
[14] Morphy, R. & Rankovic, Z. *J. Med. Chem*. **2005**, 48, 6523
[15] Ismaili, L., Refouvelet, B., Benchekroun, M., Brogi, S., Brindisi, M., Gemma, S., Campiani, G., Filipic, S., Agbabac, D., Esteban, G., Unzeta, M., Nikolic, K., Butini, S. & Marco-Contelles, J. Multitarget compounds bearing tacrine and

We embarked in the design and synthesis of the first putative dual-acting P2X$_7$-NMDA compounds, which are described in this chapter.

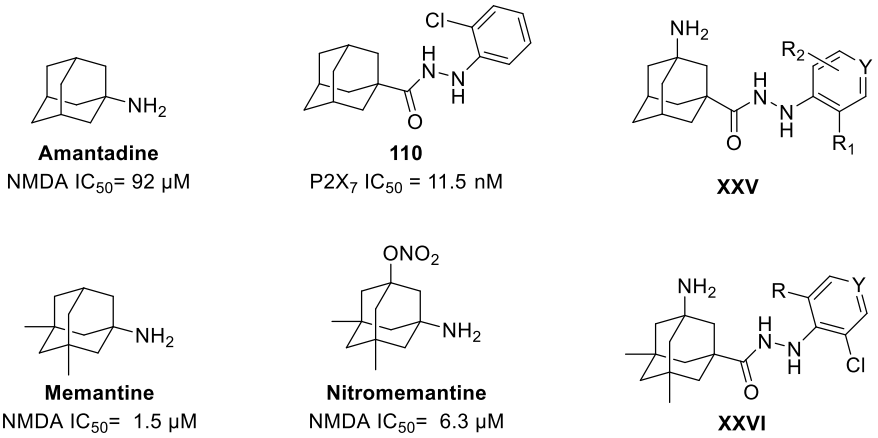

Figure 64. Rational design behind our envisaged NMDA-P2X$_7$ dual antagonists (general scaffolds **XXV** and **XXVI**).

Taking into account the structures of the clinically approved NMDA receptor antagonists amantadine and memantine and that of the P2X$_7$ inhibitor **110** developed by Abbott, we reasoned that a compound with general structures **XXV** and **XXVI** may be a dual inhibitor. Of note, Lipton and coworkers have recently found that the introduction of a substituent in the free bridgehead position of memantine is compatible with good inhibitory potency in the NMDA[17]. Thus, our assumption was that the introduction of the NH_2 group in the structure of **110** may lower the P2X$_7$ receptor antagonism, while the introduction of the hydrazine functionality in memantine may do not damage the NMDA receptor antagonism, resulting in a dual micromolar inhibition of both receptors.

donepezil-like structural and functional motifs for the potential treatment of Alzheimer's disease. *Prog. Neurobiol.* **2016** (in press).

[16] Perez, D. I., Martinez, A., Gil, C. & Campillo, N. E. From Bitopic Inhibitors to Multitarget Drugs for the Future Treatment of Alzheimer's Disease. *Curr. Med. Chem*. **2015**, 22(33), 3789–3806.

[17] Takahashi, H., Xia, P., Cui, J., Talantova, M., Bodhinathan, K., Li, W., Saleem, S., Holland, E. A., Tong, G., Piña-Crespo, J., Zhang, D., Nakanishi, N., Larrick, J. W., McKercher, S. R., Nakamura, T., Wang, Y. & Lipton, S. A. Pharmacologically targeted NMDA receptor antagonism by NitroMemantine for cerebrovascular disease. *Sci. Rep.* **2015**, 5, 14781.

8.2 Theoretical discussion

The totality of the compounds described in the manuscript was prepared in this Thesis context (Schemes 25 and 27).

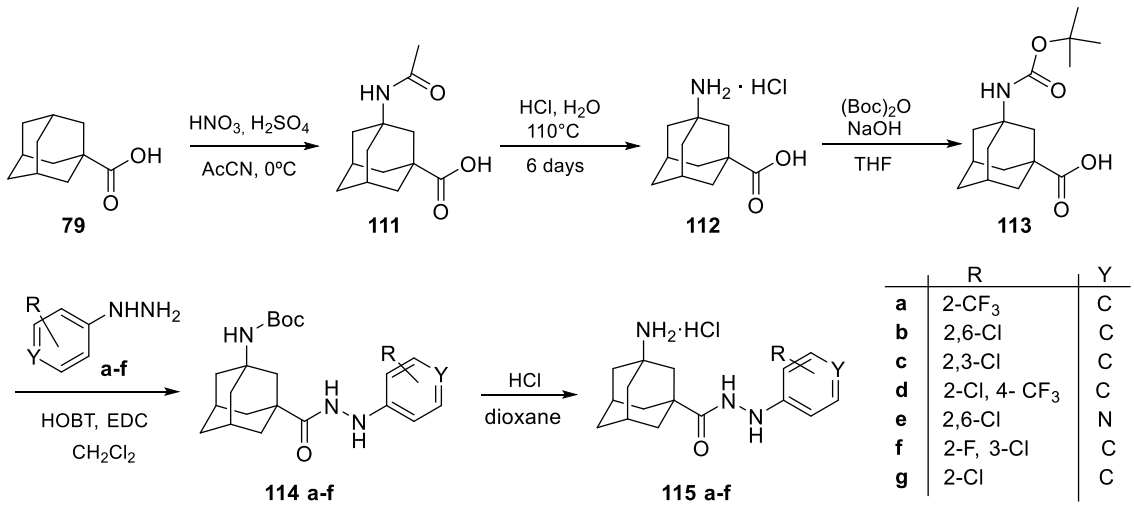

Scheme 25. Synthetic route for the first generation of compounds **115a-g**, featuring the general scaffold **XXV**.

The obtainment of the adamantane amino acid was a milestone in this project. After several unsuccessful trials, this intermediate was smoothly accessed by a Ritter-like reaction followed by a hydrolysis of the acetamide group. It is of interest commenting the first step of this synthetic route, from **79** to **111**, as despite this reaction is reported in the literature[18,19] the mechanism trough how it works has not been described to date. We propose that under the presence of strong acidic conditions, as the ones that nitric and sulfuric acid provide, an adamantyl tertiary carbocation[20] is formed through the intermediacy of a non-classical carbocation[21]. Following, the acetonitrile readily attacks this intermediate, yielding the acetamide **111** (Scheme 26).

[18] Wanka, L., Cabrelle, C., Vanejews, M. & Schreiner, P. R. γ-aminoadamantanecarboxylic acids through direct C-H bond amidations. *Eur. J. Org. Chem*. **2007**, (9), 1474–1490.
[19] Schreiner, P. R. & Wanka, L. Invention Concerning Aminoadamantane Compounds.US2008275112-A1. **2008**.
[20] Schleyer, P. R., Fort, R. C. & Watts, W. E. Stable Carbonium Ions. VIII. The 1-Adamantyl Cation. *J. Am. Chem. Soc*. **1964**, 86 (19), 4195–4197.
[21] Saunders, M., Schleyer, P. R. & Olah, G. A. Stable Carbonium Ions. XI.1 The Rate of Hydride Shifts in the 2-Norbornyl Cation. *J. Am. Chem. Soc*. **1964**, 86 (24), 5680–5681.

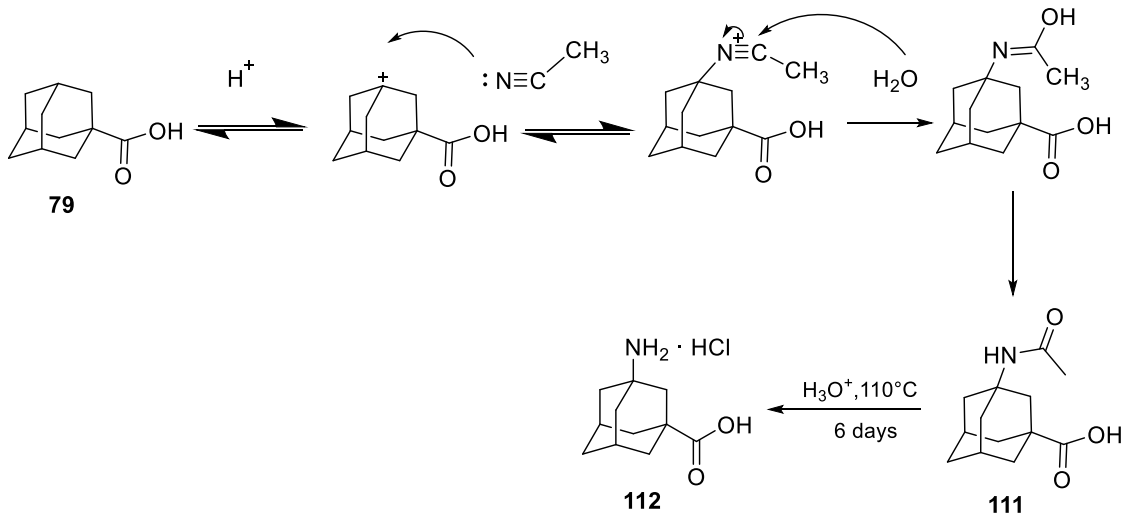

Scheme 26. Proposed mechanism for the formation of the adamantane amino acid.

A similar mechanism may take place when preparing the memantine-like structures. However, in this case, the 3,5-dimethyladamantane-1-carboxylic acid carbocation formation is more convoluted due to the two methyl groups in positions 3 and 5 produce both, induction and steric effect. The lower reactivity of this scaffold can be overcome with the addition of the superacid oleum[22] to the mixture of nitric and sulfuric acid. Remarkably the pure desired products **112** and **115** were accessed in quantitative yields.

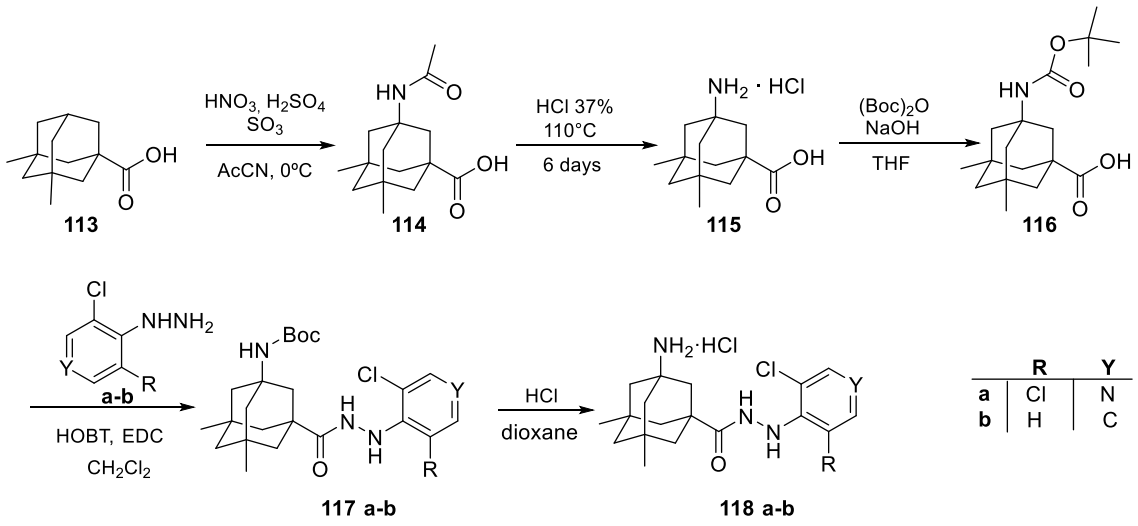

Scheme 27. Synthetic route for the second generation of compounds **118a-b**, featuring general scaffold **XXVI**.

[22] Muller, T. L. Sulfuric Acid and Sulfur Trioxide. *Kirk-Othmer Encyclopedia of Chemical Technology*. **2006**.

The compounds have been evaluated as $P2X_7$ antagonists by the group of Prof. Yong-Chul Kim and as NMDA antagonists by the group of Prof. Francesc Xavier Sureda (Universitat Rovira i Virgili, Reus). The structures and the results are shown in table 11.

Cmpd	Structure	NMDA IC_{50} (μM)[a]	$P2X_7$ % Inhibition or IC_{50} (μM)[b]
119	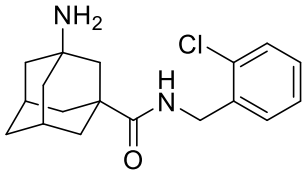	>500	NA[c]
115a	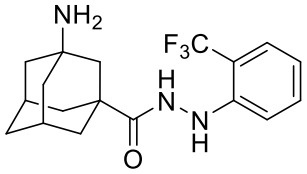	>500	63,4 %
115b	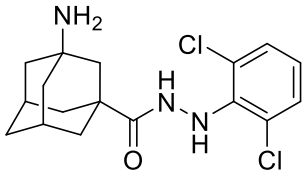	>500	84,4 %
115c	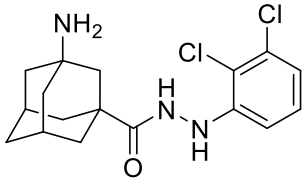	>500	82,6 %
115d	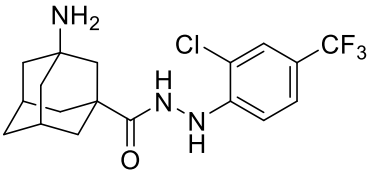	>500	79,3 %
115e	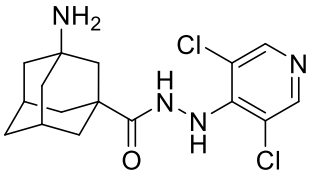	>500	73,4 %
115f	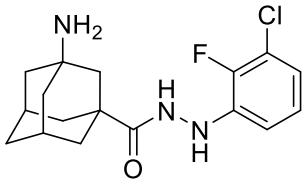	>500	82,9 %

115g	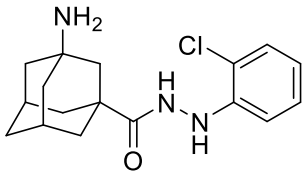	445	6.0
118a	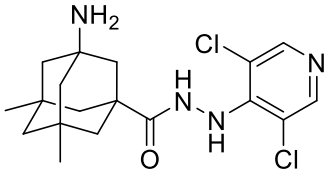	>500	16.1
118b	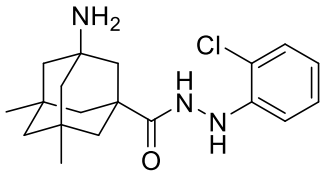	>500	9.9
Amantadine	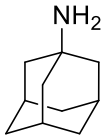	92 ± 29	ND[c]
Memantine	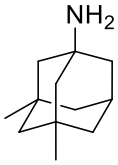	1.5 ± 0.1	ND[c]
3	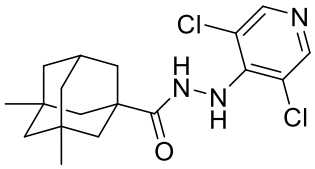	ND	0.13
120	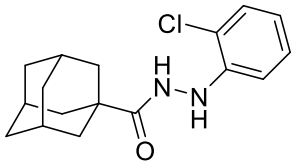	ND	11.5

Table 11. a: Functional data was obtained from primary cultures of cerebellar granule neurons by measuring the intracellular calcium concentration. Cells were challenged with NMDA as indicated. Data shown are means ± SEM of at least three separate experiments carried out on three different batches of cultured cells

b: % Inhibition values at 1 μM were expressed as a percentage, relative to maximum uptake of ethidium bromide stimulated by BzATP 6 μM and IC_{50} values were obtained from concentration response curves. All experiments were repeated at least 3-6 times. Experiments were assessed in the ethidium bromide accumulation assay using hP2X$_7$-expressing HEK293 cells.

c: ND, Not determined.

As described in the following draft manuscript, the introduction of the NH_2 group in the Abbott's compound, successfully led to **115g**, the first dual $P2X_7$/NMDA acting compound. However, the introduction of the two methyl groups when going from **115g** to **118a**, while kept the $P2X_7$ activity in the desired low μM range, unexpectedly, did not improve the NMDA activity, as when moving from Amt to memantine.

Dual $P2X_7$ - NMDA antagonists: a new strategy of potential interest for the treatment of Alzheimer's disease.

Olga Karoutzou,[#] Daina Martínez-Falguera,[∫] Francesc X. Sureda,[∫] Yong-Chul Kim,[ǂ] Santiago Vázquez[#] and Marta Barniol-Xicota[*,#]

[#]Laboratori de Química Farmacèutica (Unitat Associada al CSIC), Facultat de Farmàcia, and Institute of Biomedicine (IBUB), Universitat de Barcelona, Av. Diagonal 643, Barcelona E-08028, Spain.

[∫]Unitat de Farmacologia, Facultat de Medicina i Ciències de la Salut, Universitat Rovira i Virgili, c./St. Llorenç 21, Reus E-43201, Spain.

[ǂ]School of Life Sciences, Gwangju Institute of Science and Technology (GIST), Gwangju 500-712, Republic of Korea.

KEYWORDS. Alzheimer's Disease, dual target compounds, neuroinflammation, NMDA, $P2X_7$.

Supporting Information Placeholder

ABSTRACT: Multitarget directed ligands are a new hope for the treatment of multifactorial complex diseases as Alzheimer's Disease. Herein we present compounds targeting the NMDA and the $P2X_7$ receptors, which embody a different approach to this strategy, meanwhile on one side we are seeking to delay neurodegeneration targeting the glutamatergic NMDA, on the other side, we add on the aim to reduce the neuroinflammation, hence its exocitotoxic effects, targeting the $P2X_7$ receptors. Meanwhile the NMDA receptor is a widely recognized therapeutic target in AD, the $P2X_7$ is largely an unexplored receptor for this purpose, therefore the dual inhibitors herein presented, represent the first members – prone to a severe optimization - of a new class of multitarget-directed ligands.

Alzheimer's disease (AD) is an afflicting neurodegenerative disorder that triggers a progressive loss of neurons and synapses, leading to an irreversible cognitive decline and eventually to death.[1-3] The two groups of currently approved anti-AD drugs, cholinesterase inhibitors (donepezil, galantamine and rivastigmine)[4-6] and NMDA (N-methyl-D-aspartate) antagonists (memantine),[7-8] at their best, can only mask AD symptoms. Therefore, the development of new effective drugs that can halt the neurodegeneration process is urgently needed.[9-13]

Despite the complex pathophysiology of AD is still not completely understood, it is widely accepted that the accumulation of extracellular plaques is one of the major hallmarks in AD.[14-19] These plaques are mainly composed by beta-amyloid peptide and activated microglia, which in a first instance produces a neuroprotective inflammatory response to restore the damage.[20-21]

The ATP-gated $P2X_7$ receptors, widely expressed in the CNS,[22-24] have been recently identified as an obligate participant in activation of microglia,[25] where they are especially abundant. Moreover its physiological activation in other CNS cell lines, as granulate neurons, links to calcium-dependent neuroprotective events like cAMP response element-binding (CREB) activation,[26] responsible of protection against glutamate induced excitotoxicity and GSK3 phosphorylation, which rescues cells from apoptosis.[27] On the top of that, $P2X_7$ activation can also trigger the non-amyloidogenic cleavage of the amyloid precursor protein (APP).[28-29] On the other side, under the higher and chronic levels of ATP exposure, characteristic of AD, the $P2X_7$ receptors up-regulate in microglia.[30] This is responsible for catalysing inflammatory cascades through the release of IL-β, ATP, and other factors that lead to cell apoptosis. In addition, it has been demonstrated that $P2X_7$ also releases glutamate[31-33] which activates the ionotropic NMDA receptor.

Upon physiological levels of glutamate, the NMDA receptor is responsible for learning and memory processes,[34] however the beta amyloid oligomers that are formed in AD reduce glutamate uptake and increase glutamate release, resulting in an elevation of this neurotransmitter levels in the synaptic cleft.[35] This chronic moderate stimulation of the NMDA receptor provokes excitotoxicity, neuronal loss and the characteristic decline in memory and cognition observed in AD patients.[36-37] Clinically approved NMDA receptor antagonist memantine alleviates this process by blocking the NMDA in a non-competitive manner,[38] allowing the correct function of the receptor while preventing the excitotoxicity.[39] Despite its usefulness has been extensively proved, this drug cannot block the neurotoxic cascade of AD.

Taking into account that tackling this complex disease from only one point seems to be insufficient, in the last few years several groups have started medicinal chemistry programs aimed to design multi-target-directed (MTDL) ligands for hitting different biological targets for AD.[40-42]

Considering the aforementioned role of NMDA and $P2X_7$ receptors in AD we reasoned that a drug that could target simultaneously both receptors would be highly beneficial as a potential treatment of this disease, as it could not only halt its progression but also ameliorate its symptoms. In addition the similar double faced neuroprotective/cytotoxic behaviour that both receptors display, poses them as perfect candidates for

this purpose. In this light the ideal antagonist would be a compound that displayed inhibitory potencies in the low micromolar range, allowing the physiological function of the receptors but, in its turn, inhibiting them upon up-regulation or overactivation.

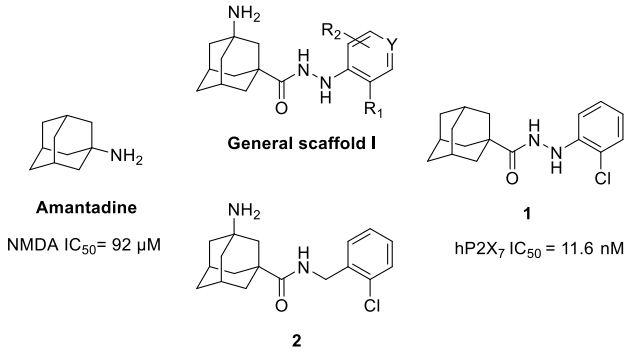

Figure 1. Rational design of the first generation of analogues.

For this we envisaged the aminoadamantylcarbohydrazides of general structure **I** as putative dual inhibitors (Figure 1). On one side **I** features the amantadine scaffold, which is known to be a micromolar NMDA antagonist (IC_{50} = 92 ± 29 μM),[43] and, on the other side, the *N'*-arylcarbohydrazide moiety of **1**, a compound endowed with nanomolar $P2X_7$ antagonist activity (IC_{50} = 11 ± 2 nM).[44] In a first instance, seven compounds featuring the general structure **I**, with diverse substitution in the aromatic moiety were prepared and pharmacologically evaluated as $P2X_7$ and NMDA antagonists. In addition and with the purpose to assess the importance of the hydrazide functionality in the linker, **2**, which features an amide group, was also prepared and pharmacologically evaluated. Upon testing of this batch of derivatives and in order to optimize the activity values obtained (see below), a second generation of dual antagonists was prepared starting from memantine, roughly sixty-fold more potent than amantadine as NMDA antagonist (IC_{50} = 1.5 ± 0.1 μM), and carbohydrazide **3**,[45] a known nanomolar $P2X_7$ antagonist (IC_{50} = 13 ± 1 nM) (Figure 2). The aim of moving from the general scaffold **I** to **II** was to improve the activity as RNMDA antagonist, shown by the previous set of molecules, while preserving the activity against the PX_7 receptor (see below).

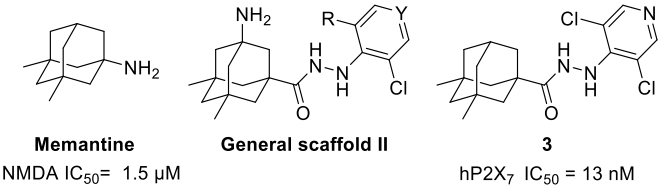

Figure 2. Design of the second generation of antagonists.

The synthetic route used to prepare the general scaffold **I**, comprehending the derivatives **9a-f** and its analogue **2** is depicted in the scheme 1.

Starting from the commercially available 1-adamantanecarboxylic acid, **4**, and following the procedure reported by Schreiner and co-workers, the *N*-Boc protected amino acid **6** was prepared in a good overall yield.[46] In order to explore the aromatic moiety SAR **6** was coupled, using EDC and HOBT, with a range of six aromatic hydrazines, **7a-f**, bearing different substituents in the phenyl group. Finally the desired compounds **9a-f** were obtained upon Boc cleavage with hydrochloric acid in 1,4-dioxane. The amide **2**, bearing a modified linker, was accessed following the aforementioned route but reacting **6** with 2-chlorobenzylamine. The pure products **9a-f** and **2**, were fully characterized and pharmacologically evaluated (see below).

Aminoacid **12** was prepared using a similar synthetic route, starting from 5,7-dimethyladamantanecarboxylic acid, **10**, but under hardened reaction conditions.[46] After *N*-protection, coupling with 2-chlorophenylhydrazine or 3,5-dichloro-4-hydrazinopyridine, and deprotection, carbohydrazides **15a-b** were obtained (Scheme 2).

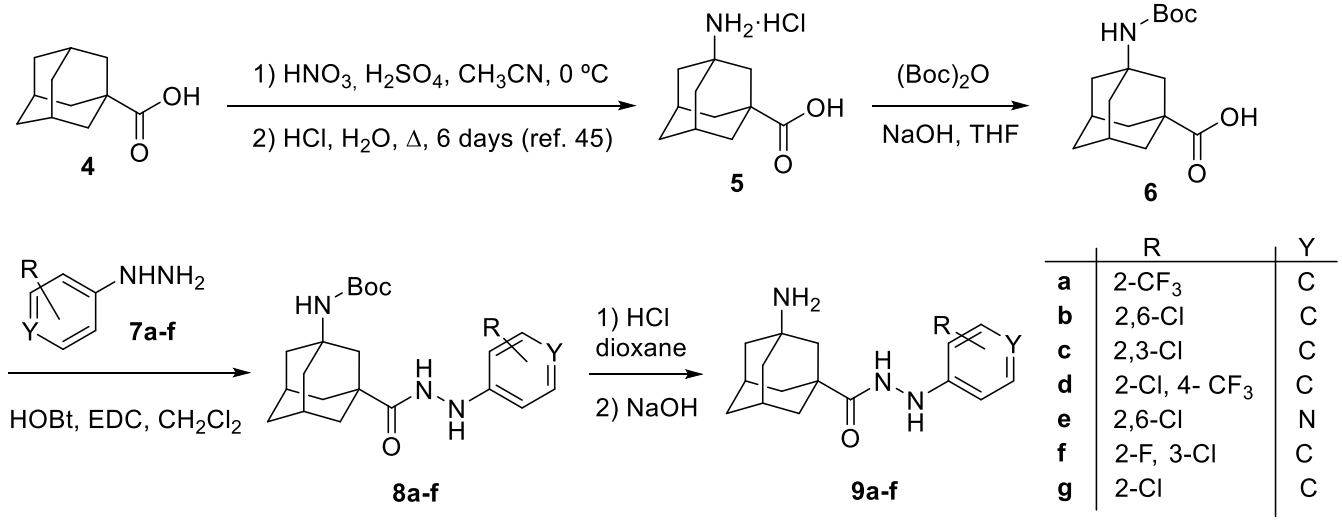

Scheme 1. Synthetic route for the first generation of compounds, featuring general scaffold I.

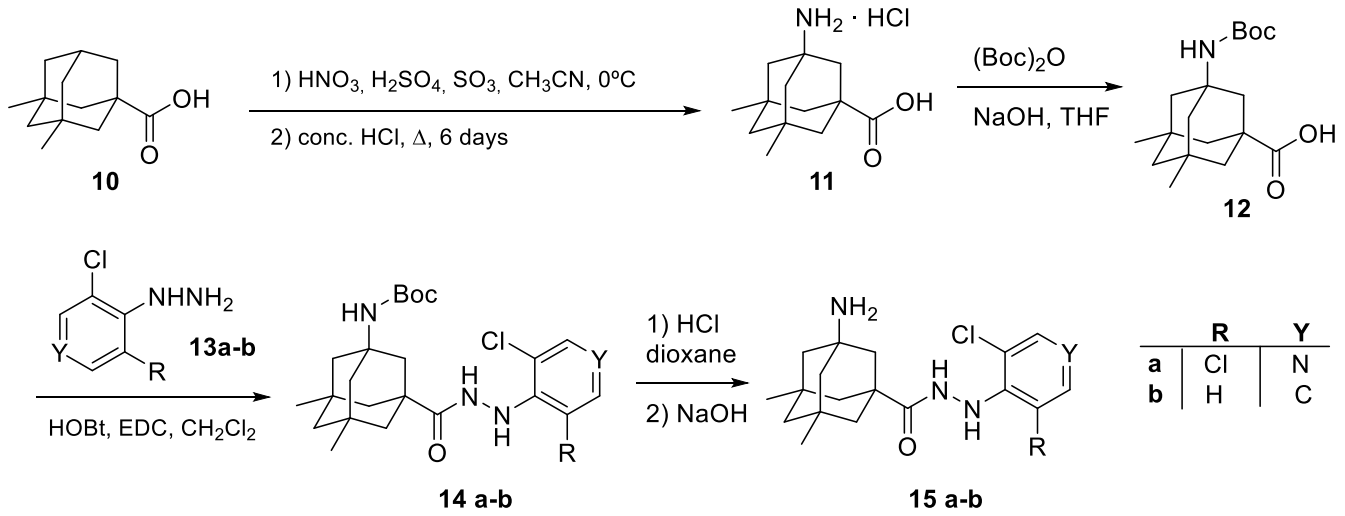

Scheme 2. Synthetic route for the second generation of compounds, featuring general scaffold **II**.

All new compounds were evaluated for their antagonistic effects on 2'(3')-*O*-(4-benzoylbenzoyl)-ATP (BzATP)-induced ethidium bromide uptake in human embryonic kidney 293 (HEK 293) cells stably expressing the human $P2X_7$ receptor, using compound AZD9056 as a positive control. Only the IC_{50} of **9g** was determined (Table 1).

Inspection of the results shown in Table 1 revealed that, with the sole exception of amide **2**, all the new compounds showed activities in the micromolar range. Suiting our purposes, **9g** displayed an IC_{50} of 6.0 ± 0.6 μM.

On another side, to evaluate if the synthesized compounds were able to antagonize NMDA receptors, we measured its effect on the increase in intracellular calcium evoked by NMDA (100 μM, in the presence of 10 μM of glycine) on rat cultured cerebellar granule neurons.[47] All the compounds were only able to inhibit NMDA in the high micromolar range (results not shown), pointing out that the addition of the phenyl hydrazide moiety is highly detrimental for NMDA activity. The best compound of the series, **9g**, with an IC_{50} = 445 μM, was roughly five fold less potent than amantadine.

Taking into account that the 3,5-dimethyl derivative of amantadine (i.e., memantine) is 60-fold more potent as NMDA inhibitor than amantadine, we envisaged a second series of derivatives featuring the memantine moiety. Reinforcing the suitability of this strategy to obtain balanced inhibitory potencies in both receptors, hydrazide **3**, featuring two methyl groups in the adamantane scaffold, was reported to be a nanomolar $P2X_7$ inhibitor.[45] Hence, while the addition of the two methyl groups to the polycyclic scaffold of the adamantane should not be detrimental for $P2X_7$ inhibition, we hoped that their insertion should optimize the activity in the NMDA receptor, leading to a dual micromolar inhibitor of both receptors.

Taking into account that the most promising compound, **9g,** in both previous pharmacological evaluations, P2X7 and NMDA, featured an *o*-chloro substitution in the phenyl ring, this motif was the one selected for the right hand side structure of our compounds. In addition we decided to prepare **15a** due to its similarity with **3** (see Figure 2).

Pleasingly upon testing in the $P2X_7$, the IC_{50} of **15a** and **15b** were only slightly higher than that of **9g**, reinforcing our hypothesis that the introduction of the two methyl groups would not be deleterious for the $P2X_7$ antagonist activity (Table 1). However, contrary to our expectations, **15a** and **15b** were unable to significantly inhibit the NMDA receptor even at milimolar concentrations.

To sum up, we have synthesized, fully characterized and evaluated a series of novel adamantylcarbohydrazides as potential dual NMDA and P2X7 antagonists. While three derivatives displayed low micromolar activities as P2X7 antagonists, only **9g** showed some activity as NMDA receptor antagonist. Compound **9g** is, to the best of our knowledge, the first dual antagonist of both receptors.

ASSOCIATED CONTENT

Supporting Information. Procedures for the synthesis and characterization of novel compounds. This material is available free of charge via the Internet at http://pubs.acs.org.

AUTHOR INFORMATION

Corresponding Author

* M. B. X.: Tel: +34 934024533. Fax: +34 934035941. E-mail: martabx@gmail.com

Funding Sources

This work was funded by the Spanish *Ministerio de Economía y Competitividad* (Grant SAF2014-57094-R to F. X. S. and S. V.). M. B.-X. acknowledges a fellowship from the Institute of Biomedicine of the University of Barcelona (IBUB). S. V. thanks the *Generalitat de Catalunya* (2014-SGR-00052)

ABBREVIATIONS

AD, Alzheimer's disease; APP, amyloid precursor protein; BzATP, 2'(3')-*O*-(4-benzoylbenzoyl)-ATP; CREB, cAMP response element-binding; EDC, 1-ethyl-3(3-dimethylaminopropyl)carbodiimide; GSK3, glycogen synthase kinase 3; HEK, human embryonic kidney; HOBT, 1-hydroxybenzotriazole; IL-β, interleukin beta; NMDA, N-methyl-D-aspartate; $P2X_7$, purinergic receptor 7; RNMDA, NMDA receptor.

Compound	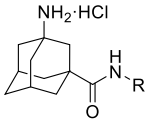	% Inhibition or IC_{50}[a] EtBr uptake in $hP2X_7$-expressing HEK293 cells[b]
no BzATP	-	0%
only BzATP	-	100%
AZD9056	-	IC_{50} = 4.1 ± 0.7 nM[d]
2	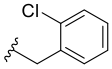	NA[c]
9a	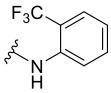	52% / 63%
9b	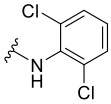	77% / 84%
9c	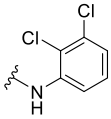	58% / 83%
9d	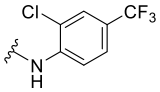	76% / 79%
9e	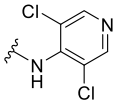	47% / 73%
9f	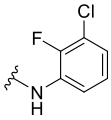	85% / 83%
9g	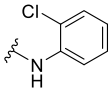	IC_{50} = 6.0 ± 0.6 μM[d]
15a	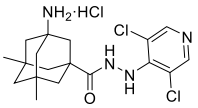	IC_{50} = 9.9 μM[d]
15b	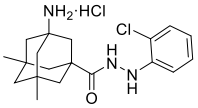	IC_{50} = 16.1 μM[d]

[a]Percentage inhibition values at 10 μM (left) and 1 μM (right) were expressed as percentages, relative to maximum uptake of ethidium bromide stimulated by BzATP 6 μM. All experiments were repeated at least 3-6 times. [b]Experiments were assessed in the ethidium bromide accumulation assay using $hP2X_7$-expressing HEK293 cells. [c]Not active. [d]IC_{50} value was obtained from concentration response curves.

REFERENCES

(1) Goedert, M.; Spillantini, M.G. A century of Alzheimer's disease. *Science* **2006**, 314, 777-781.

(2) Scheltens, P.; Blennow, K.; Breteler, M. M. B.; de Strooper, B.; Frisoni, G. B.; Salloway, S.; Van der Flier, W. M. Alzheimer's disease. *Lancet* **2016**, *388*, 505-517.

(3) Hickman, R. A.; Faustin, A.; Wisniewski, T. Alzheimer disease and its growing epidemic: risk factors, biomarkers, and the urgent need for therapeutics. *Neurol. Clin.* **2016**, *34*, 941-953.

(4) Polinsky, R. J. Clinical pharmacology of rivastigmine: a new-generation acetylcholin-esterase inhibitor for the treatment of Alzheimer's disease. *Clin Ther*. **1998**, 20, 634-47.

(5) Cheewakriengkrai, L.; Gauthier, S. A 10-year perspective on donepezil. *Expert Opin. Pharmacother*. **2013**, *14*, 331-338.

(6) Burns, A.; Bernabei, R.; Bullock, R.; Cruz Jentoft, A. J.; Frölich, L.; Hock, C.; Raivio, M.; Triau, E.; Vandewoude, M.; Came, E.; Van Baelene, B.; Hammond, G. L.; van Oene, J. C.; Schwalen, S. Safety and efficacy of galantamine (Reminyl) in severe Alzheimer's disease (the SERAD study): a randomised, placebo-controlled, double-blind trial. *Lancet Neurol.* **2009**, *8*, 39-47.

(7) Danysz, W.; Parsons, C. G. Alzheimer's disease, β-amyloid, glutamate, NMDA receptors and memantine - Searching for the connections. *Br. J. Pharmacol*. **2012**, *167*, 324–352.

(8) Parsons, C. G.; Danysz, W.; Dekundy, A.; Pulte, I. Memantine and cholinesterase inhibitors: complementary mechanisms in the treatment of Alzheimer's disease. *Neurotox. Res.* **2013**, *24*, 358-369.

(9) Winblad, B.; Amouyel, P.; Andrieu, S.; Ballard, C.; Brayne, C.; Brodaty, H.; Cedazo-Mínguez, A.; Dubois, B.; Edvardsson, D.; Feldman, H.; Fratiglioni, L.; Frisoni, G. B.; Gauthier, S.; Georges, J.; Graff, C.; Iqbal, K.; Jessen, F.; Johansson, G.; Jönsson, L.; Kivipelto, M.; Knapp, M.; Mangialasche, F.; Melis, R.; Nordberg, A.; Rikkert, M. O.; Qiu, C.; Sakmar, T. P.; Scheltens, P.; Schneider, L. S.; Sperling, R.; Tjernberg, L. O.; Waldemar, G.; Wimo, A.; Zetterberg, H. Defeating Alzheimer's disease and other dementias: a priority for European science and society. *Lancet Neurol.* **2016**, *15*, 455-532.

(10) Anand, R.; Gill, K. D.; Mahdi, A. A. Therapeutics of Alzheimer's disease: Past, present and future. *Neuropharmacology*, **2014**, *76*, 27–50.

(11) Cummings, J.; Aisen, P. S.; DuBois, B.; Frölich, L. ; Jack Jr., C. R.; Jones, R. W.; Morris, J. C.; Raskin, J.; Dowsett, S. A.; Scheltens, P. Drug development in Alzheimer's disease: the path to 2025. *Alzheimers Res. Ther.* **2016**, *8*:39, doi: 10.1186/s13195-016-0207-9.

(12) Godyń, J.; Jończyk, J.; Panek, D.; Malawska, B. Therapeutic strategies for Alzheimer's disease in clinical trials. *Pharmacol. Rep.* **2016**, *68*, 127-138.

(13) Mohamed, T.; Shakeri, A.; Rao, P. P. N. Amyloid cascade in Alzheimer's disease: recent advances in medicinal chemistry. *Eur. J. Med. Chem.* **2016**, *113*, 258-272.

(14) Mucke, L.; Selkoe, D. J. Neurotoxicity of amyloid β-protein: Synaptic and network dysfunction. *Cold Spring Harb. Perspect. Med*. **2012**, *2*, a006338

(15) Selkoe, D. J.; Hardy, J. The amyloid hypothesis of Alzheimer's disease at 25 years. *EMBO Mol. Med.* **2016**, *8*, 595-608.

(16) Luo, J.; Wärmländer, S. K.; Gräslund, A.; Abrahams, J. P. Cross-interactions between the Alzheimer disease amyloid-β and other amyloid proteins: a further aspect of the amyloid hypothesis. *J. Biol. Chem.* **2016**, *291*, 16485-16493.

(17) Iqbal, K.; Liu, F.; Gong, C. X. Tau and neurodegenerative disease: the story so far. *Nat. Rev. Neurol.* **2016**, *12*, 15-27.

(18) Harrison, J. R.; Owen, M. J. Alzheimer's disease: the amyloid hypothesis on trial. *Br. J. Phychiatry* **2016**, *208*, 1-3.

(19) Wilkins, H. M.; Swerdlow, R. H. Amyloid precursor protein processing and bioenergetics. *Brain Res. Bull.* **2016**, doi:10.1016/j.brainresbull.2016.016.08.009.

(20) Heppner, F. L.; Ransohoff, R. M.; Becher, B. Immune attack: the role of inflammation in Alzheimer disease. *Nat. Rev. Neurosci.* **2015**, *16*, 358-372.

(21) Schwartz, M.; Deczkowska, A. Neurological disease as a failure of brain-immune crosstalk: the multiple faces of neuroinflammation. *Trends Immunol.* **2016**, *37*, 668-679.

(22) Sperlágh, B.; Illes, P. P2X7 receptor: an emerging target in central nervous system diseases. *Trends Pharmacol. Sci.* **2014**, *35*, 537–547.
(23) Burnstock, G. Physiopathological roles of P2X receptors in the central nervous system. *Curr. Med. Chem.* **2015**, *22*, 819–844.
(24) Rech, J. C.; Bhattacharya, A.; Letavic, M. A.; Savall, B. M. The evolution of P2X7 antagonists with a focus on CNS indications. *Bioorg. Med. Chem. Lett.* **2016**, *26*, 3838–3845.
(25) Sanz, J. M.; Chiozzi, P.; Ferrari, D.; Colaianna, M.; Idzko, M.; Falzoni, S.; Fellin, R.; Trabace, L.; Di Virgilio, D. Activation of microglia by amyloid β requires $P2X_7$ receptor expression. *J. Immunol.* **2009**, *182*, 4378-4385.
(26) Miras-Portugal, M. T.; Gomez-Villafuertes, R.; Gualix, J.; Diaz-Hernandez, J. I.; Artalejo, A. R.; Ortega, F.; Delicado, E. G.; Perez-Sen, R. Nucleotides in neuroregeneration and neuroprotection. *Neuropharmacology* **2016**, *104*, 243–254.
(27) Ortega, F.; Pérez-Sen, R.; Morente, V.; Delicado, E. G.; Miras-Portugal, M. T. P2X7, NMDA and BDNF receptors converge on GSK3 phosphorylation and cooperate to promote survival in cerebellar granule neurons. *Cell. Mol. Life Sci.* **2010**, *67*, 1723–1733.
(28) Delarasse, C.; Auger, R.; Gonnord, P.; Fontaine, B.; Kanellopoulos, J. M. The purinergic receptor P2X7 triggers alpha-secretase-dependent processing of the amyloid precursor protein. *J. Biol. Chem.* **2011**, *286*, 2596–2606.
(29) Miras-Portugal, M.T.; Diaz-Hernández, J. I.; Gomez-Villafuertes, R.; Diaz-Hernández, M.; Artalejo, A. R.; Gualix, J. Role of P2X7 and P2Y2 receptors on α-secretase-dependent APP processing: control of amyloid plaques formation "in vivo" by P2X7 receptor. *Comput. Struct. Biotechnol. J.* **2015**, *13*, 176–181.
(30) Parvathenani, L. K.; Tertyshnikova, S.; Greco, C. R.; Roberts, S. B.; Robertson, B.; Posmantur, R. P2X7 mediates superoxide production in primary microglia and is up-regulated in a transgenic mouse model of Alzheimer's disease. *J. Biol. Chem.* **2003**, *278*, 13309–13317.
(31) Ficker, C.; Rozmer, K.; Kató, E.; Andó, R. D.; Schumann, L.; Krügel, U.; Franke, H.; Sperlágh, B.; Riedel, T.; Illes, P. Astrocyte-neuron interaction in the substantia gelatinosa of the spinal cord dorsal horn via P2X7 receptor-mediated release of glutamate and reactive oxygen species. *Glia* **2014**, *62*, 1671–1686.
(32) Cervetto, C.; Alloisio, S.; Frattaroli, D.; Mazzotta, M. C.; Milanese, M.; Gavazzo, P.; Passalacqua, M.; Nobile, M.; Maura, G.; Marcoli, M. The P2X7 receptor as a route for non-exocytotic glutamate release: dependence on the carboxyl tail. *J. Neurochem.* **2013**, *124*, 821–831.
(33) Marcoli, M.; Cervetto, C.; Paluzzi, P.; Guarnieri, S.; Alloisio, S.; Thellung, S.; Nobile, M.; Maura, G. P2X7 pre-synaptic receptors in adult rat cerebrocortical nerve terminals: a role in ATP-induced glutamate release. *J. Neurochem.* **2008**, *105*, 2330–2342.
(34) Sepulveda, F. J.; Bustos, F. J.; Inostroza, E.; Zúñiga, F. E.; Neve, R. L.; Montecino, M.; van Zundert, B. Differential roles of NMDA receptor subtypes NR2A and NR2B in dendritic branch development and requirement of RasGRF1. *J. Neurophysiol.* **2010**, *103*, 1758–1770.
(35) Fernández-Tomé, P.; Brera, B.; Arévalo, M.; de Ceballos, M. L. Beta-amyloid25-35 inhibits glutamate uptake in cultured neurons and astrocytes: modulation of uptake as a survival mechanism. *Neurobiol. Dis.* **2004**, *15*, 580–589
(36) Butterfield, D. A.; Pocernich, C. B. The glutamatergic system and Alzheimer's disease: Therapeutic implications. CNS Drugs **2003**, *17*, 641–652.
(37) Lewerenz, J.; Maher, P. Chronic glutamate toxicity in neurodegenerative diseases. What is the evidence? *Front. Neurosci.* **2015**, *9:469*.
(38) Johnson, J. W.; Kotermanski, S. E. Mechanism of action of memantine. *Curr. Opin. Pharmacol.* **2006**, *6*, 61-7.
(39) Song, M. S.; Rauw, G.; Baker, G. B.; Kar, S. Memantine protects rat cortical cultured neurons against β-amyloid-induced toxicity by attenuating tau phosphorylation. Eur. J. Neurosci. **2008**, *28*, 1989–2002.
(40) Cavalli, A.; Bolognesi, M. L.; Minarini, A.; Tumiatti, V.; Recanatini, M.; Melchiorre, C. Multi-target-directed ligands to combat neurodegenerative diseass. *J. Med. Chem.* **2008**, *51*, 347-372.
(41) Rosini, M.; Simoni, E.; Minarini, A.; Melchiorre, C. Multi-target design strategies in the context of Alzheimer's disease: acetylcholinesterase inhibition and NMDA receptor antagonism as the driving forces. *Neurochem. Res.* **2014**, *39*, 1–10.
(42) Singh, M.; Kaur, M.; Chadha, N.; Silakari, O. Hybrids: a new paradigm to treat Alzheimer's disease. *Mol. Divers.* **2016**, *20*, 271-297.
(43) Blanpied, T. A. Amantadine Inhibits NMDA receptors by accelerating channel closure during channel block. *J. Neuroscience* **2005**, *25*, 3312–3322.
(44) Nelson, D. W.; Sarris, K.; Kalvin, D. M.; Namovic, M. T.; Grayson, G.; Donnelly-Roberts, D. L.; Harris, R.; Honore, P.; Jarvis, M. F.; Faltynek, C. R.; Carroll, W. A. Structure-activity relationship studies on *N'*-aryl carbohydrazide $P2X_7$ antagonists. *J. Med. Chem.* **2008**, *51*, 3030-3034.
(45) Lee, W.-G.; Lee, S.-D.; Cho, J.-H.; Jung, Y.; Kim, J: Hien, T. T.; Kang, K.-W.; Ko, H.; Kim, Y.-C. Structure-activity relationships and optimization of 3,5-dichloropyridine derivatives as novel $P2X_7$ receptor antagonists. *J. Med. Chem.* **2012**, *55*, 3687-3698.
(46) Wanka, L.; Cabrelle, C.; Vanejews, M.; Schreiner, P. R. γ-aminoadamantanecarboxylic acids through direct C-H bond amidations. *Eur. J. Org. Chem.* **2007**, *9*, 1474–1490.
(47) Canudas, A. M.; Pubill, D.; Sureda, F. X.; Verdaguer, E.; Camps, P.; Muñoz-Torrero, D.; Jiménez, A.; Camins, A.; Pallàs, M. Neuroprotective effects of (±)-huprine Y on in vitro and in vivo models of excitotoxicity damage. *Exp. Neurol.* **2003**, *180*, 123–130.

SYNOPSIS TOC (Word Style “SN_Synopsis_TOC”).

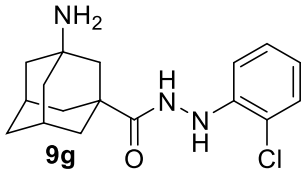

9g

Compound **9g** is the first example of a dual NMDA-P2X$_7$ antagonist, which could open up a new therapeutic strategy for the treatment of Alzheimer Disease.

Dual $P2X_7$ - NMDA antagonists: a new strategy of potential interest for the treatment of Alzheimer's disease

Olga Karoutzou ,[‡] Daina Martínez-Falguera,[#] Francesc X. Sureda,[#] Yong-Chul Kim,[§] Santiago Vázquez[‡] and Marta Barniol-Xicota*[,‡]

INDEX

1. **Chemical Synthesis**

1.1 General methods

Melting points were determined in open capillary tubes with a MFB 595010 M Gallenkamp. 400 MHz ^{1}H NMR spectra and 100.6 MHz ^{13}C NMR spectra were recorded on a Varian Mercury 400 spectrometer. The chemical shifts are reported in ppm (δ scale) relative to internal tetramethylsilane, and coupling constants are reported in hertz (Hz). Assignments given for the NMR spectra of the new compounds have been carried out on the basis of COSY $^{1}H/^{13}C$ (gHSQC and gHMBC sequences), COSY $^{1}H/^{1}H$ (standard procedures). IR spectra were run on PerkinElmer Spectrum RX I spectrophotometer. Absorption values are expressed as wavenumbers (cm^{-1}); only significant absorption bands are given. The GC/MS analysis was carried out in an inert Agilent Technologies 5975 gas chromatograph equipped with an Agilent 122-5532 DB-5MS 1b (30 m × 0.25 mm) capillary column with a stationary phase of phenylmethylsilicon (5% diphenyl−95% dimethylpolysiloxane), using the following conditions: initial temperature of 50 °C (1 min), with a gradient of 10°C/min up to 300 °C, and a temperature in the source of 250 °C, solvent delay (SD) of 4 min and a pressure of 7.35 psi. Accurate mass measurements were obtained using ESI technique. Absorption Thin-layer chromatography was performed with aluminum-backed sheets with silica gel 60 F254 (Merck, ref 1.05554), and spots were visualized with UV light and 1% aqueous solution of $KMnO_4$

1.2 Synthesis of the starting acids **6** and **12**.[1]

3-acetamidoadamantane-1-carboxylic acid.

1-Adamantane carboxylic acid, **4**, (5 g, 27.7 mmol) was suspended in 70% HNO_3 (4 mL) and cooled at 0 ^{o}C with an ice bath. Using an addition funnel, 98% H_2SO_4 (30 mL)

was added dropwise by means of an addition funnel, at such a rate that the temperature was kept at 0°C or below. The reaction mixture was stirred for 2 hours at 0 °C, whereupon acetonitrile (20 mL) was added via an addition funnel, at such a rate that the reaction mixture was kept at 0 °C. After all the acetonitrile was added, the reaction was stirred at 0 °C for 3 hours. The reaction mixture was then poured over ice (ca 200 g) with shaking and was allowed to warm to room temperature. The colorless solid was then filtered over vacuum, washed with water and dried overnight to give 5.8 g of the title compound (5.8 g, 88.1% yield). The ^{1}H NMR matched the data previously reported in the bibliography.[1]

3-Aminoadamantane-1-carboxylic acid hydrochloride, **5·HCl**

To a 3-neck round bottom flask equipped with a reflux condenser, thermometer and a mechanical stirrer were added 3-acetamidoadamantane-1-carboxylic acid (5.8 g, 24.4 mmol), water (13.5 mL) and 37% hydrochloric acid (33 mL) and the mixture was heated at reflux for 6 days. After cooling at 0°C with an ice bath, the white precipitate solid was carefully filtered. The solid obtained was then dried under vacuum for 1 day to afford **5·HCl** (2.6 g, 45.9% yield). The ^{1}H NMR matched the data previously reported in the bibliography.[1]

3-[(tert-butoxycarbonyl)amino]adamantane-1-carboxylic acid, **6**

To a mixture of **5·HCl** (2.6 g, 11.22 mmol) in THF (26 mL), aqueous 2 M NaOH (10 mL) and di-*tert*-butyl dicarbonate (2.52 g, 11.7 mmol) were added. After stirring for 16 hours at room temperature, the reaction was cooled in an ice bath. Upon neutralization with aqueous 2 M HCl, the mixture was partitioned into ethyl acetate and water. The organic layer was separated, dried over anhydrous Na_2SO_4, filtered and concentrated under reduced pressure to give impure **6** (2.66 g). After purification by crystallization

from acetonitrile, **6** (1.5 g, 45.3% yield) was obtained as a white solid. The ^{1}H NMR matched the data previously reported in the bibliography.[1]

3-acetamido-5,7-dimethyladamantane-1-carboxylic acid.

3,5-dimethyladamantane-1-carboxylic acid (2.0 g, 9.6mmol), was suspended in 70% HNO_3 (6 mL) and cooled to 0 ^oC with an ice bath. Using an addition funnel, 98% H_2SO_4 (10 mL) was added dropwise by means of an addition funnel, at such a rate that the temperature was kept at 0^oC or below. The mixture was stirred for 10 minutes and 20-30% oleum (3.5 mL) was added dropwise. The whole mixture was stirred for 30 minutes at 0 ^oC and 1 hour at room temperature. Upon cooling again at 0 ^oC, acetonitrile (6 mL) was added and the mixture stirred for 10 minutes at 0 ^oC and 3 hours at room temperature. Finally, the mixture was poured onto ice (ca 200 g) and kept at 5 ^oC overnight. The white precipitate was collected via suction filtration and dried for 1 hour to obtain the title compound as a white solid in quantitative yield.[1]

3-amino-5,7-dimethyladamantane-1-carboxylic acid hydrochloride, **11·HCl**

To a round flask equipped with a reflux condenser, thermometer and a mechanical stirrer, 3-acetamido-5,7-dimethyladamantane-1-carboxylic acid (2.5 g, 9.42 mmol) was heated in 37% HCl (60 mL) for 5 days at reflux. After removal of the acid under reduced pressure, the crude product was washed with ethyl acetate and collected via suction filtration. The compound was dried in a desiccator over P_2O_5 overnight to give **11·HCl** (1.23 g, 50% yield) as a white solid. The ^{1}H NMR matched the data previously reported in the bibliography.[1]

3-tert-butoxycarbonylamino-5,7-dimethyladamantane-1-carboxylic acid, **13**

Di-*tert*-butyl dicarbonate (1.03 g, 4.73 mmol) was added to a round flask containing 11·HCl (1.23 g, 4.73 mmol) in THF (15 mL) and aqueous 2 M NaOH (6 mL). After stirring for 16 hours at room temperature, the reaction was cooled into an ice bath. Following it was neutralized with aqueous 2 M HCl and partitioned into ethyl acetate and water. The organic layer was separated, dried over Na_2SO_4, filtered and concentrated under reduced pressure to give a white solid (1.15 g). The crude was purified by crystallization from acetonitrile to give 13 (800 mg, 52% yield). The ^1H NMR matched the data previously reported in the bibliography.[1]

1.3 General procedures for the synthesis of carbohydrazides **9a-f** and **15a-b**.

General Procedure A.

To a suspension of **6** (1 eq) in CH_2Cl_2 were added HOBT (1.2 eq) and EDC (1.2 eq) and the whole stirred at room temperature for 2 hours. The resulting mixture was then added dropwise via an addition funnel to a solution of the desired hydrazine (1 eq) in CH_2Cl_2, maintaining the temperature range between 0-10 ^oC. The mixture was washed with water and aqueous K_2CO_3, and the organic layer was dried over anhydrous Na_2SO_4, filtered and concentrated under reduced pressure, to yield the corresponding carbamate **8a-f** and **14a-b**.

General Procedure B .

To a solution of the corresponding carbamate precursor (1 eq) in CH_2Cl_2 (20 mL) was added 4 M HCl in 1,4-dioxane (10 mL) and the solution was left stirring at room temperature for 16 hours. Once the reaction was completed, the mixture was extracted with aqueous 1 M HCl and the aqueous phase was then brought to basic pH with excess of aqueous 2 M NaOH. Upon extraction with CH_2Cl_2. the joined organic extracts were dried over anhydrous Na_2SO_4, filtered and concentrated under reduced pressure. The

reaction crude was crystallized from ethyl acetate, to yield the desired pure product **9a-f** and **15a-b**.

1.4 Characterization data for **2**, **9a-f** and **15a-b**.

3-amino-N-(2-chlorobenzyl)adamantane-1-carboxamide, **2**

Following the general procedure A, but using 2-chlorobenzylamine instead of a hydrazine, the expected carbamate was obtained that was subsequently treated with the the general procedure B to yield **2** as a white solid in a 35% overall yield. mp = 186-189 ^{o}C. IR (ATR): 667, 744, 868, 1036, 1049, 1261, 1287, 1359, 1408, 1439, 1467, 1529, 1628, 2139, 2842, 2899, 3333 cm^{-1}. ^{1}H-NMR (400 MHz, $CDCl_3$) δ: 1.48 (s, 2 H, N$\underline{H_2}$), 1.56-1.63 [complex signal, 6 H, 6-H_2 and 4(10)-H_2], 1.67 (s, 2 H, 2-H_2), 1.72 -1.80 [m, 4 H, 8(9)-H_2], 2.20 [m, 2 H, 5(7)-H], 4.50 (d, *J* = 6 Hz, 2 H, NHC$\underline{H_2}$), 6.05 (s, 1 H, CON$\underline{H}$), 7.19-7.25 (complex signal, 2 H) and 7.31-7.37 (complex signal, 2 H) (Ar-H). ^{13}C-NMR (100.6 MHz, $CDCl_3$) δ: 29.5 [CH, C5(7)], 35.2 (CH_2, C6), 38.2 [CH_2, C8(9)], 41.5 (CH_2, NH$\underline{C}H_2$), 43.1 (C, C1), 45.0 [CH_2, C4(10)], 47.81 (CH_2, C2), 47.84 (C, C3), 127.1 (CH), 128.9 (CH), 129.5 (CH), 130.2 (CH), 133.6 (C, C2'), 135.8 (C, C1'), 176.8 (C, $\underline{C}$O). HRMS-ESI+ m/z [*M*+H]$^{+}$ calcd for [$C_{18}H_{23}ClN_2O^{+}H]^{+}$:319.1572, found:319.1574.

3-amino-N'-[2-(trifluoromethyl)phenyl]adamantane-1-carbohydrazide, **9a**

Compound **8a** was obtained following the general procedure A and, without further purification, **8a** was reacted with 2-(trifluoromethyl)phenylhydrazine following the general procedure B to give **9a** as a white solid (19% yield). mp = 213-216 ^{o}C. IR (ATR): 641, 695, 749, 899, 920, 1033, 1059, 1103, 1116, 1134, 1155, 1245, 1271, 1323, 1454, 1483, 1501, 1547, 1584, 1615, 1653, 2847, 2914, 3354 cm^{-1}. ^{1}H-NMR (400 MHz, $CDCl_3$) δ: 1.45 (s, 2 H, N$\underline{H}$), 1.56-1.68 [complex signal, 6 H, 6-H_2 and 4(10)-H_2],

1.78 (s, 2 H, 2-H_2), 1.82 -1.92 [m, 4 H, 8(9)-H_2], 2.26 [m, 2 H, 5(7)-H], 6.56 (s, 1 H, N<u>H</u>), 6.93 (d, *J* = 7.6 Hz, 1 H, 6'-H), 6.96 (d, J = 7.6 Hz, 1 H, 4'-H), 7.39 (t, *J* = 7.6 Hz, 1 H, 5'-H), 7.51 (d, *J* = 8.4, 1 H, 3'H). ^{13}C-NMR (100.6 MHz, $CDCl_3$) δ: 29.4 [CH, C5(7)], 35.0 (CH_2, C6), 37.9 [CH_2, C8(9)], 42.6 (C, C1), 44.9 [CH_2, C4(10)], 47.4 (CH_2, C2), 47.7 (C, C3), 113.2 (CH, C6'), 115.3 (q, *J* = 29.5 Hz , C, C2'), 120.3 (C, C4'), 124.5 (q, *J* = 269.3 Hz, C, <u>C</u>F_3), 126.6 (q, *J* = 5.4 Hz, CH, C3'), 132.9 (CH, C5'), 145.9 (C, C1'), 176.6 (C, <u>C</u>O). HRMS-ESI+ m/z $[M+H]^+$ calcd for $[C_{18}H_{22}F_3N_3O^+ H]^+$: 354.1788, found: 354.1794.

3-amino-N'-(2,6-dichlorophenyl)adamantane-1-carbohydrazide, **9b**

Compound **8b** was obtained following the general procedure A and, without further purification, **8b** was reacted with 2,6-dichlorophenylhydrazine following the general procedure B to give **9b** as a colourless solid (38% yield). mp = 153-156 ^{o}C. IR (ATR): 713, 760, 863, 935, 1085, 1304, 1418, 1444, 1524, 1576, 1594, 1653, 2020, 2847, 2914, 2930, 3136, 3322 cm^{-1}. ^{1}H-NMR (400 MHz, $CDCl_3$) δ: 1.25 (broad signal, 2 H, N<u>H</u>$_2$), 1.50-1.62 [complex signal, 6 H, 6-H_2 and 4(10)-H_2], 1.68 (s, 2 H, 2-H_2), 1.71 -1.82 [complex signal, 4 H, 8(9)-H_2], 2.19 [m, 2 H, 5(7)-H], 6.78 (d, *J* = 4.8 Hz, 1H, N<u>H</u>), 6.88 (t, *J* = 8.9 Hz, 1 H, 4'-H), 7.23 [d, *J* = 8.0 Hz, 2 H, 3'(5')-H], 7.92 (d, *J* = 5.2 Hz, 1 H, N<u>H</u>). ^{13}C-NMR (100.6 MHz, $CDCl_3$) δ: 29.4 [CH, C5(7)], 35.1 (CH_2, C6), 37.8 [CH_2, C8(9)], 42.7 (C, C1), 45.0 [CH_2, C4(10)], 47.5 (CH_2, C2), 47.6 (C, C3), 123.9 (CH, C4'), 125.8 [C, C2'(6')], 128.9 [CH, C3'(5')], 141.3 (C, C1'), 175.4 (C, <u>C</u>O). HRMS-ESI+ m/z $[M+H]^+$ calcd for $[C_{17}H_{21}Cl_2N_3O^+ H]^+$: 354.1134, found: 354.1140.

3-amino-N'-(2,3-dichlorophenyl)adamantane-1-carbohydrazide, **9c**

Compound **8c** was obtained following the general procedure A and, without further purification, **8c** was reacted with 2,3-dichlorophenylhydrazine following the general

procedure B to give **9c** as a light yellow solid (36% yield). mp = 215-219 ^{o}C. IR (ATR): 767, 912, 938, 1041, 1106, 1137, 1170, 1266, 1287, 1421, 1449, 1491, 1578, 1648, 2842, 2894, 3348 cm^{-1}. ^{1}H-NMR (400 MHz, DMSO) δ: 1.42-1.57 [complex signal, 6 H, 6-H_2 and 4(10)-H_2], 1.63 (s, 2 H, 2-H_2), 1.70 -1.80 [complex signal, 4 H, 8(9)-H_2], 2.10 [s, 2 H, 5(7)-H], 6.61 (dd, *J* = 8.0 Hz, *J* = 1.6 Hz, 1 H, 6'-H), 6.95 (dd, *J* = 8.0 Hz, *J* = 1.6 Hz, 1 H, 4'-H), 7.15 (t, *J* = 8.0 Hz, 1 H, 5'-H), 7.58 (s, 1 H, N<u>H</u>). ^{13}C-NMR (100.6 MHz, DMSO) δ: 29.3 [CH, C5(7)], 35.2 (CH_2, C6), 37.7 [CH_2, C8(9)], 41.9 (C, C1), 44.9 [CH_2, C4(10)], 47.3 (CH_2, C2), 47.6 (C, C3), 111.0 (CH, C6'), 115.1 (C, C3'), 119.5 (CH, C4'), 128.4 (CH, C5'), 131.8 (C, C2'), 147.2 (C, C1'), 176.1 (C, <u>C</u>O). HRMS-ESI+ m/z [*M*+H]$^{+}$ calcd for [$C_{17}H_{21}Cl_2N_3O$ $^{+}$H]$^{+}$: 354.1134, found: 354.1140.

3-amino-N'-[2-chloro-4-(trifluoromethyl)phenyl]adamantane-1-carbohydrazide, **9d**

Compound **8d** was obtained following the general procedure A and, without further purification, **8d** was reacted with 2-chloro-4-(trifluromethyl)phenylhydrazine following the general procedure B to give **9d** as a light orange solid (14% yield). mp = 185-186 ^{o}C. IR (ATR): 659, 822, 881, 899, 930, 1046, 1111, 1256, 1416, 1491, 1578, 1612, 1653, 2899, 2925, 3198, 3385, 3627 cm^{-1}. ^{1}H-NMR (400 MHz, DMSO) δ: 1.40-1.60 [complex signal, 6 H, 6-H_2 and 4(10)-H_2], 1.64 (s, 2 H, 2-H_2), 1.70-1.88 [complex signal, 4 H, 8(9)-H_2], 2.11 [s, 2 H, 5(7)-H], 6.81 (d, *J* = 8.0 Hz, 1H, 6'-H), 7.45-7.60 (complex signal, 2 H, 3'-H and 5'-H), 7.56 (broad s, 1 H, NH). ^{13}C-NMR (100.6 MHz, DMSO) δ: 29.2 [CH, C5(7)], 35.2 (CH_2, C6), 37.7 [CH_2, C8(9)], 41.9 (C, C1), 44.9 [CH_2, C4(10)], 47.2 (CH_2, C2), 47.6 (C, C3), 112.8 (q, *J* = 31 Hz, C, C4'), 114.9 (CH, C6'), 121.4 (C, C2'), 123.8 (q, *J* = 273 Hz, CF_3), 125.8 (broad signal, CH, C3'), 133.3 (CH, C5'), 145.8 (C, C1'), 176.1 (C, <u>C</u>O). HRMS-ESI+ m/z [*M*+H]$^{+}$ calcd for [$C_{18}H_{21}Cl\,F_3N_3O$ + H]$^{+}$: 388.1398, found: 388.1404.

3-amino-N'-(3,5-dichloropyridin-4-yl)adamantane-1-carbohydrazide, **9e**

Compound **8e** was obtained following the general procedure A and, without further purification, **8e** was reacted with 3,5-dichloro-4-hydrazinopyridine following the general procedure B to give **9e** as a white solid (30% yield). mp = 191-192 ^{o}C. IR (ATR): 729, 793, 886, 935, 1000, 1083, 1090, 1225, 1279, 1395, 1444, 1475, 1540, 1558, 1589, 1659, 1958, 1997, 2077, 2153, 2206, 2341, 2909, 3173 cm^{-1}. ^{1}H-NMR (400 MHz, $CDCl_3$) δ: 1.25 – 1.42 (broad s, 2H, NH), 1.54-1.63 [complex signal, 6 H, 6-H_2 and 4(10)-H_2], 1.71 (s, 2 H, 2-H_2), 1.74 -1.85 [complex signal, 4 H, 8(9)-H_2], 2.23 [m, 2 H, 5(7)-H], 6.81 (s, 1 H, NH), 7.87 (s, 1H, NH), 8.29 [s, 2 H, 2'(6')-H]. ^{13}C-NMR (100.6 MHz, $CDCl_3$) δ: 29.4 [CH, C5(7)], 35.0 (CH_2, C6), 37.8 [CH_2, C8(9)], 42.8 (C, C1), 44.9 [CH_2, C4(10)], 47.4 (CH_2, C2), 47.6 (C, C3), 120.6 [C, C3'(5')], 147.3 (C, C4'), 148.4 [CH, C2'(6')], 175.5 (C, CO) HRMS-ESI+ m/z [*M*+H]$^{+}$ calcd for [$C_{16}H_{20}Cl_2N_4O$+ H]$^{+}$: 355.1087, found: 355.1094.

3-amino-N'-(3-chloro-2-fluorophenyl)adamantane-1-carbohydrazide, **9f**

Compound **8f** was obtained following the general procedure A and, without further purification, **8f** was reacted with 3-chloro-2-flurophenylhydrazine following the general procedure B to give **9f** as a yellowish solid (25% yield). mp = 200-202 ^{o}C. IR (ATR): 708, 762, 814, 920, 935, 943, 1044, 1093, 1124, 1219, 1284, 1457, 1470, 1506, 1584, 1607, 1648, 1984, 2847, 2899, 3307 cm^{-1}. ^{1}H-NMR (400 MHz, DMSO) δ: 1.42-1. [complex signal, 6 H, 6-H_2 and 4(10)-H_2], 1.62 (s, 2 H, 2-H_2), 1.68-1.78 [complex signal, 4 H, 8(9)-H_2], 2.10 [broad s, 2 H, 5(7)-H], 6.61 (t, *J* = 8.0 Hz, 1 H, 6'-H), 6.82 (t, *J* = 7.6 Hz, 1 H, 4'-H), 6.99 (t, *J* = 7.6 Hz, 1 H, 5'-H), 7.83 (s, 1H, NH). ^{13}C-NMR (100.6 MHz, DMSO) δ: 29.3 [CH, C5(7)], 35.2 (CH_2, C6), 37.7 [CH_2, C8(9)], 41.9 (C, C1), 44.8 [CH_2, C4(10)], 47.2 (CH_2, C2), 47.7 (C, C3), 112.1 (CH, C6'), 118.7 (CH,

C4'), 119.5 (d, *J* = 14.6 Hz, CH, C3'), 125.2 (d, *J* = 4.2 Hz, CH. C5'), 139.9 (d, *J* = 10.2 Hz, C, C1'), 145.6 (d, *J* = 241.5 Hz, C, C2'), 176.2 (C, CO). HRMS-ESI+ m/z $[M+H]^+$ calcd for $[C_{17}H_{21}ClFN_3O+ H]^+$: 338.1430, found: 338.1439.

3-amino-N'-(2-chlorophenyl)adamantane-1-carbohydrazide, **9g**

Compound **8g** was obtained following the general procedure A and, without further purification, **8g** was reacted with 2-chlorophenylhydrazine following the general procedure B to give **9g** as a pale orange solid (28% yield). mp = 220-222 ^oC. IR (ATR): 734, 902, 925, 1033, 1046, 1292, 1442, 1496, 1545, 1586, 1594, 1646, 2904, 2925, 3322 cm^{-1}. ^1H-NMR (400 MHz, $CDCl_3$) δ: 1.42 (broad s, 2 H, NH), 1.56-1.67 [complex signal, 6 H, 6-H_2 and 4(10)-H_2], 1.75 (s, 2 H, 2-H_2), 1.76-1.87 [complex signal, 4 H, 8(9)-H_2], 2.23 [s, 2 H, 5(7)-H], 6.43 (broad s, 1 H, NH), 6.80 (dd, *J* = 8.0 Hz, *J'* = 1.6 Hz, 1 H, 6'-H), 6.83 (td, *J* = 8.0 Hz, *J'* = 1.6 Hz, 1 H, 4'-H), 7.13 (td, *J* = 8.0 Hz, *J'* = 1.6 Hz, 1 H, 5'H), 7.27 (dd, *J* = 8.0 Hz, *J'* = 1.6 Hz, 3'H), 7.54 (broad s, 1 H, NH). ^{13}C-NMR (100.6 MHz, $CDCl_3$) δ: 29.4 [CH, C5(7)], 35.1 (CH_2, C6), 37.9 [CH_2, C8(9)], 42.6 (C, C1), 44.9 [CH_2, C4(10)], 47.5 (CH_2, C2), 47.7 (C, C3), 113.4 (CH, C6'), 119.9 (C, C2'), 121.5 (CH, C4'), 127.6 (CH, C5'), 129.5 (CH, C3'), 144.1 (C, C1'), 176.5 (C, CO). HRMS-ESI+ m/z $[M+H]^+$ calcd for $[C_{17}H_{22}ClN_3O+ H]^+$: 320.1524, found: 320.1528.[2]

3-amino-N'-(3,5-dichloropyridin-4-yl)-5,7-dimethyladamantane-1-carbohydrazide, **15a**

Compound **14a** was obtained from **12** following the general procedure A. Without further purification, **14a** was reacted with 3,5-dichloro-4-hydrazinopyridine following the general procedure B to give **15a** as a white solid (25% yield). mp = 300-302 ^oC. ^1H NMR (400 MHz, $CDCl_3$) δ: 0.91 (s, 6H, CH_3), 1.12 (broad s, 2 H, 6-H_2), 1.20-1.27 [complex signal, 4 H, 4(10)-H_2], 1.42-1.48 [complex signal, 4 H, 8(9)-H_2], 1.58 (s, 2 H,

2-H_2), 6.80 (s, 1 H, NH), 7.93 (s, 1 H, NH), 8.29 [s, 2 H, 2'(6')-H]. ^{13}C-NMR (100.6 MHz, $CDCl_3$) δ: 29.6 (CH_3, $\underline{C}H_3$), 32.9 [C, C5(7)], 44.1 [CH_2, C8(9)], 44.2 (C, C1), 46.1 (CH_2, C2), 49.3 (C, C3), 49.5 (CH_2, C6), 51.4 [CH_2, C4(10)], 120.6 [CH, C3'(5')], 147.2 (C, C4'), 148.3 [CH, C2'(6')], 175.4 (C, $\underline{C}O$). HRMS-ESI+ m/z [*M*+H]$^+$ calcd for [$C_{18}H_{24}Cl_2N_4O$+ H]$^+$: 383.1400, found: 383.1404.

3-amino-N'-(2-chlorophenyl)-5,7-dimethyladamantane-1-carbohydrazide, **15b**

Compound **14b** was obtained from **12** following the general procedure A. Without further purification, **14b** was reacted with 2-chlorophenylhydrazine following the general procedure B to give **15b** as a white solid (28% yield). mp = 280-282 ^{o}C. IR (ATR): 646, 736, 1031, 1230, 1289, 1356, 1390, 1449, 1540, 1648, 2480, 2857, 2930, 3245, 3297 cm^{-1}. ^{1}H NMR (400 MHz, CD_3OD) δ: 0.96 (s, 6 H, $C\underline{H}_3$), 1.19 (broad s, 2 H, 6-H_2), 1.29-1.37 [complex signal, 4 H, 4(10)-H_2], 1.55 [broad s, 4 H, 8(9)-H_2], 1.69 (s, 2 H, 2-H_2), 6.76-6.82 (complex signal, 2 H, 4'-H and 6'-H), 7.15 (dt, *J* = 8.0 Hz, *J'* = 1.6 Hz, 1 H, 5'-H), 7.25 (dd, *J* = 8.0 Hz, *J'* = 1.6 Hz, 1 H, 3'-H). ^{13}C-NMR (100.6 MHz, CD_3OD) δ: 30.1 (CH_3, $\underline{C}H_3$), 33.9 [C, C5(7)], 45.0 (C, C1), 45.1 [CH_2, C8(9)], 45.4 (CH_2, C2), 50.5 (CH_2, C6), 50.6 [CH_2, C4(10)], 51.1 (CH_2, C3), 114.2 (CH, C6'), 120.1 (C, C2'), 121.5 (CH, C4'), 128.7 (CH, C5'), 130.3 (CH, C3'), 145.9 (C, C1'), 178.8 (C, $\underline{C}O$). HRMS-ESI+ m/z [*M*+H]$^+$ calcd for [$C_{19}H_{26}ClN_3O$+ H]$^+$: 348.1764, found: 348.1801.

2. P2X$_7$ receptor antagonist activity. Dye uptake using the ethidium ion assay.

HEK293 cells stably expressing the P2X$_7$ receptor were maintained in Dulbecco's modified Eagle's medium (DMEM) supplemented with 10% fetal bovine serum (FBS), 2 mM L-glutamine, and antibiotics (50 U/mL penicillin and 50 mg/mL streptomycin) in a humidified 5% CO_2 atmosphere at 37 ºC. We used Lipofectamine as a transfection

reagent with a pcDNA3.1 vector-based plasmid harbouring $hP2X_7R$ (Invitrogen). After diluting to $2.5x10^6$ cells/mL, 80 mL of the cell suspension was added to each well of 96-well culture plates. The test com- pounds and 20(3')-O-(4-benzoylbenzoyl)-ATP (BzATP) were then added, and the cells were incubated for 2 h in a humidified 5% CO_2 atmosphere at 37ºC. After incubation, a Bio-Tek FL600 fluorescence plate reader was used to measure the absorbance at an excitation wavelength of 530 nm and an emission wavelength of 590 nm. The inhibition (percent) of ethidium ion uptake was expressed as a relative value of the maximum accumulation when stimulated with BzATP only. To calculate IC_{50} values, we calculated a series of dose-response data using nonlinear regression analysis (i.e., percentage accumulation of ethidium bromide *vs* compound concentration).

3. NMDA receptor antagonist activity.

The functional assay of antagonist activity at NMDA receptors was performed using primary cultures of rat cerebellar granule neurons that were prepared according to established protocols.[3] Cells were grown on 10 mm poly-L-lysine coated glass cover slips, and used for the experiments after 6-10 days *in vitro*. Cells were loaded with 6 µM Fura-2 AM (Invitrogen-Molecular Probes) for 30 min. Afterwards the coverslip was mounted on a quartz cuvette containing a Locke-Hepes buffer using a special holder. Measurements were performed using a PerkinElmer LS-55 fluorescence spectrometer equipped with a fast-filter accessory, under mild agitation and at 37 ºC. Analysis from each sample was recorded real-time during 1400 s. After stimulation with NMDA (100 µM, in the presence of 10 µM glycine), increasing cumulative concentrations of the compound to be tested were added. The percentages of inhibition at every tested concentration were analyzed using a non-linear regression curve fitting (variable slope) by using the software GraphPad Prism 5.0.

4. References.

1. Wanka, L.; Cabrelle, C.; Vanejews, M.; Schreiner, P. R. γ-aminoadamantanecarboxylic acids through direct C-H bond amidations. *Eur. J. Org. Chem.* **2007**, *9*, 1474–1490.

2. Nelson, D. W.; Sarris, K.; Kalvin, D. M.; Namovic, M. T.; Grayson, G.; Donnelly-Roberts, D. L.; Harris, R.; Honore, P.; Jarvis, M. F.; Faltynek, C. R.; Carroll, W. A. Structure-activity relationship studies on *N'*-aryl carbohydrazide $P2X_7$ antagonists. *J. Med. Chem.* **2008**, *51*, 3030-3034.

3. Canudas, A. M.; Pubill, D.; Sureda, F. X.; Verdaguer, E.; Camps, P.; Muñoz-Torrero, D.; Jiménez, A.; Camins, A.; Pallàs, M. Neuroprotective effects of (±)-huprine Y on in vitro and in vivo models of excitotoxicity damage. *Exp. Neurol.* **2003**, *180*, 123–130

Chapter 9

Conclusions

In line with the stated in the objectives in this Thesis several compounds with ability to function as modulators of the Influenza A M2 viroporin, the ionotropic purinergic $P2X_7$ receptor and the ionotropic glutamatergic NMDA receptors have been successfully designed, synthesized and evaluated. In addition Multi-Target Directed Ligands for NMDA-$P2X_7$ of interest for the Alzheimer's Disease treatment, have been also designed, synthesized and evaluated.

Besides this a unique polycyclic scaffold of theoretic chemical interest, has been studied from a structural point of view.

The main conclusions that have arisen from each project follow:

Chapter 3. 3-Azatetracyclo[5.2.1.1^{5,8}.0^{1,5}]undecane derivatives as *wt* and V27A Influenza A/M2 channel blockers

- The 3-azatetracyclo[5.2.1.1^{5,8}.0^{1,5}]undecanes **25**, **26** and **27** were successfully prepared and evaluated as anti-Influenza A compounds, displaying potent M2 *wt* inhibition values which equalled or improved the ones shown by the commercial compound, Amt.

- The guanidine **27** was identified, together with some analogues reported in the same project, as a dual inhibitor of the A/M2 wt and V27A mutant channels, being the first compounds endowed with this activity reported in the literature.

- The usefulness of the 3-azatetracyclo[5.2.1.1^{5,8}.0^{1,5}]undecane scaffold for the development of bioactive compounds and/or as adamantane replacement, was successfully demonstrated.

- Several SAR information was disclosed, being that: the secondary amines perform better than its tertiary amines analogues, an increased bulkiness at the basic centre distal end improves the inhibitory activity and the guanidines are usually more potent that the corresponding amine analogues.

- Our strategy of conferring rigidity to the basic centre by including it in a heterocyclic ring was proven successful.

Chapter 4.

PART A. Easily Accessible Polycyclic Amines as wt and mutant Influenza A/M2 channel blockers

- The 4-azatetracyclo[5.4.2.$0^{2,6}$.$0^{8,11}$]trideca-9,12-diene **31** and **32** as well as its reduced analogues **33**, **34** were successfully prepared and evaluated as Influenza A/M2 channel inhibitors, all of them displaying greater A/M2 inhibition values than the reference compound and the diene **31** behaving as antiviral.

- Compound **34** was endowed with dual activity against the A/M2 wt and the A/M2 V27A.

- This family of compounds allowed us to successfully prepare potent M2 blockers with an eased synthesis. Coming from the anti-Influenza compounds of Chapter 3, which resource consuming 13 synthetic-step route involved convoluted low-yielding reactions and in some cases requiring the use of hazardous, complex handling chemicals, we developed an easy-access and high yielding route, in which the first bioactive compound can be prepared in only 2 synthetic steps.

- In this project the first triple inhibitors of A/M2 *wt*, A/M2 V27A and A/M2 L26F were developed. These compounds revealed a different binding mode for A/M2 *wt*, than for A/M2 V27A, down-binding mode and up-binding mode, respectively, which may have implications in the A/V27A drug resistance mechanism.

- The SAR trends revealed that, for V27A and L26F M2 channels, an increased bulkiness, saturation and basicity of the compound translated in an improved inhibition profile.

- The completion of this project served as a starting platform for at least three related new research expeditions.

PART B. Dimerization of a pyramidalized alkene to a hydrocarbon featuring four cyclohexane rings in boat conformations.

- An optimized and robust synthetic route towards the highly pyramidalized alkene **XII**, was developed.

- The crystal structures of the compounds **48**, **51**, **XI**, and **XIII**, were determined by X-Ray crystallography.

- The dimer **XIII**, featuring three planar cyclobutane rings and four cyclohexane rings in boat conformations was successfully prepared and studied.

- The X-ray structural studies and theoretical calculations allowed the study of the flagpole interactions occurring in this molecule. This revealed that the distances between the flagpole hydrogen atoms and the flag pole carbon atoms were smaller than the sum of the Van der Waals radius of the involved atoms.

- The dimer **XIII** presented as a sturdy structure, being highly stable to high temperatures, in sharp contrast with previously described dimers of highly pyramidalized alkenes.

Chapter 5. A/M2 wt and V27A blockade dissimilarities amongst structurally related adamantyl piperidines. Insights on drug resistance.

- In this project 12 adamantyl piperidines were successfully prepared and evaluated as Influenza A/M2 channel inhibitors. Among them, 5 were identified as dual inhibitors of the A/M2*wt* and A/M2V27A channels displaying balanced activity values.

- The SAR revealed that: (i) switching the adamantane ring from position 2 to position 4 of the piperidine, triggered faster association rate to the channel, (ii) moving the piperidine ring from the C-2 position of the adamantane, to the C-1 position led to an increase in the inhibitory activity on both channels, (iii) in the C-2 position of the adamantane, introduction of an extra methylene spacer between the adamantane and the piperidine ring, restored the inhibitory activity against the wt, but not against the V27A mutant. The previous observation that alkylation of a secondary amine to a tertiary amine reduced the activity, was also confirmed.

- The differences observed in between the isochronic inhibition tests, the TEVC electrophysiology experiments and the antiviral activity, allowed us to postulate that: (i) M2 channel blockers with potent Influenza A antiviral activity usually show slow but steady binding to the channel, however, regardless the K_{on} an antiviral displays, its K_{off} must be slow in order to display antiviral activity, (ii) caution has to be taken when defining M2 inhibitors solely by isochronic inhibition assays, as this assay may not detect

slow binders with antiviral potential and on the other hand may identify weak affinity binders (fast K_{off}) as potential antivirals.

- The fast (rapid k_{on}) but weak affinity (rapid k_{off}) behaviour observed in our compounds for the V27A A/M2 mutant channel, is the first experimental evidence of the V27A drug resistance mechanism, previously proposed by *in silico* and structural approaches.

Chapter 6. Adamantylmethylanilines and aromatic piperidines as promising scaffolds with anti-hemagglutinin activity.

- In this project 25 adamantylmethylanilines were successfully prepared and evaluated as antivirals targeting the Influenza A hemagglutinin, with some of them behaving as anti-Influenza A compounds.

- The SAR trends disclosed in this project point out that an optimal activity is achieved by a compound that features: a piperidine ring in the right hand-side and an aniline with *ortho* substitution, preferably an ethyl or isopropyl chain, in the left hand side, linked by a 2 carbon atom spacer.

Chapter 7. Adamantane scaffold optimization in the $P2X_7$ antagonists development.

- In this project it has been clearly proved that the adamantane ring can be successfully replaced by other polycyclic scaffolds without hampering the $P2X_7$ antagonistic activity profile.

- The results confirm that the adamantane ring is an unoptimized structure for the design of $P2X_7$ antagonists.

- The binding to the $hP2X_7$ and $rP2X_7$ receptors of our newly designed $P2X_7$ antagonists has been studied by *in silico* models with the homology models of $hP2X_7$ and $rP2X_7$.

- A scaffold which endows the compounds with antagonistic potencies in the low nanomolar range has been identified and submitted for patent protection.

Chapter 8. First multi-targeted directed ligands of the NMDA and $P2X_7$ receptors, with interest for the treatment of Alzheimer's Disease.

- Surprisingly, in the reported scaffolds the replacement of the amantadine moiety for memantine has little to no effect to the NMDA antagonistic activity, despite memantine is known to be one-fold more active than amantadine.

- The work disclosed in this chapter is the first prove that MTDL can be prepared for the NMDA and the $P2X_7$ receptors.

- The compound **115g** is the first compound endowed with the aforementioned dual activities ever reported in the literature.

En consonància amb l'exposat en els objectius d'aquesta Tesi, nombrosos compostos amb habilitat per funcionar com a moduladors de la viroporina M2 del virus de la Influenza A, del receptor ionotròpic de purines $P2X_7$ i del receptor ionotròpic glutamatèrgic NMDA, han estat dissenyats, sintetitzats i avaluats farmacològicament de manera satisfactòria. A més a més Lligands Dirigits a Múltiples Dianes per NMDA-$P2X_7$, de possible interès pel tractament de la malaltia d'Alzheimer han estat, així mateix, dissenyats, sintetitzats i avaluats farmacològicament.

A part d'això una estructura policíclica única, d'interès teòric, ha estat estudiada des d'un punt de vista estructural.

Les conclusions principals de cada projecte es presenten a continuació:

Capítol 3. Derivats 3-Azatetraciclo[5.2.1.1^{5,8}.0^{1,5}]undecànics com a bloquejadors del canal M2 salvatge i el mutant V27A del virus de la Influenza A.

- Els 3-azatetraciclo[5.2.1.1^{5,8}.0^{1,5}]undecans **25**, **26** i **27** van ser satisfactòriament preparats i avaluats com a agents antiinfluenza A, presentant potents valors d'inhibició del canal M2 salvatge, que van equiparar o millorar els presentats pel compost comercial, Amt.

- La guanidina **27** va ser identificada, juntament amb alguns anàlegs, com a inhibidor dual del canal A/M2 salvatge i el mutant V27A, convertint-se en el primer compost conegut dotat amb aquesta activitat.

- La utilitat de l'estructura de 3-azatetraciclo[5.2.1.1^{5,8}.0^{1,5}]undecà pel desenvolupament de compostos bioactius i/o com a substitut de l'adamantà, ha estat satisfactòriament demostrada.

- S'ha extret una gran quantitat d'informació de SAR, tal com: les amines secundàries són millors que els seus anàlegs amb amines terciàries, el volum a la part distal del centre bàsic millora la inhibició del canal i les guanidines són normalment més potents que els seus anàlegs amina.

- La nostra estratègia de donar rigidesa al centre bàsic, incloent-hi un anell heterocíclic, s'ha demostrat vàlida per incrementar la capacitat d'inhibició del canal.

Capítol 4.

PART A. Amines policícliques de fàcil accés com a bloquejadors del canal M2 salvatge i el mutant V27A del virus de la Influenza A.

- Els 4-azatetraciclo[5.4.2.$0^{2,6}$.$0^{8,11}$]trideca-9,12-diens **31** i **32** així com els seus anàlegs reduïts **33**, **34** van ser exitosament preparats i avaluats com a inhibidors del canal A/M2 del virus de la Influenza, tots ells essent millors inhibidors que el compost de referència. El dièn **31** va mostrar activitat antiviral.

- El compost **34** va presentar activitat dual contra els canals A/M2 salvatge i el A/M2 V27A.

- Aquesta família de compostos ens va permetre preparar satisfactòriament bloquejadors del canal M2 per mitjà d'una síntesi senzilla. Partint dels compostos del Capítol 3, que requerien una síntesi tediosa de 13 passos, hem desenvolupat una síntesi accessible i d'alts rendiments en la que el primer compost bioactiu es prepara en només dues etapes sintètiques.

- En aquest projecte els primers inhibidors triples del A/M2 *wt*, V27A i L26F han estat desenvolupats. Aquests compostos van revelar un mode d'unió diferent per a A/M2 *wt* que per V27A, mode d'unió *down* i mode d'unió *up*, respectivament, fet que pot tenir implicacions en el mecanisme de resistència a fàrmacs de A/V27A.

- El SAR revela que per V27A i L26F, un increment del volum, saturació i basicitat de les molècules, dóna lloc a un perfil d'inhibició millorat.

- La finalització d'aquest projecte ha servit com a punt de partida de, com a mínim, tres projectes de recerca relacionats.

PART B. Dimerització d'un alquè piramidalitzat a un hidrocarbur amb quatre anells de ciclohexà en conformació de bot.

- S'ha desenvolupat una ruta sintètica robusta i optimitzada per a l'alquè altament piramidalitzat **XII**.

- Les estructures cristal·lines dels compostos **48**, **51**, **XI**, i **XIII**, van ser determinades per cristal·lografia de Raig X.

- El dímer **XIII**, amb tres anells de ciclobutà plans i quatre anells de ciclohexà en conformació de bot, va ser exitosament preparat i estudiat.

- Els estudis estructurals de Raig X i els càlculs teòrics, van permetre estudiar les interaccions d'asta de bandera que tenen lloc en aquesta molècula.

- El dímer **XIII** va resultar ser una estructura robusta i molt estable a les altes temperatures, en marcat contrast amb els dímers d'alquens altament piramidalitzats descrits prèviament.

Capítol 5. A/M2 wt i V27A diferències de bloqueig entre adamantil piperidines relacionades estructuralment. Noves perspectives de la resistència a fàrmacs.

- En aquest projecte 12 adamantil piperidines van ser satisfactòriament preparades i avaluades com a inhibidors del canal Influenza A/M2. D'entre elles, 5 van ser identificades com a inhibidors duals del canal salvatge i del canal mutant V27A, mostrant valors d'activitat balancejats.

- El SAR va revelar que: (i) canviar l'anell d'adamantà de la posició 2 a la posició 4 de la piperidina, provoca una associació més ràpida al canal, (ii) moure l'anell de piperidina de la posició C-2 de l'adamantà a la posició C-1, dóna lloc a un increment de l'activitat inhibitòria, en ambdós canals, (iii) en la posició C-2 de l'adamantà, la introducció d'un metilè extra que el separi de l'anell de piperidina, restaura l'activitat inhibitòria contra el *wt* però no contra el canal mutant V27A. Es va confirmar que el pas d'amina secundària a terciària empobreix l'activitat.

- Les diferències observades entre els experiments d'inhibició isocrònica, d'electrofisiologia de TEVC i d'activitat antiviral, ens han permès postular que: (i) els bloquejadors potents del canal M2 amb bona activitat antiviral, normalment presenten una unió lenta però persistent al canal, en canvi, independentment de la K_{on} que tingui un compost, la seva K_{off} ha de ser lenta per tal de presentar activitat antiviral, (ii) s'ha d'anar amb compte al definir inhibidors del canal M2 només amb assajos d'inhibició isocrònica, ja que aquest assaig pot passar per alt lligands lents però amb potencial antiviral i, per contra, identificar erròniament lligands dèbils (K_{off} ràpida) com a antivirals.

- Els nostres lligands amb un comportament d'unió ràpida però dèbil (k_{on} i k_{off} ràpides) al canal mutant V27A A/M2, representen la primera evidència experimental del

mecanisme de resistència a fàrmacs del mutant V27A, prèviament proposat en models *in silico* i estructurals.

Capítol 6. Adamantilmetilanilines i piperidines aromàtiques com a estructures prometedores amb activitat anti-hemagglutinina.

- En aquest projecte 25 adamantilmetilanilines van ser preparades i avaluades com a antivirals contra la proteïna HA del virus de la Influenza A. Algunes d'elles van mostrar activitat antiviral.

- Les tendències de SAR elucidades d'aquest projecte, van recalcar que l'activitat òptima s'obté quan un compost presenta: un anell de piperidina en la part dreta de la molècula i una anilina amb un substituent en la posició *orto* – preferiblement una cadena d'etil o isopropil – a la part esquerra de la molècula, unides per un separador de dos àtoms de carboni.

Capítol 7. Optimització de l'estructura d'adamantà pel desenvolupament d'antagonistes de $P2X_7$.

- En aquest projecte s'ha demostrat satisfactòriament que l'anell d'adamantà pot ser reemplaçat per altres estructures policícliques, sense que representi un detriment del perfil antagonístic cap al receptor $P2X_7$.

- Els resultats confirmen que l'anell d'adamantà és una estructura no optimitzada pel disseny d'antagonistes de $P2X_7$.

- La unió als receptors $hP2X_7$ i $rP2X_7$ dels nostres nous antagonistes de $P2X_7$ ha estat estudiada per models *in silico*, emprant models d'homologia de $hP2X_7$ i $rP2X_7$.

- Una estructura que confereix potències en el rang nanomolar baix als antagonistes, ha estat identificada i es troba en procés de protecció per patent.

Capítol 8. Primers Lligands Dirigits a Múltiples Dianes per NMDA i $P2X_7$, de possible interès pel tractament de la malaltia d'Alzheimer.

- Sorprenentment, en les estructures descrites en aquest projecte, la substitució de la part d'amantadina per la part de memantina no té cap efecte sobre l'activitat antagonista de NMDA, tot i que la memantina és coneguda per ser un ordre de magnitud més potent que l'amantadina.

- El treball exposat en aquest capítol, és la primera proba que es poden preparar MTDL pels receptors NMDA i $P2X_7$.

- La molècula **115g** és el primer compost conegut en la literatura que està dotat amb les dues activitats anteriorment esmentades.

RESUM

L'objectiu de la present tesi doctoral consisteix en desenvolupar molècules policícliques de baix pes molecular que tinguin com a diana tres canals iònics específics: la viroporina A/M2 del virus de la grip, el receptor purinèrgic dependent de lligand $P2X_7$ i el receptor glutamatèrgic dependent de lligand N-metil-D-Aspartat, per tal de modular-los d'una manera tal que n'evitin o millorin el desenvolupament dels processos patogènics associats a aquestes proteïnes i/o que permetin ser emprades com a eines de recerca.

En el capítol 1 es presenta una introducció general del paper dels canals iònics, així com una descripció més específica de cadascun dels 3 canals objecte d'estudi en aquesta Tesi. Els objectius d'aquest treball es detallen en el capítol 2, després del qual, en el capítol 3 es presenten un seguit d'anàlegs per contracció d'anell del fàrmac comercial Amantadina, resultant-ne els primers inhibidors duals del canal M2 del virus de la Influenza A descrits en la bibliografia, actius sobre la soca salvatge (*wt*) i sobre el mutant resistent a fàrmacs V27A (Rey-Carrizo, M. *et al. J. Med. Chem.* **2013**, *56*, 9265). Seguidament en la part A del capítol 4 es millora l'accessibilitat sintètica d'aquests primers inhibidors duals de A/M2 *wt* i V27A, gràcies al desenvolupament de noves estructures policícliques que presenten reaccions de cicloaddició com a pas sintètic clau. A banda de millorar la via d'obtenció d'inhibidors de la viroporina M2, d'aquest projecte se'n deriven dos potents blocadors del canal M2 amb activitat sobre *wt*, V27A i L26F. A més a més, gràcies a estudis *in silico*, s'observa com un dels inhibidors triples presenta un mode d'unió diferent sobre els canals *wt* i V27A, que podria estar directament relacionat amb el mecanisme de resistència a fàrmacs del mutant V27A (Rey-Carrizo, M., *et al.* J. Med. Chem. **2014**, 57(13), 5738). En el capítol 5 es completa el treball sobre la proteïna M2, amb el disseny de compostos antivirals amb estructura d'adamantil piperidines. Gràcies als estudis d'activitat d'aquests compostos, en aquest capítol es presenta per primera vegada la proba experimental d'una possible explicació del mecanisme de resistència a fàrmacs del mutant V27A, consistent en la possibilitat dels inhibidors d'unir-se al canal però la incapacitat d'aquests de romandre units el temps necessari com per afectar a la viabilitat del virus (Barniol-Xicota, M., *et al*. manuscrit en revisió al *J. Med. Chem.*).

Com a continuació de la recerca de compostos que puguin actuar com a agents antivirals front el virus de la Influenza A, en el capítol 6, s'explora una diana diferent de la viroporina M2: l'hemaglutinina (HA). La raó d'aquest fet rau en la possibilitat d'emprar inhibidors d'ambdues proteïnes virals, M2 i HA, a mode de politeràpia com a tractament potent front el virus de la grip. D'aquest projecte en resulten múltiples inhibidors de la HA i, a més a

més, se n'extreu informació de relació estructura-activitat, fonamental per al disseny de futurs inhibidors d'HA (Leiva, R., *et al.* manuscrit pendent d'enviar a *J. Med. Chem.*).

El capítol 7 representa el primer treball que marca l'inici de la línia de recerca d'antagonistes del receptor $P2X_7$ en el grup. En aquest s'optimitza l'estructura adamantànica d'inhibidors ja coneguts, resultant-ne en diverses estructures equipotents al compost amb el nucli d'adamantà, així com una estructura (en procés de protecció sota patent) que millora la seva activitat i que serà emprada per al disseny dels futurs antagonistes d'aquest receptor en el grup de recerca (Barniol-Xicota, M., *et al.* manuscrit en revisió al *Bioorg. Med. Chem. Lett.*).

Finalment, en el capítol 8, es presenten els primers exemples descrits a la bibliografia de *multi-target directed ligands* (MTDL) amb els receptors NMDA i $P2X_7$ com a dianes. La implicació d'ambos receptors en l'etiologia de la malaltia d'Alzheimer fa que aquestes noves molècules siguin de gran interès com a punt de partida per desenvolupar compostos amb activitats optimitzades pel seu ús en terapèutica (Karou, O., *et al.* manuscrit pendent d'enviar a *ACS Med. Chem. Lett.*).

Deixant de banda la recerca de compostos bioactius i tenint present el rerefons purament químic orgànic del grup de recerca, en la part B del capítol 4 es descriu un estudi teòric i experimental d'un alquè altament piramidalitzat, derivat de l'estructura d'un compost bioactiu detallat en la part A del mateix capítol. En concret, es descriu la generació de l'alquè piramidalitzat, el seu atrapat en forma d'adducte Diels-Alder i la seva dimerització a un compost policíclic d'estructura molt inusual, amb anells de ciclohexà amb conformació nau congelada. Gràcies a la combinació d'estudis teòrics i a la determinació de diverses estructures de raig X es van poder determinar les interaccions entre els hidròdgens asta de bandera dels anells de ciclohexà (Rey-Carrizo, M. *et al*. *Angew. Chem. Int. Ed.* **2014**, *53*, 8195).

ABBREVIATIONS

aa – amino acid

Ach – Acetilcholine

AD - Alzheimer's disease

Amt – Amantadine

APP - Amyloid Precursor Protein

BzATP - 2'(3')-*O*-(4-benzoylbenzoyl)-ATP

CREB - cAMP response element-binding

EDC - 1-ethyl-3(3-dimethylaminopropyl)carbodiimide

EC_{50} - concentration producing 50% antiviral effect

EI -electronic impact

Et -ethyl

GSK3 - Glycogen Synthase Kinase 3

HEK - Human Embryonic Kidney

HOBT - 1-hydroxybenzotriazole

HA – Hemagglutinin

IL-1β – Interleukin beta

LDA- lithium diisopropylamide

LiHMDS- bis(trimethylsilyl)amide lithium

MCC - minimum cytotoxic concentration

MDCK - Madin Darby canine Kidney cells

Me - methyl

MTDL – Multi Target Directed Ligands

NMDA N-methyl-D-Aspartate

NP - nucleoprotein

PB1 - polymerase basic 1 protein

PB2 - polymerase basic 2 protein

Rmt – Rimantadine

SNC – Sistema Nerviós Central

SNP – Sistema Nerviós Perifèric

vRNP - viral ribonucleoprotein

TEVC – Two Electrode Voltage Clamp

WHO - World Health Organization

wt – wild type